LABORATORY OF MOLECULAR STRUCTURE AND SPECTRA

DEPARTMENT OF PHYSICS • THE UNIVERSITY OF CHICAGO

TECHNICAL REPORT

1964

For the period
1 January to 31 December 1964
OFFICE OF NAVAL RESEARCH
CONTRACT Nonr 3121(01)

For the period
1 January to 31 December 1964
ELECTRONIC SYSTEMS DIVISION, AFSC
CONTRACT AF19(628)-[illegible]

For the period
1 January to 31 December 1964
ARMY RESEARCH OFFICE
CONTRACT DA-11-022-ORD-3119

For the period
1 January to 31 December 1964
AF OFFICE OF SCIENTIFIC RESEARCH, OAR
CONTRACT AF33(657)-8891

LABORATORY OF MOLECULAR STRUCTURE AND SPECTRA

DEPARTMENT OF PHYSICS • THE UNIVERSITY OF CHICAGO

TECHNICAL REPORT

1964

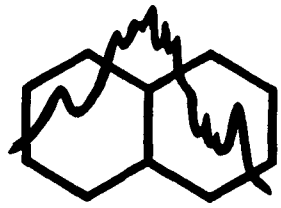

For the period
1 January to 31 December 1964
OFFICE OF NAVAL RESEARCH
CONTRACT Nonr-2121(01)

For the period
1 January to 31 December 1964
ELECTRONIC SYSTEMS DIVISION, AFSC
CONTRACT AF19(604)-6662
CONTRACT AF19(628)-2474

For the period
1 January to 31 December 1964
ARMY RESEARCH OFFICE
CONTRACT DA-11-022-ORD-3119

For the period
1 January to 31 December 1964
AF OFFICE OF SCIENTIFIC RESEARCH, OAR
CONTRACT AF33(657)-8891

CONTRACT PERSONNEL

(1 January 1964 to 31 December 1964)

Physics Faculty

#*†‡◇ Professor R. S. Mulliken

#*§ Professor C. C. J. Roothaan

Research Associates

#* Dr. Paul E. Cade (from 9-12-61)

†‡ Dr. Peter K. Carroll (thru 1-31-64). Now at Air Force Cambridge Research Laboratories, Bedford, Massachusetts.

†‡ Dr. Marshall L. Ginter (from 10-1-62)

* Dr. John B. Greenshields (thru 8-31-64). Associate Professor on leave of absence, and now returned to Duquesne University, Pittsburgh, Pennsylvania.

#* Dr. Winifred Huo (thru 9-30-64). Chemistry Ph. D. degree on March 15, 1964, now at Harvard University, Cambridge, Massachusetts.

†‡ Dr. Yerneni V. Rao (from 10-1-63)

#* Dr. John J. Sinai (thru 7-31-64). Now at the University of Louisville, Louisville, Kentucky.

#* Dr. W. Roy Wessel (from 11-1-64)

Research Assistants

#* Mr. Howard D. Cohen (from 7-16-62). Chemistry Ph. D. candidate.

#* Mr. Gurupada Das (from 10-1-61). Physics Ph. D. candidate.

#* Mr. John Detrich (from 11-1-64). Graduate student in Physics.

†‡ Mr. Fernando P. Huberman (from 12-21-59). Chemistry Ph. D. candidate.

#* Mr. Bhairav D. Joshi (from 10-1-61). Chemistry Ph. D. degree, December 18, 1964.

#* Mr. Yong-Ki Kim (from 10-1-61). Physics Ph. D. candidate.

#◇ Mr. Marvin Kroll (from 11-1-63). Chemistry Ph. D. candidate.

#* Mr. Gulzari L. Malli (thru 3-31-64). Chemistry Ph. D. degree, March 15, 1964.

#† Mr. Ramesch C. Misra (from 9-19-62). Graduate student in Physics.

#* Mr. Hideo Sambe (from 10-1-64). Graduate student in Physics.

#* Mrs. Eugenia Schwartz (from 6-17-63). Physics Ph. D. candidate.

§ Mr. Zoran Sibincic (from 4-1-62). Physics Ph. D. candidate.

#* Mr. Irving Wladawsky (from 1-1-64). Graduate student in Physics.

Mathematics Assistant

#* Mr. Tracy Kinyon

Laboratory Technicians

† Mrs. Jane Maxwell (thru 7-23-64)

† Miss Delthlyn McDonald (from 11-9-64)

#* Mr. Thomas Sherrard (from 11-16-64)

† Miss Cheryl S. Weinberg (thru 10-31-64)

Editorial Staff

#* Mrs. Helen E. Griffith

* § Mrs. Avis S. Lyles

ASSOCIATED NON-CONTRACT PERSONNEL

#◊ Dr. Ying Nan Chiu (thru 8-31-64). Now at the Catholic University of America, Washington, D. C.

\# Dr. Wlodzimierz Kolos (thru 1-31-64). Now at the Institute of Nuclear Research, Warsaw, Poland.

#◊ Dr. Tanekazu Kubota (thru 10-31-64). Now at Shionogi Research Institute, Osaka, Japan.

Mr. Joseph P. Olive (from 10-1-63). Research Assistant in Laboratory supported by ARPA contract funds. Physics Ph. D. candidate.

Dr. Sigrid Peyerimhoff (thru 4-10-64). Now at Princeton University, Princeton, New Jersey.

Mr. George Soukup (from 4-1-62). Research Assistant in Laboratory supported by ARPA contract funds thru 9-30-64, now supported by California Research Graduate Study and Research funds. Physics. Ph. D. candidate.

\# Dr. Lutoslaw Wolniewicz (thru 7-31-64). Now at Nicholas Copernicus University, Torun, Poland.

† Work assisted by the Office of Naval Research, Physics Branch, Contract Nonr-2121 (01), under Professor Mulliken.

‡ Work assisted by the Office of Aerospace Research, United States Air Force, Electronic Systems Division, Air Force Systems Command under Contract AF19(628)-2474, under Professor Mulliken.

* Work assisted by Advanced Research Projects Agency through the U. S. Army Research Office (Durham), under Contract DA-11-022-ORD-3119 with Professor Roothaan.

§ Work assisted by the U. S. Air Force through Aeronautical Systems Division, Air Force Systems Command, Wright Patterson Air Force Base, Ohio, under Contract AF33(657)-8891, with Professor Roothaan.

\# Work assisted by a grant with the National Science Foundation GP-28 which expired 31 August 1964, but is continuing under NSF grant GP-3427 which commenced 1 September 1964 under the supervision of Professors Mulliken and Roothaan for studies in molecular quantum mechanics and for studies on molecular complexes.

◊ Work assisted by a grant with the National Science Foundation G-20375, under Professor Mulliken for studies on molecular complexes. Grant expired 31 March 1964, but work continued under a supplemental grant GP-2545 which expired 30 September 1964. Work is presently continuing under the aforementioned NSF grant GP-3427 with Professors Mulliken and Roothaan.

TABLE OF CONTENTS

FOREWORD

Seven comprehensive Technical Reports were issued under Contract N6ori-20, Task Order IX, Project 019 101, with the Office of Naval Research: a Quarterly Report for the period 1 June 1947 to 31 August 1947; an Annual Report (in two parts) for the period from 1 September 1947 to 31 August 1948; a Report (in two parts) for the period 1 September 1948 to 31 March 1950; a Report (in two parts) for the period 1 April 1950 to 31 March 1951; a Report (in two parts) for the period 1 April to 31 March 1952.

The Technical Report for 1952-3, issued in two parts, and Part One of the Technical Report for 1953-4, which covered roughly the period 1 October 1953 to 31 March 1954, were issued jointly under this Laboratory's contract with the Office of Naval Research (ONR) and Contract DA-11-022-1002, Project TB2-0001 (505) with the Office of Ordnance Research (OOR). Part Two of the Technical Report for 1953-4 was issued jointly under these contracts and Contract AF18(600)-471, Project No. R-351-40-4 with the Office of Scientific Research (AFOSR) of the Air Research and Development Command (ARDC). The Technical Reports for 1955 and 1956 were issued jointly under the contracts with ONR, OOR, AFSOR, and under Contract AF19(604)1-019 with the Geophysics Research Directorate (GRD) of the Air Force Cambridge Research Center. The OOR contract was extended without additional funds from 1 October 1957 through 30 September 1958 and a Final Report was issued.

The work under the original ONR Contract N6ori-20, IX, Project 019101 was completed on 30 September 1956, and a Final Report was issued. A new contract, Nonr-2121 (01), went into effect 1 October 1956: work described in the 1956 and subsequent Technical Reports and supported by the ONR has been done under this contract.

The original GRD contract terminated 25 October 1957. This work was continued under GRD contract AF19(604)-3478 which terminated 19 December 1959. The work has further continued, beginning 15 January 1960, under contract AF19(604)-6662 with the Electronics Systems Division (AFESR) of the Air Force Systems Command (AFSC). At the termination of this contract on 14 January 1963, a final report was issued and work continues under a new contract AF19(628)-2474, for the period 15 January 1963 through 31 March 1966.

The AFOSR contract was extended for two years from 1 October 1956 without added funds but with the provision of ample computing time, for the completion of the work under the contract on the Univac Scientific (Remington-Rand 1103 and 1103A) electronic digital computers at Wright Field Air Force Base (WADC); a Final Report was issued. With the availability of these computer facilities, new funded support from a National Science Foundation (NSF) grant make it possible to carry this work further forward.

All the contract mentioned thus far were under the direction of Professor R. S. Mulliken as Principal Investigator. A one-year contract from WADC, AF33(616)-5608 with Professor C. C. J. Roothaan as Principal Investigator went into effect 1 April 1958, and the use of the computing facilities at WADC since 30 September 1958 on all the contracts and the NSF grant was under the auspices of this contract, extended on a no-cost basis through 31 May 1959. These computing facilities continued to be made available under a one-year contract AF49(638)-699 from AF Office of Scientific Research, Office of Aerospace Research which expired 30 June 1960. Continued use was made of the facilities under AFOSR, OAR contract AF49(638)-1068 which commenced 1 April 1961 and terminated 30 April 1962. Under a new contract AF33(657)-8891 which was funded 1 May 1962, use of the computing facilities at WADC was continued through September 1962. In October 1962, all computational efforts were transferred to new facilities established at the University of Chicago Computation Center, with Professor C. C. J. Roothaan as Director. These facilities originally consisted of an IBM 7090 and IBM 1401

and peripheral equipment, but in June 1963 conversion of the IBM 7090 to a 7094 was carried out, and in December of 1964 the 1401 was replaced by an IBM 7040. All computing efforts now employ the University of Chicago Computing Center IBM 7040-7094 system.

Beginning 12 June 1959, a three-year contract with the OOR (now the Army Research Office, ARO) has been in effect, sponsored under auspices of Advanced Research Projects Agency, funded under ARPA Order 368 Task 4, for theoretical computations on light molecules, under Professor C. C. J. Roothaan and Dr. B. J. Ransil as Principal Investigators, with Professor Mulliken as Consultant. At its expiration, the contract was renewed for another three-year period, and the work is continuing with Professor Roothaan as Principal Investigator and Professor Mulliken as Consultant.

The present Technical Report for 1964 is issued jointly under the contracts (ONR, AFESD, AFOSR, and ARO) which have supported our research during the period 1 January 1946 through 31 December 1964. A few papers supported largely by National Science Foundation grants are also included, because of their close relation to other work here reported and because of their partial support by the contracts. Spectroscopic equipment used in the work under the National Science Foundation Molecular Complexes grant (G-20375) was in part provided by the ONR contract.

For a complete list of papers published from 1 January 1953 up to early 1960 by personnel of the Laboratory of Molecular Structure and Spectra, reference may be made to the Technical Report 1957-9, Part Two. Papers from this Laboratory published in the period 1947-52 are listed in the ONR Final Report of 30 September 1956.

SCF EXCITED STATES AND TRANSITION PROBABILITIES OF SOME NEON-LIKE AND ARGON-LIKE IONS*

by

Paul S. Bagus

Argonne National Laboratory, Argonne, Illinois

and

Laboratory of Molecular Structure and Spectra
Department of Physics, University of Chicago
Chicago, Illinois 60637

This Work Provided the Basis for a Thesis Submitted to the Department of Physics, The University of Chicago, in Partial Fulfillment of the Requirements for the Degree of Doctor of Philosophy.

*Based on work performed under the auspices of the U. S. Atomic Energy Commission. This paper also appears as ANL-6959 Physics (TID-4500, 37th Ed.) AEC Research and Development Report.

SCF EXCITED STATES AND TRANSITION PROBABILITIES OF SOME NEON-LIKE AND ARGON-LIKE IONS

by

Paul S. Bagus

ABSTRACT

Analytic self-consistent field (SCF) wave functions were computed for the ground states of the closed-shell atomic systems F^-, Ne, Na^+; and Cl^-, Ar, and K^+, and for those ground and excited states of the open-shell systems that are obtained by removing a single electron from any one of the occupied shells of these closed-shell systems. Details of the calculation of the functions are presented with emphasis on a justification of the procedures used for the calculations for excited states. A high accuracy is obtained; the calculations for the closed-shell systems give the most accurate analytic SCF wave functions that have yet been reported. Ionization potentials are calculated and compared with experimental values. Computed ionization potentials for the removal of a 2s electron from Cl^-, Ar, and K^+, for which no direct experimental data are available, are estimated to be accurate to within 1%. It is found that the removal of an electron from the outermost s shell increases the correlation energy, in contradiction to the predictions of a recently proposed semi-empirical scheme for estimating the correlation energy. For example, the magnitude of the correlation energy of the lowest ^2S state of Ar^+ is ~4 eV greater than the magnitude of the correlation energy of neutral argon. The effect of the nonzero off-diagonal Lagrangian multipliers is considered and found to be important for the inner-shell hole states. The SCF functions have been used to compute dipole transition probabilities for photon emission. The transition probabilities are computed in several different ways to examine the effects of various approximations. In particular, the results obtained using length, velocity, and acceleration operators are compared. The calculated radiation width for the K-state of argon is combined with an experimental value of the K-fluorescence yield to obtain a value of the total K-state width in agreement with experiment.

I. INTRODUCTION

In this paper, analytical self-consistent field (SCF) functions are presented for the ground states of the closed-shell atomic systems F^-, Ne, Na^+, Cl^-, Ar, and K^+, and for those ground and excited states of the

open-shell systems that are obtained by removing a single electron from any one of the occupied shells of these closed-shell systems. Specifically, we present SCF functions for the $1s^2 2s^2 2p^5$, $1s^2 2s 2p^6$, and $1s 2s^2 2p^6$ configurations of F, Ne^+, and Na^{++}, which, for convenience, we refer to as the 2p-hole, 2s-hole, and 1s-hole states, respectively; and SCF functions for the $1s^2 2s^2 2p^6 3s^2 3p^5$, $1s^2 2s^2 2p^6 3s 3p^6$, $1s^2 2s^2 2p^5 3s^2 3p^6$, $1s^2 2s 2p^6 3s^2 3p^6$, and $1s 2s^2 2p^6 3s^2 3p^6$ configurations of Cl, Ar^+, and K^{++}, which we refer to as the 3p-hole state, 3s-hole state, etc. These states are of interest for X-ray emission and absorption phenomena. They are also useful, for example, for calculating the effect of the electronic charge distribution on electron capture by the nucleus.(1)

Several properties of the wave functions have been calculated. Expectation values of r and r^2 are given for the SCF orbitals and overlap integrals between total wave functions not orthogonal by symmetry. In the final section of this paper, dipole transition matrix elements between the wave functions are presented.

The SCF wave functions were calculated using the Roothaan analytic expansion method. This method was developed first for closed-shell systems and then extended to a large class of open-shell systems. In its present form, the method will treat a system with any number of open shells, provided there is at most one open shell for each one-electron symmetry species.(2,3,4)

Extensive investigations have led to the development of reliable and accurate numerical techniques to implement the application of the analysis. These techniques have been incorporated into computer programs, written for the IBM 704, 7090, and 7094, for the calculation of atomic SCF wave functions.(4)

Many SCF calculations have been performed, using the Roothaan analysis, with the goal of obtaining accurate representations of the Hartree-Fock functions.(5-9) However, these functions have been for ground or low-lying excited states. The functions presented here are the first analytic SCF calculations for X-ray excited states of atomic systems. To our knowledge, the only numerical Hartree-Fock calculations for such states that correctly take exchange into account are those of Sureau and Berthier on aluminum.(10)

II. THEORY

In the Roothaan expansion method, the SCF orbitals $\phi_{i\lambda\alpha}$, omitting spin, are given in terms of basis functions $\chi_{p,\lambda\alpha}$ by

$$\phi_{i\lambda\alpha} = \Sigma_p \chi_{p,\lambda\alpha} C_{i\lambda,p}. \tag{1}$$

Here λ labels the symmetry species, and α the subspecies; for atoms, these are usually denoted by ℓ and m. The principal quantum number is represented by i, and p labels different basis functions of the same symmetry. The complete spin-orbital is given by

$$\psi_{i\lambda\alpha s} = \phi_{i\lambda\alpha}\eta_s, \tag{2a}$$

where

$$\eta_s = \alpha, \text{ or } \eta_s = \beta. \tag{2b}$$

The set of basis functions used in an expansion SCF wave function is referred to as the basis set of the function.

The notation used in Eqs. (1) and (2) is that adopted by Roothaan.[3,4] Since only atomic systems are considered in this paper, the standard notation for atomic orbitals, $n\ell m$, will be used, hereafter, in place of Roothaan's more general notation, $i\lambda\alpha$.

For atomic calculations, the basis functions are given by

$$\chi_{p,\ell m}(r,\theta,\phi) = R_{\ell p}(r)Y_{\ell m}(\theta,\phi), \tag{3}$$

where $Y_{\ell m}(\theta,\phi)$ are normalized spherical harmonics, and the radial functions $R_{\ell p}(r)$ are normalized nodeless Slater-type orbitals (STO's); namely,

$$R_{\ell p}(r;n_{\ell p},\zeta_{\ell p}) = [(2n_{\ell p})!]^{-\frac{1}{2}}(2\zeta_{\ell p})^{n_{\ell p}+\frac{1}{2}} r^{n_{\ell p}-1} e^{-\zeta_{\ell p} r}. \tag{4}$$

The integer $n_{\ell p}$ is called the principal quantum number of the basis function, and $\zeta_{\ell p}$ the orbital exponent. Care should be taken not to confuse the two different uses of "principal quantum number." The principal quantum number of an orbital is the label that distinguishes that orbital from other orbitals of the same symmetry species and subspecies. The principal quantum number of an STO is merely a flexible parameter of a basis function. For example, in our calculations on argon, the 1s orbital is expanded in terms of 1s, 2s, and 3s STO's.

The choice of Slater-type orbitals for the radial functions $R_{\ell p}(r)$ is physically reasonable, and the computation of necessary integrals between STO's is simple (at least for atoms). Several expansion SCF calculations have been made on atomic systems with the goal of obtaining accurate functions using small basis sets of STO's. The results of these calculations agree quite well with Hartree-Fock (HF)* functions obtained by direct numerical integration.(9)

The many-electron wave function is constructed from one Slater determinant, or a linear combination of a few Slater determinants, of the occupied SCF orbitals. The combination is made so that the wave function is an eigenfunction of $\underset{\sim}{L}^2$, $\underset{\sim}{S}^2$, L_z, and S_z. (Methods for constructing eigenfunctions of angular momentum from Slater determinants are contained in Refs. 11 and 12.) The wave function is also an eigenfunction of the inversion operator and has a definite parity. The variational principle is applied to obtain equations for the coefficients $C_{n\ell,p}$ [$C_{i\lambda,p}$ in Eq. (1)]. These equations are then solved without further approximation. In particular, the off-diagonal Lagrangian multipliers that couple equations for open- and closed-shell orbitals of the same symmetry are treated properly. (Procedures that treat the off-diagonal Lagrangian multipliers in an approximate way are contained in Refs. 13 and 14). It will be demonstrated in the discussion of the results that neglect of the off-diagonal Lagrangian multipliers significantly affects the SCF functions of certain excited states.

Equations (1), (2), and (3) place certain restrictions on the form of the SCF orbitals that should be stated explicitly. Equation (2) requires that the spin-orbital be factored into a product of a spatial function and a spin function. Equations (1) and (3) introduce the central field approximation by requiring that the orbital be factored into a product of a radial function and a spherical harmonic. A further consequence of Eqs. (1) and (3) is that all the electrons of a given shell have the same radial function. Thus, $\phi_{n\ell m}$ may be written as**

$$\phi_{n\ell m}(r,\theta,\phi) = F_{n\ell}(r)Y_{\ell m}(\theta,\phi), \tag{5}$$

where

$$F_{n\ell}(r) = \Sigma_p R_{\ell p}(r)C_{n\ell,p}. \tag{6}$$

---

*The notations SCF and HF will be used almost interchangeably. When we wish to distinguish between analytic expansion orbitals as opposed to exact solutions of the HF equations, we will use the notation SCF orbitals as opposed to HF orbitals.

**The use of F(r) to represent the radial portion of an orbital is an unfortunate deviation from the standard notation which is, of course, R(r). We do this to avoid confusion with the notation for the basis function $R_{\ell p}(r)$.

These orbitals are symmetry-adapted; i.e., they form bases for irreducible representations of the symmetry group of the (atomic) Hamiltonian. (For a discussion of the symmetry problem in the HF scheme, see Ref. 15.)

An additional requirement is that the occupied SCF orbitals form an orthonormal set,

$$\langle \phi_{n\ell m} | \phi_{n'\ell'm'} \rangle = \delta_{n\ell m, n'\ell'm'}. \tag{7a}$$

Because the orbitals are symmetry-adapted, this reduces to the requirement that

$$\int_0^\infty F^*_{n\ell}(r) F_{n'\ell}(r) r^2 \, dr = \delta_{n,n'}. \tag{7b}$$

In matrix notation, Eq. (7b) becomes

$$\underset{\sim}{c}^\dagger_{n\ell} \underset{\sim}{S}_\ell \underset{\sim}{c}_{n'\ell} = \delta_{n,n'}, \tag{7c}$$

where $\underset{\sim}{c}_{n\ell}$ is a vector that collects the coefficients $C_{n\ell,p}$, and $\underset{\sim}{S}_\ell$ is the overlap matrix of basis functions of symmetry species ℓ,

$$S_{\ell pq} = \int_0^\infty R_{\ell p}(r) R_{\ell q}(r) r^2 \, dr. \tag{8}$$

In the numerical HF procedure, no assumption is made about the form of the radial function $F_{n\ell}(r)$. The variational principle is applied for arbitrary variations of the radial functions, subject to the constraint that they form an orthonormal set, and integro-differential equations for the $F_{n\ell}$'s are obtained.[2,3] (Reference 16 presents an excellent review of numerical Hartree-Fock procedures. Reference 17 discusses the applications of numerical techniques to high-speed digital computers.)

The solutions of the integro-differential equations satisfy the cusp condition,[18,19]

$$\left[(1/f_{n\ell}) (df_{n\ell}/dr) \right]_{r=0} = - Z/(\ell + 1), \tag{9a}$$

where

$$F_{n\ell}(r) = r^\ell f_{n\ell}(r). \tag{9b}$$

The cusp condition may be used as a criterion for the accuracy of an expansion SCF orbital near the origin. Moreover, an orbital with a poor cusp value may be a poor representation of an exact HF orbital, not only in the region $r \to 0$, but also over the entire range of the function. The cusp condition is a necessary but not a sufficient condition that the orbital be a solution of the HF equations. A basis set can be chosen so that an expansion SCF orbital will satisfy the cusp conditions exactly;[8] however, the orbital may still be a poor approximation of the exact HF orbital.

The total Hamiltonian operator $\mathscr{H}$ for an atomic system may be written, in atomic units, as

$$\mathscr{H} = \mathscr{T} + \mathscr{V}, \tag{10a}$$

where

$$\mathscr{T} = \Sigma_i \left(-\frac{1}{2} \Delta_i \right), \tag{10b}$$

and

$$\mathscr{V} = -\Sigma_i (Z/r_i) + \Sigma_{i<j} (1/r_{ij}).$$

This Hamiltonian is valid for a system with nonrelativistic Coulomb interactions and an infinitely heavy nucleus.

If Ψ is an exact eigenfunction of $\mathscr{H}$ for any bound state, then the virial theorem,

$$\langle \Psi | \mathscr{V} | \Psi \rangle / \langle \Psi | \mathscr{T} | \Psi \rangle = -2, \tag{11}$$

is satisfied. If Ψ is an approximate eigenfunction which contains a variable scale factor k such that $\Psi(x_1, \ldots, x_n) = \Psi'(kx_1, \ldots, kx_n)$, and k has been chosen to satisfy $(\partial / \partial k)(\langle \Psi' | \mathscr{H} | \Psi' \rangle / \langle \Psi' | \Psi' \rangle) = 0$, then this approximate Ψ also satisfies Eq. (11).[20]

Exact HF functions satisfy the virial theorem since arbitrary variation of the radial part of the orbitals includes, implicitly, variation of a scale factor. Expansion SCF functions for an arbitrary basis set will not, in general, satisfy the virial theorem. If, however, variation of the exponents, as well as the linear coefficients, is performed, the virial theorem will be satisfied when all parameters have been optimized. Hence, for expansion SCF functions, the virial theorem is a necessary, but by no means sufficient, condition that an optimum basis set (in the sense of satisfying variational equations) has been used.

Let $\{\Psi(a)\}$ be a set of trial functions, where the index a distinguishes different members of the set from which we wish to choose an approximate wave function for some state of a system. The index a may represent a set of variable parameters, any one of which may be discrete or continuous. Let $\Psi(A)$ be chosen from the set $\{\Psi(a)\}$ as the solution of equations determined from application of the variational principle; i.e., $\Psi(A)$ satisfies

$$\delta_a[\langle\Psi(a)|\mathcal{H}|\Psi(a)\rangle/\langle\Psi(a)|\Psi(a)\rangle] = 0. \tag{12}$$

If $\Psi(A)$ is an approximate wave function for the ground state of the system or for the lowest excited state of a symmetry (if the trial functions $\Psi(a)$ are symmetry-adapted), then $\Psi(A)$ is the best function possible for the restricted form of the trial functions - best in the sense that the expectation value of the energy for $\Psi(A)$, $\langle\Psi(A)|\mathcal{H}|\Psi(A)\rangle = E(A)$, is more nearly equal to the true energy eigenvalue E(t) than the expectation value of the energy for any of the other trial functions $\Psi(a)$. Moreover, $E(A) \geq E(t)$, and, if $E(A) = E(t)$, then $\Psi(A)$ is the true eigenfunction.[20,21]

This is not true for excited states that are not the lowest states of a symmetry unless the trial functions $\{\Psi(a)\}$ are constrained to be orthogonal to the exact eigenfunctions of all states of lower energy. The imposition of this constraint is, of course, not possible in general since the exact eigenfunctions of the lower states are not known. One procedure would be to require trial functions for excited states to be orthogonal to approximate wave functions for lower states. In the calculation of excited-state SCF functions, this is not done; no explicit requirement of orthogonality to lower SCF states is made.[8]

We rely on the physical model of the choice of the form of the SCF excited-state wave function to guarantee near-orthogonality to the SCF wave functions for lower-lying states. This physical model is, of course, the orbital or shell structure of the atom. Indeed, the only constraint that is imposed to obtain an excited-state, rather than a ground-state, wave function is the specification of the electronic configuration. For a 1s-hole state, for example, the HF operators are constructed on the assumption that the 1s orbital is occupied by only one electron. Eigenvectors of the HF operators are obtained and iterations are performed in the usual way until the condition of self-consistency is met; but the assumption that the 1s orbital is singly occupied is maintained throughout the process. The singly occupied 1s orbital is chosen at each iteration to be the eigenvector (of the appropriate HF operator) with the lowest orbital energy. This choice is easily justified by the fact that the orbital so chosen is the occupied orbital that is most similar to a hydrogenic 1s orbital.

The HF operators are functions of the electron density. The electron density of a complex atom does not change drastically in going from ground to

excited states. Thus, the HF operators for ground and excited states are not drastically different, and SCF wave functions for excited states are very nearly orthogonal to SCF wave functions for lower states. The 3s-hole state of argon is the lowest ^2S state of Ar^+; the 1s-hole state, a very highly excited ^2S state, lies about 3000 eV above the 3s-hole state. Even for this extreme case, the overlap integral between the many-electron SCF wave functions for these two states, $\langle \Psi_{SCF}(1s\text{-hole}) | \Psi_{SCF}(3s\text{-hole}) \rangle$, is 5×10^{-4}. The requirement that the 1s-hole SCF wave function be orthogonal to the 3s-hole SCF wave function would produce only a very small change in the 1s-hole wave function. Further, since the 3s-hole SCF wave function is only an approximate eigenfunction, we do not know whether the constraint of orthogonality would improve or worsen the 1s-hole wave function. Overlap integrals between many-electron SCF wave functions for all those states, presented in this paper, that are not orthogonal by symmetry are given in Table XV. [M. Cohen and A. Daglarno[22] and D. Layzer[23] have investigated the overlap of SCF excited states of the same symmetry using expansions of SCF wave functions in powers of $1/Z$ and find that the overlap is zero to order $(1/Z)^2$.]

For a certain class of excited-state SCF wave functions, it is possible to state easily tested conditions that must be fulfilled in order that the SCF energy be an upper bound to the true energy of the state.[24]

III. DETAILS OF THE CALCULATION OF THE SCF WAVE FUNCTIONS

To obtain analytic SCF orbitals that are good approximations to the exact orbitals, it is necessary to use a basis set that very nearly spans the true HF manifold. It is perhaps possible to do this by using large, more or less arbitrarily chosen, basis sets, but if this is done, several difficulties arise. Numerical processes that work well for basis sets of reasonable size become troublesome, and round-off error becomes important when large basis sets are used. Long expansions of atomic functions are poor starting points for molecular and solid-state calculations, while short expansions have proved to be excellent starting points for molecular SCF calculations.[25] By using large basis sets, one loses much of the advantage of simplicity that the analytic representation of SCF functions has over numerical tables of orbitals. For large atomic systems, the finite size of the computer becomes an important limiting factor on the size of the basis set.

For these reasons, we have used basis sets of limited size, making a careful choice of the exponents and principal quantum numbers of the STO's in order to minimize the total SCF energy. Particular emphasis is placed on varying the exponents to find optimum values. This variation is performed automatically by the computer program.[4] Our method of exponent variation is to perform several complete SCF calculations for different values of the exponents and to interpolate between these values.

While we do not explicitly solve variational equations for the exponents with this method, we do obtain a stationary value of the expectation value of the energy with respect to the exponents. The particular stationary value that we obtain is a minimum. Explicit variational equations for the exponents as well as the linear coefficients $C_{n\ell,p}$ have been given by Dehn.[26] The equations for the exponents appear to be difficult to solve. One important problem is that the basis functions used to represent an SCF orbital (to a given accuracy) are by no means uniquely determined.[27,28] Our brute-force variation of the exponents has proved to be a quite satisfactory procedure.

When basis sets of limited size are used, it is important to build up the basis set systematically to the final, accurate set. The initial calculation for a state should be made with a rather small basis set. This set can give only a crude approximation to the exact HF wave function, but for a small set it is easy to find the optimum values of the principle quantum numbers and exponents. This gives a first or base reference point for more accurate calculations on the state. Additional exponents are then introduced, usually one at a time, and the exponents reoptimized. It is not sufficient to optimize only the exponents of the new basis functions; the exponents of old functions must also be adjusted when a new function is added. In this way, it is possible to gauge the "need" for the

new basis function, and to make an educated guess about the "need" for an additional basis function. The intermediate sets, formed in this build-up process, are often useful in themselves.

Because of the many SCF calculations involved in the optimization of the basis set, the experience gained in the calculation of one state must be applied to the calculation of similar states of the same or neighboring atoms. Linear extrapolations and interpolations of the exponents for states already computed provide good approximations to the optimized exponents of a nearby state. This is particularly true for smaller basis sets, since for these sets the optimum values of the exponents are well-defined. For larger basis sets, where several different sets of values of the exponents will give functions with the same total energy, the interpolated and extrapolated values provide a good starting point for exponent variations that lead to the optimized values.

Thus the calculation of the functions of a series of states must be done systematically, and the function for each state must not be computed as a separate problem. This systematic procedure will also uncover errors in optimization of basis sets. If an extrapolation or interpolation to a neighboring state fails to work well, one has excellent reason to suspect an error in one of the previously computed states. While the calculation of the SCF wave function for a single state is laborious and time-consuming, the calculation of wave functions for a series of states is fairly economical.

It will be useful, for the following discussion, to introduce the notion of a loop of an orbital. A hydrogenic radial function with quantum numbers $n\ell$ has $n - \ell - 1$ nodes and $n - \ell$ loops between these nodes and the points $r = 0$ and $r = \infty$. Similarly, the HF radial function $F_n(r)$ generally has $n - \ell - 1$ nodes and $n - \ell$ loops. The contributions to the HF operator of exchange terms and off-diagonal Lagrangian multipliers will introduce, in exceptional cases, extra nodes and loops near the tail of the orbital;* but the function is very small in these loops, and for this discussion they may be ignored. For HF orbitals of a particular state of a system, the 1s orbital and the inner loops of the 2s and 3s orbitals, in a rough sense, occupy the same region of space. Similarly, the outer loop of the 2s orbital and the middle loop of the 3s orbital occupy the same region of space. Thus, for a given state of a system, the n^{th} loops of HF orbitals of the same symmetry roughly define a distinct range of values of r. The range is rather well-defined, except for an outer loop. The outer loop of an orbital always has a long "tail" going slowly to zero. This division of r into distinct ranges permits us to consider groups of basis functions, where each group is chosen to fit a particular loop.

*See Ref. 29 and the discussion in Section IV-E of this paper.

The computer program used for the SCF calculations has facilities for the coupled variation of the exponents of one, two, or three basis functions. The choice of the exponents to be varied, if any, is part of the input data to a run.

When the exponent of one basis function is varied, the program performs complete SCF calculations for different values of the exponent being varied while all the other exponents are held fixed. An energy minimum is found and bracketed by calculations for five values of the exponent at intervals of $\frac{1}{2}\Delta\zeta$. The optimum value of the exponent is determined by interpolation; a quartic is fit to these five points and its minimum is obtained. The exponent variation increment, $\Delta\zeta$, is a flexible input parameter.

Care must be taken in the choice of $\Delta\zeta$ so that the interpolation may be accurate. If $\Delta\zeta$ is chosen too small, the differences of the calculated SCF energies will be small and the interpolation will be in error because of the round-off errors in the SCF energies. This is not too serious since the optimum value of the exponent is indeterminate because of this round-off error in the SCF energies; however, fairly large amounts of computer time may be wasted by trying to bracket the energy minimum too closely. Moreover, if the energy differences are small enough, a true energy minimum may be missed because the round-off in the SCF energies causes an apparent, but false, minimum. Since, for calculations of the size presented here, the round-off error in the SCF energy appears to be a few units in the eighth significant figure, we tried to choose $\Delta\zeta$ so that the SCF energy changed by at least a few units in the seventh significant figure between adjacent SCF calculations.

If $\Delta\zeta$ is chosen too large, the interpolation will be in error because the points (in exponent space) at which SCF calculations are made are too far apart to be fit meaningfully by a quartic. The usual symptom of this is large changes in the SCF vector coefficients $C_{n\ell,p}$ between adjacent points. These changes indicate that the basis function is being "used" in the SCF orbitals in qualitatively different ways for different values of the exponent. The best, simple way to test whether $\Delta\zeta$ has been chosen too large is to compare the interpolated value of the total energy with the energy obtained from an SCF calculation using the interpolated value of the exponent. This SCF calculation is automatically performed by the program.

The quartic interpolation scheme is sufficiently accurate so that, for a properly chosen $\Delta\zeta$, the predicted and computed values of the energy will agree within round-off error. The range of acceptable values of $\Delta\zeta$ is, in fact, quite large, and only in exceptional cases must $\Delta\zeta$ be given to more than one or one and one-half significant figures.

The procedures for the coupled variation of two and three exponents are an extension of those described above for the variation of a single

exponent. However, while a one-dimensional variation requires at least five SCF calculations, a two-dimensional variation requires at least 25 SCF calculations, and a three-dimensional variation requires at least 125.

Multidimensional variations should couple the exponents of basis functions used to represent a loop of the orbitals. They should not couple the exponents of basis functions used to represent different loops. A multidimensional variation will usually give better values for the exponents than a series of one-dimensional variations since a larger region of exponent space is examined in a multidimensional variation. However, a multidimensional variation may use more computer time than a series of one-dimensional variations. The exponent variation procedures are described in detail elsewhere.[4]

The principal quantum numbers of the STO's of a basis set can be chosen in a special way so that the cusp condition of Eq. (9) is automatically satisfied for all the SCF orbitals.[8] We call a basis set of STO's whose principal quantum numbers have been chosen in this special way a fixed-cusp set. Extensive experience, especially for first-row atoms,[9] but also for some second-row atoms,[30] has shown that if fixed-cusp sets are not used it is possible to obtain accurate SCF orbitals with adequate cusp values using smaller basis sets. Often the best energies obtained using these free-cusp sets were lower than the best energies obtained using the larger fixed-cusp sets. For this reason, we choose to use free-cusp sets.

Whereas the exponents, being continuous parameters, were optimized by continuous variation, the principal quantum numbers of the basis functions, being integers, need to be chosen more or less arbitrarily. Our preference was to choose principal quantum numbers for the STO's that are to represent the n^{th} loop of a series of orbitals so that the STO's would have the same power of r as hydrogenic functions representing that loop have. Thus, for the states of the fluorine, neon, and sodium ions, we used 2p STO's to represent the 2p orbital; and for the states of the chlorine, argon, and potassium ions, we used 3s STO's to represent the outer loop of the 3s orbital.

This was by no means a hard and fast rule; we did limited experimentation with other values. The need for experimentation was usually indicated by one of the following three factors:

1. The failure of the automatic exponent variation procedures of our computer programs to operate efficiently. The program would vary the exponents so as to cause the basis set to become nearly redundant; that is, the basis functions at some stage of the exponent variation process would form a nearly linearly dependent set.*

* A precise measure of the redundancy of a basis set is the value of the determinant of the overlap matrix S of the basis functions. As the determinant of S goes to zero, the basis set goes to complete redundancy (exact linear dependence).

2. The failure of a subset of the full basis set to adequately represent a loop. This is indicated when a basis function that is important in a region of space outside the loop does not have a small coefficient when it contributes to the representation of the loop. Consider the 1s orbital of neutral argon, for example. For the accurate SCF function (see Table III), the principal quantum numbers of the basis functions that represent the inner s-loop are 1, 2, and 3. The coefficients of these functions for the 1s orbital are large, and the 1s coefficients $C_{1s,p}$ of the remainder of the s basis functions are of the order of 1×10^{-4}. We tried to obtain an SCF function of the same accuracy using two 1s and one 3s basis functions to represent the inner s-loop. In this case, the 1s coefficients of the remainder of the s basis functions were as large as 2×10^{-2}.

3. The desirability of keeping the basis set as nearly linearly independent as possible. For the states of the chlorine, argon, and potassium ions, we believe that we have a less redundant basis set if we use three 2p and one 4p basis functions to represent the inner p-loop, than if we were to use four 2p basis functions. This consideration is important only when we come to the final, largest basis sets used to obtain the most accurate SCF wave functions.

The minimization of the total SCF energy E_{SCF} was the fundamental criterion used to choose the basis sets for the SCF functions reported here. The analytic SCF orbitals determined by using this criterion are not uniformly good approximations to the exact HF orbitals. The orbitals of the electrons that contribute most to E_{SCF}, the core or inner-shell electrons, are determined most accurately. The orbitals of the electrons which contribute least to E_{SCF}, the valence or outer-shell electrons, are determined least accurately.

Because of the limitations of the computer, the total energy is only computed to eight significant figures. The contribution of the outer shells to E_{SCF} is masked by the large contributions of the core. A rough measure of the contribution of an electron in the $n\ell$-shell to E_{SCF} is the orbital energy $\epsilon_{n\ell}$. For neutral argon, we have the values $E_{SCF} = -526.817$, $\epsilon_{1s} = -119.610$, and $\epsilon_{3s} = -1.277$; the unit of energy is the Hartree (1 Hartree = 27.2098 eV). Thus, when exponent variations are performed on the inner s-loop basis functions, there are effectively two more significant figures in E_{SCF} to examine than when exponent variations are performed on the outer s-loop basis functions. To produce equal changes in E_{SCF}, larger changes must be made in the exponents (and therefore in the orbitals) of the basis functions used to represent outer loops than in the exponents of the basis functions used to represent inner loops.

Because it is more difficult to obtain accurate orbitals for the 3s and 3p shells than for the inner shells, we paid close attention to small changes in the total SCF energy when choosing the basis functions used to

represent the outer loops of the 3s and 3p orbitals of the states of the chlorine, argon, and potassium ions. Small improvements in the total energy obtained in fitting these loops are at least as important for the general quality of the wave function as are larger improvements obtained when fitting the inner-shell orbitals.

It was also necessary to look for small energy improvements, when the most accurate functions were computed, so that the tails of the orbitals would be fit properly. The tails of the orbitals make the smallest contribution to the total energy. Thus, small expansion sets fit the orbitals in the regions where they are large at the expense of the behavior of their tails, and larger basis sets must be chosen carefully so that the tails will be represented properly.

The calculations reported here were performed with computer programs written for the IBM 704 and 7090/4 by Professor C. C. J. Roothaan and the author, with the assistance of various members of the Laboratory of Molecular Structure and Spectra at The University of Chicago. The programs are available for distribution upon request.

IV. RESULTS AND DISCUSSION OF SCF CALCULATIONS

A. The SCF Wave Functions

Tables I-IV present the most accurate SCF function computed for each state. Tables V-VIII present a simpler, less accurate, but quite useful SCF function for each state. The simple basis sets were obtained with relatively little computational effort. They are a good starting point for extending these calculations to other states of interest (for example, to states formed in X-ray absorption). In addition, the simple basis set functions are sufficiently accurate for many purposes. Expectation values of r and r^2, dipole-transition matrix elements, and overlap of SCF wave functions were computed with the simple set SCF functions as well as the accurate set SCF functions. The values obtained usually agree quite well. Some comparisons that indicate the extent of the agreement will be given later.

The results in Tables I-VIII include the total energy for the non-relativistic, electrostatic, fixed-nucleus Hamiltonian of Eq. (10) and the virial coefficient V/T. Exponents of the basis functions are given for each state. The principal quantum number and symmetry type of each basis function are given in parentheses in the first column of each table. The different basis functions are numbered consecutively within each symmetry type. For each orbital, the SCF orbital energy $\epsilon_{n\ell}$, the cusp [defined in Eq. (9)], and the vector coefficients $C_{n\ell,p}$ are given. The numbering of the vector coefficients corresponds to the numbering of the basis functions. All energies are given in Hartrees. The results reported in Tables I-VIII are from calculations performed on an IBM 7094.

The total wave functions for the states given in Tables I-VIII are all single determinants. The ^1S and ^2S states have even parity, and the ^2P states have odd parity. The parity follows immediately from the electron configurations of the states.

The 1s-hole states of F^-, Ne, and Na^+, and the 1s-, 2s-, and 2p-hole states of Cl^-, Ar, and K^+ are not the lowest states of their symmetry species; these states are marked with asterisks in Tables I-VIII.

The 2s-hole states of Ne and Na^+, and the 3s-hole states of Ar and K^+ are the first excited states of Ne^+, Na^{++}, Ar^+, and K^{++}, respectively. They are the lowest ^2S states.

The 2s-hole state of F^- is a highly excited state of fluorine; it is, in fact, past the ionization limit. However, Moore[31] does not give any other ^2S state of even parity in the spectrum of fluorine. The 3s-hole state of Cl^- is not observed, but no ^2S states of even parity are observed in the spectrum of chlorine.[31] Thus these states may be the lowest states of their symmetry species.

TABLE I. SCF Orbitals and Energies for F^-, Ne, and Na^+, and $n\ell$-hole States of F^-, Ne, and Na^+, Accurate Basis Sets

	$F^-(^1S)$	$F(^2P)$ 2p-hole	$F(^2S)$ 2s-hole	$F(^2S)$ 1s-hole	$Ne(^1S)$	$Ne^+(^2P)$ 2p-hole	$Ne^+(^2S)$ 2s-hole	$Ne^+(^2S)^*$ 1s-hole	$Na^+(^1S)$	$Na^{++}(^2P)$ 2p-hole	$Na^{++}(^2S)$ 2s-hole	$Na^{++}(^2S)^*$ 1s-hole
E	-99.45944	-99.40933	-98.53123	-74.52412	-128.5471	-127.8178	-126.7348	-96.62571	-161.6770	-159.9974	-158.7088	-121.7424
V/T	-1.999998	-1.999996	-1.999999	-2.000000	-1.999998	-2.000003	-2.000003	-1.999992	-2.000001	-2.000003	-2.000003	-2.000006
$\zeta_1(1s)$	13.958	14.201	13.901	15.308	15.439	15.409	15.231	16.768	15.949	15.329	15.530	18.164
$\zeta_2(1s)$	7.936	7.938	7.893	8.371	8.806	8.811	8.771	9.179	9.439	9.597	9.289	9.982
$\zeta_3(3s)$	9.873	9.962	9.901	10.713	10.995	10.967	10.951	11.732	11.624	11.374	11.355	12.750
$\zeta_4(2s)$	3.426	3.332	3.288	3.522	3.764	3.824	3.758	4.070	4.384	4.462	4.372	4.566
$\zeta_5(2s)$	2.183	2.057	2.078	2.175	2.301	2.526	2.537	2.670	2.811	3.047	3.058	3.153
$\zeta_6(2s)$	1.500	. . .	. . .	. . .	. . .	. . .	. . .	. . .	. . .	. . .	. . .	. . .
$\zeta_1(2p)$	9.788	9.435	8.793	6.809	10.542	12.548	12.000	10.835	12.048	13.437	12.730	10.580
$\zeta_2(2p)$	4.446	4.249	4.181	4.058	4.956	5.759	5.718	5.567	5.703	6.030	5.939	5.829
$\zeta_3(2p)$	2.595	2.356	2.324	2.285	2.793	3.476	3.436	3.279	3.336	3.649	3.503	3.300
$\zeta_4(2p)$	1.511	1.434	1.404	1.487	1.623	2.086	2.047	2.142	2.146	2.522	2.433	2.409
$\zeta_5(2p)$	0.869	. . .	. . .	. . .	. . .	. . .	. . .	. . .	. . .	. . .	. . .	. . .
ϵ_{1s}	-25.82961	-26.38265	-26.42060	-29.53630	-32.77233	-33.61235	-33.61629	-37.16999	-40.75972	-41.86280	-41.83081	-45.82043
Cusp	-9.02404	-9.02760	-9.02411	-9.01167	-10.02496	-10.02477	-10.02401	-10.01652	-11.01520	-11.00906	-11.01874	-11.02114
$c_{1s,1}$	0.08975	0.08419	0.09403	0.04171	0.09818	0.09256	0.09927	0.05077	0.13371	0.14458	0.15929	0.05967
$c_{1s,2}$	0.94747	0.95503	0.94586	0.99591	0.94891	0.94804	0.94216	0.99596	0.91835	0.89061	0.89684	0.99466
$c_{1s,3}$	-0.04015	-0.04226	-0.04308	-0.05444	-0.04499	-0.04442	-0.04548	-0.06476	-0.05827	-0.03891	-0.06368	-0.07315
$c_{1s,4}$	0.00377	0.00301	0.00374	0.01684	0.00308	0.00299	0.00377	0.01303	0.00156	0.00420	0.00238	0.01003
$c_{1s,5}$	-0.00083	-0.00013	0.00014	0.01247	-0.00003	-0.00018	0.00004	0.01332	0.00060	-0.00067	0.00061	0.01359
$c_{1s,6}$	0.00050	. . . .	. . . .	. . . .	. . . .	. . . .	. . . .	. . . .	. . . .	. . . .	. . . .	. . . .
ϵ_{2s}	-1.07458	-1.57245	-1.70583	-1.74534	-1.93031	-2.61917	-2.75317	-2.85349	-3.07368	-3.93054	-4.06585	-4.22305
Cusp	-9.06777	-9.06608	-9.07213	-9.04294	-10.05351	-10.05387	-10.06436	-10.04150	-11.03456	-11.02316	-11.02905	-11.02846
$c_{2s,1}$	0.00560	0.00519	0.00439	0.01255	0.00645	0.00718	0.00611	0.01275	0.00581	0.01251	0.00333	0.01304
$c_{2s,2}$	-0.27435	-0.28031	-0.28538	-0.31567	-0.28821	-0.29829	-0.30146	-0.33112	-0.30875	-0.32313	-0.32328	-0.34522
$c_{2s,3}$	-0.02865	-0.02805	-0.02678	-0.03023	-0.02632	-0.02831	-0.02674	-0.02983	-0.02404	-0.03062	-0.02199	-0.02807
$c_{2s,4}$	0.49528	0.56794	0.59904	0.57594	0.56972	0.52685	0.56055	0.51259	0.49163	0.44384	0.47343	0.47638
$c_{2s,5}$	0.47665	0.52863	0.49531	0.52319	0.53066	0.56743	0.53148	0.58614	0.61232	0.65800	0.62678	0.62255
$c_{2s,6}$	0.13770	. . . .	. . . .	. . . .	. . . .	. . . .	. . . .	. . . .	. . . .	. . . .	. . . .	. . . .
ϵ_{2p}	-0.18098	-0.72994	-0.70271	-0.87141	-0.85034	-1.60663	-1.55267	-1.81602	-1.79719	-2.74429	-2.66306	-3.01964
Cusp	-4.53215	-4.51761	-4.46597	-4.40926	-5.00030	-5.06068	-5.03668	-5.00617	-5.52223	-5.58134	-5.55100	-5.49840
$c_{2p,1}$	0.00800	0.01055	0.01380	0.04764	0.00930	0.00408	0.00473	0.00566	0.00784	0.00509	0.00619	0.01168
$c_{2p,2}$	0.20342	0.26789	0.27605	0.35674	0.24154	0.13743	0.14248	0.23853	0.23017	0.19601	0.21089	0.30104
$c_{2p,3}$	0.39809	0.49083	0.48600	0.47736	0.48233	0.42831	0.43100	0.45718	0.45558	0.42481	0.46037	0.57139
$c_{2p,4}$	0.36280	0.32561	0.32218	0.21207	0.36532	0.50305	0.49736	0.37235	0.38418	0.43417	0.38511	0.17715
$c_{2p,5}$	0.17010	. . . .	. . . .	. . . .	. . . .	. . . .	. . . .	. . . .	. . . .	. . . .	. . . .	. . . .

*States which are not the lowest of a symmetry species.

TABLE II. SCF Orbitals and Energies for Cl^- and nl-hole States of Cl^-, Accurate Basis Sets

	$Cl^-(^1S)$	$Cl(^2P)$ 3p-hole	$Cl(^2S)$ 3s-hole	$Cl(^2P)^*$ 2p-hole	$Cl(^2S)^*$ 2s-hole	$Cl(^2S)^*$ 1s-hole
E	-459.5768	-459.4820	-458.9167	-452.3349	-449.7655	-356.2822
V/T	-1.999999	-2.000000	-2.000001	-2.000001	-2.000001	-2.000004
$\zeta_1(1s)$	19.955	19.840	19.830	19.955	19.955	20.000
$\zeta_2(2s)$	14.545	14.650	14.670	14.530	14.505	16.500
$\zeta_3(3s)$	16.000	16.000	16.000	16.000	16.000	18.000
$\zeta_4(3s)$	9.951	9.940	9.932	9.684	9.954	10.166
$\zeta_5(2s)$	5.748	5.745	5.743	5.867	6.010	6.062
$\zeta_6(3s)$	2.823	2.904	2.878	3.140	3.030	3.167
$\zeta_7(3s)$	1.651	1.826	1.842	1.970	1.923	1.982
$\zeta_1(2p)$	15.380	15.440	15.525	16.345	16.600	16.900
$\zeta_2(2p)$	7.535	7.550	7.555	7.790	7.845	8.310
$\zeta_3(2p)$	4.385	4.415	4.405	4.600	4.615	4.980
$\zeta_4(4p)$	7.200	7.200	7.200	7.700	7.700	8.000
$\zeta_5(3p)$	2.612	2.663	2.653	2.852	2.861	2.926
$\zeta_6(4p)$	1.826	1.976	1.932	2.091	2.100	2.136
$\zeta_7(3p)$	0.920	1.236	1.191	1.307	1.310	1.311
ϵ_{1s}	-104.50546	-104.88431	-104.95559	-106.27042	-106.04136	-112.50264
Cusp	-17.00483	-17.00224	-17.00306	-17.00187	-17.00641	-17.00392
$c_{1s,1}$	0.76554	0.77219	0.77275	0.76588	0.76542	0.77416
$c_{1s,2}$	0.43218	0.40836	0.40543	0.43389	0.43475	0.32382
$c_{1s,3}$	-0.16990	-0.15323	-0.15094	-0.17190	-0.17195	-0.07287
$c_{1s,4}$	0.00060	0.00227	0.00272	-0.00055	-0.00072	0.00487
$c_{1s,5}$	0.00005	-0.00060	-0.00082	0.00041	-0.00107	0.01344
$c_{1s,6}$	0.00003	0.00013	0.00015	-0.00006	-0.00006	-0.00217
$c_{1s,7}$	-0.00004	-0.00009	-0.00011	-0.00001	0.00000	-0.00191
ϵ_{2s}	-10.22916	-10.60741	-10.66547	-11.32032	-11.47391	-11.83135
Cusp	-16.99333	-16.99389	-16.99236	-16.98104	-17.02706	-16.94919
$c_{2s,1}$	-0.21448	-0.21639	-0.21622	-0.21855	-0.21801	-0.23204
$c_{2s,2}$	-0.21001	-0.20133	-0.20016	-0.21460	-0.22715	-0.17324
$c_{2s,3}$	0.07593	0.06997	0.06934	0.08022	0.07179	0.02477
$c_{2s,4}$	0.17263	0.17368	0.17136	0.20563	0.13283	0.17350
$c_{2s,5}$	0.90099	0.89900	0.90007	0.86777	0.94252	0.90538
$c_{2s,6}$	0.00586	0.00558	0.00719	0.00543	0.02443	0.00693
$c_{2s,7}$	-0.00023	-0.00015	0.00006	0.00042	0.00979	-0.00024
ϵ_{3s}	-0.73320	-1.07288	-1.17570	-1.22317	-1.20787	-1.23087
Cusp	-16.96224	-16.94416	-16.94540	-16.97671	-17.00251	-16.98601
$c_{3s,1}$	0.06317	0.06541	0.06693	0.07000	0.07341	0.07252
$c_{3s,2}$	0.07620	0.07656	0.07770	0.09087	0.09926	0.07018
$c_{3s,3}$	-0.02132	-0.02034	-0.02053	-0.02158	-0.02157	-0.00184
$c_{3s,4}$	-0.00604	-0.00017	-0.00059	0.01419	0.03314	0.02248
$c_{3s,5}$	-0.40771	-0.42851	-0.43667	-0.49099	-0.52027	-0.48357
$c_{3s,6}$	0.70755	0.65176	0.68652	0.64384	0.67449	0.64311
$c_{3s,7}$	0.43093	0.48089	0.44414	0.51051	0.46565	0.50431
ϵ_{2p}	-7.69557	-8.07218	-8.14619	-9.00679	-8.78960	-9.55946
Cusp	-8.44006	-8.43660	-8.44048	-8.44624	-8.47497	-8.51969
$c_{2p,1}$	0.01990	0.01930	0.01875	0.01324	0.01236	0.00767
$c_{2p,2}$	0.68564	0.68305	0.68657	0.66057	0.65222	0.63922
$c_{2p,3}$	0.19201	0.19262	0.18707	0.22510	0.23727	0.24850
$c_{2p,4}$	0.16481	0.16636	0.17024	0.14711	0.15609	0.15979
$c_{2p,5}$	0.00296	0.00516	0.00323	0.01950	0.00104	0.00535
$c_{2p,6}$	-0.00058	-0.00107	-0.00129	0.01128	0.00016	-0.00209
$c_{2p,7}$	0.00024	0.00111	0.00063	0.00531	0.00000	0.00100
ϵ_{3p}	-0.15017	-0.50640	-0.50063	-0.58967	-0.58465	-0.59605
Cusp	-8.38032	-8.35998	-8.35630	-8.38535	-8.37179	-8.40151
$c_{3p,1}$	-0.00350	-0.00346	-0.00331	-0.00274	-0.00199	-0.00022
$c_{3p,2}$	-0.18172	-0.19968	-0.20013	-0.22358	-0.20251	-0.19667
$c_{3p,3}$	-0.03172	-0.02837	-0.02733	-0.05978	-0.05454	-0.04580
$c_{3p,4}$	-0.06118	-0.07143	-0.07165	-0.07294	-0.07260	-0.07359
$c_{3p,5}$	0.59454	0.60295	0.62287	0.63710	0.63463	0.63024
$c_{3p,6}$	0.36833	0.31482	0.33734	0.32628	0.32834	0.33878
$c_{3p,7}$	0.21232	0.21687	0.17781	0.18060	0.18278	0.17251

*States which are not the lowest of a symmetry species.

TABLE III. SCF Orbitals and Energies for Argon and nl-hole States of Argon. Accurate Basis Sets

	$Ar(^1S)$	$Ar^+(^2P)$ 3p-hole	$Ar^+(^2S)$ 3s-hole	$Ar^+(^2P)^*$ 2p-hole	$Ar^+(^2S)^*$ 2s-hole	$Ar^+(^2S)^*$ 1s-hole
E	-526.8175	-526.2745	-525.5977	-517.6690	-514.8795	-409.3890
V/T	-2.000000	-1.999999	-1.999999	-1.999999	-2.000001	-2.000000
$\zeta_1(1s)$	20.750	20.750	20.735	20.700	20.615	20.080
$\zeta_2(2s)$	14.900	14.900	14.900	14.945	15.000	16.845
$\zeta_3(3s)$	16.500	16.500	16.500	16.500	16.500	18.500
$\zeta_4(3s)$	10.500	10.584	10.758	10.628	10.543	10.863
$\zeta_5(2s)$	6.206	6.224	6.253	6.451	6.498	6.544
$\zeta_6(3s)$	3.166	3.259	3.232	3.458	3.382	3.532
$\zeta_7(3s)$	1.993	2.185	2.201	2.311	2.278	2.340
$\zeta_1(2p)$	16.220	16.160	16.195	17.020	17.460	17.720
$\zeta_2(2p)$	8.230	8.180	8.200	8.410	8.500	9.055
$\zeta_3(2p)$	5.000	4.795	4.865	5.000	5.115	5.450
$\zeta_4(4p)$	8.000	8.000	8.000	8.500	8.500	8.900
$\zeta_5(3p)$	2.970	2.955	2.976	3.157	3.159	3.214
$\zeta_6(4p)$	2.211	2.209	2.242	2.359	2.358	2.385
$\zeta_7(3p)$	1.370	1.550	1.550	1.620	1.620	1.650
ϵ_{1s}	-118.61014	-119.13309	-119.19462	-120.65776	-120.39576	-127.27956
Cusp	-18.00366	-18.00349	-18.00287	-18.00005	-18.00218	-18.00163
$c_{1s,1}$	0.78751	0.78752	0.78834	0.79073	0.79512	0.83865
$c_{1s,2}$	0.41319	0.41322	0.41103	0.40339	0.38653	0.23192
$c_{1s,3}$	-0.17634	-0.17640	-0.17492	-0.17014	-0.15765	-0.05294
$c_{1s,4}$	-0.00008	-0.00004	-0.00022	0.00027	0.00121	0.00265
$c_{1s,5}$	-0.00011	-0.00016	-0.00006	-0.00047	-0.00020	0.01419
$c_{1s,6}$	0.00007	0.00011	0.00006	0.00009	0.00011	-0.00213
$c_{1s,7}$	-0.00006	-0.00008	-0.00008	-0.00008	-0.00008	-0.00203
ϵ_{2s}	-12.32193	-12.83568	-12.88311	-13.61576	-13.77370	-14.17473
Cusp	-17.99649	-18.00356	-18.01242	-18.01453	-18.02974	-17.95176
$c_{2s,1}$	-0.22353	-0.22365	-0.22356	-0.22847	-0.22912	-0.25356
$c_{2s,2}$	-0.21917	-0.22087	-0.22339	-0.23284	-0.22911	-0.15950
$c_{2s,3}$	0.08753	0.08586	0.08258	0.08007	0.07458	0.02281
$c_{2s,4}$	0.16903	0.16072	0.14166	0.13434	0.11753	0.15781
$c_{2s,5}$	0.90732	0.91795	0.93996	0.95521	0.96271	0.92791
$c_{2s,6}$	0.00708	0.00704	0.00956	0.00977	0.02490	0.00833
$c_{2s,7}$	-0.00043	-0.00048	-0.00049	-0.00085	0.00965	-0.00047
ϵ_{3s}	-1.27725	-1.71114	-1.81793	-1.89228	-1.87409	-1.90809
Cusp	-17.96890	-17.94414	-17.92541	-17.97576	-18.00103	-17.96324
$c_{3s,1}$	0.06982	0.07189	0.07327	0.07702	0.08092	0.08360
$c_{3s,2}$	0.08792	0.09287	0.09574	0.10727	0.11101	0.07415
$c_{3s,3}$	-0.02628	-0.02782	-0.02893	-0.02530	-0.02355	-0.00188
$c_{3s,4}$	0.00341	0.01304	0.01863	0.04101	0.05414	0.03755
$c_{3s,5}$	-0.45394	-0.48178	-0.49483	-0.55249	-0.58015	-0.53655
$c_{3s,6}$	0.66908	0.60576	0.63355	0.60842	0.62943	0.59459
$c_{3s,7}$	0.46963	0.53030	0.50098	0.54305	0.51521	0.55658
ϵ_{2p}	-9.57127	-10.08324	-10.14966	-11.10837	-10.86746	-11.71786
Cusp	-8.92591	-8.91125	-8.91441	-8.92308	-8.96769	-8.98739
$c_{2p,1}$	0.01876	0.01845	0.01832	0.01284	0.01174	0.00570
$c_{2p,2}$	0.63009	0.66020	0.65271	0.64006	0.61717	0.59627
$c_{2p,3}$	0.27207	0.23154	0.24110	0.25810	0.29030	0.30855
$c_{2p,4}$	0.13409	0.14874	0.14644	0.13301	0.13460	0.14165
$c_{2p,5}$	0.00309	0.00086	0.00001	0.01590	-0.00093	0.00252
$c_{2p,6}$	-0.00058	0.00171	0.00061	0.01386	0.00165	-0.00075
$c_{2p,7}$	0.00028	-0.00037	-0.00031	0.00155	-0.00088	0.00047
ϵ_{3p}	-0.59092	-1.04532	-1.03104	-1.15880	-1.15303	-1.17532
Cusp	-8.88089	-8.88838	-8.86398	-8.89927	-8.89853	-8.93455
$c_{3p,1}$	-0.00346	-0.00391	-0.00345	-0.00290	-0.00204	0.00005
$c_{3p,2}$	-0.18973	-0.20843	-0.21009	-0.22991	-0.20638	-0.19549
$c_{3p,3}$	-0.06049	-0.06140	-0.05246	-0.08803	-0.08549	-0.08377
$c_{3p,4}$	-0.06178	-0.06560	-0.07057	-0.06915	-0.06887	-0.06753
$c_{3p,5}$	0.60487	0.66790	0.65321	0.68195	0.68125	0.68076
$c_{3p,6}$	0.30887	0.33443	0.32329	0.33574	0.33983	0.33549
$c_{3p,7}$	0.22836	0.12476	0.14980	0.11967	0.11682	0.11520

*States which are not the lowest of a symmetry species.

TABLE IV. SCF Orbitals and Energies for K^+ and nf-hole States of K^+, Accurate Basis Sets

	$K^+(^1S)$	$K^{++}(^2P)$ 3p-hole	$K^{++}(^2S)$ 3s-hole	$K^{++}(^2P)^*$ 2p-hole	$K^{++}(^2S)^*$ 2s-hole	$K^{++}(^2S)^*$ 1s-hole
E	-599.0175	-597.8915	-597.1039	-587.6833	-584.6720	-466.4285
V/T	-1.999999	-2.000000	-1.999999	-2.000000	-2.000002	-1.999997
$\zeta_1(1s)$	21.530	21.545	21.685	21.480	21.390	20.400
$\zeta_2(2s)$	15.255	15.220	15.095	15.300	15.400	17.200
$\zeta_3(3s)$	17.000	17.000	17.000	17.000	17.000	19.000
$\zeta_4(3s)$	11.085	11.258	11.323	10.957	11.262	11.560
$\zeta_5(2s)$	6.687	6.724	6.711	6.878	7.010	7.025
$\zeta_6(3s)$	3.502	3.520	3.599	3.787	3.660	3.814
$\zeta_7(3s)$	2.338	2.491	2.573	2.658	2.600	2.662
$\zeta_1(2p)$	17.000	17.000	17.020	17.800	18.460	20.000
$\zeta_2(2p)$	8.890	8.820	8.855	9.075	9.210	9.920
$\zeta_3(2p)$	5.450	5.260	5.315	5.610	5.712	6.100
$\zeta_4(4p)$	8.800	8.800	8.800	9.300	9.300	9.800
$\zeta_5(3p)$	3.253	3.358	3.371	3.562	3.563	3.546
$\zeta_6(4p)$	2.412	. . .	. . .	. . .	. . .	2.726
$\zeta_7(3p)$	1.650	2.182	2.173	2.294	2.295	2.000
ϵ_{1s}	-133.75212	-134.40390	-134.45519	-136.06387	-135.76859	-143.07622
Cusp	-19.00074	-19.00027	-19.00610	-18.99684	-18.99330	-19.00584
$C_{1s,1}$	0.80888	0.80805	0.80027	0.81209	0.82183	0.88850
$C_{1s,2}$	0.38950	0.39410	0.42346	0.37982	0.34675	0.15967
$C_{1s,3}$	-0.17686	-0.18025	-0.20056	-0.17085	-0.14743	-0.03669
$C_{1s,4}$	-0.00081	-0.00177	-0.00439	-0.00043	-0.00018	0.00249
$C_{1s,5}$	-0.00024	0.00010	0.00074	-0.00055	0.00047	0.01358
$C_{1s,6}$	0.00011	0.00008	0.00001	0.00013	-0.00003	-0.00199
$C_{1s,7}$	-0.00009	-0.00008	-0.00007	-0.00011	-0.00002	-0.00208
ϵ_{2s}	-14.70798	-15.33970	-15.37648	-16.18376	-16.34603	-16.79208
Cusp	-19.00163	-19.00951	-19.01782	-19.00269	-19.03162	-18.95758
$C_{2s,1}$	-0.23231	-0.23224	-0.22961	-0.23712	-0.23933	-0.27074
$C_{2s,2}$	-0.22932	-0.23548	-0.24544	-0.23674	-0.23878	-0.15189
$C_{2s,3}$	0.09750	0.09623	0.10267	0.09486	0.07919	0.02290
$C_{2s,4}$	0.15704	0.14080	0.14292	0.15644	0.09227	0.14450
$C_{2s,5}$	0.92363	0.94521	0.94423	0.93077	0.99761	0.94824
$C_{2s,6}$	0.00901	0.00953	0.01023	0.01075	0.02701	0.00953
$C_{2s,7}$	-0.00103	-0.00166	-0.00050	-0.00133	0.00777	-0.00100
ϵ_{3s}	-1.96377	-2.47767	-2.58881	-2.68728	-2.66588	-2.71203
Cusp	-18.97447	-18.95978	-18.92907	-19.01150	-19.00299	-18.96578
$C_{3s,1}$	0.07649	0.07862	0.07904	0.08360	0.08803	0.09344
$C_{3s,2}$	0.10123	0.10710	0.11452	0.11897	0.12444	0.07854
$C_{3s,3}$	-0.05137	-0.03343	-0.03861	-0.02901	-0.02732	-0.00858
$C_{3s,4}$	0.01616	0.02255	0.02791	0.04360	0.06713	0.04315
$C_{3s,5}$	-0.50319	-0.52525	-0.54237	-0.59121	-0.62553	-0.57324
$C_{3s,6}$	0.63772	0.62378	0.57022	0.57719	0.62575	0.58974
$C_{3s,7}$	0.50386	0.51400	0.57145	0.58011	0.52008	0.56280
ϵ_{2p}	-11.73810	-12.36843	-12.42720	-13.48122	-13.21615	-14.14872
Cusp	-9.40153	-9.40961	-9.39849	-9.42043	-9.45892	-9.47034
$C_{2p,1}$	0.01736	0.01746	0.01681	0.01262	0.01054	0.00253
$C_{2p,2}$	0.60440	0.63378	0.62810	0.59657	0.57059	0.52965
$C_{2p,3}$	0.30758	0.27199	0.27634	0.31579	0.35027	0.39164
$C_{2p,4}$	0.12274	0.13211	0.13435	0.11239	0.11647	0.12198
$C_{2p,5}$	0.00147	-0.00149	-0.00177	0.01286	0.00072	0.00433
$C_{2p,6}$	0.00039	. . . .	. . . .	. . . .	. . . .	-0.00201
$C_{2p,7}$	-0.00023	0.00228	0.00077	0.01746	0.00040	0.00129
ϵ_{3p}	-1.17047	-1.71131	-1.68867	-1.85275	-1.84608	-1.88069
Cusp	-9.40818	-9.41311	-9.39637	-9.43034	-9.42898	-9.41764
$C_{3p,1}$	-0.00387	-0.00406	-0.00374	-0.00323	-0.00207	0.00057
$C_{3p,2}$	-0.19057	-0.21305	-0.21027	-0.22120	-0.19844	-0.18219
$C_{3p,3}$	-0.09892	-0.09160	-0.09122	-0.13117	-0.12730	-0.12897
$C_{3p,4}$	-0.05812	-0.06176	-0.06274	-0.06004	-0.06202	-0.06243
$C_{3p,5}$	0.67017	0.52926	0.52899	0.54360	0.54095	0.69616
$C_{3p,6}$	0.34285	. . . .	. . . .	. . . .	. . . .	0.32599
$C_{3p,7}$	0.12328	0.57550	0.57691	0.57136	0.57394	0.10617

*States which are not the lowest of a symmetry species.

TABLE V. SCF Orbitals and Energies for F^-, Ne, and Na^+ and nl-hole States of F^-, Ne, and Na^+, Simple Basis Sets

	$F^-(^1S)$	$F(^2P)$ 2p-hole	$F(^2S)$ 2s-hole	$F(^2S)^*$ 1s-hole	$Ne(^1S)$	$Ne^+(^2P)$ 2p-hole	$Ne^+(^2S)$ 2s-hole	$Ne^+(^2S)^*$ 1s-hole	$Na^+(^1S)$	$Na^{++}(^2P)$ 2p-hole	$Na^{++}(^2S)$ 2s-hole	$Na^{++}(^2S)^*$ 1s-hole
E	-99.45785	-99.40893	-98.53085	-74.52382	-128.5465	-127.8176	-126.7346	-96.62555	-161.6766	-159.9972	-158.7087	-121.7423
V/T	-2.000002	-2.000004	-1.999999	-1.999993	-2.000008	-2.000018	-2.000004	-1.999990	-2.000002	-2.000013	-1.999996	-1.999995
$\zeta_1(1s)$	13.220	13.198	12.810	12.758	14.319	13.623	13.859	12.382	15.314	14.403	14.659	12.211
$\zeta_2(1s)$	8.282	8.278	8.230	8.842	9.224	9.184	9.162	9.729	10.157	10.033	10.058	10.420
$\zeta_3(3s)$	4.952	4.982	4.962	5.225	5.619	5.627	5.576	5.926	6.254	6.233	6.172	6.676
$\zeta_4(2\phi)$	2.094	2.246	2.293	2.369	2.518	2.700	2.734	2.840	2.966	3.161	3.189	3.328
$\zeta_1(2p)$	5.219	6.165	6.112	5.695	6.620	7.588	7.405	6.665	8.000	9.058	8.759	7.515
$\zeta_2(2p)$	2.599	3.176	3.144	3.208	3.484	3.991	3.926	3.955	4.316	4.794	4.715	4.624
$\zeta_3(2p)$	1.154	1.612	1.582	1.724	1.766	2.164	2.122	2.276	2.325	2.698	2.651	2.799
ϵ_{1s}	-25.82687	-26.38217	-26.42007	-29.53598	-32.77162	-33.61208	-33.61587	-37.16972	-40.75946	-41.86265	-41.83046	-45.82011
Cusp	-9.01242	-9.01302	-9.00866	-9.02632	-10.01011	-9.99551	-10.00523	-10.02222	-11.00542	-10.98715	-10.99733	-11.01931
$C_{1s,1}$	0.07956	0.08056	0.09582	0.02797	0.08650	0.11485	0.10566	0.08021	0.09647	0.14038	0.12778	0.28471
$C_{1s,2}$	0.92438	0.92348	0.90835	0.96451	0.91716	0.88966	0.89831	0.91277	0.90707	0.86426	0.87630	0.70895
$C_{1s,3}$	0.00594	0.00580	0.00607	0.01658	0.00595	0.00408	0.00588	0.01441	0.00573	0.00315	0.00501	0.01183
$C_{1s,4}$	-0.00032	-0.00044	0.00019	0.01639	-0.00029	0.00019	0.00015	0.01595	-0.00031	0.00045	0.00034	0.01596
ϵ_{2s}	-1.07236	-1.57205	-1.70549	-1.74516	-1.92975	-2.61894	-2.75289	-2.85336	-3.07347	-3.93044	-4.06561	-4.22285
Cusp	-9.07531	-8.99798	-9.00934	-8.94043	-10.01357	-9.95997	-9.96417	-9.95186	-10.96458	-10.93106	-10.93216	-10.97567
$C_{2s,1}$	-0.00824	-0.00411	-0.00583	0.01728	-0.00431	-0.00220	-0.00127	0.03807	-0.00001	0.00192	0.00298	0.05695
$C_{2s,2}$	-0.22858	-0.24286	-0.24667	-0.29148	-0.24635	-0.26184	-0.26625	-0.32867	-0.26474	-0.28137	-0.28516	-0.36558
$C_{2s,3}$	0.33891	0.29770	0.29412	0.30914	0.29901	0.26352	0.26319	0.26448	0.26942	0.23998	0.23945	0.22166
$C_{2s,4}$	0.73161	0.76464	0.76645	0.75408	0.76514	0.79565	0.79427	0.79696	0.79097	0.81852	0.81770	0.84308
ϵ_{2p}	-0.17886	-0.72953	-0.70231	-0.87121	-0.84974	-1.60644	-1.55239	-1.81586	-1.79697	-2.74424	-2.66290	-3.01944
Cusp	-4.02916	-4.19515	-4.20656	-4.32426	-4.67506	-4.78652	-4.78530	-4.86452	-5.26728	-5.35367	-5.34729	-5.38621
$C_{2p,1}$	0.14234	0.07255	0.07692	0.13992	0.08944	0.04870	0.05544	0.11167	0.06123	0.03406	0.04050	0.10024
$C_{2p,2}$	0.56283	0.48890	0.49372	0.49635	0.50024	0.43454	0.44020	0.44736	0.45069	0.39047	0.39581	0.40934
$C_{2p,3}$	0.43109	0.53155	0.52539	0.45645	0.50722	0.58891	0.57919	0.51414	0.56481	0.63486	0.62536	0.55122

*States which are not the lowest of a symmetry species.

TABLE VI. SCF Orbitals and Energies for Cl^- and nl-hole States of Cl^-, Simple Basis Sets

	$Cl^-(^1S)$	$Cl(^2P)$ 3p-hole	$Cl(^2S)$ 3s-hole	$Cl(^2P)^*$ 2p-hole	$Cl(^2S)^*$ 2s-hole	$Cl(^2S)^*$ 1s-hole
E	-459.5736	-459.4801	-458.9148	-452.3332	-449.7638	-356.2814
V/T	-2.000000	-1.999993	-2.000007	-1.999991	-2.000000	-1.999988
$\zeta_1(1s)$	18.575	18.674	18.629	18.474	18.095	17.749
$\zeta_2(2s)$	16.329	16.439	16.385	16.245	15.621	16.424
$\zeta_3(3s)$	10.217	10.190	10.219	10.021	10.386	10.381
$\zeta_4(2s)$	5.798	5.785	5.795	5.895	6.062	6.082
$\zeta_5(3s)$	2.823	2.904	2.878	3.140	3.030	3.167
$\zeta_6(3s)$	1.651	1.826	1.842	1.970	1.923	1.982
$\zeta_1(2p)$	10.203	10.268	10.275	10.586	10.594	10.460
$\zeta_2(2p)$	5.585	5.608	5.610	5.884	5.841	6.002
$\zeta_3(3p)$	2.497	2.612	2.617	2.787	2.798	2.881
$\zeta_4(3p)$	1.224	1.465	1.459	1.570	1.576	1.607
ϵ_{1s}	-104.50086	-104.88211	-104.95369	-106.26874	-106.03937	-112.50146
Cusp	-16.96350	-16.96634	-16.96577	-16.95669	-16.95214	-17.01951
$C_{1s,1}$	0.85189	0.84517	0.84820	0.85920	0.88567	0.92623
$C_{1s,2}$	0.17649	0.18395	0.18062	0.16830	0.13937	0.07920
$C_{1s,3}$	-0.00074	-0.00011	-0.00046	-0.00234	-0.00594	0.01076
$C_{1s,4}$	0.00245	0.00217	0.00237	0.00337	0.00593	0.01019
$C_{1s,5}$	-0.00052	-0.00054	-0.00061	-0.00082	-0.00112	-0.00151
$C_{1s,6}$	0.00021	0.00024	0.00027	0.00034	0.00051	-0.00221
ϵ_{2s}	-10.22595	-10.60672	-10.66476	-11.32012	-11.47338	-11.83108
Cusp	-16.99022	-16.97968	-16.98170	-16.99964	-17.00832	-16.98680
$C_{2s,1}$	-0.23882	-0.23691	-0.23743	-0.24544	-0.25239	-0.27771
$C_{2s,2}$	-0.11908	-0.11959	-0.11987	-0.11900	-0.13056	-0.10274
$C_{2s,3}$	0.14005	0.14504	0.13795	0.17025	0.09289	0.15200
$C_{2s,4}$	0.93670	0.93089	0.93755	0.91033	0.98751	0.93066
$C_{2s,5}$	0.00654	0.00546	0.00782	0.00241	0.02434	0.00530
$C_{2s,6}$	-0.00035	0.00010	-0.00001	0.00185	0.01004	0.00059
ϵ_{3s}	-0.73031	-1.07236	-1.17505	-1.22270	-1.20752	-1.23049
Cusp	-16.76015	-16.72967	-16.74820	-16.62437	-16.83732	-16.69588
$C_{3s,1}$	0.07001	0.07132	0.07321	0.07805	0.08474	0.08627
$C_{3s,2}$	0.04802	0.05010	0.05117	0.05897	0.06448	0.05180
$C_{3s,3}$	0.01033	0.01482	0.01573	0.03488	0.04751	0.03199
$C_{3s,4}$	-0.42149	-0.44112	-0.45062	-0.50811	-0.53027	-0.49176
$C_{3s,5}$	0.70660	0.65189	0.68576	0.64632	0.67235	0.64391
$C_{3s,6}$	0.43162	0.48073	0.44446	0.50908	0.46670	0.50380
ϵ_{2p}	-7.69225	-8.07136	-8.14535	-9.00648	-8.78900	-9.55916
Cusp	-8.06915	-8.08454	-8.08774	-8.12583	-8.14560	-8.32563
$C_{2p,1}$	0.21126	0.20561	0.20543	0.17599	0.17940	0.21911
$C_{2p,2}$	0.81783	0.82121	0.82229	0.83577	0.84306	0.80592
$C_{2p,3}$	0.01585	0.02020	0.01796	0.03725	0.01956	0.01500
$C_{2p,4}$	-0.00394	-0.00457	-0.00509	0.01137	-0.00519	-0.00369
ϵ_{3p}	-0.14772	-0.50603	-0.50013	-0.58933	-0.58439	-0.59575
Cusp	-8.14508	-8.12119	-8.12953	-8.12036	-8.13553	-8.37302
$C_{3p,1}$	-0.05028	-0.05192	-0.05186	-0.05079	-0.04652	-0.05670
$C_{3p,2}$	-0.21340	-0.23694	-0.23666	-0.28976	-0.26765	-0.24645
$C_{3p,3}$	0.61008	0.56419	0.57193	0.59434	0.59193	0.58595
$C_{3p,4}$	0.52453	0.54343	0.53765	0.51794	0.52288	0.52859

*States which are not the lowest of a symmetry species.

TABLE VII. SCF Orbitals and Energies for Argon and nl-hole States of Argon, Simple Basis Sets

	$Ar(^1S)$	$Ar^+(^2P)$ 3p-hole	$Ar^+(^2S)$ 3s-hole	$Ar^+(^2P)^*$ 2p-hole	$Ar^+(^2S)^*$ 2s-hole	$Ar^+(^2S)^*$ 1s-hole
E	-526.8155	-526.2729	-525.5961	-517.6676	-514.8779	-409.3884
V/T	-2.000001	-2.000001	-1.999997	-2.000000	-2.000002	-2.000015
$\zeta_1(1s)$	19.419	19.412	19.454	19.138	19.045	18.566
$\zeta_2(2s)$	17.034	17.024	17.075	16.639	16.371	16.958
$\zeta_3(3s)$	10.943	10.941	10.896	10.896	11.085	11.082
$\zeta_4(2s)$	6.275	6.279	6.277	6.436	6.537	6.562
$\zeta_5(3s)$	3.187	3.259	3.232	3.474	3.314	3.532
$\zeta_6(3s)$	2.005	2.185	2.201	2.311	2.230	2.340
$\zeta_1(2p)$	11.027	11.073	11.095	11.402	11.417	11.208
$\zeta_2(2p)$	6.095	6.113	6.120	6.388	6.345	6.498
$\zeta_3(3p)$	2.886	2.956	2.972	3.127	3.142	3.234
$\zeta_4(3p)$	1.609	1.814	1.812	1.919	1.928	1.963
ϵ_{1s}	-118.60817	-119.13197	-119.19307	-120.65641	-120.39431	-127.27928
Cusp	-17.95816	-17.95800	-17.95995	-17.94695	-17.95166	-18.01716
$C_{1s,1}$	0.86927	0.86975	0.86693	0.88877	0.89477	0.94351
$C_{1s,2}$	0.15689	0.15636	0.15949	0.13538	0.12918	0.05966
$C_{1s,3}$	-0.00245	-0.00272	-0.00237	-0.00638	-0.00748	0.00986
$C_{1s,4}$	0.00341	0.00368	0.00348	0.00583	0.00684	0.00999
$C_{1s,5}$	-0.00079	-0.00095	-0.00096	-0.00141	-0.00142	-0.00123
$C_{1s,6}$	0.00035	0.00046	0.00045	0.00063	0.00069	-0.00244
ϵ_{2s}	-12.32139	-12.83595	-12.88297	-13.61587	-13.77364	-14.17480
Cusp	-17.98911	-17.99026	-17.99083	-18.00607	-18.02007	-18.03109
$C_{2s,1}$	-0.24687	-0.24712	-0.24592	-0.25697	-0.25799	-0.28557
$C_{2s,2}$	-0.12262	-0.12272	-0.12286	-0.12721	-0.13624	-0.10624
$C_{2s,3}$	0.12399	0.12384	0.12284	0.12539	0.08266	0.14049
$C_{2s,4}$	0.95830	0.95863	0.95768	0.96574	1.00378	0.94875
$C_{2s,5}$	0.00745	0.00727	0.00963	0.00599	0.02491	0.00724
$C_{2s,6}$	-0.00027	-0.00033	-0.00040	0.00090	0.00894	0.00010
ϵ_{3s}	-1.27666	-1.71130	-1.81793	-1.89215	-1.87392	-1.90793
Cusp	-17.75815	-17.75636	-17.74072	-17.72879	-17.83920	-17.75839
$C_{3s,1}$	0.07681	0.07917	0.08033	0.08623	0.09084	0.09367
$C_{3s,2}$	0.05492	0.05722	0.05843	0.06789	0.07238	0.05946
$C_{3s,3}$	0.02678	0.03123	0.03317	0.05377	0.05842	0.04611
$C_{3s,4}$	-0.47508	-0.49604	-0.50585	-0.56189	-0.57408	-0.54330
$C_{3s,5}$	0.65610	0.60506	0.63491	0.60870	0.67677	0.59538
$C_{3s,6}$	0.48338	0.53045	0.50004	0.54657	0.46372	0.55601
ϵ_{2p}	-9.57061	-10.08339	-10.14938	-11.10839	-10.86733	-11.71788
Cusp	-8.60975	-8.61881	-8.62450	-8.65542	-8.67770	-8.84569
$C_{2p,1}$	0.19611	0.19240	0.19107	0.16434	0.16737	0.20753
$C_{2p,2}$	0.82878	0.83062	0.83266	0.84393	0.85184	0.81457
$C_{2p,3}$	0.01861	0.02242	0.02061	0.03805	0.02168	0.01642
$C_{2p,4}$	-0.00497	-0.00547	-0.00629	0.00967	-0.00620	-0.00428
ϵ_{3p}	-0.59046	-1.04550	-1.03108	-1.15874	-1.15294	-1.17519
Cusp	-8.63989	-8.63187	-8.63848	-8.62460	-8.63667	-8.86975
$C_{3p,1}$	-0.05049	-0.05249	-0.05178	-0.04946	-0.04559	-0.05682
$C_{3p,2}$	-0.25002	-0.27029	-0.26961	-0.31930	-0.29823	-0.27652
$C_{3p,3}$	0.58087	0.55695	0.55483	0.58189	0.57570	0.56927
$C_{3p,4}$	0.53221	0.54085	0.54469	0.52121	0.52995	0.53616

*States which are not the lowest of a symmetry species.

TABLE VIII. SCF Orbitals and Energies for K^+ and nl-hole States of K^{++}, Simple Basis Sets

	$K^+(^1S)$	$K^{++}(^2P)$ 3p-hole	$K^{++}(^2S)$ 3s-hole	$K^{++}(^2P)^*$ 2p-hole	$K^{++}(^2S)^*$ 2s-hole	$K^{++}(^2S)^*$ 1s-hole
E	-599.0159	-597.8901	-597.1025	-587.6820	-584.6705	-466.4280
V/T	-2.000002	-2.000002	-2.000002	-2.000002	-1.999998	-1.999995
$\zeta_1(1s)$	20.222	20.200	20.339	19.998	20.006	19.464
$\zeta_2(2s)$	17.611	17.568	17.799	17.194	17.116	17.522
$\zeta_3(3s)$	11.812	11.804	11.603	11.868	11.962	12.155
$\zeta_4(2s)$	6.793	6.805	6.762	6.999	7.049	7.134
$\zeta_5(3s)$	3.502	3.520	3.599	3.787	3.660	3.814
$\zeta_6(3s)$	2.338	2.491	2.573	2.658	2.600	2.662
$\zeta_1(2p)$	11.838	11.880	11.890	12.210	12.228	11.965
$\zeta_2(2p)$	6.601	6.619	6.621	6.889	6.846	6.998
$\zeta_3(3p)$	3.239	3.290	3.300	3.441	3.453	3.561
$\zeta_4(3p)$	1.965	2.167	2.156	2.252	2.259	2.302
ϵ_{1s}	-133.75073	-134.40246	-134.45380	-136.06274	-135.76712	-143.07576
Cusp	-18.95218	-18.95205	-18.95638	-18.94390	-18.95098	-19.01711
$c_{1s,1}$	0.88800	0.88948	0.88039	0.90332	0.90230	0.95351
$c_{1s,2}$	0.13603	0.13446	0.14429	0.11956	0.12092	0.04811
$c_{1s,3}$	-0.00472	-0.00528	-0.00396	-0.00904	-0.00885	0.00779
$c_{1s,4}$	0.00458	0.00501	0.00448	0.00720	0.00749	0.01140
$c_{1s,5}$	-0.00112	-0.00136	-0.00132	-0.00185	-0.00174	-0.00128
$c_{1s,6}$	0.00053	0.00070	0.00066	0.00089	0.00090	-0.00243
ϵ_{2s}	-14.70793	-15.33966	-15.37635	-16.18405	-16.34594	-16.79222
Cusp	-18.99464	-19.00240	-18.99354	-19.00464	-19.01649	-19.00922
$c_{2s,1}$	-0.25518	-0.25580	-0.25269	-0.26397	-0.26285	-0.29070
$c_{2s,2}$	-0.12988	-0.13038	-0.12747	-0.14134	-0.14610	-0.12283
$c_{2s,3}$	0.09466	0.09326	0.10736	0.07830	0.05739	0.08431
$c_{2s,4}$	0.99545	0.99744	0.97862	1.02354	1.03674	1.01665
$c_{2s,5}$	0.01053	0.01133	0.01083	0.01144	0.02561	0.01163
$c_{2s,6}$	-0.00135	-0.00225	-0.00055	-0.00115	0.00869	-0.00153
ϵ_{3s}	-1.96364	-2.47755	-2.58857	-2.68729	-2.66576	-2.71209
Cusp	-18.81626	-18.82281	-18.73490	-18.82718	-18.88418	-18.86195
$c_{3s,1}$	0.08380	0.08639	0.08671	0.09277	0.09651	0.10010
$c_{3s,2}$	0.06244	0.06489	0.06623	0.07783	0.08153	0.06895
$c_{3s,3}$	0.04043	0.04354	0.05050	0.06891	0.07410	0.06040
$c_{3s,4}$	-0.52140	-0.53996	-0.55866	-0.60641	-0.62185	-0.58590
$c_{3s,5}$	0.63334	0.62015	0.57039	0.56953	0.62156	0.58244
$c_{3s,6}$	0.50598	0.51587	0.57106	0.58382	0.52239	0.56650
ϵ_{2p}	-11.73792	-12.36825	-12.42694	-13.48136	-13.21598	-14.14875
Cusp	-9.14221	-9.14897	-9.15299	-9.18073	-9.20343	-9.36415
$c_{2p,1}$	0.18371	0.18054	0.18030	0.15466	0.15745	0.19632
$c_{2p,2}$	0.83783	0.83920	0.84055	0.85107	0.85924	0.82317
$c_{2p,3}$	0.02070	0.02456	0.02220	0.03860	0.02333	0.01796
$c_{2p,4}$	-0.00591	-0.00658	-0.00725	0.00778	-0.00728	-0.00510
ϵ_{3p}	-1.17044	-1.71127	-1.68849	-1.85283	-1.84601	-1.88080
Cusp	-9.14340	-9.14264	-9.14979	-9.13004	-9.14083	-9.37069
$c_{3p,1}$	-0.05010	-0.05196	-0.05152	-0.04788	-0.04447	-0.05596
$c_{3p,2}$	-0.28036	-0.29883	-0.29718	-0.34421	-0.32398	-0.30266
$c_{3p,3}$	0.56462	0.54277	0.54510	0.58046	0.57500	0.56238
$c_{3p,4}$	0.53895	0.55028	0.54969	0.51866	0.52659	0.53909

*States which are not the lowest of a symmetry species.

The accurate basis sets for the states of the light atoms (fluorine, neon, and sodium) are composed of five s and four p basis functions. The one exception is the basis set for F^-, which is composed of six x and five p basis functions.

The accurate basis sets for the states of the heavier atoms (chlorine, argon, and potassium) are composed of seven s and either six or seven p basis functions. The seven p sets used three basis functions to represent the outer loop of the 3p orbital. The addition of a third basis function to represent this loop caused only a small improvement in the total energy. For most of the states of K^{++}, a third basis function did not cause any improvement in the total energy. Only two basis functions were used to represent the loop for these states.

The simple basis sets for the light atoms are composed of four s and three p basis functions. Two basis functions are used to represent each loop of the s orbitals. The simple basis sets for the heavier atoms are composed of six s and four p basis functions; two basis functions are used to represent each loop of the orbitals. The automatic exponent variation procedures of the SCF program converge quickly to the optimum values of the exponents of the simple basis sets; almost no manual examination of the intermediate results, and consequent readjustment of the exponent variation parameters, are required. Thus, the calculation of the simple basis set functions is extremely automatic and requires the use of little human or machine time. Of the simple basis set SCF functions, the two which give the poorest approximations to the exact HF functions are the functions for the negative ions F^- and Cl^-. (The simple basis sets for the light atoms were called nominal basis sets in an earlier paper.[9] The reasons for the use of this name were explained in that paper.)

The optimum values of the exponents are not determined in all cases to the number of significant figures given in Tables I-VIII. This is especially true for the large exponents of the basis functions used to represent inner loops, and for the large, accurate, basis sets. Some of the exponents used to represent a loop are better determined than others. The exponents of the dominant basis functions (usually the basis functions with the largest vector coefficients $C_{n\ell,p}$) are often well-determined once the exponents of the less important basis functions are fixed. The largest exponents of the accurate basis sets of the heavier atoms were rounded. The largest exponents of the p basis functions of some of the states of Ne^+ and Na^{++} were also rounded to simple values. Beyond this, we did not make a systematic attempt to round any of the other exponents but used them, rounded to three decimal places, as they were obtained from the SCF computer program. When exponents were rounded, the vector coefficients given are those determined from SCF calculations made using the rounded values of the exponents.

B. Accuracy of the SCF Wave Functions

Estimates were made of the effect of round-off errors on the SCF calculations. As a part of the round-off error, we include the extent to which the results are not self-consistent solutions of the matrix HF equations. Our estimates of round-off error are based, primarily, on information gained in the following ways:

1. The examination of the convergence thresholds, for diagonalization and self-consistency met by the SCF vector coefficients. These thresholds are part of the output of the computer program and are also set automatically by the program depending on the features of the calculation being performed.[4] Unfortunately, our experience indicates that these thresholds give a low estimate of the effects of round-off errors.

2. The comparison of the results of SCF calculations performed on the IBM 704 and on the IBM 7094. The most important difference between the 704 and 7094 programs is that in the 7094 program the results of floating-point addition and multiplication are rounded, while in the 704 program they are not. Thus a comparison of the results of SCF calculations, performed on the 704 and 7094, should provide an estimate, most likely on the high side, of the effect of rounding errors on the 7094 results.

3. The comparison of the results of two SCF calculations, both performed on the 7094 and using the same basis set, but with somewhat different initial approximations for the SCF eigenvectors.

For the calculations performed with small basis sets, viz., the simple sets for the heavier atoms (chlorine, argon, and potassium) and both the simple and accurate sets for the lighter atoms (fluorine, neon, and sodium), the estimates of round-off errors are the following: The round-off error in the total energy and V/T is probably less than or equal to five units in the eighth significant figure. For those states for which the total energy is just larger than 100 Hartrees, the round-off error in the total energy is probably less than two units in the eighth significant figure. The round-off error in the $\epsilon_{n\ell}$'s and $C_{n\ell,p}$'s is probably less than or equal to one unit in the fifth decimal place (that is, one unit in the last figure given for these quantities in Tables I-VIII). The round-off error in the cusps is usually less than one unit in the fifth decimal place, but in some cases is probably about three or four units in the fifth decimal place.

For calculations with the accurate basis sets for the heavier atoms, the estimates of round-off error are the following: The round-off error in the total energy is probably less than four to eight units in the eighth significant figure. The round-off error in V/T is usually about five units in the eighth significant figure, but in a few cases it is as large

as four in the seventh significant figure. The round-off error for the $\epsilon_{n\ell}$'s and cusps varies depending on the orbital considered (1s, 2s, 2p, etc.), but in any case is no more than one or two units in the fourth decimal place. The round-off error for the $C_{n\ell,p}$'s for s orbitals is about one unit in the fifth decimal place, and for p orbitals is less than one unit in the fourth place.

The round-off error is larger for the vector coefficients of p orbitals because the p basis functions form a more nearly linearly dependent set than the s basis functions. The diagonalization procedures lose accuracy as the basis set becomes linearly dependent. For example, for the accurate basis set for neutral argon, the determinant of the overlap matrix of the p basis functions is 0.5×10^{-6}; for the s basis functions it is 5.3×10^{-6}, a factor of 10 larger. But, because of the redundancy of the p basis functions, the round-off errors in the vector coefficients may not have a large effect on the numerical values of the p orbitals.

Although the vectors given in Tables I-VIII may not be SCF eigenvectors to the number of figures given, they do form an orthonormal set to the number of figures given.

It is important to obtain reliable estimates of the accuracy of the analytic SCF wave functions. By accuracy of the analytic functions we mean how closely they represent the exact HF solutions. Information on the accuracy of the analytic functions may be obtained in the following ways:

1. The comparison of analytic functions with solutions obtained by direct numerical integration. This method has limited usefulness; first, because numerical solutions are often not available and, second, because accurate analytic functions are often better than the available numerical solutions.

2. The comparison of different, good, analytic functions for the same state, calculated independently by different workers or with a different choice of principal quantum numbers for the basis functions, but with very nearly the same total energy. These calculations are not likely to have the same systematic errors because of individual peculiarities in the choice and optimization of the basis functions. Thus, it is reasonable that the differences between the results of these calculations should represent the random error of functions with this total energy. These differences provide a good basis for estimating the accuracy of the functions.

3. The examination of the convergence of the properties of the SCF functions obtained in the process of building up the basis set from a small set to the final accurate set. This method is very powerful when the basis set is completely reoptimized at each step of the build-up so that the effects of systematic errors on the choice of basis functions to represent a

loop are minimized. These techniques and their application to first-row atoms are discussed elsewhere.[9]

The cusp is not useful as a guide to the accuracy of any fairly good analytic SCF function. For all but very small basis sets, the cusp condition is satisfied well enough, if optimized basis functions are used, to insure against unreasonable behavior at the origin. This is because an analytic SCF radial function $P_{n\ell}(r)$, $P_{n\ell}(r) = rF_{n\ell}(r) = r\Sigma R_{\ell p}(r)C_{n\ell,p}$, goes near the origin as

$$P_{n\ell}(r) = A_0(n\ell)r^{\ell+1}[1 + (Cusp_{n\ell})r + 0(r^2)]. \qquad (13)$$

The dominant term in this expansion is $A_0(n\ell)$, not the cusp, and $P_{n\ell}$ is not overly sensitive to errors in the cusp.

Fortunately, it is not necessary to apply the tests described above to every analytic SCF function that is calculated. When the SCF functions of a series of similar states have been calculated in a systematic way, as described in Section III of this paper, the accuracy of each function in the series may be inferred from careful estimates of the accuracy of the functions of only a few states. One must take some precautions when making these inferences of estimates of accuracy. It is important, for example, to remember that it may be more difficult to determine more diffuse orbitals, e.g., orbitals of negative ions, as accurately as less diffuse ones.

Tables IX-XII present comparisons of the results of several HF calculations of Ne, F^-, Ar, and Cl^- with the results obtained with our accurate basis set functions. In each case, we give comparisons with results obtained by direct numerical integration of the HF equations;* and, except for Cl^-, we also give comparisons with analytic SCF functions with very nearly the same energy as our accurate-set functions. The analytic functions whose total SCF energies differ only in the eighth significant figure are grouped together with the accurate-set function at the left of the tables. Comparisons between these functions give information of the type 2 above. We have included, for each case, comparison with the results obtained with the simple basis set functions so that the accuracy of these functions may be determined.

For Ne and F^-, we include comparisons with the analytic SCF calculations of Allen,[36] and for Ar and Cl^-, with the analytic SCF calculations of Watson and Freeman.[37] These calculations were performed without using techniques for the automatic optimization of the exponents of the basis functions.

---

*For numerical HF calculations of Ne, F^-, Ar, and Cl^-, see Refs. 32, 33, 34, and 35, respectively.

TABLE IX. Comparison of Several Hartree-Fock Calculations of Neon

(Values are in a.u.)

		This Calculation Accurate Set	Fixed Cusp Set[a]	Clementi[b]	Worsley[c] (Numerical Integration)	This Calculation Simple Set	Allen[d]
E		-128.54709	-128.54703	-128.54701	. . . . .	-128.54648	-128.54319
ΔE		0	-0.00006	-0.00008	. . . . .	-0.00061	-0.00390
ϵ_{1s}		-32.77233	-32.77229	-32.77277	-32.77_5	-32.77162	-32.76740
$\Delta\epsilon_{1s}$		0	-0.00004	+0.00044	$+0.00_3$	-0.00071	-0.00493
$Cusp_{1s}$		-10.0250	-10.0000	-10.0049	. . . . .	-10.0101	-9.9994
$\Delta Cusp_{1s}$		+0.0250	. . . . .	+0.0049	. . . . .	+0.0101	-0.0006
$\lvert A_o(1s)\rvert$		60.777	60.741	60.750	60.77	60.761	60.746
$\Delta\lvert A_o(1s)\rvert$		-0.01	+0.03	+0.02	0	+0.01	+0.02
$\langle r\rangle_{1s}$		0.15763	0.15763	0.15763	. . . . .	0.15763	0.15764
$\Delta\langle r\rangle_{1s}$		0	0.00000	0.00000	. . . . .	0.00000	-0.00001
$\langle r^2\rangle_{1s}$		0.03347	0.03347	0.03347	. . . . .	0.03347	0.03347
$\Delta\langle r^2\rangle_{1s}$		0	0.00000	0.00000	. . . . .	0.00000	0.00000
$[\int(\Delta P_{1s})^2]^{\frac{1}{2}}$		0	0.0005	0.0004	. . . . .	0.0005	0.0006
$\lvert\Delta P_{1s}\rvert_{max}$	$0 \leq r < \infty$	0	0.0002	0.0003	0.003	0.0004	0.0005
ϵ_{2s}		-1.93031	-1.93031	-1.93048	-1.933	-1.92975	-1.92592
$\Delta\epsilon_{2s}$		0	0.00000	+0.00017	+0.003	-0.00056	-0.00439
$Cusp_{2s}$		-10.0535	-10.0000	-10.0052	. . . . .	-10.0136	-10.3010
$\Delta Cusp_{2s}$		+0.0535	. . . . .	+0.0052	. . . . .	+0.0136	+0.3010
$\lvert A_o(2s)\rvert$		14.280	14.253	14.264	14.27	14.269	14.344
$\Delta\lvert A_o(2s)\rvert$		-0.01	+0.02	+0.01	0	0.00	-0.07
$\langle r\rangle_{2s}$		0.89209	0.89207	0.89216	. . . . .	0.89135	0.89267
$\Delta\langle r\rangle_{2s}$		0	+0.00002	-0.00007	. . . . .	+0.00074	-0.00058
$\langle r^2\rangle_{2s}$		0.96694	0.96691	0.96735	. . . . .	0.96359	0.96964
$\Delta\langle r^2\rangle_{2s}$		0	+0.00003	-0.00041	. . . . .	+0.00335	-0.00270
$[\int(\Delta P_{2s})^2]^{\frac{1}{2}}$		0	0.0014	0.0015	. . . . .	0.0054	0.0061
$\lvert\Delta P_{2s}\rvert_{max}$	$0 \leq r < 1.0$	0	0.0002	0.0004	0.0003	0.0015	0.0023
	$1.0 \leq r < \infty$	0	0.0009	0.0012	0.001	0.0046	0.0046
ϵ_{2p}		-0.85034	-0.85033	-0.85048	-0.852_5	-0.84974	-0.84610
$\Delta\epsilon_{2p}$		0	-0.00001	+0.00014	$+0.002_2$	-0.00060	-0.00424
$Cusp_{2p}$		-5.0003	-5.0000	-5.0000	. . . . .	-4.6751	-4.7356
$\Delta Cusp_{2p}$		+0.0003	. . . . .	0.0000	. . . . .	-0.3249	-0.2644
$\lvert A_o(2p)\rvert$		27.804	27.732	27.861	27.87	27.159	27.479
$\Delta\lvert A_o(2p)\rvert$		+0.07	+0.14	+0.01	0	+0.71	+0.39
$\langle r\rangle_{2p}$		0.96518	0.96519	0.96537	. . . . .	0.96477	0.96489
$\Delta\langle r\rangle_{2p}$		0	-0.00001	-0.00019	. . . . .	+0.00041	+0.00029
$\langle r^2\rangle_{2p}$		1.22789	1.22787	1.22901	. . . . .	1.22516	1.23800
$\Delta\langle r^2\rangle_{2p}$		0	+0.00002	-0.00112	. . . . .	+0.00273	-0.01011
$[\int(\Delta P_{2p})^2]^{\frac{1}{2}}$		0	0.0010	0.0017	. . . . .	0.0037	0.0186
$\lvert\Delta P_{2p}\rvert_{max}$	$0 \leq r < 1.0$	0	0.0002	0.0006	0.0002	0.0011	0.0063
	$1.0 \leq r < \infty$	0	0.0006	0.0011	0.004	0.0026	0.0102

[a] P. S. Bagus, T. L. Gilbert, C. C. J. Roothaan, and H. D. Cohen (see Ref. 9).

[b] E. Clementi, C. C. J. Roothaan, and M. Yoshimine (see Ref. 7).

[c] B. H. Worsley (see Ref. 32).

[d] L. C. Allen (see Ref. 36).

TABLE X. Comparison of Several Hartree-Fock Calculations of F^-

(Values are in a.u.)

		This Calculation Accurate Set	Fixed Cusp Set[a]	Froese[b] (Numerical Integration)	Clementi[c]	Allen[d]	This Calculation Simple Set
E		-99.459440	-99.459444	. . . .	-99.459363	-99.458879	-99.457854
ΔE		0	+0.000004	. . . .	-0.000077	-0.000561	-0.001586
ϵ_{1s}		-25.82961	-25.82961	-25.822_5	-25.82944	-25.82957	-25.82687
$\Delta\epsilon_{1s}$		0	+0.00000	-0.007_1	-0.00017	-0.00004	-0.00274
$Cusp_{1s}$		-9.0240	-9.0000	. . . .	-9.0174	-9.0055	-9.0124
$\Delta Cusp_{1s}$		+0.0240	. . . . .	. . . .	+0.0174	+0.0055	+0.0124
$\lvert A_o(1s)\rvert$		51.724	51.702	51.705	51.717	51.703	51.713
$\Delta\lvert A_o(1s)\rvert$		-0.019	+0.003	0	-0.012	+0.002	-0.008
$\langle r\rangle_{1s}$		0.17576	0.17576	. . . .	0.17576	0.17577	0.17575
$\Delta\langle r\rangle_{1s}$		0	0.00000	. . . .	0.00000	-0.00001	+0.00001
$\langle r^2\rangle_{1s}$		0.04162	0.04162	. . . .	0.04162	0.04162	0.04161
$\Delta\langle r^2\rangle_{1s}$		0	0.00000	. . . .	0.00000	0.00000	+0.00001
$[\int(\Delta P_{1s})^2]^{\frac{1}{2}}$		0	$\leq$0.0002	. . . .	0.0004	0.0004	0.0006
$\lvert\Delta P_{1s}\rvert_{max}$	$0 \leq r < \infty$	0	0.0002	0.0003	0.0002	0.0004	0.0005
ϵ_{2s}		-1.07458	-1.07458	-1.076_5	-1.07435	-1.07468	-1.07236
$\Delta\epsilon_{2s}$		0	0.00000	$+0.001_9$	-0.00023	+0.00010	-0.00222
$Cusp_{2s}$		-9.0678	-9.0000	. . . .	-9.0345	-9.2576	-9.0753
$\Delta Cusp_{2s}$		+0.0678	. . . . .	. . . .	+0.0345	+0.2576	+0.0753
$\lvert A_o(2s)\rvert$		11.683	11.667	11.669	11.670	11.729	11.688
$\Delta\lvert A_o(2s)\rvert$		-0.014	+0.002	0	-0.001	-0.060	-0.019
$\langle r\rangle_{2s}$		1.03555	1.03556	. . . .	1.03540	1.03617	1.03333
$\Delta\langle r\rangle_{2s}$		0	-0.00001	. . . .	+0.00015	-0.00062	+0.00222
$\langle r^2\rangle_{2s}$		1.31886	1.31903	. . . .	1.31776	1.32219	1.30703
$\Delta\langle r^2\rangle_{2s}$		0	-0.00017	. . . .	+0.00110	-0.00333	+0.01183
$[\int(\Delta P_{2s})^2]^{\frac{1}{2}}$		0	0.0009	. . . .	0.0027	0.0035	0.0118
$\lvert\Delta P_{2s}\rvert_{max}$	$0 \leq r < 1.5$	0	0.0003	0.0005	0.0009	0.0015	0.0024
	$1.5 \leq r < \infty$	0	0.0006	0.0005	0.0018	0.0026	0.0088
ϵ_{2p}		-0.18098	-0.18098	-0.181_5	-0.18079	-0.18122	-0.17886
$\Delta\epsilon_{2p}$		0	0.00000	$+0.000_5$	-0.00019	+0.00024	-0.00212
$Cusp_{2p}$		-4.5322	-4.5000	. . . .	-4.4282	-4.1523	-4.0292
$\Delta Cusp_{2p}$		+0.0322	. . . . .	. . . .	-0.0718	-0.3477	-0.4708
$\lvert A_o(2p)\rvert$		18.861	18.882	18.849	18.740	18.268	18.017
$\Delta\lvert A_o(2p)\rvert$		-0.012	-0.033	0	+0.109	+0.581	+0.832
$\langle r\rangle_{2p}$		1.25556	1.25557	. . . .	1.25512	1.25604	1.25206
$\Delta\langle r\rangle_{2p}$		0	-0.00001	. . . .	+0.00044	-0.00048	+0.00350
$\langle r^2\rangle_{2p}$		2.20956	2.20971	. . . .	2.20516	2.21748	2.17892
$\Delta\langle r^2\rangle_{2p}$		0	-0.00015	. . . .	+0.00440	-0.00792	+0.03064
$[\int(\Delta P_{2p})^2]^{\frac{1}{2}}$		0	0.0007	. . . .	0.0024	0.0076	0.0121
$\lvert\Delta P_{2p}\rvert_{max}$	$0 \leq r < 1.5$	0	0.0002	0.0002	0.0002	0.0012	0.0021
	$1.5 \leq r < \infty$	0	0.0003_5	0.0005	0.0013	0.0034	0.0067

[a] P. S. Bagus, T. L. Gilbert, C. C. J. Roothaan, and H. Cohen (see Ref. 9).

[b] C. Froese (see Ref. 33).

[c] E. Clementi and A. D. McLean (see Ref. 36).

[d] L. C. Allen (see Ref. 36).

TABLE XI. Comparison of Several Hartree-Fock Calculations of Argon

(Values are in a.u.)

		This Calculation Accurate Set	Alternate[a] Large Set 6s and 7p	Malli[b] (Fixed Cusp Set)	Hartree[c] (Numerical Integration)	Clementi[d]	This Calculation Simple Set	Watson and Freeman[e]
E		-526.81746	-526.81745	-526.81743	. . . . .	-526.81707	-526.81553	-526.81463
ΔE		0	-0.00001	-0.00003	. . . . .	+0.00039	-0.00193	-0.00283
ϵ_{1s}		-118.61014	-118.61042	-118.61030	-118.6	-118.60987	-118.60817	-118.60950
$\Delta\epsilon_{1s}$		0	+0.00028	+0.00016	0.0	-0.00027	-0.00197	-0.00064
$Cusp_{1s}$		-18.0037	-18.0063	-18.0000	. . . . .	-18.0298	-17.9582	-17.9727
$\Delta Cusp_{1s}$		+0.0037	+0.0063	. . . . .	. . . . .	+0.0298	-0.0418	-0.0273
$\lvert A_0(1s)\rvert$		148.87	148.88	148.85	148.8	148.92	148.77	148.81
$\Delta\lvert A_0(1s)\rvert$		-0.1	-0.1	0.0	0	-0.1	0.0	0.0
$\langle r\rangle_{1s}$		0.08610	0.08610	0.08610	. . . . .	0.08610	0.08611	0.08610
$\Delta\langle r\rangle_{1s}$		0	0.00000	0.00000	. . . . .	0.00000	-0.00001	0.00000
$\langle r^2\rangle_{1s}$		0.00996	0.00996	0.00996	0.010	0.00996	0.00996	0.00996
$\Delta\langle r^2\rangle_{1s}$		0	0.00000	0.00000	0.000	0.00000	0.00000	0.00000
$[\int(\Delta P_{1s})^2]^{\frac{1}{2}}$		0	≤0.0001	≤0.0002	. . . . .	≤0.0003	0.0005	0.0004
$\lvert\Delta P_{1s}\rvert_{max}$	$0 \leq r < \infty$	0	0.0001	0.0002	0.007	0.0003	0.0008	0.0004
ϵ_{2s}		-12.32193	-12.32220	-12.32214	-12.3_3	-12.32150	-12.32139	-12.32141
$\Delta\epsilon_{2s}$		0	+0.00027	+0.00021	$+0.0_1$	-0.00043	-0.00054	-0.00052
$Cusp_{2s}$		-17.9965	-18.0049	-18.0000	. . . . .	-17.9940	-17.9891	-18.2048
$\Delta Cusp_{2s}$		-0.0035	+0.0049	. . . . .	. . . . .	-0.0060	-0.0109	+0.2048
$\lvert A_0(2s)\rvert$		42.257	42.266	42.244	42.25	42.254	42.252	42.276
$\Delta\lvert A_0(2s)\rvert$		-0.01	-0.02	+0.01	0	0.00	0.00	-0.03
$\langle r\rangle_{2s}$		0.41228	0.41227	0.41229	. . . . .	0.41228	0.41231	0.41228
$\Delta\langle r\rangle_{2s}$		0	+0.00001	-0.00001	. . . . .	0.00000	-0.00003	0.00000
$\langle r^2\rangle_{2s}$		0.20123	0.20122	0.20123	0.201	0.20122	0.20125	0.20122
$\Delta\langle r^2\rangle_{2s}$		0	+0.00001	0.00000	0.000	+0.00001	-0.00002	+0.00001
$[\int(\Delta P_{2s})^2]^{\frac{1}{2}}$		0	0.0005	0.0004	. . . . .	0.0008	0.0005	0.0006
$\lvert\Delta P_{2s}\rvert_{max}$	$0 \leq r < 0.35$	0	0.0002	0.0002	0.002	0.0002	0.0004	0.0003
	$0.35 \leq r < \infty$	0	0.0005	0.0002	0.002	0.0006	0.0006	0.0005
ϵ_{3s}		-1.27725	-1.27734	-1.27735	-1.277_5	-1.27692	-1.27666	-1.27649
$\Delta\epsilon_{3s}$		0	+0.00009	+0.00010	$+0.000_2$	-0.00033	-0.00059	-0.00076
$Cusp_{3s}$		-17.9689	-17.9517	-18.0000	. . . . .	-18.0976	-17.7582	-17.9798
$\Delta Cusp_{3s}$		-0.0311	-0.0483	. . . . .	. . . . .	+0.0976	-0.2418	-0.0202
$\lvert A_0(3s)\rvert$		13.199	13.197	13.199	13.21	13.222	13.146	13.201
$\Delta\lvert A_0(3s)\rvert$		+0.01	+0.01	+0.01	0	-0.01	+0.06	+0.01
$\langle r\rangle_{3s}$		1.42196	1.42228	1.42192	. . . . .	1.42256	1.42218	1.42252
$\Delta\langle r\rangle_{3s}$		0	-0.00032	+0.00004	. . . . .	-0.00060	-0.00022	-0.00056
$\langle r^2\rangle_{3s}$		2.34912	2.35086	2.34888	2.348	2.35144	2.34981	2.35372
$\Delta\langle r^2\rangle_{3s}$		0	-0.00174	+0.00024	+0.001	-0.00232	-0.00069	-0.00460
$[\int(\Delta P_{3s})^2]^{\frac{1}{2}}$		0	0.0009	0.0004	. . . . .	0.0025	0.0006	0.0059
$\lvert\Delta P_{3s}\rvert_{max}$	$0 \leq r < 1.2$	0	0.0008	0.0002	0.001	0.0009	0.0007	0.0003
	$1.2 \leq r < \infty$	0	0.0006	0.0002	0.001	0.0021	0.0004	0.0042

TABLE XI. Continued

(Values are in a.u.)

		This Calculation Accurate Set	Alternate[a] Large Set 8s and 7p	Malli[b] (Fixed Cusp Set)	Hartree[c] (Numerical Integration)	Clementi[d]	This Calculation Simple Set	Watson and Freeman[e]
ϵ_{2p}		-9.57127	-9.57152	-9.57146	-9.57_5	-9.57083	-9.57061	-9.57072
$\Delta\epsilon_{2p}$		0	+0.00025	+0.00019	$+0.00_4$	-0.00044	-0.00066	-0.00055
$Cusp_{2p}$		-8.9259	-8.9577	-9.0000	. . . . .	-8.9011	-8.6098	-8.7697
$\Delta Cusp_{2p}$		-0.0741	-0.0423	. . . . .	. . . . .	-0.0989	-0.3902	-0.2303
$\lvert A_0(2p)\rvert$		181.89	182.07	182.14	182.3_5	181.81	179.21	180.54
$\Delta\lvert A_0(2p)\rvert$		$+0.4_6$	$+0.2_8$	$+0.2_1$	0	$+0.5_4$	$+3.1_5$	$+1.8_1$
$\langle r\rangle_{2p}$		0.37533	0.37533	0.37533	. . . . .	0.37529	0.37527	0.37536
$\Delta\langle r\rangle_{2p}$		0	0.00000	0.00000	. . . . .	+0.00004	+0.00006	-0.00003
$\langle r^2\rangle_{2p}$		0.17434	0.17434	0.17434	0.174	0.17430	0.17427	0.17437
$\Delta\langle r^2\rangle_{2p}$		0	0.00000	0.00000	0.000	+0.00004	+0.00007	-0.00003
$[\int(\Delta P_{2p})^2]^{\frac{1}{2}}$		0	0.0005	0.0004	. . . . .	0.0009	0.0028	0.0016
$\lvert\Delta P_{2p}\rvert_{max}$	$0 \le r < \infty$	0	0.0002	0.0003	0.002	0.0007	0.0026	0.0014
ϵ_{3p}		-0.59092	-0.59102	-0.59099	-0.590_5	-0.59071	-0.59046	-0.58997
$\Delta\epsilon_{3p}$		0	+0.00010	+0.00007	-0.000_4	-0.00021	-0.00046	-0.00095
$Cusp_{3p}$		-8.8809	-8.9471	-9.0000	. . . . .	-8.9216	-8.6399	-9.1924
$\Delta Cusp_{3p}$		-0.1191	-0.0529	. . . . .	. . . . .	-0.0784	-0.3601	+0.1924
$\lvert A_0(3p)\rvert$		50.707	50.824	50.804	50.97	50.790	50.018	51.638
$\Delta\lvert A_0(3p)\rvert$		+0.26	+0.15	+0.17	0	+0.18	+0.95	-0.67
$\langle r\rangle_{3p}$		1.66276	1.66289	1.66298	. . . . .	1.66181	1.66156	1.66343
$\Delta\langle r\rangle_{3p}$		0	-0.00013	-0.00022	. . . . .	+0.00095	+0.00120	-0.00067
$\langle r^2\rangle_{3p}$		3.30917	3.31003	3.31087	3.312	3.30105	3.29947	3.32762
$\Delta\langle r^2\rangle_{3p}$		0	-0.00086	-0.00170	-0.003	+0.00812	+0.00970	-0.01845
$[\int(\Delta P_{3p})^2]^{\frac{1}{2}}$		0	0.0006	0.0019	. . . . .	0.0051	0.0051	0.0179
$\lvert\Delta P_{3p}\rvert_{max}$	$0 \le r < 1.3$	0	0.0003	0.0002	0.001	0.0009	0.0007	0.0025
	$1.3 \le r < \infty$	0	0.0004	0.0011	0.001	0.0032	0.0033	0.0096

[a] P. S. Bagus (unpublished).

[b] G. L. Malli (to be published).

[c] D. R. Hartree and W. Hartree (see Ref. 34) solved the SCF equations with exchange only for the 3s and 3p wave functions; the 1s, 2s, and 2p wave functions with exchange were obtained from the functions without exchange and interpolation between the values for Ca^{++}, K^+, and Cl^-.

[d] E. Clementi (see Ref. 39). Details of the function are not published in Clementi's paper but are available at the Library of Congress (see Ref. 40).

[e] R. E. Watson and A. J. Freeman (see Ref. 37).

TABLE XII. Comparison of Several Hartree-Fock Calculations of Cl^-

(Values are in a.u.)

		This Calculation Accurate Set	Hartree[a] (Numerical Integration)	Watson and Freeman[b]	This Calculation Simple Set
E		-459.57684	. . . . .	-459.57499	-459.57362
ΔE		0	. . . . .	-0.00185	-0.00322
ϵ_{1s}		-104.50546	-104.5_5	-104.50829	-104.50086
$\Delta\epsilon_{1s}$		0	$+0.0_4$	+0.00283	-0.00460
$Cusp_{1s}$		-17.0048	. . . . .	-16.9691	-16.9635
$\Delta Cusp_{1s}$		+0.0048	. . . . .	-0.0309	-0.0365
$\lvert A_o(1s)\rvert$		136.48	136.5	136.41	136.40
$\Delta\lvert A_o(1s)\rvert$		0.0	0	+0.1	+0.1
$\langle r\rangle_{1s}$		0.09130	. . . . .	0.09130	0.09130
$\Delta\langle r\rangle_{1s}$		0	. . . . .	0.00000	0.00000
$\langle r^2\rangle_{1s}$		0.01120	0.01_1	0.01120	0.01120
$\Delta\langle r^2\rangle_{1s}$		0	0.00_0	0.00000	0.00000
$[\int(\Delta P_{1s})^2]^{\frac{1}{2}}$		0	. . . . .	0.0004	0.0005
$\lvert\Delta P_{1s}\rvert_{max}$	$0 \leq r < \infty$	0	0.001	0.0005	0.0008
ϵ_{2s}		-10.22916	-10.23_5	-10.23225	-10.22595
$\Delta\epsilon_{2s}$		0	$+0.00_6$	+0.00309	-0.00321
$Cusp_{2s}$		-16.9933	. . . . .	-17.0174	-16.9902
$\Delta Cusp_{2s}$		-0.0067	. . . . .	+0.0174	-0.0098
$\lvert A_o(2s)\rvert$		38.238	38.24	38.254	38.238
$\Delta\lvert A_o(2s)\rvert$		0.00	0	-0.01	0.00
$\langle r\rangle_{2s}$		0.44180	. . . . .	0.44179	0.44181
$\Delta\langle r\rangle_{2s}$		0	. . . . .	+0.00001	-0.00001
$\langle r^2\rangle_{2s}$		0.23129	0.23_1	0.23129	0.23130
$\Delta\langle r^2\rangle_{2s}$		0	0.00_0	0.00000	-0.00001
$[\int(\Delta P_{2s})^2]^{\frac{1}{2}}$		0	. . . . .	0.0006	$\leq$0.0003
$\lvert\Delta P_{2s}\rvert_{max}$	$0 \leq r < 0.35$	0	0.001	0.0003	0.0002
	$0.35 \leq r < \infty$	0	0.001	0.0004	0.0003
ϵ_{3s}		-0.73320	-0.727	-0.73547	-0.73031
$\Delta\epsilon_{3s}$		0	-0.006	+0.00227	-0.00289
$Cusp_{3s}$		-16.9622	. . . . .	-17.0158	-16.7602
$\Delta Cusp_{3s}$		-0.0378	. . . . .	+0.0158	-0.2398
$\lvert A_o(3s)\rvert$		11.261	11.31	11.273	11.209
$\Delta\lvert A_o(3s)\rvert$		+0.05	0	+0.04	+0.10
$\langle r\rangle_{3s}$		1.60179	. . . . .	1.60163	1.60242
$\Delta\langle r\rangle_{3s}$		0	. . . . .	+0.00016	-0.00063
$\langle r^2\rangle_{3s}$		3.01041	3.01_2	3.01207	3.01262
$\Delta\langle r^2\rangle_{3s}$		0	-0.00_2	-0.00166	-0.00221
$[\int(\Delta P_{3s})^2]^{\frac{1}{2}}$		0	. . . . .	0.0051	0.0007
$\lvert\Delta P_{3s}\rvert_{max}$	$0 \leq r < 1.3$	0	0.001_5	0.0002	0.0010
	$1.3 \leq r < \infty$	0	0.002_5	0.0032	0.0003

TABLE XII. Continued

(Values are in a.u.)

		This Calculation Accurate Set	Hartree[a] (Numerical Integration)	Watson and Freeman[b]	This Calculation Simple Set
ϵ_{2p}		-7.69557	-7.69_5	-7.69866	-7.69225
$\Delta\epsilon_{2p}$		0	-0.00_1	+0.00309	-0.00332
$Cusp_{2p}$		-8.4401	. . . . .	-8.2818	-8.0692
$\Delta Cusp_{2p}$		-0.0599	. . . . .	-0.2182	-0.4308
$\lvert A_0(2p)\rvert$		153.63	154.1	152.46	150.73
$\Delta\lvert A_0(2p)\rvert$		+0.5	0	+1.6	+3.4
$\langle r\rangle_{2p}$		0.40538	. . . . .	0.40540	0.40525
$\Delta\langle r\rangle_{2p}$		0	. . . . .	-0.00002	+0.00013
$\langle r^2\rangle_{2p}$		0.20386	0.20_4	0.20387	0.20369
$\Delta\langle r^2\rangle_{2p}$		0	0.00_0	-0.00001	+0.00017
$[\int(\Delta P_{2p})^2]^{\frac{1}{2}}$		0	. . . . .	0.0012	0.0034
$\lvert\Delta P_{2p}\rvert_{max}$	$0 \leq r < \infty$	0	0.001	0.0009	0.0031
ϵ_{3p}		-0.15017	-0.1485_5	-0.15172	-0.14772
$\Delta\epsilon_{3p}$		0	-0.0016_2	+0.00155	-0.00245
$Cusp_{3p}$		-8.3803	. . . . .	-8.6557	-8.1451
$\Delta Cusp_{3p}$		-0.1197	. . . . .	+0.1557	-0.3549
$\lvert A_0(3p)\rvert$		37.927	38.02	38.601	37.468
$\Delta\lvert A_0(3p)\rvert$		+0.09	0	-0.58	+0.55
$\langle r\rangle_{3p}$		2.02880	. . . . .	2.03967	2.01910
$\Delta\langle r\rangle_{3p}$		0	. . . . .	-0.01087	+0.00970
$\langle r^2\rangle_{3p}$		5.10806	5.13_7	5.22941	5.01079
$\Delta\langle r^2\rangle_{3p}$		0	-0.02_9	-0.12135	+0.09727
$[\int(\Delta P_{3p})^2]^{\frac{1}{2}}$		0	. . . . .	0.0207	0.0209
$\lvert\Delta P_{3p}\rvert_{max}$	$0 \leq r < 1.5$	0	0.001_5	0.0028	0.0021
	$1.5 \leq r < \infty$	0	0.001_5	0.0102	0.0116

[a]D. R. Hartree and W. Hartree (see Ref. 35).

[b]R. E. Watson and A. J. Freeman (see Ref. 37).

Where analytic calculations of other workers are reported, we have used their basis sets to recompute their functions with our program. This was done so that all the properties of each calculation would be available for comparison. Tables IX-XII present the results obtained from our recalculations. Our recalculations agree closely with the original calculations.

The total SCF energies in Tables IX-XII are given to eight significant figures. Although round-off error affects the eighth figure, this is the only way to distinguish the energies of several of the functions. For each orbital, we give the values of the orbital energy $\epsilon_{n\ell}$, cusp, $A_0(n\ell)$, the dominant term in the expansion of the radial-wave function near the origin [defined in Eq. (13)], and the expectation values of r and r^2.

Direct comparisons are also made for the radial wave functions $P_{n\ell}(r)$. For each orbital, we give values of the quantity

$$\left[\int_0^\infty [P_{\text{accurate set}}(r) - P_{\text{comparison}}(r)]^2 dr\right]$$

denoted in the tables by $[\int(\Delta P_{n\ell})^2]^{1/2}$. This is a sum of the differences of the radial wave functions over their entire range and may be used as an overall figure of merit for the quality of the comparison function. (This comparison cannot be made with the numerical functions. The radial wave functions obtained with the accurate basis sets and by numerical methods usually agree within one or two units in the last figure given in the tabulation of the numerical functions, and $[\int(\Delta P_{n\ell})^2]^{1/2}$ calculated from these differences would only reflect rounding errors.) The tables also give the maximum value of $|\Delta P(r)| = |P_{\text{accurate set}}(r) - P_{\text{comparison}}(r)|$. For some orbitals, $|\Delta P|_{\max}$ is given for two ranges of r to indicate that the agreement between some of the radial wave functions is considerably better for the inner portion of the function than for the tail. The limit of the ranges is arbitrary. Except for a small range of values of r, usually at the tail of the orbital, $|\Delta P(r)|$ is smaller than $|\Delta P(r)|_{\max}$. Thus $|\Delta P(r)|_{\max}$ gives the worst view of the accuracy of the orbitals.

The differences given in Tables IX-XII (ΔE, $\Delta\epsilon$, etc.) are usually defined as

$$\Delta\text{Property} = \text{Property (accurate set)} - \text{Property (comparison function)}. \qquad (14a)$$

The exceptions are

$$\Delta\text{Cusp}_{n\ell} = -Z/(\ell+1) - \text{Cusp}_{n\ell}\ \text{(comparison function)}, \qquad (14b)$$

and

$$\Delta|A_0(n\ell)| = |A_0(n\ell)\ [\text{numerical calculation}]| - |A_0(n\ell)\ [\text{comparison function}]|. \quad (14c)$$

For $A_0(n\ell)$, numerical calculations were chosen as a standard of comparison because numerical techniques require that the radial functions be determined accurately at the origin. The numerical integration is started outward from $r = 0$, and the results are sensitive to any error in the function at the origin.

The values of the radial wave functions obtained from the accurate basis SCF calculations agree strikingly well with the values obtained from numerical calculations.

Worsley[32] gives the neon radial functions, tabulated at logarithmic intervals, to four decimal places except for the tail region of each orbital where they are given to only three decimal places. Worsley claims that the functions are accurate to within two or three units in the last figure given. At every point Worsley tabulates, the difference between our accurate set results and her numerical results, $|\Delta P(r)|$, is within this limit except for four points. At the great majority of tabulated points, $|\Delta P(r)|$ is 0 or 1 in the last figure Worsley gives.

Froese[33] claims that her radial wave functions for F^-, given to four decimal places, are accurate to 0.0002. The differences with our accurate-set results are within this limit with only a few exceptions. At two points, $|\Delta P_{1s}(r)| = 0.0003$; at ten points, $|\Delta P_{2s}(r)|$ is between 0.0003 and 0.0005; and at five points, $|\Delta P_{2p}(r)|$ is between 0.0003 and 0.0005.

Hartree and Hartree[34,35] give the radial wave functions for Ar and Cl^- to three decimal places; for the 3s and 3p orbitals of Cl^-, they tabulate $2P(r)$ rather than $P(r)$ in order to obtain additional accuracy. For argon, $|\Delta P_{1s}(r)|$ has its largest values at five consecutive points and is between 0.003 and 0.007; at several points of the 2s and 2p radial functions, $|\Delta P(r)|$ has its maximum value of 0.002. For the argon 3s and 3p radial functions, $|\Delta P(r)|$ is usually 0.000 and is never larger than 0.001 (i.e., 0 or 1 in the last figure that Hartree and Hartree give). The relatively large disagreements for the 1s, 2s, and 2p radial functions occur because Hartree and Hartree did not obtain these functions by direct solution of the HF integro-differential equations but rather by an interpolation between results for Cl^- and K^+. Their 3s and 3p functions, on the other hand, were obtained as self-consistent numerical solutions of the HF equations. This explanation is supported by the fact that, for the 1s, 2s, and 2p orbitals of the Hartree and Hartree calculation on Cl^-, $|\Delta P(r)|$ is never larger than 0.001. Although the agreement between our results and those

of Hartree and Hartree for the 3s and 3p orbitals of Cl^- is still good, it is not as good for these orbitals as for the others. For the 3s radial function, $2|\Delta P(r)|$ is 0.005 at one point in the tail of the function, 0.004 at the two adjacent points, and 0.002 or 0.003 at several points; for the 3p function, there are also several points for which $2|\Delta P(r)|$ is as large as 0.002 and 0.003.

For Ne, F^-, Ar, and Cl^-, the agreement between the numerical and accurate basis set analytic radial functions is, in almost all cases, within the error of the numerical calculations. The 3s and 3p radial functions of Cl^- obtained by Hartree and Hartree are slightly more accurate than the accurate basis set analytic functions.

The differences between the orbital energies $\epsilon_{n\ell}$ obtained from the accurate set analytic SCF calculations and from the numerical calculations are sometimes larger than might be expected from the small differences between the radial wave functions. This can be explained from the different way that the ϵ's are obtained by the two methods. In the analytic method, the ϵ given is obtained directly as the expectation value of the Fock operator for the orbital, $\epsilon_{n\ell} = \langle \phi_{n\ell} | F | \phi_{n\ell} \rangle$. In the numerical calculations discussed, ϵ is treated simply as a parameter to be adjusted until the solutions of the HF equations approximately satisfy the boundary conditions placed on them. The results of the accurate analytic SCF calculations should give better values of the ϵ's than the numerical calculations.

The accuracy of the accurate basis set SCF functions given in Tables I-IV has been estimated. The estimates used the techniques described above and, in large part, the information given in Tables IX-XII. The estimates are generous and probably indicate, for most of the functions, errors larger than the true errors.

The total SCF energy, E_{SCF}, represents the exact HF total energy to within two units in the seventh significant figure, and the $\epsilon_{n\ell}$'s are accurate to about five units in the same decimal place that the error enters the total energy. When $E_{SCF} < 100$, the $\epsilon_{n\ell}$'s are accurate to five units in the fifth decimal place, and when $E_{SCF} \geq 100$, to five units in the fourth decimal place.

For the states of the heavier atoms (chlorine, argon, and potassium) the 1s, 2s, and 2p radial wave functions do not differ from the exact HF solutions, for any value of r, by more than 0.0005. The 1s radial function is probably accurate to within 0.0002. The 3s and 3p radial functions are definitely accurate to within 0.0015, and over much of the range of r are accurate to within 0.0005. The only exception is the 3s radial function of Cl^-, where the error is as large as 0.0025 for a fairly small range of r near the tail of the function.

For the states of the light atoms (fluorine, neon, and sodium), the radial functions are accurate to within 0.0005. The 1s radial function is accurate to within 0.0002. The 2s and 2p radial functions have an error smaller than 0.0005.

The radial wave function of the outermost s shell (2s for the light atoms, and 3s for the heavier atoms) is the least accurate function for any given state. The outermost s shell makes the smallest contribution to the total energy and so is least well-determined by the exponent variation procedures which optimize the total energy.

The accurate set SCF functions given in Tables I-IV, except for Cl^- and the 1s-hole state of K^+, represent the limit of accuracy which can be obtained using the single-precision, eight-significant-figure, floating-point arithmetic of the IBM 704 and 7094 computers. The Cl^- SCF function could probably be improved with the addition to the basis set of an s, and possibly a p, basis function. The function for the 1s-hole state of K^+ could be improved slightly if the numerical evaluation in the exponent variation procedures were altered to minimize round-off error. (This change has already been made in the latest versions of the SCF programs.)

C. Properties of the SCF Wave Functions

Expectation values of r and r^2, for all the states computed are given in Tables XIII and XIV. These expectation values were calculated from the accurate basis set SCF functions. For each state, the expectation values of r and r^2 given are taken with respect to each occupied orbital, $\langle r\rangle_{n\ell} = \int_0^\infty [P_{n\ell}(r)]^2 r\,dr$ and $\langle r^2\rangle_{n\ell} = \int_0^\infty [P_{n\ell}(r)]^2 r^2\,dr$. In addition, the average values of the $\langle r\rangle$ and $\langle r^2\rangle$ are given. The average value of $\langle r\rangle$ is defined by $\Sigma N_{n\ell}\langle r\rangle_{n\ell}/\Sigma N_{n\ell}$, where $N_{n\ell}$ is the electron occupation of the $n\ell^{th}$ orbital and the sum is over all occupied orbitals. The values of $\langle r\rangle_{n\ell}$ and $\langle r^2\rangle_{n\ell}$ represent the exact HF values to within a few units in the last figure given. The values of $\langle r^2\rangle_{n\ell}$ for the outermost s and p orbitals of a system are least accurate, and the errors may be as large as 20 units in the last figure. These estimates of accuracy may be checked by reference to the comparisons given in Tables IX-XII.

An extra figure is given for the average values of $\langle r\rangle$ and $\langle r^2\rangle$ to avoid round-off error if these values are multiplied by the total number of electrons in the system to give $\langle \Sigma r_i\rangle$ and $\langle \Sigma r_i^2\rangle$.

Nonzero overlap integrals between many-electron SCF wave functions, calculated from the accurate basis set SCF functions, are given in Table XV. These results are presented in connection with the discussion, at the end of Section II, of the lack of orthogonality between excited- and ground-state SCF functions of the same symmetry.

TABLE XIII. Expectation Values of r and r^2 for F^-, Ne, and Na^+ and $n\ell$-hole States of F^-, Ne, and Na^+

(Values are in a.u.; 1 Bohr = 0.52917A)

	$F^-(^1S)$	$F(^2P)$ 2p-hole	$F(^2S)$ 2s-hole	$F(^2S)$ 1s-hole
$\langle r\rangle_{1s}$	0.1758	0.1757	0.1760	0.1718
$\langle r\rangle_{2s}$	1.0355	1.0011	0.9885	0.9435
$\langle r\rangle_{2p}$	1.2556	1.0847	1.0934	0.9659
$\Sigma N_i\langle r\rangle_i/\Sigma N_i$	0.99560	0.86411	0.87790	0.87267
$\langle r^2\rangle_{1s}$	0.04162	0.04161	0.04177	0.04045
$\langle r^2\rangle_{2s}$	1.3189	1.2164	1.1827	1.0836
$\langle r^2\rangle_{2p}$	2.2096	1.5429	1.5738	1.2245
$\Sigma N_i\langle r^2\rangle_i/\Sigma N_i$	1.59783	1.13672	1.18988	1.06166
	$Ne(^1S)$	$Ne^+(^2P)$ 2p-hole	$Ne^+(^2S)$ 2s-hole	$Ne^+(^2S)$ 1s-hole
$\langle r\rangle_{1s}$	0.1576	0.1576	0.1578	0.1454
$\langle r\rangle_{2s}$	0.8921	0.8603	0.8536	0.8171
$\langle r\rangle_{2p}$	0.9652	0.8759	0.8841	0.7993
$\Sigma N_i\langle r\rangle_i/\Sigma N_i$	0.78905	0.71280	0.71931	0.73159
$\langle r^2\rangle_{1s}$	0.03347	0.03344	0.03357	0.03260
$\langle r^2\rangle_{2s}$	0.9669	0.8903	0.8751	0.8056
$\langle r^2\rangle_{2p}$	1.2279	0.9820	1.0032	0.8196
$\Sigma N_i\langle r^2\rangle_i/\Sigma N_i$	0.93682	0.75081	0.77351	0.72903
	$Na^+(^1S)$	$Na^{++}(^2P)$ 2p-hole	$Na^{++}(^2S)$ 2s-hole	$Na^{++}(^2S)$ 1s-hole
$\langle r\rangle_{1s}$	0.1429	0.1428	0.1430	0.1403
$\langle r\rangle_{2s}$	0.7791	0.7530	0.7491	0.7196
$\langle r\rangle_{2p}$	0.7962	0.7385	0.7453	0.6845
$\Sigma N_i\langle r\rangle_i/\Sigma N_i$	0.66214	0.60932	0.61190	0.63182
$\langle r^2\rangle_{1s}$	0.02748	0.02744	0.02755	0.02681
$\langle r^2\rangle_{2s}$	0.7314	0.6779	0.6703	0.6210
$\langle r^2\rangle_{2p}$	0.8159	0.6889	0.7033	0.5932
$\Sigma N_i\langle r^2\rangle_i/\Sigma N_i$	0.64130	0.53945	0.54949	0.53645

TABLE XIV. Expectation Values of r and r^2 for Cl^-, Ar, and K^+ and $n\ell$-hole States of Cl^-, Ar, and K^+

(Values are in a.u.; 1 Bohr = 0.52917A)

	$Cl^-(^1S)$	$Cl(^2P)$ 3p-hole	$Cl(^2S)$ 3s-hole	$Cl(^2P)$ 2p-hole	$Cl(^2S)$ 2s-hole	$Cl(^2S)$ 1s-hole
$\langle r\rangle_{1s}$	0.09130	0.09130	0.09130	0.09121	0.09134	0.09031
$\langle r\rangle_{2s}$	0.4418	0.4417	0.4424	0.4338	0.4390	0.4226
$\langle r\rangle_{3s}$	1.6018	1.5557	1.5341	1.4696	1.4759	1.4514
$\langle r\rangle_{2p}$	0.4054	0.4057	0.4050	0.4004	0.3952	0.3776
$\langle r\rangle_{3p}$	2.0288	1.8418	1.8380	1.6928	1.6992	1.6623
$\Sigma N_i\langle r\rangle_i/\Sigma N_i$	1.04860	0.93065	0.94469	0.94988	0.94942	0.94573
$\langle r^2\rangle_{1s}$	0.01120	0.01120	0.01120	0.01117	0.01122	0.01105
$\langle r^2\rangle_{2s}$	0.2313	0.2312	0.2321	0.2225	0.2300	0.2117
$\langle r^2\rangle_{3s}$	3.0104	2.8131	2.7299	2.5069	2.5364	2.4472
$\langle r^2\rangle_{2p}$	0.2039	0.2043	0.2034	0.2020	0.1930	0.1762
$\langle r^2\rangle_{3p}$	5.1081	4.0575	4.0444	3.4404	3.4480	3.3052
$\Sigma N_i\langle r^2\rangle_i/\Sigma N_i$	2.13207	1.62498	1.68842	1.59608	1.59830	1.54220

	$Ar(^1S)$	$Ar^+(^2P)$ 3p-hole	$Ar^+(^2S)$ 3s-hole	$Ar^+(^2P)$ 2p-hole	$Ar^+(^2S)$ 2s-hole	$Ar^+(^2S)$ 1s-hole
$\langle r\rangle_{1s}$	0.08610	0.08610	0.08611	0.08602	0.08614	0.08523
$\langle r\rangle_{2s}$	0.4123	0.4121	0.4128	0.4052	0.4100	0.3954
$\langle r\rangle_{3s}$	1.4220	1.3814	1.3679	1.3162	1.3209	1.3005
$\langle r\rangle_{2p}$	0.3753	0.3756	0.3749	0.3714	0.3667	0.3515
$\langle r\rangle_{3p}$	1.6628	1.5584	1.5589	1.4560	1.4627	1.4321
$\Sigma N_i\langle r\rangle_i/\Sigma N_i$	0.89274	0.81205	0.82171	0.83576	0.83531	0.83403
$\langle r^2\rangle_{1s}$	0.00996	0.00996	0.00996	0.00994	0.00997	0.00983
$\langle r^2\rangle_{2s}$	0.2012	0.2010	0.2019	0.1940	0.2003	0.1852
$\langle r^2\rangle_{3s}$	2.3491	2.2018	2.1570	1.9980	2.0185	1.9517
$\langle r^2\rangle_{2p}$	0.1743	0.1747	0.1739	0.1730	0.1658	0.1524
$\langle r^2\rangle_{3p}$	3.3092	2.8601	2.8642	2.5102	2.5196	2.4179
$\Sigma N_i\langle r^2\rangle_i/\Sigma N_i$	1.44565	1.18672	1.22406	1.19586	1.19821	1.15911

	$K^+(^1S)$	$K^{++}(^2P)$ 3p-hole	$K^{++}(^2S)$ 3s-hole	$K^{++}(^2P)$ 2p-hole	$K^{++}(^2S)$ 2s-hole	$K^{++}(^2S)$ 1s-hole
$\langle r\rangle_{1s}$	0.08147	0.08146	0.08147	0.08139	0.08150	0.08069
$\langle r\rangle_{2s}$	0.3864	0.3861	0.3869	0.3801	0.3845	0.3715
$\langle r\rangle_{3s}$	1.2768	1.2435	1.2341	1.1922	1.1959	1.1787
$\langle r\rangle_{2p}$	0.3494	0.3496	0.3490	0.3462	0.3419	0.3287
$\langle r\rangle_{3p}$	1.4312	1.3611	1.3629	1.2850	1.2915	1.2657
$\Sigma N_i\langle r\rangle_i/\Sigma N_i$	0.78740	0.72503	0.73189	0.74991	0.74942	0.74987
$\langle r^2\rangle_{1s}$	0.00891	0.00891	0.00891	0.00889	0.00892	0.00880
$\langle r^2\rangle_{2s}$	0.1766	0.1763	0.1771	0.1706	0.1759	0.1634
$\langle r^2\rangle_{3s}$	1.8818	1.7761	1.7481	1.6320	1.6477	1.5962
$\langle r^2\rangle_{2p}$	0.1508	0.1511	0.1504	0.1497	0.1439	0.1330
$\langle r^2\rangle_{3p}$	2.4161	2.1646	2.1712	1.9402	1.9497	1.8741
$\Sigma N_i\langle r^2\rangle_i/\Sigma N_i$	1.08532	0.92071	0.94407	0.94193	0.94416	0.91592

TABLE XV. Overlap Integrals between Total SCF Wave Functions of the $n\ell$-hole States

		F^-	Ne	Na^+
^2S States	$\langle\Psi(2s\text{-hole})\|\Psi(1s\text{-hole})\rangle$	0.003984	0.003380	0.002876
		Cl^-	Ar	K^+
^2P States	$\langle\Psi(3p\text{-hole})\|\Psi(2p\text{-hole})\rangle$	0.009428	0.008299	0.007285
^2S States	$\langle\Psi(3s\text{-hole})\|\Psi(2s\text{-hole})\rangle$	0.006062	0.005469	0.004906
	$\langle\Psi(3s\text{-hole})\|\Psi(1s\text{-hole})\rangle$	0.000514	0.000486	0.000457
	$\langle\Psi(2s\text{-hole})\|\Psi(1s\text{-hole})\rangle$	0.001264	0.001131	0.001018

D. Validity of the Exponent Variation Procedure for Excited States

The basis-function exponent variation procedure, described in Section III, selects values of the exponents that minimize the total SCF energy. This is a valid procedure for ground states and excited states that are the lowest states of a symmetry species. SCF functions for these states give stationary values of the energy that are absolute minima. It is not known whether the SCF functions for the higher excited states of a symmetry species give stationary values of the energy that are relative minima or some other sort of extrema. The problem, for these excited states, is that exponents chosen to minimize the total energy may not give SCF functions that are optimum representations of the true HF solutions.

If explicit variational equations, e.g., those given by Dehn,[26] were solved for the exponents of the basis functions, there would be no difficulty with the higher excited states. In this way, stationary values of the energy would be found with respect to variation of the exponents as well as the linear coefficients, $C_{n\ell,p}$. However, when our exponent variation procedure is used, a particular stationary value of the energy with respect to variation of the exponents is found in a brute-force fashion. This point was discussed in Section III. The particular stationary value found is a minimum. For all the exponent variations performed to obtain the SCF functions reported in this paper, this stationary value was found with no more difficulty for the excited states than for the ground states.

It seems unlikely, for an analytic-expansion SCF function of a particular state, that there will be more than one stationary value of the energy. It is reasonable that the solutions of variational equations for both the $C_{n\ell,p}$'s and the exponents are unique. If this is true, then the use of our exponent variation procedure is justified.

The procedure may also be justified from the results of the SCF calculations. The virial theorem, which may be used as an indication of how well the exponents of the basis functions have been optimized, is satisfied equally well for the excited-state wave functions and the ground-state functions. The cusp condition is also satisfied equally well for the excited-state functions and the ground-state functions. This can be easily confirmed by reference to Tables I-VIII. Further, as may be seen from Table XVIII, the calculated ionization potentials, for the removal of inner-shell electrons, agree quite well with experimental values.

The success of our method of exponent variation implies that the total energy of analytic-expansion SCF functions, even for excited states, is an upper bound to the exact HF energy. The results in Table XVIII also show quite clearly that the SCF energies are, in fact, upper bounds to the exact, nonrelativistic, total energies. According to estimates made by Clementi,[43] the exact nonrelativistic energy is ~0.4 Hartree below the SCF energy for F^-, Ne, and Na^+ ($E_{nr} = E_{SCF} - 0.4$) and ~0.7 Hartree below the SCF energy for Cl^-, Ar, and K^+ ($E_{nr} = E_{SCF} - 0.7$). The calculated ionization potential $IP(\Delta E_{SCF})$ is obtained by subtracting the SCF energy of the parent from that of the ion; i.e., $IP(\Delta E_{SCF}) = E_{SCF}(\text{ion}) - E_{SCF}(\text{parent})$. Suppose the SCF energies of the inner-shell hole states were not upper bounds to the exact energies. Then $IP(\Delta E_{SCF})$ for the removal of an inner-shell electron would have to be much smaller than the true nonrelativistic ionization potential; at least 0.4 smaller for the neon-like ions and 0.7 smaller for the argon-like ions. This is obviously not the case.

E. Effect of the Off-diagonal Lagrangian Multipliers

The constraint, given in Eq. (7), that the SCF orbitals belonging to the same symmetry species be orthogonal is incorporated by introducing off-diagonal Lagrangian multipliers into the HF equations.[2-5] Orbitals of different symmetry are, of course, automatically orthogonal. For closed-shell systems, a unitary transformation can be found between the occupied orbitals that puts the matrix of Lagrangian multipliers into diagonal form. This additional requirement that the off-diagonal Lagrangian multipliers be zero serves, in fact, to uniquely define the SCF orbitals. For open-shell systems, it is possible to find a unitary transformation between the closed-shell orbitals for which the off-diagonal Lagrangian multipliers coupling the closed shells are zero. However, the Lagrangian multipliers that couple open and closed shells of the same symmetry cannot be reduced to zero.[3,4]

In other treatments, the nonzero off-diagonal Lagrangian multipliers are introduced into the HF equations as inhomogeneous terms;[16,29] i.e.,

$$F\phi_i = \epsilon_i\phi_i + \Sigma_{j\neq i}\theta_{ji}\phi_j. \qquad (15)$$

Because of the difficulty of handling these additional inhomogeneous terms, the off-diagonal Lagrangian multipliers are often treated in an approximate way.[13,14,42] Roothaan[3,4] has shown that it is possible, through the use of coupling operators, to absorb the terms involving the nonzero off-diagonal multipliers into the HF operator, thus preserving the pseudoeigenvalue form of the HF equations.

This method is especially suitable for the matrix form of the HF equations. The matrix HF operators[4] are

$$\underset{\sim}{F}_{C\ell} = \underset{\sim}{H}_{\ell} + \underset{\sim}{P}_{\ell} + \underset{\sim}{R}_{O\ell},$$

and (16)

$$\underset{\sim}{F}_{O\ell} = \underset{\sim}{H}_{\ell} + \underset{\sim}{P}_{\ell} - \underset{\sim}{Q}_{\ell} + \underset{\sim}{R}_{C\ell},$$

where $\underset{\sim}{F}_{C\ell}$ and $\underset{\sim}{F}_{O\ell}$ are closed-shell and open-shell Fock operators, respectively, for symmetry species ℓ, $\underset{\sim}{H}_{\ell}$ is the one-electron operator, $\underset{\sim}{P}_{\ell}$ and $\underset{\sim}{Q}_{\ell}$ are combinations of Coulomb and exchange operators, and $\underset{\sim}{R}_{O\ell}$ and $\underset{\sim}{R}_{C\ell}$ are the coupling operators. (The eigenvalue problem is $\underset{\sim}{F}\underset{\sim}{c} = \epsilon\underset{\sim}{S}\underset{\sim}{c}$ where $\underset{\sim}{S}$ is the overlap matrix.) Let the index k stand only for closed-shell orbitals, and m only for open-shell orbitals; the coupling operators are defined so that for self-consistent eigenvectors of $\underset{\sim}{F}_{C\ell}$ and $\underset{\sim}{F}_{O\ell}$,

$$\underset{\sim}{R}_{O\ell}\underset{\sim}{c}_{k\ell} = \Sigma(-\theta_{m\ell,k\ell}\underset{\sim}{c}_{m\ell}),$$

and (17)

$$\underset{\sim}{R}_{C\ell}\underset{\sim}{c}_{m\ell} = \Sigma(-\theta_{k\ell,m\ell}\underset{\sim}{c}_{k\ell}).$$

The $\theta_{m\ell,k\ell}$ and $\theta_{k\ell,m\ell}$ are the off-diagonal Lagrangian multipliers that couple the open and closed shells; Note that they are not symmetric, but that

$$N_{O\ell}\theta_{k\ell,m\ell} = N_{C\ell}\theta_{m\ell,k\ell}, \tag{18}$$

where $N_{C\ell}$ and $N_{O\ell}$ are the electron occupations of the closed shells and open shell, respectively, of symmetry ℓ.

The values of the nonzero off-diagonal Lagrangian multipliers for the $n\ell$-hole states of argon and neon are given in Table XVI. These values were computed with the accurate set SCF functions reported in Tables I-IV. While the off-diagonal Lagrangian multipliers are fairly small for states with open outer shells, they are more than an order of magnitude larger for states with open inner shells. The values of the off-diagonal Lagrangian multipliers for the $n\ell$-hole states of Cl^- and K^+, and F^- and Na^+ are similar to the values given in Table XVI for argon and neon.

TABLE XVI. Off-diagonal Lagrangian Multipliers for the $n\ell$-hole States of Argon and Neon*

State	Open Shell	$\theta_{\text{open shell, closed shell}}$		
		$\theta_{ns,1s}$	$\theta_{ns,2s}$	$\theta_{ns,3s}$
Ar^+(3s-hole)	3s	-0.00136	+0.01046	. . . .
Ar^+(2s-hole)	2s	+0.04518	. . . .	+0.13093
Ar^+(1s-hole)	1s	. . . .	+0.72661	-0.22742
		$\theta_{np,2p}$	$\theta_{np,3p}$	
Ar^+(3p-hole)	3p	+0.01672	. . . .	
Ar^+(2p-hole)	2p	. . . .	+0.24923	
		$\theta_{ns,1s}$	$\theta_{ns,2s}$	
Ne^+(2s-hole)	2s	+0.01644	. . . .	
Ne^+(1s-hole)	1s	. . . .	+0.37522	

*The Lagrangian multipliers are not symmetric; $\theta_{\text{closed, open}} = (N_c/N_o)\,\theta_{\text{open, closed}}$, where N_c and N_o are the electron occupations of the closed and open shells, respectively.

The most striking effect of the inclusion of the off-diagonal Lagrangian multipliers is that the 1s orbitals, of the 1s-hole states of Cl^-, Ar, and K^+, have a node. In each of these cases, $P_{1s}(r)$ goes through zero and reaches a minimum value of -0.003. For example, $P_{1s}(r)$ for Ar^+ (1s-hole) is zero for r = 0.93 Bohr and has a minimum of -0.0028 for $1.30 \leq r \leq 1.45$. For large r, the HF equation for $P_{1s}(r)$ becomes

$$\epsilon_{1s}P_{1s}(r) \cong -\theta_{2s,1s}P_{2s}(r) - \theta_{3s,1s}P_{3s}(r). \tag{19}$$

For Ar^+ (1s-hole), when the values in Tables III and XVI are used, Eq. (19) becomes

$$P_{1s}(r) \cong +0.01142P_{2s}(r) - 0.00357P_{3s}(r), \tag{20}$$

and the second term is dominant since the 2s radial function goes to zero much before the 3s radial function does. For $r \geq 1.2$ Bohrs, $P_{1s}(r)$ calculated from Eq. (20), using the accurate-set 2s and 3s radial functions, agrees with the accurate-set analytic SCF 1s radial function to within

0.00006. The error is always less than 3%; this is remarkably good agreement, especially since the analytic expansion method does not give exact solutions of the integro-differential HF equations.

The dominant terms, in the HF equations, that determine the behavior of inner-shell orbitals at large r are the nonzero off-diagonal Lagrangian multipliers with the outer-shell orbitals. With the exception of $\theta_{1s,3s}$ for the 1s-hole and 3s-hole states of Cl^-, Ar, and K^+, the off-diagonal Lagrangian multipliers, for the states reported in this paper, are positive. The effect of the positive off-diagonal Lagrangian multipliers is to extend the tails of the orbitals rather than to introduce additional nodes.

The signs of the off-diagonal Lagrangian multipliers are determined by the sign conventions used for the SCF orbitals. The signs of the orbitals have been chosen so that the 1s, 3s, and 2p radial functions are positive as $r \to 0$, and the 2s and 3p radial functions are negative as $r \to 0$. Because of this choice, the values of $P_{n\ell}(r)$ in the $(n - \ell)^{th}$ loop, usually the outermost loop of the orbital, will be positive. This is a departure from the convention usually used in numerical HF calculations,[16,32-35] which is that all radial functions are positive as $r \to 0$.

The negative value of $\theta_{3s,1s}$ should introduce a node into the 1s orbital of the 3s-hole states. However, the maximum value of $P_{1s}(r)$ in the outer loop would be only -0.00001. This is beyond the accuracy of the present calculation and too small to be of any interest.

To get further insight into the importance of the off-diagonal Lagrangian multipliers, an approximate treatment was developed. The matrices $\underset{\sim}{R}_{O\ell}$ and $\underset{\sim}{R}_{C\ell}$ were arbitrarily set equal to zero, and "self-consistent" solutions using the operators,

$$\underset{\sim}{F}'_{C\ell} = \underset{\sim}{H}_\ell + \underset{\sim}{P}_\ell$$

and (21)

$$\underset{\sim}{F}'_{O\ell} = \underset{\sim}{H}_\ell + \underset{\sim}{P}_\ell - \underset{\sim}{Q}_\ell,$$

rather than $\underset{\sim}{F}_{C\ell}$ and $\underset{\sim}{F}_{O\ell}$ of Eq. (16), were obtained. The occupied open-shell eigenvector of $\underset{\sim}{F}'_{O\ell}$ is not orthogonal to the occupied closed-shell eigenvectors of $\underset{\sim}{F}'_{O\ell}$. Since the operators of Eqs. (16) and (21) are assumed to be constructed from an orthogonal set of orbitals, the open-shell eigenvector was Schmidt-orthogonalized to the closed-shell eigenvectors. This Schmidt orthogonalization does not change the total determinantal wave function. A "self-consistent" solution was obtained when the Schmidt-orthogonalized eigenvectors of $\underset{\sim}{F}'_{O\ell}$ and $\underset{\sim}{F}'_{C\ell}$ were the same, within convergence thresholds, as the orthogonal vectors used to construct the operators $\underset{\sim}{F}'_{O\ell}$ and $\underset{\sim}{F}'_{C\ell}$ of Eq. (21).

Since this method neglects the off-diagonal Lagrangian multipliers in constructing the operators $\underset{\sim}{F}'_{O\ell}$ and $\underset{\sim}{F}'_{C\ell}$, "self-consistent" solutions obtained, using $\underset{\sim}{F}'_{O\ell}$ and $\underset{\sim}{F}'_{C\ell}$, are denoted by NLM (Neglect Lagrangian Multipliers) to distinguish them from the SCF solutions obtained using the operators of Eq. (16).

NLM calculations were performed, using the accurate basis sets of Tables I and III, for the $n\ell$-hole states of argon and neon. The results of these calculations are given in Table XVII. The NLM calculations were performed on the IBM 704 and are compared with SCF calculations also performed on the 704. The values of E(SCF) and V/T(SCF) given in Table XVII differ slightly, because of round-off, from the values given in Tables I-IV. Values of the total energy E (in Hartrees), V/T, and the overlap integrals $S_{n\ell,n'\ell}$ between the occupied eigenvector of $\underset{\sim}{F}'_{O\ell}$ and the occupied eigenvectors of $\underset{\sim}{F}'_{C\ell}$ are given. The signs of the $S_{n\ell,n'\ell}$ are determined by the sign conventions stated above for the SCF orbitals.

The NLM results for states with outer-shell vacancies are almost the same as the SCF results, and the $S_{n\ell,n'\ell}$ are quite small. However, for the states with inner-shell vacancies, where the off-diagonal Lagrangian multipliers are large, the NLM results are quite different from the SCF results, and the $S_{n\ell,n'\ell}$ are large.

F. Comparison of SCF Ionization Potentials with Experiment

Experimental data are available for most of the ionization potentials (IP's) of the closed-shell systems of F^-, Ne, Na^+, Cl^-, Ar, and K^+. This includes the IP's for the removal of an electron from any occupied shell. A comparison with experiment of IP's calculated from the SCF wave functions is presented in Table XVIII. The IP for the removal of an outer-shell electron (3s or 3p shell of the argon-like ions, and 2s or 2p shell of the neon-like ions) can usually be determined from Moore's optical data.[31] The electron affinities of F^- and Cl^- (i.e., the 2p-hole IP of F^-, and the 3p-hole IP of Cl^-) have been determined very accurately by Berry, Reimann, and Spokes.[43,44] The only state for which experimental data do not seem to be available is the 3s-hole state of Cl^-; but Varsavsky[45] reports an estimate made by Rohrlich of the term value of this state.

The IP for the removal of an inner-shell electron can be calculated from the experimental values of the energies of X-ray emission lines, combined with the IP for the removal of the appropriate outer-shell electron. For example, for the argon-like ions, the IP for the removal of a 1s electron is

TABLE XVII. Effect of Neglecting the Off-diagonal Lagrangian Multipliers for the $n\ell$-hole States of Argon and Neon (the results for the correct treatment of the off-diagonal Lagrangian multipliers are denoted by SCF, the results for the approximate treatment by NLM)

State	E(SCF)*	E(NLM) [E(SCF)-E(NLM)]	V/T(SCF)*	V/T(NLM)	Open Shell	Overlap Integrals between Open- and Closed-Shell Orbitals		
						$S_{ns,1s}$	$S_{ns,2s}$	$S_{ns,3s}$
Ar^+(3s-hole)	-525.5976	-525.5976 [0.0000]	-1.999999	-1.999972	3s	-0.0000_1	$+0.0009_3$	. . . .
Ar^+(2s-hole)	-514.8794	-514.8808 [+0.0014]	-2.000000	-2.000242	2s	$+0.0003_9$	. . . .	-0.0104_4
Ar^+(1s-hole)	-409.3890	-409.3941 [+0.0051]	-2.000000	-2.001786	1s	. . . .	-0.0062_2	$+0.0017_6$
						$S_{np,1p}$	$S_{np,2p}$	
Ar^+(3p-hole)	-526.2744	-526.2744 [0.0000]	-1.999999	-1.999966	3p	$+0.0003_5$	. . . .	
Ar^+(2p-hole)	-517.6690	-517.6746 [+0.0056]	-2.000000	-2.000464	2p	. . . .	-0.0043_8	
						$S_{ns,1s}$	$S_{ns,2s}$	
Ne^+(2s-hole)	-126.7348	-126.7348 [0.0000]	-2.000003	-1.999897	2s	$+0.0005_3$	. . . .	
Ne^+(1s-hole)	-96.62571	-96.62983 [+0.00412]	-1.999997	-2.003008	1s	. . . .	-0.0102_2	

*The results given in this table are from calculations performed on the IBM 704. Thus E(SCF) and V/T(SCF) may differ slightly from the values of these quantities given in Tables I and III, which are from calculations performed on the IBM 7094.

TABLE XVIII. Comparison of SCF and Experimental Ionization Potentials for the $n\ell$-hole States of F^-, Ne, Na^+, Cl^-, Ar, and K^+ (energies are in Hartree; 1 Hartree = 27.2098 eV = 2.194746 x 10^5 cm^{-1})

State			IP(exp)[a]	IP(nr)[a]	IP($-\epsilon_{n\ell}$)	IP(exp)[b] - IP($-\epsilon_{n\ell}$)	IP(ΔE_{SCF})	IP(exp)[b] - IP(ΔE_{SCF})
	$F^{-c,d}$		0.1273	. . . .	0.1810	-0.0537 (-1.461 eV)	0.0501	+0.0772 (+2.101 eV)
2p-hole $1s^2\underline{2s}^2\underline{2p}^5$	Ne[d]		0.7937	. . . .	0.8503	-0.0566 (-1.540 eV)	0.7293	+0.0644 (+1.752 eV)
	Na^{+d}		1.7404	. . . .	1.7972	-0.0568 (-1.546 eV)	1.6796	+0.0608 (+1.654 eV)
	$F^{-c,d}$		0.8947	. . . .	1.0746	-0.1799 (-4.895 eV)	0.9282	-0.0335 (-0.912 eV)
2s-hole $1s^2\underline{2s}^2p^6$	Ne[d]		1.7814	. . . .	1.9303	-0.1489 (-4.052 eV)	1.8123	-0.0309 (-0.841 eV)
	Na^{+d}		2.9433	. . . .	3.0737	-0.1304 (-3.548 eV)	2.9682	-0.0249 (-0.678 eV)
	F^{-e}		24.99_1[f]	24.96_7	25.8296	-0.86_3 (-23.48 eV)	24.9353	$+0.03_2$ (+0.87 eV)
1s-hole $\underline{1s}^2\underline{2s}^2\underline{2p}^6$	Ne[e]		31.970[f] 31.984[g]	31.94_5[g]	32.7723	-0.82_7 (-22.50 eV)	31.9214	$+0.02_4$ (+0.65 eV)
	Na^{+e}		39.99_9[f]	39.93_8	40.7597	-0.82_2 (-22.37 eV)	39.9345	$+0.00_3$ (+0.0_8 eV)
	$Cl^{-c,d}$		0.1341	. . . .	0.1502	-0.0161 (-0.438 eV)	0.0948	+0.0393 (+1.069 eV)
3p-hole $1s^2\underline{2s}^2\underline{2p}^6\underline{3s}^2\underline{3p}^5$	Ar[d]		0.5813	. . . .	0.5909	-0.0096 (-0.261 eV)	0.5430	+0.0383 (+1.042 eV)
	K^{+d}		1.1726	. . . .	1.1705	+0.0021 (+0.057 eV)	1.1260	+0.0466 (+1.268 eV)
	$Cl^{-c,h}$		0.52_6(?)	. . . .	0.7332	-0.20_7 (-5.63 eV)	0.6601	-0.13_4 (-3.65 eV)
3s-hole $1s^2\underline{2s}^2\underline{2p}^6\underline{3s}^2\underline{3p}^6$	Ar[d]		1.0745	. . . .	1.2773	-0.2028 (-5.518 eV)	1.2198	-0.1453 (-3.954 eV)
	K^{+d}		1.7644	. . . .	1.9638	-0.1994 (-5.426 eV)	1.9136	-0.1492 (-4.060 eV)
	Cl^{-e}	$^2P_{3/2}$	7.22_0[i] 7.24_2(?)[j]	7.22_8[i]	7.6956	-0.46_8 (-12.73 eV)	7.2420	-0.01_4 (-0.3_8 eV)
		$^2P_{1/2}$	7.27_9[i] 7.30_1(?)[j]					
2p-hole $1s^2\underline{2s}^2\underline{2p}^5\underline{3s}^2\underline{3p}^6$	Ar[3]	$^2P_{3/2}$	9.13_3[i] 9.11[j]	9.14_2[i]	9.5713	-0.42_9 (-11.67 eV)	9.1484	-0.00_6 (-0.2 eV)
		$^2P_{1/2}$	9.20_9[i] 9.20[j]					
	K^{+e}	$^2P_{3/2}$	11.30_6[i] 11.30_8[j]	11.31_5[i]	11.7381	-0.42_3 (-11.5_1 eV)	11.3342	-0.01_9 (-0.5_2 eV)
		$^2P_{1/2}$	11.41_6[i] 11.41_1[j]					
	Cl^{-k}		9.7_3(?)	. . . .	10.2292	. . . .	9.8114	. . . .
2s-hole $1s^2\underline{2s}^2\underline{2p}^6\underline{3s}^2\underline{3p}^6$	Ar		. . . .	. . . .	12.3219	. . . .	11.9380	. . . .
	K^{+k}		14.4_1(?)	. . . .	14.7080	. . . .	14.3455	. . . .
	Cl^{-e}		103.59_7[l] 103.61_9(?)[m,n]	103.1_8[l]	104.5055	-1.3_3 (-36.2 eV)	103.2947	-0.1_1 (-3.0 eV)
1s-hole $\underline{1s}^2\underline{2s}^2\underline{2p}^6\underline{3s}^2\underline{3p}^6$	Ar[e]		117.83_4[l] 117.83_5[g]	117.3_0	118.6101	-1.3_1 (-35.6 eV)	117.4284	-0.1_3 (-3.5 eV)
	K^{+e}		113.09_2[l] 133.09_5[m] 133.08_8[n]	132.4_2	133.7521	-1.3_3 (-36.2 eV)	132.5890	-0.1_7 (-4.6 eV)

[a] IP(exp) is the experimental value of the ionization potential. For ^2P terms, unless explicitly indicated otherwise, the IP is given to the center of gravity of the term. IP(exp) does not include any correction for the finite mass of the nucleus. IP(nr) is the experimental ionization potential corrected for relativistic effects and the finite mass of the nucleus. The relativistic corrections are made with data taken from Peteris (Ref. 46) and Scherr et al. (Ref. 47). For discussion of the relativistic corrections, see the text.

[b] SCF values are compared with IP(exp) unless a value of IP(nr) is given; in the latter case, comparisons are made with IP(nr).

[c] Experimental data for the electron affinity of F^- and Cl^- are from Berry and Reimann (Ref. 43).

[d] Experimental data are from Vol. I by Moore (Ref. 31) and correction for ^2P separation of the 3p-hole state of Cl^- in Vol. III.

[e] Ionization potentials are obtained by combining the ionization potentials for the outer-shell vacancy states with experimental data on X-ray emission lines. For the 1s-hole states of argon and neon, measurements of the K absorption edge are also used. For sources of X-ray data, see text.

[f] Experimental ionization potential are obtained from the relation IP(1s-hole) = $\Delta E(K\alpha_1)$ + IP(2s-hole; $^2P_{3/2}$).

[g] K absorption edge is as measured by Brogren (Ref. 49).

[h] Estimate of the 3s-hole term value is given by Varsavsky (Ref. 45).

[i] Experimental ionization potential is obtained from the relation IP(2p-hole; $^2P_{3/2,1/2}$) = $-\Delta E(K\alpha_{1,2})$ + $\Delta E(K\beta_1')$ + IP(3p-hole; $^2P_{3/2}$).

[j] Experimental ionization potential is obtained from the relation IP(2p-hole; $^2P_{3/2,1/2}$) = $\Delta E(L\beta, \eta)$ + IP(3s-hole).

[k] The experimental ionization potential is obtained from a table of normal energy levels of atoms; Table 13146 of Landolt-Börnstein (Ref. 48). A correction is added to account for the fact that the zero of energy of a free atom is not the same as that used in the Landolt-Börnstein table. The correction for K^+ is +0.56 Hartree, and for Cl^- is -0.17 Hartree.

[l] Experimental ionization potential is obtained from the relation IP(1s-hole) = $\Delta E(K\beta_1')$ + IP(3p-hole; $^2P_{3/2}$).

[m] Experimental ionization potential is obtained from the relation IP(1s-hole) = $\Delta E(K\alpha_1)$ + $\Delta E(L\beta)$ + IP(3s-hole).

[n] Experimental ionization potential is obtained from the relation IP(1s-hole) = $\Delta E(K\alpha_2)$ + $\Delta E(L\eta)$ + IP(3s-hole).

$$\begin{aligned} IP(1s\text{-hole}, {}^2S_{1/2}) &= IP(3p\text{-hole}, {}^2P_{3/2}) + \Delta E(K\beta_1) \\ &= IP(3s\text{-hole}, {}^2S_{1/2}) + \Delta E(L\ell) + \Delta E(K\alpha_1) \\ &= IP(3s\text{-hole}, {}^2S_{1/2}) + \Delta E(L\eta) + \Delta E(K\alpha_2), \end{aligned} \tag{22}$$

where the configuration and level of the final state of the ion are given in parentheses after IP, and $\Delta E(K\beta_1)$, $\Delta E(K\alpha_1)$, etc., are the energies of the X-ray emission lines $K\beta_1$, $K\alpha_1$, etc., respectively. Standard X-ray notation is used to describe the emission lines; $K\beta_1$, $K\alpha_1$, and $K\alpha_2$ denote the transitions 1s-hole, ${}^2S_{1/2} \rightarrow$ 3p-hole, ${}^2P_{3/2}(KM_{III})$, 1s-hole, ${}^2S_{1/2} \rightarrow$ 2p-hole, ${}^2P_{3/2}(KL_{III})$, and 1s-hole, ${}^2S_{1/2} \rightarrow$ 2p-hole, ${}^2P_{1/2}(KL_{II})$, respectively; and $L\ell$ and $L\eta$ denote the transitions 2p-hole, ${}^2P_{3/2} \rightarrow$ 3s-hole, ${}^2S_{1/2}(L_{III}M_I)$ and 2p-hole, ${}^2P_{1/2} \rightarrow$ 3s-hole, ${}^2S_{1/2}(L_{II}M_I)$, respectively. For the 1s-hole IP of neon and argon, the K absorption limits ($1s \rightarrow \infty$) of gaseous neon and argon, determined by Brogren,[49] may also be used. (We have used absorption limit here in the same sense as series limit is used for optical spectra; that is, the removal of the electron to infinity with zero kinetic energy.)

Except for the inert gases, argon and neon, the X-ray measurements used have not been on free atomic systems. The emission lines used to calculate IP's for the removal of inner-shell electrons were obtained from the emission spectra of atoms in crystals. The wavelength and shape of these lines will, of course, be affected by the chemical structure of the solids. The lines involving the outermost shells of the atom will be most affected. This chemical effect, for the systems considered here, appears to be small and about the same order of magnitude as the accuracy of the experimental measurements. For example, the full width at half-maximum of the $K\beta_{1,3}$ line of Cl^- in KCl, with no correction made for the unresolved doublet KM_{II} and KM_{III}, has been experimentally determined by Deslattes[50] to be 1.00 ± 0.05 eV. Deslattes estimates that 0.4 eV = 0.015 Hartree of this width is attributable to solid-state effects (i.e., the band structure of the 3p band of Cl^-). This is to be compared with the wavelength of the line, as measured by Valasek,[51] which is 4394.91 ± 0.14 XU = 103.464 ± 0.003 Hartrees. [The conversion from XU's to A's, as given in Sections 13 and 68 of Sandström's review article,[52] is 1000 XU = (1.00202 ± 0.00002) A.] The wavelength shift of the $K\beta_1$ (or $K\beta_{1,3}$) line of Cl^- as measured in various substances is also small. Valasek[51,53] gives 4394.90 ± 0.07 XU for Cl^- in NaCl, 4394.91 ± 0.14 XU for Cl^- in KCl, and 4394.61 XU for Cl^- in $CaCl_2$. The results of an earlier measurement of the $K\beta_1$ line of Cl^- in the same substances, given by Lindh and Lundquist,[54] are 4394.2 XU, 4394.1 XU, and 4394.2 XU, respectively.

In several cases, the results of more than one measurement of the same line were available. Our choice of which result to use was generally

guided by the choices made by Sandström* and Landolt-Bornstein[48] for their compilations of X-ray emission lines. When measurements were made for an atom in several compounds, the values for the atom in an alkali halide compound were usually used. The sources of the experimental data for the X-ray emission lines used are the following: F^-, $K\alpha_{1,2}$ Tyrén;[55] Ne, $K\alpha_{1,2}$ Moore and Chalklin;[56] Na^+, $K\alpha_{1,2}$ Johnson;[57] Cl^-, $K\alpha_1$ and $K\alpha_2$ Shearer;[58] $K\beta_1$ Valasek;[51] $L\eta$ and $L\ell$ Siegbahn and Magnusson;[59] Ar, $K\alpha_1$, $K\alpha_2$, and $K\beta_1$ Lindh and Nilsson;[60] $L\eta$ and $L\ell$ Bačkovský and Dolejšek;[61] K^+, $K\alpha_1$ Siegbahn and Dolejšek;[62] $K\alpha_2$ Sandström;* $K\beta_1$ Parrat and Jossem;[63] and $L\eta$ and $L\ell$ Tyrén.[64]

Unfortunately, the method described above cannot be used to determine the IP for removal of a 2s electron from the argon-like ions. According to Sandström* and Landolt-Bornstein,[48] no X-ray emission lines are observed that involve transitions from the 2s-hole state for atoms between chromium and sulfur.

Landolt-Bornstein[48] give a table of the normal energy levels of atoms in which they include values for the 2s-hole (L_I) levels of chlorine and potassium. The levels in this table were determined using a combination of X-ray emission lines and absorption limits. The procedure for determining the levels is much like that discussed above, except that X-ray absorption limits of atoms in crystals, rather than optical series limits of free atoms, are used. The values given for the 2s-hole states of chlorine and potassium were not obtained directly from experimental data; they are interpolations made by Tomboulian and Cady.[65] The interpolation was based on rules for the L_I-L_{II} (2s-hole, $^2S_{1/2}$ - 2p-hole, $^2P_{1/2}$) screening-doublet splitting.

The levels in the Landolt-Bornstein table may not be used directly as IP's of free atoms because the zero of energy chosen for the atom in the crystal is not the same as the zero of energy of the free atom.[66]

The correction for the 2s-hole IP that must be made to account for the different zeros of energy was determined by comparing the normal energy level given by Landolt-Bornstein for the 2p-hole, $^2P_{1/2}(L_{II})$ state with the IP obtained as described above. The 2s-hole experimental IP's, IP(exp), of Cl^- and K^+ given in Table XVIII are the Landolt-Bornstein values, with the corrections -0.17 and +0.56 Hartree, espectively. These values are included only to give a rough indication of the experimental values.

When the experimental IP's are compared with the IP's obtained from the SCF wave functions, the experimental values should be corrected for relativistic effects. The SCF functions were calculated using a

*See Ref. 52, Section 53. See also the discussion of the accuracy of measurements of X-ray emission spectra in Sections 50-52 in Ref. 52.

nonrelativistic, electrostatic Hamiltonian. The total experimental energy of a system E_{exp} may be written as

$$E_{exp} = E_{nr} + E_{rel}, \tag{23}$$

where E_{nr} is the exact energy eigenvalue of the Hamiltonian of Eq. (10), and E_{rel} is the relativistic correction to the total energy. (To be precise, the reduced mass of the electron should be used in the nonrelativistic Hamiltonian, and mass-polarization corrections should be included in E_{rel}.) Then the nonrelativistic IP, IP(nr), is

$$IP(nr) = E_{nr}(ion) - E_{nr}(parent) = IP(exp) - \Delta IP(rel), \tag{24}$$

and

$$\Delta IP(rel) = E_{rel}(ion) - E_{rel}(parent), \tag{25}$$

where $\Delta IP(rel)$ is the relativistic correction to IP(exp). The term ion is used here to refer to the system after an electron has been removed from the parent.

For the 1s-hole IP of an atom, $\Delta IP(rel)$ is assumed to be equal to the relativistic correction to the IP of the two-electron ion of that atom (IP for $1s^2$ to $1s^1$). Pekeris,[46] using his extremely accurate nonrelativistic wave functions, has calculated the relativistic corrections to the IP's of the two-electron ions of hydrogen through neon. His calculations include the mass polarization correction, relativistic corrections to order α^2, and the Lamb shift corrections to order α^3. Scherr and Silverman,[67] using an expansion in powers of Z^{-1}, have extrapolated Pekeris's calculations to calcium ($Z = 20$). The results of Pekeris and Scherr and Silverman have been used for $\Delta IP(rel)$ for the 1s-hole IP's.

For the 2p-hole IP of an argon-like ion, $\Delta IP(rel)$ is assumed to be equal to the relativistic correction to the IP of the ten-electron ion (IP for $1s^2 2s^2 2p^6$ to $1s^2 2s^2 2p^5$). Scherr, Silverman, and Matsen[47] have calculated these corrections using screened nuclear charges to evaluate the Dirac one-electron energy and the one-electron Lamb shift to order α^3.

For the 2p-hole IP's of the neon-like ions and the 3p-hole IP's of the argon-like ions, the only relativistic correction made is that IP(exp) in Table XVIII is given for the center of gravity of the ^2P term of the ion. No relativistic corrections are given for the 2s-hole IP's of the neon-like ions and the 2s- and 3s-hole IP's of the argon-like ions.

In several cases, IP(exp), given in Table XVIII, is determined in more than one way; this is done to indicate roughly the reliability of the experimental data. When the different ways give different values of

IP(nr), the method used to obtain IP(nr) is indicated. A correction for the finite mass of the nucleus is included in IP(nr), but not in IP(exp). This correction affects the values of IP(exp) and IP(nr) by no more than two units in the last place given.

The IP of a system can be calculated in two ways from SCF wave functions. One way is to use the frozen-orbital approximation. In the frozen-orbital approximation, an SCF calculation is performed for the parent system, and the SCF orbitals of the parent are also used as the orbitals of the ion. In this approximation, the IP for the removal of an electron from the $n\ell$-shell of a closed-shell system[2] is $-\epsilon_{n\ell}$; this result is known as Koopmans's theorem. The second way is to perform separate SCF calculations for the parent and the ion. In this case, the IP is the difference of the SCF energies ΔE_{SCF} of the two systems. The accurate-set SCF functions of Tables I-IV have been used to calculate the IP in these two ways. The results, IP($-\epsilon_{n\ell}$) and IP(ΔE_{SCF}), are given in Table XVIII together with their differences with IP(exp), or with IP(nr) when IP(nr) is given.

The true value of a quantity, in the sense that it is used in the following discussion, is the exact nonrelativistic value obtained from solutions of the Hamiltonian of Eq. (10). The error of an approximate value of a quantity is the error with respect to this true value. The values of IP(exp) or IP(nr) given in Table XVIII are taken to be good approximations to the true IP's. The choice of IP(exp) or IP(nr) depends, of course, on whether the electron has been removed from an inner or outer shell of the parent.

The data in Table XVIII show that when an electron is removed from the outermost shell (2p shell of the neon-like ions, and 3p shell of the argon-like ions), IP($-\epsilon_{n\ell}$) is a better approximation than IP(ΔE_{SCF}) to the true IP. The frozen-orbital wave function for the ion is always a poorer approximation than the SCF wave function to the true wave function of the ion. For the lowest state of a symmetry species, the error in the energy of the ion in the frozen-orbital approximation must be larger than the correlation energy of the ion (the error of the SCF energy of the ion). However, in the cases mentioned above, the correlation energy of the parent is more nearly equal to the error in the energy of the ion in the frozen-orbital approximation than to the correlation energy of the ion. The errors in the energies of the parent and ion more nearly cancel, and IP($-\epsilon_{n\ell}$) is a better approximation than IP(ΔE_{SCF}) to IP(nr).

The error in the energy of the ion in the frozen-orbital approximation is usually larger than the correlation energy of the parent. Because of this, IP($-\epsilon_{n\ell}$) is usually larger than the true IP. This is not always the case; for K^+, IP($-\epsilon_{3p}$) is 0.06 eV smaller than IP(exp) for the removal of a 3p electron.

Note that IP($-\epsilon_{n\ell}$) is larger than the true IP when an inner-shell electron has been removed. If the ion is not in the lowest state of a symmetry species, it is not necessary that the expectation value of the energy for an approximate wave function be an upper bound to the true energy. If the expectation value of the energy in the frozen-orbital approximation for ions in these states was not larger than the true energy, then IP($-\epsilon_{n\ell}$) would be considerably smaller than the true IP.

When an electron is removed from any but the outermost shell, IP(ΔE_{SCF}) is a better approximation than IP($-\epsilon_{n\ell}$) to the true IP. When an electron is removed from an inner shell (1s shell of the neon-like ions, and 1s, 2s, or 2p shell of the argon-like ions), the SCF orbitals of the ion are considerably different from the SCF orbitals of the parent (cf., $\langle r \rangle$ and $\langle r^2 \rangle$ in Tables XIII and XIV). Consequently, the error in using the orbitals of the closed-shell parent for these ions is quite large.

The SCF orbitals of the states that have a hole in the outermost s shell are not very different from the SCF orbitals of the states with a hole in the outermost p shell. The IP($-\epsilon_{n\ell}$) was a good approximation to the IP for the removal of an outermost p electron, but not for an outermost s electron. For these s-hole states, there is another reason why IP($-\epsilon_{n\ell}$) is a poorer approximation than IP(ΔE_{SCF}). As discussed in Section IV-A, these s-hole states are likely to be the lowest ^2S states of even parity of their ionic systems. The only states for which this is at all in doubt are F(2s-hole) and Cl(3s-hole). When the ion is the lowest state of a symmetry species, IP($-\epsilon_{n\ell}$) must be greater than IP(ΔE_{SCF}). Now, IP(ΔE_{SCF}) for the removal of an outermost s electron is already larger than the true IP. Since IP($\epsilon_{n\ell}$) must be still larger, it is a poorer approximation to the true IP. The surprising fact that IP(ΔE_{SCF}) is larger than the true IP is discussed in Section G below.

The agreement of IP(ΔE_{SCF}) with IP(nr) for the removal of an inner-shell electron is remarkably good. [Comparisons of IP(ΔE_{SCF}) with IP(nr) for the removal of a 2s electron from an argon-like ion cannot be made since there is no accurate experimental data available.] The error of IP(ΔE_{SCF}), for these cases, is always less than 0.2% and often no more than 0.1%. Thus, IP(ΔE_{SCF}) often agrees with IP(nr) to four significant figures.

This good agreement is due, at least in part, to the fact that the importance of the one-electron contributions to the HF operator relative to the two-electron contributions (the kinetic energy and nuclear attraction terms relative to the Coulomb and exchange terms), is considerably greater for inner-shell orbitals than for outer-shell orbitals. The best results are obtained with the HF one-electron approximation when the two-electron terms are a small perturbation on the one-electron terms. Since the error of the HF treatment of the outer-shell orbitals can be

expected to be roughly the same whether the inner-shell electron is present or not, IP(ΔE_{SCF}) for the removal of an inner-shell electron should give reasonably good agreement with the true IP.

Thus, IP(ΔE_{SCF}) for the removal of a 2s electron from an argon-like ion should be in good agreement with the true nonrelativistic IP. The relativistic correction to these IP's, estimated from the data of Scherr, Silverman, and Matsen,[47] is probably no more than 0.1 Hartree. Even without relativistic corrections, the values of IP(ΔE_{SCF}), given in Table XVIII, should agree with the correct experimental values to within 1%; because of the relativistic corrections, they should be smaller than the correct experimental values. No direct experimental data are available for these 2s-hole IP's; the values of IP(exp), given in Table XVIII, were obtained through interpolation.[65]

G. Anomalous Behavior of the Correlation Energy

The correlation energies of some of the hole-state systems have anomalous values. The correlation energy E_{corr} is the error of the total SCF energy E_{SCF} and is defined by the relation

$$E_{nr} = E_{SCF} + E_{corr}, \tag{26}$$

where E_{nr} is the exact nonrelativistic solution of the Hamiltonian of Eq. (10). The sign has been chosen so that E_{corr} is negative for all the systems considered here and is always negative for the lowest state of a symmetry species. It follows immediately from Eq. (26) that

$$IP(nr) - IP(\Delta E_{SCF}) = E_{corr}(ion) - E_{corr}(parent). \tag{27}$$

The error of IP(ΔE_{SCF}), given in the last column of Table XVIII, is the difference of E_{corr} between the parent and the ion.

Usually IP(ΔE_{SCF}) is less than the true IP. The orbitals of the ion are not drastically different from those of the parent. The ion has one fewer electron than the parent, and it is reasonable to expect that $|E_{corr}(ion)| < |E_{corr}(parent)|$. As shown in Table XVIII, this usual case occurs when an electron is removed from the outermost p shell of any of the closed-shell systems considered.

When an electron is removed from the outermost s shell, IP(ΔE_{SCF}) is larger than the true IP. The magnitude of E_{corr} of Ne^+(2s-hole) is 0.84 eV larger than the magnitude of E_{corr} of neon; $|E_{corr}|$ of Ar^+(3s-hole) is 3.95 eV larger than $|E_{corr}|$ of argon.

When an electron is removed from the 2p or the 1s shell of one of the argon-like ions, $|E_{corr}|$ of the resulting ion is also larger than $|E_{corr}|$ of the parent. The uncertainties of the experimental data and

the relativistic corrections make this conclusion somewhat doubtful for the 2p-hole states. For the 1s-hole states, however, the increase of $|E_{corr}|$ is larger than these uncertainties.

This anomalous behavior of the correlation energy is extremely important in light of the recent work of Clementi[41,68] and in particular of Allen, Clementi, and Gladney[69] to obtain semiempirical rules for the calculation of E_{corr}. Such rules, if they could be successfully applied, would be very useful since SCF wave functions may now be easily obtained for a large class of systems. The analysis of Allen, Clementi, and Gladney is based on a decomposition of E_{corr} into pair-correlation energies. For atoms, the pair-correlation energy is denoted by $E_{corr}(n,\ell,m_\ell,m_s;\ n',\ell',m'_\ell,m'_s)$, where n,ℓ,m_ℓ,m_s are the usual one-electron quantum numbers. Allen et al.[69] explicitly make the following three assumptions about this decomposition: (1) The total correlation energy is, to a very good approximation, the sum of the pair-correlation energies,

$$E_{corr} = \Sigma\, E_{corr}(n,\ell,m_\ell,m_s;\ n',\ell',m'_\ell,m'_s). \tag{28}$$

(2) The most important pair-correlation energies are for electrons which differ only in their spin quantum numbers, and these correlation energies are independent of m_ℓ; i.e., $E_{corr}(n,\ell,m_\ell,\alpha;\ n,\ell,m_\ell,\beta) = E_{corr}(n,\ell,\alpha;\ n,\ell,\beta)$. (3) The pair-correlation energy, with only minor qualifications, is a function only of the quantum numbers of the pair of electrons and the nuclear charge Z; in particular, it does not depend on the total electronic configuration of the system. The third assumption is a key one since Allen, Clementi, and Gladney obtained the pair-correlation energies for an atom by subtracting the total correlation energies of various ions of the atom.

The first two assumptions are quite reasonable. The anomalous behavior of the correlation energy, discussed above, shows that the third assumption is not correct.

From the assumptions and Eq. (27), it follows that when an electron is removed from a closed shell with quantum numbers $n\ell$,

$$-E_{corr}(n,\ell,\alpha;\ n,\ell,\beta) \cong E_{corr}(\text{ion}) - E_{corr}(\text{parent}) = IP(nr) - IP(\Delta E_{SCF}). \tag{29}$$

For neon, Allen, Clementi, and Gladney find that $-E_{corr}(2p\alpha,2p\beta) \cong +1.7$ eV, $-E_{corr}(2s\alpha,2s\beta) \cong +3.2$ eV, and $-E_{corr}(1s\alpha,1s\beta) \cong +1.2$ eV. The results given in Table XVIII show that $E_{corr}(Ne^+;2p\text{-hole}) - E_{corr}(Ne) = +1.75$ eV, $E_{corr}(Ne^+;2s\text{-hole}) - E_{corr}(Ne) = -0.84$ eV, and $E_{corr}(Ne^+;1s\text{-hole}) - E_{corr}(Ne) = +0.65$ eV. When a 2p electron is removed, Allen, Clementi, and Gladney correctly predict the change in the total correlation energy; this is hardly surprising since this change was

part of the data used in their semiempirical analysis. However, when a 2s electron is removed, they predict a decrease of $|E_{corr}|$ of ~3.2 eV; but, in fact, $|E_{corr}|$ increases by 0.84 eV. When a 1s electron is removed, they predict a decrease of ~1.2 eV, but there is a decrease of only half that. Allen, Clementi, and Gladney also give pair correlations for fluorine and sodium. Their predictions for the correlation energies of the $n\ell$-hole states of F^- and Na^+ are very similar to their predictions for neon.

Clearly the values that the Allen, Clementi, and Gladney analysis gives for $E_{corr}(2s\alpha,2s\beta)$ and $E_{corr}(1s\alpha,1s\beta)$ are not correct. Kestner[70] has considered the anomalous correlation energy of Ne^+(2s-hole) using the formalism of Sinonağlu. He claims that he has accounted for the increase of $|E_{corr}|$ to the accuracy of his calculation.

Kestner explains that the anomalous correlation energy of the 2s-hole state of neon is due to the increased importance of configuration interaction for the SCF function of this state. The $1s^22s2p^6$ configuration of the 2s-hole state of Ne^+ can interact with the configurations $1s^22s^2ep^4ns$, $1s^22s2p^5np$, and $1s^22s^22p^4nd$. The configurations $1s^22s^22p^6$ and $1s^22s^22p^5$ of neutral neon and the 2p-hole state of neon can interact only with configurations formed by exciting two electrons into orbitals with principal quantum numbers $n > 2$. The energies of some of the excited configurations that mix with the SCF configuration of the 2s-hole state of neon are closer to the energy of that state, than the energies of the exicted configurations for neon and Ne^+(2p-hole) are to the energies of these states. Thus, the mixing of configurations will be larger for the 2s-hole state than for the neutral atom or the 2p-hole state. When the effects of configuration interaction are more important, the SCF one-configuration function gives a poorer approximation to the true wave function, and the magnitude of the correlation energy is larger.

Similar arguments can be made about the 3s-hole states of the argon-like ions. It will be interesting to see if Kestner's treatment can account for the increase of $|E_{corr}|$ for these states. The increase of $|E_{corr}|$ for these states is more than four times as large as the increase of $|E_{corr}|$ for the 2s-hole states of the neon-like ions.

V. TRANSITION PROBABILITIES BETWEEN THE SCF WAVE FUNCTIONS

A. Theory

To calculate electric-dipole transition probabilities, it is necessary to evaluate matrix elements I of the form

$$I = \langle \Psi_I | \Sigma \underset{\sim}{r}(i) | \Psi_F \rangle, \tag{30}$$

where Ψ_I and Ψ_F are the normalized many-electron wave functions of the initial and final states, $\underset{\sim}{r}(i)$ is the position vector of the i^{th} electron, and the sum is over all the electrons in the atom. In this calculation, Ψ_I and Ψ_F are approximated by SCF wave functions. For the states considered here, the SCF function is given by a single Slater determinant and is an eigenfunction of L^2 and S^2, but not J^2. Since Ψ_I and Ψ_F were obtained as separate SCF solutions of the variational equations, the SCF one-electron orbitals for the two states have no special relation to each other. In particular, the overlap integrals of the orbitals $\phi^{(I)}_{n\ell m}$ of Ψ_I with the orbitals $\phi^{(F)}_{n'\ell m}$ of Ψ_F are not zero or one; that is, $\langle \phi^{(I)}_{n\ell m} | \phi^{(F)}_{n'\ell m} \rangle \neq \delta_{n,n'}$.

It is common practice[45,71,72] to approximate the dipole transition matrix element I of Eq. (30) by

$$I = \langle \Psi_I | \Sigma \underset{\sim}{r}(i) | \Psi_F \rangle \cong \underset{\sim}{W} \int_0^\infty P^{(I)}_{n\ell}(r) r P^{(F)}_{n'\ell'}(r)\, dr. \tag{31}$$

Here $P^{(I)}_{n\ell}$ and $P^{(F)}_{n'\ell'}$ are the radial wave functions of the active electron (the electron making the transition) for the initial and final states. The radial functions $P^{(I)}_{n\ell}$ and $P^{(F)}_{n'\ell'}$ need not be SCF functions.[45,71] The vector $\underset{\sim}{W}$ includes the angular integrations and also depends on the symmetry species and subspecies of the initial and final states. The approximation of Eq. (31) is equivalent to assuming that the orthonormality relations

$$\langle \phi^{(I)}_{n\ell m} | \phi^{(F)}_{n'\ell m} \rangle = \int_0^\infty P^{(I)}_{n\ell}(r)\, P^{(F)}_{n'\ell}(r)\, dr = \delta_{n,n'} \tag{32}$$

hold. We shall refer to this approximation as the active electron approximation.

With SCF functions, or with any total wave functions which are expressed as combination of Slater determinants, it is not necessary to use the active electron approximation. Löwdin[73] has given an expression for the matrix element of a one-electron operator $\Sigma O(i)$ between two arbitrary Slater determinants, Ψ_U and Ψ_V. Löwdin showed that

$$\langle \Psi_U | \Sigma O(i) | \Psi_V \rangle = \Sigma_{k,\ell} \langle \psi_k^{(U)}(1) | O(1) | \psi_\ell^{(V)}(1) \rangle D_{UV}(k|\ell), \qquad (33)$$

where $\psi_k^{(U)}$ and $\psi_\ell^{(V)}$ are spin-orbitals of the determinants Ψ_U and Ψ_V respectively, the double sum k, ℓ is over all the occupied spin-orbitals, and $D_{UV}(k|\ell)$ is the signed minor, formed by removing the k^{th} row and ℓ^{th} column, of the matrix D_{UV}. The elements of D_{UV} are the overlap integrals between the spin-orbitals of the two determinants; the $k\ell$ element of D_{UV} is

$$(D_{UV})_{k\ell} = \langle \psi_k^{(U)} | \psi_\ell^{(V)} \rangle. \qquad (34)$$

The SCF spin-orbitals were defined in Eq. (2).

The evaluation of the sum in Eq. (33) is simple because the SCF spin-orbitals are symmetry-adapted and because there is only radial function for each shell [cf., Eqs. (2) and (5)]. In fact, for the transitions considered, it was never necessary to evaluate a determinant larger than 3 x 3. The dipole transition matrix elements required for this calculation were, therefore, evaluated by means of Eq. (33).

The results of the dipole transition calculations will be given as total absolute multiplet strengths $S(M)_{IF}$. In the electric dipole approximation, $S(M)_{IF}$ is defined, in atomic units, by

$$S(M)_{IF} = \sum_{M_S, M_S'} \sum_{M_L, M_L'} |\langle \Psi_I(L,S,M_L,M_S) | \Sigma_{\underset{\sim}{r}}(i) | \Psi_F(L',S,M_L',M_S') \rangle|^2, \qquad (35)$$

where L, S, M_L, and M_S are the usual orbital and spin angular momentum quantum numbers for the many-electron system. The sum is over all the states of the initial and final terms. This sum need not be evaluated explicitly; sum rules* for the sum over M_L and M_L', and the fact that the operator $\Sigma_{\underset{\sim}{r}}(i)$ does not involve the spin, may be used to reduce the sum. For the case of interest here (transitions between ^2S and ^2P states with $\Delta L = 1$), $S(M)_{IF}$ becomes

$$S(M)_{IF} = (2S+1)(L+1)(2L+3) |\langle \Psi_I(L+1,S,M_L = L, M_S = S) | \Sigma z(i) | \Psi_F(L,S,M_L = L, M_S = S) \rangle|^2, \qquad (36)$$

where z(i) is the z coordinate of the i^{th} electron.

*Feenberg and Pake[74] present a complete statement and derivation of the sum rules.

Absolute line strengths may be obtained from $S(M)_{IF}$ by using the relative strengths of lines in multiplets. Oscillator strengths and spontaneous transition probabilities may also be obtained from $S(M)_{IF}$ by using either experimental or SCF transition energies. Summaries of current notation and definitions of terms may be found elsewhere.[75] The general problem of emission and absorption of radiation is treated in detail elsewhere; see, for example, Bethe and Salpeter.[20]

For the sake of convenience, we give here the relations that will be required later for the discussion of the width of the 1s-hole state; this width is referred to as the K-state width, or simply the K width.

The absolute line strength $S(L)_{IF}$ is defined, in atomic units, by

$$S(L)_{IF} = \sum_{M_J, M_J'} |\langle \Psi_I(J, L, S, M_J) | \Sigma \underset{\sim}{r}(i) | \Psi_F(J', L', S, M_J') \rangle|^2. \tag{37}$$

The subscripts I and F for $S(L)_{IF}$ refer to levels (i.e., $^{2S+1}L_J$), while the subscripts for $S(M)_{IF}$ refer to terms (i.e., ^{2S+1}L). For the transitions of interest here, $S(L)_{IF}$ is given in terms of $S(M)_{IF}$ by

$$\left.\begin{aligned} {}^2S_{1/2} &\longleftrightarrow {}^2P_{1/2}; \quad S(L)_{IF} = (1/3)S(M)_{IF} \\ {}^2S_{1/2} &\longleftrightarrow {}^2P_{3/2}; \quad S(L)_{IF} = (2/3)S(M)_{IF}. \end{aligned}\right\} \tag{38}$$

The transition probability for spontaneous emission of a photon A_{IF} is given, in sec^{-1}, by

$$A_{IF} = 2.1419 \times 10^{10} [(\Delta E_{IF})^3 / g_I] \, S_{IF}(L), \tag{39}$$

where $\Delta E_{IF} = E_I - E_F$ is the energy of the line in atomic units, $S_{IF}(L)$ is in atomic units, and g_I is the degeneracy of the initial level.

The total width of a level I, Γ_I, may be written as $\Gamma_I = \hbar P_I$, where P_I is the total probability of transitions from the level I to all lower-lying levels. The partial width due to radiative transitions $\Gamma^{(R)}$, called the radiative width, is

$$\Gamma_I^{(R)} = \hbar \sum_F A_{IF}, \tag{40}$$

where the sum is over all levels with lower energy, $E_F < E_I$. For inner-shell hole states, where radiationless transitions are important, the total width is given by

$$\Gamma_I = \Gamma_I^{(R)} + \Gamma_I^{(A)}, \tag{41}$$

where $\Gamma_I^{(A)}$ is called the Auger width. The fluorescence yield $\bar{\omega}_I$, the fraction of the total transition rate due to radiative transitions, may be written as

$$\bar{\omega}_I = \Gamma_I^{(R)} \Big/ \left[\Gamma_I^{(R)} + \Gamma_I^{(A)}\right] = \Gamma_I^{(R)}/\Gamma_I. \tag{42}$$

These matters are discussed in detail elsewhere.(76)

The operator $\Sigma \underset{\sim}{r}(i)$ is called the dipole length operator. It is possible, through the use of commutation relations, to find alternate expressions for the dipole transition matrix element of Eq. (30). For the many-electron Hamiltonian of Eq. (10), we have the relations

$$[\Sigma \underset{\sim}{r}(k), \mathcal{H}] = i\Sigma \underset{\sim}{p}(k) = \Sigma \underset{\sim}{\nabla}(k), \tag{43a}$$

and

$$[\Sigma \underset{\sim}{p}(k), \mathcal{H}] = -i[\Sigma \underset{\sim}{\nabla}(k)]\,\mathcal{H} = -iZ\,\Sigma \underset{\sim}{r}(k)/r(k)^3, \tag{43b}$$

where Z is the nuclear charge and the commutation relations are expressed in atomic units. If Ψ_I and Ψ_F are exact eigenfunctions of $\mathcal{H}$, the dipole transition matrix element I, in atomic units, may be evaluated, using Eq. (30) or equivalently, as either

$$I = \langle \Psi_I | [-1/\Delta E_{IF}] \Sigma \underset{\sim}{\nabla}(k) | \Psi_F \rangle, \tag{44a}$$

or

$$I = \langle \Psi_I | [Z/(\Delta E_{IF})^2] \Sigma \underset{\sim}{r}(k)/r(k)^3 | \Psi_F \rangle, \tag{44b}$$

where $\Delta E_{IF} = E_I - E_F$ is the difference between the exact nonrelativistic total energies of the initial and final states. The operators in Eqs. (44a) and (44b) are called the dipole-velocity and dipole-acceleration operators, respectively. Note that the dipole-acceleration operator was obtained from the exact many-electron potential energy and not from some average one-electron potential.

When a dipole transition matrix element is evaluated using approximate wave functions (e.g., SCF functions), the length, velocity, and acceleration forms of the matrix element will not have the same value. The values obtained using the three operators do not necessarily bound the correct value of the matrix element. Even if the three values are in close agreement, they are not necessarily correct. However, the main contributions to the matrix element come from different regions of r for the three operators. The contributions to the value of the matrix element from comparatively large r are most important for the dipole length operator, from intermediate values of r for the velocity operator, and from small values of r for the acceleration operator. Thus, if the three operators give approximately equal values for a transition matrix element, it is not unreasonable to infer that these values are close to the true value. In any event, it is interesting to see how the results obtained using the length, velocity, and acceleration operators compare. Such a comparison will be made in Section B below.

B. Results of the Dipole Transition Probability Calculations

A computer program was written for the IBM 704 to calculate all the one-electron overlap and electric-dipole transition integrals, between the expansion SCF orbitals of two states, needed for the evaluation of $S(M)_{IF}$. The one-electron overlap and transition integrals are defined in Eqs. (33) and (34). Transition integrals may be computed for the dipole-length, -velocity, and -acceleration operators. Since the angular integration follows immediately from the properties of the spherical harmonics, only the radial portions of the transition integrals are calculated by the program. For the transitions reported here, the program was modified to calculate $S(M)_{IF}$ directly, with the electric dipole transition matrix element evaluated exactly, as a matrix element between the many-electron SCF wave functions. Actually, $S(M)_{IF}$ is calculated when the length operator is used; but $(\Delta E_{IF})^2 S(M)_{IF}$ and $(\Delta E_{IF})^4 Z^{-2} S(M)_{IF}$ are calculated when the velocity and acceleration operators are used. In this way, experimental, rather than SCF, energy differences may be used when the velocity and acceleration forms of $S(M)_{IF}$ are evaluated.

For a given transition, the input to the transition moment program consists of two sets of punched cards. One of these sets contains the information necessary to describe the SCF function of the initial state; the other, the information necessary to describe the final state. While a set of cards may be prepared manually, it is available, optionally, as part of the output of an SCF calculation performed with the 7094 SCF program.

The values of $S(M)_{IF}$, in the electric dipole approximation, for all possible electric dipole transitions between the $n\ell$-hole states computed, are presented in Table XIX. The matrix elements were computed exactly, between many-electron SCF wave functions, using the expression of

Eq. (33). The matrix elements were evaluated using the dipole-length operator. The SCF functions used are the accurate-set functions reported in Tables I-IV. The values of $S(M)_{IF}$ are given in atomic units.

TABLE XIX. Total Absolute Multiplet Strengths $S(M)_{IF}$ for Transitions between the $n\ell$-hole States of F^-, Ne, Na^+, Cl^-, Ar, and K^+ (Values of $S(M)_{IF}$ are in a.u.)

	F	Ne^+	Na^{++}
2s-hole → 2p-hole ultraviolet emission line	2.0652	1.4632	1.0855
1s-hole → 2p-hole Kα emission line	0.02466	0.02193	0.01937
	Cl	**Ar^+**	**K^{++}**
3s-hole → 3p-hole ultraviolet emission line	5.3584	4.1392	3.2995
2p-hole → 3s-hole $L\ell, \eta$ emission lines	0.03430	0.02808	0.02324
2s-hole → 3p-hole not observed	0.02932	0.02991	0.02965
2s-hole → 2p-hole not observed	0.3382	0.2923	0.2549
1s-hole → 3p-hole Kβ emission line	0.0006722	0.0007010	0.0007078
1s-hole → 2p-hole Kα emission line	0.009245	0.008354	0.007588

For most of the transitions given in Table XIX, $S(M)_{IF}$, for a given transition, decreases with increasing Z. Along an isoelectronic sequence, the wave functions for a given state become more contracted as the nuclear charge increases (cf., $\langle r \rangle$ and $\langle r^2 \rangle$ given in Tables XIII and XIV). Thus, the main contributions to the dipole transition matrix element $\langle \Psi_I | \Sigma_i r(i) | \Psi_F \rangle$ come from smaller values of r for larger values of Z, and $S(M)_{IF}$ becomes smaller with increasing Z. In fact, for the hydrogenic one-electron ions, $S(M)_{IF}$ goes as $1/Z^2$.

For the 1s-hole → 3p-hole and the 2s-hole → 3p-hole transitions of Cl, Ar^+, and K^{++}, however, $S(M)_{IF}$ does not have this behavior; for the 1s-hole → 3p-hole transition, $S(M)_{IF}$ increases with increasing Z. Although all the SCF orbitals of a given state contract with increasing Z, the 3p orbitals contract more than the 1s or 2s orbitals. The region of

important "overlap," the region where $\Psi_I^* \Psi_F$ is large, will increase, and, in some cases, this increase will be more important than the fact that the "overlap" occurs in a region of smaller r. As Z becomes larger, the contraction with increasing Z, of all the orbitals of a given state, becomes more nearly the same. For large enough Z, $S(M)_{IF}$ for any transition should decrease with increasing Z along an isoelectronic sequence; $S(M)_{2s\text{-hole},3p\text{-hole}}$ is smaller for K^{++} than for Ar^+, and it is likely that $S(M)_{1s\text{-hole},3p\text{-hole}}$ will be smaller for Ca^{+3} than for K^{++}.

For transitions between the $n\ell$-hole states of neon and argon, Table XX compares the effects, on $S(M)_{IF}$, of the use of several different approximations for the evaluation of the dipole transition matrix element. The results for these transitions are very similar to the results for the transitions of the other atoms. The values of $S(M)_{IF}$ are given for the dipole length, velocity, and acceleration operators defined by Eqs. (30) and (44). For each operator, the transition matrix element was evaluated using the many-electron expression of Eq. (33), and also using the active-electron approximation of Eq. (31).

The notation $\langle \Psi(\text{ns-hole}) | \underset{\sim}{Q} | \Psi(\text{n'p-hole}) \rangle$ is used in Table XX to indicate that the matrix element for $S(M)_{\text{ns-hole,n'p-hole}}$ was evaluated between many-electron SCF wave functions. In the active-electron approximation,

$$S(M)_{\text{ns-hole,n'p-hole}} = 6 \left| \langle \phi^{(\text{ns-hole})}_{\text{n'p},m=0} | O_z | \phi^{(\text{n'p-hole})}_{\text{ns},m=0} \rangle \right|^2; \qquad (45)$$

where

$$O_z^{(\ell)} = z,$$

$$O_z^{(v)} = -(1/\Delta E_{IF}) \frac{\partial}{\partial z},$$

and

$$O_z^{(a)} = [Z/(\Delta E_{IF})^2][z/r^3]. \qquad (46)$$

The notation $\langle \phi^{(I)}_{n\ell} | \underset{\sim}{Q} | \phi^{(F)}_{n'\ell'} \rangle$ is used in Table XX to indicate that the matrix element for $S(M)_{IF}$ was evaluated using the active-electron approximation; for simplicity, the subscript m for the symmetry subspecies is not used. Matrix elements were evaluated in the active-electron approximation in two ways: first, using the appropriate orbitals from the SCF wave functions for the initial and final states of the transition, as indicated in Eq. (45); and second, using the orbitals from the SCF wave function for the closed-shell system, either neutral neon or argon.

TABLE XX. Total Absolute Multiplet Strengths $S(M)_{IF}$ Using Several Approximations for the Dipole Transition Matrix Element [$S(M)_{IF}$ and ΔE_{IF} are in a.u.]

Transition	Approximation for Matrix Element	Operator				
		Length	Velocity	Diff.*	Acceleration	Diff.*
Ne^+; 2s-hole → 2p-hole	$\langle\Psi(2s\text{-hole})\|\underset{\sim}{Q}\|\Psi(2p\text{-hole})\rangle$	1.463	1.166	20.3%	~150.	. . .
ΔE_{IF} = 0.9877	$\langle\varphi_{2p}^{(2s\text{-hole})}\|\underset{\sim}{Q}\|\varphi_{2s}^{(2p\text{-hole})}\rangle$	1.465	1.181	. . .		
	$\langle\varphi_{2p}^{(Ne)}\|\underset{\sim}{Q}\|\varphi_{2s}^{(Ne)}\rangle$	1.630	1.282	. . .		
Ne^+; 1s-hole → 2p-hole	$\langle\Psi(1s\text{-hole})\|\underset{\sim}{Q}\|\Psi(2p\text{-hole})\rangle$	0.02193	0.01979	9.8%	0.02252	2.7%
ΔE_{IF} = 39.151	$\langle\varphi_{2p}^{(1s\text{-hole})}\|\underset{\sim}{Q}\|\varphi_{1s}^{(2p\text{-hole})}\rangle$	0.02119	0.02066	. . .	0.02355	. . .
	$\langle\varphi_{2p}^{(Ne)}\|\underset{\sim}{Q}\|\varphi_{1s}^{(Ne)}\rangle$	0.01549	0.01415	. . .	0.01484	. . .
Ar^+; 3s-hole → 3p-hole	$\langle\Psi(3s\text{-hole})\|\underset{\sim}{Q}\|\Psi(3p\text{-hole})\rangle$	4.139	4.791	15.8%	~3000.	. . .
ΔE_{IF} = 0.4932	$\langle\varphi_{3p}^{(3s\text{-hole})}\|\underset{\sim}{Q}\|\varphi_{3s}^{(3p\text{-hole})}\rangle$	4.143	4.798	. . .		
	$\langle\varphi_{3p}^{(Ar)}\|\underset{\sim}{Q}\|\varphi_{3s}^{(Ar)}\rangle$	4.460	4.777	. . .		
Ar^+; 2p-hole → 3s-hole	$\langle\Psi(2p\text{-hole})\|\underset{\sim}{Q}\|\Psi(3s\text{-hole})\rangle$	0.02808	0.02150	23.4%	wrong sign**	. . .
ΔE_{IF} = 8.067	$\langle\varphi_{3s}^{(2p\text{-hole})}\|\underset{\sim}{Q}\|\varphi_{2p}^{(3s\text{-hole})}\rangle$	0.02492	0.02222	. . .	0.000003	. . .
	$\langle\varphi_{3s}^{(Ar)}\|\underset{\sim}{Q}\|\varphi_{2p}^{(Ar)}\rangle$	0.01981	0.01835	. . .	wrong sign**	. . .
Ar; 2s-hole → 3p-hole	$\langle\Psi(2s\text{-hole})\|\underset{\sim}{Q}\|\Psi(3p\text{-hole})\rangle$	0.02991	0.02413	19.3%	0.01056	64.7%
ΔE_{IF} = 11.357	$\langle\varphi_{3p}^{(2s\text{-hole})}\|\underset{\sim}{Q}\|\varphi_{2s}^{(3p\text{-hole})}\rangle$	0.02893	0.02547	. . .	0.01213	. . .
	$\langle\varphi_{3p}^{(Ar)}\|\underset{\sim}{Q}\|\varphi_{2s}^{(Ar)}\rangle$	0.01954	0.01701	. . .	0.00562	. . .
Ar^+; 2s-hole → 2p-hole	$\langle\Psi(2s\text{-hole})\|\underset{\sim}{Q}\|\Psi(2p\text{-hole})\rangle$	0.2923	0.2079	28.9%	~ 50.	. . .
ΔE_{IF} = 2.796	$\langle\varphi_{2p}^{(2s\text{-hole})}\|\underset{\sim}{Q}\|\varphi_{2s}^{(2p\text{-hole})}\rangle$	0.2842	0.2054	. . .		
	$\langle\varphi_{2p}^{(Ar)}\|\underset{\sim}{Q}\|\varphi_{2s}^{(Ar)}\rangle$	0.2967	0.2262	. . .		
Ar^+; 1s-hole → 3p-hole	$\langle\Psi(1s\text{-hole})\|\underset{\sim}{Q}\|\Psi(3p\text{-hole})\rangle$	0.0007010	0.0006519	7.0%	0.0007061	0.7%
ΔE_{IF} = 116.72	$\langle\varphi_{3p}^{(1s\text{-hole})}\|\underset{\sim}{Q}\|\varphi_{1s}^{(3p\text{-hole})}\rangle$	0.0005358	0.0005433	. . .	0.0006001	. . .
	$\langle\varphi_{3p}^{(Ar)}\|\underset{\sim}{Q}\|\varphi_{1s}^{(Ar)}\rangle$	0.0004223	0.0004011	. . .	0.0004118	. . .
Ar^+; 1s-hole → 2p-hole	$\langle\Psi(1s\text{-hole})\|\underset{\sim}{Q}\|\Psi(2p\text{-hole})\rangle$	0.008354	0.008003	4.2%	0.008683	3.9%
ΔE_{IF} = 108.16	$\langle\varphi_{2p}^{(1s\text{-hole})}\|\underset{\sim}{Q}\|\Psi_{1s}^{(2p\text{-hole})}\rangle$	0.008470	0.008347	. . .	0.009082	. . .
	$\langle\varphi_{2p}^{(Ar)}\|\underset{\sim}{Q}\|\varphi_{1s}^{(Ar)}\rangle$	0.007607	0.007208	. . .	0.007482	. . .

*This is the percent difference between $S(M)_{IF}$ evaluated using the length operator, and $S(M)_{IF}$ evaluated using the velocity or acceleration operator.

**The sign of the transition matrix element for the acceleration operator is not the same as the sign of the matrix element for the length operator.

The second case (the use of the SCF orbitals of a single state for the wave functions of both the initial and final states of a transition) may be regarded as a frozen-orbital approximation for $S(M)_{IF}$. It is, in a sense, similar to the use of Koopmans's Theorem for the IP of a system. In this case, the active-electron approximation gives the correct value for the transition matrix element since the orthonormality conditions $\langle \phi^{(I)}_{n\ell m} | \phi^{(F)}_{n'\ell m} \rangle = \delta_{n,n'}$ are satisfied.

In Table XX, the superscript on the ϕ indicates the state for which the orbital was computed. The entry "wrong sign" in the table means that the sign of the transition matrix element for the acceleration operator was not the same as the sign for the length operator; for exact eigenfunctions, the signs must be the same.

The nonrelativistic energy differences ΔE_{IF} were obtained by taking differences of the IP's given in Table XVIII; IP(exp) was used for the 3p- and 3s-hole states of the argon-like ions, and the 2p- and 2s-hole states of the neon-like ions; IP(nr) was used for the 2p-hole states of the argon-like ions, and for all the 1s-hole states; and IP(ΔE_{SCF}) was used for the 2s-hole states of the argon-like ions.

The calculations were performed using the accurate-set SCF functions given in Tables I-IV. The values of $S(M)_{IF}$ and ΔE_{IF} are given in atomic units. The column labeled "Diff." is the difference between $S(M)_{IF}$ evaluated using the dipole-length operator, and $S(M)_{IF}$ evaluated using the dipole-velocity or -acceleration operator. This difference is only given when the dipole matrix elements for $S(M)_{IF}$ have been computed between the many-electron SCF wave functions.

For all but one of the transitions given in Table XX, the dipole-length form of $S(M)_{IF}$ obtained using the orbitals of the closed-shell system (third line and first column for each transition) gives a significantly poorer result than that obtained using the orbitals for the initial and final states of the transition (first and second lines and first column for each transition). For the 3s-hole $\rightarrow$ 3p-hole transition of Ar^+, the improvement is 8%; for the 1s-hole $\rightarrow$ 3p-hole transition of Ar^+, the improvement is 40%. Only for the 2s-hole $\rightarrow$ 2p-hole transition of Ar^+ is the improvement as small as 1.5%.

For the dipole-velocity form of $S(M)_{IF}$, the frozen-orbital approximation sometimes gives a better result than the use of the SCF functions of the initial and final states of the transition. Here, we mean better in the sense of being more nearly equal to the dipole-length value of $S(M)_{IF}$ with the many-electron matrix element correctly evaluated. However, the agreement in these cases between the length and velocity forms of $S(M)_{IF}$ is not very good, and the better result of the frozen-orbital approximation does not have much meaning.

It seems, from the results given in Table XX, that the use of the SCF functions of the initial and final states of a transition gives a significantly better value for $S(M)_{IF}$ than the use of the frozen-orbital approximation.

In several cases, the value of $S(M)_{IF}$ obtained when the dipole transition matrix element is evaluated between total many-electron wave functions is quite different from the value obtained when the active-electron approximation is used. The difference is largest for transitions between the 1s-hole and the outermost p-hole states; it is smallest, and quite negligible, for transitions between the outermost s-hole and outermost p-hole states. The value of the many-electron matrix element cannot be much different from the active-electron approximation value unless the minors $D_{IF}(k|\ell)$, defined in Eqs. (33) and (34), are considerably different from one or zero. This condition is met for the former transitions, but not for the latter, where the orbitals of the initial and final states are too similar.

Note that the value of $S(M)_{IF}$ obtained using the many-electron expression for the matrix element is often larger than that obtained using the active-electron approximation. It has been suggested[77,78] that the correct evaluation of the matrix element simply corrects the active-electron approximation for overlap effects. If this were true, then the many-electron expression for the matrix element would always give a smaller result than the active-electron approximation since overlap effects always introduce a factor less than one. In several cases, transition integrals between orbitals other than the transition integral of the active-electron approximation must make significant contributions to the value of the matrix element. The best example of this is the 1s-hole → 3p-hole transition of Ar^+, where the value of dipole length form of $S(M)_{IF}$ using the many-electron matrix element is 30% larger than value in the active electron approximation.

In discussing the use of the length, velocity, and acceleration forms of the dipole matrix element, we will consider only the cases where the matrix element is evaluated between the many-electron SCF functions of the initial and final states. That is, of the values of $S(M)_{IF}$ in Table XX, only the values in the first row of each transition will be compared.

The values of the length and velocity forms of $S(M)_{IF}$ are always at least in reasonable, if not necessarily good, agreement. In the worst case, the 2s-hole → 2p-hole transition of Ar^+, the velocity form of $S(M)_{IF}$ is 30% smaller than the length form.

The acceleration form of $S(M)_{IF}$ often has absurd values. For several transitions, the acceleration form of $S(M)_{IF}$ is larger than the length and velocity forms by a factor of between 100 and 1000; and for one transition, the sign of the acceleration form of the matrix element, Eq. (44b), is

different from the signs of the length and velocity forms of the matrix element, Eqs. (30) and (44a). However, for transitions from 1s-hole states, the acceleration form of $S(M)_{IF}$ is in good agreement with the length and velocity forms. For the 1s-hole → 2p-hole transition of Ne^+ and the 1s-hole → 3p-hole transition of Ar^+, the difference between the length and acceleration forms of $S(M)_{IF}$ is, in fact, less than the difference between the length and velocity forms.

When the agreement between the length and acceleration forms of $S(M)_{IF}$ is good, the important one-electron transition integrals are between orbitals with simple structure. The orbitals involved either have no radial nodes (i.e., 1s and 2p), or the contribution to the value of the integral from the region around and past the radial node is small (i.e., 1s and 3p). When the important, one-electron transition integrals are between orbitals whose nodal structure is important in determining the value of the integral, the acceleration form of $S(M)_{IF}$ has poor values.

For transitions between outer-shell hole states, one might consider using some screened, effective, nuclear charge, Z_{eff}, for the acceleration form of the dipole transition matrix element. In place of Eq. (44b), the expression

$$I \cong \langle \Psi_I | [Z_{eff}/(\Delta E_{IF})^2] \Sigma \underset{\sim}{r}(k)/r(k)^3 \, | \, \Psi_F \rangle \tag{47}$$

would be used. For the 3s-hole → 3p-hole transition of Ar^+, $Z_{eff} = 0.7$ would be required to bring the length and acceleration forms of $S(M)_{IF}$ into agreement; for the 2s-hole → 2p-hole transition of Ne^+, $Z_{eff} = 1$ would be required. However, a reasonable value of Z_{eff} for these cases, based on arguments about the screening of the nuclear charge by the electron charge distribution (e.g., Slater's rules), must be $Z_{eff} \gtrsim 2$. Thus, even the use of a Z_{eff} will not give good values for the acceleration form of $S(M)_{IF}$.

The length form of the dipole transition matrix element has the advantage of being less sensitive than the velocity or acceleration forms to the precise shape of the approximate wave functions. The velocity operator involves derivatives of the orbitals, and the acceleration operator varies strongly and weighs different regions of r very differently. From these considerations, it would seem best to use the length form of the matrix element to evaluate $S(M)_{IF}$.

Chandrasekhar[79] has pointed out that larger values of r are more important for the evaluation of the length form of the dipole matrix element than for the evaluation of the total energy; conversely, smaller values of r are more important for the evaluation of the acceleration form of the matrix element than for the evaluation of the energy. Thus, Chandrasekhar suggests that the velocity form of the matrix element is the most suitable

form when the wave functions used have been obtained from an application of the variational principle.

He used the three forms of the matrix element for the calculation of transitions from the ground state to continuum states of the H^- ion. The use of the velocity form of the matrix element did, indeed, give better results. But, 6- and 12-term Hylleraas-type functions were used for the ground-state wave function of H^-. These functions are considerably more accurate than HF functions, and the conclusion above may not apply when HF wave functions are used to evaluate the transition matrix elements.

Weiss[80] has calculated oscillator strengths for several transitions of helium. He compared the results, for both the length and velocity forms of the matrix element, obtained by using HF functions and by using the more accurate Hylleraas-type functions. For all but three of these transitions, when HF wave functions were used, the value obtained with the length form of the matrix element was more accurate than that obtained with the velocity form. For two transitions, the use of the velocity form of the matrix element gave very poor results, while the results obtained with the length form were quite accurate. In the three cases in which the use of the velocity form of the matrix element gave better results, both the length and velocity forms gave good results; in these cases, the largest difference between the results obtained using the length and velocity forms with the HF wave functions was less than 5%. Bates and Damgaard[71] have compared the length and velocity forms of the multiplet strength, calculated using HF functions, with experimental values for several transitions of lithium and sodium. In all the cases they considered, the length form of the multiplet strength, although it sometimes gave poor values, was in better agreement with experiment than the velocity form. These calculations would seem to bear out the expectation that the use of the length form of the matrix element, when HF wave functions are used, will give more reliable results than the use of the velocity form.

The simple basis set SCF functions, given in Tables V-VIII, have also been used to calculate $S(M)_{IF}$. The agreement between the values obtained using the accurate-set SCF functions and the simple set SCF functions is quite good. For the length form of $S(M)_{IF}$, the differences between the values obtained using the simple and accurate set functions are never larger than 0.35%; for the velocity form of $S(M)_{IF}$, the differences are never larger than 0.10%. The greatest differences between the simple set and accurate set SCF orbitals are at the tails of the orbitals (c.f., Tables IX-XII). It is not surprising, then, that the differences for the velocity form of $S(M)_{IF}$ are sometimes less than those for the length form. For the acceleration form of $S(M)_{IF}$, the differences are somewhat larger than for the length and velocity forms, but only for the 2p-hole → 3s-hole transitions of Cl, Ar^+, and K^{++} is the agreement rather poor.

Varsavsky,[47] using a method based on screened nuclear charges, gives values of $S(M)_{IF}$ for a large number of ultraviolet transitions. Varsavsky's values and the values obtained from this calculation are compared in Table XXI. The values of $S(M)_{IF}$ given for this calculation are taken from Table XIX. Varsavsky's values are all approximately twice as large as the values of this calculation. It seems likely that he made an error of a factor of 2 in calculating $S(M)_{IF}$ from the value of the radial integral $\int_0^\infty P_{np}^{(I)} r\, P_{ns}^{(F)}\, dr$. The values of $S(M)_{IF}$ are, as usual, in atomic units.

TABLE XXI. Comparison of $S(M)_{IF}$ with Calculations by Varsavsky (Values of $S(M)_{IF}$ are in a.u.)

2s-hole → 2p-hole			
	F	Ne^+	Na^{++}
This calculation	2.065	1.463	1.086
Varsavsky*	5.011	2.991	1.977
3s-hole → 3p-hole			
	Cl	Ar^+	K^{++}
This calculation	5.36	4.14	3.30
Varsavsky*	11.53	8.30	6.23

*See Ref. 45.

Experimental data for the absolute or relative intensities of the X-ray lines computed here have not been found. However, a calculation of $\Gamma_K^{(R)}$, the radiative width of the 1s-hole state (or K state), can provide a comparison with experiment.

For the argon-like ions, 1s-hole → 2p-hole (Kα) and the 1s-hole → 3p-hole (Kβ) transitions make the most important contributions to $\Gamma_K^{(R)}$. All other transitions from the 1s-hole state involve at least double excitations (e.g., $1s2s^22p^63s^23p^6 \rightarrow 1s^22s^22p^63s3p^5ns$, $n \geq 4$) and are much less probable.

The value of $\Gamma_K^{(R)}$ for argon has been calculated using the values of $S(M)_{IF}$ given in Table XIX, the experimental values for the energies of the Kα and Kβ emission lines[62] [$\Delta E(K\alpha_1)$ = 108.70 Hartrees, $\Delta E(K\alpha_2)$ = 108.62 Hartrees, and $\Delta E(K\beta_1)$ = 117.26 Hartrees], and the relations of Eqs. (38-40). The value is found to be $\Gamma_K^{(R)}$ = 0.0835 eV. The K-shell

fluorescence yield for argon, as determined by Watanabe, Schnopper, and Cirillo,[81] is $\bar{\omega}_K = 0.140 \pm 0.014$. From Eq. (42), a value of the total width of the K-state $\Gamma_K = 0.60 \pm 0.06$ eV is obtained. The uncertainty in Γ_K is taken entirely from the uncertainty in the value of $\bar{\omega}_K$. Table XXII compares this value of Γ_K and values obtained directly from experimental data on X-ray emission and absorption by Watanabe[80] and by Deslattes.[52] The value which we have obtained is, within experimental uncertainties, in agreement with the experimental values.

TABLE XXII. A Comparison of Several Values of Γ_K for Argon

Author	Γ_K (eV)
Present Work	0.60 ± 0.06
Watanabe*	0.68 ± 0.03
Deslattes**	0.70 ± 0.05

*See Ref. 78.

**See Ref. 50.

ACKNOWLEDGMENTS

The author gratefully acknowledges many helpful discussions with, and encouragement from, Professor C. C. J. Roothaan and Dr. T. L. Gilbert, who jointly sponsored this research. He is indebted to Dr. Gilbert for pointing out the anomalous behavior of the correlation energy of the 2s-hole state of neon, and to Dr. A. J. Freeman for having suggested these calculations.

The author wishes to thank Dr. O. C. Simpson and the Solid State Science Division for their hospitality during his stay at Argonne National Laboratory. The author wishes to acknowledge that preliminary work, at The University of Chicago, on this publication was supported by the Advanced Research Projects Agency through the U. S. Army Research Office (Durham), under Contract No. DA-11-ORD-022-3119, and by a grant from the National Science Foundation.

REFERENCES

1. J. N. Bahcall, Phys. Rev. 129, 2683 (1963) and Phys. Rev. 131, 1756 (1963).
2. C. C. J. Roothaan, Rev. Modern Phys. 23, 69 (1951).
3. C. C. J. Roothaan, Rev. Modern Phys. 32, 179 (1960).
4. C. C. J. Roothaan and P. S. Bagus, Methods in Computational Physics (Academic Press, New York, 1963) Vol. II.
5. C. C. J. Roothaan, L. M. Sachs, and A. W. Weiss, Rev. Modern Phys. 32, 186 (1960).
6. L. M. Sachs, Phys. Rev. 124, 1283 (1961).
7. E. Clementi, C. C. J. Roothaan, and M. Yoshimine, Phys. Rev. 127, 1618 (1962).
8. C. C. J. Roothaan and P. S. Kelly, Phys. Rev. 131, 1177 (1963).
9. P. S. Bagus, T. L. Gilbert, C. C. J. Roothaan, and H. D. Cohen (to be published).
10. A. Sureau and G. Berthier, J. Phys. Radium 24, 672 (1963).
11. J. C. Slater, Quantum Theory of Atomic Structure (McGraw-Hill, New York, 1960), Vol. II.
12. R. Fieschi and P. O. Löwdin, Technical Note No. 4, Quantum Chemistry Group, Uppsala University, 1957 (unpublished).
13. R. K. Nesbet, Proc. Roy. Soc. (London) A230, 312 (1955).
14. R. E. Watson and A. J. Freeman, Phys. Rev. 123, 521 (1961).
15. P. O. Löwdin, Rev. Modern Phys. 35, 496 (1963).
16. D. R. Hartree, The Calculation of Atomic Structures (John Wiley and Sons, New York, 1957).
17. C. Froese, "Numerical Solution of the Hartree-Fock Equations" (to be published).
18. C. C. J. Roothaan and A. W. Weiss, Rev. Modern Phys. 32, 194 (1960).
19. P. O. Löwdin, Phys. Rev. 94, 1600 (1954).
20. H. A. Bethe and E. E. Salpeter, Quantum Mechanics of One- and Two-Electron Atoms (Academic Press, New York, 1957).
21. L. Pauling and E. B. Wilson, Introduction to Quantum Mechanics (McGraw-Hill, New York, 1935).

22. M. Cohen and A. Dalgarno, Rev. Modern Phys. 35, 506 (1963).

23. D. Layzer, Phys. Rev. 132, 735 (1963).

24. P. S. Bagus (to be published).

25. A. C. Wahl, Analytic Self-consistent Field Wave Functions and Computed Properties for Homonuclear Diatomic Molecules, ANL-6931 (August 1964).

26. J. T. Dehn, J. Chem. Phys. 37, 2549 (1962).

27. J. C. Slater, Phys. Rev. 42, 33 (1932).

28. P. O. Löwdin, Phys. Rev. 90, 120 (1953).

29. D. R. Hartree and W. Hartree, Proc. Roy. Soc. (London) A154, 588 (1936).

30. P. S. Bagus (in preparation).

31. C. E. Moore, Atomic Energy Levels, National Bureau of Standards Circular No. 467 (U. S. Government Printing Office, Washington, D. C., 1949) Vol. I, and corrections in Vol. II (1952) and Vol. III (1958).

32. B. H. Worsley, Can. J. Phys. 36, 289 (1958).

33. C. Froese, Proc. Cambridge Phil. Soc. 53, 206 (1957).

34. D. R. Hartree and W. Hartree, Proc. Roy. Soc. (London) A166, 450 (1938).

35. D. R. Hartree and W. Hartree, Proc. Roy. Soc. (London) A156, 45 (1936).

36. L. C. Allen, J. Chem. Phys. 34, 1156 (1961). (The cusp values given by Allen in Table 5 are incorrect.)

37. R. E. Watson and A. J. Freeman, Phys. Rev. 123, 521 (1961).

38. E. Clementi and A. D. McLean, Phys. Rev. 133, A419 (1964).

39. E. Clementi, J. Chem. Phys. 38, 1001 (1963).

40. Document No. 7440, ADI Auxiliary Publication Project, Library of Congress.

41. E. Clementi, J. Chem. Phys. 38, 2248 (1963).

42. C. Froese (private communication).

43. R. S. Berry and C. W. Reimann, J. Chem. Phys. 38, 1540 (1963).

44. R. S. Berry, C. W. Reimann, and G. N. Spokes, J. Chem. Phys. 37, 2278 (1962).

45. C. M. Varsavsky, Astrophys. J. Suppl. Ser. 6, No. 53, 75 (1961).

46. C. L. Pekeris, Phys. Rev. 112, 1649 (1958).

47. C. W. Scherr, J. N. Silverman, and F. A. Matsen, Phys. Rev. 127, 830 (1962).

48. Landolt-Bornstein (Springer-Verlag, Berlin, 1950) Vol. I, 1, Teil 8th Ed.

49. G. Brogren, Nova Acta Reg. Soc. Sci. Uppsala 14, Nr. 4 (1949).

50. R. D. Deslattes, Phys. Rev. 133, A390 (1964).

51. J. Valasek, Phys. Rev. 53, 274 (1938).

52. A. E. Sandström, Handbuch der Physik (Springer-Verlag, Berlin, 1957) Vol. XXX.

53. J. Valasek, Phys. Rev. 58, 213 (1940).

54. A. E. Lindh and O. Lundquist, Ark. Mat., Astronom. Fys. 18, Nr. 35 (1924).

55. F. Tyrén, Nova. Acta Reg. Soc. Sci. Uppsala 12, Nr. 1 (1940).

56. H. R. Moore and F. C. Chalklin, Proc. Phys. Soc. (London) A68, 717 (1955).

57. N. G. Johnson, Phys. Rev. 53, 434 (1938).

58. J. Shearer, Phil. Mag. 21, 501 (1936).

59. M. Siegbahn and T. Magnusson, Z. Physik 95, 133 (1935).

60. A. E. Lindh and A. Nilsson, Ark. Mat. Astronom. Fys. Ser. A31, Nr. 7 (1944).

61. M. Bačkovský and V. Dolejšek, Nature 136, 643 (1935).

62. M. Siegbahn and V. Dolejšek, Z. Physik 10, 159 (1922).

63. L. G. Parrat and E. L. Jossem, Phys. Rev. 97, 916 (1955).

64. F. Tyrén, Ark. Mat. Astronom. Fys. Ser. A25, Nr. 32 (1937).

65. D. H. Tomboulian and W. M. Cady, Phys. Rev. 59, 422 (1941).

66. J. C. Slater, Phys. Rev. 98, 1039 (1955).*

67. C. W. Scherr and J. N. Silverman, J. Chem. Phys. 37, 1154 (1962).

68. E. Clementi, J. Chem. Phys. 39, 175 (1963).

*Some care should be taken in using those IP's, given in this paper, that have been obtained from X-ray data. The conversion factor for wavelength from k XU's to A's, 1 k XU = 1.00202 A, has been neglected; and most of the X-ray term levels given in Table II are too large by this factor.

69. L. C. Allen, E. Clementi, and H. M. Gladney, Revs. Modern Phys. 35, 465 (1963).

70. N. R. Kestner (to be published).

71. D. R. Bates and A. Damgaard, Phil. Trans. Roy. Soc. London, Ser. A, 242, 101 (1949).

72. P. S. Kelly (to be published).

73. P. O. Löwdin, Phys. Rev. 97, 1474 (1955).

74. E. Feenberg and G. E. Pake, Notes on the Quantum Theory of Angular Momentum (Stanford University Press, Stanford, 1959).

75. R. W. Nicholls and A. L. Stewart, Atomic and Molecular Processes (Academic Press, New York, 1962) edited by D. R. Bates or C. W. Allen, Astrophysical Quantities (Athlone Press, London, 1963).

76. E. H. S. Burhop, The Auger Effect and Other Radiationless Transitions (Cambridge Press, Cambridge, 1952).

77. R. S. Knox, Phys. Rev. 110, 375 (1958).

78. T. Watanabe, Report No. 157, Materials Science Center, Cornell University (unpublished).

79. S. Chandrasekhar, Astrophys. J. 102, 223 (1945).

80. A. W. Weiss (private communication).

81. T. Watanabe, H. W. Schnopper, and F. N. Cirillo, Phys. Rev. 127, 2055 (1962).

ERRATUM

Page 44, second group, first line, last column, 0.1454 should read 0.1545; for $Ne^{+}(^{2}S)$ 1s-hole the $\langle r \rangle_{1s} = 0.1545$.

Reprinted from THE JOURNAL OF CHEMICAL PHYSICS, Vol. 41, No. 9, 2600–2611, 1 November 1964
Printed in U. S. A.

Analytic Self-Consistent Field Wavefunctions and Computed Properties for Homonuclear Diatomic Molecules*

ARNOLD C. WAHL†

Argonne National Laboratory, Argonne, Illinois and *Laboratory of Molecular Structure and Spectra, University of Chicago, Chicago, Illinois*

(Received 28 April 1964)

The analytic and computational framework for Hartree–Fock–Roothaan calculations on homonuclear diatomic molecules is presented. Several approaches to calculating the wavefunction are sketched as well as methods of computing molecular properties from the wavefunction. Emphasis is given to the efficient organization of these calculations for existing digital computers. Typical results obtained through the application of the programs and techniques developed are presented for the fluorine molecule.

I. INTRODUCTION

ALTHOUGH many calculations have been performed on diatomic molecules, few have been of sufficient depth and scope to establish the usefulness of the mathematical model. It is the purpose of this work to present the analytic and *inescapable computational* framework for Hartree–Fock–Roothaan calculations on diatomic molecules. Once the necessary one- and two-center one- and two-electron integrals are available,[1] it is possible to construct a variety of types of wavefunctions for diatomic molecules. Among these types of calculations are straight LCAO, valence-bond, atoms in molecules, limited configuration mixing, and self-consistent field molecular orbital calculations. The methods discussed in this paper apply to the calculations of analytic self-consistent field wavefunctions for homonuclear diatomic molecules via the Roothaan method. The analysis for the self-consistent field equations is well documented, and the programs available for atoms[2–4] remain virtually intact when linked to the calculation of the diatomic matrix and supermatrix elements. The methods employed to evaluate these elements have been presented recently.[1]

It should be emphasized that *even with the present large-memory high-speed digital computers* the calculations presented in this paper would be intractable unless a great deal of attention is given to possible economies in the analysis and organization of the matrix and supermatrix computations. What follows will present such an organization for the calculation of self-consistent field wavefunctions and properties for homonuclear diatomic molecules and the specific application of these programs to the F_2 molecule.

II. CHOICE OF UNITS, COORDINATE SYSTEMS, AND ATOMIC BASIS FUNCTIONS

Atomic units are used throughout this paper. In this system the unit of length is the bohr (0.52917 Å), the unit of energy the hartree ($2R_\infty hc = 27.20974$ eV), and the unit of charge that of the electron, e^-. In these units the electronic Hamiltonian for a diatomic molecule is

$$H=\sum_\mu(-\tfrac{1}{2}\Delta_\mu - Z_a/r_{a\mu} - Z_b/r_{b\mu}) + \sum_{\mu<\nu} 1/r_{\mu\nu}. \quad (1)$$

The sums are over the electrons of the molecule. The two centers are designated by subscripts a and b and their mutual separation by R. The quantities $r_{a\mu}$ and $r_{b\mu}$ are the distances from Nuclei a and b, respectively.

The position of the electrons with reference to the two centers is described in terms of the following three[1] coordinate systems:

(1) Cartesian coordinate systems centered on Nuclei a and b and on the midpoint between a and b, respectively. The z_a and z_b axes are chosen to lie along the internuclear axis pointing towards one another.

(2) Spherical coordinates centered on Nuclei a and b. The atomic orbitals are usually defined in terms of these coordinates.

(3) Prolate spheroidal coordinates with foci on Nuclei a and b. These coordinates are defined in terms of the spherical coordinates by

$$\xi=(r_a+r_b)/R; \qquad \eta=(r_a-r_b)/R; \qquad \phi=\phi_a=\phi_b. \quad (2)$$

The normalized *complex* STO's (Slater-type orbitals) are used throughout this paper. The STO's designated by $\chi_{ap\lambda a}$ or $\chi_{bp\lambda a}$ indicate the triple n, l, m and are given by

$$(n, l, m) = (2\zeta)^{n+\frac{1}{2}}[(2n)!]^{-\frac{1}{2}} r^{n-1} e^{-r\zeta} Y_{lm}(\theta, \phi), \quad (3)$$

where the spherical coordinate system is centered on Nucleus a or b and the $Y_{lm}(\theta, \phi)$ are the normalized

* Based on work performed under the auspices of the U.S. Atomic Energy Commission, and by Advanced Research Projects Agency through the U.S. Army Research Office (Durham) under Contract No. DA-11-022-ORD-3119, and by a grant from the National Science Foundation, NSF GP-28.

† NSF fellowship, 1961–1962.

[1] A. C. Wahl, P. E. Cade, and C. C. J. Roothaan, "A Study of Two Center Integrals Useful in Calculations on Molecular Structure" J. Chem. Phys. 41, 2578 (1964) (preceding article).

[2] C. C. J. Roothaan, Rev. Mod. Phys. 23, 69 (1951).

[3] C. C. J. Roothaan, Rev. Mod. Phys. 32, 179 (1960).

[4] C. C. J. Roothaan and P. S. Bagus, "Atomic Self-Consistent Field Calculations by the Expansion Method" Methods of Computational Physics, Vol. II (Academic Press Inc., New York).

complex spherical harmonics defined by

$$Y_{lm}(\theta, \phi) = \mathcal{P}_{lm}(\cos\theta)\Phi_m(\phi),$$

and

$$\Phi_m(\phi) = (2\pi)^{-\frac{1}{2}}e^{im\phi}; \tag{4}$$

and the normalized associated Legendre functions are defined by

$$\mathcal{P}_{lm}(\cos\theta) = \frac{1}{2^l l!}\left[\frac{2l+1}{2}\frac{(l-m)!}{(l+m)!}\right]^{\frac{1}{2}} \times(-\sin\theta)^m\left[\frac{d}{d\cos}\right]^{l+m}(\cos^2\theta-1)^l, \tag{5}$$

where $-l\leq m\leq l$.

In Eq. (3), n is taken as being a positive integer and zeta (ζ) is completely flexible.

The normalized associated Legendre functions are related to the unnormalized associated Legendre functions by

$$\mathcal{P}_{lm}(x) = \left[\frac{(2l+1)}{2}\frac{(l-m)!}{(l+m)!}\right]^{\frac{1}{2}}P_{lm}(x).$$

The $P_{lm}(x)$ functions are defined by

$$P_{lm}(x) = \frac{(-1)^m}{2^l l!}(1-x^2)^{\frac{1}{2}m}\frac{d^{l+m}}{dx^{l+m}}(x^2-1)^l. \tag{6}$$

For the calculation of the exchange integrals we make use of similar functions defined for $1\leq x\leq\infty$ by

$$\hat{P}_l^m(x) = \frac{(-1)^m}{2^l l!}(x^2-1)^{\frac{1}{2}m}\frac{d^{l+m}}{dx^{l+m}}(x^2-1)^l. \tag{7}$$

Details of these considerations are presented elsewhere.[1]

III. REVIEW OF GENERAL THEORY

The total N-electron wavefunction is put forth as an antisymmetrized product of MSO's[3]

$$\Phi = (N!)^{\frac{1}{2}}[\psi_1[1]\cdots\psi_N[N]] \tag{8}$$

where $[1, 2, \cdots N]$ indicates the operation of "alternation" and

$$\psi_\kappa{}^\mu = \varphi_{i(\alpha)}{}^\mu\eta_\kappa{}^\mu, \tag{9}$$

where the superscript μ stands for the space and spin coordinates of the μth electron, and the subscripts κ and i label the different MSO's and MO's, respectively. In the following we drop the superscript μ and subscript κ in order to simplify salient features of the MO $\varphi_{i(\alpha)}{}^\mu$ for the homonuclear diatomic molecule. In the expansion form of the self-consistent field method the molecular orbital φ_i is expanded in terms of a set of suitable functions called basis functions χ_p,

$$\varphi_i = \sum_p \chi_p C_{ip}, \tag{10}$$

where the C_{ip} are the expansion coefficients which are determined by the variational procedure. It is convenient to group the basis functions χ_p according to the symmetry of the molecular orbital

$$\chi_p \rightarrow \chi_{p\lambda\alpha}, \tag{11}$$

so that

$$\varphi_{i\lambda\alpha} = \sum_p \chi_{p\lambda\alpha}C_{i\lambda p}, \tag{12}$$

where λ is the symmetry species and α is the subspecies of symmetry λ.

The total electronic energy of the system is expressed in terms of matrices and supermatrices, whose elements are one- and two-electron integrals over the basis functions $\chi_{p\lambda\alpha}$, and suitably defined density matrices built from the coefficients $C_{i\lambda p}$.[2-4] The variational principle is applied to minimize the energy with respect to the linear parameters $C_{i\lambda p}$. By proper manipulation, the variational equations determining the coefficients $C_{i\lambda p}$ can be written in the form of pseudo-eigenvalue equations. These equations are customarily solved by the iterative SCF procedure. A complete and authoritative discussion of the self-consistent-field equations and process for atoms has been given recently by Roothaan and Bagus.[4] The reader is encouraged to refer to this work for details since the formalism for atoms is virtually the same as that for molecules.

IV. APPLICATION TO THE HOMONUCLEAR DIATOMIC MOLECULE

For the homonuclear diatomic molecule two-center symmetry basis functions belonging to the rotation–reflection group $D_{\infty h}$ are introduced by

$$\chi_{p\lambda\alpha} = (1/\sqrt{2})(\chi_{ap\lambda\alpha}+\sigma_\lambda\chi_{bp\lambda\alpha}), \tag{13}$$

where the subscripts a and b refer to the two atoms. In order for $\chi_{p\lambda\alpha}$ to have proper symmetry, it is obvious that $\chi_{ap\lambda\alpha}$ must be the mirror image of $\chi_{bp\lambda\alpha}$ when reflected through a plane midway between atoms a and b perpendicular to the internuclear axis. The parameter σ_λ is determined by the gerade or ungerade symmetry of the basis function $\chi_{p\lambda\alpha}$ and is given by $\sigma_\lambda = (-1)^{m_\lambda}$ for g symmetry and $\sigma_\lambda = (-1)^{m_\lambda+1}$ for u symmetry.

For given symmetry λ, the subspecies α permits two values; namely, $\alpha = \pm m_\lambda$ where m_λ is the value of the projection of orbital angular momentum on the internuclear axis. Henceforth the notation $\bar{m}_\lambda$ in lieu of $-m_\lambda$ is used. The introduction of symmetry basis functions permits considerable computational economies.

The variational principle is applied to minimize the total energy of the molecule yielding the Roothaan equations determining the linear coefficients $C_{i\lambda p}$. The expression for the total energy of the molecule is given by[3,4]

$$E = H^\dagger D_T + \tfrac{1}{2}D_T{}^\dagger\mathcal{P}D_T - \tfrac{1}{2}D_0{}^\dagger\mathcal{Q}D_0. \tag{14}$$

In the above expression the elements of the H matrix, which is a collection of all one-electron integrals between basis functions and is considered as a supervector, and the $\mathcal{P}$ and $\mathcal{Q}$ supermatrices, which are ordered collections of all two-electron integrals between basis functions, are only dependent upon the set of basis functions $\chi_{p\lambda\alpha}$ employed. The total density matrix D_T and the open-shell density matrix D_0, however, are constructed from the expansion coefficients $C_{i\lambda p}$ which are determined by the self-consistent-field process.[3,4]

The bulk of the diatomic SCF calculation is the evaluation of the matrix elements $H_{\lambda pq}$ and the supermatrix elements $\mathcal{P}_{\lambda pq,\mu rs}$ and $\mathcal{Q}_{\lambda pq,\mu rs}$, where λ and μ designate the symmetry of the basis functions, and p, q, r, s label the functions within a given symmetry. For the homonuclear diatomic molecule we have

$$H_{\lambda pq}=d_\lambda^{-1}\int\chi^*_{p\lambda\alpha}[-\tfrac{1}{2}\Delta-Z(r_a^{-1}+r_b^{-1})]\chi_{q\lambda\alpha}dV, \quad (15)$$

$$\mathfrak{J}_{\lambda pq,\mu rs}=(d_\lambda d_\mu)^{-1}\sum_{\alpha\beta}\iint\chi^*_{p\lambda\alpha}(1)\chi^*_{r\mu\beta}(2)\,(r_{12})^{-1}\times\chi_{q\lambda\alpha}(1)\chi_{s\mu\beta}(2)dV_1dV_2, \quad (16)$$

$$\mathfrak{K}_{\lambda pq,\mu rs}=(d_\lambda d_\mu)^{-1}\sum_{\alpha\beta}\iint\chi^*_{p\lambda\alpha}(1)\chi^*_{s\mu\beta}(2)\,(r_{12})^{-1}\times\chi_{r\mu\beta}(1)\chi_{q\lambda\alpha}(2)dV_1dV_2, \quad (17)$$

and

$$\mathcal{P}_{\lambda pq,\mu rs}=\mathfrak{J}_{\lambda pq,\mu rs}-\tfrac{1}{2}\mathfrak{K}_{\lambda pq,\mu rs},$$
$$\mathcal{Q}_{\lambda pq,\mu rs}=\alpha\mathfrak{J}_{\lambda pq,\mu rs}-\tfrac{1}{2}\beta\mathfrak{K}_{\lambda pq,\mu rs}, \quad (18)$$

where d_λ and d_μ are the dimensions of the representation λ, and the basis functions are given in terms of atomic functions by Eq. (13).

From Eq. (13) it is clear that $H_{\lambda pq}$ reduces to a sum of one- and two-center one-electron integrals, which can be evaluated in a straightforward manner. However, the evaluation of the supermatrix elements, $\mathfrak{J}_{\lambda pq,\mu rs}$ and $\mathfrak{K}_{\lambda pq,\mu rs}$ presents a formidable computational problem for any large molecular calculation. One of the economies which makes these calculations feasible in practice is that no single two-electron integral is ever computed as such. Instead the scalar product of a total ***symmetrized charge distribution*** with a ***one-center potential*** yields all ***Coulomb***[5,6] and ***hybrid***[5,6] integrals contributing to a given supermatrix element. Similarly, all ***exchange***[7] contributions are evaluated as the scalar product of a pair of two-center ***exchange functions*** symmetrized for the homonuclear diatomic molecule. Another important principle which leads to considerable economy is to confine all numerical work to a *manifold of points characteristic of the particular molecule being studied* and *chosen to be physically significant.* Finally the saving and interlacing of reusable information during the course of a lengthy calculation leads to a significant extension of computer capacity (particularly during the variation of orbital exponents).

[5] C. C. J. Roothaan, J. Chem. Phys. **19**, 1445 (1951).
[6] K. Ruedenberg, C. C. J. Roothaan, and W. Jaunzemis, J. Chem. Phys. **24**, 201 (1956).
[7] K. Ruedenberg, J. Chem. Phys. **19**, 1449 (1951).

V. CALCULATION OF THE MATRIX ELEMENTS

We write down the explicit expressions used for the evaluation of matrix elements, $H_{\lambda pq}$ and $S_{\lambda pq}$, for the homonuclear diatomic molecule, although the methods employed may be easily used to evaluate matrix elements for other operators. The formulas are

$$S_{\lambda pq}=d_\lambda^{-1}\sum_\alpha\int\chi^*_{p\lambda\alpha}\chi_{q\lambda\alpha}dV, \quad (19)$$

$$U_{\lambda pq}=d_\lambda^{-1}\sum_\alpha\int\chi^*_{p\lambda\alpha}(r_a^{-1}+r_b^{-1})\chi_{q\lambda\alpha}dV, \quad (20)$$

$$T_{\lambda pq}=-\tfrac{1}{2}d_\lambda^{-1}\sum_\alpha\int\chi^*_{p\lambda\alpha}\Delta\chi_{q\lambda\alpha}dV, \quad (21)$$

$$H_{\lambda pq}=T_{\lambda pq}-ZU_{\lambda pq}. \quad (22)$$

If we now introduce the explicit form of the symmetry basis function given by Eq. (13) and carry out the summation over α, we obtain

$$S_{\lambda pq}=\int\chi^*_{ap\lambda\alpha}\chi_{aq\lambda\alpha}dV+\sigma_\lambda\int\chi^*_{ap\lambda\alpha}\chi_{bq\lambda\alpha}dV, \quad (23)$$

$$U_{\lambda pq}=\int\chi^*_{ap\lambda\alpha}r_a^{-1}\chi_{ap\lambda\alpha}dV+\sigma_\lambda\int\chi^*_{ap\lambda\alpha}r_a^{-1}\chi_{bq\lambda\alpha}dV+\sigma_\lambda\int\chi^*_{ap\lambda\alpha}r_b^{-1}\chi_{bq\lambda\alpha}dV+\int\chi^*_{ap\lambda\alpha}r_b^{-1}\chi_{aq\lambda\alpha}dV, \quad (24)$$

$$T_{\lambda pq}=-\tfrac{1}{2}\int\chi^*_{ap\lambda\alpha}\Delta\chi_{aq\lambda\alpha}dV-\tfrac{1}{2}\sigma_\lambda\int\chi^*_{ap\lambda\alpha}\Delta\chi_{bq\lambda\alpha}dV. \quad (25)$$

The one-center integrals occurring in Eqs. (23–25) are easily computed via the functions[4]

$$V_i(x)=x^{-i-1}i!=\int_0^\infty dr\,r^ie^{-xr}. \quad (26)$$

The two-center Coulomb integral

$$\int\chi^*_{ap\lambda\alpha}r_b^{-1}\chi_{aq\lambda\alpha}dV$$

can be computed by applying the Laplace expansion[1] to r_b^{-1}.

The remaining two-center integrals are of the type

$$\int\chi^*_{ap\lambda\alpha}M\chi_{bq\lambda\alpha}dV,$$

where M is a one-electron operator. They are computed via the auxiliary functions $L_{\alpha\beta}^{\gamma\delta\epsilon}(\tau, \rho)$.[1,8]

The amalgamation of the various one-electron programs into the diatomic matrix program was done in a straightforward manner. Note that all integrals reduce to analytical expressions. The main programming consideration was to avoid any redundant computation. In any event, the evaluation of the one-electron matrix elements constitutes only a small fraction of the total computation time.

VI. REDUCTION OF THE SUPERMATRIX ELEMENTS TO INTEGRALS OVER CHARGE DISTRIBUTIONS

After introducing into Eqs. (16) and (17) the explicit form for $\chi_{p\lambda\alpha}$ given by Eq. (13), it is clear that the general supermatrix element may be considered to be the sum of electrostatic interactions of charge distributions built from products of atomic basis functions. A given charge distribution occurs in many supermatrix elements, and we use these distributions to achieve great computational economy in the evaluation of the supermatrices. The charge distributions which are particularly useful for the homonuclear molecule are

$$\Omega^{a}{}_{p\lambda\alpha,r\mu\beta}=\tfrac{1}{2}\chi^{*}{}_{ap\lambda\alpha}\chi_{ar\mu\beta},$$
$$\Omega^{ab}{}_{p\lambda\alpha,r\mu\beta}=\sigma_{\mu}\chi^{*}{}_{ap\lambda\alpha}\chi_{br\mu\beta}+\sigma_{\lambda}\chi^{*}{}_{bp\lambda\alpha}\chi_{ar\mu\beta}. \tag{27}$$

It is easily established that

$$\Omega_{p\lambda\alpha,r\mu\beta}=(-1)^{\alpha+\beta}\Omega^{*}{}_{p\lambda-\alpha,r\mu-\beta}, \tag{28}$$

which holds for charge distributions with the superscripts a or ab.

If we recast the expressions for the supermatrices $\mathcal{J}$ and $\mathcal{K}$ as given by Eqs. (16) and (17) in terms of these charge distributions (27) we obtain

$$\mathcal{J}_{\lambda pq,\mu rs}=\mathcal{J}^{c}{}_{\lambda pq,\mu rs}+\mathcal{J}^{x}{}_{\lambda pq,\mu rs},$$
$$\mathcal{K}_{\lambda pq,\mu rs}=\mathcal{K}^{c}{}_{\lambda pq,\mu rs}+\mathcal{K}^{x}{}_{\lambda pq,\mu rs}, \tag{29}$$

where

$$\begin{aligned}\mathcal{J}^{c}{}_{\lambda pq,\mu rs}=&[\Omega^{a}{}_{p\lambda\alpha,q\lambda\alpha}(1)\mid\Omega^{*a}{}_{r\mu\beta,s\mu\beta}(2)\\&+\Omega^{*ab}{}_{r\mu\beta,s\mu\beta}(2)+\Omega^{*b}{}_{r\mu\beta,s\mu\beta}(2)]\\&+[\Omega^{a}{}_{r\mu\beta,s\mu\beta}(1)\mid\Omega^{*a}{}_{p\lambda\alpha,q\lambda\alpha}(2)+\Omega^{*ab}{}_{p\lambda\alpha,q\lambda\alpha}(2)\\&+\Omega^{*b}{}_{p\lambda\alpha,q\lambda\alpha}(2)],\end{aligned} \tag{30}$$

$$\begin{aligned}\mathcal{K}_{\lambda pq,\mu rs}=&d_{\mu}^{-1}\sum_{\beta}\{[\Omega^{a}{}_{p\lambda\alpha,r\mu\beta}(1)\mid\Omega^{*a}{}_{q\lambda\alpha,s\mu\beta}(2)\\&+\Omega^{*ab}{}_{q\lambda\alpha,s\mu\beta}(2)+\sigma_{\lambda}\sigma_{\mu}\Omega^{*b}{}_{q\lambda\alpha,s\mu\beta}(2)]\\&+[\Omega^{a}{}_{q\lambda\alpha,s\mu\beta}(1)\mid\Omega^{*a}{}_{p\lambda\alpha,r\mu\beta}(2)\\&+\Omega^{*ab}{}_{p\lambda\alpha,r\mu\beta}(2)+\sigma_{\lambda}\sigma_{\mu}\Omega^{*b}{}_{p\lambda\alpha,r\mu\beta}(2)]\},\end{aligned}$$

$$\mathcal{J}^{x}{}_{\lambda pq,\mu rs}=\tfrac{1}{4}[\Omega^{ab}{}_{p\lambda\alpha,q\lambda\alpha}(1)\mid\Omega^{*ab}{}_{r\mu\beta,s\mu\beta}(2)], \tag{31}$$

$$\mathcal{K}^{x}{}_{\lambda pq,\mu rs}=\tfrac{1}{4}d_{\mu}^{-1}\sum_{\beta}[\Omega^{ab}{}_{p\lambda\alpha,r\mu\beta}(1)\mid\Omega^{*ab}{}_{q\lambda\alpha,s\mu\beta}(2)].$$

[8] C. C. J. Roothaan, J. Chem. Phys. 24, 947 (1956).

The methods which will be used for the evaluation of these supermatrix elements divide them naturally into two classes. The first class, Eqs. (30), consisting of the Coulomb and hybrid integrals, will be evaluated as scalar products between two vectors—one having as its components the values of a *reduced charge distribution*, the other having as its components the *weighted* values of the electrostatic *potential* arising from a one-center charge distribution. Both of these vectors occur over a two-dimensional manifold of points used for numerical integration. The second class, Eqs. (31), consisting of the exchange integrals, will also be evaluated as scalar products between two vectors; however, for this class the components of each vector are the values of a *weighted exchange function* over a one-dimensional manifold of points. This exchange function is obtained through the analysis[1] recently presented, organized specifically for distributions of the form $\Omega^{ab}{}_{p\lambda\alpha,r\mu\beta}$.

VII. COULOMB AND HYBRID INTEGRALS

For the evaluation of the supermatrix contributions $\mathcal{J}^{c}{}_{\lambda pq,\mu rs}$ and $\mathcal{K}^{c}{}_{\lambda pq,\mu rs}$ the analysis given recently[1] was organized for the computation of large batches of integrals and for the symmetry $D_{\infty h}$. Since the integration over the angle ϕ is done analytically, the functions necessary for the numerical evaluation of the Coulomb and hybrid integrals need to be tabulated only over a two-dimensional manifold of points. The selection of this manifold is strongly influenced by the particular two-dimensional integration scheme used. In principle this integration can be performed over *any* two-dimensional coordinate system; in practice, however, the accuracy and reliability obtained strongly depends on the specific choice of the manifold. After various attempts, it was found that a grid constructed as the direct product of two Gaussian grids over the prolate spheroidal coordinates ξ and η was most satisfactory.

Since all numerical work for the evaluation of the Coulomb and hybrid integrals is confined to the chosen manifold, which is referred to as P, it is useful to define the *reduced atomic basis functions* $\chi_{ap\lambda\alpha}(P)$ by means of

$$\chi_{ap\lambda\alpha}(P,\phi)=\chi_{ap\lambda\alpha}(P)e^{i\alpha\phi}/(2\pi)^{\frac{1}{2}}. \tag{32}$$

From these reduced atomic basis functions we can build the *reduced one-center charge distributions*

$$\Omega^{a}{}_{p\lambda\alpha,r\mu\beta}(P)=\tfrac{1}{2}\chi_{ap\lambda\alpha}(P)\,\chi_{ar\mu\beta}(P), \tag{33}$$

and a *reduced symmetrized two-center charge distribution*

$$\begin{aligned}\Omega^{ab}{}_{p\lambda\alpha,r\mu\beta}(P)=&\sigma_{\mu}\chi_{ap\lambda\alpha}(P)\,\chi_{br\mu\beta}(P)\\&+\sigma_{\lambda}\chi_{bp\lambda\alpha}(P)\,\chi_{ar\mu\beta}(P).\end{aligned}$$

At this point it is convenient to limit considerations to the use of $\alpha=m_{\lambda}$ and $\beta=\pm m_{\mu}$ and to the *only* combination of the reduced distributions of Eqs. (33) which will appear in the working formulas for the super-

matrices of the homonuclear diatomic molecule. We accordingly define *reduced homonuclear distributions* by

$$\Omega'^{+}_{p\lambda r\mu}(P)=\Omega^{a}_{p\lambda m_\lambda,r\mu m_\mu}(P)+\Omega^{ab}_{p\lambda m_\lambda,r\mu m_\mu}(P)+\sigma_\lambda\sigma_\mu\Omega^{b}_{p\lambda m_\lambda,r\mu m_\mu}(P), \quad (34)$$

$$\Omega'^{-}_{p\lambda r\mu}(P)=\Omega^{a}_{p\lambda m_\lambda,r\mu \bar{m}_\mu}(P)+\Omega^{ab}_{p\lambda m_\lambda,r\mu \bar{m}_\mu}(P)+\sigma_\lambda\sigma_\mu\Omega^{b}_{p\lambda m_\lambda,r\mu \bar{m}_\mu}(P).$$

It is easily shown from the properties of the spherical harmonics[1,9] that

$$\Omega'^{-}_{p\lambda r\mu}(P)=(-1)^{m_\mu}\Omega'^{+}_{p\lambda r\mu}(P). \quad (35)$$

The second quantity necessary for the evaluation of the Coulomb and hybrid integrals as scalar products over the manifold P is the weighted potential arising from a one-center distribution. These weighted potentials may be developed from the familiar[1] one-center potentials obtained by the integration over the coordinates of one electron

$$U^{+}_{p\lambda r\mu}(2)=\int\Omega^{a}_{p\lambda m_\lambda,r\mu m_\mu}(1)\,(r_{12})^{-1}dV_1,$$

$$U^{-}_{p\lambda r\mu}(2)=\int\Omega^{a}_{p\lambda m_\lambda,r\mu \bar{m}_\mu}(1)\,(r_{12})^{-1}dV_1, \quad (36)$$

where the above integration is performed *analytically* in a *spherical* coordinate system centered on Nucleus a. The definition of the potential Eqs. (36) has been limited to Center a since reference to only one center is necessary for the final evaluation of the integrals due to the $D_{\infty h}$ symmetry of the distributions Eqs. (34). The specific reference to Electrons 1 and 2 in Eqs. (36) is only necessary to formally define these potentials. Once defined, they may be considered as functions of three dimensions and the reference to the coordinates of Electron 2 dropped. Since we will need only the dependence of this function over the manifold P we define the *reduced potentials by*

$$U^{\pm}_{p\lambda r\mu}(P,\phi)=\mathrm{U}^{\pm}_{p\lambda r\mu}(P)\exp[-i(m_\lambda\mp m_\mu)\phi]. \quad (37)$$

From this reduced potential we construct the *reduced weighted potentials* over the manifold P defined by

$$\mathrm{V}^{\pm}_{p\lambda r\mu}(P)=W(P)\,\mathrm{U}^{\pm}_{p\lambda r\mu}(P), \quad (38)$$

where $W(P)$ is the weight factor necessary for the numerical integration over the manifold P. It arises from the Gaussian weight factors and the volume element in the prolate spherical coordinate system.

For the $\mathcal{J}$ supermatrix only the limited class of distributions $\Omega'^{+}_{p\lambda q\lambda}$ and potentials $\mathrm{V}^{+}_{p\lambda q\lambda}$ are needed. We therefore introduce the abbreviated notation defined by

$$\Omega'_{\lambda pq}(P)=\Omega'^{+}_{p\lambda q\lambda}(P),$$

$$\mathrm{V}_{\lambda pq}(P)=\mathrm{V}^{+}_{p\lambda q\lambda}(P). \quad (39)$$

[9] M. E. Rose, *Elementary Theory of Angular Momentum* (John Wiley & Sons, Inc., New York, 1957), Chap. III.

The working expressions for the Coulomb and hybrid integral contributions then become

$$\mathcal{J}^{a}_{\lambda pq,\mu rs}=\mathrm{V}_{\lambda pq}\cdot\Omega'_{\mu rs}+\mathrm{V}_{\mu rs}\cdot\Omega'_{\lambda pq},$$

$$\mathcal{K}^{a}_{\lambda pq,\mu rs}=\tfrac{1}{2}[\mathrm{V}^{+}_{\lambda p\mu r}+(-1)^{m_\mu}\mathrm{V}^{-}_{\lambda p\mu r}]\cdot\Omega'^{+}_{\lambda q\mu s}+\tfrac{1}{2}[\mathrm{V}^{+}_{\lambda q\mu s}+(-1)^{m_\mu}\mathrm{V}^{-}_{\lambda q\mu s}]\cdot\Omega'^{+}_{\lambda p\mu r}. \quad (40)$$

VIII. EXCHANGE INTEGRALS

The exchange supermatrix contributions, $\mathcal{J}^{x}_{\lambda pq,\mu rs}$ and $\mathcal{K}^{x}_{\lambda pq,\mu rs}$, were evaluated by a straightforward application of the methods presented recently.[1] Again the incorporation of the $D_{\infty h}$ symmetry of the charge distributions $\Omega^{ab}_{p\lambda\alpha,r\mu\beta}$ into the analysis leads to significant computational economies. Both $\mathcal{J}^{x}_{\lambda pq,\mu rs}$ and $\mathcal{K}^{x}_{\lambda pq,\mu rs}$ can be considered as special cases of the general integral

$$X_{p\lambda\alpha,r\mu\beta;m_\nu\gamma,n\kappa\delta}=[\Omega^{ab}_{p\lambda\alpha,r\mu\beta}(1)\mid\Omega^{*ab}_{m_\nu\gamma,n\kappa\delta}(2)], \quad (41)$$

where ν and κ indicate symmetry species, and γ and δ subspecies. It is computationally convenient to formulate this integral as the scalar product of two vectors over a one-dimensional manifold of points, where the manifold is defined by the numerical aspects of the exchange integral analysis. Each of these vectors arises from an *exchange function* determined by a charge distribution.

It is easily shown[1,7] that the basis function product $\chi_{ap\lambda\alpha}\chi^{*}_{br\mu\beta}$ may be expanded in prolate spheroidal coordinates by

$$(-1)^{\beta}(\tfrac{1}{2}R)^{3}(\xi^2-\eta^2)\chi_{ap\lambda\alpha}\chi_{br\mu-\beta}=(-1)^{\beta}K_{ab}\omega(\xi,\eta)\exp(-\rho\xi-\tau\rho\eta)\times[(\xi^2-1)(1-\eta^2)]^{\frac{1}{2}M}\Phi_\alpha(\phi)\Phi_{-\beta}(\phi), \quad (42)$$

where

$$\omega(\xi,\eta)=\sum_n\sum_j a_{nj}\xi^n\eta^j,$$

and

$$M=\alpha-\beta.$$

The normalization factor K_{ab}, the parameters ρ and τ, and the expansion coefficients a_{nj} are determined by the product $\chi_{ap\lambda\alpha}\chi_{br\mu-\beta}$. Since the distribution $\Omega^{*ab}_{p\lambda\alpha,r\mu\beta}$ is a linear combination of two basis function products which differ only by the inversion of the centers a and b, it may be expanded by

$$(\tfrac{1}{2}R)^{3}(\xi^2-\eta^2)\Omega^{*ab}_{p\lambda\alpha,r\mu\beta}=(-1)^{\beta}K_{ab}[(\xi^2-1)(1-\eta^2)]^{\frac{1}{2}M}\times\Phi_\alpha(\phi)\Phi_{-\beta}(\phi)e^{-\rho\xi}[\sigma_\lambda\omega(\xi,\eta)e^{-\tau\rho\eta}+\sigma_\mu\omega(\xi,-\eta)e^{\tau\rho\eta}]. \quad (43)$$

The introduction of these expanded distributions into the expression (41) is followed by familiar steps.[1,7] First the Neuman expansion for $1/r_{12}$ is introduced and the trivial integration over the angles ϕ_1 and ϕ_2 performed. Then, the results of the analytic integrations over η_1 and η_2 are expressed in terms of the

auxiliary functions[1,7] defined by

$$B_j^{Ml}(\rho\tau)=\int_{-1}^{1}d\eta\,\eta^j(1-\eta^2)^{\frac{1}{2}M}\mathcal{P}_l^M(\eta), \qquad (44)$$

for which it is easily verified that

$$B_j^{Ml}(-\rho\tau)=(-1)^{l+M+j}B_j^{Ml}(\rho\tau).$$

Finally, several partial integrations over the variables ξ_1 and ξ_2 lead to the following expression:

$$X_{p\lambda\alpha,r\mu\beta;ms\gamma,nu\delta}=(-1)^{\beta+\delta}\sum_{l=l\,\min}^{\infty}I^l{}_{p\lambda\alpha,r\mu\beta;ms\gamma,nu\delta}, \qquad (45)$$

where

$$I^l{}_{p\lambda\alpha,r\mu\beta;ms\gamma,nu\delta}$$
$$=4R^{-1}[\sigma_\lambda+\sigma_\mu(-1)^{l+M}][\sigma_\nu+\sigma_\kappa(-1)^{l+M}]$$
$$\times\int_1^\infty\frac{d\xi}{(\xi^2-1)[\hat{P}_l^M(\xi)]^2}$$
$$\times F^M{}_{l;p\lambda\alpha,r\mu\beta}(\xi;\rho,\tau)\,F^M{}_{l;ms\gamma,nu\delta}(\xi;\rho,\tau)$$

and

$$F^M{}_{l;p\lambda\alpha,r\mu\beta}(\xi;\rho,\tau)=K_{ab}\int_1^\xi dx\,\hat{P}_l^M(x)\,(x^2-1)^{\frac{1}{2}M}$$
$$\times\sum_j B_j^{Ml}(\rho\tau)\sum_n a_{nj}x^n\sigma_{\overline{\gamma}}^{\overline{m}}. \qquad (46)$$

Note that the $I^l{}_{p\lambda\alpha,r\mu\beta,ms\gamma,nu\delta}$ integral vanishes identically unless $\sigma_\lambda\sigma_\mu=\sigma_\nu\sigma_\kappa$ and $\alpha-\beta=\gamma-\delta$. The parameters ρ and τ, the indices n and j, and the coefficients a_{nj} entering into this auxiliary function are determined by the charge distribution $\Omega^{ab}{}_{p\lambda\alpha,r\mu\beta}$ through Eqs. (42) and (43).

The numerical scheme presented recently[1] was used to evaluate the integrals $I^l{}_{p\lambda\alpha,r\mu\beta;ms\gamma,nu\delta}$, namely, Simpson's rule integrations over the variables ξ and x. This numerical procedure was used to avoid many complications[7] which arise in the analytic evaluation of these integrals over the numerous orbital products appearing as integrands. The Simpson's rule integration introduces in a natural way the manifold S as the selection of points used for the numerical integrations (see Appendix). For the purpose of organizing the numerical work in the simplest possible terms it is useful to define the *weighted exchange function* over this manifold S by

$$\mathbf{G}^+{}_{l;p\lambda r\mu}(S)$$
$$=(-1)^{m_\mu}2R^{-1}[W(S)]^{\frac{1}{2}}[(S^2-1)^{\frac{1}{2}}\hat{P}_l^{m_\lambda-m_\mu}(S)]^{-1}$$
$$\times F^{m_\lambda-m_\mu}{}_{l;p\lambda m_\lambda,r\mu\overline{m}_\mu}(S;\rho,\tau),$$

$$\mathbf{G}^-{}_{l;p\lambda r\mu}(S)$$
$$=(-1)^{m_\mu}2R^{-1}[W(S)]^{\frac{1}{2}}[(S^2-1)^{\frac{1}{2}}\hat{P}_l^{m_\lambda+m_\mu}]^{-1}$$
$$\times F^{m_\lambda+m_\mu}{}_{l;p\lambda m_\lambda,r\mu m_\mu}(S;\rho,\tau), \qquad (47)$$

where $W(S)$ is the necessary weight factor for the Simpson's rule integration over the manifold.

For the exchange contribution to the supermatrix $\mathcal{G}$ only the limited class of exchange functions, namely, $\mathbf{G}^+{}_{l;p\lambda q\lambda}$ will be needed. As was done for the Coulomb hybrid contribution we introduce the abbreviated notation

$$\mathbf{G}_{l;\lambda pq}(S)=\mathbf{G}^+{}_{l;p\lambda q\lambda}(S). \qquad (48)$$

The final working expression for the exchange integral contribution to the supermatrices in terms of scalar products are

$$\mathcal{J}^x{}_{\lambda pq,\mu rs}=\sum_{l=0}^{\infty}{}^{2}\mathbf{G}_{l;\lambda pq}\cdot\mathbf{G}_{l;\mu rs}$$

$$\mathcal{K}^x{}_{\lambda pq,\mu rs}=\sum_{l=\left[\frac{m_\lambda-m_\mu}{m_\lambda-m_\mu+1}\right]}^{\infty}{}^{2}\mathbf{G}^+{}_{l;p\lambda r\mu}\cdot\mathbf{G}^+{}_{l;q\lambda s\mu}$$
$$+\sum_{l=\left[\frac{m_\lambda+m_\mu}{m_\lambda+m_\mu+1}\right]}^{\infty}{}^{2}\mathbf{G}^-{}_{l;p\lambda r\mu}\cdot\mathbf{G}^-{}_{l;q\lambda s\mu}, \qquad (49)$$

where in the summations over l, the smaller lower limit is used if $\sigma_\lambda\sigma_\mu(-1)^{m_\lambda+m_\mu}=1$ and the larger lower limit if $\sigma_\lambda\sigma_\mu(-1)^{m_\lambda+m_\mu}=-1$. Also note that the summation over l proceeds in steps of two. This economy results from the inversion symmetry of the distributions Eq. (43).

IX. CALCULATION OF THE WAVEFUNCTION

Fully automatic computer programs were built which incorporated the analysis and organization discussed in Secs. I–VIII of this paper.[3,4] These programs, which computed the H matrix and the supermatrices, $\mathcal{P}$ and $\mathcal{Q}$, were linked to a modified version of the atomic SCF program written at the University of Chicago and Argonne National Laboratory.[4] The modifications which had to be made in the atomic SCF programs were, of course, complete replacement of the atomic integral computation, new closed- and open-shell weight factors, and extensive changing of the "screening" of input data and printing of results to fit the diatomic molecule. The specifications for the preparation of input and use of the molecular program are given in Appendix B.

Once such a program exists it is possible to use it in a variety of ways ranging from the calculation of very crude SCF wavefunctions[11,12] to an attempt to reach the molecular Hartree–Fock function for the ground and excited states of diatomic molecules.[12–16] There are, of course, an infinite number of crude functions

[10] Laboratory of Molecular Structure and Spectra, University of Chicago (Arnold C. Wahl).
[11] B. J. Ransil, Rev. Mod. Phys. **32**, 245 (1960).
[12] J. Eve, Proc. Roy. Soc. (London) **246**, 582 (1958).
[13] P. E. Cade, K. D. Sales, and A. C. Wahl, "The Electronic Structure of the Nitrogen Molecule", J. Chem. Phys. (to be published).
[14] W. Huo, "The Electronic Structure of CO and BF," Ph.D. thesis, University of Chicago.
[15] A. C. Wahl, "SCF Wavefunction and Properties for Cl_2" (to be published).
[16] A. C. Wahl and T. L. Gilbert, "A Theoretical Study of the Cl_2^- Molecule–Ion," Phys. Rev. (to be published).

which may be calculated depending upon the use for which they are desired and in many cases personal taste. There is within the framework of the analysis, however, only one molecular Hartree–Fock function. It has been the goal of this work to make it possible to approach very closely the molecular Hartree–Fock function with a truncated expansion. Since this function may be represented by several choices of basis sets, and currently the path to the "final" function depends on computer economics, program capacity, intuition, and previous data, a brief discussion of the approaches used in this work is in order.

The gradual improvement of the molecular wavefunction depends upon the judicious addition of basis functions $\chi_{p\lambda\alpha}$ and the optimization of the orbital exponents of the added functions in order to make them most effective. This improvement process may be done in many different ways. Two distinct methods were employed in this work.

The first method was to start with a minimal basis set, optimize the basis function exponents in a coupled way, using chemical intuition and computer experimentation to determine which functions should influence each other, gradually add new basis functions, and optimize the new exponents. This process was continued until the total molecular energy showed little further improvement upon the addition of new functions or until program capacity was exhausted. The second method was to start the molecular calculation with a large basis set which was obtained *independently* for the constituent *atoms*, singly optimize each basis function exponent, and add functions with higher quantum numbers to each molecular symmetry with optimization of the new exponents. Ideally these two methods would lead to the same result; however, since computer economics makes extensive coupled optimization of the molecular basis function exponents intractable, the *exhaustively* optimized *atomic basis sets*[17] appear to be an energetically better representation of the molecular wavefunction after the exponents are merely singly optimized and functions with higher l values added to each molecular symmetry. These considerations will be elaborated in forthcoming work.[13–16] It is sufficient to say here that the atomic Hartree–Fock function is a dominant contributor to the molecular Hartree–Fock function and forms a very good starting point for the further development of the molecular wavefunction. Currently attempts are being made to develop some wavefunction "prescription" which by starting with atomic basis sets will efficiently lead to the molecular Hartree–Fock function with a minimum of effort.

X. CALCULATION OF MOLECULAR PROPERTIES

In order to evaluate any molecular property characterized by an operator M which has cylindrical symmetry, the matrix elements defined by

$$M_{\lambda pq}=\int \chi^*_{p\lambda\alpha} M \chi_{q\lambda\alpha} dV \tag{50}$$

are necessary. We may conveniently evaluate the matrix element $M_{\lambda pq}$ as the scalar product of two vectors over the manifold P. For this purpose we introduce still *another reduced homonuclear distribution* defined by

$$\Omega_{\lambda pq}(P)=\Omega^a{}_{p\lambda\alpha,q\lambda\alpha}(P)+\tfrac{1}{2}\Omega^{ab}{}_{p\lambda\alpha,q\lambda\alpha}(P)+\Omega^b{}_{p\lambda\alpha,q\lambda\alpha}(P) \tag{51}$$

and the *weighted property operator* defined by

$$\mathbf{M}(P)=W(P)M(P),$$

where $M(P)$ is the value of the property operator over the manifold P and as before $W(P)$ is the weight factor necessary for the numerical integration over the manifold. We may integrate analytically over the angle ϕ. The general expression for the property matrix elements are then

$$M_{\lambda pq}=\mathbf{M}\cdot\Omega_{\lambda pq}. \tag{52}$$

The molecular property is given as the inner product of the density matrix with the property matrix (52) where both are considered as supervectors by

$$M=D_T\cdot M. \tag{53}$$

A quantity often of interest, the contribution of a given orbital to this property, may be defined in terms of the contribution of the ith orbital to the density matrix:

$$M_i=D_i\cdot M, \tag{54}$$

where D_i contains only coefficients from Orbital i. This numerical scheme is conceptually simple, and a very large class of properties can be evaluated in this way, particularly since most differential operators can be expressed as multiplicative ones.[1] An important feature of this method is its generality and easy extendability. The basic quantities needed are only the charge distributions $\Omega_{\lambda pq}$ and the weighted property operator $\mathbf{M}$ over the manifold of points P. Properties characterized by operators which have strong singular behavior at one of the nuclei can be evaluated by this method if a suitable manifold P is designed; however, better methods exist for the calculation of this type of operator.

For the evaluation of spectroscopic constants, use must be made of the computed SCF potential curve for the molecule. This computed potential curve has two serious shortcomings. The first is that the molecular orbital wavefunction dissociates properly only for a limited class of systems. For all others it dissociates into a sum of neutral and ionic atomic states. Although this error is largest at $R=\infty$ it probably also tends to raise the molecular energy even at the equilibrium internuclear distance. Even if the proper dissociation

[17] P. Bagus and T. L. Gilbert, "Accurate SCF Wavefunctions for First Row Atoms and Ions," Phys. Rev. (to be published).

took place, there is the second error which tends to raise the molecular energy. This is the increased correlation energy in the molecule. Both of these factors lower the computed dissociation energy which in this work is defined as

$$D_e = E_{\text{molecule}} - 2E_{\text{atom}}, \tag{55}$$

where E_{atom} is the Hartree–Fock atomic energy. Often the sum of these two errors is sufficient to completely overshadow the comparatively small binding energy of many diatomic systems. However, the failure of the molecular wavefunction to show binding on this basis (55) does not completely obviate the significance of the SCF potential energy curve. We may certainly say that

$$E_{\text{exact}} = E_{\text{Hartree–Fock}} + \Delta E, \tag{56}$$

where ΔE is the correction energy. It is not *unreasonable* to expect that over *any small* range of R, for instance, near the computed potential minimum ($R_e - \Delta R < R < R_e + \Delta R$ where $\Delta R \sim 0.25$ a.u.) that ΔE is roughly constant so that

$$dE_{\text{exact}}/dR \sim dE_{\text{Hartree–Fock}}/dR. \tag{57}$$

This should allow the equilibrium internuclear distance and the *first*-order spectroscopic constants to be predicted fairly well. In this work a Dunham analysis was used over the region near the equilibrium internuclear distance, and the first-order spectroscopic constants thus obtained show fair agreement with experiment.

Total electronic charge densities for the molecule are defined by

$$\Omega = \sum_{\lambda}\sum_{p}\sum_{q} D_{\lambda pq}\Omega_{\lambda pq}. \tag{58}$$

In order to visualize these densities they are normally plotted as contour lines in the x, z plane. These lines are defined by

$$\Omega(x, z) = C, \tag{59}$$

where C is the value of the density for which a contour is desired. Although the total charge density is significant, orbital densities, obtained by including only the contributions of a given orbital to the density matrix, should be of even greater interest. These orbital densities should prove useful in studying the visual aspect of molecular and atomic orbital comparisons, concepts like S–P hybridization, and the difference between bonding and antibonding orbitals. These contours are currently produced and plotted automatically by the computer.

XI. DETAILS OF THE COMPUTATION

The following is a list of some general computational considerations which make these calculations possible with existing computing facilities.

(1) The reliability and accuracy of the methods used to evaluate the supermatrices depend upon the proper selection of the manifolds P and S. This selection is discussed in the Appendix. It should be noted that the three basic working functions $\mathbf{V}^{\pm}_{p\lambda r\mu}$, $\mathbf{\Omega}'^{+}_{p\lambda r\mu}$, and $\mathbf{G}^{\pm}_{l;p\lambda r\mu}$ depend only upon a single pair of basis functions. This retains the computational identity of Electrons 1 and 2, and thus the most arduous part of the supermatrix evaluation, namely, the evaluation of these three types of functions, need be done for approximately $\sum_{\mu}\sum_{\lambda} n_\lambda n_\mu$ basis function pairs as opposed to the square of this dependence which would arise if this identity were sacrificed. (n_λ is the number of basis functions in symmetry λ.) Also the conceptual simplicity of this formulation makes it easily extendable to polyatomic systems. The main further developments necessary are the selection of the manifolds, characteristic of the molecule under study, over which numerical work will be done and a general reorganization for the multicenter geometry.

(2) In order to avoid extensive redundant computation in the evaluation of the supermatrices it is necessary to have *all* vectors $\mathbf{V}^{\pm}_{p\lambda r\mu}$ available when *a* vector $\mathbf{\Omega}'^{+}_{p\lambda r\mu}$ is constructed. The size of existing computer memories make this impossible for a moderately large basis set. Therefore the manifold P was divided into regions determined by values of the prolate spheroidal coordinate ξ. The vector tabulations were then made only over a region in the manifold and the total supermatrix contribution evaluated as the sum of the regional integrations.

(3) The convergence of the Coulomb and hybrid integrals as a function of the number of points in the manifold P was a matter of experimentation and depended upon the molecule under investigation. It was found that the ξ integration should be truncated at $\xi < 50/\zeta_{\min} R$, where $\zeta_{\min}$ is the minimum exponent in the basis set, and that a grid of 20 points on each of the variables ξ and η was sufficient for studies of first-row diatomic systems. For investigations of second-row molecules, however, grids of 36 points were found to be necessary.

The convergence of the exchange integrals as a function of l in the Neumann expansion is controlled by a single threshold. When all contributions arising from a given vector $\mathbf{G}^{\pm}_{l;p\lambda r\mu}$ are below this threshold in absolute value, the calculation of this vector is terminated. The iteration on l is terminated when the contributions for all vectors $\mathbf{G}^{\pm}_{l;p\lambda r\mu}$ lie below this threshold *or* when $l = 30$. Should the latter occur, a record is made of the largest last contribution and the calculations continued. In practice, the exchange contributions have converged well before $l = 30$. It was found that 40 points in the manifold S were sufficient for all exchange integrals occurring in studies of first- and second-row molecules.

(4) Due to the numerical characteristics of the exchange integral analysis it was necessary to scale the functions $P_l^M(x)$, e^{-x}, and $B_j^{lm}(x)$.

(5) During the variation of orbital exponents a great deal of machine time may be saved by the saving and

TABLE I. Near Hartree-Fock wavefunction for the ground state of F_2.

	Internuclear distance = 2.68 (bohrs)						
Molecular symmetry species	Basis functions (quantum numbers, orbital exponents)						
	σ_g			σ_u		π_u	π_g
	1S 8.27336			1S 8.28062		2P 1.67164	2P 1.58741
	1S13.17191			1S13.16925		2P 3.20350	2P 3.18020
	3S 4.90649			3S 5.03602		2P 6.11692	2P 6.15863
	2S 2.26251			2S 2.23962		3D 2.49433	3D 2.43222
	2P 1.84915			2P 1.44746		4F 2.85001	4F 2.56431
	2P 3.26935			2P 3.00518			
	2P 5.85912			2P 6.35647			
	3D 2.44269			3D 3.60759			
	4F 2.83176			4F 1.52251			
	Total energy (hartrees) −198.76825			Potential energy (hartrees) −397.35489		Kinetic energy (hartrees) 198.58664	Virial theorem −2.0009145
Molecular orbital	$1\sigma_g$	$2\sigma_g$	$3\sigma_g$	$1\sigma_u$	$2\sigma_u$	$1\pi_u$	$1\pi_g$
Orbital energy (hartrees)	−26.42269	−1.75654	−0.74604	−26.42244	−1.49499	−0.80523	−0.66290
	+0.92243	−0.23113	+0.04801	+0.92318	−0.24801	+0.50684	+0.57948
	+0.08175	−0.00452	+0.00260	+0.08074	−0.00368	+0.45168	+0.51156
	+0.00560	+0.29092	−0.05578	+0.00618	+0.29569	+0.07153	+0.07716
	−0.00037	+0.67105	−0.25752	−0.00098	+0.82366	+0.02122	−0.00102
Vector components	+0.00032	+0.06396	+0.58162	−0.00036	−0.02437	+0.00992	+0.00352
	−0.00066	+0.05373	+0.30716	−0.00033	−0.08330		
	+0.00145	+0.00749	+0.08509	+0.00120	−0.00927		
	−0.00025	+0.02017	+0.04571	−0.00043	−0.00633		
	−0.00000	+0.00931	+0.01416	+0.00005	+0.00264		

reuse of the vectors $V^{\pm}_{p\lambda r\mu}$ and $G^{\pm}_{l,p\lambda r\mu}$ which are not built from a basis function being varied. Therefore the program was designed to save and reuse those vectors during the variation of exponents.

(6) Due to the large amount of computer time needed for any sizable molecular computation, a true interrupt procedure and an emergency feature were built into the molecular program. The interrupt procedure allows the calculations to be interrupted and recommenced when scheduling permits with virtually no backtracking necessary. The emergency procedure periodically saves sufficient information to restart the computation. Thus, should some catastrophe occur calculations may be continued with the loss of only a small fraction of the computing done previous to the disaster.

TABLE II. Computed properties for near Hartree-Fock ground state wavefunction[a] of F_2.

Molecular property	R (bohrs)	E (hartrees)	μ	Q e(bohrs)^2	q e/(bohrs)^3	Ip (hartrees)	De (hartrees)	$\langle r_a+r_b\rangle_{hy}$ (bohrs)	$\langle\rho^2\rangle_{hy}$ (bohrs)^2
Computed	2.68	−198.7683	0	0.659	6.868	0.6689	−0.060	3.689	0.7772
Experiment	2.68	−199.670	0	...	...	0.5990	0.062	...	...

	Spectroscopic constants via Dunham analysis				
	ω_e(cm^{-1})	ω_eX_e(cm^{-1})	B_e(cm^{-1})	α_e(cm^{-1})	R_e(Å)
Computed	1257	9.85	1.003	0.0108	1.33
Experiment	919.0	13.6	0.8901	0.0146	1.42

[a] The basis set was constructed by starting with the nominal atomic set of Bagus and Gilbert: (1) singly optimizing all setas; (2) addition of 3d functions with single optimization; (3) addition of 4f functions with single optimization.

TABLE III. Comparison of arduously[a] built up molecular basis set with set obtained starting from atomic[b] functions for F_2.

Basis set				R (bohrs)	E (hartrees)	μ	Q e(bohrs)^2	Ip (hartrees)	De (hartrees)	$\langle r_a+r_b\rangle_{Av.}$ (bohrs)	$\langle\rho^2\rangle_{Av.}$ (bohrs)^2
σ_g	σ_u	π_u	π_g								
Atomic start											
$1s$	$1s$	$2p$	$2p$	2.68	−198.7683	0	0.6589	0.66290	−0.048	3.689	0.7772
$1s'$	$1s'$	$2p'$	$2p'$								
$2s$	$2s$	$2p''$	$2p''$								
$3s$	$3s$	$3d$	$3d$								
$2p$	$2p$	$4f$	$4f$								
$2p'$	$2p'$										
$2p''$	$2p''$										
$3d$	$3d$										
$4f$	$4f$										
Arduously built											
$1s$	$1s$	$2p$	$2p$	2.68	−198.7563	0	0.5753	0.66894	−0.060	3.695	0.7874
$1s'$	$1s'$	$2p'$	$2p'$								
$2s$	$2s$	$2p''$	$2p''$								
$2s$	$2s$	$3d$	$3d$								
$2p$	$2p$	$4f$	$4f$								
$2p'$	$2p'$										
$2p''$	$3d$										
$3p$	$4f$										
$4f$											

[a] Arduous refers to starting with a small basis set and gradually adding functions with coupled optimization of zetas at each addition.
[b] Starting point was the "nominal" atomic set: the result of a very careful investigation of first-row atoms of Bagus and Gilbert (Argonne National Laboratory) to be published.

XII. RESULTS FOR THE FLUORINE MOLECULE

The fluorine molecule was selected as a prototype system for investigation through the use of the techniques developed in the preceding sections. The reasons for this choice were several: (1) the comparative lack of experimental and theoretical information on this system, (2) the fact that if fluorine could be successfully studied with these programs it should clear the way for studies of smaller systems and provide a guidepost for the investigation of larger systems, and (3) it was estimated to be the largest system for which extensive optimization of basis function exponents would be economically feasible and for which the molecular Hartree–Fock function might be attainable.

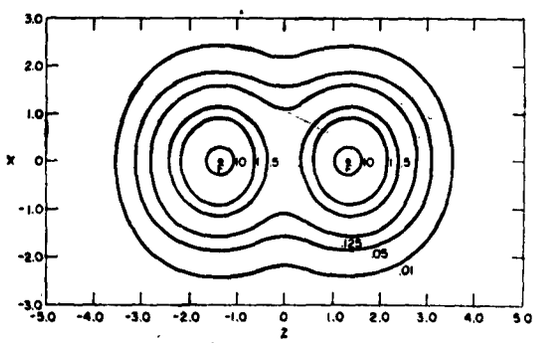

FIG. 1. Total molecular change density contours for the fluorine molecule.

Previous calculations on F_2 consist of SCF calculations by Ransil[11] and Eve[12] yielding total energies of −197.87694 a.u. and −197.87017 a.u., respectively. Eve[12] also performed a limited configuration mixing calculation yielding a total energy of −197.95036 a.u. The best wavefunction presented in this work yields an energy of −198.76825 a.u.

The above F_2 function is presented in Table I along with the orbital energies. Table II presented additional properties computed from this function. The ionization potential (IP) was evaluated by Koopman's theorem. The spectroscopic constants are given in conventional units. There are no experimental comparisons available for the molecular quadrupole moment (Q), the field gradient at the nucleus (q), or, of course, the average molecular size $\langle r_a+r_b\rangle_{Av}$, and the size of the average cylinder enclosing the molecule $\langle\rho^2\rangle_{Av}$.

Table III compares the function (atomic start) obtained by starting with the atomic Hartree–Fock results with the molecular wavefunction which was built up gradually (arduous). The *atomic-start* function is energetically superior and represents far less computation.

Table IV presents a hierarchy of functions ending with the final function. Note the convergence of the energy as contrasted to the wide variation of several of the properties as basis set size is increased.

Figure 1 is a contour diagram of the total electronic charge density in the x, z plane, where the wavefunction

TABLE IV. Summary of basis set (expansion) buildup for F_2.

Basis set				Functions added				R (bohrs)	E (hartrees)	Q e(bohrs)^2	q e/(bohrs)^2	Ip (hartrees)	$\langle r_a+r_b\rangle_{hf}$ (bohrs)	$\langle \rho^2\rangle_{hf}$ (bohrs)^2
σ_g	σ_u	π_u	π_g	σ_g	σ_u	π_u	π_g							
3	× 3	× 1	× 1											
1s	1s	2p	2p											
2s	2s							2.68	−197.8865	0.2379	5.349	0.47497	3.618	0.6411
2p	2p													
5	× 5	× 2	× 2											
1s	1s	2p	2p	2s	2s	2p	2p							
2s	2s	2p′	2p′	2p	2p									
2s′	2s′													
2p	2p													
2p′	2p′							2.68	−198.7075	0.3474	6.939	0.66496	3.694	0.7717
Nominal atom buildup														
7	× 7	× 3	× 3											
1s	1s	2p	2p	3s	3s	2p	2p	[a]2.68	−198.7364	0.2622	7.107	0.68199	3.704	0.7906
1s′	1s′	2p′	2p′	2p	2p			[b]2.68	−198.7418	0.3235	7.042	0.67562	3.699	0.7832
2s	2s	2p″	2p″	−2s	−2s									
3s	3s													
2p	2p													
2p′	2p′													
2p″	2p″													
8	× 8	× 4	× 4											
1s	1s	2p	2p	3d	3d	3d	3d							
1s′	1s′	2p′	2p′											
2s′	2s′	2p″	2p″					2.68	−198.7639	0.7843	6.950	0.66402	3.689	0.7817
3s	3s	3d	3d											
2p	2p													
2p′	2p′													
2p″	2p″													
3d	3d													
9	× 9	× 5	× 5											
1s	1s	2p	2p	4f	4f	4f	4f							
1s′	1s′	2p′	2p′											
2s′	2s′	2p″	2p″					2.68	−198.7683	0.6589	6.868	0.66290	3.689	0.7772
3s	3s	3d	3d											
2p	2p	4f	4f											
2p′	2p′													
2p″	2p″													
3d	3d													
4f	4f													
Experimental values								2.68	−199.670	...	...	0.5990	...	...

[a] Straight nominal atom function (from atomic studies of Bagus and Gilbert).[17]
[b] Single optimization of all nominal atom setas.

normalization is $\int\psi\psi^*dV=2\pi N$ (N is the number of electrons).

The computed dissociation energy (D_e) is poor; in fact, of the wrong sign. Evidently the two shortcomings of the molecular wavefunction discussed in Sec. X, namely, the increased correlation energy in the molecule and the improper description of molecular dissociation, are serious enough to completely mask the relatively small binding energy for this molecule. This failure to yield energetic binding, however, should not be considered a total condemnation of the wavefunction. It should be noted that the calculated ionization potential, internuclear distance, and the first-order spectroscopic constants show fair agreement with experiment. Further it should be kept in mind that the binding energy is a very subtle quantity and that the definition of it employed in this work is a particularly hard test of the theory. Less rigorous definitions would yield almost any binding energy desired.

In conclusion it can be said that the results obtained for F_2 are encouraging but that only through a consistent study of the Hartree–Fock–Roothaan wavefunction for a large series of molecules will the ultimate usefulness of this function become established. Such a study is now possible with existing "computing machinery" and is, in fact, under way. The molecular Hartree–Fock function is clearly lower in energy than any limited configuration mixing wavefunction currently available which suggests that a next logical step is to add the one additional configuration which would lead to the proper description of the dissociation of the molecule. Significant improvement of the potential curve would then be expected resulting in the more reliable computation of the spectroscopic constants. Hopefully, studies of this sort for a series of molecules will aid in the development of a set of consistent rules which will allow us to use the Hartree–Fock function more effectively without enormous computational effort. It is also clear that the *atomic* Hartree–Fock functions are necessary to efficiently evaluate the molecular Hartree–Fock function, as *diatomic* Hartree–Fock functions may prove to be the dominant contributors to polyatomic and ultimately solid wavefunctions.

ACKNOWLEDGMENTS

The author is indebted to Professor C. C. J. Roothaan for his continued interest and guidance in this work, to Dr. T. L. Gilbert for many encouraging and helpful discussions and for making available the computer at Argonne National Laboratory, to Dr. P. S. Bagus for his generous cooperation in making available to the author his version of the atomic self-consistent field program, to Dr. G. Goodman, and to the Chemistry Division at Argonne National Laboratory for sponsoring the last year of this research and in particular the computations on F_2. The author is particularly grateful to S. Derenzo for his very able and enthusiastic assistance in the computer programming of this problem. Finally the very competent and patient assistance of Miss M. J. Ewens in the preparation of this manuscript is gratefully acknowledged.

APPENDIX A: THE MANIFOLDS P AND S

The existence of a series of manifolds P which will yield increasingly accurate results by numerical integration is basic to the very definition of the Riemann integral. In practice the problem is to find an *optimal small set* of points which will yield results of a desired accuracy. The development of this set is a matter of experimentation guided by a knowledge of the spatial behavior of the charge distributions which appear as integrands. These distributions show their steepest variation in the region near the nuclei, thus requiring a manifold which concentrates points about the two nuclei and distributes points more diffusely as the distance in every direction from the internuclear axis increases. After experimentation with several coordinate systems it was found that the manifold P obtained by a crossed Gaussian numerical integration over the prolate spheroidal coordinates ξ and η yielded the most satisfactory results where the inverse transformation $\xi=(1+\beta)/(1-\beta t)$ was employed. The parameter β was chosen to confine the manifold P inside an ellipsoid of revolution outside of which the wavefunction of the molecule under study is no longer computationally significant.

The manifold S, used for the numerical integration necessary for the evaluation of the exchange integrals, must concentrate points near the internuclear axis ($\xi=1$). The inverse transformation $\xi=1/T$ where a Simpson-rule integration is performed over the variable T was found to be satisfactory. It is important to use an equal interval numerical integration procedure so that the inner integrations over the variables x may be performed efficiently.[1] If the selection of the manifold S does not extend to infinity, a correction term is added to the formula Eqs. (46) given for the $I^l_{p\lambda\alpha,r\mu\beta;m\nu\gamma,n\kappa\delta}$ integral. This truncation correction term is defined by

$$\begin{aligned}\mathfrak{I}^l_{p\lambda\alpha,r\mu\beta;m\nu\gamma,n\kappa\delta}=&4R^{-1}[\sigma_\lambda+\sigma_\mu(-1)^{M+l}]\\&\times[\sigma_\nu+\sigma_\kappa(-1)^{M+l}][(l-M)!/(l+M)!](-1)^M\\&\times[Q_l{}^M(\xi_{\max})/\hat{P}_l{}^M(\xi_{\max})]F^M{}_{l;p\lambda\alpha,r\mu\beta}(\xi_{\max};\tau,\rho)\\&\times F^M{}_{l;m\nu\gamma,n\kappa\delta}(\xi_{\max};\tau,\rho),\end{aligned}\quad(60)$$

where $\xi_{\max}$ is the finite upper limit of the ξ integration and $Q_l{}^M(x)$ is the associated Legendre function of the second kind.[1] The analysis of Sec. VIII was presented for the infinite upper limit of the ξ integration since the above correction is a consideration which complicates formulas unnecessarily while representing no real computational difficulty.

APPENDIX B

THE COMPUTER PROGRAM

1. General Considerations

A fully automatic program that computes the SCF wave function for homonuclear diatomic molecules was constructed for the IBM 7094 computer. It incorporates the features discussed previously in this paper. An SCF run using the first basis set presented in Table IV requires about 40 sec; the "final" basis set requires about 45 minutes.

The orbital exponents are varied automatically by an essentially brute-force technique, which is the same as that presented for atoms.[4] The program handles a limited number of open shell cases, among which are $\sigma_{g,u}$, $\pi_{g,u}$, $\delta_{g,u}$, $\pi^2_{g,u}$, $\delta^2_{g,u}$, $\pi^3_{g,u}$, $\delta^3_{g,u}$. The necessary α and β coefficients are presented in Table V. The homonuclear diatomic SCF program is designed to include certain open-shell configuration cases. Table V lists the vector coupling coefficients for the open-shell configuration cases now acceptable by the program. The number of basis functions permissible is determined by

$$\sum_{\lambda}\left(\frac{1}{2}\right)(N_\lambda)(N_\lambda + 1) \leq 144,$$

where N_λ is the total number of symmetry basis functions, Eq. (13), of symmetry λ. The restrictions on basis function quantum numbers are $1 \leq N \leq 6$, $0 \leq \ell \leq 3$, and $-\ell \leq m \leq \ell$. Experience has shown that this program is useful for obtaining near Hartree-Foch wave functions for molecular systems ranging in size from H_2 through Cl_2.

Table V

VECTOR COUPLING COEFFICIENTS FOR HOMONUCLEAR OPEN-SHELL CONFIGURATIONS

Open-shell Case(s)	State(s)		
$\sigma_{g,u}$	$^2\Sigma^+_{g,u}$	1	-1/2
$\pi_{g,u}$, $\delta_{g,u}$	$^2\Pi_{g,u}$, $^2\Delta_{g,u}$	1	-1/2
$\pi^2_{g,u}$, $\delta^2_{g,u}$	$^3\Sigma^-_g$, $^3\Sigma^-_g$	0	1/2
	$^1\Delta_g$, $^1\Gamma_g$	1/2	-1/2
	$^1\Sigma^+_g$, $^1\Sigma^+_g$	1	-3/2
$\pi^3_{g,u}$, $\delta^3_{g,u}$	$^2\Pi_{g,u}$, $^2\Delta_{g,u}$	1/9	-1/18

2. Loading Conventions

The input to the program is specified as follows on FAP (Fortran Assembly Program) cards:

Location	Operation	Contents
10	BCD	Heading sentence. Inserted in first line of input and final output page. Also inserted in heading of each interrupt page.
20	DEC	Nuclear charge. Floating or fixed point number.
21	DEC	Internuclear separation, R. Floating point number. Up to nine R values permitted to be run consecutively.
30	DEC	Number of symmetry-orbitals basis functions, according to symmetry. Order is $\#\sigma_g$, $\#\sigma_u$, $\#\pi_u$, $\#\pi_g$, $\#\delta_g$, $\#\delta_u$, $\#\gamma_u$, $\#\gamma_g$. The total number of symmetry-orbitals basis functions is limited by $\sum_\lambda \left(\frac{1}{2}\right) N_\lambda (N_\lambda + 1) \leq 144,$ where N_λ is the total number of symmetry-orbital basis functions of λ symmetry.
40	DEC	Number of closed-shell molecular orbitals, according to symmetry. Order is $\#\sigma_g$, $\#\sigma_u$, $\#\pi_u$, $\#\pi_g$, $\#\delta_g$, $\#\delta_u$, $\#\gamma_u$, and $\#\gamma_g$ closed shells.
50	DEC	Number of open-shell electrons, according to symmetry. Order is $\#\sigma_g$, $\#\sigma_u$, $\#\pi_u$, $\#\pi_g$, $\#\delta_g$, $\#\delta_u$, $\#\gamma_u$, and $\#\gamma_g$ open-shell electrons. No more than one open shell per symmetry is permitted.
60	DEC	Open-shell alpha coefficients. Listed in Table V.
80	DEC	Open-shell beta coefficients. Listed in Table V.
100	DEC	Quantum number N for symmetry-orbitals basis functions given above. Order is $\sigma_g, \sigma_g', \ldots, \sigma_u, \sigma_u', \ldots, \pi_u, \pi_u', \ldots, \pi_g, \pi_g', \ldots, \delta_g, \delta_g', \ldots, \delta_u, \delta_u', \ldots, \gamma_u, \gamma_u', \ldots, \gamma_g, \gamma_g', \ldots$ Limit is $N \leq 6$.
133	DEC	Quantum number L for symmetry-orbitals basis functions given above. Order is same as for quantum numbers N order. $L \leq 3$.

Location	Operation	Contents
166	DEC	Orbital exponents for the symmetry-orbitals basis functions given above. The order coincides with that of N and L just preceding. All orbital exponents must exceed the input threshold (normally 0.100). In addition, the difference between orbital exponents for symmetry-orbitals basis functions with the same N and L value must be greater in absolute magnitude than a given threshold (also normally 0.100).
200	DEC	SCF input vectors. No more than 200 total vector components are permitted.
400	DEC	Indices of symmetry-orbitals basis functions whose orbital exponents are to be varied and mutually optimized. One, two, or three orbital exponents may be simultaneously optimized. Each set of indices must be separated by a zero. The basis functions are numbered in the order given above where the N, L, and orbital exponent values are listed. A typical variational chain might be 1, 2, 0, 3. This would specify that the orbital exponents of symmetry-orbital functions 1 and 2 are simultaneously optimized, and then the orbital exponents of symmetry-orbital function 3 is singly optimized. In preparing the coupling chains, always put the most energy-sensitive orbital exponent first in the indices.
420	DEC	Increment for the variation of the symmetry-orbitals basis functions orbital exponents. Loaded in the same manner and sequence as the indices immediately preceding, except that the increments replace the indices. If any particular increment or all the increments are not explicitly given, or if any are less than 0.001, 10% of the orbital exponent involved is employed in the variation. The set of increments is called the mesh of the variation.
		SCF Convergence Control
440	DEC	N Diagonalization SCF Threshold Bias. $1 \leq N \leq 5$, and normally program is set to N = 1.
441	DEC	N Number of SCF Extrapolations. $5 \leq N \leq 25$, and normally program is set to N = 5.
442	DEC	N Number of Prior SCF Extrapolations. $0 \leq N \leq 25$, and normally program is set to N = 0.

Location	Operation	Contents
443	DEC	N Number of Diagonalization Iterations. $5 \leq N \leq 25$, and normally program is set to N = 5.
444	DEC	Number of Locked Passes Prior to SCF. $0 \leq N \leq 9$, and normally program is set to N = 0.
445	DEC	N Maximum Number of Extrapolations. $5 \leq N \leq 100$, and normally program is set to N = 50.
446	DEC	N Extrapolation Method. N = 1 for Hartree-Roothaan Method, N = 2 for Sack Method. Normally program is set to N = 1.
447	DEC	N Diagonalization Method. N = 1 for SVDG (Single Vector Diagonalization), and N = 2 for Jacobi. Normally program is set to N = 1.
448	DEC	25 Computes expectation values of 1, $(\sin^2\theta_a)/r_a$ $(\cos^2\theta_a)/r_a$, $3z_a^2 - r_a^2$, $1/r_a$, ξ, r_a^2, z_a^2, and $x_a^2 + y_a^2$.
449	DEC	Quadratic one-dimensional exponent variation employed.
		Intermediate Output Requests
460	DEC	*Intermediate matrices printout. S, U, T, , and matrices are printed in format*.
461	DEC	*S-Matrix, its eigenvalues, and vectors are printed in format*.
462	DEC	*Final matrices S,H,P,Q, D-Open, D-Total, F-Open, F-Closed, R-Open, and R-Closed are printed in format*.
463	DEC	*Integrals between final orbitals, H-integrals, P-integrals. Q-integrals, and La Grangian multipliers are printed in format*.
464	DEC	*F Matrix, its eigenvalues, and vectors are printed in format*.
465	DEC	1 SCF iterations are printed.
		*Gives the printout format (always off line): If * equals 1, the output will be eight-column floating point decimal.
		If * equals 2, the output will be eight-column fixed point decimal.
466	DEC	Print final vectors of intermediate results during variation run.

Location	Operation	Contents
470	DEC	Integration truncation cutoff value in floating decimal. If omitted, a standard value is used: RTRUN = 60. This assumes no STO's are more diffuse than a hydrogen IS function.
476	DEC	Only used in variation runs. Number of Neumann expansion terms to be included in exchange integral calculations. The maximum number of terms permitted is $(30 - M_{max})$, after which record is kept of any exchange integral that does not meet the threshold of 10^{-6}, and computations are continued.
477	DEC	1 Save current input flag. Current input will be reused with any modifications as read in for the next case; it does not save itself.
480	OCT	NSIMP000001. Number of Simpson's-rule points in octal. The maximum number of points is 70.
481	OCT	NPETA0000NPXI. Number of Gaussian points in octal used in the double Gaussian numerical integrations. NPETA and NPXI may take any of the values 12, 16, 20, 24, 30, or 36 points (in decimal). If no grid is specified, a 30 x 30 grid is employed.
482	DEC	1 Output flag to call for eight-column floating point decimal print-out (off line) to addends to J and K supermatrix elements for exchange and coulomb passes.
500	BCD	Symmetry symbol list, only if order of molecular orbitals departs from the order 1 σ_g, 2 σ_g, . . . , 1 σ_u, 2 σ_u, . . . , 1 π_u, 2 π_u, . . . , 1 π_g, 2 π_g, . . . , 1 δ_g, 2 δ_g, . . . , 1 δ_u, 2 δ_u, . . . , 1 γ_u, 2 γ_u, . . . , 1 γ_g, 2 γ_g, . . .

3. Operating Instructions

a. To Start Any Run

1. Mount LMSS-AA-SCF No. 1 tape on B7.
2. Mount blanks on B3, B4, B5, A5, A6, and A7.
3. Mount output tape on A3.
4. Place deck in card reader headed by molecule card.
5. Clear, put SSW 1, 4, and 5 down.
6. Load cards.

Program will load cards and proceed with computation.

b. To Interrupt

1. Place SSW 3 down.
2. Within 1-60 minutes, run will stop and print out on-line interrupt sentence.
3. Unload tapes B7 and B5, and save these tapes for subsequent continuation of computation.

c. To Restart Interrupted Run

1. Mount tapes B7, and B5 saved in interrupt procedure.
2. Place blanks on B3, B4, and A3, A5, A6, and A7.
3. Place INTERRUPT-RESTART card in card reader.
4. Clear, put SSW 1, 4, and 5 down.
5. Load INTERRUPT-RESTART card.
6. Computations will be continued from interrupted point.

d. Also Note

1. Description of emergency procedure on page 40.
2. Details of interrupt output option on pages 39 and 40.
3. Channel a tape option on page 40.
4. Program STOP with END in IR 4, 5, 6, 7 lights is normal conclusion.

e. Sense Switch Controls

SSW	Function
1.	If down, program considers current input to be last case.
2.	If down, exponent variation will be terminated at current iteration, and final output page printed.
3.	If down, computation will be interrupted and tapes written for subsequent continuence of computation at point of interruption. See following paragraphs for output option at this point.
4.	If down, input is called from cards. If up, input is called from tape A2.
5.	If down, tapes A5 and A6 are used for saving and editing of two electron potentials during exponent variation. If up, tapes A5 and A6 are not used at the expense of computer time.
6.	If down, current internuclear distance in a series of values is considered as last one.

f. Interrupt

The depression of SSW 3 interrupts the current molecular computation. The computer will come to a program stop after printing an interrupt message on the one-line printer.* The stop will occur within 1-60 minutes of the time SSW 3 is pressed. Tape B5 must be saved for restarting of computations.

*If a full requested output at the time of interruption is desired, push SSW 3 up after the stop has occurred, and press the START button. The output will be written on tape A3, and the computer will come to a second program stop.

For restarting of interrupted computation, tape B5 should be remounted with program tape on B7. Blanks on B3, B4, A5, A6, and A7. Machine is cleared and interrupt restart card loaded. Computations will restart at point of interruption.*

g. Emergency Procedure

Should computations stop at an unexpected point, or should the tapes give trouble, provide new tapes as follows:**

1. Ready EMERGENCY RESTART AND RECOVERY card in reader.
2. Clear machine; load cards.

USE OF EMERGENCY PROCEDURE WILL LEAD TO A LOSS OF NO MORE THAN 60 MINUTES OF COMPUTATION.

h. Channel A Tape Option

If the heavy use of tapes A5 and A6 leads to continued difficulty after new tapes have been provided, computations may be continued less efficiently without the use of these tapes as follows:

1. Clear machine at any time other than when tape B3 is being referenced.
2. Put SSW 5 up.
3. Load EMERGENCY RESTART AND RECOVERY CARD.

---

*If the restart fails (very unlikely), use the emergency procedure.

**Directions will appear on on-line printer.

THE ELECTRONIC STRUCTURE OF DIATOMIC MOLECULES. III. A. HARTREE-FOCK WAVE FUNCTIONS AND ENERGY QUANTITIES FOR $N_2(X\ ^1\Sigma_g^+)$ AND $N_2^+(X\ ^2\Sigma_g^+,\ A\ ^2\Pi_u,\ B\ ^2\Sigma_u^+)$ MOLECULAR-IONS.*

Paul E. Cade and K. D. Sales†

Laboratory of Molecular Structure and Spectra
Department of Physics, University of Chicago
Chicago, Illinois 60637

Arnold C. Wahl

Chemistry Division, Argonne National Laboratory
Argonne, Illinois‡

and

Laboratory of Molecular Structure and Spectra
Department of Physics, University of Chicago
Chicago, Illinois 60637

ABSTRACT

The problem of the convergence of a sequence of Hartree-Fock-Roothaan wave functions and energy values to the true Hartree-Fock results is examined for $N_2(X\ ^1\Sigma_g^+)$. This critical study is based on a hierachy of Hartree-Fock-Roothaan wave functions which differ in the size and composition of the expansion basis set in terms of STO symmetry orbitals. The concluding basis set gives a total Hartree-Fock energy of -108.9956 Hartrees and $R_e(HF) = 2.0132$ Bohr for $N_2(X\ ^1\Sigma_g^+)$.

Results are also presented from direct calculations for three states of the N_2^+ molecular-ion ($X\ ^2\Sigma_g^+$, $A\ ^2\Pi_u$, $B\ ^2\Sigma_u^+$) which are also thought to be very close approximations to the true Hartree-Fock values. The results give $E_{HF} = -108.4079$ H., -108.4320 H., and -108.2702 H. and $R_e(HF) = 2.0385$ B., 2.134 B., and 1.934 B. for the $X\ ^2\Sigma_g^+$, $A\ ^2\Pi_u$, and $B\ ^2\Sigma_u^+$ states of N_2^+, respectively. Extensive calculations for various R values establishes that the $X\ ^2\Sigma_g^+$ and $A\ ^2\Pi_u$ states are reversed in order relative to experiment, a shortcoming ascribed to the Hartree-Fock approximation.

I. INTRODUCTION

This is the third in a planned series of papers from this laboratory whose objective is to obtain Hartree-Fock wave functions for the ground state and certain excited states of diatomic molecules, and from these wave functions to calculate many expectation values of the electronic coordinates, certain molecular properties, and the electronic charge and momentum density for each molecular orbital as well as for the entire molecule. All of these calculations are made for several internuclear separations. The longer range objective of this series is to provide a solid and

*Research reported in this publication was supported by Advanced Research Projects Agency through the U.S. Army Research Office (Durham), under Contract DA-11-022-ORD-3119, and by a grant from the National Science Foundation, NSF GP-28.

†Present address: Department of Chemistry, Queen Mary College, London, England.

‡Present address.

extensive platform from which to begin a critical re-examination of the theory of the electronic structure of small molecules. This extensive platform will consist of calculations for homologous and isoelectronic series of diatomic molecules to approximately the same level of accuracy.

In another perspective, this series of theoretical studies might be viewed as "dry" experiments. One may recall the immense early successes Mulliken, Herzberg and others had in the interpretation of the electronic structure of diatomic and polyatomic molecules in terms of the nature of their molecular orbitals as gleaned from the electronic spectra of these systems. In as much as this series of studies is able to obtain accurate molecular orbitals, we hope to extend these studies to molecules yet unobserved, and in particular to explore a host of expectation values and molecular properties not available from the corresponding spectral data.

The first paper in this series[1] dealt with the Hartree-Fock-Roothaan equations for diatomic molecules, especially for homonuclear diatomic molecules, and discusses at length the organization of the computer program to calculate efficiently and rapidly the supermatrix elements and perform the SCF procedure. Results are also presented by Wahl[1] for $F_2(X\ ^1\Sigma_g^+)$ as a prototype molecule. The second paper of this series[2] deals primarily with extensive calculations on $CO(X\ ^1\Sigma_g^+)$ and $BF(X\ ^1\Sigma_g^+)$ and also discusses the partner heteronuclear diatomic SCF computer program with emphasis on any differences from the description given by Wahl.[1] Further members of this series will include results for $Li_2(X\ ^1\Sigma_g^+)$, $Be_2(^1\Sigma_g^+)$, $B_2(X\ ^3\Sigma_g^-)$, $C_2(a\ ^1\Sigma_g^+, A'\ ^3\Sigma_g^-)$, and $O_2(X\ ^3\Sigma_g^-, a\ ^1\Delta_g, b\ ^1\Sigma_g^+)$ to complete this study of the first row homonuclear diatomic molecules; results for $Na_2(X\ ^1\Sigma_g^+)$, $C\ell_2(X\ ^1\Sigma_g^+)$, and eventually all ground configuration states for all second row homonuclear diatomic molecules; results for the first and second row hydride molecules, AH; results for first row oxides, AO, and fluorides, AF, a number of other important heteronuclear diatomic molecules (including $BN(a\ ^1\Sigma^+)$, $NO(X\ ^2\Pi, A\ ^2\Sigma^+)$, $CN(X\ ^2\Sigma^+, A\ ^2\Pi)$, $LiC\ell(X\ ^1\Sigma^+)$, and a number of other small heteronuclear diatomic molecules some of which have not been experimentally identified).[3] As a matter of course each presentation will usually include calculations for several positive and/or negative ions of the parent system and potential curves as well for all ground configuration states.

---

[1] A. C. Wahl, J. Chem. Phys. 41, 2600 (1964).

[2] W. Huo, "SCF Wave Functions and Computed Properties for CO and BF", to be published in J. Chem. Phys.

[3] The scope of this study will eventually include certain excited states of a given diatomic system and thus the specific state(s) involved will have to be clearly designated. It is therefore convenient to employ the spectroscopic designation for the state in question where it is available and applicable.

The three general objectives of the present paper are:

i) To report the Hartree-Fock-Roothaan wave functions for $N_2(X\ ^1\Sigma_g^+)$ and $N_2^+(X\ ^2\Sigma_g^+,\ A\ ^2\Pi_u,\ B\ ^2\Sigma_u^+)$, molecules and molecule-ions for a range of R values. A number of expectation values of electronic coordinates, certain molecular properties and charge density contours of the various molecular orbitals are given in subsequent members of this series, III. B and III. C.

ii) To provide considerable documentation of the study of the convergence of the expansion method (see Section II) toward limiting behavior with respect to the total energy and certain molecular properties. This limit should be the Hartree-Fock result. This study is essentially a problem in numerical analysis, but since the results in this series are intended to represent the Hartree-Fock results as closely as practically possible, it is a rather important item to be considered. In addition, the reasons for the choice of many of the methods employed, in this and later members of this series, to obtain the expansion basis set will become evident. In paper IV of this series a similar documentation is given for $Li_2(X\ ^1\Sigma_g^+)$.

iii) To give the general prospectus for this and projected remaining members of the series in regard to objectives, methods, and nomenclature.

The general discussion of the behavior of the electronic charge distributions is deferred to contributions dealing with various homologous and isoelectronic series. Such studies are primarily being developed directly in terms of charge density contours and charge density difference contours and will eventually also include population analysis and localized molecular orbitals. Such an effort for the first row homonuclear diatomic molecules is now in progress.

The remainder of this section is devoted to a consideration of the importance of certain new experimental methods for measuring directly the properties of individual molecules and a brief review of previous calculations on the nitrogen molecule. In Section II the basic theory underlying this series of papers is briefly reviewed for completeness and to emphasize certain practical difficulties.

The electronic structure of the nitrogen molecule has been studied experimentally and theoretically by many investigators and using a variety of experimental methods. A large part of our present understanding of the electronic structure of nitrogen has come from years of careful study of the electronic spectra of nitrogen and nitrogen molecular-ions. This has provided accurate dissociation energies for $N_2(X\ ^1\Sigma_g^+)$ and $N_2^+(X\ ^2\Sigma_g^+)$, ionization potentials, much information about the nature of the molecular orbitals, and other useful molecular quantities. The electronic spectra

of the nitrogen-(nitrogen-molecular-ions) system is one of the most well understood (though far from completely), and thoroughly studied.[4,5] The easy availability, relatively great stability, and traditionally important chemical status of nitrogen, has often led to the use of nitrogen in experimental studies employing new high resolution apparatus or in the introduction of innovative experimental methods to study simple physical processes. One might recall the innovative experimental studies of Fox and Hickam[6] and Frost and McDowell[7] in determining several electron impact molecular-ion appearance potentials or vertical ionization potentials of nitrogen for various excited states of the N_2^+ molecular-ion formed, studies which nicely complement the far ultraviolet Rydberg-series spectra of nitrogen; the new work of Al-Joboury and Turner[8] on Photoelectron Spectroscopy which is particularly useful for determining higher ionization potentials as is demonstrated for the ionization of N_2 to N_2^+ and this method is also suggestive as to the bonding type of the molecular orbital involved in the ionization process; the recent success of Buckingham and associates[9] in the direct measurement of the electric quadrupole moment of simple molecules, including N_2, and for the first time providing unambigously the sign of the electric quadrupole moment. Previous experimental estimates of the electric quadrupole moment of simple molecules have come chiefly from line broadening measurements and pressure induced rotational or vibration-rotational spectra[10] and give only the magnitude of the electric quadrupole moment.

---

[4]R. S. Mulliken, in The Threshold of Space, edited by E. B. Armstrong and A. Dalgarno, (Pergamon Press, Inc., New York, 1957), p. 169. A complete survey of the nitrogen spectra and state through 1956.

[5]A. Lofthus, "The Molecular Structure of Nitrogen", University of Oslo, 1960, Blindern, Norway.

[6]R. E. Fox and W. H. Hickman, J. Chem. Phys. 22, 2059 (1954).

[7]D. C. Frost and C. A. McDowell, Proc. Roy. Soc. (London), A230, 227 (1955).

[8]M. I. Al-Joboury and D. W. Turner, J. Chem. Soc. (London), 983 (1963).

[9]A. D. Buckingham, J. Chem. Phys. 30, 1580 (1959); A. D. Buckingham and R. L. Disch, Proc. Roy. Soc. (London) A275, 275 (1963), and private communication.

[10]J. A. A. Ketelaar and R. P. H. Rettschnick, J. Molecular Phys. 7, 191 (1963), give one of the latest result of this kind.

Molecular beam magnetic and electric resonance measurements have continued to provide an additional and potentially very valuable source of information about the electronic structure of simple molecules. N. F. Ramsey and associates[11] have recently begun an extensive program to measure the molecular magnetic rotational moment of small molecules and have measured the magnetic rotational moment of $N^{15}N^{15}$. In addition, the spin-rotational interaction constant, that is, the interaction constant between the nuclear magnetic moment and the rotational magnetic moment, has been measured for $N^{15}N^{15}$ and have yielded the nuclear magnetic antishielding constant for the nitrogen nucleus.[12] The corresponding measurements have not been made for $N^{14}N^{14}$ due to experimental difficulties and hence no nuclear quadrupole coupling constant, eqQ, is yet available from molecular beam magnetic resonance methods since N^{15} nuclei have spin $\frac{1}{2}$ and no electric quadrupole moment. The nuclear quadrupole coupling constant at the N^{14} nucleus has, however, been measured in the solid phase of nitrogen, most recently by Scott.[13] These experimental quantities, the magnetic rotational moment, the spin-rotation coupling constant(s), the quadrupole coupling constant, and the related quantities are relatively new sources of valuable information about the charge distribution in simple molecules.

The study of collision or scattering processes involving small molecules has also provided much new and interesting information relating to the electronic structure of simple molecules, including nitrogen. The variety of these newer experimental methods ranges from elastic and inelastic scattering of slow electrons from molecules, through electron impact spectroscopy,[14] a new tool which offers great promise of complementing optical spectroscopy in providing means of studying usually forbidden electronic transitions in atoms and molecules, to the difficult problems involving the collision of charged or neutral atoms or molecules with molecules, or simply, chemical reactions. Gerjuoy and Stein[15] have theoretically studied the rotational excitation of homonuclear diatomic molecules by slow electron collisions and in particular have made calculations for nitrogen. This theory makes use in an important way of the

---

[11] N. F. Ramsey, Bull. Amer. Phys. Soc. 9, 89 (1964), and paper presented at the American Physical Society Meeting, January 25, 1964.

[12] M. R. Baker, C. H. Anderson, and N. F. Ramsey, Phys. Rev. 133, A1533 (1964).

[13] T. A. Scott, J. Chem. Phys. 36, 1459 (1962).

[14] A. Kuppermann and L. M. Raff, Disc. Faraday Soc. 35, 30 (1963).

[15] E. Gerjuoy and S. Stein, Phys. Rev. 97, 1671 (1955).

details of the electronic charge distribution of the nitrogen molecule. Schulz[16] has recently suggested the existence of a short-lived intermediate species, $N_2:e^-$, in the interpretation of his experimental data on the scattering of slow electrons from nitrogen. An excellent review of these and other low energy collision processes has been given by Biondi,[17] where many additional references are listed.

The scattering of fast electrons (30 to 50 kev) from molecules has long been useful in determining molecular geometry from the electron diffraction of gases. As in X-ray diffraction of crystals (or gases), the X-ray scattering factors of the constituent atoms of the molecule are universally employed to interpret the electron diffraction measurements. In both X-ray crystallography and electron diffraction, the molecular scattering factor is simply assumed to be the superposition of the atomic scattering factors for the constituent atoms and except for vibrational corrections, no account is taken of the effects of chemical bonding and the modification of the superimposed atomic electronic charge distribution due to molecule formation. This is almost always an excellent approximation, but very careful X-ray measurements have revealed small effects in certain cases which may be ascribed to the intrinsic molecular character of the scattering system. The recent improvements in the techniques and interpretation of electron diffraction measurements for diatomic molecules have initiated studies by Bartell and Kuchitsu,[18] to detect anharmonic vibrational effects in N_2, O_2, NO, and $C\ell_2$, and Hansen[19] has recently suggested a method for obtaining atomic scattering factors from high precision electron diffreaction measurements on simple molecules. In addition, Swick[20] has been able to measure the elastic and inelastic electron diffraction scattering pattern for N_2 and other simple molecules.

---

[16] G. J. Schulz, Phys. Rev. 116, 1141 (1959); 125, 229 (1962).

[17] M. A. Biondi, "Advances in Electronic and Electron Physics", 18, 67 (1963),(Academic Press, Inc., New York).

[18] L. S. Bartell and K. Kuchitsu, J. Phys. Soc. (Japan), 17, Suppl. B-11, 20 (1962). Proce dings of the International Conference on Magnetism and Crystallography, Kyoto, Japan, 1961.

[19] H. P. Hansen, J. Chem. Phys. 36, 1043 (1962).

[20] D. A. Swick, J. Phys. Soc. (Japan), 17, Suppl. B-11, 12 (1962). Proceedings of the International Conference on Magnetism and Crystallography, Kyoto, Japan, 1961.

It is not too optimistic to expect that further improvements will eventually provide evidence for "shifts" of the atomic scattering factors for atoms in different molecular environments which are due to differential bonding situations. A review of the calculations of X-ray and electron diffraction scattering factors for atoms and molecules has been given by Roux and Cornille[21] who emphasize the basic association of these quantities with the electronic charge density of the atom or molecule. The experimental measurement of the scattering of X-rays by simple molecules in the gaseous phase seems to have been completely abandoned in recent years although measurements were made by Gajewski[22] for nitrogen and several other simple molecules over thirty years ago. The molecular scattering factor might play a more important role in understanding the electronic structure of simple molecules if these experimental developments are indeed realized and use made of the effects already observed. The X-ray and electron diffraction scattering factors do contain the closest means available of direct (or semi-direct) measurement of the electronic charge density (coherent scattering) and as Coulson has emphasized, the electronic momentum density (incoherent scattering).

The preceding paragraphs have purposely emphasized newer, and to some extent chemically unorthodox, kinds of experimental information measuring the behavior and properties of the electronic charge distribution of small molecules. Experimental results of this kind are partially available for N_2 and a few other small molecules, and it is hoped that further results will be rapidly forthcoming. There are many other types of experimental studies involving the physical properties of small molecules which could also be mentioned here. In addition, the variation of molecular properties with vibrational state of the molecule, and hence information about the change of the electronic charge density with nuclear separation, is possible. It is the general contention of this paper, and indeed of this series of papers, that these molecular properties, these newer and more demanding probes into the electronic charge density of small molecules, should and will play a more prominent role in understanding more fully the electronic structure of small molecules. Paper III. B of this series will deal with certain of these molecular properties for N_2 and N_2^+ molecular ions, but others, and particularly the scattering problems remain temporarily beyond the scope of this series.

---

[21] M. Roux and M. Cornille, Cahier Phys. 16, 45 (1962).

[22] H. Gajewski, Phys. Z. 33, 122 (1932).

The theoretical attempts to understand the nitrogen molecule, and in particular to explain the great stability and inertness of nitrogen, began rather early and two simple molecular models were those discussed by Langmuir and Sommerfeld. The model of Langmuir, which was a static model[23] based on empirical chemical evidence and the Lewis octet theory, envisioned the nitrogen molecule as arising from two nitrogen atoms with unchanged K shells, eight of the remaining electrons forming a Lewis octet, and the last two electrons were embedded in the octet such that an increase in stability resulted (see Fig. 1a). The dynamical model of Sommerfeld (which was first suggested by N. Bohr in 1913) was one of the several, now forgotten, attempts to extend and test the Bohr model of atomic hydrogen to other atoms and to diatomic molecules. Sommerfeld's nitrogen molecule (shown in Fig. 1b), consisted of two nitrogen atom cores, with a charge of +3 each separated by a distance R, and the six remaining electrons all revolving in the same orbit and direction half-way between these two nitrogen atom cores.

It is interesting to note that fifty years later a "Modified" Lewis-Langmuir octet model based on the necessity of coulombic and exclusion repulsion between the electrons of a molecule has been proposed by Linnett.[24] The Linnett model for nitrogen is illustrated by Figs. 1c and 1d and only the ten valence shell electrons are considered. Five electrons are assigned to each spin and these five electrons of each set will be situated at the corners of two tetrahedra having a common face (Fig. 1c for spin up and Fig. 1d for spin down). These two sets are superimposed, but the two triangular sets in the bond region may be staggered with respect to one another.

The first major attempt of any kind to calculate the electronic density of N_2 (and also F_2), after the advent of quantum mechanics, was the effort by Hund in 1932 using the Thomas-Fermi approximation. The valence bond, or Heitler-London-Slater-Pauling, method could suggest a reasonable interpretation for the nitrogen molecule, but since at least three "bonding pairs" were involved, ab initio valence-bond calculations for the full six (or ten) valence shell electrons were very difficult. Kopineck[25] did, however, make certain valence bond calculations in 1952 for both the six and ten electron cases following the methods of Hellmann. The most extended valence

---

[23] It is interesting to read the heroic attempts on the part of A. Lande in 1917 and 1918 to provide a dynamical justification of the octet model.

[24] J. W. Linnett, "The Electronic Structure of Molecules", (John Wiley and Sons, Inc., New York, 1964).

[25] H. Kopineck, Z. Naturforschg. 7a, 22, 314 (1952).

bond (or atomic orbital) method calculations seem to be the unpublished results of T. Itoh,[26] obtained in this laboratory, which yielded a dissociation energy of 5.03 eV. Huber and Thorsen[27] have also made certain valence-bond calculations for the $X\ ^1\Sigma_g^+ - A\ ^3\Sigma_u^+$ excitation energy for N_2.

Molecular orbital calculations have proved much more manageable and there has been a steady stream of LCAO-MO-SCF calculations for N_2 from this laboratory and others. Scherr[28] made calculations in which the molecular orbitals were approximated by 1s, 2s, 2pσ, and $2p\pi^{\pm}$ STO orbitals on each nucleus. In his pioneering study, Scherr used the Slater orbital exponents with no optimization of these non-linear parameters. Ransil,[29] and Fraga and Ransil[30] then determined LCAO-MO-SCF wave functions for N_2 at R_e(Exptl.), and for a range of R values, again using the minimal valence shell Slater-type expansion functions, but the orbital exponents were optimized at R_e(Exptl.). Fraga and Ransil[31] also made limited configuration interaction calculations based on the minimal basis set just mentioned. Clementi[32] made the next small improvement by adding a $3d\pi$ STO to the minimal set and optimizing the orbital exponent of the new function. Richardson[33] has given the real start of the extended basis set LCAO-MO-SCF calculations for N_2 in his "double-ζ" expansion set, in which the molecular orbitals are approximated by one 1s, two 2s, two 2pσ, and two $2p\pi$ STO functions on each nucleus. Richardson was able to perform only crude optimization of the non-linear variational parameters. In unpublished research, Richardson also made several useful calculations of certain N_2^+ states of this same quality. Only recently, Nesbet[34] has published a much more extended LCAO-MO-SCF calculation for N_2. This last calculation and parallel ones for several other molecules are near the depth of study intended in this series.

---

[26] R. S. Mulliken, in lectures on "Problems Concerning the Electronic Structure of Diatomic Molecules", Autumn quarter, 1961, University of Chicago.

[27] L. M. Huber and W. Thorsen, J. Chem. Phys. 41, 1829 (1964).

[28] C. W. Scherr, J. Chem. Phys. 23, 569 (1955).

[29] B. J. Ransil, Rev. Modern Phys. 32, 245 (1960).

[30] B. J. Ransil and S. Fraga, J. Chem. Phys. 35, 669 (1961).

[31] S. Fraga and B. J. Ransil, J. Chem. Phys. 36, 1127 (1962).

[32] E. Clementi, Gazz. Chimica Ital. 91, 722 (1961).

[33] J. W. Richardson, J. Chem. Phys. 35, 1829 (1961).

[34] R. K. Nesbet, J. Chem. Phys. 40, 3619 (1964).

In the present endeavor, no critical comparison of these various LCAO-MO-SCF results for N_2 with the results here given is attempted. This is chiefly because the present calculations contain a hierachy of different results, certain of which are comparable to these earlier results, and these seem more suitable for the comparative investigations herein discussed.

II. THE HARTREE-FOCK AND HARTREE-FOCK-ROOTHAAN EQUATIONS

In the Hartree-Fock approximation the electronic wave function is written

$$\Phi_\Omega = [(2N)!]^{\frac{1}{2}} (\varphi_1\alpha)[1(\varphi_1\beta)^2 \ldots\ (\varphi_N\alpha)^{2N-1}(\varphi_N\beta)^{2N}] \quad , \qquad \text{II.1}$$

for the system containing 2N electrons with the closed shell configuration specified by the set of N orthonormal space orbitals φ_i, and having the state symmetry symbol $\Omega(^1\Sigma^+$ or $^1\Sigma_g^+)$.[35] A single Slater determinant suffices for a closed shell configuration, for a closed shell configuration plus one extra electron in an open shell or a closed shell configuration with one hole to form an open shell, and for those open shell configurations which arise if all open shell φ_i have the same spin function (that is, states for $M_S = \pm S$). If there are several electrons in a single open shell, or electrons distributed in open shells of <u>different</u> symmetry, the wave functions for the open shell configuration of definite state symmetry Ω can be written in the form,

$$\Phi_\Omega = \sum_K C_K \Phi_{(\Omega)}^K \quad , \qquad \text{II.2}$$

where the $\Phi_{(\Omega)}^K$ are single Slater determinants of the form in Eq. II.1 ordered by the superscript K. This index K identifies the possible various choices from the degenerate members of molecular spin orbitals available to the electrons in the incomplete shells.[36] The C_K in Eq. II.2 are determined <u>entirely</u> by symmetry requirements, that is, by combining the $\Phi_{(\Omega)}^K$ to form Φ_Ω of a definite state symmetry, Ω. The short sum in Eq. II.2 is <u>not</u> to be confused with "configuration interaction" and indeed configuration interaction wavefunctions for open shell systems might be written as <u>sums</u>

[35] The notation given in this section follows that employed in C. C. J. Roothaan, Rev. Modern Phys. <u>23</u>, 69 (1951); <u>ibid</u>, <u>32</u>, 179 (1960); C. C. J. Roothaan and P. S. Bagus, in <u>Methods in Computational Physics</u>, edited by B. Adler, S. Fernbach and M.Rotenberg, (Academic Press, Inc., New York, 1963), p. 47ff. These three papers will be referred to as T1, T2, and T3, respectively.

[36] Numerous examples of wave functions of the form of II.2 occur in the literature and basic texts. A convenient collection of such forms for $D_{\infty h}$ or $C_{\infty v}$ symmetry molecules is given by S. Fraga and B. J. Ransil in "Formulae for the Evaluation of Electronic Energies in the LCAO-MO-SCF Approximation", Technical Report 1961, Laboratory of Molecular Structure and Spectra, University of Chicago, pp. 236ff. The formulae given by Fraga and Ransil really have nothing to do with the LCAO approximation.

of selected Φ_Ω with coefficients determined by the variational method. It is quite proper to refer to both expressions II.1 and II.2 as "single configurations" since in both cases a unique set of space orbitals, φ_i, is implied. In open shell cases this set of space orbitals, φ_i, may give rise to several states (Ω) in which only the set of coefficients C_K will differ. (For example the X $^3\Sigma_g^-$, a $^1\Delta_g$, and b $^1\Sigma_g^+$ states of O_2).

The total energy expression for a wave function of the form of II.2 (and also II.1) may be written

$$E_\Omega = \sum_{\lambda,i} N_{i\lambda} H_{i\lambda} + \tfrac{1}{2} \sum_{\lambda,i} \sum_{\mu,j} N_{i\lambda} N_{j\mu} \mathcal{P}_{\lambda i,\mu j} - \tfrac{1}{2} \sum_{\lambda,m} \sum_{\mu,n} N_{m\lambda} N_{n\mu} \mathcal{Q}_{\lambda m,\mu n} + \sum_{\alpha>\beta} \frac{Z_\alpha Z_\beta}{R_{\alpha\beta}} , \qquad \text{II.3}$$

where the sums over both closed and open shell molecular orbitals of symmetry λ or μ are indicated by i and j, and sums over only open shell molecular orbitals are indicated by m and n. The last sum, over $\alpha>\beta$, is just the nuclear repulsion term(s). $N_{i\lambda}$ is the number of electrons in molecular orbital i of symmetry λ, and $H_{i\lambda}$ is the familiar one-electron integral contributions. The second and third terms here parallel those given by Roothaan and Bagus[35] in T3 and are valid for a wide range of open shell configuration cases. (But please note, no expansion method, or LCAO molecule orbitals, has been introduced at this point.) The expressions for $\mathcal{P}_{\lambda i,\mu j}$ and $\mathcal{Q}_{\lambda m,\mu n}$ are

$$\mathcal{P}_{\lambda i,\mu j} = \mathcal{J}_{\lambda i,\mu j} - \tfrac{1}{2} \mathcal{K}_{\lambda i,\mu j}$$

and

$$\mathcal{Q}_{\lambda m,\mu n} = \sum_\nu \alpha_{\lambda\mu\nu} \mathcal{J}^\nu_{\lambda m,\mu n} - \tfrac{1}{2} \sum_\nu \beta_{\lambda\mu\nu} \mathcal{K}^\nu_{\lambda m,\mu n} \quad . \qquad \text{II.4}$$

The $\mathcal{J}_{\lambda i,\mu j}$ and $\mathcal{K}_{\lambda i,\mu j}$ are two-electron integrals involving both closed and open shell molecular orbitals, φ_i, and the $\mathcal{J}^\nu_{\lambda m,\mu n}$ and $\mathcal{K}^\nu_{\lambda m,\mu n}$ are two-electron integrals involving only the open shell molecular orbitals, φ_m. The $\alpha_{\lambda\mu\nu}$ and $\beta_{\lambda\mu\nu}$ are the open shell coefficients and are obtained from the C_K of Eq. II.2.

If the total energy, as expressed by Eq. II.3, is minimized with respect to the orthonormal set of functions φ_i (the molecular orbitals), which occur in the integrals, $H_{i\lambda}$, $\mathcal{P}_{\lambda i,\mu j}$, and $\mathcal{Q}_{\lambda m,\mu n}$, one obtains the usual Hartree-Fock equations:

and

$$\left.\begin{aligned} F_C(\varphi_k, \varphi_m)\varphi_\ell &= \epsilon_\ell \varphi_\ell \quad , \\ F_O(\varphi_k, \varphi_m)\varphi_n &= \epsilon_n \varphi_n \quad , \end{aligned}\right\} \qquad \text{II.5}$$

for the closed shell molecular orbitals (indicated by φ_k and φ_ℓ) and for the open shell molecular orbitals (indicated by φ_m and φ_n), respectively. Solution of this set of coupled integro-differential equations for the φ_k and φ_m molecular orbitals and using Eq. II.3, gives the lowest energy possible for a wave function of the form of Eq. II.1 or II.2. Since the operators $F_C(\varphi_k,\varphi_m)$ and $F_O(\varphi_k,\varphi_m)$ depend on the φ_k and φ_m sets, an iterative procedure is required which yields the self-consistent field (SCF) wave function which is by definition the Hartree-Fock wave function. Thus when a direct numerical solution of Eqs. II.5 is possible, SCF wave functions and Hartree-Fock wave functions are identical.

The above program is indeed realized for atoms as was vigorously exploited by Hartree and many others. For electronic systems possessing less symmetry, direct numerical solution of Eqs. II.5 becomes much less inviting. If one considers diatomic molecules and writes the φ_i in terms of prolate spheroidal coordinates as

$$\varphi_i(r) = f_i(\xi,\eta)g_\alpha(\phi) \ , \qquad \text{II.6}$$

with the nuclei at the foci, then the Hartree-Fock equations, Eqn. II.5, for a diatomic molecule reduce to the general form

$$A\frac{\partial^2}{\partial\xi^2} f_i(\xi,\eta) + B\frac{\partial}{\partial\xi} f_i(\xi,\eta) + C\frac{\partial^2}{\partial\eta^2} f_i(\xi,\eta) + D\frac{\partial}{\partial\eta} f_i(\xi,\eta)$$
$$+ E\, f_i(\xi,\eta) + \sum_j \int G_i[f_j(\xi,\eta)]\, d\xi d\eta\, f_i(\xi,\eta) = \epsilon_i f_i(\xi,\eta) \ . \qquad \text{II.7}$$

The coefficients A, B, C, D, and E are simple functions of ξ, η, and the internuclear separation, R, and the integrand $G[f_i(\xi,\eta)]$ is only intended to show the integro-differential character of these equations. The explicit form follows simply from equations and a discussion given by Lennard-Jones and Pople.[37] The Hartree-Fock wave function for a diatomic molecule is thus to be gained from the numerical solution of this set of coupled elliptic partial integro-differential equations in ξ and η. Except for an approximate treatment by Berthier[38] for H_2, no serious attempts have been published. The numerical solution of partial differential equations in two variables has

---

[37] J. Lennard-Jones and J. A. Pople, Proc. Roy. Soc. (London), A210, 190 (1951).

[38] G. Berthier, in Calcul Des Fonctions D'Onde Moleculaire, Colloques Internationaux du CNRS LXXXII. (Paris, 1958), p. 115.

experienced some progress, but apparently the numerical solution of the coupled set of Eqs. II.7 still represents a formidable problem in this embryonic field of applied mathematics (see Fox[39] and Young[40] for surveys of methods useful for simpler forms of elliptic partial differential equations). It may not be too optimistic to think that it will be feasible to solve the Hartree-Fock equations for a few representative diatomic molecules (for example, H_2, Li_2, LiH, N_2 and CO) by direct numerical methods in the next decade.

If an analytical form for the molecular orbitals, φ_i, is now assumed, that is, if they are expanded in terms of certain known functions;[35]

$$\varphi_{i\lambda\alpha} = \sum_p \chi_{p\lambda\alpha}\, C_{i\lambda p} \ , \qquad \text{II.8}$$

the problem resolves to finding the linear expansion coefficients, $C_{i\lambda p}$, and an adequate expansion in terms of the expansion functions, $\chi_{p\lambda\alpha}$. Following Roothaan and Bagus[35] in T3 the energy expression is written

$$E_\Omega = \mathbf{H}^\dagger \mathbf{D}_T + \tfrac{1}{2}\, \mathbf{D}_T^\dagger \boldsymbol{\mathcal{P}}\, \mathbf{D}_T - \tfrac{1}{2}\, \mathbf{D}_0^\dagger \boldsymbol{\mathcal{Q}}\, \mathbf{D}_0 + \sum_{\alpha>\beta} \frac{Z_\alpha Z_\beta}{R_{\alpha\beta}} \ , \qquad \text{II.9}$$

where $\boldsymbol{\mathcal{P}}$ and $\boldsymbol{\mathcal{Q}}$ are now supermatrices with elements[35]

$$\mathcal{P}_{\lambda pq,\mu rs} = \mathcal{J}_{\lambda pq,\mu rs} - \tfrac{1}{2}\mathcal{K}_{\lambda pq,\mu rs}$$

and

$$\mathcal{Q}_{\lambda pq,\mu rs} = \sum_\nu \alpha_{\lambda\mu\nu} \mathcal{J}^\nu_{\lambda pq,\mu rs} - \tfrac{1}{2} \sum_\nu \beta_{\lambda\mu\nu} \mathcal{K}^\nu_{\lambda pq,\mu rs} \ . \qquad \text{II.10}$$

Equation II.10 corresponds to elements of Eqn. II.4. The supermatrix elements are thus constructed from electronic integrals involving the expansion functions $\chi_{p\lambda\alpha}$. The Hartree-Fock equations now become[35]

$$\left.\begin{aligned} \mathbf{F}_c \mathbf{C} &= \epsilon \mathbf{S} \mathbf{C} \\ \mathbf{F}_c \mathbf{C} &= \epsilon \mathbf{S} \mathbf{C} \end{aligned}\right\} \qquad \text{II.11}$$

and

---

[39] L. Fox, Numerical Solution of Ordinary and Partial Differential Equations, (Addison-Wesley Publ. Co., Inc., Reading, Massachusetts, 1962).

[40] David M. Young, in a Survey of Numerical Analysis, edited by J. Todd, (McGraw-Hill Book Co., Inc., New York, 1962), chap. 11.

This series of papers deals with the solution of Eqs. II.11 for diatomic molecules and specifically for the lowest state of any symmetry type arising from closed shells configurations or configurations which have several open shells of different symmetry (for example σ, π^n, $\sigma\pi^n$, and so forth). These equations are here reproduced to serve as a touchstone for this and following members of this series.

In choosing to solve the Eqs. II.11, one has thus bypassed relative incompetence at the numerical solution of the Hartree-Fock equations for diatomic molecules (Eq. II.7) and substituted the relatively well developed machinery of matrix methods and calculation of electronic integrals over analytic functions. In addition one has also assumed the task of exploring the convergence of expansions given by Eq. II.8 such that true Hartree-Fock wave functions are obtained.

The expansion method has been referred to in the literature as the "Roothaan Method", "Roothaan Scheme","extended basis set SCF", and called various other names. We would like to propose that one refer instead to the expansion method in terms of the Hartree-Fock-Roothaan Equations as given by Eq. II.11. This would thus imply on expansion form as systematized by Roothaan[35] in T1, indicate the adoption of the open-shell formalism given by Roothaan and Bagus[35] in T3, and, of course, imply the iterative solution to invariance in the $C_{i\lambda p}$ coefficients. One would thus be referring to a specific genera of equations, flexible in regard to the extent of the expansion and the nature of the expansion functions $\chi_{p\lambda\alpha}$.

This suggestion is primarily motivated by an attempt to clarify the term "Self-Consistent-Field". The solution of the Hartree-Fock Equations (Eq. II.5) yields the Hartree-Fock wavefunction which is identical with the Self-Consistent Field wavefunction, that is, only if the φ_i are exactly determined is the true self-consistency of the independent particle model really achieved. In contrast, one may have a hierachy of Hartree-Fock-Roothaan Equations and Hartree-Fock-Roothaan wavefunctions, where the members of the hierachy perhaps arise from different size or kinds of expansions of the form of Eq. II.8. The hierachy of Hartree-Fock-Roothaan wavefunctions thus gradually approaches the Hartree-Fock wavefunction in a limiting manner. One must remember that in speaking of LCAO-MO-SCF wavefunctions, or, as we propose, of Hartree-Fock-Roothaan (HFR) wavefunctions, that the self-consistency merely means a certain degree of invariance in the $C_{i\lambda p}$ coefficients and does not mean the true self-consistency of the independent particle model, except as the expansion converges to the true Hartree-Fock orbitals φ_i.

A remaining practical point may be noted before concluding this section. The basic limitation on how large an expansion basis set may be employed depends on the total number of unique $\mathcal{P}_{\lambda pq,\mu rs}$ and $\mathcal{Q}_{\lambda pq,\mu rs}$ supermatrix elements generated. The present versions of the Homonuclear and Heteronuclear diatomic SCF programs perform the contraction of the supermatrices such that the entire $\mathcal{P}$ or $\mathcal{Q}$ supermatrix must occupy the rapid access memory of the computer (the 32K core for an IBM 7094). Thus approximately 20000 total supermatrix elements are permitted. In terms of the total number of expansion functions, $\chi_{p\lambda\alpha}$ this requires that

$$\sum_{\lambda} \tfrac{1}{2}\, n_\lambda (n_\lambda + 1) \leq N_{max} \,, \qquad \text{II.12}$$

where n_λ is the number of expansion functions of symmetry λ. The present limit for N_{max} is 144 for homonuclear diatomic molecules and 172 for heteronuclear diatomic molecules. Even as this is written, modifications are underway to remove these limits, but the problem of computation time will go up sharply as still larger basis sets are employed.

III. THE DETERMINATION OF THE BEST HARTREE-FOCK-ROOTHAAN WAVE FUNCTION

The most time consuming and tedious task leading to the results presented here was the exhaustive study to determine the best basis set expansion, the optimal non-linear parameters (orbital exponents) of the expansion functions, the behavior towards convergence, and the effects of these various characteristics of the calculation on certain expectation values and molecular properties of the nitrogen molecule, to be discussed subsequently. This study on nitrogen and the following one for Li_2, was particularly exhaustive in order to provide useful general guidelines for similar studies on other first row homonuclear diatomic molecules. This section will display in detail the methods employed and conclude by presenting the final choice of the Hartree-Fock-Roothaan wave function for nitrogen. Evidence will be presented in support of the belief, herein advanced, that this final result is a very close approximation to the true Hartree-Fock wave function.

A. Basis Expansion Functions and Molecular Parameters

The ground electronic configuration of nitrogen in terms of molecular orbitals as established by molecular spectroscopy is written

$$N_2(X\ ^1\Sigma_g^+)\ 1\sigma_g^{\,2}1\sigma_u^{\,2}2\sigma_g^{\,2}2\sigma_u^{\,2}1\pi_u^{\,4}3\sigma_g^{\,2}\ ,$$

where the molecular orbitals are in the order of decreasing orbital energy as obtained from the analysis of the relative positions of the several Rydberg series ionization limits of $N_2(X\ ^1\Sigma_g^+)$. The use of the simply numbered symbols, $1\sigma_g$, $2\sigma_g$, $3\sigma_g$, $1\sigma_u$, $1\pi_u$, ..., is more suitable when dealing with extended basis set expansions for the molecular orbitals. The familiar symbols, $\sigma_g 1s$, $\sigma_g 2s$, $\sigma_g 2p$, $\sigma_u 1s$, $\pi_u 2p$, ..., which denote the parentage of the molecular orbitals with respect to the separated atoms limit, will be employed here instead to denote the individual STO symmetry molecular orbitals, as is explained below. Another useful notation suggested by Mulliken, that is, writing only the outer shell molecular orbitals as $z\sigma$, $y\sigma$, $x\sigma$, $w\pi$, $v\pi$, ..., is most useful when dealing with homologous series of molecules involving different numbers of closed inner shells of the separated atoms and for isoelectronic series of homonuclear and heteronuclear diatomic molecules. This last notation will be employed in this series only for such series of molecules. All of the calculations in this section for nitrogen ($X\ ^1\Sigma_g^+$) employ the experimental equilibrium separation, $R_e(\text{Exptl.}) = 2.068$ Bohr.

The general expansion form of the various molecular orbitals was given in Eq. II.8. The expansion functions, $\chi_{p\lambda\alpha}$, employed in this series of papers for homonuclear diatomic molecules are given by

$$\chi_{p\lambda\alpha} = 2^{-\frac{1}{2}} \left[\chi_{n_p \ell_p \lambda_\alpha}(\vec{r}_a) + \sigma_\lambda \chi_{n_p \ell_p \lambda_\alpha}(\vec{r}_b) \right], \qquad \text{III.1}$$

or explicitly

$$\chi_{p\lambda\alpha} = (2\zeta_p)^{n_p + \frac{1}{2}} [2(2n_p)!]^{-\frac{1}{2}} \left\{ r_a^{n_p - 1} e^{-\zeta_p r_a} Y_{\ell_p \lambda_\alpha}(\theta_a, \phi) + \sigma_\lambda r_b^{n_p - 1} e^{-\zeta_p r_b} Y_{\ell_p \lambda_\alpha}(\theta_b, \phi) \right\}. \qquad \text{III.2}$$

Detailed definition of the spherical harmonics, $Y_{\ell m}(\theta,\phi)$, and the coordinate systems employed are given by Wahl, Cade and Roothaan.[41] This rather cumbersome subscript notation on the expansion functions and the Slater-Type-Orbitals (STO's) should be interpreted as follows: the expansion function $\chi_{p\lambda\alpha}$, hereafter called a <u>STO symmetry molecular orbital</u>, specifies basis function p (which defines n_p, ℓ_p, and ζ_p of the STO's on centers <u>a</u> and <u>b</u>) of symmetry λ (that is, σ_g, σ_u, π_u, π_g, ...) which defines $|\lambda_\alpha|$ ($|\lambda_\alpha|$ is the projection of the orbital angular momentum on the molecular axis such that $|\lambda_\alpha| = 0, 1, 2, \ldots$ lead to $\sigma,\pi,\delta, \ldots$ STO symmetry orbitals) and σ_λ. If $\sigma_\lambda = (-)^{\lambda_\alpha}$, $\chi_{p\lambda\alpha}$ is a gerade (g) function and $\sigma_\lambda = (-)^{\lambda_\alpha + 1}$ implies $\chi_{p\lambda\alpha}$ is an ungerade (u) function. The subscript α on $\chi_{p\lambda\alpha}$ designates the subspecies of symmetry λ and specifies the λ_α values from among $\pm \lambda_\alpha$ or zero. The STO symmetry molecular orbitals, as well as linear combinations to form the $\Psi_{i\lambda\alpha}$, belong to an irreducible representation of the $D_{\infty h}$ point group.

A simple shorthand procedure will be employed in discussing the expansion basis sets. This is most easily conveyed by a few examples:

$$\sigma_g 1s = 2^{-\frac{1}{2}} \left[\chi_{1s}^{(a)} + \chi_{1s}^{(b)} \right], \quad \sigma_g 2p = 2^{-\frac{1}{2}} \left[\chi_{2p\sigma}^{(a)} + \chi_{2p\sigma}^{(b)} \right],$$

$$\sigma_g 3d = 2^{-\frac{1}{2}} \left[\chi_{3d\sigma}^{(a)} + \chi_{3d\sigma}^{(b)} \right], \qquad \text{III.3}$$

and analogous symbols for corresponding σ_u STO symmetry orbitals except with minus signs. The π_u, π_g, and higher type STO symmetry orbitals are similarly abbreviated by

[41] A. C. Wahl, P. Cade and C. C. J. Roothaan, J. Chem. Phys. <u>41</u>, 2578 (1964).

$\pi_u 2p$, $\pi_g 2p$, $\pi_u 3d$, $\pi_g 3d$, where for example

$$\pi_u 2p \equiv \left\{ \begin{array}{l} 2^{-\frac{1}{2}}[\chi_{2p\pi_+}^{(a)} + \chi_{2p\pi_+}^{(b)}] \quad , \\ 2^{-\frac{1}{2}}[\chi_{2p\pi_-}^{(a)} + \chi_{2p\pi_-}^{(b)}] \quad , \end{array} \right\} \qquad \text{III.4}$$

that is, includes the degenerate members of different α subspecies. The distinction between STO symmetry orbitals having the same symbol but different orbital exponents will be made by primes. The basis set composition will refer to the specific make-up (that is the set of n_p, ℓ_p, ζ_p of the expansion functions for each symmetry).

The restriction of these calculations to the employment of symmetry-adapted expansion functions, $\chi_{p\lambda\alpha}$, and hence symmetry-adapted molecular orbitals, $\varphi_{i\lambda\alpha}$, is not necessary and there has been doubts expressed by Löwdin[42] that such a choice really represents an absolute minimum even to Hartree-Fock approximation. The employment of symmetry-adapted molecular orbitals does, however, provide considerable simplification in dealing with the large number of supermatrix elements as is discussed by Wahl.[1] Even if it is useful to relax the restriction that the molecular orbitals, $\varphi_{i\lambda\alpha}$, be symmetry adapted, it is important to realize that in so doing the expansion basis set size would have to be considerably reduced for molecules as small even as nitrogen, especially if any optimization of orbital exponents is desired, not to mention other difficulties.

In the STO symmetry orbitals of Eqs. III.1 and III.2, it is of course, necessary that the functions centered on nuclei a and b be identical, that is, n_p, ℓ_p, λ_α, and ζ_p must be the same. Finally, it should be noted that basis set compositions for σ_g and σ_u type molecular orbitals, $\varphi_{i\lambda\alpha}$, are completely independent. Thus, the corresponding σ_g and σ_u STO symmetry orbitals (if indeed they are corresponding sets) do not have to have the same orbital exponents as was the case in the calculations by Ransil and Fraga. The usefulness of this extra degree of functional freedom was first pointed out by Huzinaga,[43] and Phillipson and Mulliken,[44] and is discussed in part B of this section.

---

[42] P. O. Löwdin, Rev. Modern Phys. 35, 496 (1963).

[43] S. Huzinaga, Proc. Theoret. Phys. (Japan) 19, 125 (1957).

[44] P. E. Phillipson and R. S. Mulliken, J. Chem. Phys. 28, 1248 (1958).

B. General Principles in Synthesizing the Expansion Basis Set; Illustration for $N_2(X\ ^1\Sigma_g^+)$.[45]

In these calculations on nitrogen and in general in seeking solutions to the Hartree-Fock-Roothaan equations, the problem of synthesizing the expansion basis set may be conveniently analyzed in terms of the following questions:

1st) How is the basis set composition decided? That is, how many STO symmetry expansion functions are needed to adequately represent each molecular orbital symmetry type and what kind of STO symmetry orbitals with respect to the n_p, ℓ_p, and ζ_p values? If several STO symmetry orbitals with the same n_p and ℓ_p, but different ζ_p values (such as, for example, $\sigma_g 2p$ and $\sigma_g 2p'$), are used, how many of such multiple form are recommended and with what spread or values of ζ_p's? What is the quickest and best manner to decide the basis set composition in terms of computer time? Associated with these questions is the problem of deciding what role the related atomic Hartree-Fock-Roothaan wave functions should play in contributing to representing at least the inner shell molecular orbitals. These questions must all find answers such that the total number of matrix elements satsifies Eq. II.12.

2nd) What sequence, combination, and extent of optimization of the orbital exponents, ζ_p, of the STO symmetry orbitals chosen to form the basis set composition is necessary and useful? This question is more inextricably tied to the preceding questions for small or inadequate basis sets, but may be treated as approximately separated when large expansion basis sets are employed. As the existing program permits one, two, or three ζ_p's to be optimized simultaneously, this question also involves the assessment of the relative merits of the many possible combination schemes of exponent optimizations. Also, how does the relative importance of optimization of the ζ_p's depend on the original source of the starting ζ_p's, for example ζ_p's from atomic results for inner shells and ζ_p's from interpolation or extrapolation schemes?

---

[45] The basic problem considered in this section has also been dealt with extensively by Bagus, Gilbert, Roothaan, and Cohen,[46] for the first row atoms. While the general procedures to obtain very accurate approximations to the Hartree-Fock wave function are basically similar in atoms and diatomic molecules, practical difficulties prevent the more exhaustive methods used for atoms from being used for diatomic molecules.

[46] P. Bagus, T. L. Gilbert, C. C. J. Roothaan, and H. D. Cohen, "Analytic Self-Consistent Field Functions for First-Row Atoms", to be submitted to Phys. Rev. for publ.

3rd) How close is the best Hartree-Fock-Roothaan SCF wave function to the true Hartree-Fock SCF wave function? How is this to be measured? For atoms, many cases exist where numerical Hartree-Fock wave functions have been determined and a direct point by point comparison with the Hartree-Fock-Roothaan wave functions is possible. These comparisons have been very encouraging in most cases.[46] Such a direct comparison with diatomic molecules is not possible unless a few Hartree-Fock wave functions are obtained by the numerical solution of Eq. II.7. Other means must then be found to indicate the convergence of these calculations toward the true Hartree-Fock result.

In the broader and purely mathematical sense, the problem of the rate of convergence of the approximation of the molecular orbitals, $\varphi_{i\lambda\alpha}$, should also deal with the nature and form of the expansion functions, $\chi_{p\lambda\alpha}$. That is, whether other analytic forms of $\chi_{p\lambda\alpha}$ might be generally or specifically advantageous. Even the consideration of different kinds of expansion functions for different purposes might be useful. The commitment to the STO symmetry expansion functions of Eq. III.2 in this series of papers, is based largely on a background of success and no serious practical competitors and not on any formal demonstration that such a form minimized the number of terms in the expansion of Eq. II.8.

4th) What role can the various molecular properties and expectation values play as criteria of the convergence towards Hartree-Fock results? Strictly speaking the progression of calculations steadily and monotonously improves the total energy, but this gradual improvement provides no assurance that the wave function is an equally good approximation to the true Hartree-Fock wavefunction in all regions of space. The convergence of the total energy may mask serious deficiencies in the wave function and the problem is to discover how to measure this and correct for it. This aspect will be considered for N_2 and N_2^+ molecular-ions in paper III.B of this series.

The four items above stress the purely numerical and empirical nature of the problem under consideration and introduce some nomenclature. The predominate influence, so long as small, or minimal, expansion basis sets are employed, has been from chemical or physical intuition, couched in terms of distorted, hybridized, or polarized atoms in the molecule, and there is good reason to retain these ideas if possible. There is, however, great difficulty in properly and uniquely assessing these intuitive aspects when the basis set is large and for molecular orbitals which depart radically from the distorted one-center problem, or atom, are involved. The problem, especially for the outer molecular orbitals, becomes more properly one of a purely mathematical nature,

namely to best approximate the molecular orbitals with as few terms as possible. This purely mathematical aspect has been largely and necessarily ignored in the past when considering the expansion functions and really takes the form of curve fitting of a most tedious kind. Physical intuition still can play a measured role and is certainly desirable, and chemically significant interpretations can be won, but less so in terms of the simple single expansion coefficients, $C_{i\lambda p}$. This is partially why the interpretative and chemical aspects of this series of papers is reserved for homologous and isoelectronic series of diatomic molecules where a direct approach in terms of molecular orbital charge density contours is proposed.

Previous calculations of the kind considered in this series have also probed the problem of choosing the basis set composition. These calculations include the results of Richardson[33] for N_2, Lefebvre-Brion, Moser, and Nesbet[47] for CO, Clementi[48] and Nesbet[49] for HF, Manneback[50] for Li_2, Kahalas and Nesbet[51] for LiH, and more recently the results of McLean[52] for LiF, Yoshimine[53] for BeO, Nesbet[34] for the 14 electron systems N_2, CO, and BF, and finally the HCℓ results of Nesbet.[54] In general these efforts, all for extended basis sets, seem to suffer from two defects. First, practical considerations have usually forced the authors to restrict, often severely, the size of the expansion basis set, the extent of optimization of orbital exponents, and most importantly, to restrict exhaustive tests of the basic assumptions made in support of the particular calculations. The second defect is associated with the fact that these are, with one exception, studies of individual molecules and do not permit the study of whole homologous and/or isoelectronic series. The present investigations generously relax these restraints.

Mulliken[55] has given an interesting discussion on criteria for the construction of good LCAO-MO-SCF wave functions, but the specific suggestions made were based mostly on the results on HF by Clementi.[48] In particular several specific warnings

[47] H. Lefebvre, C. Moser and R. K. Nesbet, J. Chem. Phys. 35, 1702 (1961).

[48] E. Clementi, J. Chem. Phys. 36, 33 (1962).

[49] R. K. Nesbet, J. Chem. Phys. 36, 1518 (1962).

[50] C. Manneback, Physica 29, 769 (1963).

[51] S. L. Kahalas and R. K. Nesbet, J. Chem. Phys. 39, 529 (1963).

[52] A. D. McLean, J. Chem. Phys. 39, 2653 (1963).

[53] M. Yoshimine, J. Chem. Phys. 40, 2970 (1964).

[54] R. K. Nesbet, J. Chem. Phys. 41, 100 (1964).

[55] R. S. Mulliken, J. Chem. Phys. 36, 3428 (1962).

given by Mulliken about "balanced" sets and other matters seem particularly relevant only when small or marginal expansion basis sets are employed. This matter will be reconsidered later.

Answers to the four groups of questions given cannot claim to be either unique or complete and are "general" only within certain bounds. The remainder of this section is devoted to describing the calculations on N_2 as a start to answering these questions.

Three different and relatively independent schemes were employed in synthesizing the expansion basis set for $N_2(X\ ^1\Sigma_g^+)$ at R_e = 2.068 Bohr. The first scheme takes the perspective that the N_2 wavefunction should be built up completely from scratch and the relationship to the two $N(^4S)$ atoms be gleaned directly. The second and third scheme consider the N_2 molecule to be formed by two distorted $N(^4S)$ atoms separated by R_e, and the Hartree-Fock-Roothaan wavefunctions for the $N(^4S)$ atom play a key role. In these last two schemes the calculations of Bagus, Gilbert, Roothaan and Cohen[46] for atoms are employed and the two differ in which atomic basis set is used as the starting point.

A quick preview of the progress of two of these schemes to build up the expansion basis set, expressed in terms of certain energy quantities, is given in Figs. 2, 3, 4, and 5, and in Tables I and II. In Table I, the total energy, kinetic and potential energy, virial, and orbital energies are documented for the first and second schemes. The variation of these quantities as the basis set synthesis progresses for both schemes is illustrated in Figs. 2 (total energy), 3 (orbital energies), 4(kinetic energy), and 5 (potential energy). In these figures the lines connecting the points do not correspond to any curve fitting, but merely serve to connect the points in sequence. The following discussion will define these Tables and Figures completely.

The construction of basis set 1 started with the reproduction of Ransil's Best-Minimal-Molecular-Orbitals (BMMO) set[29], called set 1A here, with the ζ_p's of $\chi_{p\sigma_g}$ and $\chi_{p\sigma_u}$ complements equal (g = u constraint). The general procedure was then to add new STO symmetry orbitals one or two at a time and optimize certain combinations of orbital exponents. The overall basic logic was simply to add $\chi_{p\lambda\alpha}$ STO symmetry orbitals of lowest permitted ℓ_p until no further improvement was evident and then add $\chi_{p\lambda\alpha}$ with the next highest ℓ_p value. For example, in σ_g symmetry, $\sigma_g$ns and $\sigma_g$np, and $\sigma_g$ns' and $\sigma_g$np' types were practically exhausted before starting to add σ_gnd STO symmetry orbitals. The next step, however, from the BMMO results of Ransil[29] (Set 1A) was the relaxation of the g = u constraint which gave a small improvement. Set 1B was

obtained from Set 1A by double (i.e. simultaneous) optimizations of the ζ_p's for each of the $\sigma_g 1s$ and $\sigma_u 1s$; $\sigma_g 2s$ and $\sigma_u 2s$; and $\sigma_g 2p$ and $\sigma_u 2p$ pairs. Then, in addition, certain other double optimizations were carried out of ζ_p's only in σ_g or σ_u symmetry and several single optimizations which finally gave what may be termed the BMMO ($g \neq u$) set. Sets 1C through 1G, represented by the first, and steepest drop, of the solid curve in Fig. 2, correspond to the gradual improvement to the "double zeta" approximation (Set 1G). At each intermediate point the ζ_p's of the new STO symmetry orbitals, that is $\sigma_g 1s'$ and $\sigma_u 1s'$ (Set 1C), $\sigma_g 2s'$ and $\sigma_u 2s'$ (Set 1D), $\pi_u 2p'$ (Set 1E), $\sigma_g 2p'$ (Set 1F), or $\sigma_u 2p'$ (Set 1G), respectively, were simultaneously optimized with the original unprimed analog and a few other ζ_p's, usually from those $\chi_{p\lambda\alpha}$ which are important in the same symmetry, were single reoptimized. Thus when a second $\sigma_g 2s$ was added, $\sigma_g 2s'$, the ζ_p's of $\sigma_g 2s$ and $\sigma_g 2s'$ were doubly optimized and then the ζ_p's of $\sigma_g 1s$ and $\sigma_g 1s'$ were singly reoptimized. An exhaustive and complete reoptimization of all ζ_p's was not carried out at each stage, however. Set 1G should be comparable with Richardson's best double zeta calculation,[33] but actually the energy for Set 1G is much lower than Richardson's result (i.e. -108.8914 Hartree versus -108.785 Hartree). Although Richardson's set did not have $\sigma_g 1s'$ and $\sigma_u 1s'$ STO symmetry orbitals, most of the improvement through Set 1G is due to more thorough optimization of orbital exponents. The first plateau of the solid curve in Fig. 2, corresponding to Set 1H through Set 1K, represents the addition of new STO symmetry orbitals such as $\pi_u 2p''$, $\sigma_g 2p''$, and $\sigma_g 3s$, that is, additional $\chi_{p\lambda\alpha}$ of already existing kinds, differing only in different ζ_p's or n_p values, but no new ℓ_p values. The new ζ_p's were optimized in a similar fashion as before, except now, with up to three $\chi_{p\lambda\alpha}$ identical except for ζ_p's, successive double optimizations were employed (a few triple optimizations indicated that well chosen consecutive double optimizations were as effective). This also increases the lability towards degeneracy of the expansion basis set; so not only did this stage contribute only slight improvement in the energy, it was difficult to keep the calculation in production.

The last major improvement in constructing basis set 1, shown by the second and smaller drop of the solid curve in Fig. 2, was obtained by the introduction of a new ℓ_p value, namely the addition of $\sigma_g 3d$ (Set 1L) and $\pi_u 3d$ (Set 1M) STO symmetry orbitals. The ζ_p's of the new STO symmetry orbitals were singly optimized and there was no exhaustive back optimizations to permit readjustment of the ζ_p's of the $\chi_{p\lambda\alpha}$ already present. Basis sets 1N through 1R were formed by introducing $\sigma_u 3d$, $\sigma_g 3d'$, and $\pi_u 3d'$ STO symmetry orbitals and also adding $\sigma_g 4f$ and $\pi_u 4f$ STO symmetry orbitals.

Again the new functions were either doubly optimized with analogous unprimed forms or just single optimized. This last stage (1N through 1R) gives rise the second plateau of the solid curve in Fig. 2 and here the next new ℓ_p value, involving $\ell_p = 3$, shows no significant drop off. Set 1R consists of 11 STO symmetry orbitals representing σ_g molecular orbitals, 7 representing σ_u molecular orbitals, and 6 representing the single $1\pi_u$ molecular orbital, or in short this is a 11×7×6 set. This set (1R) gives rise to 115 matrix elements thus leaving room for a few additional basis functions. To test what additions might be useful, a few additional STO symmetry orbitals were added to each symmetry type holding the other two fixed. These single SCF runs, called "saturation" runs, tested the usefulness of adding $\sigma_g 4d$, $\sigma_g 5f$, $\sigma_g 3d''$, $\pi_u 3p$, $\pi_u 3d''$, $\sigma_u 3s$, $\sigma_u 3p$, $\sigma_u 4f$, and certain other STO symmetry orbitals. This series of single SCF saturation runs suggested the addition of $\sigma_g 3d''$ and $\sigma_u 3s$ basis functions which yielded set 1S, a 12×8×6 set, which concluded the buildup of basis set 1 and the first scheme of synthesizing the basis set. The ζ_p's of these two new STO symmetry orbitals were optimized either singly or together with analogous types already present as in the preceding steps.

It may be profitable to make several points here before going on to the description of the second scheme of synthesizing the expansion basis set. In the first place, and most important for assessment of the convergence towards the true Hartree-Fock results, is the striking appearance of the solid curve in Fig. 2 which displays the progressive improvement in the total energy (see Table II for energy differences). Particularly encouraging is the fact that this curve seems to have leveled off and is only very slightly affected (in the third or fourth decimal place) by adding more STO symmetry functions of types already present or even new types of functions from the remaining possibilities (STO symmetry functions with $n_p \leq 6$ and $\ell_p \leq 3$ permitted). The leveling off follows two substantial drops in the energy improvement curve associated with doubling the minimal basis set and the introduction of basis functions with $\ell_p = 2$, respectively.

The second point is that the total energy for basis set 1S is -108.9888 Hartree compared to the experimental value of -109.586 Hartree. This difference, about 16.244 e.v., reflects not only the improvement yet to be obtained to Hartree-Fock limits, but the intrinsic shortcomings of the Hartree-Fock approximation. It seems that the bulk of improvement must lie with the latter and only a rather small amount remains to be gained within the Hartree-Fock approximation.

To achieve a Hartree-Fock-Roothaan result which is an even closer approximation to the true Hartree-Fock result than the results of basis set 1S, the remaining source of improvement is most likely to be gained from either, i) continued and relentless optimization and reoptimization of ζ_p's, and substitution of one $\chi_{p\lambda\alpha}$ for another (for example, replace a $\sigma_g 2p$ function by a $\sigma_g 3p$ function) within basis set 1S, or, ii) continued extension of the expansion basis set with the addition of more functions of types already present or new types. This second possibility seems unlikely to be too useful except perhaps in giving overwhelming conviction that convergence has indeed been achieved. Remarks already made have indicated the likelihood that the addition of many new functions will give only a small reward for much extra effort. Besides, this second possibility is presently beyond the capability of the existing computer program, which does not permit basis sets giving rise to more than 144 matrix elements. Any small improvement which remains must then come from the pursuit of i), that is by extensive reoptimizations of the ζ_p's of set 1S. In building up set 1S, the ζ_p's of the new $\chi_{p\lambda\alpha}$ were optimized either singly or in combination with the $\chi_{p\lambda\alpha}$'s of <u>like</u> symmetry and ℓ_p already present. Therefore any improvement via i) must come from the back optimizations and reoptimizations of the ζ_p's of the <u>whole</u> basis set at <u>each</u> stage to permit the old $\chi_{p\lambda\alpha}$ to readjust to the addition of the new $\chi_{p\lambda\alpha}$. It is likely that the bulk of this readjustment for STO symmetry orbitals of the same symmetry but different ℓ_p values is absorbed in the vector components, but perhaps the small residue is only to be gained by following path i). For a large basis set, optimization of the ζ_p's is very expensive, especially if double optimizations are desired, so this problem was postponed until the second and third schemes were explored. See Table III for the terminal wave function resulting from this first scheme (that is, basis set 1S).

The synthesis of the basis set in the second and third schemes was based on the use of the Bagus, Gilbert, Roothaan, and Cohen results for the $N(^4S)$ atom.[46] The basic plan was to employ STO symmetry functions constructed from the atomic basis sets and then to add $\chi_{p\lambda\alpha}$, especially those with $\ell_p = 2$, which seem <u>necessary</u> from the results of scheme one. The Bagus, Gilbert, Roothaan and Cohen results give several Hartree-Fock-Roothaan wave functions for $N(^4S)$ which differ in the size of the basis set, that is, in the number of <u>s</u> and <u>p</u> Slater-Type-Orbitals employed. These results for the first row atoms are the fruit of a dedicated effort to obtain the best possible expansion set for several arbitrary levels of approximation. For each set exhaustive optimization, reoptimization, and back optimization of the ζ_p's was carried out.

The depth of study of this effort is emphasized to point out the care that was devoted to insuring that both inner and outer shell atomic orbitals were very close to the true Hartree-Fock orbital results. Translated into practical terms, this means that these sets are particularly valuable for these molecular calculations since the atomic cores are accurately represented by as <u>few</u> terms as possible, thus permitting more flexibility in the addition of <u>new</u> $\chi_{p\lambda\alpha}$. The second and third scheme to construct the basis set for N_2 differ only in the choice of which Hartree-Fock-Roothaan wave function for $N(^4S)$ was employed. Since the third scheme (really the second chronologically) was abandoned when it became evident scheme two (really the third chronologically) was superior, only the results of the second scheme are presented.

The two Hartree-Fock-Roothaan wave functions for $N(^4S)$ which are of particular interest here are the "nominal" set and the "accurate" set of Bagus, Gilbert, Roothaan and Cohen.[46] The basis set composition of the <u>nominal</u> set is; 1s(ζ = 6.346), 1s"(10.507), 2s(1.697), 3s(3.715); 2p(1.352), 2p'(2.555), and 2p"(5.573), which yields -54.40080 Hartrees for the total energy. The <u>accurate</u> set has the basis set composition; 1s(ζ = 6.037), 1s'(10.586), 2s(1.588), 2s'(2.539), 3s(7.334); 2p(1.222), 2p'(1.890), 2p"(3.270), and 2p"'(7.677), and gives a total energy of -54.40093 Hartrees for $N(^4S)$. A number of <u>single</u> SCF runs were made for $N_2(X\ ^1\Sigma_g^+)$ at R_e = 2.068 Bohr to explore the merits of using these atomic basis sets, either unchanged or mixed, together with <u>other</u> $\chi_{p\lambda\alpha}$ involving ℓ_p = 2 and 3 based on the results of the first scheme. It was decided from these calculations, to employ as a starting set for the second scheme a composite set of STO symmetry functions constructed by using the five s-functions of the <u>accurate</u> set in σ_g and σ_u symmetry, the three p-functions from the <u>nominal</u> set in σ_g and π_u symmetry, the two p-functions from the <u>marginal</u> set in σ_u, and then $\sigma_g 3d$, $\sigma_g 4f$, $\sigma_u 3d$, $\pi_u 3d$, and $\pi_u 4f$ STO symmetry orbitals as recommended from the build up of Set 1 but with independent ζ_p's.[56] The actual <u>starting</u> basis set for

---

[56] This choice was also influenced by collateral calculations and suggestions by various members of this group, especially those by Dr. J. B. Greenshields.

the second scheme was therefore,

$\sigma_g 1s(\zeta = 6.037)$, $\sigma_g 1s'(10.586)$, $\sigma_g 2s(1.588)$, $\sigma_g 2s'(2.539)$, $\sigma_g 3s(7.334)$, $\sigma_g 2p(1.352)$, $\sigma_g 2p'(2.555)$, $\sigma_g 2p''(5.573)$, $\sigma_g 3d(1.352)$, $\sigma_g 3d'(2.555)$, $\sigma_g 3d''(5.573)$, $\sigma_g 4f(1.917)$; $\sigma_u 1s(6.037)$, $\sigma_u 1s'(10.586)$, $\sigma_u 2s(1.588)$, $\sigma_u 2s'(2.539)$, $\sigma_u 3s(7.334)$, $\sigma_u 2p(1.497)$, $\sigma_u 2p'(3.247)$, $\sigma_u 3d(1.917)$; $\pi_u 2p(1.352)$, $\pi_u 2p'(2.555)$, $\pi_u 2p''(5.573)$, $\pi_u 3d(1.497)$, $\pi_u 3d'(3.247)$, and $\pi_u 4f(1.917)$. This is Set 2B in Tables I and II, and Figs. 2,3,4,5.

Set 2A, which is obtained from set 2B by deleting all $\chi_{\lambda p\alpha}$ with $\ell_p = 2$ or 3, is only a single SCF result with no "molecular" optimizations of the ζ_p's and is included purely for comparative purposes. Set 2A is an 8×7×3 size set which gives a total energy for N_2 of -108.8967 Hartrees and may be compared with the gradual build up set 1I, which is a 7×6×3 size set with total energy -108.8992 Hartrees. Set 1I is the smallest set in the gradual build up scheme which gives a lower energy than set 2A and lacks only $\sigma_g 3s$ and $\sigma_u 3s$ STO symmetry orbitals from being equivalent to set 2A [except for the ζ_p's, of course]. How can the smaller basis set, set 1I [7×6×3 in size], give a better energy than the larger set, set 2A [8×7×3 in size]? The answer ζ_p's and certainly set 2A would give the better result if the ζ_p's were all optimized. However, if set 2B, which also has no "molecular" optimization of the ζ_p's, and is a 12×8×6 size set, is now compared with 1S, the result of extensive optimizations as described before and also is a 12×8×6 size set, the surprising result is that the proposed starting set of scheme two, set 2B, is already lower in energy than the laborous result of scheme one, set 1S [the energy of set 2B is -108.9897 Hartree and the energy of set 1S is -108.9888 Hartree, a difference of |0.0009| Hartree]! In addition, except for the ζ_p's, set 1S and 2B are identical in basis set composition; thus the small difference must be attributed entirely to the ζ_p values. Two possible explanations may be advanced to understand this paradox.

A first possible explanation suggests that this small energy difference reflects the inadequacy in scheme one of the optimization of those ζ_p values for $\chi_{p\lambda\alpha}$ which significantly affect the $1\sigma_g$ and $1\sigma_u$ molecular orbitals, these being very important contributors to the total energy. Although there was considerable optimization of the ζ_p's in scheme one, the procedure followed was certainly not comparable to the exhaustive optimizations of Bagus, Gilbert, Roothaan and Cohen,[46] for $N(^4S)$ and a small improvement in the quality of the $1\sigma_g(\sim 1s_N)$ and $1\sigma_u(\sim 1s_N)$ molecular orbitals might account for this small deficiency of the gradual build up set 1S. As may be noted, the $\epsilon_{1\sigma_g}$ and $\epsilon_{1\sigma_u}$ values are lower for the starting set 2B than for the final

set 1S by small amounts and both are lower than the ϵ_{1s} value for N(^{4}S). Argument based solely on this evidence is weak and unconvincing and in light of the comparison of basis sets 1I and 2A cited earlier, this explanation is not the major reason why the proposed starting set, set 2B, is better than the final set of the gradual build up, set 1S.

The second proposed explanation is that extensive optimizations of the ζ_p's should be performed only after the basis set composition as a whole, that is the entire set of n_p, ℓ_p, and starting ζ_p's of the $\chi_{p\lambda\alpha}$ for each symmetry, has been decided. This explanation thus suggests that the gradual build up of basis set 1S failed to permit sufficient readjustment of the entire set of ζ_p's at each stage. Therefore, through basis set 1K, which is the last set in scheme one before STO symmetry orbitals with ℓ_p = 2 and 3 were added, a better result is obtained than from basis sets based on unoptimized atomic sets only (and no σ_g3d, π_u3d STO symmetry orbitals) because the optimizations through set 1K permit the important outer shell distortions due to molecule formation but probably at the slight expense of representing the inner parts of the molecular orbitals involving σ_g2p, σ_u2p, and π_u2p type STO symmetry orbitals (as well as the $1\sigma_g$ and $1\sigma_u$ molecular orbitals). Then continuing to set 1S by addition of $\chi_{p\lambda\alpha}$ with ℓ_p = 2 and 3 and only optimizing the newly added STO symmetry orbitals, the σ_g2p, σ_g2p', σ_g2p", π_u2p, π_u2p', and π_u2p" basis functions were trapped in a manner which prevented their readjustment except through the linear expansion coefficients. This readjustment of the ζ_p's of the $\chi_{p\lambda\alpha}$ with ℓ = 0 and 1 would permit higher quality representation of the inner parts of the molecular orbitals since the σ_g3d and π_u3d types were now also available for representing the outer parts, or polarization, of these molecular orbitals. Conversely, set 2B, which is an unoptimized atom set with the addition of σ_g3d, σ_g4f, σ_u3d, π_u3d, and π_u4f type STO symmetry orbitals, was able to well represent the inner parts of the molecular orbitals by using atomic ζ_p's and obtain a substantially good representation of the outer parts from $\chi_{p\lambda\alpha}$ with ℓ_p = 2 and 3 together with some flexibility in the $\chi_{p\lambda\alpha}$ with ℓ_p = 0 and 1. Set 2B thus was large enough in size, and versatile enough in original composition, to slightly eclispe set 1S entirely through atomic ζ_p's and the vector components.

The second argument seems much more plausible and it was decided to start scheme two with the full 12x8x6 size set (set 2B) and carry out the optimization of the ζ_p's with the whole set present.

Set 2C was obtained from set 2B by singly optimizing all ζ_p's in order of most important vector components in any symmetry. The improvement in total energy from set

2B to set 2C was from -108.9897 Hartree to -108.9926 Hartree with the major improvements coming from the optimization of the ζ_p's for the $\sigma_g 2s(\Delta E = 0.00071)$, $\sigma_g 2p(\Delta E = 0.00018)$, $\sigma_g 2s'(\Delta E = 0.00009)$, $\pi_u 3d(\Delta E = 0.00049)$, $\sigma_g 4f(\Delta E = 0.00027)$, and $\pi_u 4f(\Delta E = 0.00078)$ STO symmetry orbitals. The relatively large energy improvements from the $\pi_u 3d$, $\sigma_g 4f$, and $\pi_u 4f$ basis functions reflects more the starting choices of the ζ_p's rather than the importance of these basis functions. The concluding set, set 2D, was obtained by <u>again</u> singly optimizing <u>all</u> ζ_p's from the preceding set, set 2C. The <u>total</u> improvement in the energy in going from set 2C to set 2D was rather small ($\Delta E = 0.00025$) with the <u>largest</u> improvement from a single optimization contributing only 0.00005 H. This indicated that further passes of single optimizations, either in total or partially, would not be rewarding. The last feasible prospect would be to perform various double optimizations and these were considered to be potentially unproductive relative to the machine time involved. Thus set 2D is the final result for scheme two and this wave function is given in Table IV.

The dashed line in Fig. 2 shows the energy values for basis sets 2A, 2B, 2C, and 2D. This curve is less emphatic as a testimony of convergence except that it indicates an energy limit in the close neighborhood of the limit of the curve from the gradual build up scheme. That other schemes could be divised is not unlikely, but it is doubtful that the energy result could be significantly lower than the results of set 2D (actually the energy difference between basis sets 1S and 2D is not very large, $|\Delta E| = 0.0040$ Hartrees of 0.1088 ev.).

How have these results (and other minor excursions of calculations on N_2 not presented here) helped in suggesting answers to the questions posed at the beginning of this section? For calculations on diatomic molecules it seems imperative to start with <u>atomic</u> Hartree-Fock-Roothaan wavefunctions whose basis set are large enough to adequately represent the <u>atomic</u> orbitals, <u>but</u> small enough to permit the addition of new $\chi_{p\lambda\alpha}$ and if still possible leave room for further exploration. In addition to the $\chi_{p\lambda\alpha}$ arising from the atomic results, it is <u>essential</u> to have at least one, and preferably two, $\chi_{p\lambda\alpha}$ STO symmetry orbitals with $\ell_p = 2$. Multiple $\chi_{p\lambda\alpha}$, differing only in ζ_p, for example $\sigma_g 2p$, $\sigma_g 2p'$, and $\sigma_g 2p''$, are <u>necessary</u> either from atom parentage or possibly for addition functions (for example $\pi_u 3d$ and $\pi_u 3d'$ in basis sets 1S and 2D). It is also clear that the "double-zeta" approximation[33] leaves much to be desired since this result would do no better than level off on the first and upper plateau of the solid curve of Fig. 2. In addition, the expectation values for the "double-zeta" approximation are suspect as discussed in paper III. B. The requirements on the size

and composition of the basis set suggested by the preceding remarks can be satisfied within the present restriction of the total number of matrix elements for all first row homonuclear diatomics, but perhaps without crushing conviction for O_2 and F_2.

The optimization of orbital exponents is crucial for small basis sets but can never alone absorb the deficiency due to a lack of expansion functions. The number and secondly, the kind of STO symmetry orbitals are still the most important considerations and the energy improvement to be gained by exponent optimization decreases sharply as skill in picking a starting basis set composition improves. This has been illustrated in this section for $N_2(X\ ^1\Sigma_g^+)$. After the set of n_p and ℓ_p for the $\chi_{p\lambda\alpha}$ representing each symmetry type is decided and a set of ζ_p is chosen from either atomic results, interpolation, extrapolation, or elsewhere, optimization of certain orbital exponents seems obligatory. As emphasized before it seems essential to do these optimizations with either the whole set present (which is preferable) or to back optimize the ζ_p's very extensively as the basis set is built up. The calculations reported here, and others to be reported, indicate that optimization of certain ζ_p's make no significant improvement. Recognition of these certain ζ_p's, or more properly the $\chi_{p\lambda\alpha}$, permits a curtailment of the optimization of the ζ_p's with confidence that little or nothing is lost and this considerably reduces the computation time. Such curtailment has been practiced in the present paper only for the potential curve points of $N_2(X\ ^1\Sigma_g^+)$ and for the $N_2^+(X\ ^2\Sigma_g^+$, $A\ ^2\Pi_u$, and $B\ ^2\Sigma_u^+)$ molecule-ions.

Although not exhaustively tested, triple optimizations seem to accomplish no more than arranged combinations of double and/or single optimizations and are not recommended. Carefully chosen combinations of single optimizations, or exhaustive and repetitive single optimizations, seem to accomplish almost as much as a double optimization involving the same two ζ_p. This is based only on a few test cases and probably depends on the particular case and very importantly on the size of the basis set. The major argument against extensive double and/or triple optimizations is the tremendous time investment necessary for molecules. The general problem of the simultaneous optimization of all orbital exponents is thus not definitively solved and this represents a defect in the present efforts. It is our belief, however, that for large basis sets series of single optimizations are as effective as such a general solution would be.

Before leaving the discussion of basis set composition and the ζ_p values, a few remarks about the "split-zeta" method proposed by Huzinaga[43] and Phillipson and Mulliken[44] was promised. The Best-Minimal-Molecular-Orbital (BMMO g = u) sets of Ransil[29] restricted the ζ_p such that $\zeta_{\sigma_g 1s} = \zeta_{\sigma_u 1s}$, $\zeta_{\sigma_g 2s} = \zeta_{\sigma_u 2s}$, and $\zeta_{\sigma_g 2p} = \zeta_{\sigma_u 2p}$,

and, of course, that equal numbers of $\chi_{p\lambda\alpha}$ represent the σ_g and σ_u molecular orbitals. The improvement to be gained by relaxing the $\zeta_{\sigma_g} = \zeta_{\sigma_u}$ restraint to give the BMMO($g \neq u$) results were indicated in going from set 1A (BMMO $g = u$) to set 1B (BMMO $g \neq u$) on the solid curve of Fig. 2. That this is a significant improvement is not to be doubted relative to the BMMO($g = u$) result, but this degree of flexibility seems far less important relative to extending the basis set and permitting $\sigma_g 3d$, $\pi_u 3d$, and other such $\chi_{p\lambda\alpha}$. It is our present conclusion that the complete separation of, for example, σ_g and σ_u, basis function sets is most important only in permitting different numbers of $\chi_{p\lambda\alpha}$ for the two symmetries due to having more σ_g type molecular orbitals than σ_u, and due to the fact, as has been discovered, that fewer σ_u expansion functions are necessary even when an equal number σ_g and σ_u molecular orbitals are present.[57] Any exhaustive treatment should keep them separated but as the ζ_p's in Tables III and IV show analogous ζ_p's differ only slightly.

The question of measuring how closely our best results (basis set 2D) compares with the true Hartree-Fock results is less easy to answer conclusively. This comparison refers to a point by point comparison of the final Hartree-Fock-Roothaan wave function and a comparison of certain expectation values and molecular properties. In the paper by Bagus, Gilbert, Roothaan, and Cohen[46] this question is considered at length for first row atoms and the very favorable comparison of the Hartree-Fock-Roothaan wave functions with the numerical Hartree-Fock wave functions is delivered with crushing conviction. Lacking even one molecular Hartree-Fock wave function (from solving Eq. II-17 numerically) our discussion must be based almost entirely on observing the convergence of the calculation. If all the functional parameters were exercised to exhaustion with no further improvement, it would be a very strong indication of convergence. In the results[58] for $Li_2(X\ ^1\Sigma_g^+)$ this was more comfortably achieved, that is, by virtue of having only two σ_g molecular orbitals and one σ_u molecular orbital, relatively huge basis sets could be employed to go far beyond what is really needed. For N_2 the situation is somewhat less favorable since the problem and present computer program do not permit comfortable margins for such exploration. The problem is thus to determine from a series of "improving" approximations how close the last result is

[57] J. B. Greenshields, "The Electronic Structure of Diatomic Molecules. VII. Carbon and Carbon Molecule Ions", to be submitted for publication in J. Chem. Phys.

[58] P. E. Cade, K. D. Sales, and A. C. Wahl, "The Electronic Structure of Diatomic Molecules. IV. $Li_2(X\ ^1\Sigma_g^+)$ and $Li_2^+(^2\Sigma_g^+, ^2\Pi_u)$ Ions", to be submitted for publication in J. Chem. Phys.

from the unknown quantity sought. The quantity sought may be considered as any Hartree-Fock computed value, such as the total energy, orbital energies, expectation values, or molecular property, but especially the molecular orbitals and the molecular orbital charge densities.

To therefore measure how certain molecular quantities do vary or "converge" as the wave function assumes greater and greater flexibility, one may construct tables of differences between results of the Nth and (N+1)th approximation for the various quantities and examine the behavior as N increases. In Table II is presented $\Delta E = E_{N+1} - E_N$, ΔT, ΔV, and the set of $\Delta\epsilon_i$ for the basis set synthesis in both scheme one and two. The differences in Table II arise from the results given in Table I. Difference tables are given and discussed in paper III. B for various expectation values and molecular properties. Figs. 2, 3, 4, and 5 also indicate the manner of convergence for the total energy, orbital energies, kinetic energy, and potential energy, respectively.

The ΔE increments of Table II show explicitly the relative saturation at the various stages shown in the solid curve of Fig. 2 as the basis set progresses from set 1A to set 1S. Similarly the relative improvements in going from set 2A to set 2D indicates that the true Hartree-Fock energy value has been obtained to at least two decimal places and perhaps to three decimal places.

The other quantities considered here are not of course, bound to a predictable course toward the Hartree-Fock result and their differences show this. Most disturbing is the erratic behavior of the kinetic and potential energy values displayed in the solid lines of Figs. 4 and 5. Thus while the total energy in the solid curve of Fig. 2 is relatively well behaved and always descending, the differences in Table II show that the gains in energy may be due chiefly to a decrease in the kinetic energy (always positive) or an increase in the potential energy (always negative), or finally a combined change of a subtle nature. The major feature of the ΔT and ΔV differences is that they also gradually decrease in size. Though less convincing when compared to the ΔE values, the ΔT and ΔV progressions indicate that the kinetic and potential energy are also converging, but more slowly, to perhaps the true Hartree-Fock values. Not much else can safely be stated. The dashed curves in Figs. 4 and 5 for the synthesis of basis set 2D show a more reasonable behavior which suggests that the erratic behavior of ΔT and ΔV in scheme one arises from the crude approximation of the molecular orbitals in scheme one at the intermediate stages and the relative sensitivity of $\langle T \rangle$ and $\langle V \rangle$ to these changes. A question of "internal balancing" of the representation of

various molecular orbitals may also be responsible (see paper III. B ior a discussion).

The various ϵ_i's shown in Fig. 3 and $\Delta\epsilon_i$'s in Table II indicate that the ϵ_i's are not greatly sensitive to improving the wave function, but also show an unsystematic behavior (see $\Delta\epsilon_i$ values) at the intermediate points of scheme one. These $\Delta\epsilon_i$ also exhibit decreasing values for all ϵ_i columns as larger basis sets are obtained.

It should be emphasized that the erratic behavior in certain regions of the solid curves of Figs. 4 and 5, which display the variation of the kinetic and potential energy, respectively, should not be taken as condemnation of the convergence of scheme one or cause alarm generally in this context. The gradual build up of the basis set in scheme one was purposely constructed step at a time to more effectively measure the defects of the various intermediate basis sets when viewed in the overall sequence of the converging series. The last points of the solid curves, for example points, 1P, 1Q, 1R, and 1S, should certainly be given more weight than the points on the left hand side of Figs. 4 and 5 because these sets are gradually larger and better able to make up defects in basis set composition and exponent optimizations due to greater flexibility through the linear expansion coefficients. In this light the last several points in the solid curve should perhaps be set at greater intervals and not strictly linear as they are given. In such a perspective the erratic behavior of $\langle T \rangle$ and $\langle V \rangle$ would still be present and condemn intermediate sets, but it would not mask as much the apparent gradual convergence of these values.

It would be desirable to also construct a table of charge density differences for each molecular orbital and for the total wavefunction, a quantity, for example, such as $D(\xi,\eta,\phi)$,

$$D(\xi,\eta,\phi) = \frac{\rho_N(\xi,\eta,\phi) - \rho_{N+1}(\xi,\eta,\phi)}{\rho_{N+1}(\xi,\eta,\phi)} \quad , \qquad \text{III.5}$$

for an octant of the molecule. $\rho_N(\xi,\eta,\phi)$ is either a partial or total electron charge density. As the sequence of Hartree-Fock-Roothaan wavefunctions approach the Hartree-Fock wavefunction then $D(\xi,\eta,\phi) \rightarrow 0$ all over the octant. This would, however, be only a necessary and not sufficient condition. The resulting massive table, or the equivalent, is not included in this paper.

The well known test could also be made to investigate the constancy of $\epsilon_\ell(\xi,\eta,\phi)$ and/or $\epsilon_n(\xi,\eta,\phi)$ in the expressions

$$\frac{F_c(\varphi_k,\varphi_m)\varphi_\ell}{\varphi_\ell} = \epsilon_\ell(\xi,\eta,\phi) \quad , \qquad \text{III.6}$$

for closed shells, and

$$\frac{F_0(\varphi_k,\varphi_m)\varphi_n}{\varphi_n} = \epsilon_n(\xi,\eta,\phi) \quad , \qquad \text{III.7}$$

for open shells, over the range of (ξ,η,ϕ) points in the unique octant. It is contemplated that this test may be undertaken in the future for a few diatomic systems.

Certain additional manifestations of the convergence of the Hartree-Fock-Roothaan wavefunctions to the Hartree-Fock wavefunctions is discussed in paper III. B concerning certain expectation values and a few molecular properties.

This discussion of convergence is the most satisfactory the authors though could be presented with the calculations performed. It is especially unsatisfactory from the viewpoint of numerical analysis, in which a more meaningful discussion would consider the best approximation in terms of the measure $M_N(\varphi_{i\lambda\alpha})$,

$$M_N(\varphi_{i\lambda\alpha}) = \underset{C_{i\lambda p}}{\text{Min}} \; \| \varphi_{i\lambda\alpha} - \sum_p^N \chi_{p\lambda\alpha} C_{i\lambda p} \| \quad , \qquad \text{III.8}$$

and then study $M_N(\varphi_{i\lambda\alpha})$ as N increases to its present limitations (that is if $\varphi_{i\lambda\alpha}$ was known). Eq. III.8 defines the measure, M, of the best approximation of the molecular orbital $\varphi_{i\lambda\alpha}$ to Nth degree, $M_N(\varphi_{i\lambda\alpha})$, as equal to the norm of the quantity

$$\varphi_{i\lambda\alpha} - \sum_p^N \chi_{p\lambda\alpha} C_{i\lambda p} \quad , \qquad \text{III.9}$$

minimized with respect to the expansion coefficients. A detailed discussion of an analysis of this sort and its ramifications as regards expectation values and molecular properties would be very interesting and useful.

It is to be noted that the general conclusions drawn here closely parallel those discussed by Huo[2] for the calculations on CO and BF. In assessing the relative approach to the true Hartree-Fock results for the N_2 calculation compared to the calculations on CO and BF, one must remember that relatively huge sets are employed for N_2 compared to CO and BF. This arises since <u>symmetry</u> expansion orbitals are employed for homonuclear diatomic molecules. Therefore, the 12 σ_g, 8 σ_u, and 6 π_u basis set for N_2 really corresponds, in terms of the heteronuclear problem, to 20 σ-type functions and 6 π-type STO's on <u>each</u> nitrogen nucleus, while the largest set employed by Huo[2] has 8 σ-type STO's on O, 8 σ-type STO's on C, 4 π-type STO's on O, and 4 π-type STO's on C for CO. The employment of <u>symmetry</u> expansion functions is thus a tremendous

practical advantage.

Certain of the conclusions presented here are also well known from the works of Nesbet[34] (who first draws attention to the necessity of introducing d-type orbitals), McLean[52] (who also stresses the importance of optimizing orbital exponents with the entire basis set present), and others.

In closing Sec. III-B, it may be useful to pinpoint the deficiencies of the preceding results as viewed by the authors. The major shortcomings are:

1st) It would be very desirable to be able to add even more basis functions to clinch our view that convergence is achieved. The present computer program for homonuclear diatomic molecules just does not permit a <u>comfortable</u> margin beyond what we believe is really needed to obtain Hartree-Fock results for N_2.

2nd) Simultaneous optimization of <u>all</u> orbital exponents would be desirable. At our present level, it would be desirable to be able to do exhaustive double and triple optimizations, but the expense seems unjustified.

3rd) It would be interesting to be able to add $\chi_{p\lambda\alpha}$ with $\ell_p > 3$ to confirm our belief that, at least for first row diatomic molecules in their ground states, STO symmetry orbitals <u>beyond</u> $\sigma_g 4f$, $\sigma_u 4f$, $\pi_u 4f$, and $\pi_g 4f$ are unnecessary.

4th) It is not now feasible, or in light of the 1st) defect mentioned, perhaps even necessary, to painstakingly attempt to weed out the one or two functions, if indeed there are any functions, not really needed as Bagus, Gilbert, Roothaan and Cohen have done for the first row atoms.[46] This defect is most objectionable if these sets are to be used as the starting point for perturbation calculations, such as involved in obtaining the electric polarizability or magnetic susceptibility of diatomic molecules.

C. <u>Final Hartree-Fock-Roothaan Wave Functions For $N_2(X\ ^1\Sigma_g^+)$ and $N_2^+(X\ ^2\Sigma_g^+,\ A\ ^2\Pi_u,\ B\ ^2\Sigma_u^+)$ Ions.</u>

The concluding wave functions from the synthesis of the expansion basis set using scheme one (Set 1S) and scheme two (Set 2D) are given in Table III and IV, respectively. The total energy, kinetic and potential energy, virial, and the orbital energies for these wave functions are given in the appropriate rows of Table I and are repeated here for completeness. Basis set 2D will be considered the final result at R_e(Exptl.) and is taken as the Hartree-Fock wave function for $N_2(X\ ^1\Sigma_g^+)$ when a single definite choice is required, or unless it is otherwise stated.

The wave function for $N_2(X\ ^1\Sigma_g^+)$, set 2D, was now used for the starting basis set composition to obtain the Hartree-Fock-Roothaan wave functions for the following singly ionized states of N_2:

$$N_2^+(1\sigma_g^2 1\sigma_u^2 2\sigma_g^2 2\sigma_u^2 1\pi_u^4 3\sigma_g),\quad X\ ^2\Sigma_g^+ ,$$
$$N_2^+(1\sigma_g^2 1\sigma_u^2 2\sigma_g^2 2\sigma_u^2 1\pi_u^3 3\sigma_g^2),\quad A\ ^2\Pi_u ,$$
$$N_2^+(1\sigma_g^2 1\sigma_u^2 2\sigma_g^2 2\sigma_u 1\pi_u^4 3\sigma_g^2),\quad B\ ^2\Sigma_u^+ ,$$

The order of the molecular orbitals and the state specifications are in accordance with experimental assignments.[4] These three states of N_2^+ participate in two well-known band systems of N_2^+, that is,[5]

$$B\ ^2\Sigma_u^+ - X\ ^2\Sigma_g^+ \text{ (First Negative System)},$$

and

$$A\ ^2\Pi_u - X\ ^2\Sigma_g^+ \text{ (Meinel System)}.$$

It should be emphasized that these calculations on the $N_2^+(X\ ^2\Sigma_g^+,\ A\ ^2\Pi_u,\ B\ ^2\Sigma_u^+)$ ions are direct calculations for the open shell system resulting from the removal of one electron from a $3\sigma_g$, $1\pi_u$, or $2\sigma_u$ molecular orbital, respectively, and are not simply taken from the $N_2(X\ ^1\Sigma_g^+)$ results. Accordingly, full rearrangement of the molecular orbitals (and therefore full rearrangement within the Hartree-Fock approximation) is achieved for the N_2^+ ions resulting from the ionization processes:

$$N_2(\ldots 2\sigma_u^2 1\pi_u^4 3\sigma_g^2,\ X\ ^1\Sigma_g^+) \rightarrow \begin{cases} N_2^+(\ldots 2\sigma_u 1\pi_u^4 3\sigma_g^2,\ B\ ^2\Sigma_u^+) + e^- \\ N_2^+(\ldots 2\sigma_u^2 1\pi_u^3 3\sigma_g^2,\ A\ ^2\Pi_u) + e^- \\ N_2^+(\ldots 2\sigma_u^2 1\pi_u^4 3\sigma_g,\ X\ ^2\Sigma_g^+) + e^- \end{cases} .$$

Thus we have obtained Hartree-Fock-Roothaan wave functions for these three states of N_2^+ which are also to be employed in subsequent research on the reorganization of the electronic charge distribution of nitrogen upon ionization, and for calculating the transition moments for the First Negative and Meinel systems of N_2^+.

It seemed reasonable that the final $N_2(X\ ^1\Sigma_g^+)$ wave function should provide the starting expansion basis set for each of these three states of $N_2^+(X\ ^2\Sigma_g^+,\ A\ ^2\Pi_u,\ B\ ^2\Sigma_u^+)$. This choice was far more practical than starting anew for each of these states of N_2^+ and is not unreasonable on simple physical arguments. The reorganization of the charge distribution, and hence modification of the molecular

orbitals, for these various states was thus effected through the linear expansion coefficients and reoptimization of certain ζ_p values as is discussed below. In the case of the $N_2^+(X\ ^2\Sigma_g^+)$, however, a parallel study was also made which makes use of the Hartree-Fock-Roothaan wavefunctions for the $N^+(^3P)$ atomic ion.

Let us consider first the calculations on the $N_2^+(B\ ^2\Sigma_u^+)$ molecular-ion. The basis set composition of N_2, set 2D (Table IV), provided the starting set using $R = R_e(\text{Exptl.}) = 2.0315$ Bohr. This Hartree-Fock-Roothaan wave function gave an energy of -108.2533 Hartrees before any reoptimizations of the orbital exponents. The ζ_p values for all eight $\chi_{p\lambda\alpha}$ of σ_u symmetry were singly reoptimized, including those which contribute mainly to the $1\sigma_u$ molecular orbital (that is $\sigma_u 1s$, $\sigma_u 1s'$, and $\sigma_u 3s$ STO symmetry orbitals). The total improvement in the energy after these eight single optimizations was 0.00163 Hartrees (E = -108.2549 Hartrees), with 0.00148 of the improvement coming from the slight expansion of the $\sigma_u 2s'$ STO symmetry function and 0.00010 improvement coming from the reoptimization of $\zeta_{\sigma_u 3d}$. Clearly then, the reoptimization of most of the ζ_p for σ_u symmetry was fruitless and apparently the bulk of the reorganization to this point is effected by the linear expansion coefficients and the slight expansion of the first σ_u STO symmetry function optimized ($\sigma_u 2s'$). The next step was to singly reoptimize the ζ_p's for nine of the twelve σ_g STO symmetry functions (neglecting only the $\sigma_g 1s$, $\sigma_g 1s'$, and $\sigma_g 4f$ functions). This step gave an additional energy lowering of 0.00108 Hartrees (E = -108.2560 Hartrees) with the only large contributions arising from two contracting σ_g STO symmetry functions, that is, 0.00077 Hartree lowering from $\sigma_g 2s$ optimization (the first σ_g function optimized) as $\zeta_{\sigma_g 2s}$ increases from 1.45349 to 1.61093, and 0.00023 Hartree lowering from $\sigma_g 2p$ ($\zeta_{\sigma_g 2p}$ goes from 1.28261 to 1.39078). The attempted optimization of the ζ_p for the other seven σ_g STO symmetry functions clearly gave very little improvement.

The last set of reoptimizations of the non-linear parameters (ζ_p's) for the $N_2^+(B\ ^2\Sigma_u^+)$ wave function involved π_u STO symmetry functions. All six ζ_p's for the π_u basis functions were singly reoptimized, lowering the energy to E = -108.2596 Hartrees (a further improvement of 0.00354 Hartree). In fact, the largest improvement of all (that is, from any symmetry) came from optimizing the energy with respect to $\zeta_{\pi_u 2p}$, which also contracted ($\zeta_{\pi_u 2p}$ went from 1.38436 to 1.53707) and alone gave a lowering of 0.00352 Hartree. This last result provided what was taken as the Hartree-Fock wave function for $N_2^+(B\ ^2\Sigma_u^+)$, which is given in Table VII. The most surprising fact in this sequence of reoptimizations was that any rearrangement of the molecular orbitals not accomplished by the linear expansion coefficients, $C_{i\lambda p}$, seems to come chiefly from

the contraction of the $\pi_u 2p$, $\sigma_g 2s$, and $\sigma_g 2p$ STO symmetry functions. This is surprising since it is an electron from the $2\sigma_u$ molecular orbital which is removed to form the $N_2^+(B\ ^2\Sigma_u^+)$ ion. The total energy decreased from -108.2533 Hartrees to -108.2596 Hartrees (which gives $\Delta E = 0.0063$) as a result of these three sequences of single optimizations. A few additional further calculations were also made for $N_2^+(B\ ^2\Sigma_u^+)$ and these are discussed a little later.

It is known from experimental data that the $B\ ^2\Sigma_u^+$ state of N_2^+ is several electron volts above the $A\ ^2\Pi_u$ and $X\ ^2\Sigma_g^+$ states, whereas these latter two states have potential curves which are relatively close together over a range of internuclear separations. The calculations of the Hartree-Fock-Roothaan wave functions and energies for the $N_2^+(X\ ^2\Sigma_g^+,\ A\ ^2\Pi_u)$ states closely paralleled the calculations for the $B\ ^2\Sigma_u^+$ state. The basis set composition used as the starting point was again set 2D for $N_2(X\ ^1\Sigma_g^+)$ and in both cases three sequences of selected single reoptimizations of ζ_p's were carried out; one sequence for each symmetry type occupied.

The starting basis set (Table IV) gave an energy of -108.4208 Hartrees for $N_2^+(A\ ^2\Pi_u)$ at R = 2.222 Bohr (the experimental R_e value). This energy value decreased to -108.4239 Hartrees ($\Delta E = 0.0031$ Hartree) after all six ζ_p's of the π_u STO symmetry orbitals were single optimized. Only the first optimization, however, was effective, namely that for $\zeta_{\pi_u 2p}$. This single optimization alone gave a lowering of $\Delta E = 0.00308$ Hartree as the basis function contracted and $\zeta_{\pi_u 2p}$ increased from 1.38436 to 1.54195. The total energy was next optimized in sequence, or singly, with respect to the ζ_p's for seven of the twelve STO symmetry functions, $\chi_{p\lambda\alpha}$, of σ_g symmetry. Three of these optimizations on σ_g functions were significant; $\sigma_g 2s$, which contracted as $\zeta_{\sigma_g 2s}$ went from 1.45349 to 1.62293, gave an $\Delta E = 0.00080$ Hartree, $\sigma_g 2p$ gave an $\Delta E = 0.00048$ Hartree and also contracted ($\zeta_{\sigma_g 2p}$ went from 1.28261 to 1.42818), and $\sigma_g 3d$ which gave an improvement of only 0.00015 Hartree as it's orbital exponent also increased. The total energy for $N_2^+(A\ ^2\Pi_u)$ after these seven single optimizations was -108.4254 Hartrees ($\Delta E = 0.0015$ Hartree for the σ_g sequence). The last sequence of optimizations of orbital exponents involved only $\chi_{p\lambda\alpha}$ of σ_u symmetry. Thus the ζ_p's for the $\sigma_u 2s$ and $\sigma_u 2s'$ expansion functions were simultaneously optimized and the ζ_p of $\sigma_u 2p$, $\sigma_u 2p'$, and $\sigma_u 3d$ STO symmetry orbitals were each singly optimized. The double optimization of $\sigma_u 2s$ and $\sigma_u 2s'$ ζ_p values gave an energy lowering of 0.00149 Hartree, which was the <u>entire</u> improvement from this sequence of optimizations. The total energy, at the conclusion of all three sequences of optimization of orbital exponents for $N_2^+(A\ ^2\Pi_u)$ at $R = R_e(\text{Exptl.}) = 2.222$ Bohr, was E = -108.4270 Hartrees (the total $\Delta E = 0.0062$ Hartree)

and this result and wave function was taken as the final result (Table VI). Several further calculations were, however, made and these are discussed subsequently.

Two separate calculations were made for the $N_2^+(X\ ^2\Sigma_g^+)$ molecular ion. Both were made with R = R_e(Exptl.) = 2.113 Bohr and the two efforts differed only in the source of the ζ_p values employed in the starting set, although their composition was otherwise identical, that is the usual 12x8x6 basis set. The first set of calculations started with the basis set composition of $N_2(X\ ^1\Sigma_g^+)$, Set 2D in Table IV, while the second set, to be discussed later, started anew with ζ_p values obtained from an atomic Hartree-Fock-Roothaan wave function for $N^+(^3P)$. Starting with the basis set composition from Table IV, an energy of -108.3974 Hartrees was obtained for $N_2^+(X\ ^2\Sigma_g^+)$, the ground state of N_2^+. It may be noted already that some thing is amiss, as the starting energy value for the $N_2^+(A\ ^2\Pi_u)$ ion was lower. This had also been noted earlier from the fact that $|\epsilon_{3\sigma_g}| > |\epsilon_{1\pi_u}|$ for the results of basis set 2D for N_2 and for <u>each</u> set in the gradual build up scheme.

Three sequences of reoptimizations of orbital exponents were again performed. Eight of the twelve ζ_p's of σ_g STO symmetry functions were singly optimized (omitting the functions σ_g1s, σ_g1s', σ_g3s, and σ_g3d", all having large ζ_p values) giving a total energy improvement of ΔE = 0.00120 Hartree (E = -108.3986 Hartrees). This improvement came chiefly from only two of the single optimizations; the optimization of the energy with respect to $\zeta_{\sigma_g 2s}$ gave a gain of 0.00068 Hartree as $\zeta_{\sigma_g 2s}$ increased from 1.45349 to 1.67662, and the optimal value of $\zeta_{\sigma_g 2p}$ gave an energy lowering of 0.00038 as $\zeta_{\sigma_g 2p}$ increased from 1.28261 to 1.47252. The next sequence of reoptimizations involved all six π_u STO symmetry functions. Thus ζ_p values for the π_u2p, π_u2p', π_u2p", and π_u4f STO symmetry functions were adjusted by single optimizations of the energy, and the ζ_p's from the π_u3d and π_u3d' STO symmetry functions were simultaneously optimized. The total energy was lowered to -108.4023 Hartrees (ΔE = 0.00364 Hartree), and 0.00362 Hartree improvement of this came from the contraction of the π_u2p basis function ($\zeta_{\pi_u 2p}$ increased from 1.38436 to 1.53784). Finally, optimal values of five to eight STO symmetry functions of σ_u symmetry were obtained. Of these five single optimizations, only that involving σ_u2s' was significant. The total energy was thus lowered to -108.4037 Hartree. The concluding wave function for the ground state of N_2^+, the $X\ ^2\Sigma_g^+$ state, at R_e(Exptl.) = 2.113 Bohr is given in Table V. Thus it appears that the $A\ ^2\Pi_u$ and $X\ ^2\Sigma_g^+$ states of N_2^+ are reversed in order. Several subsequent calculations on the $X\ ^2\Sigma_g^+$ state were also carried out and are discussed below. The total energy improvement after these three sequences of reoptimizations is ΔE = 0.0063 Hartree.

A few general remarks about the Hartree-Fock-Roothaan wave functions displayed in Table III through VII, about certain trends in the optimization of the non-linear parameters, and about the quality of the results for the $N_2^+(X\ ^2\Sigma_g^+,\ A\ ^2\Pi_u,\ B\ ^2\Sigma_u^+)$ molecular ions may be useful at this point. As a preliminary, however, it seems advisable to emphasize that caution should be exercised in considering discussion of the $C_{i\lambda p}$ and ζ_p values, and in general no great significance should be placed on discussions which attempt to relate these quantities to the physical properties of the electronic system. The viewpoint taken here is conservative in this regard and is primarily concerned with the $C_{i\lambda p}$ and ζ_p values in a purely numerical approximation perspective. It is usually impossible to objectively, or uniquely, untangle the relative merits of the linear ($C_{i\lambda p}$) and non-linear (ζ_p) degrees of freedom in the representation of a given molecular orbital. This perspective underlies the following remarks.

When the wave functions for $N_2(X\ ^1\Sigma_g^+)$ in Table III (Set 1S from the gradual basis set synthesis) and Table IV (Set 2D from using HFR wave functions for N in ^4S state) are compared, one major quantitative difference may be observed. Although the basis set compositions are equivalent, that is, each has the same number and kind of $\chi_{p\lambda\alpha}$ except for the ζ_p values, in each symmetry, basis set 2D is always better distributed among the important $\chi_{p\lambda\alpha}$ for each molecular orbital, $\varphi_{i\lambda\alpha}$. For example, in Set 1S, $C_{2\sigma_g,\sigma_g 2s} = 0.01437$ and $C_{2\sigma_g,\sigma_g 2s'} = 0.72687$, but for set 2D, $C_{2\sigma_g,\sigma_g 2s} = 0.14106$ and $C_{2\sigma_g,\sigma_g 2s'} = 0.59948$. This better balance among expansion functions for set 2D relative to set 1S is observed again for the $2\sigma_g$ vector components involving $\sigma_g 2p$ and $\sigma_g 2p'$ STO symmetry orbitals and in the $3\sigma_g$, $2\sigma_u$, and $1\pi_u$ vector components. This is suggestive that the small improvement of set 2D over set 1S might be due to making better use of the several important $\chi_{p\lambda\alpha}$ and thus implies that set 2D is perhaps a better representation of the various molecular orbitals on grounds other than only yielding a lower energy value. That set 1S could not spread the contributions from the important $\chi_{p\lambda\alpha}$ more evenly is due to insufficient back reoptimizations of the ζ_p values as suggested earlier.

Before noting the changes in the Hartree-Fock-Roothaan wave functions in going from $N_2(X\ ^1\Sigma_g^+)$ to $N_2^+(X\ ^2\Sigma_g^+,\ A\ ^2\Pi_u,\ B\ ^2\Sigma_u^+)$, the major features of the sequences of reoptimizations of the ζ_p for the N_2^+ ions is now summarized. The three sequences of reoptimizations, for σ_g, σ_u, and π_u symmetry, gave identical total improvements of $\Delta E = 0.0063$ Hartree for each the $X\ ^2\Sigma_g^+$, $A\ ^2\Pi_u$, $B\ ^2\Sigma_u^+$ states. Thus, the reorganization effected by reoptimization of the ζ_p values was apparently insensitive to the state involved, although the details differ somewhat. The second major feature was that for

each state the total gain from reoptimizing the orbital exponents came from the $\sigma_g 2s$, $\sigma_g 2p$, $\sigma_u 2s'$, and $\pi_u 2p$ STO symmetry orbitals only. These basis functions are among the most important contributors to the $2\sigma_g$, $3\sigma_g$, $2\sigma_u$, and $1\pi_u$ molecular orbitals and they were usually (except for $\sigma_g 2p$) the first STO symmetry function of that symmetry optimized. Thus, there was apparently little connection between the symmetry of the molecular orbital which lost the electron and the symmetry of the $\chi_{p\lambda\alpha}$ which made the largest improvement upon reoptimization of the ζ_p values. In as much as ζ_p reoptimizations are able to reflect the reorganization of the $\varphi_{i\lambda\alpha}$, spatial readjustment is relatively symmetry-independent. These observations are incorporated in future calculations on A_2^+ molecular ions.

Consider now the wave functions for the $N_2^+(X\ ^2\Sigma_g^+,\ A\ ^2\Pi_u,\ B\ ^2\Sigma_u^+)$ molecular-ions and recall the procedure employed to obtain these results, all starting from basis set 2D for $N_2(X\ ^1\Sigma_g^+)$. It is our belief that results close to Hartree-Fock have been obtained for these states of N_2^+ at their respective R_e(Exptl.) values. This argument lacks the alleged thoroughness of the argument for $N_2(X\ ^1\Sigma_g^+)$, except indirectly, and suggests in particular two questions; 1st) Should the calculations for these ions have started with HFR wave functions for $N(^4S)$ and $N^+(^3P)$ atoms and paralleled exactly the N_2 calculations instead of starting with the HFR wave function for N_2? 2nd) Was sufficient and/or judicious reoptimization of the ζ_p values performed? The problem of the basis set composition, that is the number of $\chi_{p\lambda\alpha}$ and kind with respect to n_p and ℓ_p values, but not ζ_p values, is considered to be analogous with that for N_2 as discussed in section III-C.

In regard to this first question, it may have been desirable to completely parallel the $N_2(X\ ^1\Sigma_g^+)$ calculations for each ion, but the computation time for each ion would have increased very considerably. By starting with the $N_2(X\ ^1\Sigma_g^+)$ wave function, the major features are already present, and presumably the loss of a $3\sigma_g$, $1\pi_u$, or $2\sigma_u$ electron from N_2 is a less drastic change, than that resulting from the formation N_2^+ from an $N(^4S)$ atom and an $N^+(^3P)$ ion. However, it was decided to make a completely alternative calculation for the $X\ ^2\Sigma_g^+$ state using results from $N^+(^3P)$ calculations. This was motivated by the observation that the $X\ ^2\Sigma_g^+$ and $A\ ^2\Pi_u$ states are reversed relative to experiment and the desire to remove any doubts that this result is indeed a Hartree-Fock result and not a shortcoming of the Hartree-Fock-Roothaan results themselves. A Hartree-Fock-Roothaan wave function for the $N^+(^3P)$ was thus obtained of a quality comparable to the results of Bagus, Gilbert, Roothaan and Cohen.[46] This result for $N^+(^3P)$ gave an energy of -53.88799 Hartrees and had the basis set

composition 1s(ζ = 5.8503), 1s'(10.3582), 2s(1.8480), 2s'(2.6759), 3s(7.0804); 2p(1.6880), 2p'(2.9459), and 2p"(6.7416). Several single SCF runs were made for $N_2^+(X\ ^2\Sigma_g^+)$ using basis sets constructed from $N^+(^3P)$ and a 12×8×6 basis set was finally chosen which took the ζ_p values for $\chi_{p\lambda\alpha}$ with ℓ_p = 0,1 as the <u>average</u> of the ζ_p's for $N(^4S)$ and $N^+(^3P)$ results. The $\chi_{p\lambda\alpha}$ with ℓ_p = 2,3 were taken from Table V, the previous calculation for $N_2^+(X\ ^2\Sigma_g^+)$. Three sequences of single optimizations were then carried out in the manner described before. The starting energy was -108.4009 Hartrees and at the conclusion of the three sequences of single optimizations the energy had been lowered to -108.4031 Hartrees, that is, ΔE = 0.0022 Hartree. Thus, although the <u>starting</u> energy is lower than the initial result using set 2D, the improvement after twenty-two single optimizations did not give an energy as low as that starting from set 2D (in Table V). The pattern of which $\chi_{p\lambda\alpha}$ made the largest improvements as the ζ_p were optimized was roughly the same, <u>except</u> $\sigma_g 2s$ and $\sigma_u 2s$ or $\sigma_u 2s'$ gave only very small contributions. Thus the result, using ζ_p values from $N(^4S)$ and $N^+(^3P)$ wave functions, is 0.0006 Hartree above the previous result. This investigation was certainly not equivalent to the more exhaustive effort for $N_2(X\ ^1\Sigma_g^+)$, but it does indicate that the procedure of using the N_2 set 2D as the starting set for the N_2^+ ions is probably satisfactory when gauged only in terms of the total energy.

In regard to the question about the sufficiency of the optimization of the ζ_p values, several supplementary double optimizations were carried out with negative results. The fact that only a few of the ζ_p reoptimizations were effective reinforces our contention that the $C_{i\lambda p}$ have absorbed the bulk of the reorganization of the molecular orbitals.

The inspection of the wave functions in Tables V, VI, and VII reveals the single distrubing feature, namely the change in the vector components of the $2\sigma_u$ molecular orbital. Thus in basis set 2D for $N_2(X\ ^1\Sigma_g^+)$ it is observed that $C_{2\sigma_u,\sigma_u 2s}$ = 0.36437 and $C_{2\sigma_u,\sigma_u 2s'}$ = 0.54702, but for $N_2^+(B\ ^2\Sigma_u^+)$, the worse case, these two vector components are -0.40083 and 1.13692, respectively (but of course with newly optimized ζ_p values for $\sigma_u 2s$ and $\sigma_u 2s'$ STO symmetry functions). This can be rationalized several ways, but disproportionate vector components sometimes indicate unsatisfactory behavior in a basis set composition and arguments given earlier would indicate that the representation of the $2\sigma_u$ molecular orbital is less good with such an unbalanced distribution (see particularly the $2\sigma_u$ coefficients in Tables V and VI). No such behavior was noted for the $2\sigma_g$, $3\sigma_g$, or $1\pi_u$ molecular orbitals of the N_2^+ molecular-ions. This problem was investigated since it may indicate the N_2^+ basis sets are deficient in σ_u symmetry and

hence further, substantial improvement might be possible. For all three ions a number of double optimizations involving $\sigma_u 2s$ and $\sigma_u 2s'$ STO symmetry functions were carried out to improve the distribution between these two functions. Every attempt, however, which gave a better distribution did so at the expense of the total energy, and conversely when the double optimizations were followed step at a time, it was observed that as the energy lowered the distribution between $\sigma_u 2s$ and $\sigma_u 2s'$ became worse and worse. The possibility of degeneracy or near-degeneracy was also investigated using $\sigma_u 3s'$ and other functions with negative results. We have been forced to conclude that this unequal distribution is indicative of no difficulties. A similar, but less emphatic, shift in vector components was noted also in going from $N(^4S)$ to $N^+(^3P)$ for atoms.

Therefore with <u>slight</u> trepidation, we repeat our conviction that these results for N_2^+ are very near the Hartree-Fock values. This is an important point since the results for $N_2^+(X\ ^2\Sigma_g^+)$ and $N_2^+(A\ ^2\Pi_u)$ are reversed relative to experiment at their respective R_e(Exptl.) values. If this reversal persists as E(R) is obtained for these ions, if one is convinced that the error between these results and the true Hartree-Fock values is too small to explain the discrepancy, then this reversal must be due to a <u>differential</u> shortcoming of the Hartree-Fock approximation for these two states, $A\ ^2\Pi_u$ and $X\ ^2\Sigma_g^+$, of N_2^+. This indeed is the conclusion of this research as is discussed fully in a later section.

In the course of the calculations to obtain the final wave functions of $N_2^+(X\ ^2\Sigma_g^+,\ A\ ^2\Pi_u,\ B\ ^2\Sigma_u^+)$ several recurrent features were noted which are clearly associated with the readjustment of the molecular orbitals, or to be more precise, are associated with the rearrangement of the electronic charge distribution. Since each calculation was made for R_e(Exptl.) of the particular ion in question, these observations are superimposed on the relatively smaller and non-specific changes in the $\varphi_{i\lambda\alpha}$ over this small range of R values. As section III-D will show, these changes are negligible in comparison. As expected, the major change, expressed in $C_{i\lambda p}$ and ζ_p values, was that the $\varphi_{i\lambda\alpha}$, and the total wave function in general, contracted. Thus one can notice that relative to the N_2 wave function, the $C_{i\lambda p}$ of the N_2^+ ions in $2\sigma_g$, $3\sigma_g$, $2\sigma_u$, and $1\pi_u$ molecular orbitals are shifted to favor the $\chi_{p\lambda\alpha}$ with larger ζ_p value for the important vector components. As noted also in the discussion of the optimization of the ζ_p's for each state of N_2^+, the ζ_p values usually increased also, shrinking the orbitals. This discussion in terms of $C_{i\lambda p}$ and ζ_p values is obviously awkward and in this series of papers we seek to examine these questions more directly.

In a companion contribution, Wahl and Cade[59] consider the reorganization of the electronic charge distribution as N_2 is ionized to form the three $N_2^+(X\ ^2\Sigma_g^+,\ A\ ^2\Pi_u,\ B\ ^2\Sigma_u^+)$ molecular-ions. This study extensively employs charge density contours directly.

Calculations have also been made for several states of N_2^{+2}, N_2^{+3}, and N_2^{+4} molecular-ions. These results are, however, unoptimized Hartree-Fock-Roothaan results using set 2D and no attempt is made to modify and improve the basis set composition. In Table VIII the energy values for these calculations are presented with no claim that these results are very close to the Hartree-Fock values.

D. Calculation of Potential Curves for $N_2(X\ ^1\Sigma_g^+)$ and $N_2^+(X\ ^2\Sigma_g^+,\ A\ ^2\Pi_u,\ B\ ^2\Sigma_u^+)$ Molecular-Ions.

It is well known that the regular Hartree-Fock wave functions for molecules go over into usually a mixture of ground and/or excited state wave functions for the separated constituent parts (e.g. atoms or ions for diatomic molecules) as the internuclear distance(s) become very large. The exceptions are cases in which the separated constituent parts are themselves closed shell systems or one separated part is a bare nucleus. This behavior is well illustrated for $HeH^+(^1\Sigma^+)$ and $NeH^+(^1\Sigma^+)$ by the calculations of Peyerimhoff.[60] Thus with relatively few exceptions, potential curves for diatomic molecules are expected to be rather poorly represented by the usual Hartree-Fock results when viewed over the whole range of internuclear separations. Especially, however, the calculated potential curve, $E_{HF}(R)$, depreciates rapidly at intermediate to large R values as $E_{HF}(R)$ rises very steeply and often exceeds even the dissociation limit at intermediate R values (e.g. two or three times R_e). For R values less than R_e(Exptl.) and for perhaps a restricted range of R values on both sides of R_e(Exptl.), $E_{HF}(R)$ might be expected to be more successful in representing at least the shape of the true potential curve (that is, a potential curve constructed from a Rydberg-Klein-

---

[59] A. C. Wahl and P. E. Cade, "The Reorganization of the Electronic Charge Distribution in the (Nitrogen Molecule-Nitrogen Molecular-Ion) System", to be submitted for publication in J. Chem. Phys.

[60] S. Peyerimhoff, "Hartree-Fock-Roothaan Wave Functions, Potential Curves, and Charge Density Contours for $HeH^+(X\ ^1\Sigma^+)$ and $NeH^+(X\ ^1\Sigma^+)$ Molecular Ions", submitted for publication in J. Chem. Phys.

Rees analysis[61] of experimental results for the molecule and state in question) although $E_{HF}(R)$ calculated is elevated substantially by virtue of the intrinsic shortcomings of the Hartree-Fock approximation.

If consideration is limited to R values in a narrow range around R_e(Exptl.), the quality of the representation of the shape of the true potential curve is measured by

$$\Delta(R) \equiv E_{RKR}(R) - E_{HF}(R) = \int [\Psi - \Psi_{HF}] H [\Psi - \Psi_{HF}]dV + 2 \int [\Psi - \Psi_{HF}] H \Psi_{HF} dV , \quad \text{III.10}$$

where Ψ is the exact wave function and the true potential curve is taken as that obtained from an RKR analysis, i.e. obtained by employing the turning points, R_{min} and R_{max}, and the height of each vibrational state known. If $\Delta(R)$ is constant, or slowly varying, over the range of R values considered, then the Hartree-Fock potential curve, $E_{HF}(R)$, will be a good approximation to the shape of the RKR potential curve, $E_{RKR}(R)$. The crux of the matter thus clearly depends on the differential shortcomings of the Hartree-Fock results as a function of R, or more conventionally stated, it depends on the variation of the "correlation" energy with R. It is, of course, true that for each R value within the narrow range around R_e that $E_{HF}(R)$ is correct to second order, but this knowledge offers no security that $\Delta(R)$ is slowly varying or constant, it merely means that second and higher order corrections are more important for some R values than for others, presumably in a systematic manner. The authors know of no general predictions as to the quantitative behavior of $\Delta(R)$ over a restricted range of R values. For $H_2(X\ ^1\Sigma_g^+)$ and $He_2^{++}(^1\Sigma_g^+)$, Kolos and Roothaan[62] have given curves for the variation of the correlation energy over a range of R values around R_e.

These few preliminary remarks are intended to support the value of calculations now to be presented for potential curves for $N_2(X\ ^1\Sigma_g^+)$ and $N_2^+(X\ ^2\Sigma_g^+,\ A\ ^2\Pi_u,\ B\ ^2\Sigma_u^+)$ molecular-ions. The R_e(HF) value may be slightly displaced and the $E_{HF}(R)$ curve may be arcuated or flattened relative to $E_{RKR}(R)$, but as mentioned earlier, $E_{HF}(R)$ may be an accurate representation of the shape of the true potential curve. Thus one objective is to obtain a quantitative measure of the accuracy of the shape of $E_{HF}(R)$

[61] See J. T. Vanderslice, E. A. Mason, W. G. Maisch, and E. Lippincott, J. Mol. Spec. 3, 17 (1959); 5, 83 (1960). Also F. R. Gilmore, unpublished researches. Rydberg-Klein-Rees abbreviated RKR henceforth, although Gilmore's results do not include Rees' quadratic procedure.

[62] W. Kolos and C. C. J. Roothaan, Rev. Modern Phys. 32, p. 231, Fig. 6 (1960).

over a small range of R values around R_e(Exptl.). This evaluation of the quality of the shape of the potential energy curve might just as well be considered in terms of vibrational states (via the R_{min} and R_{max} or turning points from an RKR analysis). This then exposes a second objective, namely to give expectation values and molecular properties for specific vibrational states (for example for $v \leq 5$) and therefore quantities more readily comparable to experimental results. Thus a careful consideration of the shape of $E_{HF}(R)$ between $R_{min}(v)$ and $R_{max}(v)$ will give some idea of the quality of the molecular property calculated for the vibrational state v. The final objective was to obtain spectroscopic constants by several independent means and consider the relative merits of the different methods.

The preceding discussion is applicable only for the Hartree-Fock potential curve, so that before considering the results obtained argument is necessary to explain how the calculated potential curve was obtained and to support our belief that this curve is a very close approximation to $E_{HF}(R)$. A related matter also considered, and seldom critically studied, is the practical problem of discovering what extent of optimization of orbital exponents as a function of internuclear distance is necessary.

Tables IX through XIII give the final wave functions and energy quantities for $N_2(X\ ^1\Sigma_g^+)$ at five R values, that is, for R = 1.85 B., 1.95 B., 2.05 B., 2.15 B., and 2.45 B. For these particular R values, as well as for R = 1.65 B. and 2.90 B., which are not presented, considerable reoptimization of orbital exponents was carried out. Other results for $N_2(X\ ^1\Sigma_g^+)$ were obtained using interpolated ζ_p values and a number of parallel calculations (but without optimizing ζ_p values) were made for $N_2^+(X\ ^2\Sigma_g^+,\ A\ ^2\Pi_u,\ B\ ^2\Sigma_u^+)$ molecular-ions. In the calculations by Nesbet[34] on nitrogen, five R values were chosen which are roots of an appropriately scaled fifth-order Chebyshev polynomial.[63] This permits rather excellent interpolated values of E(R) and is a commendable method for getting flexibility in the range of E(R) values. We have, alternatively, obtained results for the eight R values indicated above to permit freedom in selection of the R values and also to obtain $\zeta_p(R)$ curves which afford full flexibility to calculate the wavefunctions and subsequently expectation values for any R value. The details of the calculations for $N_2(X\ ^1\Sigma_g^+)$ will now be briefly considered.

---

[63] A. F. Tidman, Theory of Approximation of Functions of a Real Variable, (The MacMillan Company, New York, 1963), Chap. II.

The development of $E_{HF}(R)$ and the wave functions in Tables IX through XIII for $N_2(X\ ^1\Sigma_g^+)$ were the results of a rather lengthy series of calculations.[64] Two R values (R = 1.85 Bohr and 2.15 Bohr), one on either side of R_e(Exptl.) and substantially away from the calculated minimum, were chosen as starting points to obtain $E_{HF}(R)$. The calculations began with basis set 2D (Table IV) and all ζ_p values except those for $\sigma_g 1s'$, $\sigma_u 1s'$, and $\pi_u 2p''$, which have relatively large ζ_p values, were individually reoptimized for these two R values. For R = 1.85 Bohr, basis set 2D gave an energy of -108.9629 Hartrees before any optimization, and after the twenty-three single reoptimizations, this value was decreased only slightly to -108.9635 Hartrees. Most of these optimizations gave no substantial energy lowering and only the ζ_p for $\pi_u 2p$ and $\sigma_g 4f$ STO symmetry orbitals give ΔE increments greater than 0.0001 Hartree. For R = 2.15 Bohr, basis set 2D gave a starting energy of -108.9798 Hartrees and after the same twenty-three single ζ_p optimizations the energy was -108.9799 Hartrees. Using these results for R = 1.85 Bohr and 2.15 Bohr, as well as the result for R = R_e(Exptl.) = 2.068 Bohr, calculations were made for R = 1.95 Bohr and 2.05 Bohr starting again with set 2D (obtained for R = 2.068 Bohr), and this time singly optimizing only the ζ_p which may produce any significant improvement. Thus for these two additional points, at most only eight ζ_p were singly optimized. The final wave functions for R = 1.85, 1.95, 2.05, and 2.15 Bohr are given in Tables IX, X, XI, and XII, respectively, and careful comparison of the ζ_p values and vector components, $C_{i\lambda p}$, of each with each other and the results in Table IV for set 2D, indicates which ζ_p's were optimized and how these quantities changed for the various R values.

Finally, to obtain values for the potential curve to the limits of R_{min} and R_{max} given from the RKR analysis (v = 21) and to obtain more points to employ for interpolation purposes, calculations were also made for R = 1.65, 2.45, and 2.90 Bohr again starting with set 2D. For each of these internuclear separations, seventeen ζ_p's were reoptimized (neglecting those $\chi_{p\lambda\alpha}$ which are significant only for the inner shells) and the final wave function for R = 2.45 Bohr is given in Table XIII. The results now included reoptimized ζ_p values for the same basis set composition at eight R values and curves for interpolation purposes were drawn for all ζ_p which do show a

---

[64] We will refer to the calculated Hartree-Fock-Roothaan potential curve as simply $E_{HF}(R)$. That is, we believe our best result is sufficiently close to the true Hartree-Fock potential curve to avoid introducing an $E_{HFR}(R)$ curve.

significant variation with R (these were curves for $\zeta_p(R)$ for the $\sigma_g 2s$, $\sigma_g 2s'$, $\sigma_g 2p$, $\sigma_g 2p'$, $\sigma_g 3d$, $\sigma_g 3d'$, $\sigma_g 4f$; $\sigma_u 2s$, $\sigma_u 2p$; $\pi_u 2p$, $\pi_u 3d$, and $\pi_u 4f$ STO symmetry functions). The $\chi_{p\lambda\alpha}$ functions which have ζ_p's which change significantly as a function of R are either important in the $2\sigma_g$, $3\sigma_g$, $2\sigma_u$, or $1\pi_u$ molecular orbitals (that is, have large vector components) or involve high ℓ_p values ($\ell_p = 2$ or 3). The STO symmetry functions in this latter category contribute improvements in the energy upon optimization of ζ_p's for various R values to an extent which belies the size of their vector components. All of these curves of ζ_p versus R are smoothly varying, though more than half are not linear. It was therefore relatively easy to interpolate ζ_p values for these STO symmetry orbitals for internuclear separations between R = 1.80 and 2.50 Bohr to three or four significant figures. These results have afforded us the flexibility to calculate $E_{HF}(R)$ at many points, as further investigations required, with a reasonable expectation that the results (wave function, energies, and so forth) are as accurate as possible and equivalent to optimizing the orbital exponents again for each R value needed.

The preceding procedure of starting with the Hartree-Fock-Roothaan wave function for N_2 with R = R_e(Exptl.) = 2.068 Bohr (Set 2D) and carrying out a long sequence of single ζ_p optimizations, with no double optimizations or reconsideration of the basis set composition, is believed to be quite satisfactory to obtain the Hartree-Fock potential curve over a small range of R values around R_e. This belief depends strongly on the quality of the Hartree-Fock-Roothaan result at R_e(Exptl.), that is, on the quality of approximation to the true Hartree-Fock result as argued in Sec. III. B. This is supported by noting the relatively small improvements in the energy upon optimization of the orbital exponents, and is presumably due in large part to the small change in the Hartree-Fock field with R over this limited range of R values and the adequacy of the large expansion basis set used to absorb these changes via the $C_{i\lambda p}$ vector components which indicate only a small readjustment as R goes from 1.85 Bohr to 2.45 Bohr.

The conclusion suggested from these calculations is that reoptimization of orbital exponents for different R values is not very important for a large basis set composition if the R values are near R_e(Exptl.). (Or rather, if the R values are near the R for which the basis set was originally constructed.) This conclusion is supported from other results for Li_2 and C_2 molecules.[57,58] Little direct evidence is available, but presumably for small expansion basis sets, and especially for minimal or double-ζ basis sets, reoptimization of the ζ_p for different R values becomes more

important. These calculations show that as $|R-R_e(\text{Exptl.})|$ becomes larger, reoptimization of the non-linear variational parameters becomes more important and especially so for $\chi_{p\lambda\alpha}$ with $\ell_p = 2$ or 3. Fig. 6 clearly illustrates this former point. The energy improvement, ΔE, is the magnitude of the difference between $E_{HF}(R)$ calculated using set 2D with <u>reoptimized</u> ζ_p values and $E_{HF}(R)$ calculated using ζ_p values of set 2D. The open squares are for R = 1.85, 1.95, 2.05, 2.15, and 2.45 Bohr, as discussed above, and the solid circles are for R values using interpolated ζ_p values. The plot of ΔE versus R thus clearly shows the sequence of reoptimizations of ζ_p performed here contribute an additional lowering of less than 0.001 Hartree for R near $R_e(\text{Exptl.})$. The fact that ΔE is not zero at $R_e(\text{Exptl.})$ is no doubt indicative that <u>another</u> sequence of single reoptimizations of ζ_p at $R_e(\text{Exptl.})$ would lower the energy by ~0.00005 Hartree which is consistent with our earlier belief expressed in III-B. The scale in Fig. 6 is such that this improvement appears large, but a clearer perspective of this relatively small effect is more evident in Fig. 7.

The final results for the potential curve of $N_2(X\ ^1\Sigma_g^+)$ include the original result from set 2D at R = 2.068 Bohr, results for seven other R values with ζ_p values reoptimized, results using <u>interpolated</u> ζ_p values for the twelve turning points,[61] $R_{min}(v)$ and $R_{max}(v)$, with v = 0,1,2,3,4,5, and finally a number of additional points using <u>interpolated</u> orbital exponents which are chosen to fill gaps in the curve. A summary of the energy quantities for $N_2(X\ ^1\Sigma_g^+)$ is given in Table XIV for a selected group of R values.

The quantitative comparison of the calculated potential curve $E_{HF}(R)$, with the curve obtained by Gilmore[61] for $N_2(X\ ^1\Sigma_g^+)$ will now be considered. The $E_{HF}(R)$, the solid line in Fig. 7, is constructed from the calculations at the turning points, $R_{min}(v)$ and $R_{max}(v)$, given by Gilmore.[61] Thus for $R_{min}(v = 0,1,2,3,4,5) = 1.994$, 1.941, 1.905, 1.878, 1.858, and 1.839 Bohr, respectively, and $R_{max}(v = 0,1,2,3,4,5)$ = 2.166, 2.239, 2.292, 2.340, 2.383, and 2.423 Bohr, respectively, two set of calculations are shown on the solid curve of Fig. 7. The solid circles are results using interpolated or reoptimized ζ_p values and the open squares are results using the ζ_p values directly from set 2D. Several other points not at $R_{min}(v)$ or $R_{max}(v)$ are also shown, but this curve emphasized again how inconsequential reoptimization of the ζ_p values was for various R values. The dashed curve was derived from Gilmore's results for the first six vibrational states, use of $E_{exptl.} = -109.586$ Hartrees, and then <u>vertically</u> elevating the resulting "experimental" curve so that the minimum was <u>parallel</u> with the minimum of $E_{HF}(R)$. This maneuver is to facilitate examination of the displacement of R_e and assess the quality of the <u>shape</u> of $E_{HF}(R)$ for various

vibrational states. The experimental curve was therefore uniformly elevated by the amount $|E_{exptl.} - E_{HF}(R_e)| = |109.586 - 108.9956| = 0.590$ Hartrees, in which both E(R) values are taken at their respective minimum.

The shortcomings of $E_{HF}(R)$ when compared to the E_{RKR} curve are that: i) the $E_{HF}(R)$ curve is generally much too high, ii) the $E_{HF}(R)$ curve is shifted as a whole inward to smaller R values relative to E_{RKR}, and iii) the $E_{HF}(R)$ curve is sharply arcuated in contrast to $E_{RKR}(R)$ and this is especially evident on the large R side of $E_{HF}(R)$. The effect of ii) and iii) is such that lines drawn between $E_{HF}[R_{max}(v)]$ and $E_{HF}[R_{min}(v)]$ for various v are <u>not</u> horizontal, as for the $E_{RKR}(R)$ curve, but are tilted with the angle above horizonal increasing sharply as v increases (see Fig. 7). If one now imagines that the solid curve of Fig. 7 is moved to the right such that the minimum coincides with that of the dashed curve, then one would see that for v = 0 or 1 the <u>shape</u> is quite reasonable, but for $v \geq 2$ the $E_{HF}(R)$ already rises much too high on the large R side. Thus one might expect that molecular properties computed for v = 0, 1 using $E_{HF}(R)$ would reflect properly the <u>shape</u> effects of the true potential curve, but that for v = 2 or higher the shape effects would progressively be less well represented. There would still be defects, however, since the nuclei would come to close together in vibration and would vibrate in a potential well much too shallow. We will continue this discussion in terms of the $\Delta(R)$ function below. A more significant gauge of the quality of $E_{HF}(R)$, and the effects of i), ii), and iii) above, would be to solve the vibrational-rotational problem using $E_{HF}(R)$ and compare the results with experiment. This latter investigation is now in progress.

The foregoing discussion indicated that reoptimization of the orbital exponents contributed very little towards improving $E_{HF}(R)$ for $N_2(X\ ^1\Sigma_g^+)$. It seems certain that the major features of $E_{HF}(R)$ are only slightly altered by such reoptimizations for A_2 molecules when a large expansion basis set is employed and in light of the overall poor quality of the potential curves given by $E_{HF}(R)$, reoptimizations of ζ_p values for $N_2^+(X\ ^2\Sigma_g^+, A\ ^2\Pi_u, B\ ^2\Sigma_u^+)$ molecular-ions were abandoned. The largest energy gain in the reoptimizations for $N_2(X\ ^1\Sigma_g^+)$ was ~ 0.001 Hartree and the only other N_2^+ reoptimization (that for the $X\ ^2\Sigma_g^+$ state at R = 2.0132 Bohr) gave an energy gain of 0.00006 Hartrees relative to the results obtained using the ζ_p's optimized at $R = R_e(Exptl.) = 2.113$ Bohr for $N_2^+(X\ ^2\Sigma_g^+)$. It is a reasonable estimate that reoptimization of the orbital exponents would produce no gains greater than ~ 0.002 Hartrees and probably half of this size. Therefore $E_{HF}(R)$ curves for $N_2(X\ ^2\Sigma_g^+, A\ ^2\Pi_u, B\ ^2\Sigma_u^+)$ were calculated using the wave functions given in Tables V, VI, and VII, respectively, obtained at the

R_e(Exptl.) values. The resulting points for the potential curves are found in Tables XV, XVI, and XVII for these three states of N_2^+.

is the orbitals satisfying the physical self-consistency requirement of this model, we can now examine how the model behaves in this regard. Thus, although all R_e(HF) values are shifted inward relative to the corresponding R_e(Exptl.) values and in spite of the fact that the $N_2^+(X\ ^2\Sigma_g^+)$ and $N_2^+(A\ ^2\Pi_u)$ states are reversed, there is a strikingly close analogy between the ΔR_e shifts of theory and experiment upon ionization of $N_2(X\ ^1\Sigma_g^+)$. Thus for the loss of the strongly bonding electron in $1\pi_u$ symmetry, R_e(Exptl.) goes from 2.0741 Bohr (N_2, $X\ ^1\Sigma_g^+$) to 2.222 Bohr (N_2^+, $A\ ^2\Pi_u$), an increase of 0.148 Bohr or + 6.13%, while R_e(HF) goes from 2.0132 Bohr (N_2, $X\ ^1\Sigma_g^+$) to 2.134 Bohr (N_2^+, $A\ ^2\Pi_u$), a parallel increase of 0.121 Bohr or + 6.0%. In an exactly analogous fashion ΔR_e(Exptl.) for the loss of a weakly bonding $3\sigma_g$ electron is + 1.88% compared to the calculated value of + 1.26% and for the loss of an antibonding $2\sigma_u$ electron, ΔR_e(Exptl.) = -2.05% and ΔR_e(HF) = -3.93%. Thus in every case the model gives good agreement and predicts in each case less bonding in terms of ΔR_e than the experimental results give. To good approximation then, the far reaching concept of bonding and antibonding orbitals predicted by the theory seems relatively immune to the shortcomings of the Hartree-Fock approximation. This tool can thus be extensively exploited in further investigations of this series. Although no new information is provided in this paragraph, we wish to stress that having obtained the results of the Hartree-Fock model, it seems obligatory to critically examine how close the orbital concept, so solidly entrenched in molecular spectroscopy, conforms with the model it assumes. In a companion paper to the present effort[59] the rearrangement of the electronic charge distribution upon loss of either a $3\sigma_g$, $1\pi_u$, or $2\sigma_u$ electron is considered in terms of the electronic charge density contours for the various orbitals themselves. This latter study could not be done by using only virtual orbitals, but requires directly calculated wave functions for $N_2^+(X\ ^2\Sigma_g^+,\ A\ ^2\Pi_u,\ B\ ^2\Sigma_u^+)$ ions as obtained here.

Let us now consider more quantitative aspects of the total energy values, $E_{HF}(R)$, namely ionization potentials, dissociation energies, and the energy quantity $\Delta(R)$, defined in Eq. III.10. Since relativistic effects are completely neglected in these calculations, $\Delta(R)$ is not the variation of the usually defined correlation energy with R because $E_{RKR}(R)$ implicitly contains all the physics of the problem as communicated by the experimental data used in the RKR analysis. Therefore, we will refer to $\Delta(R)$ as a quantity which measures the variation with R of the shortcomings of a given approximate wave function, or in the present case, of the Hartree-Fock wave function. The $\Delta(R) = E_{RKR}(R) - E_{HF}(R)$ curves for $N_2(X\ ^1\Sigma_g^+)$ and $N_2^+(X\ ^2\Sigma_g^+,\ A\ ^2\Pi_u,\ B\ ^2\Sigma_u^+)$ states are given in Fig. 11. The numbers used to obtain these curves come from the calculated

IV. DISCUSSION OF ENERGY QUANTITIES

The principal energy results are summarized in Tables XIV, XV, XVI, and XVII for $N_2(X\ ^1\Sigma_g^+)$ and $N_2^+(X\ ^2\Sigma_g^+,\ A\ ^2\Pi_u,\ B\ ^2\Sigma_u^+)$, respectively. The variation of $E_{HF}(R)$, $T_{HF}(R)$, $V_{HF}(R)$, and $\epsilon_1(R)$ with internuclear separation for these four molecular systems are shown in Fig. 8a, 9a, 9b, and 10a,b,c,d in that order. These results are claimed to Hartree-Fock accuracy within at least 0.005 Hartree for $E_{HF}(R)$ and less for the other quantities.

The potential curves for $N_2(X\ ^1\Sigma_g^+)$ and $N_2^+(X\ ^2\Sigma_g^+,\ A\ ^2\Pi_u,\ B\ ^2\Sigma_u^+)$ are given in Fig. 8a and 8b. Figure 8a is the result of the present calculations as already described and Fig. 8b is replotted from data of F. R. Gilmore.[61] The Rydberg-Klein curves of Gilmore and Fig. 8b have been juxtaposed so that the calculated and "experimental" minima of $N_2(X\ ^1\Sigma_g^+)$ are exactly parallel. But note, that although the ordinate scale is the same in Figs. 8a and 8b, and the abscissa scale and range is identical, the ordinate ranges of Figs. 8a and 8b are different. The objective is simply to measure the internal spacings and relationships among the four states as calculated and compare these with the experimental results. The small numbered horizontal struts in Fig. 8b indicate the various vibrational states.

The first general impression in comparing the calculated $E_{HF}(R)$ curves with the $E_{RKR}(R)$ curves is that the N_2^+ states are all nearly correctly spaced above the $N_2(X\ ^1\Sigma_g^+)$ curve. One notes that all $E_{HF}(R)$ curves are shifted inward relative to the corresponding $E_{RKR}(R)$ curves, all $E_{HF}(R)$ curves rise much too rapidly at large R, and that some significant relative shifting has occured among the N_2^+ states. The most significant feature, however, as noted earlier, is the reversal of the $N_2^+(X\ ^2\Sigma_g^+)$ and $N_2^+(A\ ^2\Pi_u)$ states over a substantial range of R values. This reversal of levels involves energy differences of the order of ~0.02 Hartree which is considerably too large to be explained as due to differential shortcomings of our approximation to the Hartree-Fock result for these two states. We are confident that this reversal is a characteristic feature of the Hartree-Fock approximation and hence must find an explanation in the differential shortcomings of the Hartree-Fock results, or differential correlation energy, for these two states of N_2^+.

It may be recalled that the concept of bonding, antibonding, or non-bonding orbitals first arose in considering the change in R_e(Exptl.) which resulted when an electron vacated the particular molecular orbital in question. In as much as our claims of having obtained to good approximation the molecular orbitals are valid, that

results for $E_{HF}(R)$ at $R_{min}(v)$ and $R_{max}(v)$ and the results of Gilmore for $E_{RKR}(R)$ at the corresponding R values. These curves all show the characteristic degeneration as R increases and are not slowly varying (the gradient varys from about 0.11 Hartree/Bohr for N_2^+, X $^2\Sigma_g^+$ to about 0.23 Hartree/Bohr for a part of the N_2^+, B $^2\Sigma_u^+$ curve) functions of R around R_e(Exptl.). It is also observed that the shortcomings of $E_{HF}(R)$ are only slightly worse for $N_2^+(X\ ^2\Sigma_g^+)$ than for $N_2(X\ ^1\Sigma_g^+)$, but these two $\Delta(R)$ curves are closely parallel over a substantial range of R values. This is also seen in the potential curves for $N_2(X\ ^1\Sigma_g^+)$ and $N_2^+(X\ ^2\Sigma_g^+)$ states in Fig. 8a. Thus, except for a constant relative elevation of the $N_2^+(X\ ^2\Sigma_g^+)$ $E_{HF}(R)$ curve, these two curves behave very similarly to their counterparts in Fig. 8b. The point to be made here is that apparently breaking of the $3\sigma_g^2$ pair in going to the X $^2\Sigma_g^+$ state of N_2^+ is of but minor consequence as far as the correlation energy is concerned. Or another way of putting it, these Hartree-Fock calculations on $N_2(X\ ^1\Sigma_g^+)$ and $N_2^+(X\ ^2\Sigma_g^+)$ are closely comparable in quality. In contrast to this, the $\Delta(R)$ curve for the A $^2\Pi_u$ state of N_2^+ indicates that, relatively speaking, the Hartree-Fock result is much better for this state than for N_2, and the final $\Delta(R)$ curve shows that the B $^2\Sigma_u^+$ state of N_2^+ is, relatively, the worse treated by Hartree-Fock approximation. Thus the calculated $E_{HF}(R)$ curve for the A $^2\Pi_u$ state of N_2^+ is relatively lower than its experimental counterpart in Fig. 8a,b because somehow the Hartree-Fock result for $N_2^+(A\ ^2\Pi_u)$ is much better than corresponding results for $N_2^+(X\ ^2\Sigma_g^+)$ and $N_2(X\ ^1\Sigma_g^+)$. It is certainly no coincidence that this behavior is associated with the loss of a strongly bonding $1\pi_u$ electron in forming $N_2^+(A\ ^2\Pi_u)$ from $N_2(X\ ^1\Sigma_g^+)$. In terms of breaking electron pairs the results of $\Delta(R)$ for the $N_2^+(B\ ^2\Sigma_u^+)$ state resulting from breaking up the $2\sigma_u^2$ pair also is significant. Clearly there is substantial information in considerations of this kind about correlation energy, but until more results are obtained for other homonuclear systems, the authors decline attempts at any synthesis. The authors have no explanation of the reversal of the X $^2\Sigma_g^+$ and A $^2\Pi_u$ states of N_2^+ relative to experiment and know of no explanations in the literature. Several attempts have been made by Clementi[65] and others to construct empirical correlation energy corrections to be added on to the Hartree-Fock energies for molecules to give accurate dissociation energies. The view in this paper is that insufficient data is presently available to attempt to construct such an empirical recipe and this is why the quantity $\Delta(R)$ was introduced. It is, we feel, imperative to get more results for more electron configurations, for variable differences of nuclear charges, and to obtain these results as a function of internuclear separation.

[65] E. Clementi, J. Chem. Phys. 38, 2780 (1963); 39, 487 (1963).

In Sec. III.D the defects of calculated potential curves for $N_2(X\ ^1\Sigma_g^+)$ were considered to be loosely divisable into an elevation factor, a shift factor, and a shape factor. We may now ask what these divisions means, if anything, in terms of the $\Delta(R)$ quantity and can any useful quantitative or interpretative advantage be gained in their employment? Let us first define the quantity

$$\delta R = R_e(HF) - R_e(Exptl.) \quad , \qquad IV.1$$

that is, just the difference between the calculated equilibrium value, $R_e(HF)$, and the experimental R_e value. For the $N_2(X\ ^1\Sigma_g^+)$ and $N_2^+(X\ ^2\Sigma_g^+,\ A\ ^2\Pi_u,\ B\ ^2\Sigma_u^+)$ states the shift in the position of the minimum is δR = 0.061, 0.075, 0.088, and 0.098 Bohr, respectively. A constant elevation factor for each state may also be defined as

$$\mathcal{E} = E_{RKR}[R_e(Exptl.)] - E_{HF}[R_e(HF)] \quad , \qquad IV.2$$

which in magnitude is just the height the minimum of $E_{HF}(R)$ is above the minimum of $E_{RKR}(R)$. The quantity $\Delta(R)$ can now be written

$$\Delta(R) = E_{RKR}(R) - E_{HF}(R) = \mathcal{E} + E^o_{RKR}(R) - E^o_{HF}(R)$$

$$= \mathcal{E} + [E^o_{RKR}(R) - E^o_{HF}(R - \delta R)] - \alpha(R) \quad , \qquad IV.3$$

in which $E^o_{RKR}(R)$ and $E^o_{HF}(R)$ refer to energies relative to their respective minima and thus are to the same zero and are always positive. By definition $\alpha(R)$ is

$$\alpha(R) = E^o_{HF}(R) - E^o_{HF}(R-\delta R) \quad . \qquad IV.4$$

The constant $\mathcal{E}$ is thus the elevation factor, $\alpha(R)$ is the shift factor, or the correction to be subtracted at each R value to bring $E_{HF}(R)$ upon $E_{RKR}(R)$ such that the minima are coincident, and $E^o_{RKR}(R) - E^o_{HF}(R-\delta R)$ is the shape factor[66] measuring how the two curves with coincident minima differ in details of their shape with R.

The major theoretical shortcomings of $E_{HF}(R)$ relative to $E_{RKR}(R)$ are that: i) $E_{HF}(R)$ does not go to the correct atom states upon dissociation, ii) $E_{HF}(R)$ is a result which does not take account of the instantaneous interactions between the electrons, the usually defined correlation defect, and iii) $E_{HF}(R)$ is the result of a calculation in which relativistic effects are neglected. Can these theoretical defects be meaningfully associated with the elevation, shift, and shape factors just defined? Now the constant $\mathcal{E}$ is -0.590, -0.605, -0.539, and -0.627 Hartree for $N_2(X\ ^1\Sigma_g^+)$ and $N_2^+(X\ ^2\Sigma_g^+,\ A\ ^2\Pi_u,\ B\ ^2\Sigma_u^+)$ respectively, and it is reasonable to associate this R-independent elevation factor primarily to the neglect of correlation and relavistic effects in the inner shells, defects also present in the corresponding calculations for the separated $N(^4S)$ atom and $N^+(^3P)$ ion. Not all of $\mathcal{E}$ can, however, be association with this source since, as we will discuss below, the rationalized dissociation energy is

[66] A related quantity is defined by A. D. McLean in J. Chem. Phys. 40, 243 (1964).

is still only about 50% of the experimental value and therefore the remainder must be due to an R-independent part associated with the correlation energy and relativistic effects for the valence shell electrons of the atom as the molecule is formed. These conjectures are consistent with the relative sizes of the $\mathcal{E}$ values for these four electronic systems of N_2 and N_2^+, and, presumably, the difference in $\mathcal{E}$ for these states is largely associated with their differences in correlation energy since one might expect that relativistic defects for the molecules is approximately the same as for the separated atoms, except if R is very small.

The shape factor given by $E^o_{RKR}(R) - E^o_{HF}(R)$, which was already obliquely discussed in Sec. III-D, seems to be dominated by the fact that $E_{HF}(R)$ does not approach the energy of the separated ground state atoms (or atom and ion) as R increases. The shift factor, expressed either in terms of $\alpha(R)$ or δR, indicates that, in the Hartree-Fock approximation for the N_2 molecule and the N_2^+ molecular-ions, the nuclei are more shielded from one another by electron charge distribution between them than is actually the case.[67] Thus, as might be anticipated, the neglect of the instantaneous interactions between the electrons will increase the electron density in regions where it is already high (and, of course, the instantaneous interactions are more important) and tend to decrease the electron density in regions where it is too low. The shift factor is thus largely ascribable to the R-dependent portion of the correlation energy although it must also be associated with a sort of "stove-pipe" effect due to the rapid rise of $E_{HF}(R)$ for large R.[34,66]

In summary then, the arbitrary division of the defects manifested in $\Delta(R)$ and the association of the elevation, shift, and shape parts with known theoretical shortcomings seems at this point only heuristic. This discussion was intended to attempt an assessment of the shortcomings of $E_{HF}(R)$, staying as close to experiment as possible, and to emphasize our belief in considering the various defects as a function of internuclear separation. The usefulness of $\Delta(R)$, $\mathcal{E}$, $\alpha(R)$, and δR will be critically examined for entire homologous and/or isoelectronic series of molecules at a latter data. These concepts may offer an alternative or supplement to the present few empirical schemes to obtain dissociation energies for diatomic molecules by estimating correlation energies, and possesses the advantage of being a quasi-direct comparison with experiment. The proposed analysis in terms of this division of defects of an arbitrarily calculated potential curve, for example, from results beyond the Hartree-Fock approximation by configuration interaction or perhaps by completely alternative methods, might also serve as an objective standard for interpretive comparison of merits. It must be

67 All δR values calculated have been positive for other unpublished diatomic molecules and ions.

remembered, however, that such a division is completely arbitrary and it is probable that a sequence of approximate wave functions would lead to potential curves which approach the true curve along a contorted geodesic. Some useful data is expected to emerge, however, such as studies of δR versus $|Z_A - Z_B|$ or other parameters representing the molecular system.

The calculated dissociation energy, $D_e(R)$ is the "rationalized" value, which is defined for a diatomic molecule, AB, by

$$-D_e(R) = E_{HF}^{(AB)}(R) - (E_{HF}^{(A)} + E_{HF}^{(B)}) \quad , \qquad \text{IV.5}$$

where $D_e(R)$ includes the zero point energy and is given here as a function of R. The energy quantities, $E_{HF}^{(AB)}(R)$, $E_{HF}^{(A)}$, and $E_{HF}^{(B)}$ are, respectively the calculated Hartree-Fock energies of the diatomic molecule, AB, and the infinitely separated parts, A and B, all in the appropriate electron configuration and state. $D_e(R)$ as defined can be positive or negative, the latter simply corresponding to no binding if true for all R values. The rationalization is that, ideally, one expects the molecular Hartree-Fock result to approach the appropriate atomic Hartree-Fock results as R becomes very large, so that $D_e(R)$ at $R_e(HF)$ would be a good approximation to the true dissociation energy (D_e) except for the difference between the correlation (and relativistic) corrections for the AB and A+B systems.

In calculating $D_e(R)$ we have used $E_{HF}(N, {}^4S) = -54.40093$ H.[46] and $E_{HF}(N^+, {}^3P) = -53.88799$ H. and find that $D_e(R = 2.0132$ B.$) = 0.1937$ H. (5.27 eV) for $N_2(X\ {}^1\Sigma_g^+)$, $D_e(R = 2.0385$ B.$) = 0.1190$ H. (3.24 eV) for $N_2^+(X\ {}^2\Sigma_g^+)$, $D_e(R = 2.134$ B.$) = 0.1431$ H. (3.89 eV) for $N_2^+(A\ {}^2\Pi_u)$, and $D_e(R = 1.934$ B.$) = -0.01874$ H. (-0.509 eV), unbound, for $N_2^+(B\ {}^2\Sigma_u^+)$. These $D_e(R)$ values are quoted for $R = R_e(HF)$ and not for $R = R_e(Exptl.)$. These results again reflect the shortcomings already discussed, but compared to the experimental results of 9.90 eV for $N_2(X\ {}^1\Sigma_g^+)$ and 8.86 eV for $N_2^+(X\ {}^2\Sigma_g^+)$, these D_e values are far better than most previous approximate results, being 53% and 37%, respectively of the true value. In Fig. 2, which shows the improvement in the total energy as the expansion basis set is built up in scheme one, it is evident that $N_2(X\ {}^1\Sigma_g^+)$ is bound relative to the Hartree-Fock atom results (also indicated on Fig. 2) from set 1E onwards. The $D_e(R)$ curve can be obtained from polynomial curves for $E_{HF}(R)$ and $E_{HF}(N, {}^4S)$ and $E_{HF}(N^+, {}^3P)$. There have been several recent proposals of alternative ways of calculating D_e, such as that given by Stanton,[68] and the method suggested by Richardson and Pack.[69]

[68] R. E. Stanton, J. Chem. Phys. 36, 1298 (1962).

[69] J. W. Richardson and A. K. Pack, J. Chem. Phys. 41, 897 (1964).

A rationalized ionization potential, $I_e(R)$ can also be defined and is given by

$$-I_e(R) = E_{HF}^{(AB)}(R) - E_{HF}^{(AB^+)}(R) \quad , \qquad \text{IV.6}$$

for the ionization of AB to form AB^+. This definition includes ionization potentials corresponding to excited states of the molecular ion AB^+, in which case the appropriate $E_{HF}^{(AB^+)}(R)$ curves must be employed, and <u>double</u> ionization potentials can be similarly defined. The ionization potential curve in Eq. IV.6, $I_e(R)$, is the "vertical" ionization potential for AB if $R = R_e(HF)$, except that $I_e(R)$ <u>includes</u> the zero point energy of AB, and with this correction is the quantity allegedly measured as electron impact ionization potentials. The related "adiabatic" ionization potential is defined here by

$$-I_e^{(a)} = E_{HF}^{(AB)}(R_e) - E_{HF}^{(AB^+)}(R_e') \quad , \qquad \text{IV.7}$$

that is, the difference between the <u>minimal</u> energy of AB at R_e and AB^+ at R_e' (R_e and R_e' are the Hartree-Fock minimal values). The experimental "adiabatic" ionization potential measures the difference between the energy of $AB(v = 0, J = \Omega)$ and $AB^+(v = 0, J = \Omega)$, so that $I_e^{(a)}$ is slightly modified by the <u>difference</u> of the zero point energies of AB and AB^+. It should be recalled again, however, that the energy values, $E_{HF}^{(AB^+)}(R)$, are for direct calculations for the molecular ions in question and are not obtained from virtual orbital results for AB.

The "vertical" ionization potentials of $N_2(X\ ^1\Sigma_g^+)$ to form $N_2^+(X\ ^2\Sigma_g^+,\ A\ ^2\Pi_u,\ B\ ^2\Sigma_u^+)$ molecular-ions, using results for <u>each</u> obtained for $R = R_e(HF) = 2.0132$ B., the minimum for the $E_{HF}(R)$ curve of $N_2(X\ ^1\Sigma_g^+)$, are calculated to be $I_e(R = 2.0132\ B.) =$ 16.01 eV, 15.67 eV, and 19.93 eV, respectively. The experimental values of Frost and McDowell[7] after adding on the zero point energy of $N_2(X\ ^1\Sigma_g^+)$ are 15.77 eV, 16.98 eV, and 18.90 eV, again in the same order (although no state specification is obtained by the electron impact measurements). The directly calculated "vertical" ionization potentials are thus 1.5% and 5.4% too high for formation of $N_2^+(X\ ^2\Sigma_g^+)$ and $N_2^+(B\ ^2\Sigma_u^+)$ and 7.7% too low for the formation $N_2^+(A\ ^2\Pi_u)$. Fig. 10a indicates the variation of the orbital energys, $\epsilon_{2\sigma_u}$, $\epsilon_{3\sigma_g}$, and $\epsilon_{1\pi_u}$, of $N_2(X\ ^1\Sigma_g^+)$ over a small range of internuclear separation and for $R = 2.0132$ B., the "vertical" ionization potentials using Koopmans' Theorem are 17.36 eV (+10.1% in error) for the loss of an $3\sigma_g$ electron, 17.10 eV (+0.71% in error) for the loss of an $1\pi_u$ electron, and 20.92 (+10.7% in error) for the loss of an $2\sigma_u$ electron. These values indicate that, as expected, the directly calculated values are generally better and are especially good (1.5%) when the correlation effects in the neutral and ionized state are very similar. It is also to be noted

that the "vertical" ionization potential to form $N_2^+(A\ ^2\Pi_u)$ given by Koopmans' Theorem is astonishingly, and probably fortuitously, good. The full $I_e(R)$ curves can be obtained by use of the $E_{HF}(R)$ polynomial curves.

One final set of "vertical" ionization potentials might also be mentioned which involves the loss of two electrons by $N_2(X\ ^1\Sigma_g^+)$ to form $N_2^{+2}(?)$. Certain double ionization processes involving nitrogen have recently been re-examined by Dorman and Morrison,[70] who find two such potentials,[71] one at 42.7 eV and another at 43.8 eV, but no clear-cut association with particular states of N_2^{+2} is available from these electron impact measurements. It is not unlikely that there is a number of N_2^{+2} states in this energy range above N_2 and certain of these states are represented in Table VIII. These N_2^{+2} calculations are crude compared to the N_2 and N_2^+ results in that no reoptimization of orbital exponents was attempted, but these are direct calculations again for the states in question. For the double "vertical" ionization potentials of $N_2(X\ ^1\Sigma_g^+)$ we calculate that $I_e(R = 2.0132\ B.) = 43.77$ eV to form $N_2^{+2}(2\sigma_u^{\ 2}3\sigma_g^{\ 2}1\pi_u^{\ 2}, {}^3\Sigma_g^-)$, 45.20 eV to form $N_2^{+2}(2\sigma_u^{\ 2}3\sigma_g^{\ 2}1\pi_u^{\ 2}, {}^1\Delta_g)$, and 46.18 eV to form $N_2^{+2}(2\sigma_u^{\ 2}3\sigma_g^{\ 0}1\pi_u^{\ 4}, {}^1\Sigma_g^+)$ respectively. The $N_2^{+2}(2\sigma_u^{\ 2}3\sigma_g^{\ 2}1\pi_u^{\ 2}, {}^1\Sigma_g^+)$ state is probably also close by as are a number of other states involving $2\sigma_u^{\ 2}3\sigma_g1\pi_u^{\ 3}$, $2\sigma_u3\sigma_g1\pi_u^{\ 4}$, and $2\sigma_u3\sigma_g^{\ 2}1\pi_u^{\ 3}$ electronic configurations. Explicit knowledge as to which of these states are bound is not available from calculations performed. The $I_e(R = 2.0132\ B.)$ given are probably uniformly too high by about 0.2 - 0.5 eV due to relative crudeness of the N_2^{+2} wave functions when compared to the $N_2(X\ ^1\Sigma_g^+)$ results. We are not able to convincingly make any identification of the states of N_2^{+2}involved in the measurements of Dorman and Morrison since it seems that N_2^{+2}has an abundance of closely grouped low lying states (about ten states). N_2^{+3} is about 90 eV and N_2^{+4} is about 145 eV above $N_2(X\ ^1\Sigma_g^+)$.

The "adiabatic" ionization potentials of $N_2(X\ ^1\Sigma_g^+)$ to form $N_2^+(X\ ^2\Sigma_g^+, A\ ^2\Pi_u, B\ ^2\Sigma_u^+)$ are well known from spectroscopic observations of Rydberg series of N_2 and, in general, ionization potentials measured in this way are the most accurate obtained. For ionization of $N_2(X\ ^1\Sigma_g^+)$ to the $X\ ^2\Sigma_g^+$, $A\ ^2\Pi_u$, and $B\ ^2\Sigma_u^+$ states of N_2^+, the experimental adiabatic ionization potentials are $I_e^{(a)} = 15.585$ eV, 16.74 eV, and 18.744 eV, respectively, using the values quoted by McDowell[72] and the relationship

---

[70] F. H. Dorman and J. D. Morrison, J. Chem. Phys. 39, 1906 (1963).

[71] No correction for the zero-point energy of $N_2(X\ ^1\Sigma_g^+)$ is made since the measured values may be off by more than the zero-point correction (0.143 eV).

[72] C. A. McDowell, in Mass Spectrometry, edited by C. A. McDowell, (McGraw-Hill Book Co., Inc., New York, 1963), p. 544.

$$I_e^{(a)} = I_0^{(a)} + \tfrac{1}{2}(\omega_e - \omega_e') - \tfrac{1}{4}(\omega_e x_e - \omega_e x_e') + \tfrac{1}{8}(\omega_e y_e - \omega_e y_e') \quad , \qquad \text{IV.8}$$

where the unprimed quantities are for $N_2(X\ ^1\Sigma_g^+)$ and the primed values are for the various states of N_2^+, and $I_0^{(a)}$ is the experimental "adiabatic" ionization potential. The zero point corrections which are smaller than the uncertainty in $I_0^{(a)}$ are neglected (usually the last two terms in Eq. IV.8). The adiabatic ionization potentials calculated here are $I_e^{(a)}$ = 15.99 eV. ($X\ ^2\Sigma_g^+$), 15.34 eV. ($A\ ^2\Pi_u$), and 19.74 eV. ($B\ ^2\Sigma_u^+$) and it should be noted that the calculated, and not the experimental, R_e values are taken as the minimal point in the $E_{HF}(R)$ curves of N_2 and N_2^+. The adiabatic ionization potentials are again in very good agreement as might be expected since the R_e(HF) values are not shifted very far in going from N_2 to N_2^+ and the vertical ionization potentials were good.

From these calculations on the ionization potentials we see that ionization potentials can be calculated to within 10% at worse (using Koopmans' Theorem), but to within about 5% for the directly calculated results. Furthermore, in those few cases where the Hartree-Fock approximation is equally good for both neutral and ionized system, then ionization potentials can be predicted to within 1 or 2%. Therefore it is likely that Hartree-Fock calculations of the type described here, guided by more experience, can help to identify the state of the ion that a Rydberg series is convergent upon. It should also be feasible to construct empirical schemes based upon Hartree-Fock results and estimates of differential correlation energies of AB and AB^+ to give $I_e(R)$ or $I_e^{(a)}$ just as schemes are now being proposed to calculate D_e by Clementi[65] and others.

It is traditional to calculate spectroscopic constants once a potential curve, such as $E_{HF}(R)$, has been calculated. This is usually done by performing the analysis introduced by Dunham[73] in which a polynomial fit is made to $E_{HF}(R)$. We have conformed to this tradition, but with certain misgivings. As is abundantly evident from the potential curves in Fig. 7, the sharp rise of $E_{HF}(R)$ for large R considerably perils any conclusions which might be drawn about quantities calculated using $E_{HF}(R)$ at large R values. Stanton,[68] Leies,[74] Goodisman,[75] and McLean,[66,76] among others, have

[73] J. L. Dunham, Phys. Rev. 41, 713, 721 (1932).

[74] G. M. Leies, J. Chem. Phys. 39, 1137 (1963).

[75] J. Goodisman, J. Chem. Phys. 39, 2396 (1963).

[76] A. D. McLean, J. Chem. Phys. 40, 2774 (1964).

recently expressed certain ideas about the quality of potential curves, and especially the quality of spectroscopic constants calculated from Hartree-Fock results for various internuclear separations. In particular, Stanton has conjectured, "that Hartree-Fock potential energy surfaces and exact potential energy surfaces are parallel over short distances". McLean[66] has questioned certain of Stanton's ideas based on calculations for H_2 and LiF and the results of the present paper are also in disagreement with Stanton's conjecture quoted above. The spectroscopic constants presented in Table XVIII are not given with the expectation that results of great accuracy are possible, but rather to examine their deficiencies.

A number of different polynomial fits were made to $E_{HF}(R)$ for $N_2(X\ ^1\Sigma_g^+)$ in which the number of points was varied from 4 to 10, and the overall symmetry of distribution of points was also independently studied. Certain of the less stable spectroscopic constants were observed to vary wildly, especially when a small left or right asymmetric distribution of points on $E_{HF}(R)$ was employed, and to be worse when one point was very near the minimum of the curve. For example, it was observed in this study for $N_2(X\ ^1\Sigma_g^+)$ that $2681 \leq \omega_e \leq 2773$, $2.85 \leq \omega_e x_e \leq 39.75$, $-7.072 \leq \omega_e y_e \leq 5.588$, $2.119 \leq B_e \leq 2.124$, and $0.0091 \leq \alpha_e \leq 0.0187$ for the various extremes of these results. Clearly then a reasonable choice and distribution of points is obligatory and the use of a symmetrical 10 point polynomial in R was adopted for these states of N_2 and N_2^+.

The resulting spectroscopic constants obtained from the usual Dunham analysis are compared in Table XVIII with the experimental results. It is thus concluded that most spectroscopic constants are quite unreliable, but that at least for B_e, α_e, and ω_e the calculated results are always wrong in the same direction, i.e. too high or too low. It may be possible for the theory to discount the assignment of a certain observed state if the observed B_e or ω_e values are outside the ranges implied above, but positive predictions seem impossible with this accuracy for A_2 type molecules. The remarks, however, are made from the results on N_2 and N_2^+ molecular-ions and for other cases, for example, the diatomic hydrides, AH, the situation may be more favorable.

It has been suggested by Goodisman[76] that spectroscopic constants might be more accurately calculated employing the force on the nuclei as a function of internuclear separation. This is explored in paper III.B where expectation values and molecular properties are considered. Leies,[74] who states that "vibrational properties derived from the SCF function would be valid", which contradicts the results cited, suggests the direct comparison of ΔG values from the numerical solution of the nuclear vibration-rotational problem using $E_{HF}(R)$ and this study is in progress for N_2 and N_2^+ molecular ions. These two alternative methods to the calculation of spectroscopic constants are

important since the Dunham analysis is, generally speaking, rather crude. In a Dunham analysis performed using the turning points and energy values calculated as described in Sec. III.D for $N_2(X\ ^1\Sigma_g^+)$, the spectroscopic constants were found to be $B_e = 2.00087$, $\omega_e = 2271.4\ cm^{-1}$, $\alpha_e = 0.0406$, and $\omega_e x_e = 71.65\ cm^{-1}$. This included only the potential curve for v = 0 through 5, which is why $\omega_e x_e$ was so bad, but it does indicate the best quality of results for B_e and ω_e that can be obtained from a Dunham analysis.

Embellishments of the Hartree-Fock potential curve to improve the spectroscopic constants, such as suggested by McLean,[76] seems to be of neglible importance in view of the apparent intrinsic shortcomings of $E_{HF}(R)$ in this regard.

The variation of the kinetic and potential energy with internuclear separation for $N_2(X\ ^1\Sigma_g^+)$ and $N_2^+(X\ ^2\Sigma_g^+,\ A\ ^2\Pi_u,\ B\ ^2\Sigma_u^+)$ is shown in Figs. 9a and 9b, respectively. The potential energy curves include the nuclear repulsion term. The major, and well-known, feature is the decrease in magnitude of both the kinetic and potential energy as R increases. The rate of decrease is large when R is small, for example, less than R_e(Exptl.), and gradually becomes smaller as $R \rightarrow \infty$. It is interesting to note that the order of the four states are identical for both T(R) and V(R) and that no curve-crossing between the $A\ ^2\Pi_u$ and $X\ ^2\Sigma_g^+$ states of N_2^+ is observed in either T(R) or V(R). In fact, except for the $B\ ^2\Sigma_u^+$ state of N_2^+, the T(R) and V(R) curves seem nearly completely parallel over the entire range of R values considered. That T(R) and V(R) for the $A\ ^2\Pi_u$ and $X\ ^2\Sigma_g^+$ states of N_2^+ are nearly parallel is <u>not</u> inconsistent with the result shown in Fig. 8, in which the $E_{HF}(R)$ curves for these two states cross at approximately R = 1.92 Bohr. It is also noted that the loss of an electron from $N_2(X\ ^1\Sigma_g^+)$, regardless of the resulting N_2^+ state, <u>lowers</u> the kinetic energy curve, T(R), much less than it <u>raises</u> the potential energy curve, V(R). These curves are plotted from results given in Tables XIV through XVII.

A relatively narrow cross-section through the molecular orbital correlation diagram for N_2 and N_2^+ are shown in Figs. 11a,b,c,d. These plots of $\epsilon_{2\sigma_g}(R)$, $\epsilon_{3\sigma_g}(R)$, $\epsilon_{2\sigma_u}(R)$, and $\epsilon_{1\pi_u}(R)$ are linear except for slight curvature over this narrow range of R values. The ϵ_i for the N_2^+ ions are, of course, substantially lower than those for N_2 although the internal spacings and gross characteristics is about the same. The only feature of interest here is the crossing of the $\epsilon_{3\sigma_g}(R)$, $\epsilon_{2\sigma_u}(R)$, and $\epsilon_{1\pi_u}(R)$ curves. The order of the orbital energies at large R is $\epsilon_{2\sigma_g} < \epsilon_{2\sigma_u} < \epsilon_{3\sigma_g} < \epsilon_{1\pi_u}$ for $N_2(X\ ^1\Sigma_g^+)$ and $N_2^+(X\ ^2\Sigma_g^+,\ A\ ^2\Pi_u,\ B\ ^2\Sigma_u^+)$ although their <u>relative</u> separations vary. The $\epsilon_{1\pi_u}$ is seen to cut across both $\epsilon_{2\sigma_u}$ and $\epsilon_{3\sigma_g}$ (except for the $X\ ^2\Sigma_g^+$ and $B\ ^2\Sigma_u^+$ states, in which cases the second crossing seems to be for R less than the smallest R shown).

Similarly the $\epsilon_{2\sigma_u}$ curve rises and apparently crosses both $\epsilon_{3\sigma_g}$ and $\epsilon_{1\pi_u}$. The order at small R thus is $\epsilon_{2\sigma_g} < \epsilon_{1\pi_u} < \epsilon_{3\sigma_g} < \epsilon_{2\sigma_u}$. Therefore the <u>actual</u> ϵ_i values seem to behave well in correlating with the separated and united atom situations and the only new information is the precise behavior of the $\epsilon_i(R)$ over a narrow range of R and the intersections of these $\epsilon_i(R)$.

V. CONCLUSIONS

The extensive set of calculations which form the substantive basis of the presentation in this paper and the study by Huo[2] for CO and BF comprise the only thoroughly documented attempts at a critical study of the convergence of a heirachy of Hartree-Fock-Roothaan wave functions to the true Hartree-Fock wave function for molecules, except for the study by Kolos and Roothaan[62] for the hydrogen molecule. On the basis of these calculations and on the strength of the discussions given, the following conclusions are submitted.

(1) The solution of the Hartree-Fock-Roothaan equations for a carefully selected, and sufficiently large, expansion basis set in terms of STO functions seems to approach the true Hartree-Fock solution as evidenced in terms of certain energy quantities. This conclusion is not very surprizing in light of the remarkably successful Hartree-Fock calculations for first row atoms by Bagus, Gilbert, Roothaan, and Cohen[46] and the reasonable extension of these methods to another electronic system which differs basically only in having a bicentric character. Moreover, the accurate representation of the molecular orbitals is realized by a practicable procedure, feasible for all first row homonuclear diatomic molecules once sufficient information is available from a few exhaustive pilot calculations.

(2) It is imperative to introduce expansion basis functions in σ_g or σ_u and π_u or π_g symmetry which have $\ell_p = 2$ and 3 (d-type and f-type STO functions) as is also emphasized by Nesbet.[34] This is evident from the discussion given in Sec. III and other important manifestations will be considered in paper III.B in regard to certain molecular properties for N_2 and N_2^+ ions. The minimal basis set[29,30] and the double-zeta basis set[33] are seen to have serious shortcomings when viewed comparatively in the overall perspective of the basis set synthesis. The conclusion is that there is no particular reason to obtain such intermediate results if the objective is to obtain the Hartree-Fock wave functions and the concomitant molecular properties. These observations should suggest the exercise of caution in considering the merits of results for diatomic molecules or polyatomic molecules which employ minimal basis sets. Ramifications of this problem are also considered in paper III.B in relation to certain molecular properties.

(3) A certain degree of flexibility should be exercised in employment of the term "molecular orbital". We are referring here to the molecular orbital, that is the canonical set of functions $\phi_{i\lambda\alpha}$ which satisfy the independent particle model, and not

simply functions which are of proper symmetry and are "delocalized". The molecular orbitals inferred in the study of molecular electronic spectroscopy are clearly only approximately the molecular orbitals as given by the independent particle model. This is exhibited in the present study in the reversal of the levels of the $N_2^+(A\ ^2\Pi_u)$ and $N_2^+(X\ ^2\Sigma_g^+)$ states and the $\epsilon_{3\sigma_g}$ and $\epsilon_{1\pi_u}$ for $N_2(X\ ^1\Sigma_g^+)$ relative to experiment. It is claimed by Sinanoglu and Szasz that major vestiges of the orbital concept are retained in elaborate theories beyond the Hartree-Fock model which include the instantaneous interactions of the electrons of the system. This or similar explanations must reconcile the molecular orbital of theory and experiment in certain (and hopefully few) key situations.

(4) Although the calculated "rationalized" dissociation energies are still quite bad and the potential curves are all much too high relative to experimental results, both not especially unexpected results, the calculated internal spacings of ionized states are quite well predicted. The prospects of careful studies of the variation of the correlation energy with internuclear separation and upon selective ionizations are thus quite good. For complete homologous series and certain isoelectronic series such raw data for the possible success of empirical correlation energy is thus close at hand.

(5) Spectroscopic constants from Hartree-Fock calculations obtained by the Dunham analysis of the potential curve are quite unreliable.

(6) A very encouraging result of these calculations is the relatively high accuracy obtained for the directly calculated ionization potentials. The accuracy, which should be relatively the same for other systems, indicates that we can calculate ionization potentials to within about 5%. We have also seen that in some cases the Koopmans' Theorem ionization potential may be much more accurate.

One final note may be made in this section about configuration interaction calculations. Caution should always be exercised to distinguish generic and practical improvements in wave functions. Thus configuration interaction calculations, such as those of Fraga and Ransil,[30] are actually inferior in quality to the Hartree-Fock results given here. Configuration interaction itself does not necessarily imply a blanket and automatic improvement on inferior, but more exhaustively pursued approximations.

ACKNOWLEDGEMENTS

The authors have profited considerably from the assistance of our colleagues in the execution of the research described herein. We are grateful to Dr. P. S. Bagus and Dr. T. L. Gilbert of the Solid State Division, Argonne National Laboratory, for free use of their unpublished Hartree-Fock wave functions for the first row atoms and for useful advice. Frequent conversations with Dr. J. B. Greenshields, Dr. Winifred Huo, Dr. B. J. Ransil, and Dr. B. Joshi, among others, have been most helpful in serving as useful criticisms of this work in progress. Professor Clemens C. J. Roothaan has generously provided seasoned and welcome criticisms of the arguments and results given here and it is a pleasure to acknowledge his sustained encouragement and support. Finally, it is a privilege to thank Professor Robert S. Mulliken for many useful suggestions and for a critical reading of a rough draft of certain parts of this paper. We are particularly happy to offer this contribution as a tribute to Professor Mulliken, since nitrogen is more or less his favorite molecule.

TABLE I. SYNTHESIS OF BASIS SET 1 AND 2 — ENERGY QUANTITIES — $N_2(X^1\Sigma_g^+)$, R = 2.068 BOHRS

Basis Set*	Symmetry STO, $\chi_{p\lambda\alpha}$, Basis Set Composition†	E‡	T	V	$-\frac{V}{T}$	$\epsilon_{1\sigma_g}$	$\epsilon_{1\sigma_u}$	$\epsilon_{2\sigma_g}$	$\epsilon_{2\sigma_u}$	$\epsilon_{3\sigma_g}$	$\epsilon_{1\pi_u}$	$\epsilon_{3\sigma_u}$
Set 1A (BMMO g = u)	σ_g1s,σ_g2s,σ_g2p; σ_u1s,σ_u2s,σ_u2p;π_u2p;(g = u)	-108.6336	108.7306	-217.3642	1.9991	-15.6471	-15.6442	-1.4211	-0.7137	-0.5555	-0.5454	1.2262
Set 1B (BMMO g ≠ u)	σ_g1s,σ_g2s,σ_g2p; σ_u1s,σ_u2s,σ_u2p;π_u2p;(g ≠ u)	-108.6459	108.7541	-217.4000	1.9990	-15.6436	-15.6405	-1.4262	-0.7185	-0.5499	-0.5435	1.3608
Set 1C (4x4x1)	Set 1B + σ_g1s' and σ_u1s'	-108.6908	108.7386	-217.4294	1.9996	-15.6573	-15.6539	-1.4307	-0.7150	-0.5434	-0.5397	1.4020
Set 1D (5x5x1)	Set 1C + σ_g2s' and σ_u2s'	-108.7713	108.5154	-217.2867	2.0024	-15.7089	-15.7056	-1.4718	-0.7477	-0.5932	-0.5691	0.9002
Set 1E (5x5x2)	Set 1D + π_u2p'	-108.8691	108.7975	-217.6666	2.0007	-15.7116	-15.7082	-1.5069	-0.7702	-0.6193	-0.6172	0.8848
Set 1F (6x5x2)	Set 1E + σ_g2p'	-108.8896	108.8933	-217.7829	2.0000	-15.7140	-15.7104	-1.5257	-0.7770	-0.6291	-0.6272	0.8807
Set 1G (6x6x2)	Set 1F + σ_u2p'	-108.8914	108.9084	-217.7999	1.9998	-15.7157	-15.7122	-1.5293	-0.7780	-0.6309	-0.6298	0.8417
Set 1H (6x6x3)	Set 1G + π_u2p"	-108.8926	108.9286	-217.8212	1.9997	-15.7108	-15.7072	-1.5249	-0.7750	-0.6275	-0.6277	0.8446
Set 1I (7x6x3)	Set 1H + σ_g2p"	-108.8992	108.9698	-217.8691	1.9994	-15.7070	-15.7034	-1.5235	-0.7739	-0.6293	-0.6257	0.8468
Set 1J (8x6x3)	Set 1I + σ_g2s"	-108.9022	108.8488	-217.7510	2.0005	-15.7115	-15.7078	-1.5246	-0.7738	-0.6294	-0.6256	0.8474
Set 1K (8x6x3)	Set 1I + σ_g3s	-108.9022	108.8522	-217.7544	2.0004	-15.7113	-15.7076	-1.5246	-0.7738	-0.6294	-0.6255	0.8474
Set 1L (9x6x3)	Set 1K + σ_g3d	-108.9298	108.8556	-217.7854	2.0007	-15.6988	-15.6952	-1.5119	-0.7742	-0.6369	-0.6144	0.8596
Set 1M (9x6x4)	Set 1L + π_u3d	-108.9819	108.8291	-217.8110	2.0014	-15.6725	-15.6689	-1.4644	-0.7692	-0.6262	-0.6080	0.8757

TABLE I. SYNTHESIS OF BASIS SET 1 AND 2 – ENERGY QUANTITIES – $N_2(X^1\Sigma_g^+)$, R = 2.068 BOHRS (Continued)

Basis Set*	Symmetry STO $\chi_{p\lambda\alpha}$ Basis Set Composition†	E‡	T	V	$-\frac{V}{T}$	$\epsilon_{1\sigma_g}$	$\epsilon_{1\sigma_u}$	$\epsilon_{2\sigma_g}$	$\epsilon_{2\sigma_u}$	$\epsilon_{3\sigma_g}$	$\epsilon_{1\pi_u}$	$\epsilon_{3\sigma_u}$
Set 1N (10x6x4)	Set 1M + $\sigma_g 4f$	-108.9832	108.8361	-217.8192	2.0014	-15.6716	-15.6679	-1.4640	-0.7690	-0.6258	-0.6078	0.8760
Set 1O (10x6x5)	Set 1N + $\pi_u 4f$	-108.9855	108.8387	-217.8242	2.0013	-15.6694	-15.6657	-1.4612	-0.7680	-0.6237	-0.6077	0.8775
Set 1P (10x6x6)	Set 1O + $\pi_u 3d'$	-108.9868	108.8207	-217.8076	2.0015	-15.6753	-15.6716	-1.4662	-0.7718	-0.6281	-0.6110	0.8740
Set 1Q (10x7x6)	Set 1P + $\sigma_u 3d$	-108.9869	108.8208	-217.8076	2.0015	-15.6752	-15.6716	-1.4660	-0.7719	-0.6280	-0.6109	0.8710
Set 1R (11x7x6)	Set 1Q + $\sigma_g 3d'$	-108.9875	108.8249	-217.8124	2.0015	-15.6749	-15.6713	-1.4665	-0.7721	-0.6283	-0.6112	0.8707
Set 1S (12x8x6)	Set 1R + $\sigma_g 3d''$ and $\sigma_u 3s$	-108.9888	108.8083	-217.7971	2.0017	-15.6747	-15.6710	-1.4657	-0.7720	-0.6275	-0.6104	0.8437
Set 2A (8x7x3)	$\sigma_g 1s, \sigma_g 1s', \sigma_g 2s, \sigma_g 2s', \sigma_g 3s, \sigma_g 2p, \sigma_g 2p', \sigma_g 2p''; \sigma_u 1s, \sigma_u 1s', \sigma_u 2s, \sigma_u 2s' \sigma_u 3s, \sigma_u 2p, \sigma_u 2p'; \pi_u 2p, \pi_u 2p', \pi_u 2p''$	-108.8967	108.8987	-217.7954	2.0000	-15.7169	-15.7133	-1.5381	-0.7823	-0.6374	-0.6311	0.8887
Set 2B (12x8x6)	Set 2A + $\begin{cases} \sigma_g 3d, \sigma_g 3d', \sigma_g 3d'', \sigma_g 4f; \\ \sigma_u 3d; \pi_u 3d, \pi_u 3d', \pi_u 4f. \end{cases}$	-108.9897	108.8067	-217.7964	2.0017	-15.6791	-15.6755	-1.4723	-0.7761	-0.6339	-0.6126	0.8748
Set 2C (12x8x6)	Set 2B + Optimization of all ζ's	-108.9926	108.7954	-217.7880	2.0018	-15.6826	-15.6790	-1.4746	-0.7788	-0.6357	-0.6161	0.7975
Set 2D (12x8x6)	Set 2C + Optimization of all ζ's	-108.9928	108.7911	-217.7839	2.0019	-15.6820	-15.6783	-1.4736	-0.7780	-0.6350	-0.6154	0.8077

*The designation of the various basis sets given here are those employed in the text. The symbols under the basis set designation, for example (6x6x2) under basis set 1G, refer to the number of symmetry basis functions in the σ_g, σ_u, and π_u symmetry, respectively.

†This column gives only the n_p and ℓ_p of the symmetry STO basis functions for each stage of the build up of basis set 1. The basis set composition refers in addition to the orbital exponents of the basis functions which may change from case to case. The full wavefunction including the orbital exponents and the vectors for each member of the build up is available from the authors upon request.

‡All energy quantities are in Hartrees.

TABLE II. SYNTHESIS OF BASIS SET 1 AND 2 — ENERGY DIFFERENCES — $N_2(X^1\Sigma_g^+)$, R = 2.068 Bohrs

Basis Set	Symmetry STO, $\chi_{p\lambda\alpha}$ Basis Set Composition	ΔE^*	ΔT	ΔV	$\Delta(-\frac{V}{T})$	$\Delta\epsilon_{1\sigma_g}$	$\Delta\epsilon_{1\sigma_u}$	$\Delta\epsilon_{2\sigma_g}$	$\Delta\epsilon_{2\sigma_u}$	$\Delta\epsilon_{3\sigma_g}$	$\Delta\epsilon_{1\pi_u}$	$\Delta\epsilon_{3\sigma_u}$
Set 1A (BMMO g = u)	σ_g1s,σ_g2s,σ_g2p; σ_u1s,σ_u2s,σ_u2p;π_u2p; (g = u)	———	———	———	———	———	———	———	———	———	———	———
Set 1B (BMMO g ≠ u)	σ_g1s,σ_g2s,σ_g2p; σ_u1s,σ_u2s,σ_u2p;π_u2p; (g ≠ u)	-0.0123	+0.0235	-0.0358	-0.0001	+0.0035	+0.0037	-0.0051	-0.0048	+0.0056	+0.0019	+0.1346
Set 1C (4x4x1)	Set 1B + σ_g1s' and σ_u1s'	-0.0449	-0.0155	-0.0294	+0.0006	-0.0137	-0.0134	-0.0045	+0.0035	+0.0065	+0.0038	+0.0412
Set 1D (5x5x1)	Set 1C + σ_g2s' and σ_u2s'	-0.0805	-0.2232	+0.1427	+0.0028	-0.0516	-0.0517	-0.0411	-0.0327	-0.0498	-0.0294	-0.5018
Set 1E (5x5x2)	Set 1D + π_u2p'	-0.0978	+0.2821	-0.3799	-0.0017	-0.0027	-0.0026	-0.0351	-0.0225	-0.0261	-0.0481	-0.0154
Set 1F (6x5x2)	Set 1E + σ_g2p'	-0.0205	+0.0958	-0.1163	-0.0007	-0.0024	-0.0022	-0.0188	-0.0068	-0.0098	-0.0100	-0.0041
Set 1G (6x6x2)	Set 1F + σ_u2p'	-0.0018	+0.0151	-0.0170	-0.0002	-0.0017	-0.0018	-0.0036	-0.0010	-0.0018	-0.0026	-0.0390
Set 1H (6x6x3)	Set 1G + π_u2p"	-0.0012	+0.0202	-0.0213	-0.0001	+0.0049	+0.0050	+0.0044	+0.0030	+0.0034	+0.0021	+0.0029
Set 1I (7x6x3)	Set 1H + σ_u2p"	-0.0066	+0.0412	-0.0479	-0.0003	+0.0038	+0.0038	+0.0014	+0.0011	-0.0018	+0.0020	+0.0022
Set 1J (8x6x3)	Set 1I + σ_g2s"	-0.0030	-0.1210	+0.1181	+0.0011	-0.0045	-0.0044	-0.0011	+0.0001	-0.0001	+0.0001	+0.0006
Set 1K (8x6x3)	Set 1I + σ_g3s	0.0000	+0.0034	-0.0034	-0.0001	+0.0002	+0.0002	0.0000	0.0000	0.0000	+0.0001	0.0000
Set 1L (9x6x3)	Set 1K + σ_g3d	-0.0276	+0.0034	-0.0310	+0.0003	+0.0125	+0.0124	+0.0127	-0.0004	-0.0075	+0.0111	+0.0122
Set 1M (9x6x4)	Set 1L + π_u3d	-0.0521	-0.0265	-0.0256	+0.0007	+0.0263	+0.0263	+0.0475	+0.0050	+0.0107	+0.0064	+0.0161

TABLE II. SYNTHESIS OF BASIS SET 1 AND 2 — ENERGY DIFFERENCES — $N_2(X\,^1\Sigma_g^+)$, R = 2.068 Bohrs (Continued).

Basis Set	Symmetry STO, $\chi_{p\lambda\alpha}$, Basis Set Composition	ΔE^*	ΔT	ΔV	$\Delta(-\frac{V}{T})$	$\Delta\epsilon_{1\sigma_g}$	$\Delta\epsilon_{1\sigma_u}$	$\Delta\epsilon_{2\sigma_g}$	$\Delta\epsilon_{2\sigma_u}$	$\Delta\epsilon_{3\sigma_g}$	$\Delta\epsilon_{1\pi_u}$	$\Delta\epsilon_{3\sigma_u}$
Set 1N (10×6×4)	Set 1M + $\sigma_g 4f$	-0.0013	+0.0070	-0.0082	0.0000	+0.0009	+0.0010	+0.0004	+0.0002	+0.0004	+0.0002	+0.0003
Set 1O (10×6×5)	Set 1N + $\pi_u 4f$	-0.0023	+0.0026	-0.0050	-0.0001	+0.0022	+0.0022	+0.0028	+0.0010	+0.0021	+0.0001	+0.0015
Set 1P (10×6×6)	Set 1O + $\pi_u 3d'$	-0.0013	-0.0180	+0.0166	+0.0002	-0.0059	-0.0059	-0.0050	-0.0038	-0.0044	-0.0033	-0.0035
Set 1Q (10×7×6)	Set 1P + $\sigma_u 3d$	-0.0001	+0.0001	0.0000	0.0000	+0.0001	0.0000	+0.0002	-0.0001	+0.0001	+0.0001	-0.0030
Set 1R (11×7×6)	Set 1Q + $\sigma_g 3d'$	-0.0006	+0.0041	-0.0048	0.0000	+0.0003	+0.0003	-0.0005	-0.0002	-0.0003	-0.0003	-0.0003
Set 1S (12×8×6)	Set 1R + $\sigma_g 3d''$ and $\sigma_u 3s$	-0.0013	-0.0166	+0.0153	+0.0002	+0.0002	+0.0003	+0.0008	+0.0001	+0.0008	+0.0008	-0.0270
Set 2A (8×7×3)	$\sigma_g 1s, \sigma_g 1s', \sigma_g 2s, \sigma_g 2s', \sigma_g 3s, \sigma_g 2p, \sigma_g 2p', \sigma_g 2p''; \sigma_u 1s, \sigma_u 1s', \sigma_u 2s, \sigma_u 2s', \sigma_u 3s, \sigma_u 2p, \sigma_u 2p'; \pi_u 2p, \pi_u 2p', \pi_u 2p''$	———	———	———	———	———	———	———	———	———	———	———
Set 2B (12×8×6)	Set 2A + $\begin{cases} \sigma_g 3d, \sigma_g 3d', \sigma_g 3d'', \sigma_g 4f \\ \sigma_u 3d, \pi_u 3d, \pi_u 3d', \pi_u 4f \end{cases}$	-0.0930	-0.0920	-0.0010	+0.0017	+0.0378	+0.0378	+0.0658	+0.0062	+0.0035	+0.0185	-0.0139
Set 2C (12×8×6)	Set 2B + Optimization of all ζ's	-0.0029	-0.0113	+0.0084	+0.0001	-0.0035	-0.0035	.0.0023	.0.0027	-0.0018	-0.0035	-0.0773
Set 2D (12×8×6)	Set 2C + Optimization of all ζ's	-0.0002	-0.0043	+0.0041	+0.0001	+0.0006	+0.0007	+0.0010	+0.0008	+0.0007	+0.0007	+0.0102

*The differences in the various columns are differences between the (N+1)th and Nth row quantities from Table I. All energy changes are in Hartrees.

TABLE III.

HFR Wave Function 1S for $N_2(1\sigma_g^2 1\sigma_u^2 2\sigma_g^2 2\sigma_u^2 3\sigma_g^2 1\pi_u^4, X^1\Sigma_g^+)$, R = 2.068 Bohr.

E = -108.9888 H., T = 108.8083 H., V = -217.7971 H., V/T = -2.00166

$\epsilon_{1\sigma_g}$ = -15.67467, $\epsilon_{2\sigma_g}$ = -1.46565, $\epsilon_{3\sigma_g}$ = -0.62749, $\epsilon_{1\sigma_u}$ = -15.67101, $\epsilon_{2\sigma_u}$ = -0.77203, $\epsilon_{1\pi_u}$ = -0.61037

$\chi_{p\sigma_g}$ \ $C_{i\lambda p}$	$C_{1\sigma_g,p}$	$C_{2\sigma_g,p}$	$C_{3\sigma_g,p}$	$\chi_{p\sigma_u}$ \ $C_{i\lambda p}$	$C_{1\sigma_u,p}$	$C_{2\sigma_u,p}$	$\chi_{p\pi_u}$ \ $C_{i\lambda p}$	$C_{1\pi_u,p}$
σ_g1s (ζ = 6.34808)	0.91893	-0.26088	0.07517	σ_u1s (6.42643)	0.95623	-0.21563	π_u2p (1.63543)	0.67240
σ_g1s'(10.44794)	0.08480	0.00624	-0.00172	σ_u1s'(11.79782)	0.04946	0.00128	π_u2p'(3.29947)	0.20651
σ_g2s (1.15656)	-0.00156	0.01473	-0.30107	σ_u2s (1.35580)	-0.01279	0.27631	π_u2p"(7.66609)	0.00797
σ_g2s'(2.19475)	0.00657	0.72687	-0.28580	σ_u2s'(2.12224)	0.01276	0.79805	π_u3d (0.51707)	0.05303
σ_g3s (8.34237)	0.00149	-0.02834	0.00347	σ_u3s (9.60739)	-0.00250	-0.02039	π_u3d'(2.33801)	0.06928
σ_g2p (1.34282)	-0.00178	0.00835	0.23567	σ_u2p (1.44387)	-0.00380	-0.24628	π_u4f (3.45922)	0.01041
σ_g2p'(2.36027)	0.00228	0.31756	0.58490	σ_u2p'(3.04456)	0.00294	-0.16958		
σ_g2p"(6.31659)	0.00089	0.01389	0.03064	σ_u3d (4.36861)	0.00037	-0.00240		
σ_g3d (1.34301)	-0.00110	-0.01061	-0.03648					
σ_g3d'(2.62151)	0.00144	0.05116	0.05095					
σ_g3d"(5.36005)	-0.00023	-0.00134	-0.00199					
σ_g4f (3.31101)	0.00041	0.00876	0.00443					

TABLE IV

HFR Wave Function 2D for $N_2(1\sigma_g^2 1\sigma_u^2 2\sigma_g^2 2\sigma_u^2 3\sigma_g^2 1\pi_u^4, X^1\Sigma_g^+)$, R = 2.068 Bohr

E = -108.9928 H., T = 108.7911 H., V = -217.7839 H., V/T = -2.00185

$\epsilon_{1\sigma_g}$ = -15.68195, $\epsilon_{2\sigma_g}$ = -1.47360, $\epsilon_{3\sigma_g}$ = -0.63495, $\epsilon_{1\sigma_u}$ = -15.67833, $\epsilon_{2\sigma_u}$ = -0.77796, $\epsilon_{1\pi_u}$ = -0.61544

$\chi_{p\sigma_g}$ \ $C_{i\lambda p}$	$C_{1\sigma_g,p}$	$C_{2\sigma_g,p}$	$C_{3\sigma_g,p}$	$\chi_{p\sigma_u}$ \ $C_{i\lambda p}$	$C_{1\sigma_u,p}$	$C_{2\sigma_u,p}$	$\chi_{p\pi_u}$ \ $C_{i\lambda p}$	$C_{1\pi_u,p}$
σ_g1s (ζ = 5.68298)	0.92319	-0.27931	0.07484	σ_u1s (5.95534)	0.93406	-0.24370	π_u2p (1.38436)	0.46921
σ_g1s'(10.34240)	0.15204	-0.00615	0.00262	σ_u1s'(10.65879)	0.11483	-0.00000	π_u2p'(2.53288)	0.39869
σ_g2s (1.45349)	0.00090	0.14106	-0.45859	σ_u2s (1.57044)	-0.01156	0.36437	π_u2p"(5.69176)	0.03141
σ_g2s'(2.43875)	-0.00003	0.59948	-0.17662	σ_u2s'(2.48965)	0.00479	0.54702	π_u3d (2.05707)	0.05938
σ_g3s (7.04041)	-0.08501	-0.02333	-0.00678	σ_u3s (7.29169)	-0.05343	-0.03054	π_u3d'(2.70650)	0.01738
σ_g2p (1.28261)	0.00041	0.11602	0.42914	σ_u2p (1.48549)	-0.00679	-0.41355	π_u4f (3.06896)	0.01233
σ_g2p'(2.56988)	0.00104	0.25907	0.48453	σ_u2p'(3.49990)	0.00294	-0.10945		
σ_g2p"(6.21698)	0.00109	0.01092	0.02478	σ_u3d (1.69003)	-0.00121	-0.03553		
σ_g3d (1.34142)	0.00017	0.03626	0.04696					
σ_g3d'(2.91681)	0.00098	0.03984	0.03065					
σ_g3d"(5.52063)	-0.00018	-0.00275	-0.00158					
σ_g4f (2.59449)	0.00032	0.01334	0.01086					

TABLE V

HFR Wave Function for $N_2^+(1\sigma_g^2 1\sigma_u^2 2\sigma_g^2 2\sigma_u^2 3\sigma_g 1\pi_u^4, X^2\Sigma_g^+)$, R = 2.113 Bohr

E = -108.4037 H., T = 108.1612 H., V = -216.5649 H., V/T = -2.00224

$\epsilon_{1\sigma_g}$ = -16.18273, $\epsilon_{2\sigma_g}$ = -1.88073, $\epsilon_{3\sigma_g}$ = -1.12345, $\epsilon_{1\sigma_u}$ = -16.18002, $\epsilon_{2\sigma_u}$ = -1.15688, $\epsilon_{1\pi_u}$ = -1.02369

$\chi_{p\sigma_g}$ \ $C_{i\lambda p}$	$C_{1\sigma_g,p}$	$C_{2\sigma_g,p}$	$C_{3\sigma_g,p}$	$\chi_{p\sigma_u}$ \ $C_{i\lambda p}$	$C_{1\sigma_u,p}$	$C_{2\sigma_u,p}$	$\chi_{p\pi_u}$ \ $C_{i\lambda p}$	$C_{1\pi_u,p}$
σ_g1s (ζ = 5.68298)	0.92380	-0.28356	0.08485	σ_u1s (5.95534)	0.93479	-0.25955	π_u2p (1.53784)	0.47956
σ_g1s'(10.34240)	0.15194	-0.00622	0.00249	σ_u1s'(10.65879)	0.11476	0.00040	π_u2p'(2.54788)	0.38728
σ_g2s (1.67652)	0.00156	0.20359	-0.43210	σ_u2s (0.95819)	-0.00098	-0.01418	π_u2p"(5.61486)	0.03526
σ_g2s'(2.50020)	-0.00082	0.58070	-0.14364	σ_u2s'(2.20484)	0.00109	0.88861	π_u3d (2.24311)	0.07876
σ_g3s (7.04041)	-0.08537	-0.02826	-0.00497	σ_u3s (7.29169)	-0.05302	-0.02107	π_u3d'(3.68750)	-0.00183
σ_g2p (1.47252)	0.00014	0.09449	0.37297	σ_u2p (1.49449)	-0.00080	-0.38798	π_u4f (3.04069)	0.01516
σ_g2p'(2.56008)	0.00064	0.22626	0.51555	σ_u2p'(3.52453)	0.00112	-0.10141		
σ_g2p"(6.51387)	0.00053	0.00962	0.02345	σ_u3d (1.58465)	-0.00007	-0.03958		
σ_g3d (1.57033)	0.00021	0.02886	0.02899					
σ_g3d'(2.87912)	0.00034	0.03387	0.02357					
σ_g3d"(5.52063)	0.00010	-0.00235	-0.00070					
σ_g4f (2.79841)	0.00020	0.01271	0.01570					

TABLE VI

HFR Wave Function for $N_2^+(1\sigma_g^2 1\sigma_u^2 2\sigma_g^2 2\sigma_u^2 3\sigma_g^2 1\pi_u^3, A^2\Pi_u)$, R = 2.222 Bohr

E = -108.4270 H., T = 108.1820 H., V = -216.6089 H., V/T = -2.00226

$\epsilon_{1\sigma_g}$ = -16.18050, $\epsilon_{2\sigma_g}$ = -1.86435, $\epsilon_{3\sigma_g}$ = -1.03491, $\epsilon_{1\sigma_u}$ = -16.17820, $\epsilon_{2\sigma_u}$ = -1.20616, $\epsilon_{1\pi_u}$ = -1.02888

$\chi_{p\sigma_g}$ \ $C_{i\lambda p}$	$C_{1\sigma_g,p}$	$C_{2\sigma_g,p}$	$C_{3\sigma_g,p}$	$\chi_{p\sigma_u}$ \ $C_{i\lambda p}$	$C_{1\sigma_u,p}$	$C_{2\sigma_u,p}$	$\chi_{p\pi_u}$ \ $C_{i\lambda p}$	$C_{1\pi_u,p}$
σ_g1s (ζ = 5.68298)	0.92406	-0.27186	0.09871	σ_u1s (5.95534)	0.93494	-0.26169	π_u2p (1.54195)	0.50577
σ_g1s'(10.34240)	0.15190	-0.00599	0.00238	σ_u1s'(10.65879)	0.11463	0.00030	π_u2p'(2.55318)	0.36203
σ_g2s (1.62293)	0.00115	0.18359	-0.44381	σ_u2s (2.21503)	-0.00296	0.87726	π_u2p"(5.60093)	0.03573
σ_g2s'(2.48547)	-0.00073	0.56677	-0.18261	σ_u2s'(3.13473)	0.00366	0.00836	π_u3d (2.15014)	0.09281
σ_g3s (7.04041)	-0.08552	-0.02640	-0.00558	σ_u3s (7.29169)	-0.05416	-0.02388	π_u3d'(4.00627)	-0.00193
σ_g2p (1.42818)	-0.00014	0.13471	0.39371	σ_u2p (1.50366)	-0.00211	-0.38275	π_u4f (2.80565)	0.01410
σ_g2p'(2.55362)	0.00123	0.23594	0.48071	σ_u2p'(3.54115)	0.00254	-0.10310		
σ_g2p"(6.21698)	0.00164	0.01123	0.02620	σ_u3d (1.65063)	-0.00002	-0.04804		
σ_g3d (1.52969)	-0.00010	0.04759	0.05017					
σ_g3d'(2.87017)	0.00100	0.03538	0.03206					
σ_g3d"(5.52063)	-0.00027	-0.00224	-0.00208					
σ_g4f (2.37367)	0.00019	0.01767	0.01161					

TABLE VII

HFR Wave Function for $N_2^+(1\sigma_g^2 1\sigma_u^2 2\sigma_g^2 2\sigma_u 3\sigma_g^2 1\pi_u^4, B^2\Sigma_u^+)$, R = 2.0315 Bohr

E = -108.2596 H., T = 107.8350 H., V = -216.0946 H., V/T = -2.00394

$\epsilon_{1\sigma_g}$ = -16.16271, $\epsilon_{2\sigma_g}$ = -1.89302, $\epsilon_{3\sigma_g}$ = -1.00569, $\epsilon_{1\sigma_u}$ = -16.15837, $\epsilon_{2\sigma_u}$ = -1.25973, $\epsilon_{1\pi_u}$ = -1.03593

$\chi_{p\sigma_g}$ \ $C_{i\lambda p}$	$C_{1\sigma_g,p}$	$C_{2\sigma_g,p}$	$C_{3\sigma_g,p}$	$\chi_{p\sigma_u}$ \ $C_{i\lambda p}$	$C_{1\sigma_u,p}$	$C_{2\sigma_u,p}$	$\chi_{p\pi_u}$ \ $C_{i\lambda p}$	$C_{1\pi_u,p}$
σ_g1s (ζ = 5.68298)	0.92217	-0.28050	0.09191	σ_u1s (5.90826)	0.93825	-0.25604	π_u2p (1.53707)	0.47174
σ_g1s'(10.34240)	0.15250	-0.00611	0.00323	σ_u1s'(10.69717)	0.11717	-0.00078	π_u2p'(2.55041)	0.38718
σ_g2s (1.61093)	0.00087	0.15461	-0.49521	σ_u2s (1.65689)	-0.00279	-0.40083	π_u2p"(5.61323)	0.03537
σ_g2s'(2.49340)	0.00018	0.56562	-0.15239	σ_u2s'(2.10568)	0.00229	1.13692	π_u3d (2.10647)	0.06439
σ_g3s (7.02110)	-0.08461	-0.02788	-0.00612	σ_u3s (7.31519)	-0.05994	-0.02072	π_u3d'(2.70650)	0.01331
σ_g2p (1.39078)	0.00070	0.12146	0.38610	σ_u2p (1.51874)	-0.00141	-0.47612	π_u4f (3.06104)	0.01352
σ_g2p'(2.58075)	0.00088	0.28087	0.48916	σ_u2p'(3.48920)	0.00045	-0.11921		
σ_g2p"(6.25817)	0.00012	0.01305	0.02453	σ_u3d (1.37167)	-0.00014	-0.03593		
σ_g3d (1.41676)	0.00021	0.03355	0.04293					
σ_g3d'(2.93434)	0.00106	0.04265	0.02525					
σ_g3d"(4.46937)	-0.00019	-0.00512	-0.00121					
σ_g4f (2.59449)	0.00039	0.01354	0.01213					

TABLE VIII. ENERGY QUANTITIES FOR CERTAIN STATES OF N_2^{+2}, N_2^{+3}, AND N_2^{+4} (R = 2.0132 Bohr).†

Ion	Outer Shells	E(H.)	$\epsilon_{1\sigma_g}$	$\epsilon_{1\sigma_u}$	$\epsilon_{2\sigma_g}$	$\epsilon_{2\sigma_u}$	$\epsilon_{3\sigma_g}$	$\epsilon_{1\pi_u}$	$-\frac{\langle V \rangle}{\langle T \rangle}$
$N_2^{++}(^3\Sigma_g^-)$	$2\sigma_u^2 3\sigma_g^2 1\pi_u^2$	-107.3871	-16.7170	-16.7129	-2.5000	-1.6373	-1.5207	-1.6495	1.9894
$N_2^{++}(^1\Delta_g)$	$2\sigma_u^2 3\sigma_g^2 1\pi_u^2$	-107.3344	-16.7201	-16.7160	-2.5036	-1.6386	-1.5223	-1.5977	1.9890
$N_2^{++}(^1\Sigma_g^+)$	$2\sigma_u^2 3\sigma_g^0 1\pi_u^4$	-107.2985	-16.7400	-16.7368	-2.4089	-1.5570	-1.0668*	-1.5242	1.9966
$N_2^{+3}(^2\Pi_u)$	$2\sigma_u^2 3\sigma_g^2 1\pi_u^1$	-105.6941	-17.3286	-17.3247	-3.0792	-2.1202	-2.0114	-2.0114	1.9796
$N^{+4}(^1\Sigma_g^+)$	$2\sigma_u^2 3\sigma_g^2 1\pi_u^0$	-103.6322	-17.9820	-17.9783	-3.6956	-2.6293	-2.5256	———	1.9684

†These calculations are all direct calculations for the ion and state in question. No claim is made that these are Hartree-Fock results or that the states considered are bound states. All results employ set 2D of Table IV.

*Virtual orbitals.

TABLE IX

HFR Wave Function for $N_2(1\sigma_g^2 1\sigma_u^2 2\sigma_g^2 2\sigma_u^2 3\sigma_g^2 1\pi_u^4,\ X^1\Sigma_g^+)$, R = 1.85 Bohr.

E = -108.9635 H., T = 109.7690 H., V = -218.7325 H., V/T = -1.99266

$\epsilon_{1\sigma_g}$ = -15.63888, $\epsilon_{2\sigma_g}$ = -1.55836, $\epsilon_{3\sigma_g}$ = -0.64458, $\epsilon_{1\sigma_u}$ = -15.63096, $\epsilon_{2\sigma_u}$ = -0.73869, $\epsilon_{1\pi_u}$ = -0.67089

$\chi_{p\sigma_g}$ \ $C_{i\lambda p}$	$C_{1\sigma_g,p}$	$C_{2\sigma_g,p}$	$C_{3\sigma_g,p}$	$\chi_{p\sigma_u}$ \ $C_{i\lambda p}$	$C_{1\sigma_u,p}$	$C_{2\sigma_u,p}$	$\chi_{p\pi_u}$ \ $C_{i\lambda p}$	$C_{1\pi_u,p}$
σ_g1s (ζ = 5.94056)	0.91434	-0.29387	0.06704	σ_u1s (5.93353)	0.93359	-0.23852	π_u2p (1.41982)	0.43150
σ_g1s'(10.34240)	0.12958	0.00030	0.00166	σ_u1s'(10.65879)	0.11715	0.00002	π_u2p'(2.53835)	0.41612
σ_g2s (1.41866)	-0.00036	0.09577	-0.47425	σ_u2s (1.54143)	-0.01416	0.28143	π_u2p"(5.69176)	0.03159
σ_g2s'(2.44464)	0.00411	0.61729	-0.17010	σ_u2s'(2.47023)	0.00476	0.53707	π_u3d (1.97411)	0.03959
σ_g3s (7.13249)	-0.04846	-0.03655	-0.00149	σ_u3s (7.25156)	-0.05577	-0.02971	π_u3d'(2.68119)	0.04179
σ_g2p (1.31201)	-0.00051	0.08691	0.38339	σ_u2p (1.48871)	-0.00764	-0.48016	π_u4f (3.27677)	0.01276
σ_g2p'(2.60843)	0.00229	0.31261	0.49517	σ_u2p'(3.57859)	0.00307	-0.10993		
σ_g2p"(6.42640)	0.00088	0.01146	0.02187	σ_u3d (1.68711)	-0.00113	-0.03842		
σ_g3d (1.32508)	-0.00032	0.02099	0.02244					
σ_g3d'(3.01776)	0.00162	0.04471	0.03548					
σ_g3d"(6.01250)	-0.00018	-0.00212	-0.00156					
σ_g4f (3.41264)	0.00062	0.00890	0.00740					

TABLE X

HFR Wave Function for $N_2(1\sigma_g^2 1\sigma_u^2 2\sigma_g^2 2\sigma_u^2 3\sigma_g^2 1\pi_u^4,\ X^1\Sigma_g^+)$, R = 1.95 Bohr.

E = -108.9914 H., T = 109.2666 H., V = -218.2580 H., V/T = -1.99748

$\epsilon_{1\sigma_g}$ = -15.65864, $\epsilon_{2\sigma_g}$ = -1.51944, $\epsilon_{3\sigma_g}$ = -0.64009, $\epsilon_{1\sigma_u}$ = -15.65324, $\epsilon_{2\sigma_u}$ = -0.75699, $\epsilon_{1\pi_u}$ = -0.64381

$\chi_{p\sigma_g}$ \ $C_{i\lambda p}$	$C_{1\sigma_g,p}$	$C_{2\sigma_g,p}$	$C_{3\sigma_g,p}$	$\chi_{p\sigma_u}$ \ $C_{i\lambda p}$	$C_{1\sigma_u,p}$	$C_{2\sigma_u,p}$	$\chi_{p\pi_u}$ \ $C_{i\lambda p}$	$C_{1\pi_u,p}$
σ_g1s (ζ = 5.68298)	0.92264	-0.28799	0.07170	σ_u1s (5.95534)	0.93372	-0.23944	π_u2p (1.40557)	0.45036
σ_g1s'(10.34240)	0.15208	-0.00630	0.00302	σ_u1s'(10.65879)	0.11493	0.00012	π_u2p'(2.53288)	0.40619
σ_g2s (1.41988)	0.00080	0.11221	-0.45954	σ_u2s (1.57044)	-0.01325	0.36698	π_u2p"(5.69176)	0.03177
σ_g2s'(2.43875)	0.00035	0.61377	-0.18152	σ_u2s'(2.48965)	0.00495	0.52425	π_u3d (2.05707)	0.05238
σ_g3s (7.04041)	-0.08473	-0.02472	-0.00460	σ_u3s (7.29169)	-0.05315	-0.02888	π_u3d'(2.70650)	0.02669
σ_g2p (1.30312)	0.00042	0.10205	0.40187	σ_u2p (1.49395)	-0.00747	-0.43100	π_u4f (3.15158)	0.01267
σ_g2p'(2.58558)	0.00138	0.28682	0.48928	σ_u2p'(3.49990)	0.00308	-0.11382		
σ_g2p"(6.21698)	0.00105	0.01172	0.02407	σ_u3d (1.69003)	-0.00123	-0.03346		
σ_g3d (1.34142)	0.00015	0.02816	0.03107					
σ_g3d'(2.95065)	0.00122	0.04322	0.03434					
σ_g3d"(5.52063)	-0.00016	-0.00254	-0.00176					
σ_g4f (3.02076)	0.00045	0.01087	0.00858					

TABLE XI

HFR Wave Function for $N_2(1\sigma_g^2 1\sigma_u^2 2\sigma_g^2 2\sigma_u^2 3\sigma_g^2 1\pi_u^4, X^1\Sigma_g^+)$, R = 2.05 Bohr.

E = -108.9944 H., T = 108.8567 H., V =-217.8511 H., V/T = -2.00127

$\epsilon_{1\sigma_g}$ = -15.67829, $\epsilon_{2\sigma_g}$ = -1.48034, $\epsilon_{3\sigma_g}$ = -0.63550, $\epsilon_{1\sigma_u}$ = -15.67446, $\epsilon_{2\sigma_u}$ = -0.77472, $\epsilon_{1\pi_u}$ = -0.61940

$\chi_{p\sigma_g}$ \ $C_{i\lambda p}$	$C_{1\sigma_g,p}$	$C_{2\sigma_g,p}$	$C_{3\sigma_g,p}$	$\chi_{p\sigma_u}$ \ $C_{i\lambda p}$	$C_{1\sigma_u,p}$	$C_{2\sigma_u,p}$	$\chi_{p\pi_u}$ \ $C_{i\lambda p}$	$C_{1\pi_u,p}$
σ_g1s (ζ = 5.68298)	0.92312	-0.28047	0.07462	σ_u1s (5.95543)	0.93400	-0.24310	π_u2p (1.39040)	0.46819
σ_g1s'(10.34240)	0.15205	-0.00625	0.00277	σ_u1s'(10.65879)	0.11485	0.00012	π_u2p'(2.53288)	0.39794
σ_g2s (1.42218)	0.00085	0.13329	-0.44444	σ_u2s (1.57044)	-0.01201	0.33824	π_u2p"(5.69176)	0.03166
σ_g2s'(2.43875)	0.00006	0.60508	-0.18936	σ_u2s'(2.44572)	0.00495	0.56306	π_u3d (2.05707)	0.04664
σ_g3s (7.04041)	-0.08498	-0.02420	-0.00480	σ_u3s (7.29169)	-0.05335	-0.02721	π_u3d'(2.47469)	0.02968
σ_g2p (1.29712)	0.00042	0.11600	0.41592	σ_u2p (1.48549)	-0.00690	-0.41678	π_u4f (3.06896)	0.01231
σ_g2p'(2.56733)	0.00108	0.26133	0.48640	σ_u2p'(3.49990)	0.00296	-0.11016		
σ_g2p"(6.21698)	0.00108	0.01149	0.02476	σ_u3d (1.69003)	-0.00121	-0.03467		
σ_g3d (1.34142)	0.00017	0.03561	0.03763					
σ_g3d'(2.91681)	0.00103	0.04156	0.03355					
σ_g3d"(4.95183)	-0.00018	-0.00357	-0.00236					
σ_g4f (2.59449)	0.00034	0.01344	0.01011					

TABLE XII

HFR Wave Function for $N_2(1\sigma_g^2 1\sigma_u^2 2\sigma_g^2 2\sigma_u^2 3\sigma_g^2 1\pi_u^4, X^1\Sigma_g^+)$, R = 2.15 Bohr.

E = -108.9799 H., T = 108.5254 H., V = -217.5053 H., V/T = -2.00419

$\epsilon_{1\sigma_g}$ = -15.69694, $\epsilon_{2\sigma_g}$ = -1.44205, $\epsilon_{3\sigma_g}$ = -0.63057, $\epsilon_{1\sigma_u}$ = -15.69411, $\epsilon_{2\sigma_u}$ = -0.79183, $\epsilon_{1\pi_u}$ = -0.59736

$\chi_{p\sigma_g}$ \ $C_{i\lambda p}$	$C_{1\sigma_g,p}$	$C_{2\sigma_g,p}$	$C_{3\sigma_g,p}$	$\chi_{p\sigma_u}$ \ $C_{i\lambda p}$	$C_{1\sigma_u,p}$	$C_{2\sigma_u,p}$	$\chi_{p\pi_u}$ \ $C_{i\lambda p}$	$C_{1\pi_u,p}$
σ_g1s (ζ = 5.93769)	0.91506	-0.27096	0.07613	σ_u1s (5.93368)	0.93446	-0.24717	π_u2p (1.37528)	0.48352
σ_g1s'(10.34240)	0.13012	-0.00004	0.00062	σ_u1s'(10.65879)	0.11689	-0.00026	π_u2p'(2.53388)	0.39163
σ_g2s (1.42470)	-0.00063	0.14616	-0.42794	σ_u2s (1.56045)	-0.01043	0.33335	π_u2p"(5.69176)	0.03156
σ_g2s'(2.42328)	0.00425	0.60892	-0.19210	σ_u2s'(2.43781)	0.00474	0.58812	π_u3d (2.08982)	0.06310
σ_g3s (7.08574)	-0.04949	-0.03311	-0.00298	σ_u3s (7.25407)	-0.05648	-0.02702	π_u3d'(2.56540)	0.01117
σ_g2p (1.29398)	-0.00072	0.11748	0.42535	σ_u2p (1.48774)	-0.00621	-0.40233	π_u4f (2.93505)	0.01228
σ_g2p'(2.55118)	0.00148	0.24127	0.48416	σ_u2p'(3.53093)	0.00285	-0.10346		
σ_g2p"(6.12719)	0.00101	0.01085	0.02593	σ_u3d (1.68538)	-0.00115	-0.03610		
σ_g3d (1.35983)	-0.00052	0.03900	0.04278					
σ_g3d'(2.94342)	0.00100	0.03636	0.03053					
σ_g3d"(5.53943)	-0.00024	-0.00295	-0.00220					
σ_g4f (2.58964)	0.00015	0.01333	0.01015					

TABLE XIII

HFR Wave Function for $N_2(1\sigma_g^2 1\sigma_u^2 2\sigma_g^2 2\sigma_u^2 3\sigma_g^2 1\pi_u^4, X^1\Sigma_g^+)$, R = 2.45 Bohr.

E = -108.8792 H., T = 107.8664 H., V = -216.7456 H., V/T = -2.00939

$\epsilon_{1\sigma_g}$ = -15.74469, $\epsilon_{2\sigma_g}$ = -1.33758, $\epsilon_{3\sigma_g}$ = -0.61231, $\epsilon_{1\sigma_u}$ = -15.74327, $\epsilon_{2\sigma_u}$ = -0.83927, $\epsilon_{1\pi_u}$ = -0.54184

$\chi_{p\sigma_g}$ \ $C_{i\lambda p}$	$C_{1\sigma_g,p}$	$C_{2\sigma_g,p}$	$C_{3\sigma_g,p}$	$\chi_{p\sigma_u}$ \ $C_{i\lambda p}$	$C_{1\sigma_u,p}$	$C_{2\sigma_u,p}$	$\chi_{p\pi_u}$ \ $C_{i\lambda p}$	$C_{1\pi_u,p}$
σ_g1s (5.68298)	0.92428	-0.26335	0.07791	σ_u1s (5.95534)	0.93493	-0.25651	π_u2p (1.33036)	0.51817
σ_g1s'(10.34240)	0.15191	-0.00607	0.00175	σ_u1s'(10.65879)	0.11462	0.00010	π_u2p'(3.53355)	0.38388
σ_g2s (1.43321)	0.00102	0.19474	-0.36773	σ_u2s (1.62946)	-0.00755	0.42890	π_u2p"(5.69176)	0.03135
σ_g2s'(2.40158)	-0.00069	0.61766	-0.19982	σ_u2s'(2.47750)	0.00457	0.56616	π_u3d (2.02067)	0.06791
σ_g3s (7.04041)	-0.08571	-0.01902	-0.00644	σ_u3s (7.29169)	-0.05404	-0.02780	π_u3d'(2.92400)	-0.00057
σ_g2p (1.32165)	0.00036	0.12585	0.47105	σ_u2p (1.48555)	-0.00484	-0.32965	π_u4f (2.69290)	0.01139
σ_g2p'(2.56043)	0.00042	0.17350	0.45587	σ_u2p'(3.49774)	0.00265	-0.09231		
σ_g2p"(6.21698)	0.00125	0.00827	0.02573	σ_u3d (1.65747)	-0.00106	-0.03239		
σ_g3d (1.40283)	0.00020	0.04476	0.05141					
σ_g3d'(2.90518)	0.00052	0.02455	0.02455					
σ_g3d"(5.52063)	-0.00020	-0.00221	-0.00207					
σ_g4f (2.15310)	0.00016	0.01583	0.01344					

TABLE XIV

SUMMARY OF ENERGY QUANTITIES AS A FUNCTION OF INTERNUCLEAR DISTANCE

$N_2(1\sigma_g^2 1\sigma_u^2 2\sigma_g^2 2\sigma_u^2 3\sigma_g^2 1\pi_u^4, X^1\Sigma_g^+)$

R	E*	T	V	V/T	$\epsilon_{2\sigma_g}$	$\epsilon_{2\sigma_u}$	$\epsilon_{3\sigma_g}$	$\epsilon_{1\pi_u}$
1.65†	-108.7887	111.1275	-219.9162	-1.97895	-1.6292	-0.7002	-0.6534	-0.7355
1.82	-108.9489	109.9386	-219.8874	-1.99100	-1.5699	-0.7331	-0.6459	-0.6798
1.85†	-108.9635	109.7690	-218.7325	-1.99266	-1.5584	-0.7387	-0.6446	-0.6709
1.905	-108.9825	109.4792	-218.4617	-1.99546	-1.5372	-0.7489	-0.6422	-0.6558
1.95†	-108.9914	109.2666	-218.2580	-1.99748	-1.5194	-0.7570	-0.6401	-0.6438
2.0132	-108.9956	108.9959	-217.9914	-2.00000	-1.4953	-0.7687	-0.6379	-0.6285
2.05†	-108.9944	108.8567	-217.8511	-2.00127	-1.4803	-0.7747	-0.6355	-0.6194
2.068†	-108.9928	108.7911	-217.7839	-2.00185	-1.4736	-0.7780	-0.6350	-0.6154
2.0741	-108.9922	108.7698	-217.7620	-2.00205	-1.4712	-0.7790	-0.6346	-0.6140
2.09	-108.9904	108.7152	-217.7055	-2.00253	-1.4651	-0.7818	-0.6338	-0.6106
2.15†	-108.9799	108.5254	-217.5053	-2.00419	-1.4421	-0.7918	-0.6306	-0.5974
2.20	-108.9679	108.3824	-217.3502	-2.00540	-1.4235	-0.8001	-0.6280	-0.5872
2.292	-108.9397	108.1586	-217.0983	-2.00722	-1.3902	-0.8149	-0.6226	-0.5693
2.34	-108.9226	108.0587	-216.9813	-2.00799	-1.3736	-0.8224	-0.6196	-0.5606
2.45†	-108.8792	107.8664	-216.7456	-2.00939	-1.3376	-0.8393	-0.6123	-0.5418
2.90†	-108.6828	107.4409	-216.1236	-2.01156	-1.2217	-0.9009	-0.5759	-0.4824

*All energy quantities are in Hartree units (27.2097 eV) and internuclear separations are in Bohr units (0.529172 Å).

†The ζ_p values for these R values were separately optimized. Interpolated ζ_p values were used for the remaining R values.

TABLE XV

SUMMARY OF ENERGY QUANTITIES AS A FUNCTION OF INTERNUCLEAR DISTANCE

$N_2^+(1\sigma_g^2 1\sigma_u^2 2\sigma_g^2 2\sigma_u^2 3\sigma_g 1\pi_u^4, X^2\Sigma_g^+)$

R	E*	T	V	V/T	$\epsilon_{2\sigma_g}$	$\epsilon_{2\sigma_u}$	$\epsilon_{3\sigma_g}$	$\epsilon_{1\pi_u}$
1.80	-108.3389	109.5230	-217.8618	-1.98919	-2.0226	-1.1092	-1.1531	-1.1223
1.85	-108.3674	109.2387	-217.6061	-1.99202	-2.0002	-1.1170	-1.1485	-1.1045
1.95	-108.3999	108.7539	-217.1539	-1.99674	-1.9543	-1.1322	-1.1393	-1.0713
2.00	-108.4064	108.5488	-216.9552	-1.99869	-1.9313	-1.1398	-1.1344	-1.0559
2.0132	-108.4073	108.4984	-216.9056	-1.99916	-1.9252	-1.1417	-1.1331	-1.0519
2.035	-108.4079	108.4184	-216.8263	-1.99990	-1.9153	-1.1450	-1.1310	-1.0454
2.0375	-108.4079	108.4095	-216.8174	-1.99998	-1.9141	-1.1453	-1.1307	-1.0447
2.0385	-108.4079	108.4060	-216.8139	-2.00002	-1.9137	-1.1455	-1.1306	-1.0444
2.040	-108.4079	108.4007	-216.8086	-2.00007	-1.9130	-1.1457	-1.1304	-1.0440
2.050	-108.4078	108.3657	-216.7735	-2.00039	-1.9084	-1.1472	-1.1294	-1.0411
2.113†	-108.4037	108.1612	-216.5649	-2.00224	-1.8807	-1.1569	-1.1235	-1.0237
2.15	-108.3986	108.0582	-216.4568	-2.00315	-1.8635	-1.1618	-1.1188	-1.0134
2.30	-108.3643	107.7187	-216.0830	-2.00599	-1.7995	-1.1832	-1.1012	-0.9757
2.40	-108.3333	107.5569	-215.8902	-2.00722	-1.7597	-1.1970	-1.0883	-0.9529
2.60	-108.2626	107.3457	-215.6083	-2.00854	-1.6878	-1.2232	-1.0598	-0.9118

*All energy quantities are in Hartree units (27.2097 eV) and internuclear separations are in Bohr units (0.529172 Å).

†The ζ_p values for this R value were re-optimized. The calculations for the other R values employed the same set of orbital exponents.

TABLE XVI

SUMMARY OF ENERGY QUANTITIES AS A FUNCTION OF INTERNUCLEAR DISTANCE

$N_2^+(1\sigma_g^2 1\sigma_u^2 2\sigma_g^2 2\sigma_u^2 3\sigma_g^2 1\pi_u^3,\ A^2\Pi_u)$

R	E*	T	V	V/T	$\epsilon_{2\sigma_g}$	$\epsilon_{2\sigma_u}$	$\epsilon_{3\sigma_g}$	$\epsilon_{1\pi_u}$
1.80	-108.3088	109.8977	-218.2065	-1.98554	-2.0767	-1.1570	-1.0838	-1.1779
1.85	-108.3484	109.6076	-217.9560	-1.98851	-2.0517	-1.1633	-1.0780	-1.1573
1.95	-108.4010	109.1093	-217.5102	-1.99351	-2.0006	-1.1755	-1.0664	-1.1187
2.00	-108.4165	108.8962	-217.3127	-1.99559	-1.9750	-1.1814	-1.0607	-1.1006
2.0132	-108.4196	108.8436	-217.2632	-1.99610	-1.9682	-1.1830	-1.0592	-1.0960
2.05	-108.4262	108.7045	-217.1307	-1.99744	-1.9494	-1.1872	-1.0549	-1.0833
2.125	-108.4319	108.4524	-216.8843	-1.99981	-1.9117	-1.1956	-1.0463	-1.0586
2.134	-108.4320	108.4248	-216.8568	-2.00007	-1.9072	-1.1966	-1.0452	-1.0558
2.140	-108.4320	108.4067	-216.8386	-2.00023	-1.9043	-1.1973	-1.0445	-1.0539
2.145	-108.4319	108.3918	-216.8237	-2.00037	-1.9018	-1.1978	-1.0440	-1.0523
2.15	-108.4318	108.3770	-216.8088	-2.00051	-1.8993	-1.1984	-1.0434	-1.0507
2.222†	-108.4270	108.1820	-216.6089	-2.00226	-1.8644	-1.2062	-1.0349	-1.0289
2.30	-108.4154	108.0020	-216.4174	-2.00383	-1.8278	-1.2143	-1.0256	-1.0065
2.40	-108.3936	107.8136	-216.2072	-2.00538	-1.7833	-1.2245	-1.0132	-0.9799
2.60	-108.3357	107.5462	-215.8819	-2.00734	-1.7031	-1.2435	-0.9874	-0.9324

*All energy quantities are in Hartree units (27.2097 eV) and internuclear separations are in Bohr units (0.529172 Å).

†The ζ_p values for this R value were re-optimized. The calculations for the other R values employed the same set of orbital exponents.

TABLE XVII

SUMMARY OF ENERGY QUANTITIES AS A FUNCTION OF INTERNUCLEAR DISTANCE

$N_2^+(1\sigma_g^2 1\sigma_u^2 2\sigma_g^2 2\sigma_u 3\sigma_g^2 1\pi_u^4, B^2\Sigma_u^+)$

R	E*	T	V	V/T	$\epsilon_{2\sigma_g}$	$\epsilon_{2\sigma_u}$	$\epsilon_{3\sigma_g}$	$\epsilon_{1\pi_u}$
1.75	-108.2159	109.3476	-217.5635	-1.98965	-2.0205	-1.2217	-1.0288	-1.1281
1.80	-108.2430	109.0145	-217.2575	-1.99292	-1.9990	-1.2291	-1.0246	-1.1100
1.85	-108.2600	108.7123	-216.9724	-1.99584	-1.9767	-1.2362	-1.0205	-1.0926
1.90	-108.2685	108.4384	-216.7069	-1.99843	-1.9540	-1.2430	-1.0164	-1.0761
1.925	-108.2700	108.3112	-216.5813	-1.99962	-1.9424	-1.2463	-1.0143	-1.0681
1.9325	-108.2702	108.2743	-216.5445	-1.99996	-1.9390	-1.2473	-1.0137	-1.0657
1.934	-108.2702	108.2670	-216.5372	-2.00003	-1.9383	-1.2475	-1.0136	-1.0653
1.95	-108.2699	108.1902	-216.4601	-2.00074	-1.9309	-1.2496	-1.0123	-1.0603
2.00	-108.2652	107 9655	-216.2307	-2.00278	-1.9076	-1.2559	-1.0083	-1.0451
2.0132	-108.2631	107.9098	-216.1728	-2.00327	-1.9015	-1.2575	-1.0072	-1.0413
2.0315†	-108.2596	107.8350	-216.0945	-2.00394	-1.8930	-1.2597	-1.0057	-1.0359
2.05	-108.2554	107.7621	-216.0176	-2.00458	-1.8845	-1.2620	-1.0042	-1.0306
2.15	-108.2240	107.4122	-215.6362	-2.00756	-1.8387	-1.2735	-0.9960	-1.0034
2.30	-108.1565	107.0061	-215.1626	-2.01075	-1.7728	-1.2892	-0.9833	-0.9665
2.40	-108.1034	106.7994	-214.9028	-2.01221	-1.7314	-1.2989	-0.9745	-0.9443
2.60	-107.9885	106.5032	-214.4917	-2.01395	-1.6558	-1.3163	-0.9557	-0.9046

*All energy quantities are in Hartree units (27.2097 eV) and internuclear separations are in Bohr units (0.529172 Å).

†The ζ_p values for this R value were re-optimized. The calculations for the other R values employed the same set of orbital exponents.

TABLE XVIII. COMPARISON OF CALCULATED AND EXPERIMENTAL SPECTROSCOPIC CONSTANTS FOR $N_2(X\ ^1\Sigma_g^+)$ AND $N_2^+(X\ ^2\Sigma_g^+,\ A\ ^2\Pi_u,\ B\ ^2\Sigma_u^+)$.

System	Source	B_e	α_e	ω_e	$\omega_e x_e$	$\omega_e y_e$	R_e(B.)	$k_e \times 10^{-6}$
$N_2(X\ ^1\Sigma_g^+)$	Experimental*	1.9987	0.01781	2358.07	14.188	-0.0124	2.0741	2.291
	Calculated†	2.121	0.01347	2729.6	8.378	-0.4745	2.0134	3.073
	% Error	+6.1%	-24.4%	+15.8%	-41.0%		-2.9%	+34.1%
$N_2^+(X\ ^2\Sigma_g^+)$	Experimental	1.932	0.020	2207.19	16.14	—	2.113	2.009
	Calculated	2.065	0.01481	2570.5	9.809	-0.2462	2.0405	2.726
	% Error	+6.9%	-25.9%	+16.4%	-39.2%		-3.4%	+35.7%
$N_2^+(A\ ^2\Pi_u)$	Experimental	1.740	0.018	1902.84	14.91	—	2.222	1.493
	Calculated	1.887	0.01550	2312.5	6.082	0.9114	2.1344	2.206
	% Error	+8.4%	-13.9%	+21.5%	-59.2%		-4.0%	+47.8%
$N_2^+(B\ ^2\Sigma_u^+)$	Experimental	2.073	0.020	2419.84	23.19	—	2.0315	2.415
	Calculated	2.296	0.01280	3101.8	19.88	2.087	1.935	3.969
	% Error	+10.8%	-35.9%	+28.2%	-14.3%		-4.8%	+64.3%

*These experimental values are taken from the review of Loftus.[5]

†The calculated values are the results from a Dunham analysis using 10 points of the $E_{HF}(R)$ curves.

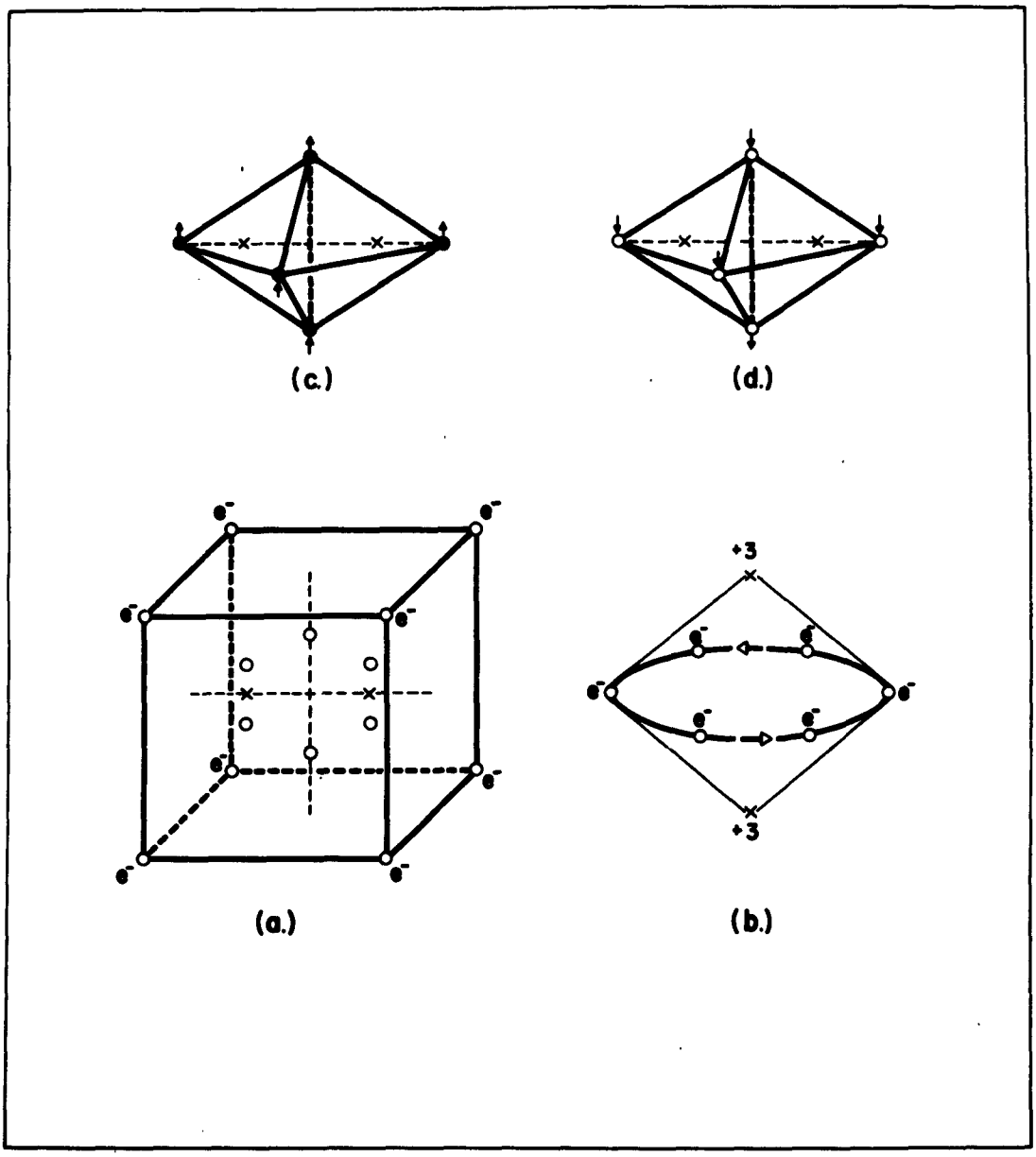

Fig. 1. **Models of the Nitrogen Molecule:** (a) the Lewis-Langmuir "Imbedded Pair" octet model (1919), (b) the Bohr-Sommerfeld dynamic model (1921), and (c) and (d), the Linnett "Modified Lewis-Langmuir" octet model. (c) With electron spins up and (d) with electron spins down.

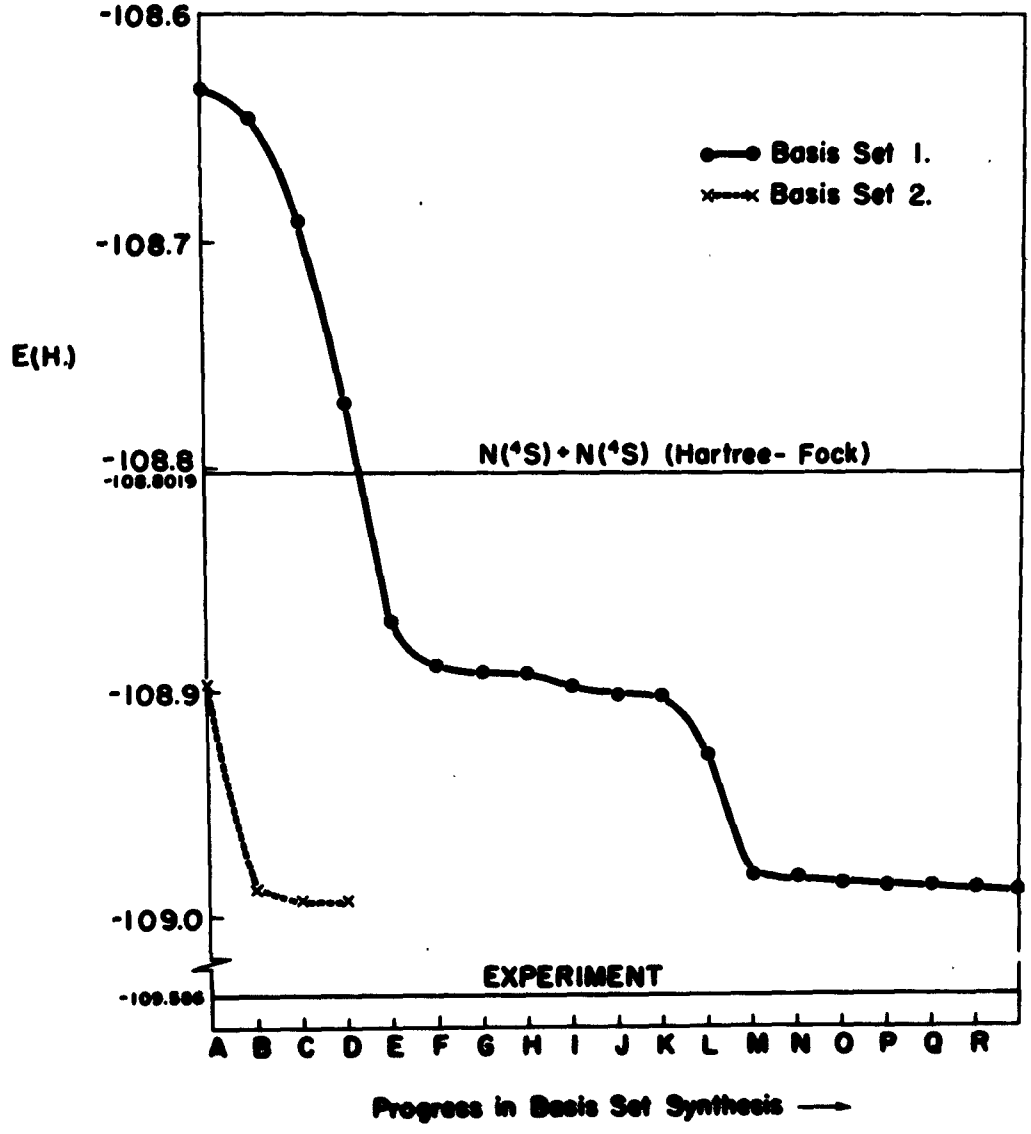

Fig. 2. Synthesis of expansion basis set - Improvement in total energy for $N_2(X\ ^1\Sigma_g^+)$, R = 2.068 Bohr.

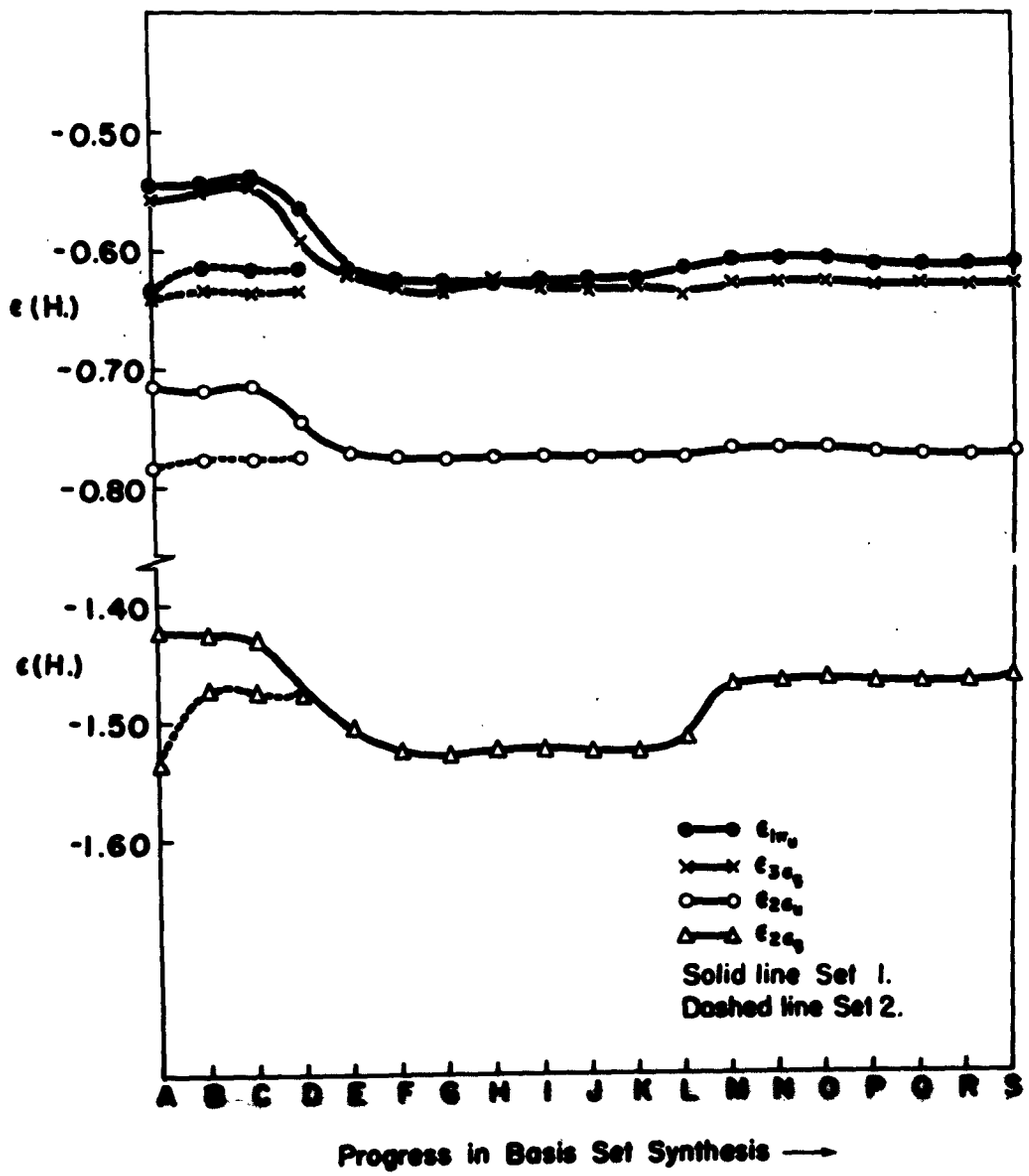

Fig. 3. Synthesis of expansion basis set - variation in orbital energies for $N_2(X\ ^1\Sigma_g^+)$, R = 2.068 Bohr.

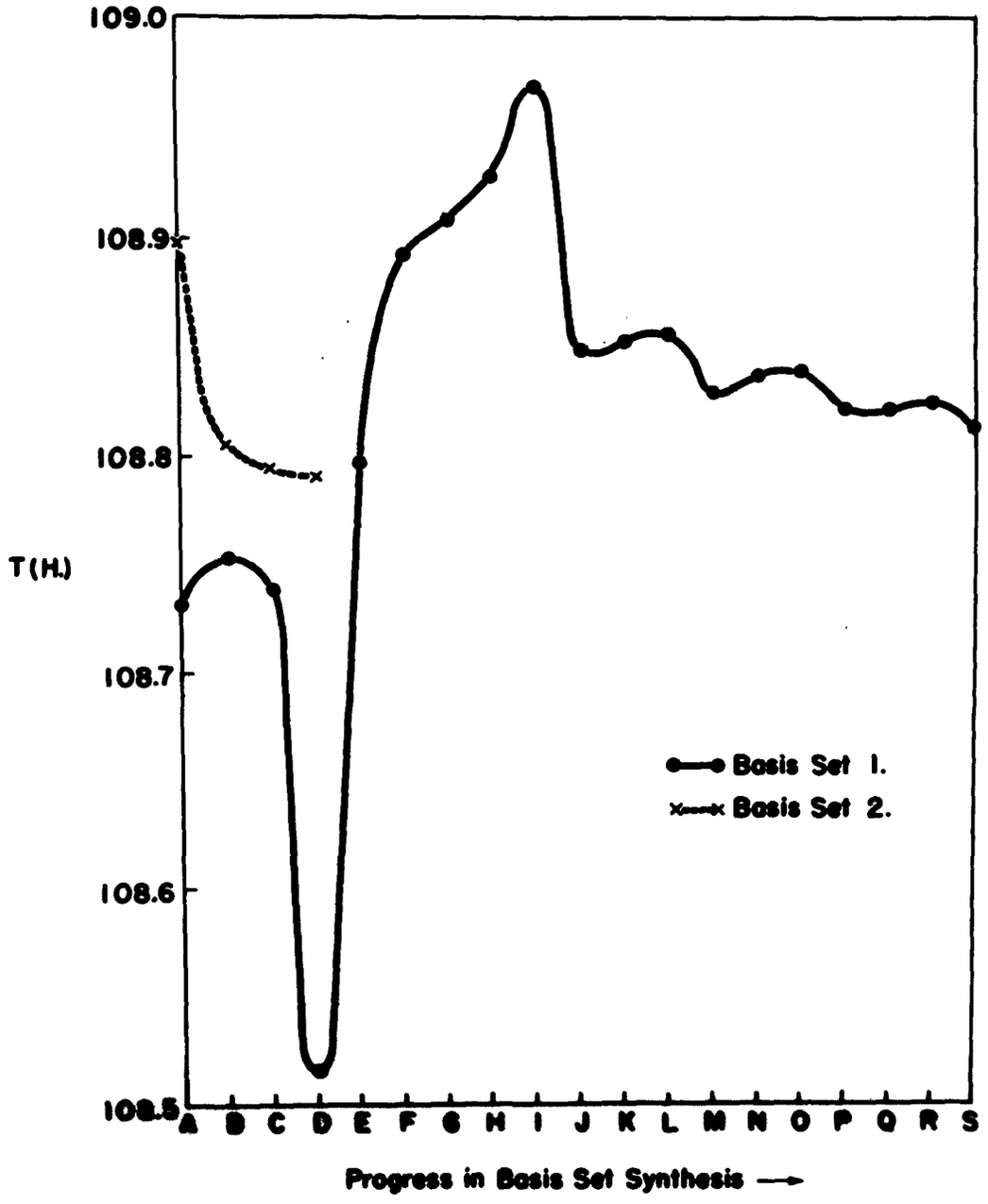

Fig. 4. Synthesis of expansion basis set - variation in total kinetic energy for $N_2(X\ ^1\Sigma_g^+)$, R = 2.068 Bohr.

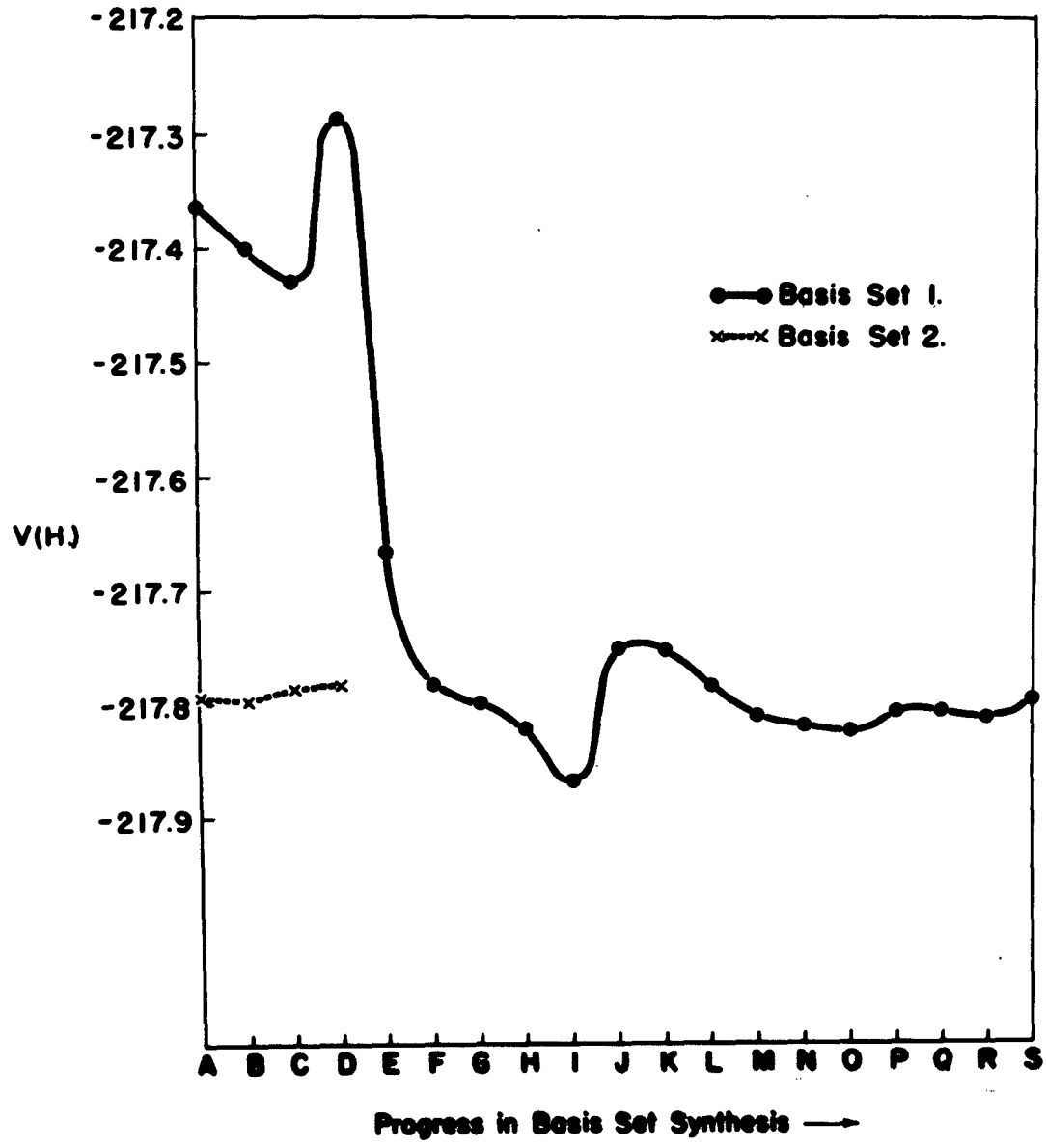

Fig. 5. Synthesis of expansion basis set - variation in total potential energy for $N_2(X\ ^1\Sigma_g^+)$, R = 2.068 Bohr.

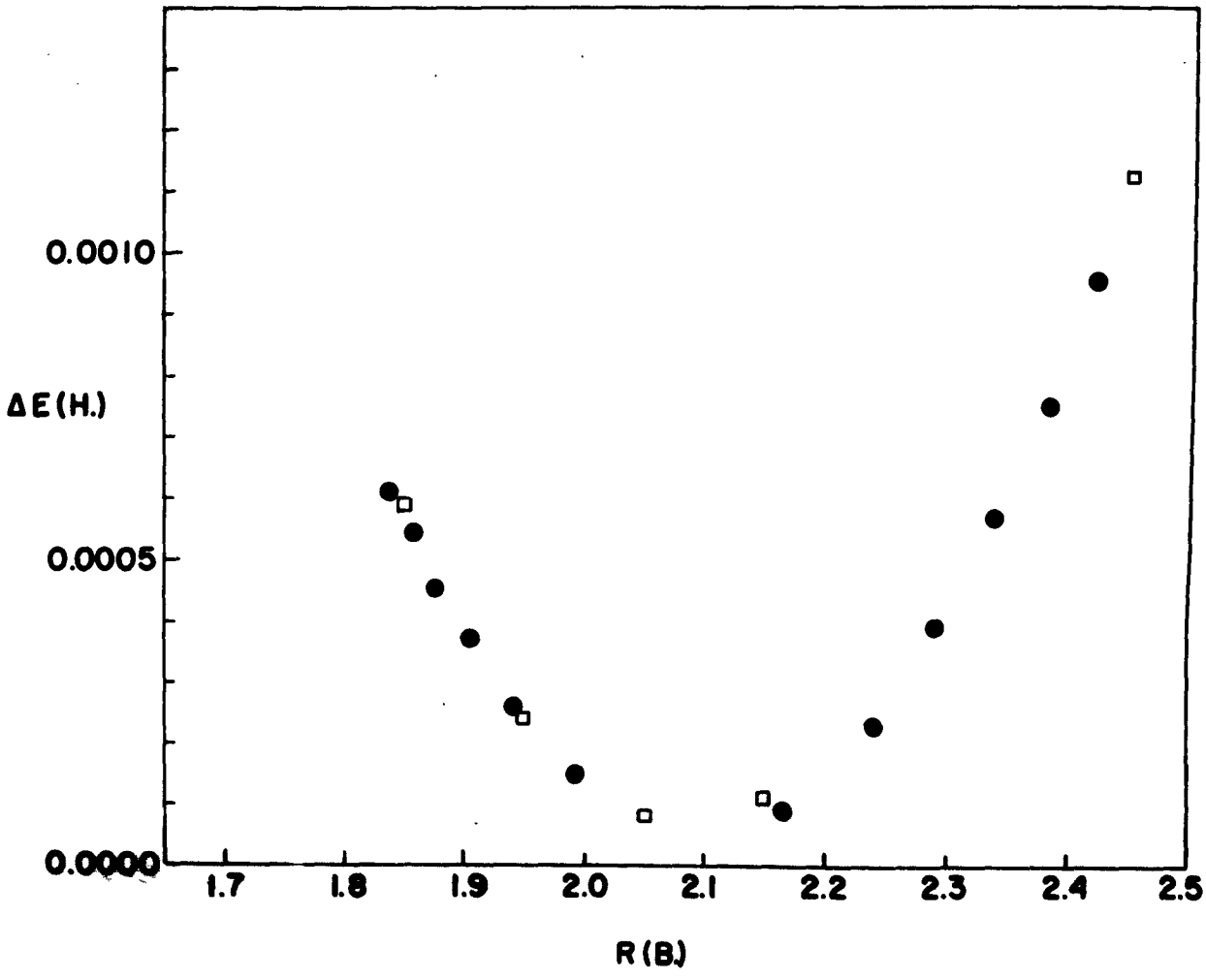

Fig. 6. Improvement of $E_{HF}(R)$ for $N_2(X\ ^1\Sigma_g^+)$ by re-optimization of orbital exponents for various R values (• indicates interpolated ζ_p values and are results using re-optimized ζ_p values).

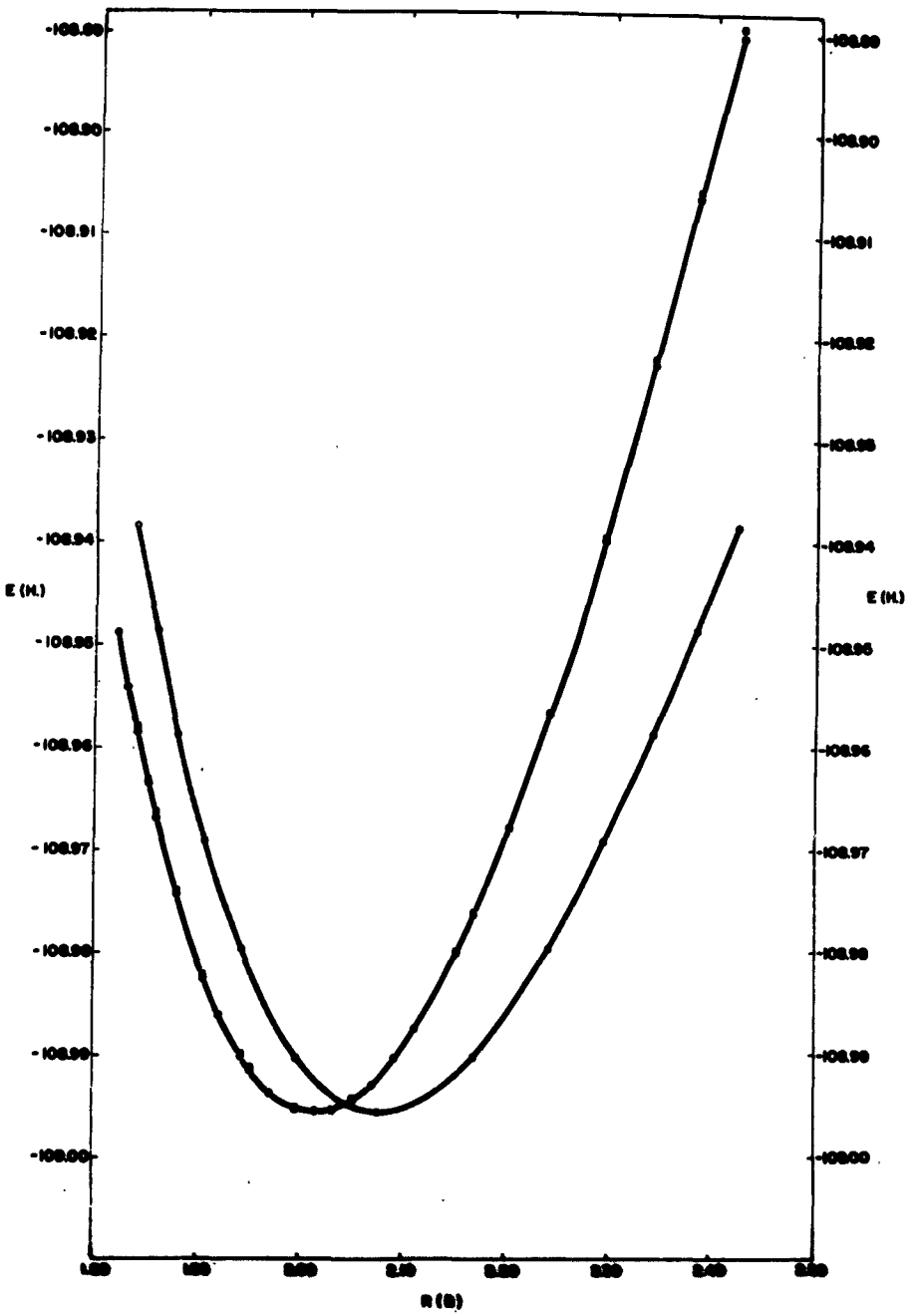

Fig. 7. Comparison of the shape of the $E_{HF}(R)$ and $E_{RKR}(R)$ potential curves for $N_2(X\ ^1\Sigma_g^+)$. (• indicates calculated results using interpolated ζ_p values and indicates calculated results using re-optimized ζ_p values. The o points derive from the RKR analysis of Gilmore).

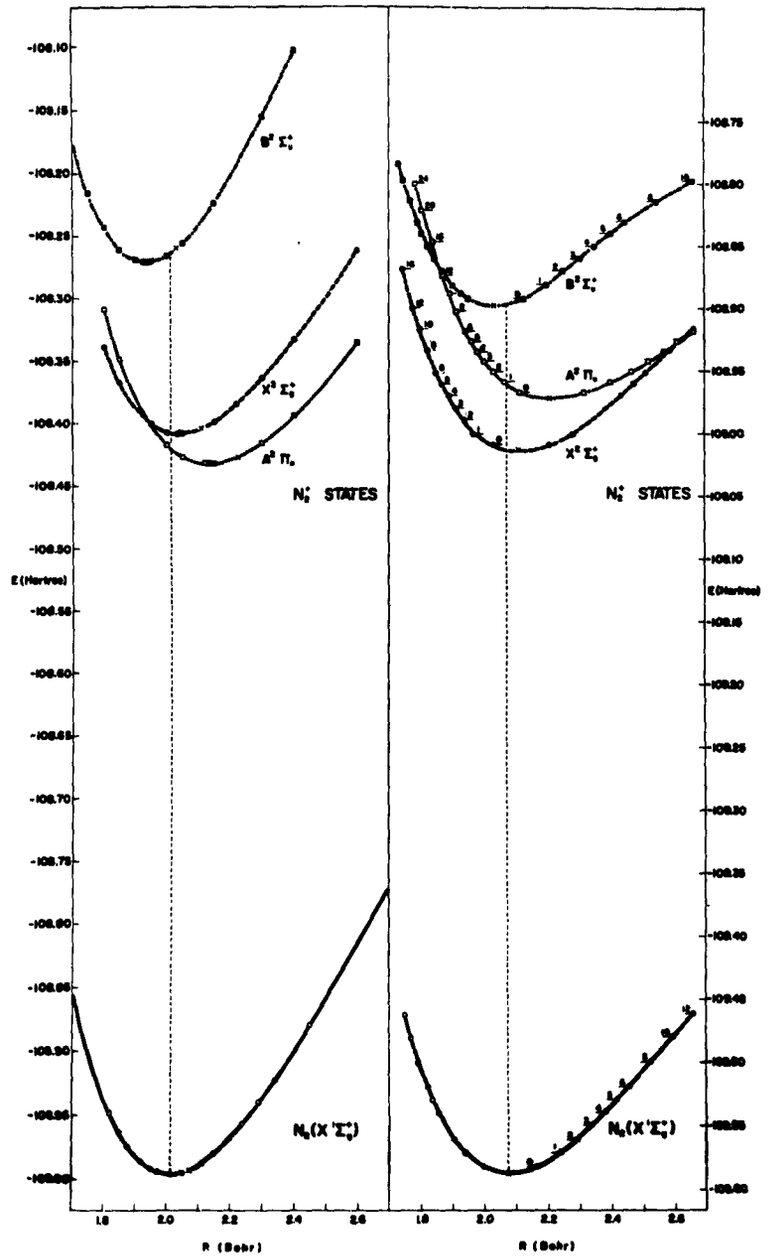

Fig. 8. Potential curves, E(R), for $N_2(X\ ^1\Sigma_g^+)$ and $N_2^+(X\ ^2\Sigma_g^+,\ A\ ^2\Pi_u,\ B\ ^2\Sigma_u^+)$. (a), Left Figure, is calculated $E_{HF}(R)$ results. (b), Right Figure, is $E_{RKR}(R)$ results of Gilmore.

Figure 9; KINETIC ENERGY, T(R), AND POTENTIAL ENERGY, V(R), CURVES FOR $N_2(X\,^1\Sigma_g^+)$ AND $N_2^+(X\,^2\Sigma_g^+,\ A\,^2\Pi_u,\ AND\ B\,^2\Sigma_u^+)$

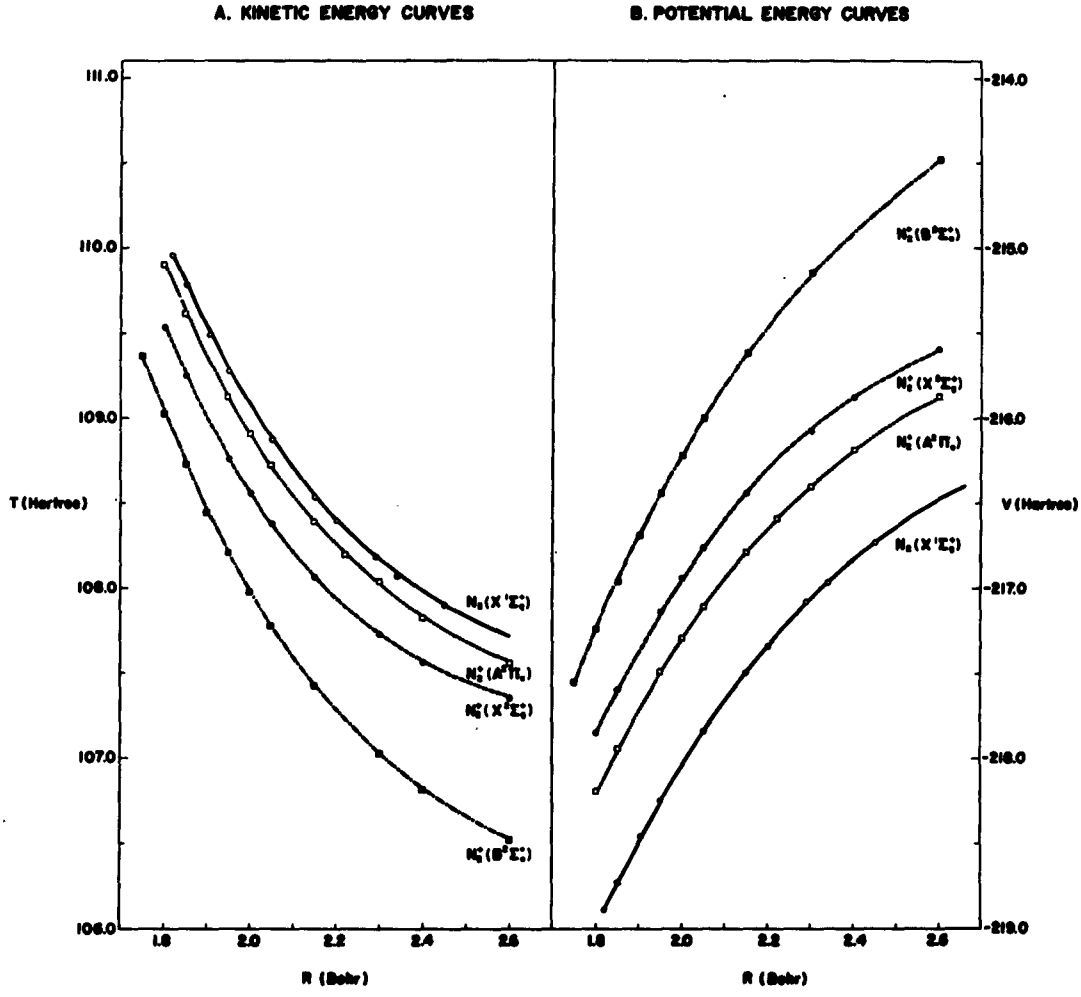

Fig. 9. Calculated kinetic energy, T(R), and potential energy, V(R), curves for $N_2(X\,^1\Sigma_g^+)$ and $N_2^+(X\,^2\Sigma_g^+,\ A\,^2\Pi_u,\ B\,^2\Sigma_u^+)$. (a) kinetic energy curve and (b) potential energy curve.

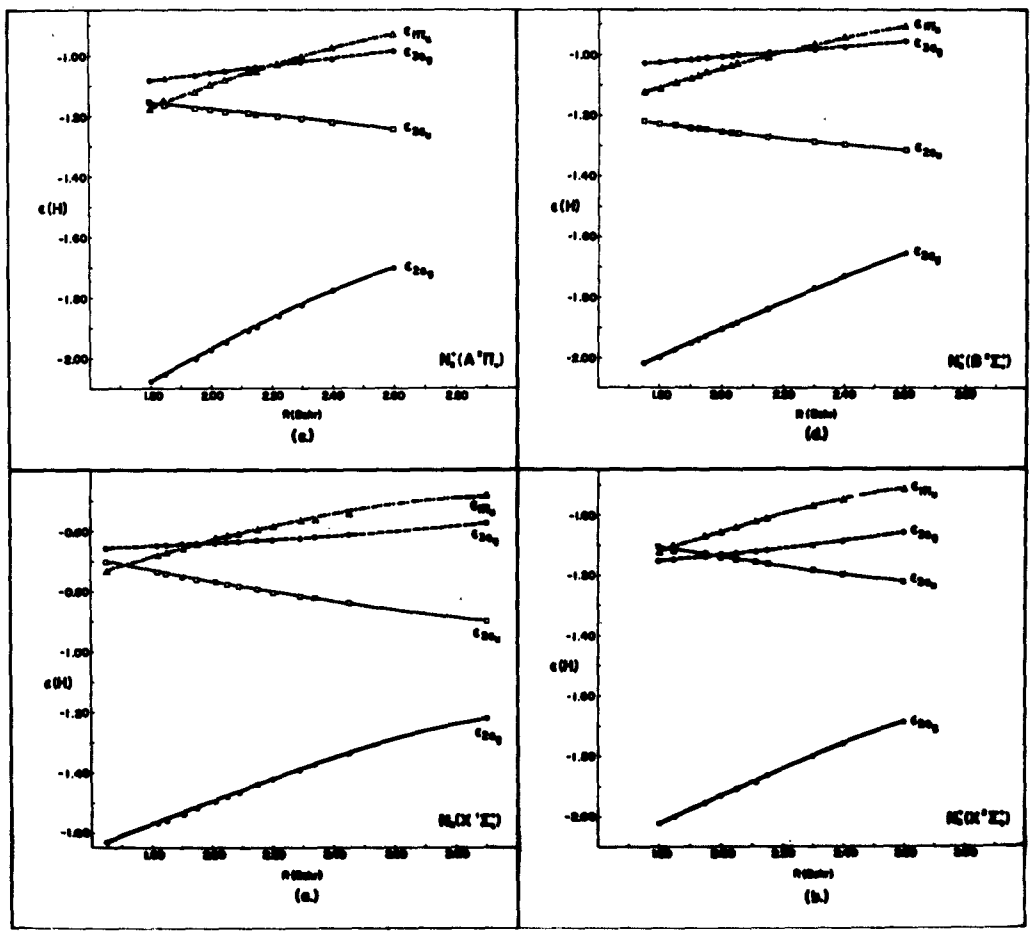

Fig. 10. Variation of orbital energies, $\epsilon_{2\sigma_g}$, $\epsilon_{3\sigma_g}$, $\epsilon_{2\sigma_u}$, and $\epsilon_{1\pi_u}$ with internuclear separation. (a) $N_2(X\ ^1\Sigma_g^+)$, (b) $N_2^+(X\ ^2\Sigma_g^+)$, (c) $N_2^+(A\ ^2\Pi_u)$, and (d) $N_2^+(B\ ^2\Sigma_u^+)$.

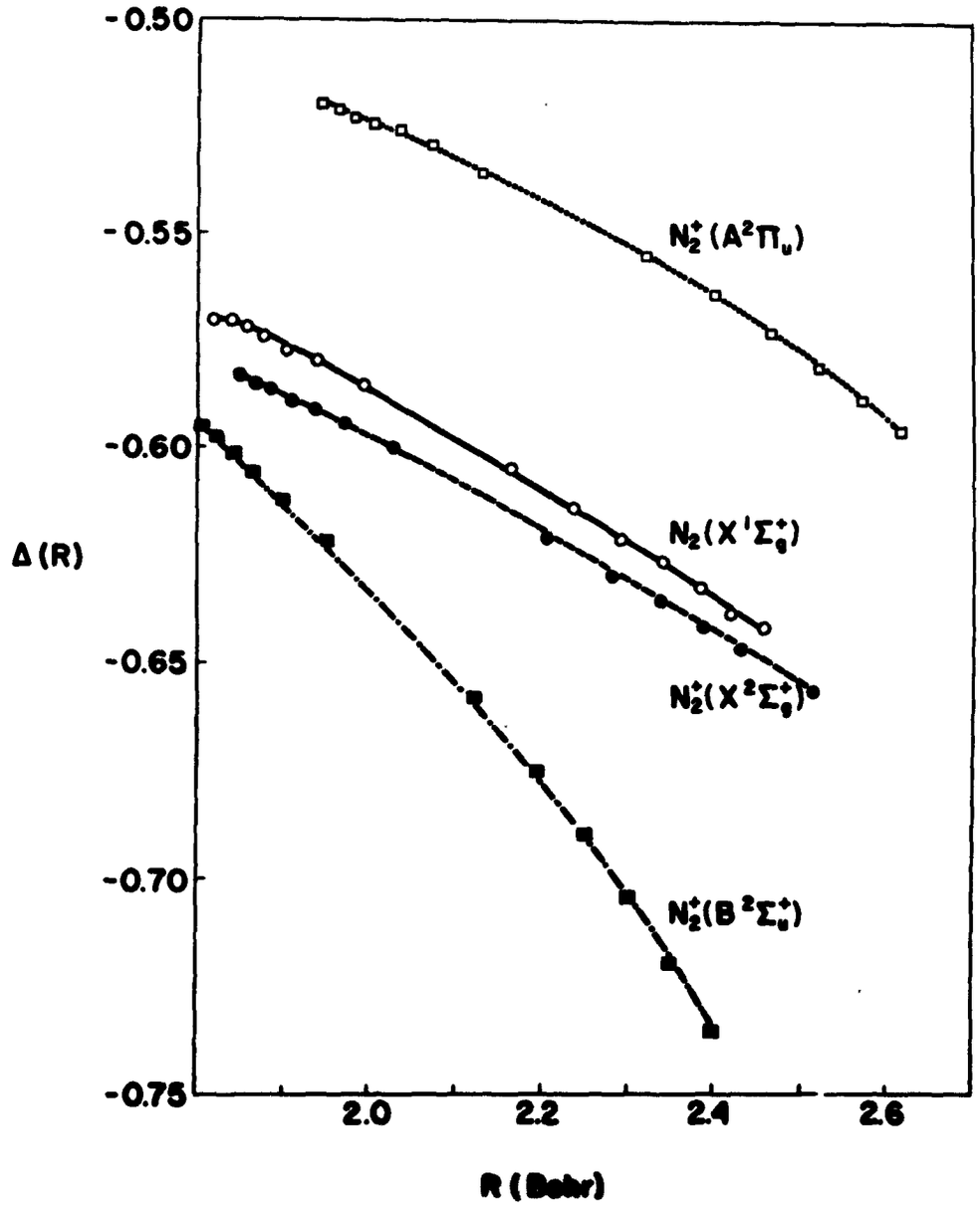

Fig. 11. The Δ(R) functions for $N_2(X\ ^1\Sigma_g^+)$, $N_2^+(X\ ^2\Sigma_g^+)$, $N_2^+(A\ ^2\Pi_u)$, and $N_2^+(B\ ^2\Sigma_u^+)$.

ELECTRONIC STRUCTURE OF CO AND BF*†

Winifred M. Huo‡
Laboratory of Molecular Structure and Spectra
Department of Physics, University of Chicago
Chicago, Illinois 60637

ABSTRACT

Single determinantal Self-Consistent Field wave functions calculated by the expansion method are reported for the ground state of CO and BF. These calculations were performed at four different internuclear distances, including the experimental equilibrium internuclear distance. Exponents are optimized at all four distances. Potential curves and dipole moment curves are obtained. From the potential curve, spectroscopic constants are calculated via the Dunham analysis. An SCF calculation was then performed at the calculated R_e. Exponents are also optimized. Expectation values of a number of one-electron operators, including the electric dipole moment, the gradient of the electric field at the nucleus and the Hellmann-Feynman force, are presented and compared with experimental data available. Contour diagrams for the total charge densities and orbital charge densitites are included.

---

*Research reported in this publication was supported by Advanced Research Projects Agency through the U. S. Army Research Office (Durham), under Contract No. DA-11-ORD-022-3119.

†Based on a thesis, submitted to the Department of Chemistry, University of Chicago, in partial fulfillment of the Ph.D. degree.

‡Present address: Department of Chemistry, Harvard University, Cambridge, Massachusetts.

I. INTRODUCTION

In recent years, several single determinantal SCF wave functions with extended basis set[1-8] for first row diatomic molecules have been calculated. They are fairly good approximations to the Hartree-Fock functions. Three useful points emerge from past experiences. First, the orbital exponents should be optimized. Second, in order to describe adequately the distortion of atomic orbitals to form molecular orbitals, functions with suitable angular characteristics, i.e., dσ, dπ, etc., should be added to the basis set.[9,10,3] Third, the calculated dipole moment, besides the total energy, is reasonable compared with experimental results.

It was shown by Brillouin,[11] and also by Møller and Plesset,[12] using a perturbation treatment of an n-electron system in which the Hartree-Fock solution is the zero order approximation, that the Hartree-Fock charge distribution is a representation of the exact charge distribution correct to first order. Consequently, we expect one-electron atomic or molecular properties, calculated from the Hartree-Fock functions, to be rather good approximations to experimental quantities. A rather instructive example of this was given by Cohen and Dalgarno,[13] who calculated the expectation values of a number of one-electron operators for helium with an SCF function[14] and with an accurate wave function.[15] The expectation values calculated from the two wave functions differ by less than 3 per cent, while the difference in total energy is 1.5 per cent.

---

[1] W. Kolos and C. C. J. Roothaan, Revs. Modern Phys. 32, 205 (1960); ibid. 32, 219 (1960).

[2] E. Clementi, J. Chem. Phys. 36, 33 (1962).

[3] R. K. Nesbet, J. Chem. Phys. 36, 1518 (1962).

[4] S. L. Kahalas and R. K. Nesbet, J. Chem. Phys. 39, 529 (1963).

[5] A. D. McLean, J. Chem. Phys. 39, 2653 (1963).

[6] R. K. Nesbet, J. Chem. Phys. 40, 3619 (1964).

[7] M. Yoshimine, J. Chem. Phys. 40, 2970 (1964).

[8] A. C. Wahl, J. Chem. Phys. 41, 2600 (1964).

[9] R. S. Mulliken, J. Chem. Phys. 8, 234 (1940).

[10] R. S. Mulliken, J. Chem. Phys. 36, 3428 (1962).

[11] L. Brillouin, Actualites sci. et ind. No. 71 (1933); ibid. No. 159 (1934).

[12] Chr. Møller and M. S. Plesset, Phys. Rev. 46, 618 (1934).

[13] M. Cohen and A. Dalgarno, Proc. Phys. Soc. 77, 748 (1961).

[14] L. C. Green, M. M. Mulder, M. N. Lewis and J. W. Woll, Phys. Rev. 93, 757 (1954).

[15] C. L. Pekeris, Phys. Rev. 115, 1216 (1959).

The determination of a molecular Hartree-Fock function is tedious and expensive. At present we have to work with the expansion SCF technique using a limited basis set, and we therefore obtain only an approximation to the molecular Hartree-Fock functions. It is of interest to know how well the energy and other molecular properties can be calculated from these. From calculations of first row atoms[14,16-20] it has become clear that if the basis set is sufficiently large and well chosen, an expansion SCF function is virtually the same as the numerical Hartree-Fock function and Brillouin's theorem can also be applied to it. In the case of the 14-electron molecular systems we dealt with, the maximum possible basis set allowed by the current program is not large enough to expect the same degree of agreement as in the atoms. Convergence was observed as the size of the basis set was allowed to expand and orbital exponents were reoptimized upon addition of new basis functions. However, the rate of convergence of the SCF energy with respect to the Hartree-Fock value may not be the same as that of other expectation values.[21] This indicates expectation values of one-electron operators should be used as criteria, besides energy, to judge how well an expansion SCF function with limited basis set approximates the Hartree-Fock functions. Furthermore, different operators are more sensitive in different regions of space, so their expectation values are tests on how well the charge distribution in a certain region is represented.

Recently in the Laboratory of Molecular Structure and Spectra, computer programs for the IBM 7094 have been completed to calculate SCF wave functions for diatomic molecules. A systematic study is under way to determine, with these programs, the best approximate Hartree-Fock functions of diatomic molecules composed of first and second row atoms. The present paper is a report on the calculations on CO and BF. These two molecules, together with N_2,[22] form an isoelectronic system. Furthermore, CO is an

---

[16] P. O. Löwdin, Phys. Rev. 90, 120 (1953).

[17] C. C. J. Roothaan, L. M. Sachs and A. W. Weiss, Revs. Modern Phys. 32, 186 (1960); E. Clementi, C. C. J. Roothaan and M. Yoshimine, Phys. Rev. 127, 1618 (1962); C. C. J. Roothaan and P. S. Kelly, Phys. Rev. 131, 1177 (1963).

[18] L. M. Sachs, Phys. Rev. 124, 1283 (1961).

[19] L. C. Allen, J. Chem. Phys. 34, 1156 (1961).

[20] P. S. Bagus, T. L. Gilbert, C. C. J. Roothaan and H. D. Cohen, (to be published).

[21] J. Goodisman, J. Chem. Phys. 38, 304 (1963).

[22] P. E. Cade, K. D. Sales and A. C. Wahl, (to be published).

important heteronuclear molecule because of the abundance of experimental data on it. These two particular molecules were therefore chosen for the pilot calculations with the heteronuclear diatomic SCF program.

II. REVIEW OF GENERAL THEORY AND APPLICATION TO HETERONUCLEAR DIATOMIC MOLECULES

In the atomic unit system,[23] the non-relativistic electronic Hamiltonian for a heteronuclear diatomic molecule is

$$\mathcal{H} = \sum_{\mu} (-\tfrac{1}{2} \Delta_{\mu} - Z_A/r_{A\mu} - Z_B/r_{B\mu}) + \sum_{\mu} \sum_{\nu} 1/r_{\mu\nu} , \qquad (1)$$

where the summations are over the electrons; Z_A and Z_B are charges of the nuclei A and B; $r_{A\mu}$ and $r_{B\mu}$ are the distances from electron μ to the two nuclei.

The SCF wave function is an antisymmetrized product of one-electron molecular orbitals $\varphi_{i\lambda\alpha}$, where λ refers to the symmetry species to which the orbital belongs, α to the subspecies, and i labels orbitals not distinguishable by symmetry. The orbital $\varphi_{i\lambda\alpha}$ is expanded in terms of a set of basis functions $\chi_{p\lambda\alpha}$ according to

$$\varphi_{i\lambda\alpha} = \sum_{p} \chi_{p\lambda\alpha} C_{i\lambda p} . \qquad (2)$$

The basis functions used are normalized Slater-type functions

$$\chi_{p\lambda\alpha}(N) = R_{\lambda p}(r_N) Y_{\ell_{\lambda p} m_{\lambda\alpha}}(\theta_N, \varphi_N) , \qquad (3)$$

where N represents the nucleus A or B, depending on where the basis function is centered. It is the origin of the spherical coordinates r_N, θ_N, φ_N. The coordinate system on either nucleus is so orientated that the positive Z-axis points <u>toward</u> the other nucleus, as shown in Fig. 1.

---

[23] In the atomic unit system, unit energy is 1 Hartree (1H) = 27.20976 ev, unit length is 1 Bohr (1B) = 0.529172 Å. See E. R. Cohen, K. M. Crowe and J. W. M. DuMond, Fundamental Constants of Physics (Interscience Publishers, Inc., New York, 1957).

The radial functions $R_{\lambda p}(r_N)$ are given by

$$R_{\lambda p}(r_N) = [(2n_{\lambda p})!]^{-\frac{1}{2}}(2\zeta_{\lambda p})^{n_{\lambda p}+\frac{1}{2}} r_N^{n_{\lambda p}-1} e^{-\zeta_{\lambda p} r_N} , \tag{4}$$

and $Y_{\ell_{\lambda p} m_\lambda}(\theta_N, \varphi_N)$ are the spherical harmonics in complex form as defined by Rose.[24]

The expansion coefficients $C_{i\lambda p}$ in Eq. (2) are determined by the Roothaan procedure,[25-27] in which the variation principle is applied to minimize the total energy of the molecule. The total energy is given by the expression

$$E = H^\dagger D_T + \tfrac{1}{2} D_T^\dagger \mathcal{P} D_T - \tfrac{1}{2} D_O^\dagger \mathcal{Q} D_O , \tag{5}$$

where

$$D_{i\lambda} = N_{i\lambda} c_{i\lambda} c_{i\lambda}^\dagger . \tag{6}$$

The index pair $i\lambda$ represents a shell which is composed of all orbitals $\varphi_{i\lambda\alpha}$ belonging to the same i and λ; $N_{i\lambda}$ is the occupation number of the shell. The closed shell, open shell and total density matrices are defined as

$$\left.\begin{aligned} D_{C\lambda} &= \textstyle\sum_{i \in \text{closed}} D_{i\lambda} , \\ D_{O\lambda} &= \textstyle\sum_{i \in \text{open}} D_{i\lambda} , \\ D_{T\lambda} &= D_{C\lambda} + D_{O\lambda} . \end{aligned}\right\} \tag{7}$$

For the heteronuclear diatomic molecule, the one-electron matrix elements $H_{\lambda pq}$ and two-electron supermatrix elements $\mathcal{P}_{\lambda pq,\mu rs}$ and $\mathcal{Q}_{\lambda pq,\mu rs}$ are given by,

$$H_{\lambda pq} = d_\lambda^{-1} \sum_\alpha \int \chi^*_{p\lambda\alpha}[-\tfrac{1}{2}\Delta - (Z_A r_A^{-1} + Z_B r_B^{-1})]\chi_{q\lambda\alpha} dV , \tag{8}$$

$$\mathcal{J}_{\lambda pq,\mu rs} = (d_\lambda d_\mu)^{-1} \sum_{\alpha\beta} \iint \chi^*_{p\lambda\alpha}(1)\, \chi^*_{r\mu\beta}(2)(1/r_{12})\, \chi_{q\lambda\alpha}(1)\, \chi_{s\mu\beta}(2) dV_1 dV_2 , \tag{9}$$

$$\begin{aligned} \mathcal{K}_{\lambda pq,\mu rs} = (d_\lambda d_\mu)^{-1} \sum_{\alpha\beta} \tfrac{1}{2} \Big\{ &\iint \chi^*_{p\lambda\alpha}(1)\, \chi^*_{r\mu\beta}(2)(1/r_{12})\, \chi_{s\mu\beta}(1)\, \chi_{q\lambda\alpha}(2) dV_1 dV_2 \\ &+ \iint \chi^*_{p\lambda\alpha}(1)\, \chi^*_{s\mu\beta}(2)(1/r_{12})\, \chi_{r\mu\beta}(1)\, \chi_{q\lambda\alpha}(2) dV_1 dV_2 \Big\} \end{aligned} \tag{10}$$

$$\mathcal{P}_{\lambda pq,\mu rs} = \mathcal{J}_{\lambda pq,\mu rs} - \tfrac{1}{2}\mathcal{K}_{\lambda pq,\mu rs} , \tag{11}$$

---

[24] M. E. Rose, Elementary Theory of Angular Momentum (John Wiley and Sons, Inc., New York, 1957) Appendix III.

[25] C. C. J. Roothaan, Revs. Modern Phys. 23, 69 (1951).

[26] C. C. J. Roothaan, Revs. Modern Phys. 32, 179 (1960).

[27] C. C. J. Roothaan and P. S. Bagus, Methods in Computational Physics (Academic Press, New York, 1963), Vol. 2, pp. 47-94.

and for a molecule with one open shell, we have

$$2_{\lambda pq,\mu rs} = a\mathcal{J}_{\lambda pq,\mu rs} - \tfrac{1}{2}b\mathcal{K}_{\lambda pq,\mu rs} \ . \qquad (12)$$

The constants a and b are determined by the symmetry and configuration of the open shell.

The heteronuclear diatomic SCF program makes use of a very efficient and accurate integration method for two center integrals as described by Wahl, Cade and Roothaan.[28] The SCF procedure is described by Roothaan and Bagus.[27] One of its significant operational features is that it provides automatic exponent optimization. A single optimization[27] is to determine the value of a single exponent ζ so that the energy becomes a minimum. This is achieved by varying this exponent until five energy values bracketing the energy minimum have been obtained, fitting a fourth degree curve through these five points, so that the minimum energy and corresponding ζ-value can be determined by interpolation. A double optimization[27] is to obtain the value of two exponents, ζ_1 and ζ_2, corresponding to the minimum of the energy surface spanned by them. This is achieved by a procedure analogous to the single optimization, and requires at least twenty-five independent SCF calculations. Double optimization is used when two exponents are strongly "coupled"; i.e., the optimization of one exponent greatly depends on the value of the other.

Matrices and supermatrices in the SCF program are stored in triangular form with maximum economy; no redundant elements are stored and neither are elements which are necessarily zero. The number of matrix elements N_{mx} is related to the number of basis functions by

$$N_{mx} = \sum_{\lambda} \tfrac{1}{2}N_\lambda(N_\lambda + 1) \ , \qquad (13)$$

where N_λ is the number of basis functions of symmetry λ. The number of supermatrix elements N_{smx} is given by

$$N_{smx} = \tfrac{1}{2}N_{mx}(N_{mx} + 1) \ . \qquad (14)$$

The heteronuclear diatomic SCF program allows a maximum of 172 matrix elements and therefore 14,878 supermatrix elements, which, for our present case of σ and π symmetries, limits the number of basis functions to the values given in Table I. In

[28] A. C. Wahl, P. E. Cade and C. C. J. Roothaan, J. Chem. Phys. 41, 2578 (1964).

addition to this limitation, the efficient organization of the numerical integration process[8] necessitated an upper limit to the number of basis function in any given symmetry; in our program this number was set at 16.

III. CALCULATION OF WAVE FUNCTIONS AT EXPERIMENTAL R_e

The ground state for both CO and BF is a $^1\Sigma^+$ state with the electronic configuration $1\sigma^2 2\sigma^2 3\sigma^2 4\sigma^2 1\pi^4 5\sigma^2$. The experimental equilibrium internuclear distance, R_e, is 2.132 B[29] for CO and 2.391 B[30] for BF. These data, together with nuclear charges, specification of the basis set and an approximate set of expansion coefficients, are required as input[31] to the SCF calculations.

The size and composition (n, ℓ, ζ) of the basis set determine how good an SCF wave function we can acquire. Since the maximum size of the basis set is limited by the program, it is necessary to spend a great deal of effort on the choice of a suitable basis set within the allowable size. We also want to find out how to build up such a set in the most economical way. For CO and BF, two completely independent approaches were used to build up the basis set at the experimental R_e.

Gradually Built Up Set

Ransil[32] reported a minimal basis set for both CO and BF where the exponents are obtained by Slater's empirical rule. The basis functions used were 1s, 2s, 2pσ and 2pπ functions on each nucleus. We used these functions as a starting point, and optimized all the exponents. This optimized set shall be referred to as the minimal set. To the minimal set we gradually added basis functions, one or two at a time, until the basis set reached the maximum allowable size. Each time when new basis functions were added, their exponents were optimized with, in general, a sequence of single and double optimizations. If a new basis function was optimized with a double optimization, it was coupled with one already in the basis set or another new basis function. Sometimes a single optimization was carried out on a basis function the exponent of which seemed to be affected by the addition of new basis functions.

---

[29] D. H. Rank, A. H. Guenther, G. D. Saksena, J. N. Shearer and T. A. Wiggins, J. Opt. Soc. Am. 47, 686 (1957).

[30] R. Onaka, J. Chem. Phys. 27, 374 (1957).

[31] A detailed description of the input convention for the heteronuclear diatomic SCF program is available at the Laboratory of Molecular Structure and Spectra, U. of Chicago.

[32] B. J. Ransil, Revs. Modern Phys. 32, 245 (1960).

It is, of course, desirable to subject all exponents in a basis set to repeated optimizations so that a true minimum of the energy as a function of all the non-linear parameters is assured. This, however, would be such a time-consuming process that, even for the fastest computer currently available, it would be very impractical for the size of basis set necessary for this type of calculation. Instead, only a limited number of single and double opitmizations were used. Presumably, if optimizations are done in a suitable order and the exponents are coupled correctly, we can obtain a result close to what would be obtained from a complete exponent optimization. However, there is no straightforward guide to the correct procedure. Experience gained from similar calculations is of course very valuable, but even so, a new molecule often requires experimentation peculiar to it. In this research, exponents important in the inner orbitals were optimized first, and then those important in the outer orbitals. The importance of a basis function was judged by the magnitude of its coefficients in the expansion of the one electron orbitals. The general rule used for double optimization was: when a new basis function was added to the set, we looked for the orbital to which it made a significant contribution; the basis function most important to this orbital was then coupled with this new basis function and a double optimization was carried out on them.

If the addition of a basis function, after optimization as just described, yielded a significant energy improvement, it was kept in the set and other trial basis functions were added. If the contribution to the total energy by the addition of this basis function was small (usually less than 0.0015 H), it was rejected.

After the basis set reached its maximum possible size, all exponents were subjected to single optimizations until the energy improvement from further optimization was less than 0.0001H. The basis set was then considered "completely" optimized.

Atomic Built Up Set

After the gradually built up set was well under way, it occurred to us that, if we used a basis set from atomic calculations on the two constituents of the molecule as a starting point, we could, in a much shorter time, obtain a molecular SCF function which was as good an approximate Hartree-Fock function as that calculated from the gradually built up set. We used the atomic results calculated by Bagus, Gilbert, Roothaan and Cohen.[20] They made some very careful studies on the size and composition of basis sets needed to represent the atomic Hartree-Fock functions with a given accuracy. For the first row atoms, they obtained four basis sets for each state they calculated, i.e., the accurate, nominal, marginal and minimal sets. We picked their

nominal set, which is the next to largest set; the differences in total energy as calculated from the accurate and nominal sets are 0.00004 H, 0.00008 H, 0.00025 H and 0.00041 H for the ground state of B, C, O and F respectively. We then made modifications and additions to this set, based on the experience gained from working on the gradually built up set. Exponents were optimized until the energy improvement from further optimizations was less than 0.0001 H.

Table II presents, in chronological order, the total energy and dipole moment of CO as the gradually built up set was allowed to expand. Table III presents the same quantities for the atomic built up set at different stages of exponent optimizations. The final basis set compositions and eigenvectors of coefficients are presented in Table IV and V for CO and BF, respectively.

The total amount of machine time used for the gradually built up set was longer than for the atomic built up set, even though exponent optimizations for the former were inexpensive initially when the size of basis set was small. However, as the basis set expanded, repeated optimizations were necessary, since otherwise basis functions added first would sometimes take too heavy a load. At worst, the exponent set might be "trapped" during the process. The exponents are trapped when the optimized values have settled in an auxiliary minimum rather than the absolute minimum of the energy surface. It is to be noted that if the basis set is large enough, auxiliary minima almost always exist. A bad initial choice of exponent values, and/or an injudiciously chosen order of adding basis functions, may cause trapping.

An actual case of trapped exponents occurred for the gradually built up set of CO. Since both the gradually and atomic built up sets were large and carefully optimized, their orbitals could be expected to be close if they were good approximations to the Hartree-Fock function. Furthermore, since the basis functions for π symmetry were of the same type, in the sense that exponent variations could bring about the identity of the two sets, their exponents and coefficients should be close. However, they were not so for the $2p\pi_0$ functions, as seen in the first two columns of Table VI. If we assumed, then, that the σ orbitals were physically the same in spite of not strictly comparable basis sets, we concluded that the $2p\pi_0$ basis functions were trapped in one case, most likely in the gradually built up set. Hence, we replaced the $2p\pi_0$ exponents in the gradually built up set with the atomic built up values and reoptimized the set. The energy improvement was significant, as seen in the third column of Table VI.

The atomic built up set was more economical to attain because it started out with exponents that were already carefully optimized in the atomic SCF calculations. It also had the benefit that exponents were optimized with all constituents of the final basis set present. "Trapping" thus was much less likely to happen than with the gradually built up set, and, so far as we know, did not occur. There is no guarantee, however, that trapping cannot occur in the atomic built up set.

Even after taking advantage of many economies possible within current computational technology, our program apparently still does not allow a large enough basis set to obtain the molecular Hartree-Fock functions for 14 electron systems with sufficient accuracy. This is evident from the fact that calculations by the two approaches of building up basis sets do not give identical results, as discussed in Section V. From our experience with the two approaches, it appears that if a sufficiently large basis set is allowed, it is advisable to start out from an accurate atomic basis set[20] and add enough other basis functions for an adequate description of the formation of the chemical bond. Essentially the same conclusion was drawn from recent work on LiF,[5] F_2[8] and N_2.[22]

IV. CALCULATION OF POTENTIAL CURVES

It is desirable to calculate SCF functions at several different internuclear distances besides the experimental R_e. From these calculations we can then determine a potential curve, and also the dependence of molecular properties on the internuclear separation.

To obtain a meaningful potential curve, it is necessary that all points on the curve are calculated equally well. If we insisted on full optimization for each value of R, this would necessitate a very large amount of computer time. Instead we calculated at three internuclear distances besides the experimental R_e, partially optimized SCF functions, starting in each case from the unoptimized atomic built up set, and optimizing all the exponents once, singly (i.e., uncoupled), and in the same order. After these were done, considerably more optimizations were carried out at the experimental R_e only. These further optimizations yielded an improvement in the total energy of 0.00017 H for CO and 0.00022 H for BF, compared to 0.00203 H for CO and 0.00168 H for BF from the first series of optimizations. Of course, the intermediate results for R_e, when all exponents were optimized singly, and which are comparable to the calculations for the other R values, were used for the construction of the potential curve.

We found it desirable to obtain more points on the potential curve by direct computation. Since the optimized exponents were found to be smooth functions of R, it was possible to interpolate for other R values. Using the interpolated exponents, we made single SCF calculations (with no exponent optimization) at three other R values for CO and BF. These results were also used for the construction of the potential curve.

For BF the exponent optimizations were first carried out at R = 2.385 B, which had one time been reported as the experimental value of R_e.[33] However, when the computation was well under way, it was realized that more recently the value 2.391 B had been obtained.[30] We later reoptimized all exponents for R_e = 2.391 B, but used the calculations for 2.385 B for the potential curve, so that all points on the curve were obtained in a consistent manner.

The calculated points of the potential curves for CO and BF are given in Tables VII and VIII; the curves themselves are shown in Figs. 2 and 3. From the calculated curves we computed the spectroscopic constants for $C^{12}O^{16}$ and $B^{11}F^{19}$ via the Dunham analysis.[34] The results are compared with experimental data in Tables IX and X. The differences between the calculated and experimental values are partly due to the fact that our calculations have not completely converged to the Hartree-Fock functions. However, we believe that most of the discrepancy is due to the basic shortcoming of the molecular orbital theory. In most cases, including CO and BF, molecular orbital type wave functions do not dissociate to the proper limit of two ground state atoms, but rather to a mixture of ionic and neutral states. Therefore, the wave function is a better representation of the molecular system at $R \leq R_e$ than $R > R_e$. Consequently, the computed potential curve is somewhat different from the correct curve.

In addition to the two final SCF functions calculated at the experimental R_e, we present in Tables IV and V for CO and BF, respectively, the SCF functions calculated at the three additional internuclear distances where exponent optimizations were done.

Since molecular properties evaluated at the SCF calculated R_e are to be compared with experimental quantities, we computed SCF functions for both molecules at the <u>calculated</u> R_e. For this calculation we started with interpolated exponents as mentioned above, and optimized part of the exponent set. An exponent was singly

---

[33] G. Herzberg, Spectra of Diatomic Molecules (D. Van Nostrand Co., Inc., Princeton, New Jersey, 1950).

[34] J. L. Dunham, Phys. Rev. <u>41</u>, 721 (1932).

optimized if its optimization at the experimental R_e yielded an energy change of more than 0.00004 H, or if its optimization at the next closest R on the potential curve yielded more than 0.00013 H. These SCF functions are also included in Tables IV and V.

V. CALCULATION OF MOLECULAR PROPERTIES

The expectation value of a one electron operator which has $C_{\infty v}$ symmetry is given by the expression

$$\langle \Phi | \mathbf{M} | \Phi \rangle = \mathbf{M}^{\dagger} D \ , \tag{15}$$

where the elements of the matrix $\mathbf{M}$ is written as

$$\mathbf{M}_{\lambda pq} = d_{\lambda}^{-1} \sum_{\alpha} \int \chi^{*}_{p\lambda\alpha} \mathbf{M} \chi_{q\lambda\alpha} \, dV \ . \tag{16}$$

We can then define shell properties as

$$\langle \mathbf{M} \rangle_{i\lambda} = \mathbf{M}_{\lambda}^{\dagger} D_{i\lambda} \ . \tag{17}$$

Obviously we have the relation

$$\langle \mathbf{M} \rangle = \langle \Phi | \mathbf{M} | \Phi \rangle = \sum_{\lambda} \sum_{i} \langle \mathbf{M} \rangle_{i\lambda} \ . \tag{18}$$

It should also be pointed out that the wave function is normalized to the number of electrons in the system, N;

$$\langle \Phi | \Phi \rangle = \mathbf{S}^{\dagger} D = N \ , \tag{19}$$

where $\mathbf{S}$ is the overlap matrix

$$\mathbf{S}_{\lambda pq} = d_{\lambda}^{-1} \sum_{\alpha} \int \chi^{*}_{p\lambda\alpha} \chi_{q\lambda\alpha} \, dV \ . \tag{20}$$

The computed molecular properties for the ground state of CO at both the experimental and calculated R_e are summarized in Table XI. Table XII presents the corresponding quantities for BF. For the results at the experimental R_e, we present those computed with the two final sets, namely the gradually built up set and the atomic built up set, as well as those obtained from the minimal set. In addition, results intermediate between our minimal and final sets obtained by Nesbet[6] are also included. All the exponents in his basis set, with the exception of the 3d functions, were not optimized. We reproduced his functions with our programs and, in order to make the comparison with our results complete, we calculated from his functions a few additional expectation values which he did not compute.

The properties at the calculated R_e are evaluated with the atomic built up set because this is the only set we used to obtain an optimized SCF function at that R value. In addition, we present Nesbet's values[6] for the dipole moment, dipole derivative and molecular quadrupole moment of the two molecules evaluated at the R_e determined from his potential curve. These values, however, are not directly computed with an SCF function at the calculated R_e; rather, they are interpolated from the results computed at other R's.

A number of experimental data available for the two molecules are also presented in Tables XI and XII. It is to be emphasized that our calculations use the Born-Oppenheimer approximation and are carried out at a particular internuclear distance. Most experimental data, however, apply to the ground vibrational state as a whole. To make the experimental and calculated quantities strictly comparable, we should therefore integrate the calculated molecular property over the ground vibrational wave function. This is of course desirable, but has as yet not been carried out. However, if the ground vibrational wave function is symmetrical around R_e, and if the calculated property has a linear dependence on R, then the molecular property evaluated at R_e is the same as that integrated with the ground vibrational wave function. This is certainly approximately the case, so that a molecular property computed at the R_e of the SCF potential curve (calculated R_e) can be considered as an SCF property. Therefore, it can be meaningfully compared with the corresponding experimental value.

In order to compare SCF properties calculated with different basis sets, it is necessary to obtain a potential curve for each basis set and make SCF calculations at the R_e of each potential curve. Obviously this will require too large an amount of computer time. On the other hand, if two SCF functions are very close to the Hartree-Fock function, their computed properties at the experimental R_e should also converge. Therefore, even though molecular properties computed at the experimental R_e are not, strictly speaking, SCF molecular properties, they are very useful for the comparison of different basis sets when results at the calculated R_e are not available for every basis set.

We notice that, in the molecular properties calculated at the experimental R_e from the gradually built up set and the atomic built up set, there are some significant differences, indicating that we have not yet reached the Hartree-Fock function. On the other hand, we are rather confident that the charge distribution calculated with either function resembles the Hartree-Fock value to two figures, since the expectation values of one-electron operators calculated from the two independent approaches all

agree with each other to two or three places.

For the same size of basis set, energy values calculated from the atomic built up sets are better than those calculated from the gradually built up sets, although much less effort was spent on the former.

The expectation values of several one-electron operators related to the geometry of the charge distribution, $\langle r_C^2 \rangle$, $\langle r_O^2 \rangle$, $\langle z_C^2 \rangle$, $\langle z_O^2 \rangle$, $\langle x^2 \rangle$, $\langle r_C + r_O \rangle$ and the corresponding quantities for B and F are all larger for the final sets than for the minimal set, indicating that outer regions are better described when the basis set is allowed to expand.

Since no comparable SCF calculations have been completed yet for the low lying states of the positive ions of CO and BF, the ionization potentials of these two molecules are, instead, calculated by means of Koopmans' theorem,[35,25] which states that the vertical ionization potentials are, to a good approximation, the negative of the orbital energies. The validity of the theorem, at least for the two molecules we deal with, is essentially confirmed: the differences between calculated and experimental[36] values, for the first three ionization potentials, are all within 10 per cent.

The difference between the experimental total energy[37] and that calculated from the Hartree-Fock approximation consists of the sum of the correlation energy E_C and the relativistic contributions E_R, i.e.,

$$E_{exp} - E_{SCF} = E_C + E_R \ . \qquad (21)$$

For the isoelectronic sequence N_2,[22] CO and BF, their values are quite uniform, as seen in Table XIII. The uncertainty in the value for BF is due to the experimental error of its dissociation energy.[38] Since there is no reliable estimation of the

[35] T. Koopmans, Physica 1, 104 (1933); G. G. Hall and J. Lennard-Jones, Proc. Roy. Soc. (London), A202, 155 (1950).

[36] For CO the first ionization potential is taken from F. H. Field and J. L. Franklin, Electron Impact Phenomena and The Properties of Gaseous Ions (Academic Press, New York, 1957), p. 110. Second and third ionization potentials are taken from Données Spectroscopiques Concernant les Molecules Diatomiques (Hermann and Cie, Paris, 1951), p. 69. For BF the first ionization potential is estimated by D. W. Robinson, Journal of Molecular Spectroscopy, 11, 275 (1963).

[37] B. J. Ransil, Revs. Modern Phys. 32, 239 (1960).

[38] A. G. Gaydon, Dissociation Energies and Spectra of Diatomic Molecules (Chapman and Hall Ltd., London, 1953), second edition (revised).

relativistic effects, we cannot draw any conclusion about the correlation energies of this isoelectronic sequence.

Another interesting quantity in the comparison of the isoelectronic series N_2, CO and BF is the orbital order of these molecules. Table XIV presents the orbital energies of the three highest occupied orbitals of these molecules, and the change in orbital ordering across the series is shown in Fig. 4.

The virial coefficient[39] is given by

$$\langle V \rangle / \langle T \rangle = -2 - (R/\langle T \rangle)(dE/dR) \ . \tag{22}$$

At the minimum of the potential curve, the second term on the right hand side of Eq. (22) drops out. Therefore, at R_e we have

$$\langle V \rangle / \langle T \rangle = -2 \ . \tag{23}$$

Also by virtue of the shape of potential curve for diatomic molecules, at $R < R_e$ we have

$$| \langle V \rangle / \langle T \rangle | < 2 \ , \tag{24}$$

and at $R > R_e$ we have

$$| \langle V \rangle / \langle T \rangle | > 2 \ . \tag{25}$$

Hence the virial coefficient is useful in testing whether a particular internuclear distance is at the minimum of the potential curve. The virial coefficient at the calculated R_e satisfied Eq. (22) to five figures both for CO and BF.

An important molecular quantity is the average value of the gradient of the electric field at the nucleus. This quantity, for the nucleus A, is given by the expression

$$q_A = e[(2Z_B/R^3) - \langle (3\cos^2\theta_A - 1)/r_A^3 \rangle] \ . \tag{26}$$

Experimental measurement of the quadrupole hyperfine splitting of an atom or a linear molecule containing a nucleus with a quadrupole moment Q_N is expressible in terms of the combined parameter eqQ_N. Therefore, the nuclear quadrupole moment Q_N can be

[39] J. C. Slater, Quantum Theory of Molecules and Solids (McGraw-Hill Book Company, Inc., 1963), Vol. I, pp. 30-33.

evaluated from the experimental value of eqQ_N and the calculated q. The two center integrals $\langle \chi_p(A)|(3\cos^2\theta_A-1)/r_A^3|\chi_q(B)\rangle$ and $\langle \chi_p(B)|(3\cos^2\theta_A-1)/r_A^3|\chi_q(B)\rangle$ were evaluated by the Coulson-Barnett method,[40] in which the Slater-type functions on center B are expanded in terms of radial functions and spherical harmonics on center A, followed by an analytical integration of the angular part, and then a numerical integration of the radial part.

Rosenblum and Nethercot[41] measured the hyperfine splitting caused by the O^{17} quadrupole moment in CO^{17} and found eqQ_N to be 4.43 ± 0.40 Mc/sec. Using this result and the calculated q at the oxygen nucleus, Q_N of O^{17} is evaluated and shown in Table XV. The previously reported value[42] for Q_N of O^{17}, evaluated from atomic data, is also presented. The atomic result is obtained from Harvey's experimental data[43] and the evaluation of $\langle(3\cos^2\theta-1)/r^3\rangle$ by Bessis, Lefebvre-Brion and Moser,[42] where Φ is a superposition of configurations based on the ground state configuration calculated with the expansion SCF technique. The agreement between the atomic result and our values is good.

The dipole moment μ is given by the expression

$$\mu = e[\tfrac{1}{2}(Z_B - Z_A)R - \langle z\rangle] \ . \qquad (27)$$

The coordinate system used for the evaluation of $\langle\Phi|z|\Phi\rangle$ is such that the origin is at the midpoint of the two nuclei, with the positive Z-axis pointing toward center B (carbon or boron).

The values of the dipole moment of CO as calculated for the R values where the exponents were optimized are presented in Table XVI. By least square fitting to a quadratic equation, we obtained the following expression for the dipole moment of CO

$$\mu_{CO} = 0.158 + 5.4\rho + 1.7\rho^2 \ , \qquad (28)$$

where $\rho = (R - R_e)/R_e$; the calculated R_e is used for the expression of ρ. The dipole moment μ is in Debye units, and is defined as positive for C^+O^-.

The solid curve in Fig. 5 shows the calculated dipole moment curve of CO. It is seen that this curve is almost linear, so that it is meaningful to compare the

---

[40] C. A. Coulson and M. P. Barnett, Conference on Quantum-Mechanical Methods in Valence Theory (Long Island, N. Y., September, 1951).

[41] B. Rosenblum and A. H. Nethercot, Jr., J. Chem. Phys. 27, 828 (1957).

[42] N. Bessis, H. Lefebvre-Brion and C. Moser, Phys. Rev. 128, 213 (1963).

[43] S. Harvey (to be published).

dipole moment of CO calculated at R_e with the experimental value. In Fig. 5 are also shown two other curves, which are based on the semi-empirical equation given by Mulliken[44]

$$\mu_{CO} = \mp 0.118 + 9.1\rho + 3.7\rho^2 , \qquad (29)$$

where the experimental R_e is used for the expression of ρ. Eq. (29) is based on the experimental data by Matheson[45] and the resonance structures of CO, namely $C^-\equiv O^+$, C=O, and C^+-O^-, as suggested by Pauling[46] and Mulliken.[44] For intermediate ranges of R, where Eq. (29) holds, the triple bond structure $C^-\equiv O^+$ is important at smaller R values, so the dipole moment is C^-O^+; the single bond structure C^+-O^- becomes predominant as R becomes larger, so the dipole moment is C^+O^-. Near R_e the two structures C^+-O^- and $C^-\equiv O^+$ contribute almost equally, thus producing a very small dipole moment. This chemical behavior can also be used to interpret Eq. (28) that we obtained.

At the time when Eq. (29) was obtained, the absolute sign of the dipole moment of CO was not experimentally known; therefore, there was an uncertainty in the sign of the first term in the equation. Subsequently, the sign of the dipole moment of CO was deduced by Rosenblum, Nethercot and Townes[47] to be C^-O^+ from a measurement of the shift of the magnetic moment in the J = 1 rotational state of varying isotopic species of CO, namely $C^{12}O^{16}$, $C^{13}O^{16}$, $C^{14}O^{16}$ and $C^{12}O^{18}$. Our calculated results are in disagreement with their conclusion (see Table XI). As mentioned earlier, the expectation values of one-electron operators are probably good to two significant figures in our wave functions. Furthermore, the magnitude of our calculated dipole moment is comparable to the experimental value.[48] If our estimation of accuracy is correct, a more accurate SCF function is not likely to give C^-O^+. We believe that a further investigation of the experimental situation as to the sign of the dipole moment of CO is in order.

The comparison of dipole moment of CO calculated with different basis sets is a good illustration on the convergence of computed molecular properties. In Figs. 6 and 7, the solid lines represent, respectively, the dipole moment and total energy of

---

[44] R. S. Mulliken, J. Chem. Phys. 2, 400 (1934).

[45] L. A. Matheson, Phys. Rev. 40, 813 (1932).

[46] L. Pauling, The Nature of the Chemical Bond (Cornell University Press, Ithaca, New York, 1948), 2nd edition, p. 135.

[47] B. Rosenblum, A. H. Nethercot, Jr. and C. H. Townes, Phys. Rev. 109, 400 (1958).

[48] C. A. Burrus, J. Chem. Phys. 28, 427 (1958).

CO, calculated at the experimental R_e at different stages of the gradually built up set; the dotted lines give the same quantities at different stages of optimization of the atomic built up set. The comparison of these two figures clearly shows that the dipole moment does not converge at the same rate as the energy, and that if a calculation with a moderate basis set gives a dipole moment in close agreement with experiment, this must be regarded as fortuitous.

Table XVI also presents the values of the dipole moment of BF calculated at the four values of R with optimized exponents. From these four values of μ we obtained the following expression by least square fitting to a quadratic equation

$$\mu_{BF} = -1.05 + 6.9\rho + 4.3\rho^2 \; ; \qquad (30)$$

the negative sign of μ_{BF} corresponds to B^-F^+. The above equation is also supported by the resonance structures B^+F^-, B-F, $B^-=F^+$ and $B^{--}\equiv F^{++}$. For intermediate ranges of R where Eq. (30) holds, the double bond and triple bond structures are predominant at smaller R values, and the dipole moment is B^-F^+; the single bond structure is more important at larger R, so the dipole moment becomes B^+F^-. Fig. 8 shows the dipole moment curve for BF. There are no experimental data on the dipole moment of BF.

At the midpoint of the two nuclei, the molecular quadrupole moment Q is given by

$$Q = (\tfrac{1}{2}R)^2(Z_A + Z_B) - \tfrac{1}{2}\langle 3z^2 - r^2\rangle . \qquad (31)$$

The molecular quadrupole moment for a polar molecule is not invariant upon coordinate transformation. At present, no directly measured experimental values for the Q of the two molecules are available.

The Lermor term of molar diamagnetic susceptibility is given by

$$\chi_L = -1/6\; N_{Av}\; r_o \langle r^2\rangle , \qquad (32)$$

where N_{Av} is Avogadro's number, $r_o = e^2/mc^2$ is the classical electron radius. No comparable experimental data is available for this quantity either.

The total Hellmann-Feynman force[49] on a heteronuclear diatomic molecule, calculated with the exact Hartree-Fock function at the R_e as defined by the Hartree-Fock

[49] H. Hellmann, Einführung in die Quantenchemie (Deuticke, Leipzig and Vienna, 1937); R. P. Feynman, Phys. Rev. 56, 340 (1939).

potential curve, can be shown[50] to satisfy the relation

$$\mathcal{F}_A + \mathcal{F}_B = 0 , \tag{33}$$

where of course $\mathcal{F}_A$ is the force on nucleus A, and is expressed by

$$\mathcal{F}_A = Z_A\, e^2[\langle \cos\theta_A / r_A^2 \rangle - Z_B/R^2] . \tag{34}$$

In Tables XI and XII, it is seen that the total Hellmann-Feynman force, computed at the calculated R_e, does not satisfy Eq. (33) identically. This shows that our wave function has not reached the Hartree-Fock function.

The molecular charge density at a point r is given by

$$P(\underset{\sim}{r}) = \sum_{\lambda}\sum_{i} P_{i\lambda}(\underset{\sim}{r}) = \underset{\sim}{P}(\underset{\sim}{r})^{\dagger}\underset{\sim}{D}. \tag{35}$$

The elements of the matrix $\underset{\sim}{P}(r)$ is written as

$$\underset{\sim}{P}_{\lambda pq}(\underset{\sim}{r}) = d_{\lambda}^{-1} \sum_{\alpha} \chi^{*}_{p\lambda\alpha}(\underset{\sim}{r})\, \chi_{q\lambda\alpha}(\underset{\sim}{r}) . \tag{36}$$

The charge density of a shell $i\lambda$ is given as

$$P_{i\lambda}(\underset{\sim}{r}) = \underset{\sim}{P}_{\lambda}(\underset{\sim}{r})^{\dagger}\underset{\sim}{D}_{i\lambda} . \tag{37}$$

and the orbital charge density is

$$P_{i\lambda\alpha}(\underset{\sim}{r}) = d_{\lambda}^{-1}\, P_{i\lambda}(\underset{\sim}{r}) . \tag{38}$$

It should be pointed out that the charge density of a π shell is the sum of the densities of π and $\bar{\pi}$ orbital.

A contour line of given charge density C on the xz plane is defined as

$$P(xz) = C . \tag{39}$$

Fig. 9 shows the total molecular charge density contours for CO, calculated with the atomic built up set at the experimental R_e. Figs. 10-13 show the corresponding orbital density contours of the 3σ, 4σ, 5σ and 1π orbitals of CO. The total and partial contours for BF shown in Figs. 14-18 are also calculated with the atomic built up set at the experimental R_e.

[50] C. W. Kern and M. Karplus, J. Chem. Phys. 40, 1374 (1964).

In the comparison of the contour diagrams of the two molecules, we notice the strong resemblance in the general shape of their orbital contours. For both molecules, the 3σ orbital has the largest amount of charge between the two nuclei. The orbital contours of both molecules have molecular type nodal planes besides the atomic type. For example, the 3σ orbital of CO as a $2S_0$ nodal plane, but there is another nodal plane near carbon which is not of atomic origin. Furthermore, the number of nodal planes is not directly related to the orbital ordering, as in the atomic case.

The average position along z-axis of an electron in an $i\lambda\alpha$ orbital is $\langle 1/N_{i\lambda}\rangle\langle z\rangle_{i\lambda}$. This corresponds to the position of maximum charge density in the orbital contour. Their values for CO and BF, are given in Table XVII.

The difference between the total charge densities of two wave functions Φ_1 and Φ_2 is

$$\Delta_{12}(\underset{\sim}{r}) = P_1(\underset{\sim}{r}) - P_2(\underset{\sim}{r}) = \sum_{\lambda}\sum_{i} P^1_{i\lambda}(\underset{\sim}{r}) - P^2_{i\lambda}(\underset{\sim}{r}) \ . \qquad (40)$$

The total charge density difference contours between the atomic built up set and gradually built up set at the experimental R_e are shown in Fig. 19 for CO and Fig. 20 for BF.

VI. DISCUSSION

In the comparison of various molecular properties with experimental data or their theoretical limits, we can conclude that the calculated wave functions for CO and BF are good approximations to the Hartree-Fock functions. After a study of this kind on a series of molecules, we will have better knowledge on the reliability of this type of wave functions. They can then be employed as useful tools in the understanding of molecular structure and as building blocks for more elaborate calculations in the future.

ACKNOWLEDGMENTS

The author expresses her gratitude to Professor C. C. J. Roothaan, who sponsored this research, for many stimulating discussions and fruitful suggestions, to Professor R. S. Mulliken, for some very valuable conversations, to Dr. A. C. Wahl, for his cooperation in the construction of the heteronuclear diatomic SCF program, and to Dr. P. E. Cade, who made some valuable suggestions on the manuscript. Thanks are also due to Dr. R. K. Nesbet, for a preprint of his paper prior to publication.

TABLE I. MAXIMUM NUMBERS OF BASIS FUNCTIONS FOR σ AND π SYMMETRY

Basis functions of σ symmetry	16	15	14	13
Basis functions of π symmetry	8	9	11	12
Total number of matrix elements	172	165	171	169

TABLE II. TOTAL ENERGY AND DIPOLE MOMENT OF CO CALCULATED FROM DIFFERENT STAGES OF EXPANSION IN THE GRADUAL BUILT UP SET[a,b]

Run No.	Basis Set Description	Total Energy (H)	Dipole Moment (D)
1	$1s_O$, $2s_O$, $2p\sigma_O$, $2p\pi_O$ $1s_C$, $2s_C$, $2p\sigma_C$, $2p\pi_C$	-112.39103	0.464 (C^-O^+)
2	Above set + $1s'_O$, $1s'_C$	-112.43784	0.450 (C^-O^+)
3	Above set + $2s'_O$, $2s'_C$	-112.52244	0.416 (C^-O^+)
4	Above set + $2p\pi'_O$, $2p\pi'_C$	-112.66252	0.623 (C^+O^-)
5	Above set + $2p\sigma'_O$, $2p\sigma'_C$	-112.70152	0.393 (C^+O^-)
6	Above set + $3d\sigma_O$, $3d\sigma_C$	-112.72942	0.368 (C^+O^-)
7	Above set + $3d\pi_O$, $3d\pi_C$	-112.77394	0.107 (C^+O^-)
8	Above set + $2p\pi''_O$	-112.77653	0.143 (C^+O^-)
9	Above set + $4f\pi_C$	-112.77810	0.147 (C^+O^-)
10	Above set + $3s_O$	-112.78023	0.147 (C^+O^-)
11	Above set + $3s_C$	-112.78164	0.137 (C^+O^-)
12	Single optimization on all exponents in above set except the 1s type	-112.78283	0.208 (C^+O^-)
13[c]	Single optimization on $2s_C$, $2s'_C$, $2p\sigma_C$, $2p\sigma'_C$, $3s_C$	-112.78335	0.189 (C^+O^-)
14	Use atomic built up oxygen π functions, and single optimization on <u>all</u> π functions	-112.78437	0.188 (C^+O^-)
15[d]	Single optimization on $2s_C$, $2s'_C$, $2p\sigma_C$, $3s_C$, $2p\pi_O$, $3d\pi_O$	-112.78452	0.183 (C^+O^-)
16[e]	Single optimization on $2s_C$, $2s'_C$	-112.78459	0.181 (C^+O^-)

[a] The results presented here are from additions of basis functions kept in the final set. The results from other trial functions which are not kept in the final set are omitted.

[b] Each run was carried out with exponent optimizations.

[c] This run reoptimized all the exponents whose optimizations in run 12 lowered the total energy by more than 0.00010 H.

[d] This run optimized all the exponents whose optimizations in run 13 and 14 lowered the total energy by more than 0.00004 H.

[e] This run reoptimized all the exponents whose optimizations in run 15 lowered the total energy by more than 0.00002 H.

TABLE III. TOTAL ENERGY AND DIPOLE MOMENT OF CO CALCULATED FROM DIFFERENT STAGES OF OPTIMIZATION IN THE ATOMIC BUILT UP SET

Run No.	Basis Set Description	Total Energy (H)	Dipole Moment (D)
1	$1s_O$, $1s'_O$, $2s_O$, $3s_O$, $2p\sigma_O$, $2p\sigma'_O$, $2p\sigma''_O$, $3d\sigma_O$, $2p\pi_O$, $2p\pi'_O$, $2p\pi''_O$, $3d\pi_O$, $1s_C$, $1s'_C$, $2s_C$, $3s_C$, $2p\sigma_C$, $2p\sigma'_C$, $2p\sigma''_C$, $3d\sigma_C$, $2p\pi_C$, $2p\pi'_C$, $3d\pi_C$, $4f\pi_C$ unoptimized exponents	-112.78380	0.326 (C^+O^-)
2	Single optimizations on $1s_O$, $1s'_O$, $1s_C$, $1s'_C$, $2s_O$, $3s_O$, $2s_C$, $3s_C$	-112.78516	0.284 (C^+O^-)
3	Single optimizations on $2p\sigma_O$, $2p\sigma'_O$, $2p\sigma_C$, $2p\sigma'_C$, $2p\pi_O$, $2p\pi'_O$, $2p\pi_C$, $2p\pi'_C$	-112.78526	0.290 (C^+O^-)
4	Single optimizations on $2p\sigma''_O$, $2p\sigma''_C$, $2p\pi''_O$, $3d\sigma_O$, $3d\sigma_C$, $3d\pi_O$, $3d\pi_C$, $4f\pi_C$	-112.78583	0.289 (C^+O^-)
5	Double optimization on $2s_O$, $3s_O$	-112.78589	0.296 (C^+O^-)
6	Double optimization on $2s_C$, $3s_C$	-112.78600	0.274 (C^+O^-)
7	Double optimization on $3d\sigma_O$, $3d\sigma_C$	-112.78600	0.274 (C^+O^-)

TABLE IV. BASIS FUNCTIONS AND EIGENVECTORS OF COEFFICIENTS FOR THE GROUND STATE OF CO

R (Bohr)	Nucleus	Basis Function	Orbital Exponent	Eigenvectors 1σ	2σ	3σ	4σ	5σ	Basis Function	Orbital Exponent	Eigenvector 1π
2.132[a,b]	C	1s	5.37234	-0.00040	-0.91861	-0.12870	-0.13900	-0.14260	2pπ	1.58163	0.33139
		1s	9.06997	0.00022	-0.08773	0.00147	0.00094	0.00072	2pπ	3.40692	0.05053
		2s	1.18958	0.00097	0.00282	-0.02351	0.26793	0.37863	3dπ	2.04840	0.06379
		2s	1.97355	-0.00116	-0.00579	0.27944	0.37322	0.39348	4fπ	2.71153	0.01462
		3s	6.91029	0.00047	0.00029	-0.01962	-0.01911	-0.01954			
		2pσ	1.26795	-0.00032	0.00177	0.04198	0.09714	-0.38052			
		2pσ	2.45306	-0.00022	-0.00318	0.15681	0.07480	-0.25086			
		3dσ	2.44036	-0.00045	-0.00095	0.03150	0.02331	-0.03082			
	O	1s	7.36941	0.94168	0.00080	-0.23075	0.11561	0.01869	2pπ	1.44012	0.42218
		1s	12.63896	0.06137	-0.00007	0.00799	-0.00487	-0.00007	2pπ	2.82360	0.39477
		2s	1.25577	-0.00227	-0.00125	0.09245	-0.40101	0.12489	2pπ	5.86534	0.04272
		2s	2.54861	0.00791	-0.00036	0.71698	-0.42789	-0.07173	3dπ	2.51766	0.03519
		3s	9.09265	0.00111	-0.00015	-0.02711	0.00349	0.00763			
		2pσ	2.23196	0.00048	-0.00074	0.18093	0.54634	-0.28557			
		2pσ	4.76903	0.00119	-0.00032	0.03052	0.09689	-0.04792			
		3dσ	2.94826	0.00058	-0.00029	0.02647	0.02209	-0.01234			
2.132[a,c]	C	1s	5.37427	0.00002	-0.91928	-0.12135	-0.13073	-0.11115	2pπ	1.58358	0.32617
		1s	9.06462	-0.00000	-0.08724	-0.00239	-0.00552	-0.01163	2pπ	3.34444	0.05288
		2s	1.30803	0.00070	0.00045	-0.00418	0.11105	0.68860	3dπ	2.06686	0.06070
		3s	2.95658	0.00002	-0.00484	0.19832	0.26508	0.21163	4fπ	2.80937	0.01315
		2pσ	1.18707	0.00055	0.00050	-0.03822	-0.07028	-0.21623			
		2pσ	2.17085	0.00005	-0.00202	0.19795	0.13200	-0.33496			
		2pσ	5.82068	0.00002	-0.00096	0.00428	0.00164	-0.01234			
		3dσ	2.75585	0.00010	-0.00104	0.02907	0.01291	-0.02098			
	O	1s	7.30920	0.92173	0.00074	-0.20517	0.10223	0.01435	2pπ	1.47330	0.44164
		1s	11.80975	0.08281	-0.00001	-0.00411	0.00434	0.00051	2pπ	2.84829	0.37506
		2s	1.92860	-0.00135	0.00038	0.58501	-0.42530	-0.06762	2pπ	5.78456	0.04463
		3s	4.33335	0.00606	-0.00076	0.26224	-0.14013	-0.01853	3dπ	2.38286	0.03871
		2pσ	1.48825	-0.00034	0.00073	0.09840	0.36668	-0.20817			
		2pσ	2.83326	0.00029	-0.00128	0.13062	0.35823	-0.17850			
		2pσ	5.89845	0.00117	0.00003	0.00975	0.03985	-0.02008			
		3dσ	2.44797	0.00022	-0.00015	0.03134	0.03566	-0.02167			
1.898[c]	C	1s	5.36810	0.00002	-0.91776	-0.14380	-0.11999	-0.11632	2pπ	1.63932	0.33733
		1s	9.05065	0.00000	-0.08851	-0.00268	-0.00292	-0.01113	2pπ	3.30085	0.05865
		2s	1.31732	0.00088	0.00007	0.00567	0.00179	0.73627	3dπ	2.15839	0.06821
		3s	2.95997	-0.00016	-0.00596	0.21403	0.22240	0.20235	4fπ	2.99661	0.01434
		2pσ	1.17046	0.00061	0.00036	-0.02077	-0.06853	-0.23780			
		2pσ	2.26306	-0.00011	-0.00318	0.22281	0.16153	-0.31575			
		2pσ	6.18550	0.00007	-0.00079	0.00446	0.00199	-0.00946			
		3dσ	2.85091	0.00003	-0.00168	0.03391	0.01633	-0.01956			
	O	1s	7.30391	0.92016	0.00159	-0.20974	0.10158	0.02642	2pπ	1.53900	0.41157
		1s	11.76836	0.08435	-0.00001	-0.00357	0.00364	0.00114	2pπ	2.85677	0.36465
		2s	1.98881	-0.00181	0.00158	0.50750	-0.44359	-0.11254	2pπ	5.67626	0.04670
		3s	4.25750	0.00678	-0.00158	0.26796	-0.11752	-0.03809	3dπ	2.72431	0.03662
		2pσ	1.46535	-0.00039	0.00131	0.06312	0.37215	-0.13294			
		2pσ	2.85673	0.00083	-0.00203	0.18030	0.40846	-0.14627			
		2pσ	6.07698	0.00096	-0.00007	0.01021	0.03849	-0.01229			
		3dσ	2.83335	0.00053	-0.00052	0.02656	0.02945	-0.01619			

TABLE IV. BASIS FUNCTIONS AND EIGENVECTORS OF COEFFICIENTS FOR THE GROUND STATE OF CO (Continued)

R		Basis	Orbital	Eigenvectors					Basis	Orbital	Eigenvector
(Bohr)	Nucleus	Function	Exponent	1σ	2σ	3σ	4σ	5σ	Function	Exponent	1π
2.366[c]	C	1s	5.37827	0.00000	-0.92100	-0.10043	-0.14794	-0.10423	2pπ	1.52960	0.31612
		1s	9.10101	0.00000	-0.08573	-0.00312	-0.00791	-0.00885	2pπ	3.37338	0.04963
		2s	1.37243	0.00062	0.00075	0.02903	0.22397	0.65888	3dπ	1.98152	0.05463
		3s	2.92702	0.00001	-0.00394	0.18150	0.30736	0.15312	4fπ	2.60502	0.01236
		2pσ	1.22654	0.00049	0.00041	-0.02394	-0.08384	-0.20919			
		2pσ	2.08499	0.00008	-0.00088	0.16841	0.10269	-0.33965			
		2pσ	5.09108	-0.00000	-0.00144	0.00486	0.00001	-0.01923			
		3dσ	2.60543	0.00013	-0.00063	0.02621	0.00979	-0.02247			
	O	1s	7.31100	0.92274	0.00037	-0.20701	0.10080	0.00113	2pπ	1.41884	0.46331
		1s	11.84400	0.08192	-0.00000	-0.00385	0.00385	-0.00030	2pπ	2.84310	0.38729
		2s	1.95497	-0.00112	-0.00035	0.61927	-0.40159	-0.01022	2pπ	5.87134	0.04309
		3s	4.32853	0.00564	-0.00027	0.25267	-0.13709	0.00486	3dπ	2.13884	0.03891
		2pσ	1.49543	-0.00029	0.00010	0.09475	0.34674	-0.29158			
		2pσ	2.83606	0.00001	-0.00078	0.09417	0.29818	-0.21131			
		2pσ	5.83429	0.00132	0.00005	0.00767	0.03710	-0.02829			
		3dσ	2.18005	0.00005	-0.00012	0.03063	0.03875	-0.03013			
2.600[c]	C	1s	5.38035	-0.00001	-0.92145	-0.08509	-0.16820	-0.08934	2pπ	1.48049	0.30445
		1s	9.10207	0.00001	-0.08538	-0.00312	-0.00938	-0.00616	2pπ	3.36594	0.04831
		2s	1.41267	0.00066	0.00086	0.04837	0.35914	0.57962	3dπ	1.90688	0.04870
		3s	2.92323	-0.00005	-0.00341	0.16120	0.33432	0.10008	4fπ	2.46841	0.01121
		2pσ	1.30767	0.00057	0.00016	-0.01797	-0.09081	-0.24031			
		2pσ	2.03593	-0.00000	0.00008	0.14239	0.07188	-0.31280			
		2pσ	4.59809	-0.00001	-0.00187	0.00442	-0.00354	-0.02681			
		3dσ	2.46789	0.00016	-0.00041	0.02219	0.00704	-0.02485			
	O	1s	7.31588	0.92402	0.00021	-0.20958	0.09444	-0.01194	2pπ	1.37459	0.48065
		1s	11.87308	0.08060	0.00000	-0.00414	0.00362	-0.00100	2pπ	2.83929	0.40058
		2s	1.93893	-0.00106	-0.00062	0.65046	-0.37221	0.05672	2pπ	5.93775	0.04202
		3s	4.34964	0.00558	0.00001	0.25915	-0.13294	0.02394	3dπ	1.94542	0.03823
		2pσ	1.48598	-0.00034	-0.00029	0.09104	0.29245	-0.35158			
		2pσ	2.84672	-0.00007	-0.00042	0.06126	0.24109	-0.24697			
		2pσ	5.87222	0.00136	0.00002	0.00623	0.02971	-0.03334			
		3dσ	2.02064	-0.00008	-0.00016	0.02886	0.03635	-0.03651			
2.081[c,d]	C	1s	5.37427	0.00002	-0.91927	-0.12604	-0.12731	-0.11253	2pπ	1.58536	0.33201
		1s	9.06462	-0.00001	-0.08717	-0.00235	-0.00505	-0.01181	2pπ	3.34444	0.05409
		2s	1.30188	0.00073	0.00042	-0.00807	0.08940	0.69364	3dπ	2.03939	0.06601
		3s	2.95650	0.00001	-0.00514	0.20282	0.25615	0.21683	4fπ	2.80937	0.01466
		2pσ	1.18707	0.00056	0.00048	-0.04169	-0.07000	-0.21616			
		2pσ	2.17085	0.00002	-0.00223	0.20704	0.14086	-0.33462			
		2pσ	5.82068	0.00003	-0.00094	0.00468	0.00202	-0.01249			
		3dσ	2.77588	0.00008	-0.00115	0.03024	0.01381	-0.02107			
	O	1s	7.30920	0.92172	0.00087	-0.20567	0.10219	0.01720	2pπ	1.46796	0.42364
		1s	11.80975	0.08279	-0.00001	-0.00398	0.00433	0.00066	2pπ	2.84829	0.38323
		2s	1.92860	-0.00140	0.00059	0.57333	-0.43231	-0.07631	2pπ	5.78456	0.04323
		3s	4.33335	0.00618	-0.00088	0.26411	-0.13786	-0.02410	3dπ	2.55453	0.03562
		2pσ	1.48825	-0.00035	0.00087	0.09361	0.36605	-0.18759			
		2pσ	2.83326	0.00037	-0.00142	0.14034	0.36997	-0.17149			
		2pσ	5.89845	0.00113	0.00002	0.01019	0.04045	-0.01845			
		3dσ	2.54463	0.00028	-0.00020	0.03024	0.03385	-0.01968			

[a] Experimental R_e.

[b] Gradually built up set.

[c] Atomic built up set.

[d] Calculated R_e.

TABLE V. BASIS FUNCTIONS AND EIGENVECTORS OF COEFFICIENTS FOR THE GROUND STATE OF BF

R (Bohr)	Nucleus	Basis Function	Orbital Exponent	Eigenvectors 1σ	2σ	3σ	4σ	5σ	Basis Function	Orbital Exponent	Eigenvector 1π
2.391[a,b]	B	1s	4.38952	0.00039	0.90775	-0.07969	-0.13792	-0.18206	2pπ	1.27692	0.06789
		1s	7.50431	-0.00013	0.10047	0.00488	0.00949	0.00606	2pπ	2.12197	0.06032
		2s	1.07039	0.00469	-0.00089	-0.08901	-0.05001	0.66926	3dπ	2.14366	0.02482
		2s	1.52977	0.00059	0.00508	0.12432	0.27539	0.39001			
		2pσ	0.95973	0.00332	-0.00118	-0.03003	0.00442	-0.18307			
		2pσ	1.93697	-0.00033	0.00434	0.09861	0.15714	-0.20953			
		3dσ	2.39361	0.00017	0.00110	0.02006	0.02436	-0.01683			
	F	1s	8.38343	0.95557	-0.00069	-0.24948	0.05809	0.02187	2pπ	1.63505	0.55210
		1s	14.81039	0.04705	-0.00002	0.00591	-0.00193	-0.00093	2pπ	3.20654	0.41802
		2s	1.45346	-0.00976	-0.00195	0.20822	-0.11347	-0.13795	2pπ	6.09410	0.07149
		2s	2.86225	0.01145	0.00196	0.82707	-0.22239	-0.09052	3dπ	2.07841	0.04312
		3s	1.23108	-0.00048	-0.00018	-0.02349	0.00326	-0.00076	4fπ	2.59737	0.01227
		2pσ	2.33613	-0.00336	-0.00231	0.02518	0.13943	-0.10809			
		2pσ	4.97508	0.00107	0.00218	0.08543	0.61611	-0.13219			
		2pσ	2.49090	0.00070	0.00042	0.01749	0.16809	-0.04213			
		3dσ	12.07491	-0.00043	0.00005	0.01838	0.03501	-0.00890			
2.391[a,c]	B	1s	4.41374	0.00001	0.92007	-0.07071	-0.12174	-0.15057	2pπ	1.33032	0.07082
		1s	7.73118	-0.00000	0.08772	0.00049	0.00034	-0.00904	2pπ	2.16451	0.05462
		2s	1.08378	0.00029	-0.00083	0.00466	0.02912	0.74552	3dπ	2.13826	0.02441
		3s	2.43726	0.00032	0.00477	0.04853	0.13535	0.24189			
		2pσ	1.05601	0.00042	-0.00149	0.00543	-0.00453	-0.28213			
		2pσ	2.10282	0.00015	0.00456	0.07164	0.13113	-0.15210			
		3dσ	2.17836	0.00019	0.00123	0.01985	0.01951	-0.02418			
	F	1s	8.27971	0.92337	-0.00078	-0.23237	0.05180	0.02006	2pπ	1.62192	0.54979
		1s	13.18833	0.08049	0.00003	-0.00336	0.00209	0.00095	2pπ	3.20512	0.42353
		2s	2.23259	-0.00136	-0.00045	0.72281	-0.20222	-0.13100	2pπ	6.10240	0.07050
		3s	4.98303	0.00664	0.00138	0.27356	-0.07818	-0.01747	3dπ	2.05584	0.04380
		2pσ	1.66269	-0.00037	-0.00145	0.07745	0.49989	-0.13756	4fπ	2.58714	0.01230
		2pσ	3.15922	-0.00001	0.00245	0.04725	0.38730	-0.09101			
		2pσ	6.02635	0.00089	-0.00018	0.00745	0.07257	-0.01747			
		3dσ	2.10013	-0.00010	-0.00009	0.02678	0.05223	-0.00918			
		4fσ	2.61144	-0.00004	0.00019	0.00874	0.01289	-0.00256			
2.000[c]	B	1s	4.40582	0.00000	0.91678	-0.11680	-0.14249	-0.13933	2pπ	1.23511	0.06343
		1s	7.70548	-0.00001	0.08992	0.00080	0.00436	-0.00890	2pπ	2.15256	0.09804
		2s	1.05528	0.00033	-0.00041	0.00754	-0.02434	0.76331	3dπ	2.34194	0.02995
		3s	2.44969	0.00035	0.00541	0.07237	0.08472	0.22210			
		2pσ	1.06205	0.00044	-0.00091	0.01146	-0.02914	-0.29240			
		2pσ	2.17483	0.00012	0.00558	0.11272	0.15305	-0.15637			
		3dσ	2.36218	0.00010	0.00230	0.02957	0.02041	-0.02225			
	F	1s	8.27178	0.92143	-0.00246	-0.23601	0.05907	0.02584	2pπ	1.71226	0.53009
		1s	13.13543	0.08252	0.00004	-0.00177	0.00174	0.00080	2pπ	3.18893	0.40388
		2s	2.33188	-0.00180	-0.00056	0.67557	-0.24368	-0.15288	2pπ	6.12120	0.07214
		3s	4.88682	0.00704	0.00334	0.25773	-0.06866	-0.02193	3dπ	2.37301	0.04769
		2pσ	1.69651	-0.00035	-0.00079	0.06143	0.47374	-0.06045	4fπ	3.03050	0.01173
		2pσ	3.13122	0.00020	0.00465	0.09984	0.43159	-0.07403			
		2pσ	6.12492	0.00083	0.00015	0.00874	0.07285	-0.00850			
		3dσ	2.44268	0.00006	0.00161	0.02531	0.04646	-0.00955			
		4fσ	2.99518	0.00002	0.00112	0.00692	0.01090	-0.00266			

TABLE V. BASIS FUNCTIONS AND EIGENVECTORS OF COEFFICIENTS FOR THE GROUND STATE OF BF (Continued)

R (Bohr)	Nucleus	Basis Function	Orbital Exponent	Eigenvectors 1σ	2σ	3σ	4σ	5σ	Basis Function	Orbital Exponent	Eigenvector 1π
2.770[c]	B	1s	4.41300	-0.00002	0.92019	-0.04162	-0.11404	-0.15998	2pπ	1.28284	0.07797
		1s	7.73200	0.00001	0.08809	-0.00048	-0.00297	-0.00869	2pπ	2.24954	0.02973
		2s	1.12289	0.00028	-0.00052	0.00657	0.09595	0.72549	3dπ	1.85112	0.02347
		3s	2.40848	0.00011	0.00328	0.04550	0.18997	0.24432			
		2pσ	0.98743	0.00031	-0.00196	-0.00002	-0.01016	-0.22565			
		2pσ	1.86165	0.00011	0.00418	0.05594	0.13363	-0.18685			
		3dσ	1.99483	0.00018	0.00079	0.01507	0.02109	-0.02786			
	F	1s	8.27800	0.92335	-0.00030	-0.23222	0.04321	0.01539	2pπ	1.57692	0.55023
		1s	13.19800	0.08062	0.00002	-0.00454	0.00201	0.00078	2pπ	3.17600	0.43863
		2s	2.19877	-0.00088	-0.00026	0.73366	-0.17397	-0.10222	2pπ	6.07471	0.07286
		3s	4.99251	0.00615	0.00069	0.28907	-0.06894	-0.01212	3dπ	1.94229	0.03483
		2pσ	1.61907	-0.00023	-0.00133	0.05656	0.48477	-0.20193	4fπ	2.40335	0.01035
		2pσ	3.19256	-0.00008	0.00162	0.02538	0.37519	-0.12758			
		2pσ	6.16500	0.00081	-0.00023	0.00434	0.06218	-0.02379			
		3dσ	2.05720	-0.00011	-0.00046	0.01818	0.04349	-0.00830			
		4fσ	2.52957	-0.00003	-0.00014	0.00628	0.01037	-0.00160			
3.155[c]	B	1s	4.41696	-0.00003	0.92096	-0.02531	-0.12371	-0.16210	2pπ	1.21320	0.07022
		1s	7.72894	0.00002	0.08732	-0.00050	-0.00451	-0.00780	2pπ	2.35328	0.01921
		2s	1.16164	0.00035	-0.00065	0.01159	0.20686	0.68717	3dπ	1.65980	0.02004
		3s	2.38735	-0.00003	0.00283	0.03222	0.21867	0.24043			
		2pσ	0.96931	0.00035	-0.00208	0.00379	-0.00482	-0.20077			
		2pσ	1.76488	0.00003	0.00374	0.03728	0.10525	-0.18429			
		3dσ	1.77005	0.00021	0.00050	0.01105	0.01876	-0.03241			
	F	1s	8.28471	0.92519	-0.00012	-0.23285	0.03551	0.01003	2pπ	1.52770	0.55176
		1s	13.25067	0.07869	0.00001	-0.00502	0.00175	0.00043	2pπ	3.17796	0.45781
		2s	2.17529	-0.00088	0.00009	0.73880	-0.14594	-0.06546	2pπ	6.16215	0.06855
		3s	4.99460	0.00628	0.00027	0.30145	-0.05889	-0.00588	3dπ	1.76827	0.02943
		2pσ	1.55724	-0.00022	-0.00092	0.04167	0.45936	-0.27668	4fπ	2.23459	0.00905
		2pσ	3.20861	-0.00008	0.00110	0.01219	0.35506	-0.18426			
		2pσ	6.13641	0.00070	-0.00021	0.00286	0.05550	-0.03194			
		3dσ	1.86514	-0.00012	-0.00053	0.01365	0.04031	-0.01228			
		4fσ	2.23366	-0.00002	-0.00028	0.00529	0.01075	-0.00270			
2.354[c,d]	B	1s	4.41374	0.00001	0.92003	-0.07462	-0.12356	-0.14941	2pπ	1.33032	0.06775
		1s	7.73118	0.00000	0.08769	0.00068	0.00083	-0.00909	2pπ	2.16451	0.05843
		2s	1.08027	0.00029	-0.00084	0.00463	0.02403	0.74630	3dπ	2.21019	0.02364
		3s	2.43726	0.00035	0.00487	0.04791	0.12794	0.24093			
		2pσ	1.07335	0.00044	-0.00143	0.00645	-0.00339	-0.28955			
		2pσ	2.12829	0.00015	0.00460	0.07314	0.13022	-0.14630			
		3dσ	2.17836	0.00019	0.00129	0.02054	0.01975	-0.02470			
	F	1s	8.27971	0.92337	-0.00086	-0.23249	0.05259	0.02058	2pπ	1.62732	0.55055
		1s	13.18833	0.08048	0.00003	-0.00322	0.00208	0.00095	2pπ	3.20512	0.42127
		2s	2.23598	-0.00141	-0.00043	0.72122	-0.20522	-0.13172	2pπ	6.10240	0.07074
		3s	4.98303	0.00669	0.00146	0.27207	-0.07878	-0.01865	3dπ	2.03846	0.04577
		2pσ	1.65760	-0.00038	-0.00137	0.07948	0.49951	-0.12882	4fπ	2.58714	0.01281
		2pσ	3.15922	0.00000	0.00253	0.05057	0.39231	-0.09018			
		2pσ	6.02635	0.00090	-0.00016	0.00770	0.07239	-0.01635			
		3dσ	2.10013	-0.00010	0.00001	0.02791	0.05339	-0.00900			
		4fσ	2.61144	-0.00004	0.00026	0.00908	0.01331	-0.00262			

[a] Experimental R_e.

[b] Gradually built up set.

[c] Atomic built up set.

[d] Calculated R_e.

TABLE VI. EXPONENTS AND EXPANSION COEFFICIENTS OF $2p\pi_0$ FUNCTIONS FROM DIFFERENT BASIS SETS OF CO.

		Set A*	Set B†	Set C‡
Exponents	$2p\pi_0$	0.98035	1.47330	1.45228
	$2p\pi_0'$	1.91497	2.84829	2.82360
	$2p\pi_0''$	4.07397	5.78456	5.86534
Expansion Coefficients	$2p\pi_0$	0.11122	0.44163	0.42529
	$2p\pi_0'$	0.56952	0.37505	0.39023
	$2p\pi_0''$	0.18908	0.04463	0.04340
Total Energy	(H)	-112.78335	-112.78600	-112.78437

*Gradually built up set.

†Atomic Built up Set.

‡Gradually Built up Set with Atomic Built up Oxygen π Functions. (Exponents were reoptimized.)

TABLE VII. POINTS USED FOR THE CONSTRUCTION OF THE POTENTIAL CURVE OF CO.

R(B)	E(H)
1.898[a]	-112.7554
2.015[b]	-112.7841
2.132[a]	-112.7858
2.249[b]	-112.7700
2.366[a]	-112.7428
2.483[b]	-112.7088
2.600[a]	-112.6710

[a]Calculated with optimized exponents.

[b]Calculated with interpolated exponents.

TABLE VIII. POINTS USED FOR THE CONSTRUCTION OF THE POTENTIAL CURVE OF BF.

R(B)	E(H)
2.000[a]	-124.1077
2.1925[b]	-124.1567
2.385[a]	-124.1658
2.5775[b]	-124.1547
2.770[a]	-124.1343
2.9625[b]	-124.1103
3.155[a]	-124.0857

[a]Calculated with optimized exponents.

[b]Calculated with interpolated exponents.

TABLE IX. SPECTROSCOPIC CONSTANTS FOR THE GROUND STATE OF $C^{12}O^{16}$

	Calculated	Experimental[a]
ω_e (cm^{-1})	2431	2169.829
$\omega_e x_e$ (cm^{-1})	11.69	13.295
B_e (cm^{-1})	2.027	1.931285
α_e (cm^{-1})	0.01525	0.017535
R_e (B)	2.081	2.132
k (10^5 dyne cm^{-1})	23.86	19.02

[a]See reference 29.

TABLE X. SPECTROSCOPIC CONSTANTS FOR THE GROUND STATE OF $B^{11}F^{19}$

	Calculated	Experimental[a]
ω_e (cm^{-1})	1496	1402.1
$\omega_e x_e$ (cm^{-1})	12.07	11.8
B_e (cm^{-1})	1.559	1.510
α_e (cm^{-1})	0.01851	0.016
R_e (B)	2.354	2.391
k (10^5 dyne cm^{-1})	9.189	8.071

[a]See Reference 30.

TABLE XI. SUMMARY OF RESULTS[a] FOR THE GROUND STATE OF CO

	Experimental R_e[b]				Calculated R_e		
	Minimal Set	Nesbet Set[c]	Gradually Built up Set	Atomic Built up Set	Nesbet Set[c,d]	Atomic Built up Set[e]	Experimental
Total energy	-112.3910	-112.7588	-112.7846	-112.7860		-112.7879	-113.377[f]
Dissociation energy (ev)[g]	-2.91	7.09	7.80	7.84		7.89	-11.242[h]
Potential energy $\langle V \rangle$	-225.0690	-225.3763	-225.4405	-225.4280		-225.5844	-226.754[f]
Kinetic energy $\langle T \rangle$	112.6779	112.6175	112.6559	112.6420		112.7965	113.377[f]
Virial coefficient $\langle V \rangle / \langle T \rangle$	-1.997454	-2.001252	-2.001143	-2.001278		-1.999924	-2.000000
Orbital energies 1σ	-20.66794	-20.69373	-20.66243	-20.66123		-20.66124	
2σ	-11.28564	-11.39129	-11.35998	-11.35927		-11.34817	
3σ	-1.48115	-1.54931	-1.52062	-1.51920		-1.53938	
4σ	-0.72785	-0.82522	-0.80418	-0.80235		-0.80595	
5σ	-0.48416	-0.57040	-0.55347	-0.55304		-0.55048	
1π	-0.55824	-0.65309	-0.63905	-0.63771		-0.65073	
Vertical ionization potential $X^2\Sigma^+$	13.174	15.520	15.060	15.048		14.978	14.01[i]
(ev) to upper state $^2\Pi$	15.190	17.770	17.388	17.352		17.706	16.92[i]
$^2\Sigma^+$	19.805	22.454	21.882	21.832		21.930	19.66[i]
$\langle z \rangle$[j]	-1.9494	-2.2882	-2.2033	-2.2399	-2.26	-2.1412	-2.088[k]
$\langle z \rangle 1\sigma$	-2.1311	-2.1314	-2.1313	-2.1313		-2.0803	
$\langle z \rangle 2\sigma$	2.1301	2.1303	2.1306	2.1305		2.0790	
$\langle z \rangle 3\sigma$	-1.0050	-0.95190	-0.96661	-0.96826		-0.89567	
$\langle z \rangle 4\sigma$	-1.9648	-2.2136	-2.1601	-2.1820		-2.2931	
$\langle z \rangle 5\sigma$	2.7899	3.1740	3.1616	3.1399		3.1917	
$\langle z \rangle 1\pi$	-1.7684	-2.2957	-2.2374	-2.2288		-2.1428	
Dipole Moment (D)	0.464 (C^-O^+)	0.397 (C^+O^-)	0.181 (C^+O^-)	0.274 (C^+O^-)	0.361 (C^+O^-)	0.153 (C^+O^-)	0.112 ± 0.005[k] (C^-O^+)
$(d\mu/dR)_{R_e}$ (D/Å)					1.508	4.89	
$\langle 1/r_C \rangle$	18.457	18.370	18.396	18.397		18.502	
$\langle 1/r_O \rangle$	25.027	25.034	25.065	25.065		25.135	
$\langle \sum_{i,j<i} 1/r_{ij} \rangle$[j]	85.893	85.115	85.455	85.483		86.506	
$\langle 3z_C^2 - r_C^2 \rangle$	74.509	76.151[m]	76.154	76.439		72.841	
$\langle 3z_O^2 - r_O^2 \rangle$	57.885	56.637	57.365	57.336		55.018	
Molecular Quadrupole Moment (10^{-26} esu)	-1.72[j]	-1.79[n]	-2.10[j]	-2.19[j]	-1.81[n]	-2.22[j]	

TABLE XI. CONTINUED

	Experimental R_e[b]				Calculated R_e		
	Minimal Set	Nesbet Set[c]	Gradually Built up Set	Atomic Built up Set	Nesbet Set[c,d]	Atomic Built up Set[e]	Experimental
$\langle \sin^2\theta_C/r_C \rangle$	10.263	10.190[m]	10.186	10.186		10.232	
$\langle \sin^2\theta_C/r_O \rangle$	15.398	15.447[m]	15.444	15.443		15.463	
$\langle \cos^2\theta_C/r_C \rangle$	8.1946	8.1797[m]	8.2100	8.2108		8.2698	
$\langle \cos^2\theta_C/r_O \rangle$	9.6295	9.5871[m]	9.6204	9.6216		9.6726	
$\langle r_C + r_O \rangle$	47.360	48.341[m]	48.087	48.049		47.375	
$\langle r_C^2 \rangle$	57.883	61.538[m]	60.829	60.768		58.875	
$\langle r_O^2 \rangle$	49.571	51.781[m]	51.434	51.217		49.963	
χ_L (10^{-6} erg/gauss^{2}mole)	-30.0[j]	-32.3[j]	-31.9[j]	-31.8[j]		-31.1[j]	
$\langle z_C^2 \rangle$	44.131	45.896[m]	45.661	45.736		43.905	
$\langle z_O^2 \rangle$	35.819	36.140[m]	36.266	36.184		34.994	
$\langle x^2 \rangle^O$	13.753	15.642[m]	15.168	15.032		14.969	
$\langle P_1(\cos\theta_C)/r_C^2 \rangle$	1.5665	1.6993[m]	1.7351	1.7844		1.8592	
$\langle P_1(\cos\theta_O)/r_O^2 \rangle$	0.98383	1.3012[m]	1.3168	1.3373		1.3965	
$\mathcal{Z}_C^p$	-1.16	-0.364[m]	-0.149	0.146		0.0712	
$\mathcal{Z}_C^q$	-2.69	-0.150[m]	-0.0261	0.138		0.0876	
$\mathcal{Z}_C + \mathcal{Z}_O^p$	1.53	-0.214[m]	-0.123	0.0077		-0.0163	
$\langle P_2(\cos\theta_C)/r_C^3 \rangle$	1.3331	1.4091[m]	1.3746	1.4139		1.4772	
$\langle P_2(\cos\theta_O)/r_O^3 \rangle$	1.2010	0.93248[m]	0.94688	0.95847		1.0644	
q_C	-1.02	-1.17[m]	-1.10	-1.18		-1.18	
q_O	-1.16	-0.627[m]	-0.655	-0.679		-0.797	

TABLE XI. FOOTNOTES

[a]All the quantities in this table, unless explicitly specified, are in atomic units of Hartree; see reference 23.

[b]The experimental R_e of CO is 2.132 B; see reference 29.

[c]See reference 6.

[d]Interpolated values to the calculated R_e of 2.115 B.

[e]The calculated R_e of the atomic built up set is 2.081 B.

[f]See reference 37.

[g]The calculation of dissociation energies takes the energies of the ground state separated atoms to be: C + O = -112.49800 H. See reference 20.

[h]See reference 38.

[i]See reference 36.

[j]The origin of the coordinate used in the calculation of this quantity is at the midpoint of the two nuclei, and positive Z-axis points toward carbon.

[k]See references 47 and 48.

[l]The indices i and j sum over electrons.

[m]Calculated with our program, using Nesbet's function.

[n]The origin of the coordinate system used in the evaluation of this quantity is at the center of mass.

[o]$\langle x_C^2 \rangle = \langle x_O^2 \rangle = \langle x^2 \rangle$.

[p]Attractive force towards carbon is positive.

[q]Attractive force towards oxygen is positive.

TABLE XII. SUMMARY OF RESULTS[a] FOR THE GROUND STATE OF BF

	Experimental R_e[b]				Calculated R_e		
	Minimal Set	Nesbet Set[c]	Gradually Built up Set	Atomic Built up Set	Nesbet Set[c,d]	Atomic Built up Set[e]	Experimental
Total energy	-123.6463	-124.1404	-124.1636	-124.1659		-124.1664	-124.777 ± 0.018[f]
Dissociation energy (ev)[g]	-7.95	5.48	6.11	6.18		6.19	8.58 ± 0.5[h]
Potential energy $\langle V \rangle$	-247.1480	-248.1959	-248.3138	-248.2809		-248.3313	-249.554[f]
Kinetic energy $\langle T \rangle$	123.5016	124.0556	124.1503	124.1150		124.1649	124.777[f]
Virial coefficient $\langle V \rangle / \langle T \rangle$	-2.001172	-2.000684	-2.000107	-2.000411		-2.000011	2.000000
Orbital energies 1σ	-26.42200	-26.39718	-26.37408	-26.37504		-26.37967	
2σ	-7.63301	-7.72822	-7.70866	-7.70897		-7.70382	
3σ	-1.64543	-1.71601	-1.69711	-1.69759		-1.70806	
4σ	-0.73827	-0.86828	-0.85292	-0.85373		-0.86190	
5σ	-0.36124	-0.41387	-0.40470	-0.40424		-0.40162	
1π	-0.62179	-0.75269	-0.74390	-0.74447		-0.75210	
Vertical ionization potential $X^2\Sigma^+$	9.8293	11.261	11.012	10.999		10.928	(10.969)[i]
(ev) to upper state $^2\Pi$	16.919	20.481	20.241	20.257		20.464	
$^2\Sigma^+$	20.088	23.626	23.208	23.230		23.452	
$\langle z \rangle^j$	-4.2310	-4.5072	-4.4326	-4.4103	-4.57	-4.2976	
$\langle z \rangle 1\sigma$	-2.3906	-2.3847	-2.3907	-2.3906		-2.3536	
$\langle z \rangle 2\sigma$	2.3888	2.3823	2.3888	2.3885		2.3514	
$\langle z \rangle 3\sigma$	-1.9302	-1.9117	-1.9349	-1.9353		-1.8859	
$\langle z \rangle 4\sigma$	-2.2150	-2.3208	-2.3092	-2.3061		-2.3118	
$\langle z \rangle 5\sigma$	3.6483	3.9855	3.9790	4.0020		3.9842	
$\langle z \rangle 1\pi$	-3.7324	-4.2577	-4.1656	-4.1687		-4.0819	
Dipole moment (D)	1.40 (B^-F^+)	0.668 (B^-F^+)	0.888 (B^-F^+)	0.945 (B^-F^+)	0.617 (B^-F^+)	1.04 (B^-F^+)	
$(d\mu/dR)_{R_e}$ (D/Å)					1.921	5.56	
$\langle 1/r_B \rangle$	15.178	15.109	15.119	15.117		15.182	
$\langle 1/r_F \rangle$	28.495	28.586	28.608	28.605		28.633	
$\langle \sum_{i,j<i} 1/r_{ij} \rangle^k$	85.197	84.618	84.753	84.750		85.280	
$\langle 3z_B^2 - r_B^2 \rangle$	104.80	107.33[l]	107.32	107.47		104.10	
$\langle 3z_F^2 - r_F^2 \rangle$	64.334	64.329	64.922	65.293		63.637	
Molecular quadrupole moment (10^{-26} esu)	-3.05[j]	-4.39[m]	-4.09[j]	-4.27[j]	-4.38[m]	-4.23[j]	

TABLE XII. CONTINUED

	Experimental R_e[b]				Calculated R_e		
	Minimal Set	Nesbet Set[c]	Gradually Built up Set	Atomic Built up Set	Nesbet Set[c,d]	Atomic Built up Set[e]	Experimental
$\langle \sin^2\theta_B/r_B \rangle$	7.9006	7.8559[f]	7.8543	7.8506		7.8730	
$\langle \sin^2\theta_F/r_F \rangle$	18.132	18.212[f]	18.209	18.200		18.205	
$\langle \cos^2\theta_B/r_B \rangle$	7.2774	7.2529[f]	7.2646	7.2665		7.3089	
$\langle \cos^2\theta_F/r_F \rangle$	10.363	10.373[f]	10.399	10.405		10.429	
$\langle r_B + r_F \rangle$	50.759	51.584[f]	51.467	51.478		50.993	
$\langle r_B^2 \rangle$	73.835	77.164[f]	76.706	76.718		75.019	
$\langle r_F^2 \rangle$	53.603	55.665	55.509	55.628		54.786	
χ_L (erg/gauss^{2}mole)	-34.6[j]	-36.8[f,j]	-36.5[j]	-36.6[j]		-36.06[j]	
$\langle z_B^2 \rangle$	59.545	61.497[f]	61.340	61.397		59.707	
$\langle z_F^2 \rangle$	39.312	39.998[f]	40.143	40.307		39.474	
$\langle x^2 \rangle$	14.291	15.667[f]	15.365	15.321		15.311	
$\langle P_1(\cos\theta_B)/r_B^2 \rangle$	1.4599	1.5363[f]	1.5406	1.5466		1.5935	
$\langle P_1(\cos\theta_F)/r_F^2 \rangle$	0.56704	0.85787[f]	0.86703	0.88122		0.90616	
$\mathcal{A}_B^o$	-0.572	-0.230[f]	-0.168	-0.138		-0.153	
$\mathcal{A}_F^p$	-2.77	-0.190[f]	-0.0758	0.0595		0.0346	
$\mathcal{A}_B + \mathcal{A}_F^o$	2.20	-0.0394[f]	-0.0922	-0.198		-0.188	
$\langle P_2(\cos\theta_B)/r_B^3 \rangle$	0.90502	0.91952[f]	0.91950	0.92575		0.96045	
$\langle P_2(\cos\theta_F)/r_F^3 \rangle$	0.19708	0.033028[f]	0.0091887	0.070862		0.12083	
q_B	-0.493	-0.512[f]	-0.522	-0.535		-0.541	
q_F	0.337	0.671[f]	0.713	0.590		0.525	

TABLE XII. FOOTNOTES

[a]All quantities in this table, unless explicitly specified, are in atomic units of Hartree, see reference 23.

[b]The experimental R_e of BF is 2.391 B; see reference 30.

[c]See reference 6. Calculation at experimental R_e is carried out at an older reported R_e of 2.385 B.

[d]Interpolated values to the calculated R_e of 2.404 B.

[e]The calculated R_e of the atomic built up set is 2.354 B.

[f]See reference 37.

[g]The calculation of dissociation energies takes the energies of the ground state separated atoms to be: B + F = -123.93893 H. See reference 20.

[h]See reference 38.

[i]See reference 36.

[j]The origin of the coordinate system used in the calculation of this quantity is at the midpoint of the two nuclei, and positive Z-axis points toward boron.

[k]The indices i and j sum over electrons.

[l]Calculated with our program, using Nesbet's function.

[m]The origin of the coordinate system used in the calculation of this quantity is at the center of mass.

[n]$\langle x_B^2 \rangle = \langle x_F^2 \rangle = \langle x^2 \rangle$.

[o]Attractive force towards boron is positive.

[p]Attractive force towards fluorine is positive.

TABLE XIII. DIFFERENCES BETWEEN EXPERIMENTAL AND SCF TOTAL ENERGY (H) FOR N_2, CO AND BF

N_2[a]	CO	BF[b]
0.5904	0.5891	0.5926 ~ 0.6286

[a]See reference 22.

[b]The uncertainty is originated from the error in the experimental measurement of the dissociation energy of BF. See reference 38.

TABLE XIV. ORBITAL ENERGIES (H) OF THE THREE HIGHEST OCCUPIED ORBITAL OF N_2, CO AND BF

	N_2[a]	CO	BF
4σ ($2\sigma_u$)	-0.76870	-0.80595	-0.86190
5σ ($3\sigma_g$)	-0.63789	-0.55048	-0.40162
1π ($1\pi_u$)	-0.62845	-0.65073	-0.75210

[a]See reference 22.

TABLE XV. NUCLEAR QUADRUPOLE MOMENT OF O^{17} (BARN)

Molecular Result[a,b]	-0.0236 ± 0.0021
Atomic Result[c]	-0.024

[a]The field gradient used in the calculation is evaluated with the atomic built up set at calculated R_e.

[b]The error associated with the molecular results is due to the error in the experimental measurement of eqQ_N. See reference 41.

[c]See reference 42.

TABLE XVI. DIPOLE MOMENT OF CO AND BF AT DIFFERENT VALUES OF R.

CO		BF	
R(B)	μ(D)	R(B)	μ(D)
1.898	0.302 (C^-O^+)	2.000	1.99 (B^-F^+)
2.132	0.289 (C^+O^-)	2.385	0.967 (B^-F^+)
2.366	0.930 (C^+O^-)	2.770	0.315 (B^+F^-)
2.600	1.61 (C^+O^-)	3.155	1.80 (B^+F^-)

TABLE XVII. AVERAGE POSITION OF AN ELECTRON ALONG Z-AXIS

	CO[a,c]	BF[b,c]
1σ	0.0004	0.0002
2σ	2.1313	2.3898
3σ	0.5819	0.2279
4σ	0.0250	0.0424
5σ	2.6360	3.1965
1π	0.5138	0.1533

[a]Origin at oxygen nucleus.

[b]Origin at fluorine nucleus.

[c]Calculated in Bohr unit with the atomic built up set at experimental R_e.

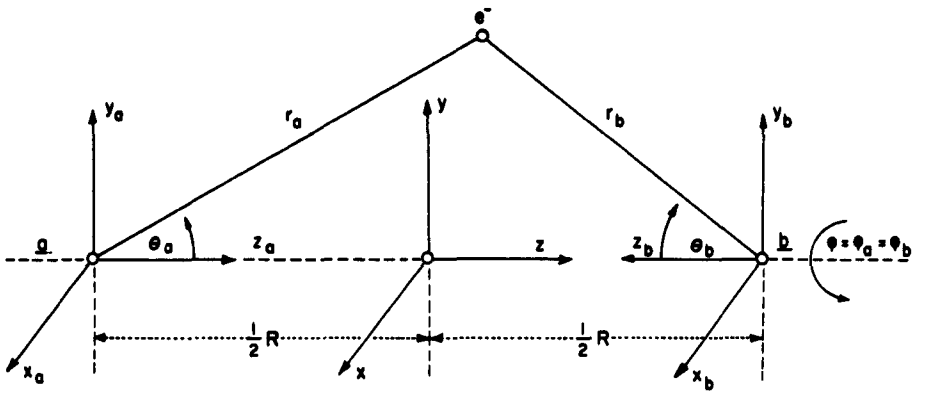

Fig. 1. Coordinate systems used for heteronuclear diatomic molecule

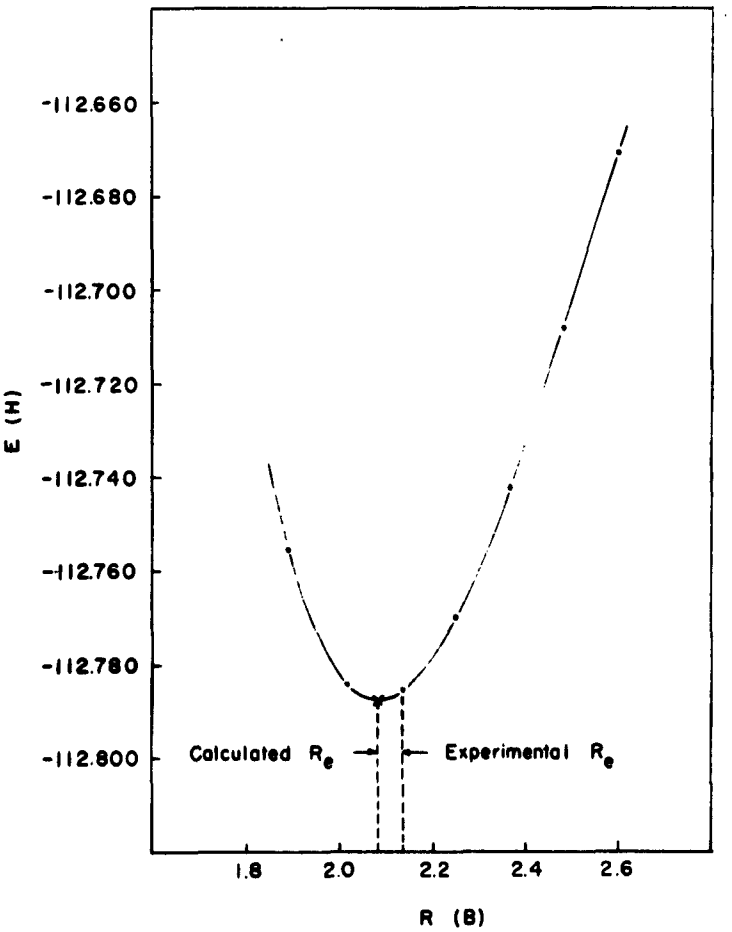

Fig.2. Calculated Potential Curve of CO

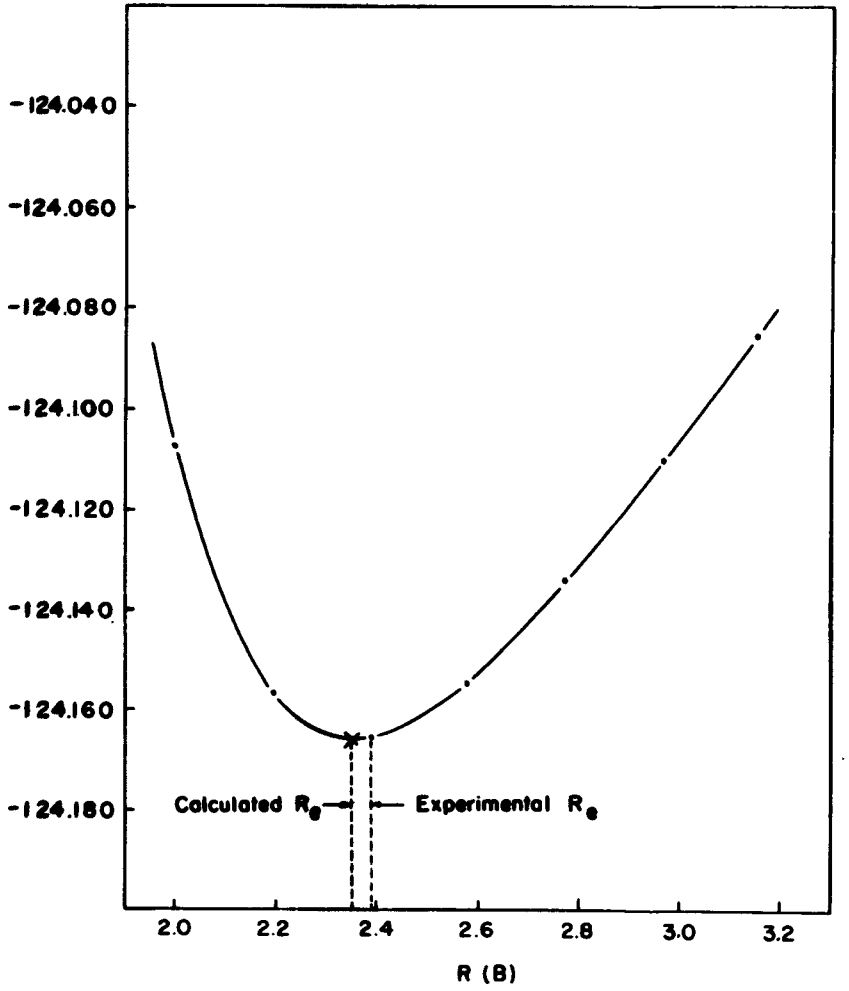

Fig. 3. Calculated Potential Curve of BF

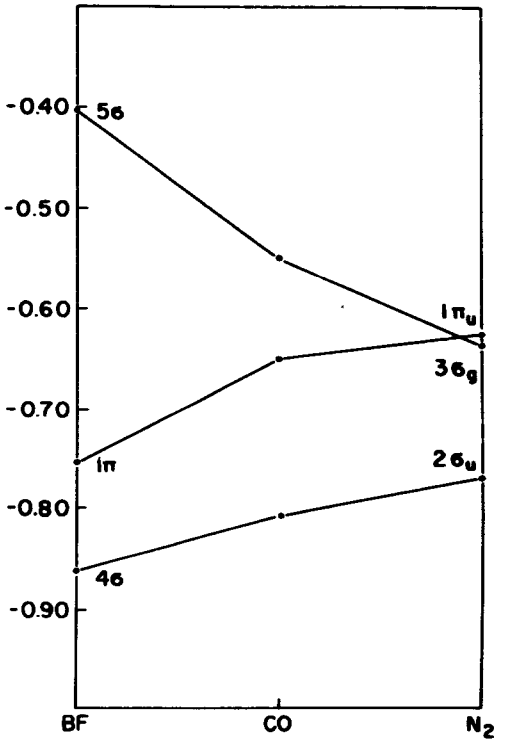

Fig. 4. Orbital Energies of the three Highest Occupied Orbitals of BF, CO, N_2.

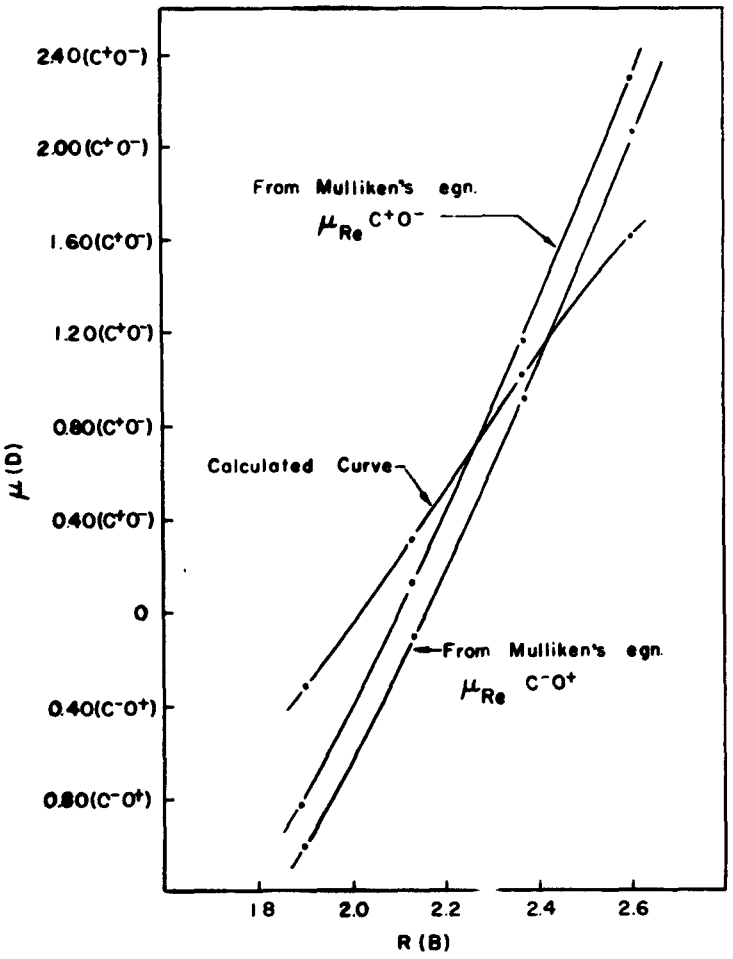

Fig. 5. Dipole Moment Curve of CO

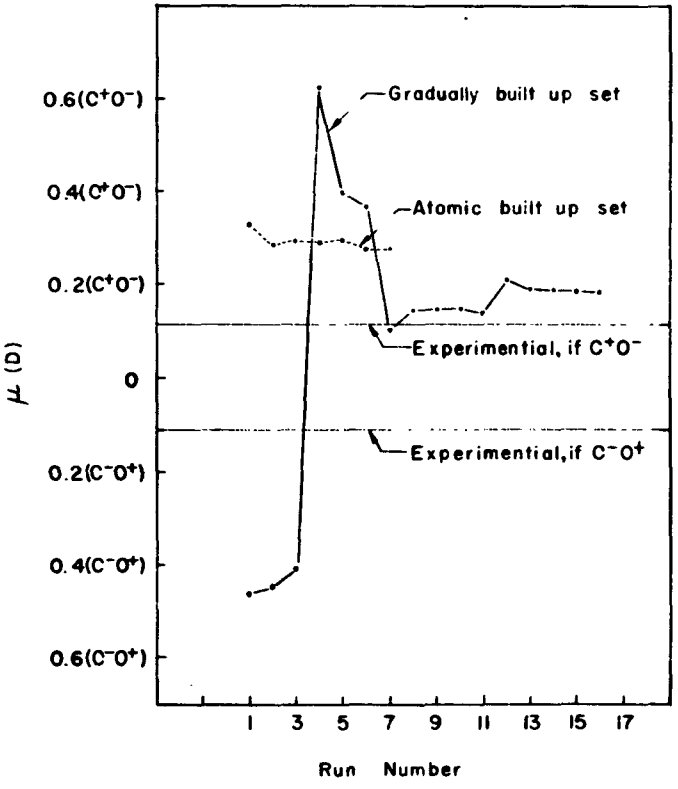

Fig. 6 Dipole Moment of CO Calculated at Different Stages of the Gradually and Atomic Built Up Sets.

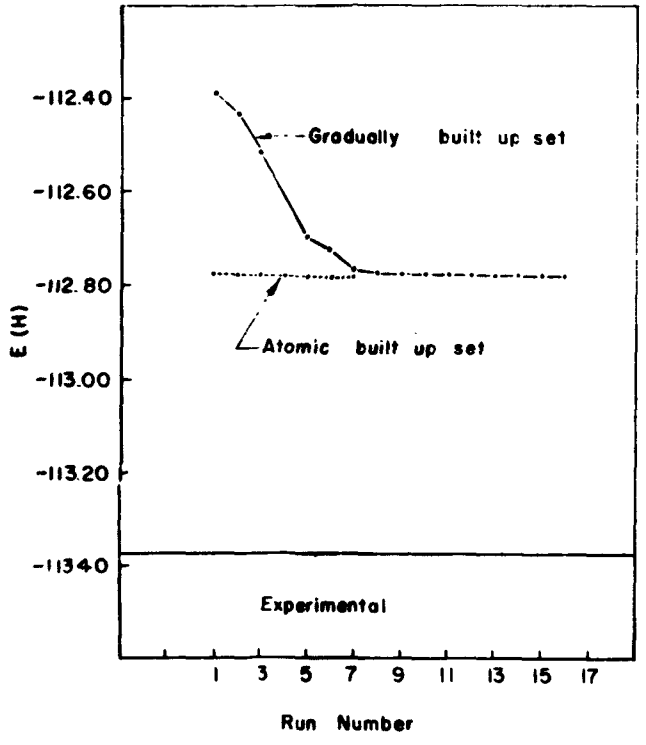

Fig 7. Total Energy of CO Calculated at Different Stages of the Gradually and Atomic Built up Sets.

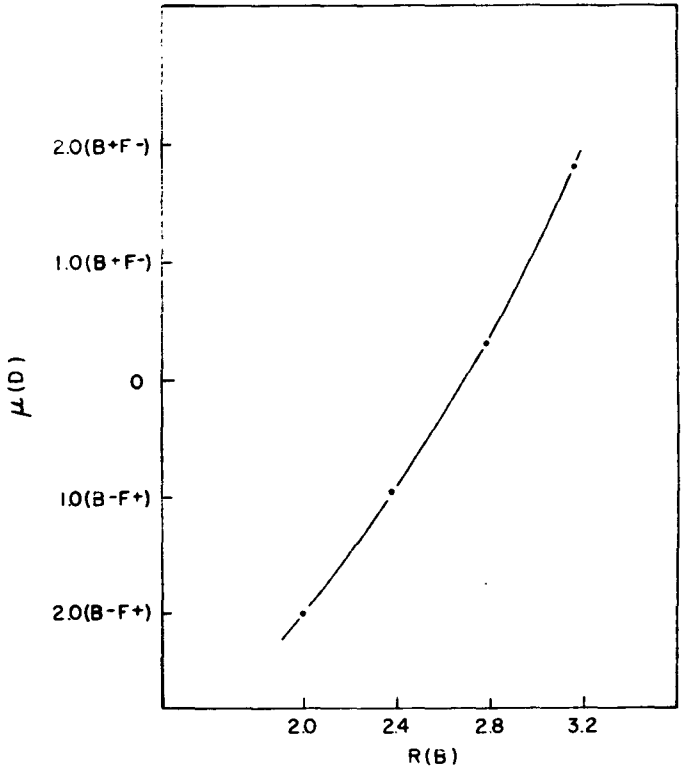

Fig. 8. Dipole Moment Curve of BF

TOTAL MOLECULAR CHARGE DENSITY CONTOURS FOR CO

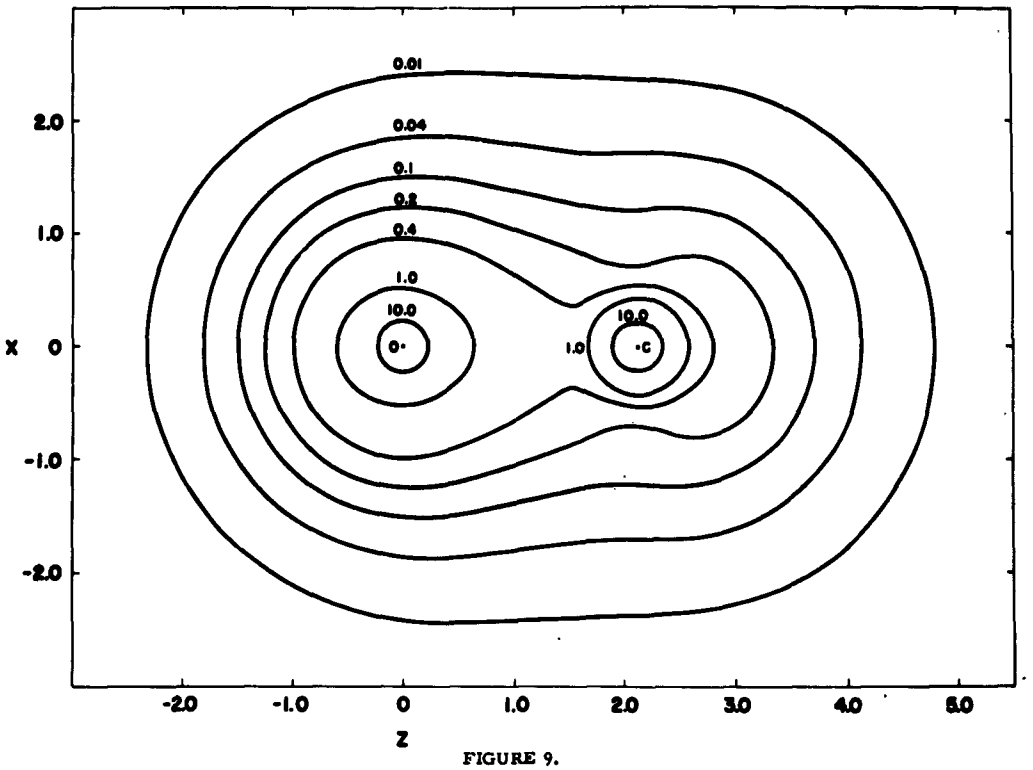

FIGURE 9.

MOLECULAR ORBITAL CHARGE DENSITY CONTOURS
3σ ORBITAL OF CO

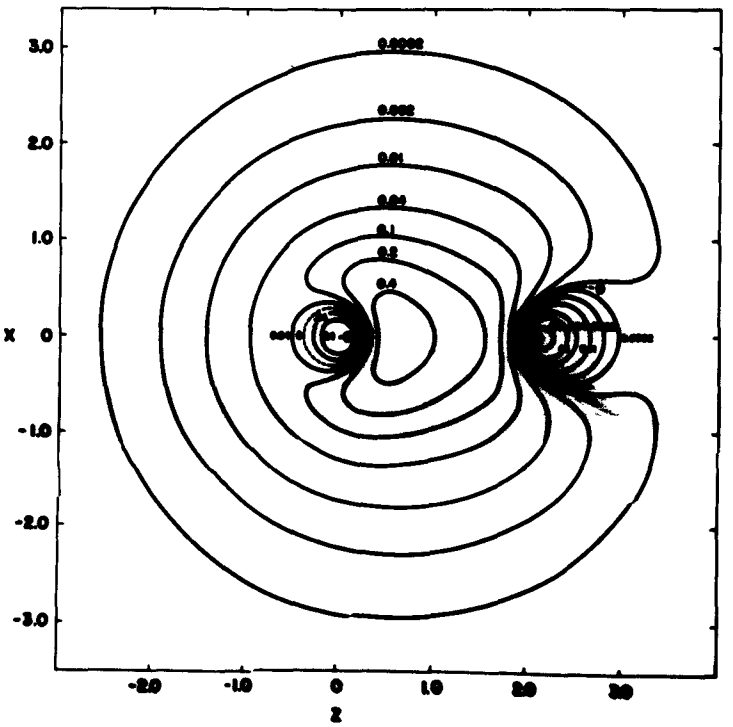

FIGURE 10.

MOLECULAR ORBITAL CHARGE DENSITY CONTOURS
4σ ORBITAL OF CO

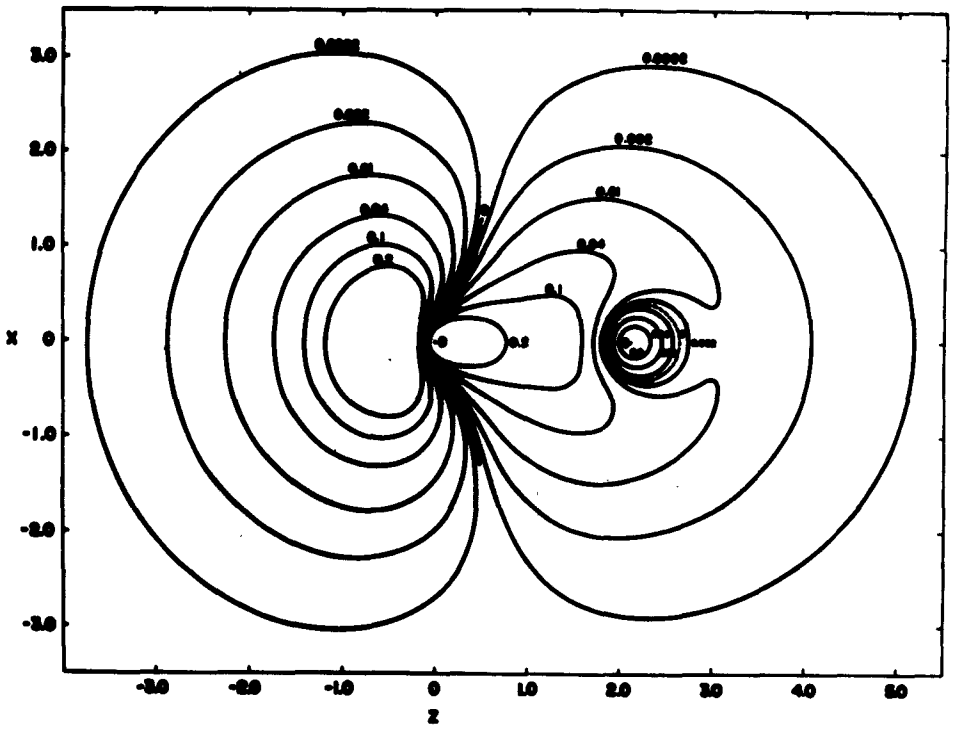

FIGURE 11.

MOLECULAR ORBITAL CHARGE DENSITY CONTOURS
5σ ORBITAL OF CO

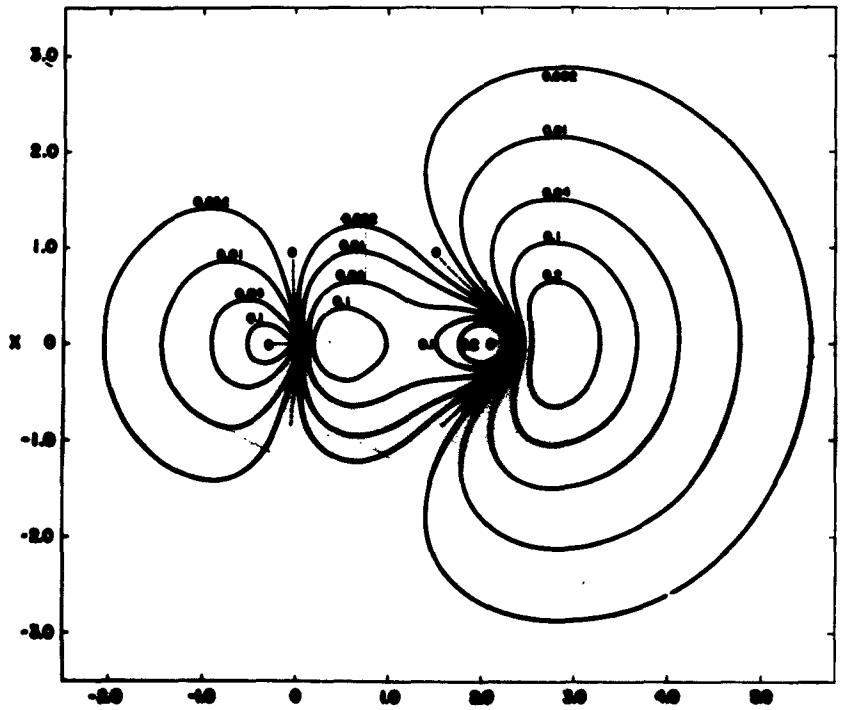

FIGURE 12.

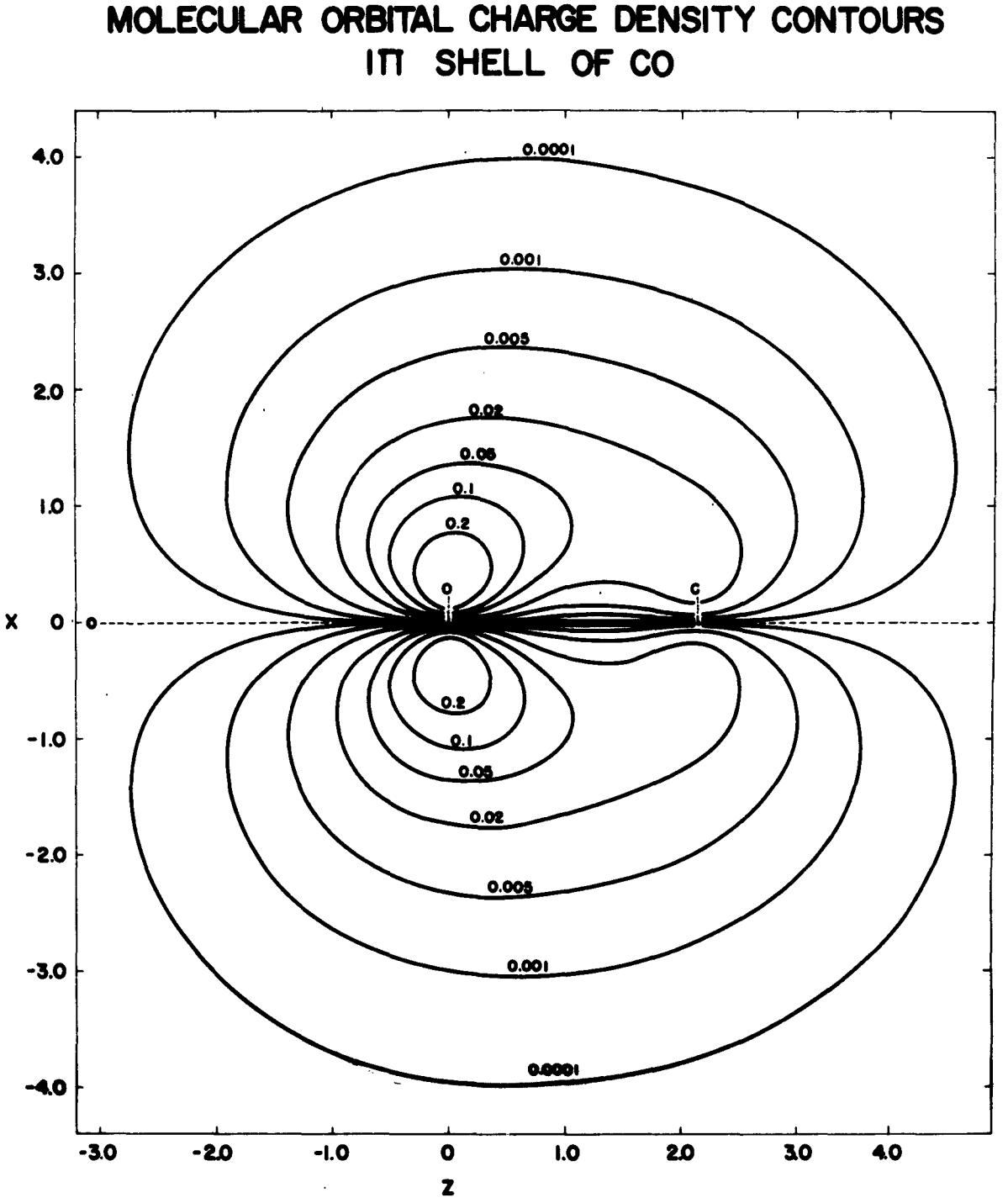
MOLECULAR ORBITAL CHARGE DENSITY CONTOURS
ITT SHELL OF CO
0.0001
0.001
0.005
0.02
0.05
0.1
0.2
O
C
X
Z
4.0
3.0
2.0
1.0
0
-1.0
-2.0
-3.0
-4.0
-3.0
-2.0
-1.0
1.0
2.0
3.0
4.0

FIGURE 13.

TOTAL MOLECULAR CHARGE DENSITY CONTOURS FOR BF

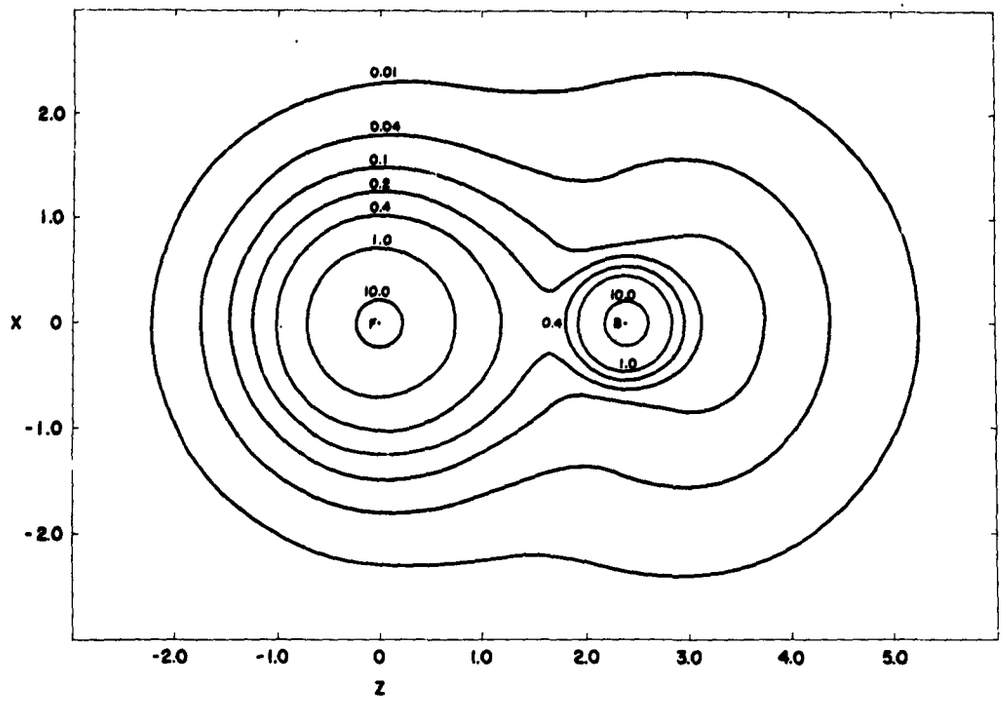

FIGURE 14.

MOLECULAR ORBITAL CHARGE DENSITY CONTOURS 3σ ORBITAL OF BF

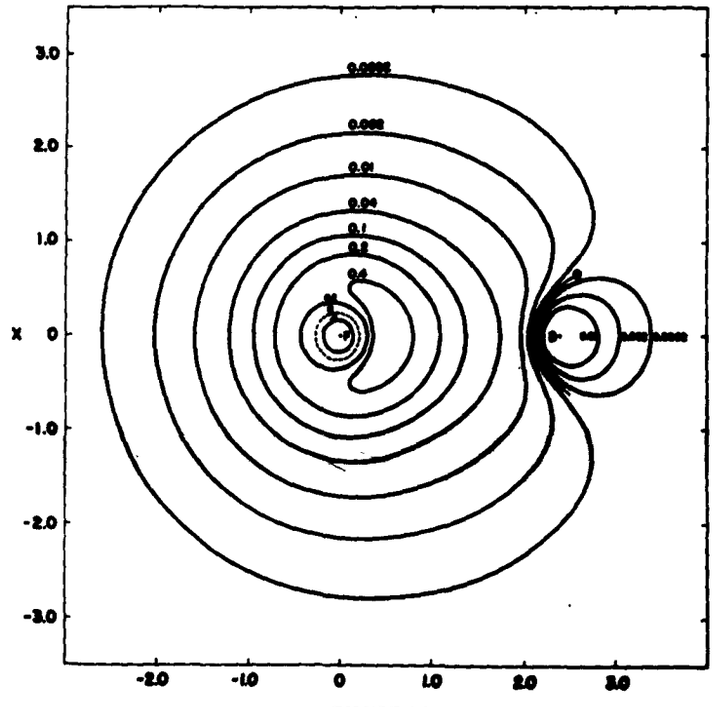

FIGURE 15.

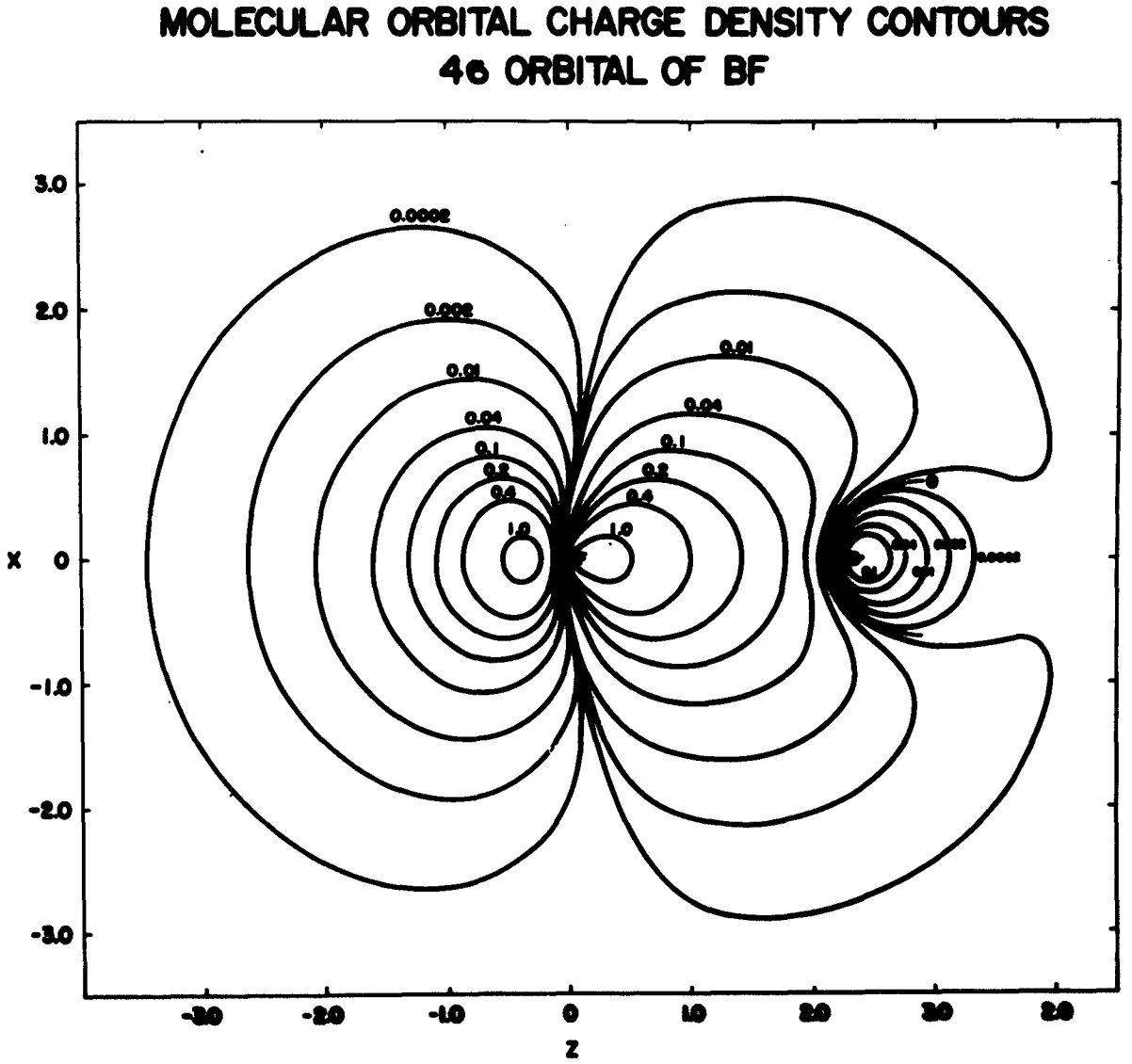
MOLECULAR ORBITAL CHARGE DENSITY CONTOURS
4σ ORBITAL OF BF
3.0
2.0
1.0
0
-1.0
-2.0
-3.0
X
-3.0
-2.0
-1.0
0
1.0
2.0
3.0
4.0
Z
0.0002
0.002
0.01
0.04
0.1
0.2
0.4
1.0

FIGURE 16.

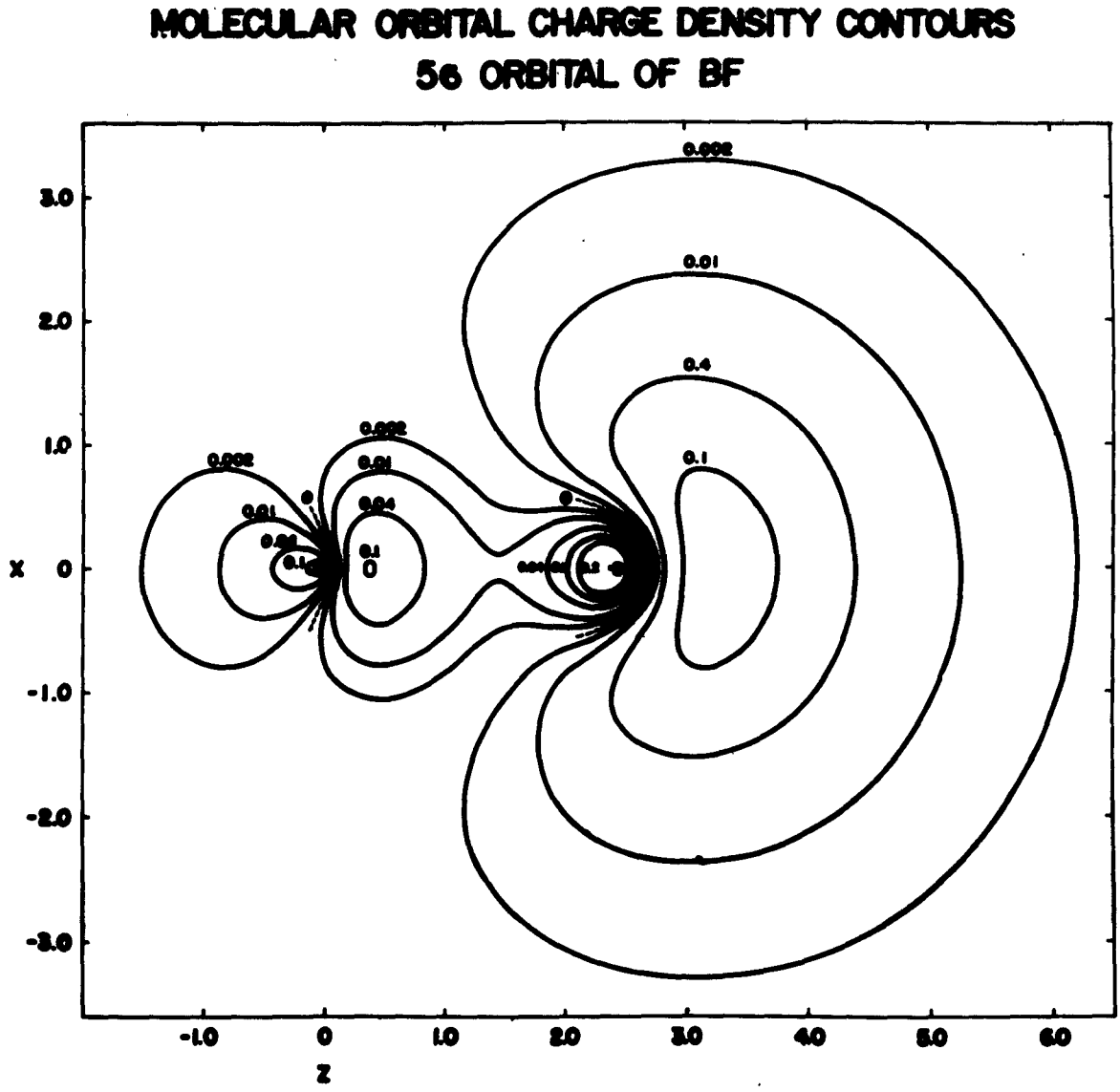
MOLECULAR ORBITAL CHARGE DENSITY CONTOURS
5σ ORBITAL OF BF
0.002
0.01
0.4
0.1
0.002
0.01
0.004
0.1
O
3.0
2.0
1.0
X 0
-1.0
-2.0
-3.0
-1.0
0
1.0
2.0
3.0
4.0
5.0
6.0
Z

FIGURE 17.

MOLECULAR ORBITAL CHARGE DENSITY CONTOURS
1IT SHELL OF BF

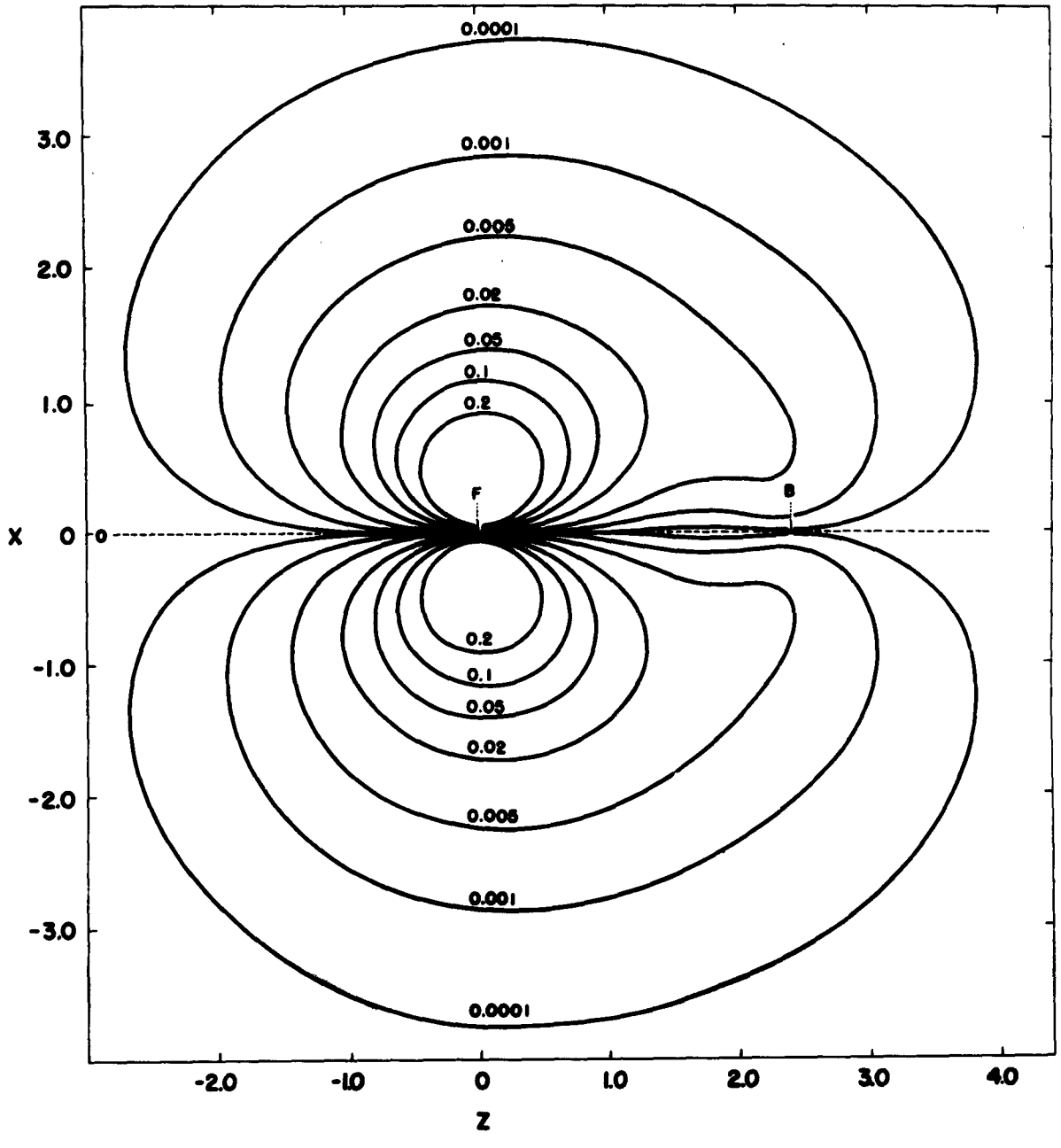

FIGURE 18.

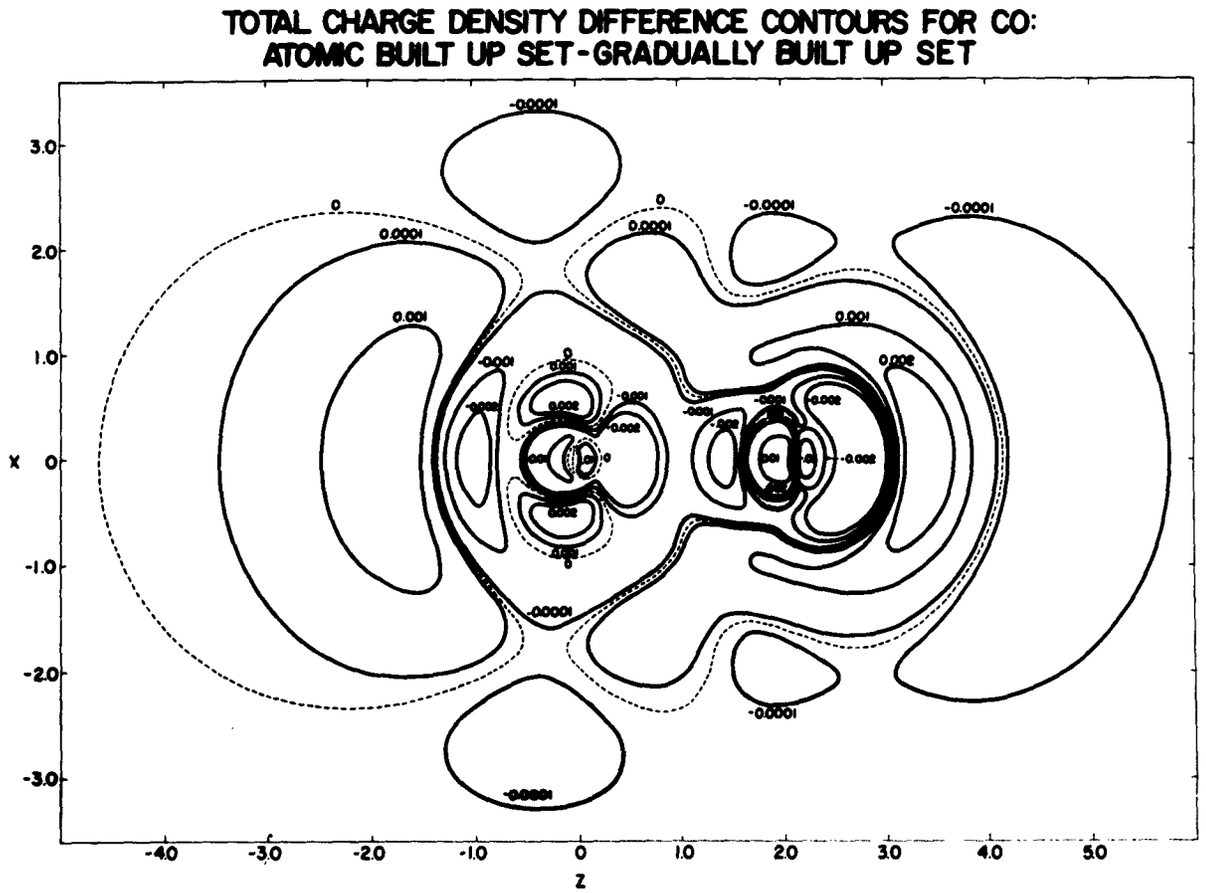
TOTAL CHARGE DENSITY DIFFERENCE CONTOURS FOR CO:
ATOMIC BUILT UP SET-GRADUALLY BUILT UP SET
X
Z
3.0
2.0
1.0
0
-1.0
-2.0
-3.0
-4.0
-3.0
-2.0
-1.0
0
1.0
2.0
3.0
4.0
5.0

FIGURE 19.

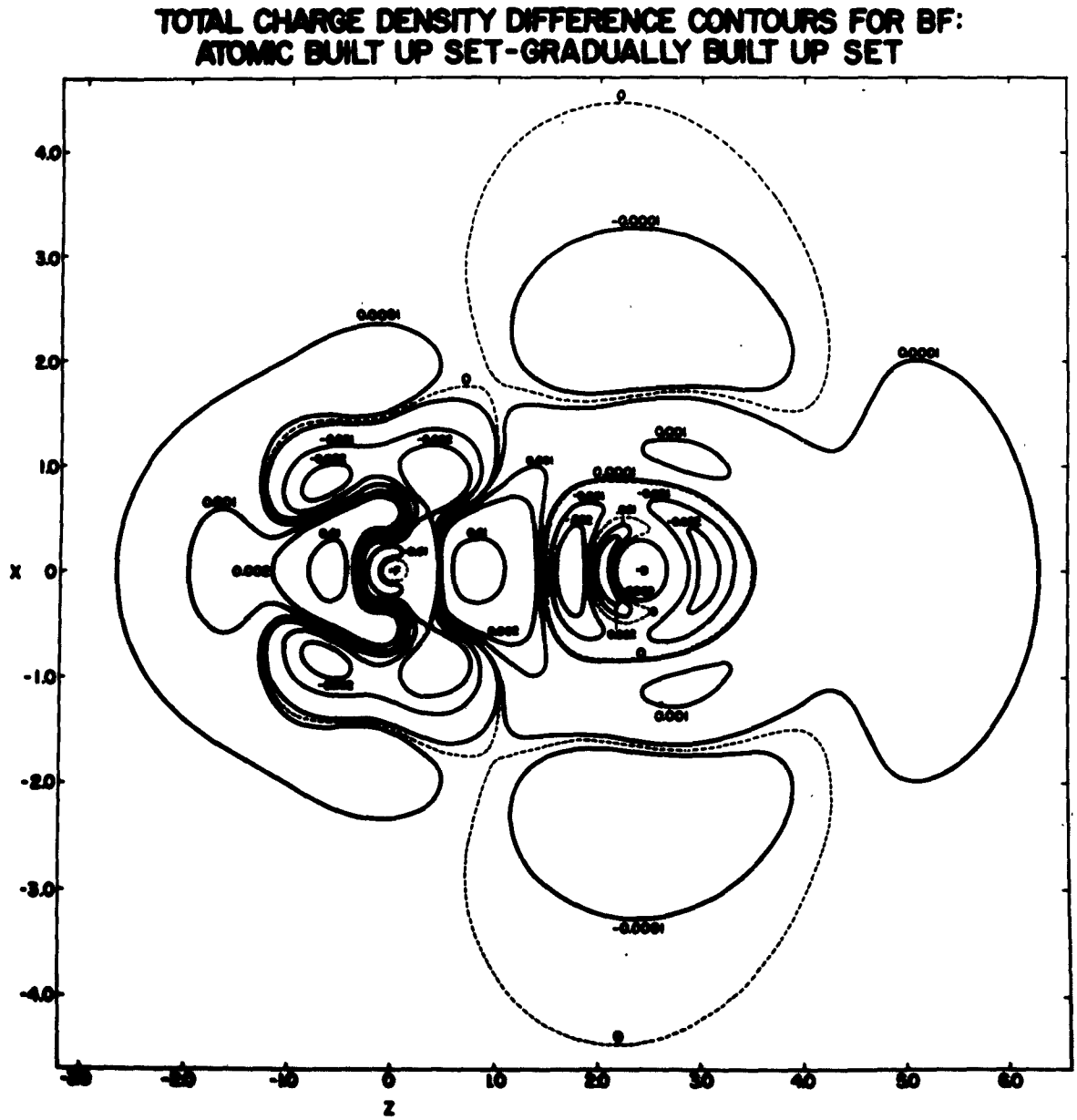
TOTAL CHARGE DENSITY DIFFERENCE CONTOURS FOR BF:
ATOMIC BUILT UP SET-GRADUALLY BUILT UP SET
X
Z
4.0
3.0
2.0
1.0
0
-1.0
-2.0
-3.0
-4.0
-1.0
0
1.0
2.0
3.0
4.0
5.0
6.0

FIGURE 20.

HARTREE-FOCK-ROOTHAAN WAVE FUNCTIONS, POTENTIAL CURVES, AND CHARGE DENSITY CONTOURS FOR THE $HeH^+(X^1\Sigma^+)$ AND $NeH^+(X^1\Sigma^+)$ MOLECULE IONS.[†]

Sigrid Peyerimhoff[*]
Laboratory of Molecular Structure and Spectra
Department of Physics, University of Chicago
Chicago, Illinois 60637

ABSTRACT

Hartree-Fock-Roothaan wave functions for the ground state of the HeH^+ ion and the NeH^+ ion are reported. The potential curves for HeH^+ and NeH^+ are calculated using wavefunctions, which are optimized at the equilibrium distance and also at each internuclear distance, and their relative behavior is discussed. The Hellmann-Feynman forces on the nuclei are studied as a function of the internuclear distance with regard to the size of the basis set and optimization of the wave function. Spectroscopic data are calculated in different ways, a dissociation energy of 1.74 eV for HeH^+ and 2.03 eV for NeH^+ is computed, and calculations made to find the center of negative charge for every internuclear separation. Electron density maps are plotted for several internuclear distances in HeH^+ and for the total wave function and the individual molecular orbitals of NeH^+ at the equilibrium distance.

I. INTRODUCTION

Rare gas hydride ions (HeH^+, NeH^+, AH^+) were first observed in mass spectrometers around 1933,[1] and in recent years a number of experiments have been carried out

---

[†]Computations reported in this paper were supported by Advanced Research Projects Agency thru the U.S. Army Research Office (Durham), under Contract DA-11-022-ORD-3119.

[*]Present address: Department of Chemistry, Princeton University, Princeton, New Jersey. On leave from Department of Theoretical Physics, Justus Liebig University, Giessen, Germany.

[1]H. Lukanow, W. Schuetze, Z. Physik 82, 610 (1933); K. T. Bainbridge, Phys. Rev. 43, 103 (1933); J. W. Hiby, Ann. Phys. Lpz. 34, 473 (1939).

to study their properties, especially their formation and reactions.[2] These ions have only a short lifetime and are formed in low concentrations which makes the experimental measurement of their properties by conventional means difficult. It is therefore, highly desirable to obtain accurate wave functions for these molecules which enable us to calculate the spectroscopic constants for the ground state and other molecular expectation values and properties.

The $(HeH)^+$ rare gas hydride ion is of particular theoretical interest because it is the simplest two electron system among the heteronuclear diatomic molecules and therefore plays a prototype role, similar to the role the hydrogen molecule plays among the homonuclear diatomic molecules. Besides this, there has been considerable interest in this ion - or more exactly in the $(He^3H)^+$ ion, since it is the resulting ion when tritium of the TH molecules undergoes β-decay.

The two recent calculations on $(HeH)^+$ which also present spectroscopic data are the calculation by Evett,[3] who employs a James-Coolidge type wave function, and the configuration interaction calculation using one-electron basis functions in confocal elliptical coordinates by Anex.[4] Unfortunately, these methods can be applied to systems with more electrons only with great difficulty at the present.[5] On the other hand, it has recently become possible to obtain SCF-LCAO-MO wave functions to the Hartree-Fock accuracy for systems with several electrons using high speed digital computers and programs constructed in this laboratory. Furthermore, it is well known that the expectation value for any one-electron operator computed in the Hartree-Fock approximation should coincide with the exact values to second order terms in a perturbation expansion of the exact wave function, in which the zeroth order term is the Hartree-Fock function for the system. Therefore, one purpose of this work was to

---

[2] D. P. Stevenson, D. O. Schissler, J. Chem. Phys. 24, 926 (1956); H. Gutbier, Z. Naturforsch. 12a, 499 (1957); T. F. Moran, L. F. Friedmann, J. Chem. Phys. 39, 2491 (1963) and references therein.

[3] A. A. Evett, J. Chem. Phys. 24, 150 (1956).

[4] B. G. Anex, J. Chem. Phys. 38, 1651 (1963).

[5] After this work was completed, a calculation on HeH^+ using a one-center wavefunction was published by J. D. Stuart and F. A. Matsen, J. Chem. Phys. 41, 1646 (1964).

obtain Hartree-Fock-Roothaan wave functions for the ground state of the first two molecules, $(HeH)^+$ and $(NeH)^+$, in the series of the rare gas hydride ions and then calculate expectation values, which should predict the experimental values with reasonable accuracy.

There are reasons to believe that the correlation energy in the rare gas hydride ions is approximately the same for the whole range of the internuclear distances, from the united atom to the separated atoms (rare gas atom and proton); this assumption will be discussed further in a later section of this paper. It implies that the Hartree-Fock and the exact potential energy curve are of the same shape and therefore, the potential curve for both molecules were calculated. Thus, in this special case the depth of the potential curve should also give a good value for the dissociation energy which cannot usually be obtained in such a direct way from a Hartree-Fock calculation for molecules other than the rare gas hydride ions. Such a potential curve will also be useful in proton-helium and proton-neon scattering calculations.

Charge density contours have also been calculated to give some insight into the electronic structure of these systems.

Since calculations for both molecules are treated to a comparable level of sophistication, I assume that conclusions based on the comparison of the present results for $(HeH)^+$ with those of Evett[3] and Anex[4] (which are assumed to be close to the exact solution of the Schrödinger equation) should apply in a similar manner to a comparison of the $(NeH)^+$ results to the exact solution.

II. GENERAL METHODS OF CALCULATION

The well known theoretical basis for this type of calculation is given by Roothaan,[6] the computational details are described in two recent articles by Wahl and Huo.[7] The calculations were carried out on a IBM 7094 using the HETEROPOLAR DIATOMIC SCF PROGRAM of this laboratory, chiefly written by Dr. W. Huo.

[6] C. C. J. Roothaan, Rev. Modern Phys. 23, 69 (1951).

[7] A. C. Wahl, "Analytic Self-Consistent Field Wave Functions and Computed Properties of Homonuclear Diatomic Molecules", J. Chem. Phys. 41, 2600 (1964).
W. Huo, "The Electronic Structures of CO and BF", (to be submitted for publication to J. Chem. Phys.).

A. The Construction of the Wave Function

The molecular wave function is an antisymmetrized product of molecular orbitals (MO's) which are expanded in terms of Slater-Type-Orbitals (STO's) centered on the nuclei. The set of STO's which is used in constructing the MO's is referred to as basis set composition for the total molecular wave function.

There exist no unique general rules concerning the number and the type of atomic orbitals which are necessary to represent a molecular orbital set with respect to accuracy and economy in computer time. However, considerable experience has been obtained in this laboratory in constructing Hartree-Fock-Roothaan wave functions with extended basis sets for different diatomic molecules, and the main features of this problem are discussed at length by Cade, Sales and Wahl.[8] Apparently the best way is to start with the Hartree-Fock basis set(s) for the substituent atoms and augment this basis set by additional functions which take polarization effects into account, and then to optimize all the orbital exponents of the basis set.

The Hartree-Fock energy for $He(1s^2, {}^1S)$ is obtained from a basis set of three functions ($1s(\zeta = 1.45)$, $2s(\zeta = 1.732)$, $2s'(\zeta = 2.641)$). Three additional functions were added to this basis set and then the energy was calculated for the $^1\Sigma^+$ state of $(HeH)^+$ at an internuclear distance of R = 1.44 B, which is, according to earlier publications,[3,4] close to the equilibrium internuclear distance. The exponents of the three additional functions were singly optimized first, and then the exponents of all six functions were singly reoptimized proceeding from the most important to least important STO in the expansion of the 1σ molecular orbital. Among all basis sets with a total number of six functions which were tried, the basis set with a supplementary polarizing σ3d STO centered at the He-nucleus and a σ1s and a σ2p STO at the H-nucleus seemed best. For this 4 × 2 set, as we shall subsequently refer to it, various double optimizations ($\sigma 1s_{He}$ and $\sigma 2s_{He}$, $\sigma 2s_{He}$ and $\sigma 2s'_{He}$, and $\sigma 1s_H$ and $\sigma 2p_H$) i.e., optimizations of two exponents simultaneously, were carried out in addition to the single optimizations mentioned previously. Part of the potential curve was calculated using this function and then at the value of the internuclear distance which corresponds to the minimum of this curve (R = 1.455 B., slightly larger than the first assumed value of 1.44 B.) all of the orbital exponents were again singly optimized.

---

[8] P. E. Cade, K. D. Sales and A. C. Wahl, "The Electronic Structure of Diatomic Molecules III. N_2 and N_2^+ Ions", (to be submitted to J. Chem. Phys. for publication).

Further extension of the basis set composition gave only a small improvement in the total energy, and with eleven functions in the MO-expansion the energy was almost independent of the basis set composition. (Calculations were made with several 7×4, 6×5 and one 5×5 set.) Finally, we chose a 7×5 set that gave a value for the energy which changed by less than 3×10^{-6} H. when another STO was added. All orbital exponents of this set were then optimized using both single and certain double optimizations. Thus two different final wave functions were obtained for HeH^+, a 4×2 set and a 7×5 set, both at R_e (calculated).

For NeH^+ we started with a basis set of 10 functions for Ne,[9] and made a few preliminary calculations with a molecular basis set of 14 functions, in which only the exponents of the 4 additional functions have been optimized, to find the approximate value for the equilibrium internuclear distance. At R = 1.9 a.u., which seemed to be close to R_e, various calculations were carried out in order to find the best basis set. Most of these calculations were done with a basis set of 24 functions. For NeH^+ a basis set of this size seems necessary to get a wave function with Hartree-Fock accuracy, and it is the upper limit which can be handled by the present program. It was not feasible to optimize exhaustively each of the different basis sets (an optimization of all exponents in the 4×2 set took approximately 20 min., in the 7×5 set $2\frac{1}{2}$ hours and for a set of 24 functions about 30 hours computation time on a IBM 7094) and therefore it was sometimes very difficult or even impossible to decide which of two basis sets, giving almost the same energy, would give better results after the optimization. The comparison could be made only with respect to the energy as no other properties of NeH^+ are known. The final choice of the $11 \times 5 \times 6 \times 2$ basis set with eleven σ-functions and six π-functions at the Ne-nucleus and five σ-functions and two π-functions at the H-nucleus might thus be arbitrary to some extent. The exponents of this set were then optimized at R = 1.9 B, but without any double optimizations. After part of the potential curve had been calculated with this function, R = 1.83 B. seemed to be a better approximation to R_e, and therefore we reoptimized all exponents at R = 1.83 B.

B. The Calculation of the Potential Curves

The potential curve for $(HeH)^+$ was first calculated using the 4×2 and 7×5 functions with orbital exponents optimized at R = 1.455 B., and the potential curve of

[9] P. S. Bagus, T. L. Gilbert, C. C. J. Roothaan and H. D. Cohen, "Analytic Self-Consistent Field Wave Functions for First-Row Atoms", (to be submitted to Phys. Rev.)

$(NeH)^+$ using the 11 × 5 × 6 × 2 basis set with orbital exponents optimized at R = 1.83 B.. These curves progressively lose accuracy at R values gradually decreasing or increasing from R_e(HF) since the orbital exponents in the wave functions have their optimal values only at the minimum of the curve. Therefore, one can expect to obtain a reliable Hartree-Fock potential curve only if the orbital exponents are optimized in some manner at several internuclear separations. In both the 4 × 2 and 7 × 5 basis sets for $(HeH)^+$ all orbital exponents were singly reoptimized at each R value considered. For the 11 × 5 × 6 × 2 basis set of $(NeH)^+$, fifteen of the twenty-four orbital exponents, mainly those which seemed to be the most important and sensitive to a change in the internuclear distance, were singly reoptimized at most R values employed.

C. The Calculation of the Charge Density Contours

The total electronic charge density, $\rho(\vec{r})$, for a single determinant wave function, constructed from N doubly occupied MO's can be obtained as;

$$\rho(\vec{r}) = \sum_{i=1}^{N} 2 \, |\varphi_i(\vec{r})|^2 \, , \tag{1}$$

where φ_i are the MO's, or in terms of STO's, χ_{ki} as;

$$\rho(\vec{r}) = \sum_{i=1}^{N} 2 \, |\sum_k c_{ik} \, \chi_{ki}|^2 \, , \tag{2}$$

where c_{ik} are the linear expansion coefficients of the molecular orbital, $\varphi_i(\vec{r})$. The corresponding partial charge density for a single MO, $\rho(\vec{r})$, can be calculated from:

$$\rho_i(\vec{r}) = 2 \, |\sum_k c_{ik} \, \chi_{ki}|^2 \, . \tag{3}$$

These calculations for $(HeH)^+$ and $(NeH)^+$ for several R values were carried out using a charge density program constructed by Dr. Sinai and Mr. Olive of this laboratory.

III. RESULTS AND DISCUSSION

A. The $(HeH)^+$ Molecule Ion

Tables 1 and 2 present the 4 × 2 and 7 × 5 Hartree-Fock-Roothaan wave functions for $(HeH)^+$ at R_e(HFR), respectively and also the energy quantities for the ground state. Inspection of the results in these two tables shows that the improvement of the larger basis set (7 × 5 basis set) is small with regard to the total energy.

The contribution of all six atomic orbitals in the 4 × 2 set is considerable, whereas the $6 3d_{He}$, the second $6 2s_{H}$, the $6 3d_{H}$ and especially the $6 4f_{He}$ orbital in the 7 × 5 set seem to be of little importance. However, this $6 4f_{He}$ function gave an energy improvement of approximately 1.5×10^{-5} H. which could not be obtained from the set without this orbital just by changing the exponents of the other remaining functions. Several calculations have also been performed with additional 61s, 62s, 62p or 3d AO's for He, and 62p and 64f orbitals for H, using two or three different values for their exponents, but we did not include these functions in the final basis set because their effect seemed negligible. The largest energy variation (adding the $6 2p_{H}$ or $6 4f_{H}$ orbital) was approximately 3×10^{-6} H.. A second optimization of the exponents of the original basis set (without additional functions) gave about the same value.

In Fig. 1, we plotted the potential energy curves for HeH^{+}, which we obtained by using the different basis sets. Curves A and B result from the 4 × 2 and 7 × 5 sets respectively, with the exponents optimized only at the equilibrium internuclear distance. The 7 × 5 basis set yields the curve B', if the optimization is done at each internuclear separation. Table 3 lists the corresponding values and also the results for the 4 × 2 basis set optimized at each internuclear distance (column A'). In the scale of Fig. 1 this curve could hardly be distinguished from curve B' and for this reason has not been included there. The few energy values which are in brackets have not been calculated by carrying out the optimization for the exponents but by using ζ-values that have been interpolated for that particular R-value from the neighboring calculated exponents. For two R-values the energy has been determined in both ways and the agreement found to be better than 10^{-6}B.. Thus, we expect these values in brackets to have the same accuracy as the other values given in this table.

The wave functions for the different points on the potential curve have also been obtained but are not listed here. These results are available upon request.

An interesting feature of Fig. 1 is the fact that the general behavior of the potential energy curves is correct for large internuclear separations; the curve approaches the Hartree-Fock energy of the separated atoms He and H^{+} (the horizontal dashed line in Fig. 1). This behavior cannot usually be obtained by a single determinant wave function, but rather requires at least mixing of several configurations. However, in this special case of the rare gas hydride ions we expected it. Assuming that the correlation energy in the separated atoms and in the molecule at every internuclear separation is approximately the same, one should be able to calculate a potential curve which is shifted in comparison to the exact one by the correlation energy of He,

major
but shifted as a whole without/distortions. This assumption seems reasonable because both in the separated atoms and in the molecule we have a 2-electron system with one doubly occupied shell; in terms of configuration mixing He - H^+ is the most important configuration, and a configuration with significantly different correlation energy (He^+ - H) should be of little importance (perhaps very small R values excluded) since the ionization energy of He is much higher than that of H.

The 7 × 5 set has more flexibility than the 4 × 2 set and therefore at larger R values gives much better values for the energy than the 4 × 2 set, so that the difference between the two curves A and B, which is relatively small at the equilibrium separation, increases considerably when moving further apart from R_e. The behavior of the curve B' compared to B is to be expected. The corresponding values from the 4 × 2 set also behave as expected as can be seen from column A and A' in Table 3. Remarkable is the fact that for R = 2.8 B. and all larger R values the numbers in column A' are lower than those in column B , which means that the larger and more flexible basis set with non-optimized exponents is not able to give the same improvement in the energy as a poorer function with properly chosen exponents.

One further comment may be of some interest: the energy values at larger internuclear distances are approximately proportional to R^{-4}, as one would have expected for the potential between a charge and an induced dipole. Stuart and Matsen[5] noticed also this E vs. R^{-4} behavior in their calculation and discussed it in detail.

From the description of the whole calculation it has probably become clear that great effort has been made to get an energy as low as possible. There exist no exact experimental data with which to compare our results; therefore, it is difficult to ascertain how closely convergence has been obtained in the procedure of adding basis functions to a small set. In comparison to extended calculations which have been performed in a similar way for several other molecules where such comparisons are possible,[10] our calculated energy should certainly be within Hartree-Fock accuracy. The same conclusion can be drawn from Table 4 which compares the energy values of the optimized 7 × 5 function with the most accurate values for HeH^+ that are so far available. The difference between these values is fairly constant over the whole range of R values from 1 B. to 2.2 B. but is slightly smaller than the correlation energy of He (0.042044 H.), probably due to the fact that the values in the first row are still not exact, especially at larger R values where the difference should certainly approach

[10] Private communications from W. Huo for CO and BF, P. Cade for N_2 and Li_2, and P. Cade and W. Huo for first row hydrides. Also see Refs. 7 and 8.

the correlation energy of He. Furthermore, the last row of this table supports our assumption concerning the shape of the potential energy curve.

Very recently the Hellmann-Feynman forces acting on the nuclei in a molecule have been investigated and they turned out to be very sensitive with respect to a small deviation in the wave function from the exact Hartree-Fock solution. Kern and Karplus[11] have shown that even wave functions yielding the same total energy may give results for these forces which differ considerably, especially for the force acting on the heavier nucleus. The Hellmann-Feynman force $\vec{F}_N$, acting on the nucleus N is defined by the relation:

$$\vec{F}_N = -\langle\psi|\nabla_N \mathcal{H}|\psi\rangle = -Z_N e^2\left[\sum_{\alpha \neq N} \frac{Z_\alpha \vec{R}_{\alpha N}}{R_{\alpha N}^3} - \langle\psi|\sum_k \frac{\vec{r}_{Nk}}{r_{Nk}^3}|\psi\rangle\right], \qquad (4)$$

where k refers to the electrons and α to the nuclei of the system.

It is a necessary condition that the exact Hartree-Fock wave function for HeH^+ must satisfy the relation $\vec{F}_{He} = \vec{F}_H = 0$ for the equilibrium internuclear distance and $\vec{F}_{He} = \vec{F}_H$ at each internuclear distance. Any difference between these two quantities indicates that one still does not have the exact Hartree-Fock function and moreover, that not only the force but also the other calculated properties might differ from their corresponding exact values by the same order of magnitude.

For a linear molecule such as HeH^+ only the force component along the internuclear axis is of importance since all the other components are zero by symmetry. Fig. 2 represents these forces on the He and H nucleus obtained from the 4 × 2 set and 7 × 5 set where the optimization is carried out at each R value, and the curve for the 7 × 5 set where the exponents have been optimized only at R = 1.455 B.. The force F_N is chosen to be positive if the force points from the nucleus N toward the other nucleus.

For the force on the proton only the curve for the 7 × 5 set optimized at each internuclear distance was plotted: the two other curves would lie (in the medium range of R values) within about .002 a.u. on either side of the plotted curve, the 7 × 5 curve (exponents optimized at R_e) above and the 4 × 2 curve below, and would intersect with the 0-line at R = 1.463 B.. But there are fairly sizeable differences between the three plotted curves for the force on the He-nucleus, although the potential energy curve obtained from the corresponding wave functions almost coincide.

[11] C. W. Kern and M. Karplus, J. Chem. Phys. 40, 1374 (1964).

These facts are consistent with the results Kern and Karplus[11] found in comparing several wave functions for the HF molecule. At the equilibrium distance where the forces should be zero, the proton force differed in the five wave functions under consideration from +.084 a.u. to -.017 a.u.,[12] but only by .005 a.u. for the two wave functions yielding almost the same energy; whereas the difference in the fluorine force for these two wave functions was .676 a.u., and including the other three wave functions the values for the F-force varied from .103 to 3.10 a.u..

Since the general appearance of curve A' and B' of Fig. 2 is the same, the difference between the 4 × 2 and 7 × 5 basis set seems to be reflected mainly in the He-force which is too high for the smaller set. From this we may conclude that the 4 × 2 set is a good representation for the He- core, which is necessary to give a good value for the total energy, but it does not account satisfactorily for polarization effects: that is, too much charge is concentrated around the He-nucleus and there is a deficiency of charge in the bonding region between the two nuclei. The greater flexibility of the larger basis set is able to build up a higher density between the two nuclei and thus reduces the force on the He-nucleus; this shift of charge into the bonding region is, as we shall learn later from the charge density calculations, the main difference between the two basis sets.

The shortcoming of a calculation in which a wave function with the orbital exponents optimized only at the equilibrium distance is used to calculate the whole potential curve can clearly be seen from the curve B. This curve even predicts values for the He-force at large internuclear distances where all curves should approach zero. This behavior can be explained by recalling the fact that the exponents are related to a special electron distribution at R_e, but that the distribution changes at larger R. In fact the charge cloud is concentrating towards the He-nucleus and the flexibility in the wave function due to the linear coefficients in the MO expansion alone is not sufficient to give a proper description of this readjustment. Thus, if the exponents are held fixed, charge is shifted too far from the He-nucleus and the second term in the above formula (4) becomes too small and eventually the first term outweighs the second.

The condition $F_{He} = F_H$ is satisfied to high accuracy, only by the large basis set, and only if the exponents are optimized at each internuclear distance. In Fig. 2 the force on the He-nucleus appears to be reflected image of the force on the proton.

[12] 1 a.u. of force = 8.2378×10^{-3} dyn.

However, a more careful consideration shows that the forces are not exactly of equal magnitude; the difference between the He-force and the H-force is approximately .003 a.u.. This difference is approximately constant over the whole range of the internuclear distances, which is certainly of importance. The fact that it is not exactly zero might be somewhat disappointing at first, although this result is superior to the results found for the HF functions.[11] On the other hand, for a point of the potential curve which we had obtained both by carrying out the optimization procedure for the exponents and by using the interpolated exponents we found the energy differed by only a few units in the 7th decimal place, yet the difference between the $F_{He} - F_H$ values was about .0005. Therefore, we feel the difference of .003 to be very close to the lower limit that we can hope to get with a function such as we are using, at least over a whole range of internuclear distances.[13]

Table 5 lists the spectroscopic data obtained from the several calculations. The first and second row contains for comparison the data given in the earlier calculations.[3,4] The values in the 3rd and 4th row and in the 6th and 7th row have been calculated as described in Herzberg[14] from a polynomial fitted through the different points of the potential energy curve. In each case we averaged over six calculations using polynomials of 8th, 9th and 10th degree through different combinations of points. The difference between values obtained in this way from the different basis sets is small, as we had already expected, since the shape of the corresponding potential energy curve near the minimum, which is the important part for the calculation of the spectroscopic constants, is almost the same. Optimizing the exponents at each R value decreases the curvature and is reflected in the slightly larger R_e- and $\omega_e x_e$- values. The values for the equilibrium internuclear distance given in the 5th and 8th row is obtained from the virial theorem, which requires the ratio of kinetic energy T and potential energy V to be -2 at R_e. These R_e values are interpolated from the E/V values at R = 1.4, 1.455 and 1.5 B.. The 9th and 10th row contain the equilibrium

[13] For some R values $F_{He} = F_H$ might be exactly satisfied. This is true for the 7 × 5 set (opt. at 1.455 B.) between R = 1.0 B. and 1.2 B. and between 1.3 B. and 1.4 B. where the difference $F_{He} - F_H$ changes sign, but we assume this exact equality to be coincidental. See also the corresponding discussion for NeH^+.

[14] G. Herzberg, Spectra of Diatomic Molecules (D. Van Nostrand Co., Inc., Princeton New Jersey, 1950), 2nd ed. pp. 90 ff.

distance and the force constant derived from the force curve of Fig. 2. The F_{He} and F_H curve have been approximated by a parabola through the points R = 1.4, 1.455 and 1.5 B.; the first value is derived from the F_H curve, the second from the intersection of both curves.

From all these calculations of the equilibrium distance we may draw the conclusion that this value is certainly larger than the values given in the two earlier calculations although we are not able to give the exact figure for the third decimal place, which is consistent with the fact that $F_{He} - F_H$ is zero only to approximately 3 figures. The dissociation energy listed in the last column of the above table is in good agreement with the calculated value of Anex and also with the experimental value listed in the last row, the accuracy of which is not exactly known.[15]

One remark might be necessary here: the binding energy has been calculated as the difference between the calculated total molecular energy, which is believed to be within Hartree-Fock accuracy, and the Hartree-Fock energy of the separated atoms. Therefore, the deviation of the number given in the above table from the exact value depends only on the correlation energy in both systems. A difference of 0.001 H. in the correlation energy, which might occur, would change the calculated binding energy by about .03 eV.

One of the important properties of a diatomic molecule that can be calculated, is its dipole moment. Since this depends for an ion on the location of the origin of the coordinate system, we calculated a related quantity, the center of negative charge. Table 6 gives the distance of the center of negative charge from the He-nucleus. We also include the results of the 4 × 2 basis set to show the difference which arises when such an expectation value is calculated from both basis sets directly and not determined from energy values. We will come back to this difference in the discussion of the NeH^+ results. All our values differ from those calculated by Anex[4] by approximately the same amount as did the values for the equilibrium distance. It can be seen from this table that the values have a maximum near the equilibrium distance and decrease at larger R values. This means that if the proton is within a distance from the He-nucleus smaller than R_e the charge cloud tends to follow it, but as the distance between proton and He-nucleus increases from R_e the charge cloud moves steadily back towards the unperturbed position which it would have in the He atom.

[15] W. Kaul, U. Lauterbach, R. Taubert, Z. Naturforsch. 16a, 624 (1961).

This behavior of the charge cloud is also reflected in some other expectation values which have also been calculated; for instance in the expectation value of z^2, and to some extent in those of r_{He}^{-1} and r_{He}^{2}, where the expectation value of r_{He} is the mean distance of the charge cloud from the He-nucleus. The expectation value of x^2(x-axis perpendicular to the molecular axis through the He-nucleus) which is a measure for the size of the charge cloud in a plane including the He-nucleus perpendicular to the molecular axis, increases monotonically with R toward a certain limit. The charge cloud behavior can also be illustrated by the charge density contours, which we plotted for several internuclear distances in Fig. 3, a-d. We chose values for the internuclear separation which correspond to points on the replusive and the attractive part of the potential energy curve, to the equilibrium distance, and to a point close to the dissociation limit. The solid lines in all 4 figures refer to the same density contours respectively; additional dashed lines have been included at times to give more detailed information about the contour in a particular region.

A look at this whole series of figures might give us a very instructive picture of the way in which the dissociation in such a rare gas hydride ion might occur. Fig. 4 shows the charge density along the internuclear axis for several R values.

On the whole, we would have expected this shape of the density contours: in the immediate neighborhood of the He-nucleus they resemble spherical ellipsoids, slightly polarized and the degree of this polarization depending on the position of the proton; in the outer region of the molecule they approach ellipses whose eccentricity is smaller at small R values where the dissociation almost occurs; in the intermediate region a pear shape is evident.

The general appearance is the same regardless which function we use to calculate the electron density. Only a careful study shows that there are differences: the 4×2 set with only two orbitals at the H-nucleus tends to pile up charge around the proton, consequently there appears in Fig. 4 a small but rather distinct peak at the position of the proton, whereas the 7×5 set distributes the charge more equally in the bonding region, so that rather a shoulder than a peak appears. This increase of electron density in the bonding region is partly due to a shift of charge from the H-nucleus into that region, but mainly to such a shift from the He-nucleus towards the proton, which is also the reason for the decrease of the He-force mentioned previously.

A consideration of Fig. 3 would suggest that a one-center expansion might give reasonable results for the total energy; but a basis set of 10 partly optimized functions gave an energy of only -2.910 H. which was not very encouraging; and since computational difficulties (degeneracies) arose when going to larger basis sets, this study has not been carried further.[16]

[16] The extensive calculation by Stuart and Matsen (see Ref. 5) shows indeed, that a one-center expansion is able to give excellent results for HeH^+.

B. The $(NeH)^+$ Molecule Ion

The calculations for NeH^+ were analogous to the calculations for HeH^+ and the results are listed in the same order.

Table 7 presents details about the 11 × 5 × 6 × 2 basis set which we have used for the NeH^+ calculations and shows the energy for the ground state of NeH^+ obtained with this function. From the coefficients in this table it may be seen that the several orbitals which we have added to the atomic set (d and f functions on the Ne-nucleus and all hydrogen orbitals) are negligible in the 1σ MO, but they contribute to all of the other three molecular orbitals.

Fig. 5 shows the potential energy curve for NeH^+. The dashed curve is the result if the orbital exponents are optimized only at R = 1.83 B.. The solid curve results if those exponents which seem to be most sensitive with respect to a variation in the internuclear distance are optimized at each R value. The optimized ζ value for the $\sigma 1s_{Ne}$ exponent remains the same when varying the internuclear distance. This was to be expected considering the fact that its value in the free atom and in the molecule is practically the same. Most sensitive are of course the values of the outer orbitals, especially of those which have been added to the atomic set. Furthermore, it is worthwhile to note that among these the orbital exponents in the π symmetry are more sensitive with respect to a change in the internuclear separation than the corresponding orbital exponents in the σ symmetry. A reoptimization at each R value was also important for some of the $2p_{Ne}$ exponents; they do not change as much as the $3d_{Ne}$ or $2s_H$, $2p_H$ or $3d_H$ exponents, but the magnitude of the 2p orbital contribution to the total energy is quite large. A reoptimization of the 2s exponent was found to have little influence.

The wave functions for the different points at the potential curve have been tabulated but are not included here for the same reason as before.

Table 8 lists the numerical data for the potential curves. The values in brackets have been obtained (as in Table 3) from calculations in which we used interpolated values for the exponents.

The general appearance for the potential energy curve for NeH^+ is the same as for HeH^+. For large internuclear distances the curve approaches the Hartree-Fock energy of the separated atoms (the dashed line in Fig. 5). The effect of lowering the energy at larger distances due to the optimization of the exponents at each R value is greater than it was for the 7 × 5 set of HeH^+ but smaller than for the 4 × 2 set. This

might lead to the conclusion that the flexibility of the NeH^+ basis is better than of the 4 × 2 set but inferior to that of the 7 × 5 set as we would expect, since the flexibility is primarily due to the number of basis functions of each symmetry which were added to the Hartree-Fock atomic set. However, we should be very careful at this point since we did not optimize all the exponents at each internuclear distance.

The behavior of the force curve in the neighborhood of the equilibrium distance is similar to the behavior of the corresponding curve of the 4 × 2 set in Fig. 2. The force on the Ne-nucleus is too large, and therefore the difference between the force on the neon and on the hydrogen nucleus is not zero; at R = 1.83 B. this value is .028 a.u., only slightly smaller than the corresponding difference for the 4 × 2 basis set of HeH^+ which might suggest that the accuracy of this neon function at R_e is only slightly better than that of the smaller HeH^+ basis set but much inferior to the accuracy of the large basis set of HeH^+. However, this difference does not remain constant over the range of the internuclear separations; it decreases with increasing R values and at R = 2.7 B. it is only .0004 a.u.. This behavior seems to be due to the combination of two effects which can be seen from Fig. 2 from the dashed and dotted curve: the general shortcoming representing the electron density accurately in the bond region and the consequent high force on the He-nucleus (this corresponds to the dashed line) is partly overcome by the fact that the orbital exponents are not fully optimized (this is indicated by the dotted curve). The result is an exact equality of the forces near R = 2.7 B.. This might happen for any wave function at a particular R value, even if the energy is far off from the correct value.[17] Therefore, we have to be very careful in judging a wavefunction only with respect to the equality condition for the forces at one particular point of the potential curve and must remember that this equality condition is only a necessary condition for a Hartree-Fock solution.

At large values the F_{Ne} curve approaches zero but does not take negative values. From this we may estimate the error arising from the fact that the optimization has not been carried out for all 24 orbital exponents (see Fig. 2). In summarizing all our considerations concerning the accuracy of our NeH^+ function we may conclude that this function is slightly better at the equilibrium distance and slightly

[17] The well known situation, where a poor function gives good values for some properties and gives poorer values when the function is improved by an optimization of the orbital exponents or an expansion of the basis set, might be explained in a similar way.

worse for R values farther away, than the 4 × 2 set is for HeH^+ (optimized at each R). The same is consequently also true for the expectation values for a one electron operator. How much such a value differs from an expectation value calculated with a function of much higher accuracy might be seen from Table 6. With respect to the energy this means that we can expect the NeH^+ potential energy curve to lie compared to the HeH^+ curves approximately at the same point or slightly below the dashed line of Fig. 1 at the equilibrium distance and at larger R values between the solid and the dotted curve close to the latter.

Table 9 presents the spectroscopic data for NeH^+. The first row contains the data which Moran and Friedmann[18] obtained by using Platt's electrostatic model. The next few rows present the results of our calculations. The main difference between the next two rows is again the larger $\omega_e x_e$ value which results from the optimization at each internuclear distance. The R_e value in the 4th row has been calculated by interpolating between the E/V values at R = 1.8, 1.83 and 1.9 B.. The R_e value in the next to the last row has been determined from a plotted force curve; a correct interpolation could not be carried out since the available calculated values were not grouped close enough to the minimum. For the same reason the k_e value is missing in that row. The calculated dissociation energy is in good agreement with the experimental value.[15,19]

It can be seen from Table 10 that the general behavior of the charge cloud for NeH^+ is the same as for HeH^+, and the expectation values of z^2, r_{Ne}^{-1} and r_{Ne}^{2} again indicate this behavior. The absolute values for the distance of the center of negative charge from the Ne-nucleus are smaller.

The general appearance of the total electron distribution in Fig. 6 resembles that of HeH^+. At the equilibrium distance the proton has penetrated the same distance into the charge cloud in both molecules, and a preliminary study of AH^+ showed that the proton at the equilibrium distance is also just within the .2 contour. This fact is not surprising if one remembers the success of the Platt model which has recently been applied to hydride ions and which assumes that the total charge beyond a sphere of radius R_e is the same for all three molecules. Fig. 7. a-d, shows the charge density maps of the different molecular orbitals, and Fig. 8 the corresponding charge along the internuclear axis.

[18] T. F. Moran, L. Friedmann, J. Chem. Phys. 40, 860 (1964).

[19] T. F. Moran, L. Friedmann, J. Chem. Phys. 39, 2491 (1963).

From Fig. 7a and Fig. 8, it is clear that the 1σ MO is almost unaffected by the presence of the proton. We came to the same conclusion in considering the expansion coefficients of Table 7. The π electron density also is not very perturbed, as may be seen from Fig. 7d; the contours are slightly asymmetrical with respect to the x axis (perpendicular to the molecular axis through the Ne-nucleus). Most affected are the 2σ and 3σ MO's. The 3σ orbital is strongly polarized towards the proton and almost resembles a 62p function. However, the charge distribution in the immediate neighborhood of the Ne-nucleus and in the region opposite the hydrogen seems to be little affected, although there is a small shift of the nodal plane (Fig. 8). On the other hand, the polarization of the 2σ orbital is quite large in the region relatively close to the Ne-nucleus and in the region opposite the proton. Charge is piled up in the bond region and decreased on the other side of the Ne-nucleus, which gives rise to the asymmetric shape of the contour close to the Ne-nucleus. This asymmetry increases at smaller internuclear separations which means that in Fig. 7b more of these "moon shape" contours will appear.

From these considerations it appears that both the 2σ and 3σ MO's play a role in the formation of the bond. The magnitude of their contribution varies in the different areas of the bonding region, the 2σ being more important near the Neon and the 3σ becoming more important near the Hydrogen nucleus.

ACKNOWLEDGMENTS

I am very grateful to Professor Mulliken and Professor Roothaan for their hospitality in the Laboratory of Molecular Structure and Spectra. I wish to express my thanks to all the members of the Laboratory for many stimulating discussions, and finally, to the Cusanuswerk for financial support.

TABLE 1. THE 4 × 2 HARTREE-FOCK-ROOTHAAN WAVEFUNCTION FOR THE GROUND STATE OF HeH^+ ($1\sigma^2, {}^1\Sigma^+$) AND ENERGY QUANTITIES AT R = 1.455 B.[a]

Basis Functions χ_k		$c_{1\sigma,k}$
$\sigma 1s_{He}$	(ζ = 1.83692)	.91271
$\sigma 2s_{He}$	(3.18073)	-.04743
$\sigma 2s'_{He}$	(1.60271)	-.03009
$\sigma 2p_{He}$	(2.26480)	.03513
$\sigma 1s_{H}$	(1.51431)	.23680
$\sigma 2p_{H}$	(1.91503)	.04154
$\epsilon_{1\sigma}$	-1.63751	
E	-2.932325	

[a] $c_{1\sigma,k}$ are coefficients of normalized AO's χ_k, ζ orbital exponents; total energy E and orbital energy $\epsilon_{1\sigma}$ in Hartree, 1 H = 27.2097 eV, internuclear distance R in Bohr, 1 B = 0.52917×10^{-8} cm.

TABLE 2. THE 7 × 5 HARTREE-FOCK-ROOTHAAN WAVEFUNCTIONS FOR THE GROUND STATE OF HeH^+ ($1\sigma^2, {}^1\Sigma^+$) AND ENERGY QUANTITIES AT R = 1.455 B.[a]

Basis Functions χ_k		$c_{1\sigma,k}$
$\sigma 1s_{He}$	(ζ = 1.37643)	1.19873
$\sigma 1s'_{He}$	(3.87107)	.04345
$\sigma 2s_{He}$	(1.54335)	-.46038
$\sigma 2p_{He}$	(2.64576)	.06404
$\sigma 2p_{He}$	(3.24082)	-.03015
$\sigma 3d_{He}$	(2.54147)	.00593
$\sigma 4f_{He}$	(3.73526)	.00119
$\sigma 1s_{H}$	(1.00949)	.40973
$\sigma 2s_{H}$	(1.18036)	-.21100
$\sigma 2s'_{H}$	(2.56229)	.00692
$\sigma 2p_{H}$	(1.79089)	.04454
$\sigma 3d_{H}$	(2.41228)	.00642
$\epsilon_{1\sigma}$	-1.63748	
E	-2.933126	

[a] Notation as in Table 1.

TABLE 3. THE TOTAL ENERGY OF $HeH^+(1\sigma^2, {}^1\Sigma^+)$ AS A FUNCTION OF INTERNUCLEAR SEPARATION

R (B.)	Energy (H.)			
	4 × 2 Basis Set[a]		7 × 5 Basis Set[a]	
	A	A'	B	B'
1.0	-2.857919	-2.860478	-2.860566	-2.861036
1.2	-2.916006	-2.916651	-2.917221	-2.917390
1.3	-2.927219	-2.927431	-2.928148	-2.928206
1.4	-2.931777	-2.931800	-2.932588	-2.932594
1.455	-2.932525	-2.932325	-2.933126	-2.933126
1.5	-2.932010	-2.932026	-2.932825	-2.932830
1.6	-2.929500	-2.929644	-2.930403	-2.930450
1.7	-2.925336	-2.925693	-2.926376	-2.926500
1.8	-2.920236	-2.920883	-2.921462	-2.921683
2.0	-2.909106	-2.910421	-2.910760	-2.911205
2.2	-2.898462	-2.900422	-2.900535	-2.901201
2.5	-2.885294		-2.887848	-(2.888782)
2.8	-2.875905	-2.879129	-2.878680	-2.879782
3.15	-2.868938		-2.871666	-(2.872847)
3.5	-2.864957	-2.868262	-2.867442	-2.868619
4.0	-2.862206		-2.864273	-(2.865341)
4.5	-2.861094	-2.863593	-2.862837	-2.863752

[a]Columns A and B, for the 4 × 2 and 7 × 5 set respectively, were obtained using the orbital exponents optimized only at R = 1.455 Bohr. Columns A' and B', for the 4 × 2 and 7 × 5 set respectively, were obtained using optimal orbital exponents at each R value cited or interpolated values (in parenthesis).

TABLE 4. COMPARISON OF THE TOTAL ENERGY FOR HeH^+ FROM THE CALCULATION OF ANEX[4] AND THIS CALCULATION.[a]

R	1.0	1.4	1.8	2.2
E (Anex)	-2.90160	-2.97424	-2.96471	.2.94035
E (This calculation)	-2.86104	-2.93259	-2.92168	-2.90120
Difference	.04056	.04165	.04103	.03915

[a]Energy values in H., values of the internuclear separation in B.

TABLE 5. SPECTROSCOPIC DATA FOR HeH^+ OBTAINED FROM THE DIFFERENT CALCULATIONS

Calculation	R_e (B.)	B_e (cm^{-1})	ω_e (cm^{-1})	$\omega_e x_e$ (cm^{-1})	k_e ($10^5 \frac{dyn}{cm}$)	α_e (cm^{-1})	D_o (eV)	Zero point energy (eV)	D_e (eV)
Evett[a]	1.432		3500				1.9	.22	1.68
Anex[b]	1.446		3286				1.931	.204	1.727
4×2 Set A (Dunham)[c]	1.4550	35.32	3306	157	5.18	2.75	1.9219	.205	1.717
4×2 Set A' (Dunham)	1.4451	35.31	3229	179	4.95	2.84	1.9219	.200	1.722
4×2 Set A (Virial)[d]	1.4553								
7×5 Set B (Dunham)	1.4553	35.30	3257	167	5.03	2.71	1.9437	.202	1.742
7×5 Set B' (Dunham)	1.4554	35.30	3233	176	4.96	2.82		.200	1.743
7×5 Set B (Virial)	1.4557								
7×5 Set B(F_N curve)[e]	1.452				4.97				
	1.459				4.925				
Experiment[f]									1.79

[a] See Ref. 3.
[b] See Ref. 4.
[c] Calculated using the Dunham analysis.
[d] Calculated using $\partial E/\partial R$ and the Virial theorem.
[e] Calculated using the force curve, F_N.
[f] See Ref. 15.

TABLE 6. DISTANCE z OF THE CENTER OF NEGATIVE CHARGE FROM THE He-NUCLEUS FOR DIFFERENT INTERNUCLEAR DISTANCES R.

R(Bohr)	z(Bohr)		
	4×2 Set	7×5 Set	Anex[a]
1.0	.2214	.2202	.22554
1.2	.2326	.2315	
1.3	.2348	.2337	
1.4	.2348	.2338	.24624
1.455	.2340	.2331	
1.5	.2329	.2320	
1.6	.2293	.2286	
1.7	.2242	.2236	
1.8	2179	.2174	.23427
2.0	.2022	.2019	
2.2	.1838	.1837	.20027
2.8	.1254	.1259	
3.5	.0730	.0743	
4.5	.0368	.0377	

[a]See Ref. 3. Also note that the values of Anex are corrected values, not the values given originally in this paper. (B. G. Anex, private communication.) Exponents optimized at each R-value.

TABLE 7. THE 11 × 5 × 6 × 2 HARTREE-FOCK-ROOTHAAN WAVE FUNCTIONS FOR THE GROUND STATE OF $NeH^+(1\sigma^2 2\sigma^2 3\sigma^2 1\pi^4, {}^1\Sigma^+)$ AND ENERGY QUANTITIES AT R = 1.83 B.[a]

Basis Functions χ_k		$c_{1\sigma,k}$	$c_{2\sigma,k}$	$c_{3\sigma,k}$	$c_{1\pi,k}$
$\sigma 1s_{Ne}$	(ζ = 8.91020)	.94299	-.28499	.04349	
$\sigma 1s'_{Ne}$	15.25118	.08902	.00826	-.00139	
$\sigma 2s_{Ne}$	2.35322	-.00081	.48004	-.08490	
$\sigma 2s'_{Ne}$	3.67914	.00394	.58099	-.10651	
$\sigma 3s_{Ne}$	11.15634	-.03390	-.02502	.00424	
$\sigma 2p_{Ne}$	1.64063	-.00002	.01418	.16696	
$\sigma 2p'_{Ne}$	2.51232	-.00046	.04777	.54621	
$\sigma 2p''_{Ne}$	4.88404	.00072	.01214	.25216	
$\sigma 2p'''_{Ne}$	11.15553	.00030	.00096	.00743	
$\sigma 3d_{Ne}$	2.48734	-.00016	.01169	.03695	
$\sigma 4f_{Ne}$	3.14362	-.00003	.00320	.00824	
$\sigma 1s_{H}$	1.73096	.00036	-.10150	.13756	
$\sigma 1s'_{H}$	2.12470	-.00017	.12141	.02273	
$\sigma 2s_{H}$	2.17392	.00019	.04441	.04288	
$\sigma 2p_{H}$	2.32609	.00018	.01563	.02087	
$\sigma 3d_{H}$	3.10413	.00003	.00341	.00269	
$\pi 2p_{Ne}$	1.81230				.34210
$\pi 2p'_{Ne}$	2.77094				.46612
$\pi 2p''_{Ne}$	4.92893				.25683
$\pi 2p'''_{Ne}$	10.61784				.00939
$\pi 3d_{Ne}$	2.39912				.02098
$\pi 4f_{Ne}$	3.22623				.00492
$\pi 2p_{H}$	1.79232				.01929
$\pi 3d_{H}$	2.54963				.00482
ϵ_i(H.)		-33.35881	-2.49750	-1.45857	-1.38468
E (H.)		-128.62836			

[a] $c_{i,k}$ are coefficients of normalized AO's χ_k, ζ orbital exponents, ϵ_i orbital energies and E the total energy.

TABLE 8. THE TOTAL ENERGY OF $NeH^+(1\sigma^2 2\sigma^2 3\sigma^2 1\pi^4, {}^1\Sigma^+)$ AS A FUNCTION OF INTERNUCLEAR SEPARATION.[a]

R (B.)	Energy (H.)	
	A	A'
1.35	-128.53871	-128.53942
1.5	-128.59536	(-128.59568)
1.6	-128.61454	-128.61469
1.7	-128.42663	(-128.62448)
1.8	-128.62812	-128.62812
1.83	-128.62836	-128.62836
1.9	-128.62773	-128.62773
2.0	-128.62472	(-128.62479)
2.1	-128.62010	(-128.62026)
2.2	-128.61457	-128.61492
2.4	-128.60260	-128.60330
2.7	-128.58579	-128.58728
3.0	-128.57248	(-128.57470)
3.5	-128.55826	-128.56128
4.0	-128.55110	-128.55418
4.5	-128.54776	-128.55089

[a]Calculation A employs orbital exponents optimized only at R = 1.83 Bohr. Calculation A' employs orbital exponents optimized at each R value except those in parenthesis which interpolated orbital exponents were used.

TABLE 9. SPECTROSCOPIC DATA FOR NeH^+

Calculation	R_e (B.)	B_e (cm^{-1})	ω_e (cm^{-1})	$\omega_e x_e$ (cm^{-1})	k_e ($10^5 \frac{dyn}{cm}$)	α_e (cm^{-1})	D_o eV	Zero point energy (eV)	D_e (eV)
Platt Model[a]	1.53				5.52				
Set A (Dunham)[b]	1.836	18.52	3069	122	5.35	1.13	2.212	.190	2.022
Set A' (Dunham)	1.836	18.52	3053	141	5.29	1.21	2.212	.189	2.023
Set A (Virial)[c]	1.833								
Set A (F_N curve)[d]	1.81-1.82								
Experimental[e]									2.15±.25

[a]See Moran and Friedmann, Refs. 18 and 19.
[b]Calculated using the Dunham analysis.
[c]Calculated using $\partial E/\partial R$ and the Virial theorem.
[d]Calculated using the force curve, F_N.
[e]See Ref. 15.

TABLE 10. DISTANCE z OF THE CENTER OF NEGATIVE CHARGE FROM THE Ne-NUCLEUS FOR DIFFERENT INTERNUCLEAR DISTANCE R.[a]

R (Bohr)	1.35	1.6	1.83	2.2	2.7	3.5	4.5
z (Bohr)	.0550	.0592	.0604	.0574	.0472	.0383	.0238

[a]Values are calculated using the basis set with exponents optimized at each R.

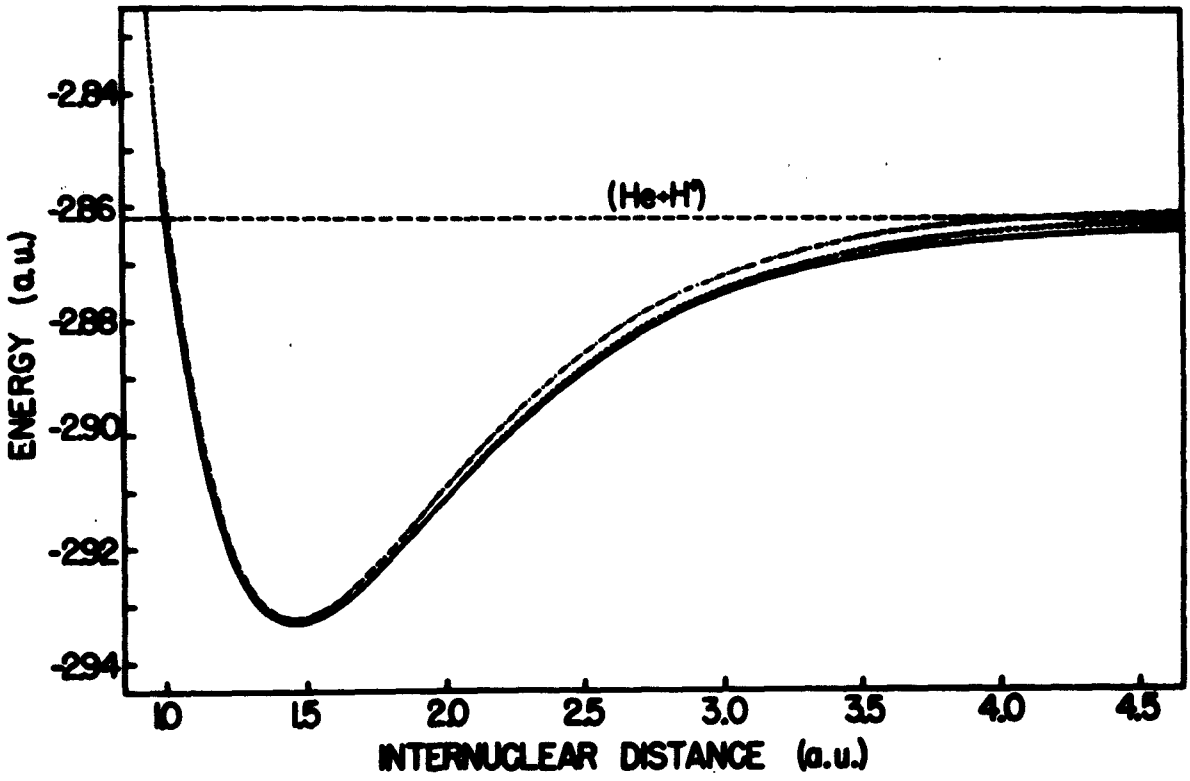

Fig. 1. Potential curve for $HeH^+(X^1\Sigma^+)$ and Hartree-Fock energy of the separated atoms ($He + H^+$).

—·—·—·— A, 4 × 2 basis set, optimized at R = 1.455 Bohr.

--------- B, 7 × 5 basis set, optimized at R = 1.455 Bohr.

———— B', 7 × 5 basis set, optimized at each R.

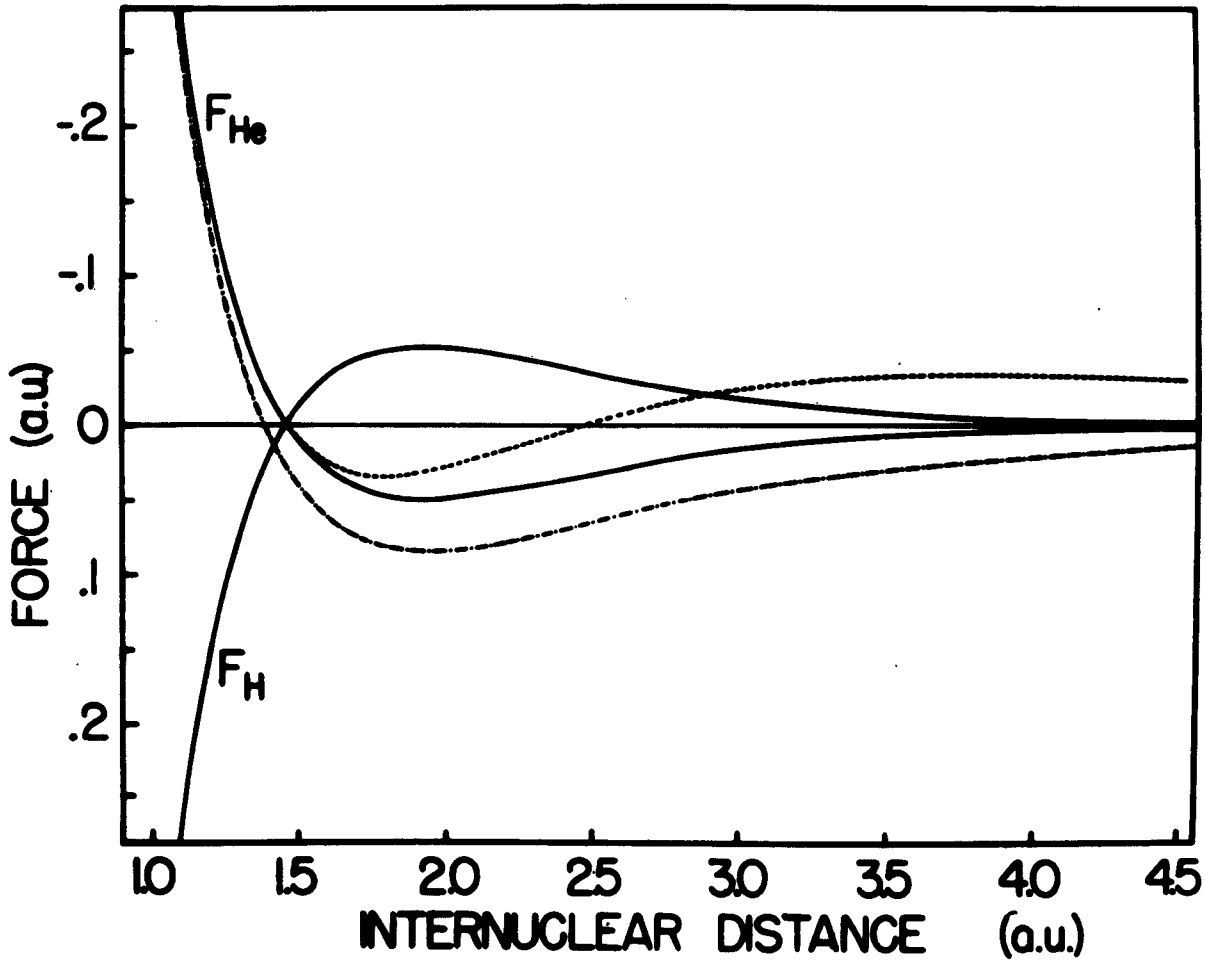

Fig. 2. Force on the He-nucleus (F_{He}) and on the H-nucleus (F_H) at different internuclear distances.

-·-·-·-·- A', 4 × 2 basis set, optimized at each R.

--------- B, 7 × 5 basis set, optimized at R = 1.455 Bohr.

———— B', 7 × 5 basis set, optimized at each R.

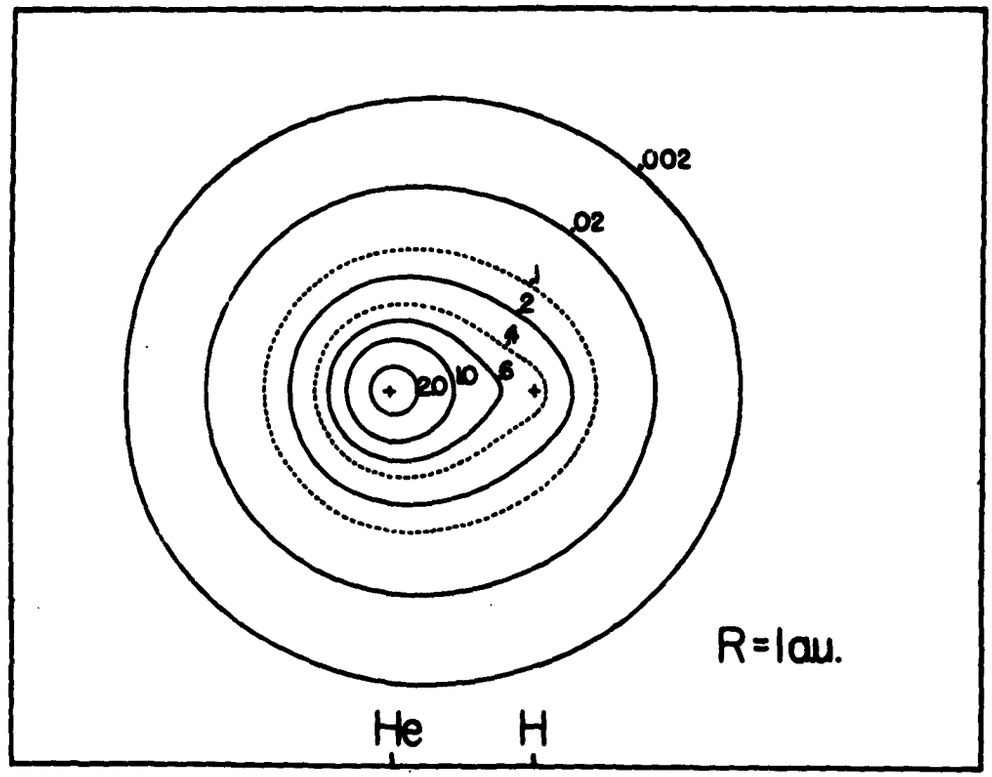

Fig. 3a. Charge density contours for HeH^+ for R = 1.0 Bohr. Calculated using the 7 x 5 basis set with exponents optimized at R = 1.0 Bohr.

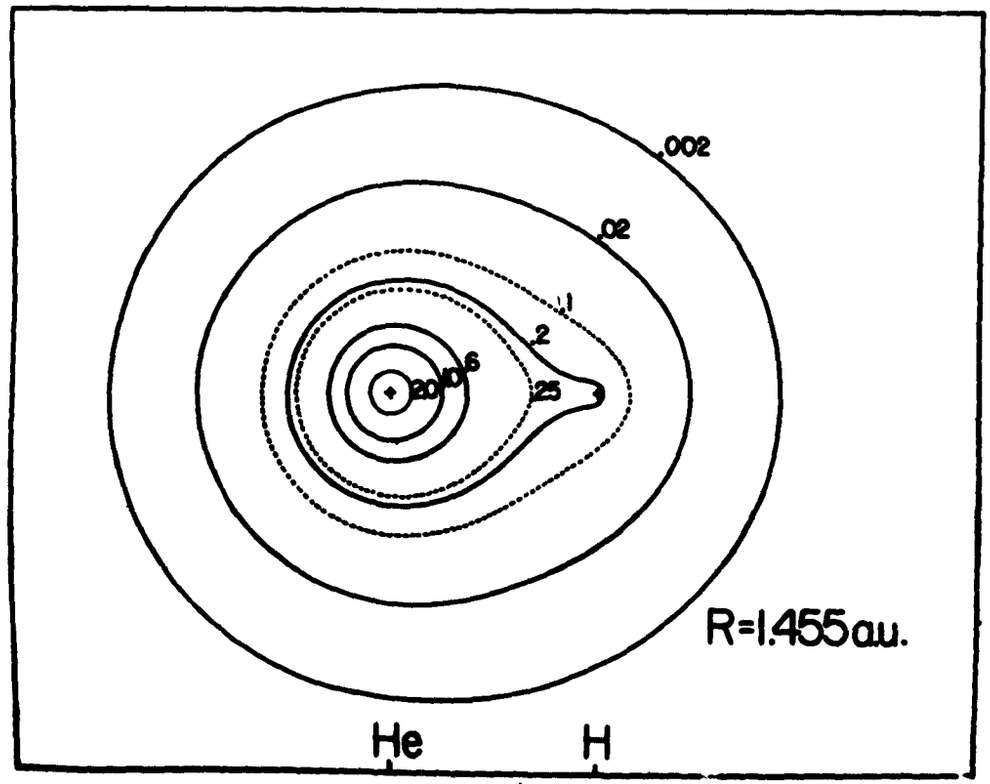

Fig. 3b. Charge density contours for HeH^+ for R = 1.455 Bohr. Calculated using the 7 x 5 basis set with exponents optimized at R = 1.455 Bohr.

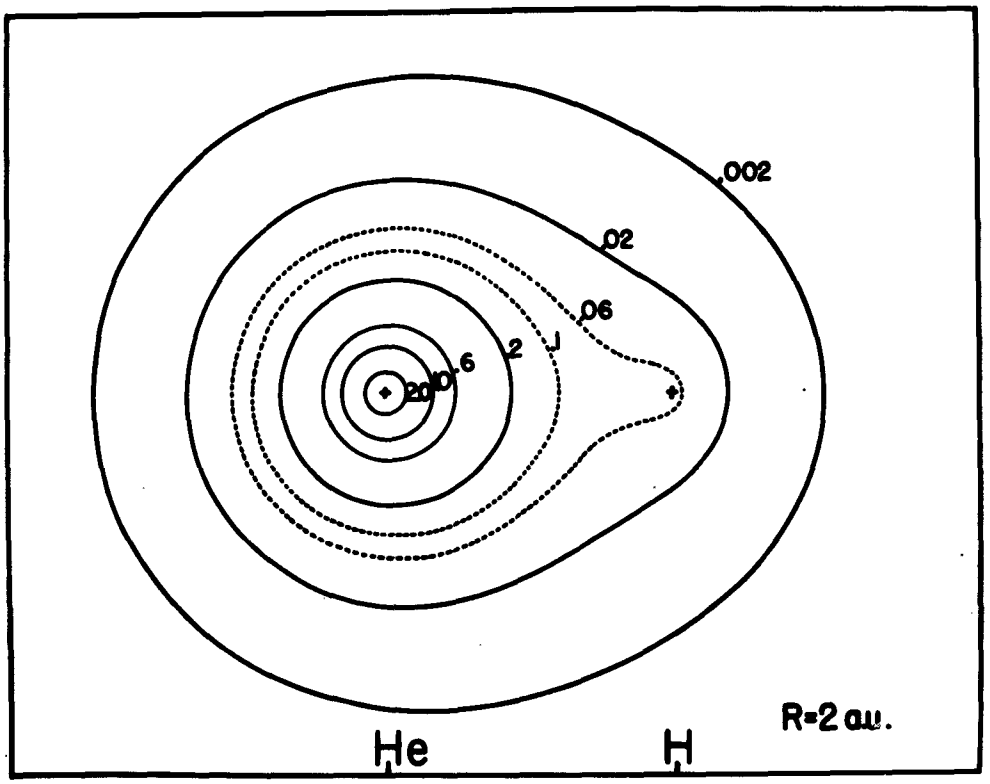

Fig. 3c. Charge density contours for HeH^+ for R = 2.0 Bohr. Calculated using the 7 × 5 basis set with exponents optimized at R = 2.0 Bohr.

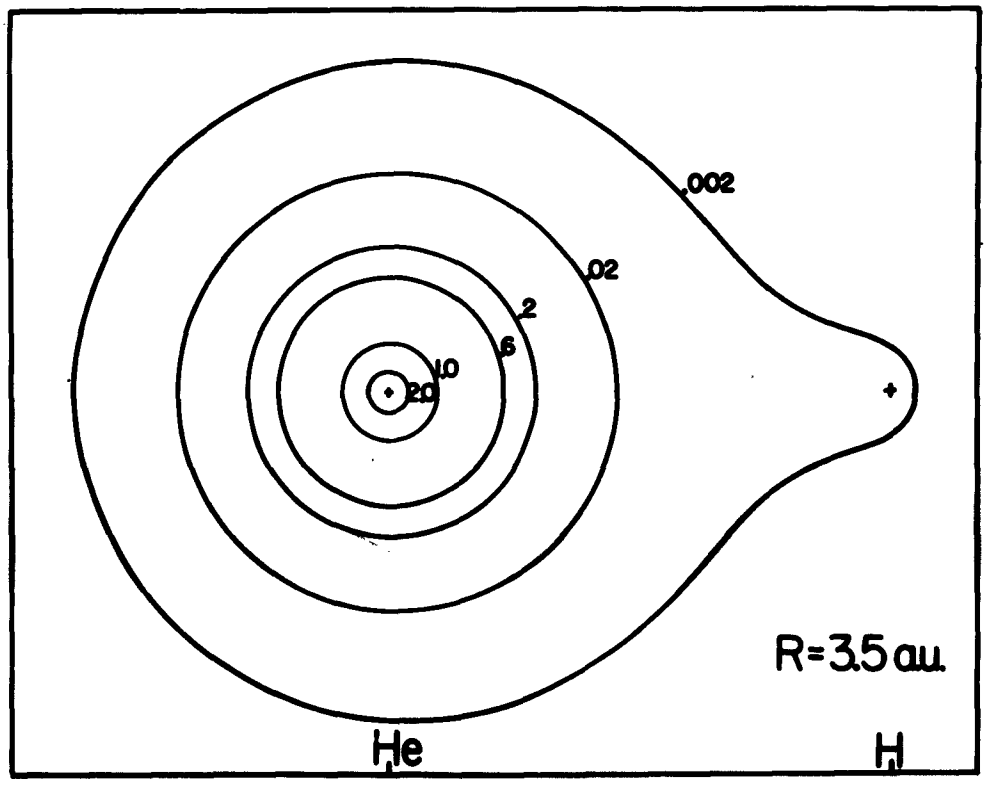

Fig. 3d. Charge density contours for HeH^+ for R = 3.5 Bohr. Calculated using the 7 × 5 basis set with exponents optimized at R = 3.5 Bohr.

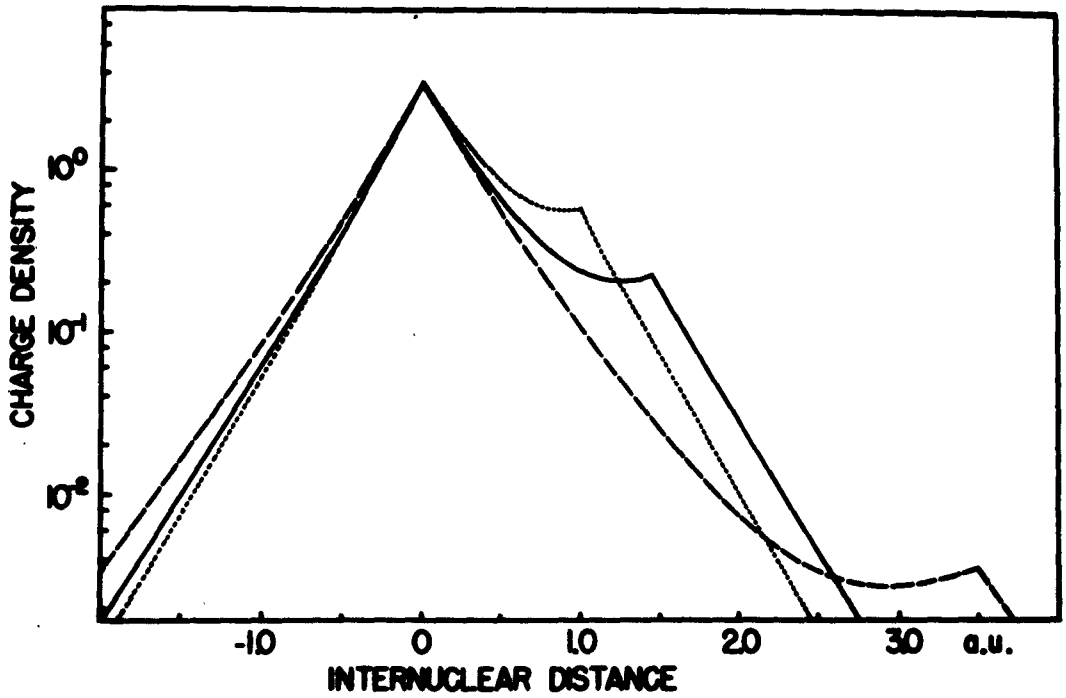

Fig. 4. Charge density for HeH^+ along the internuclear axis. Calculated using the 7 × 5 basis set with exponents optimized at each R.

---------- R = 1.0 Bohr.

———————— R = 1.455 Bohr.

– – – – – R = 3.5 Bohr.

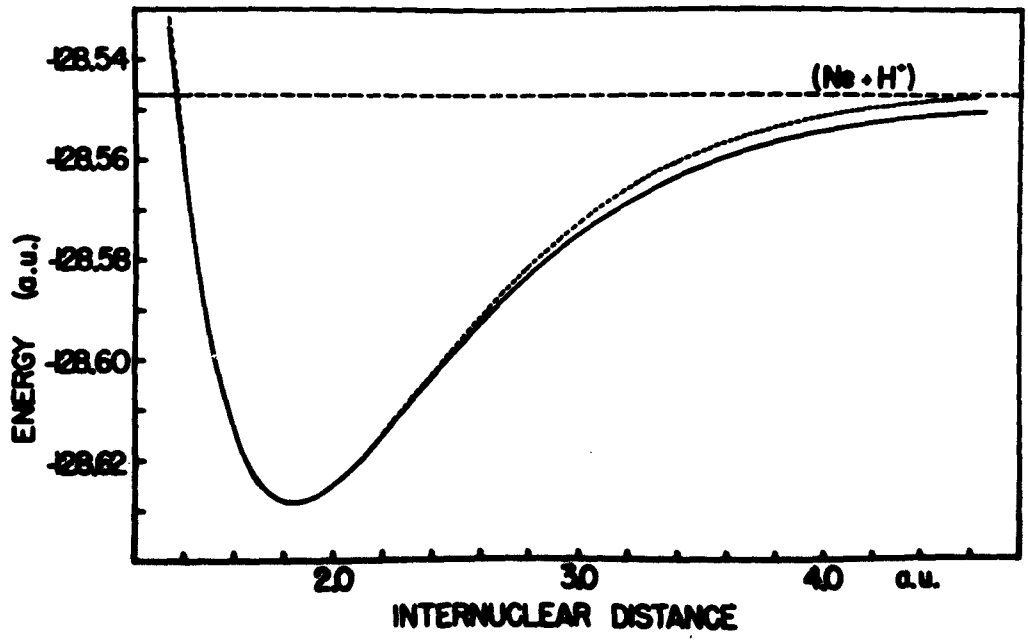

Figure 5: Potential curve for $NeH^+(X^1\Sigma^+)$ and Hartree-Fock energy of the separated atoms ($Ne + H^+$).

– – – – – A, basis set optimized at R = 1.83 Bohr.

———————— A', basis set optimized at each R.

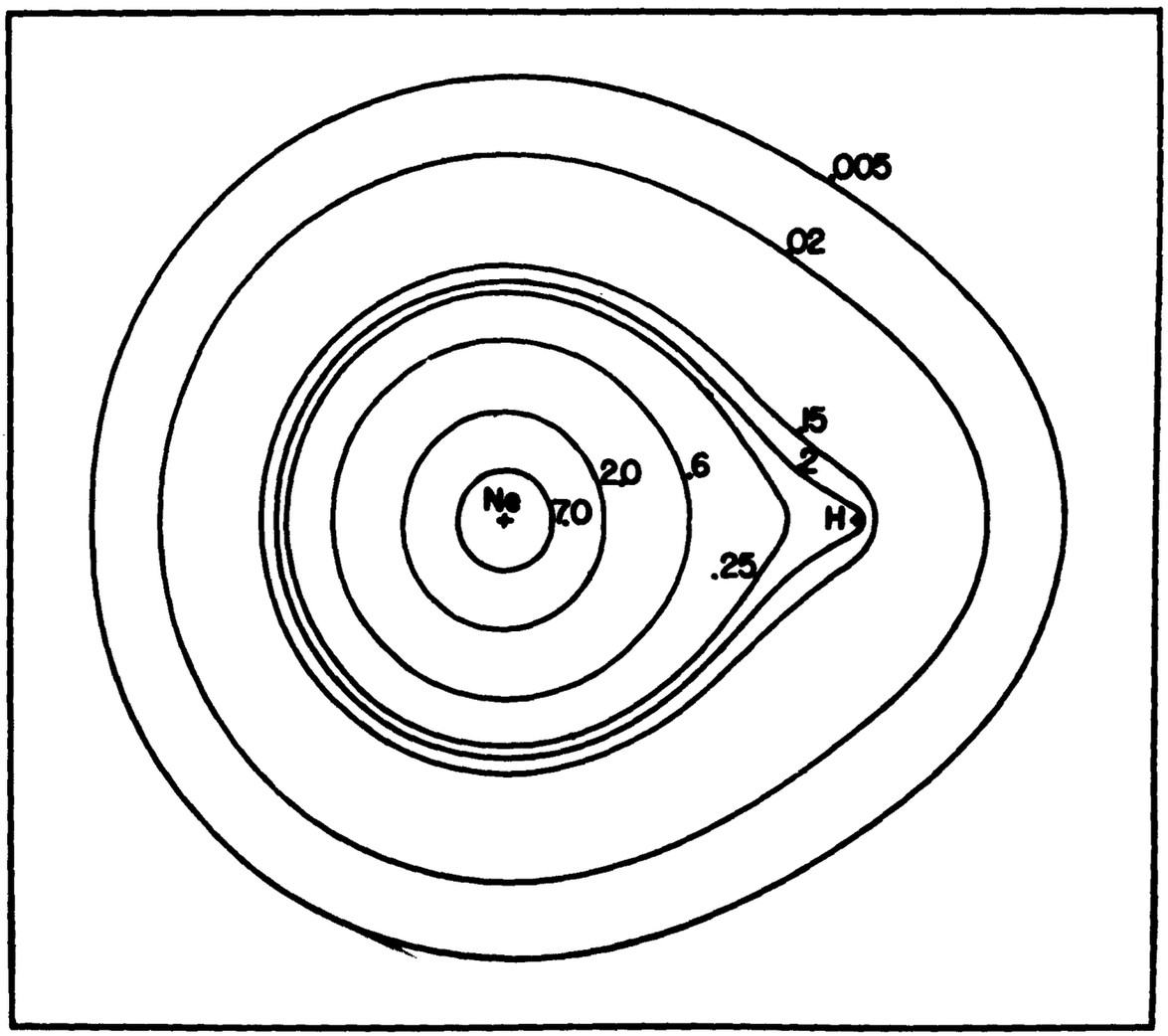

Figure 6: Charge density contours for NeH^+, R = 1.83 Bohr.

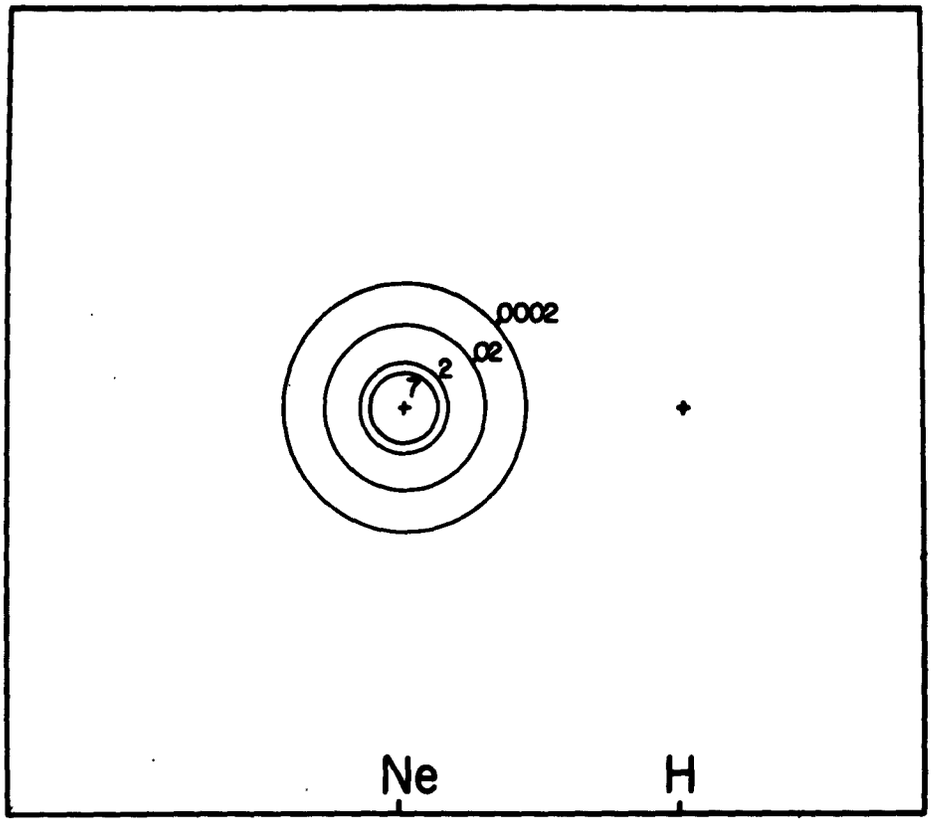

Figure 7a: Charge density contours for the 1σ MO of NeH^+ (R = 1.83 Bohr).

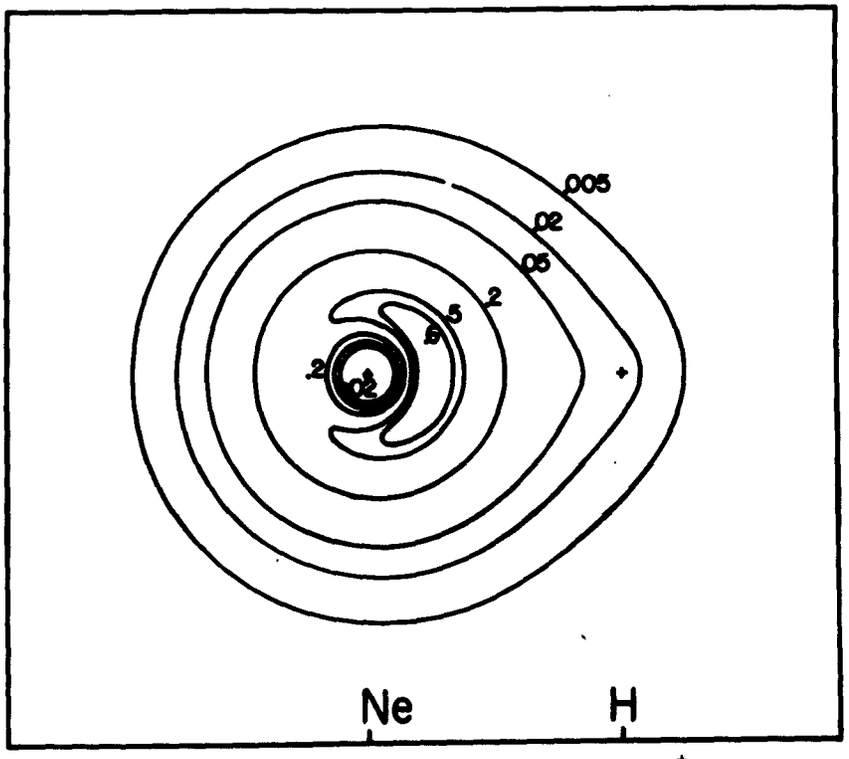

Figure 7b: Charge density contours for the 2σ MO of NeH^+ (R = 1.83 Bohr).

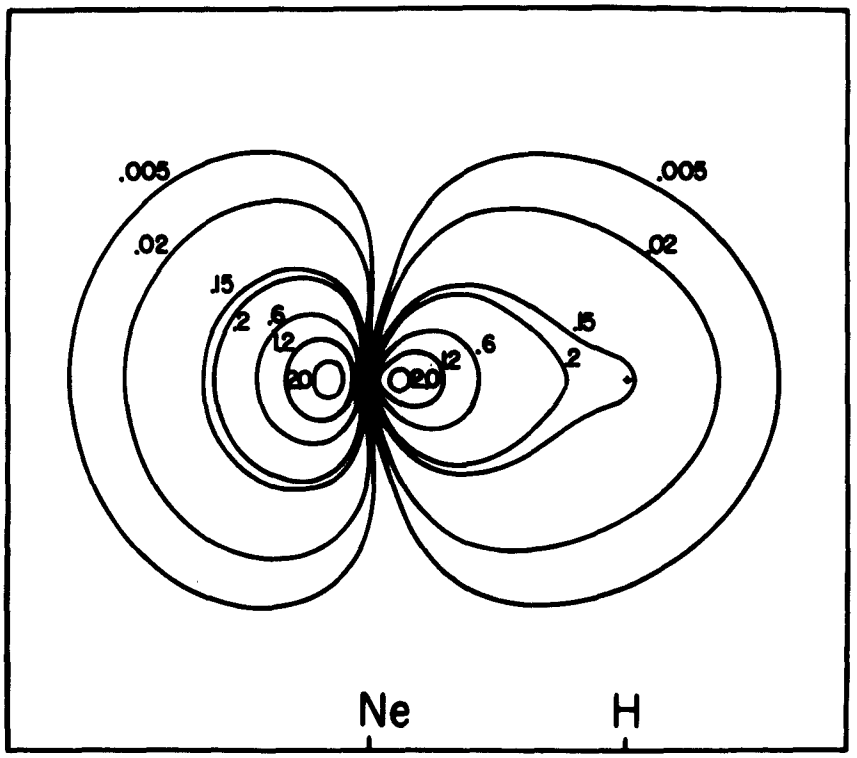

Figure 7c: Charge density contours for the 3σ MO of NeH^+ (R = 1.83 Bohr).

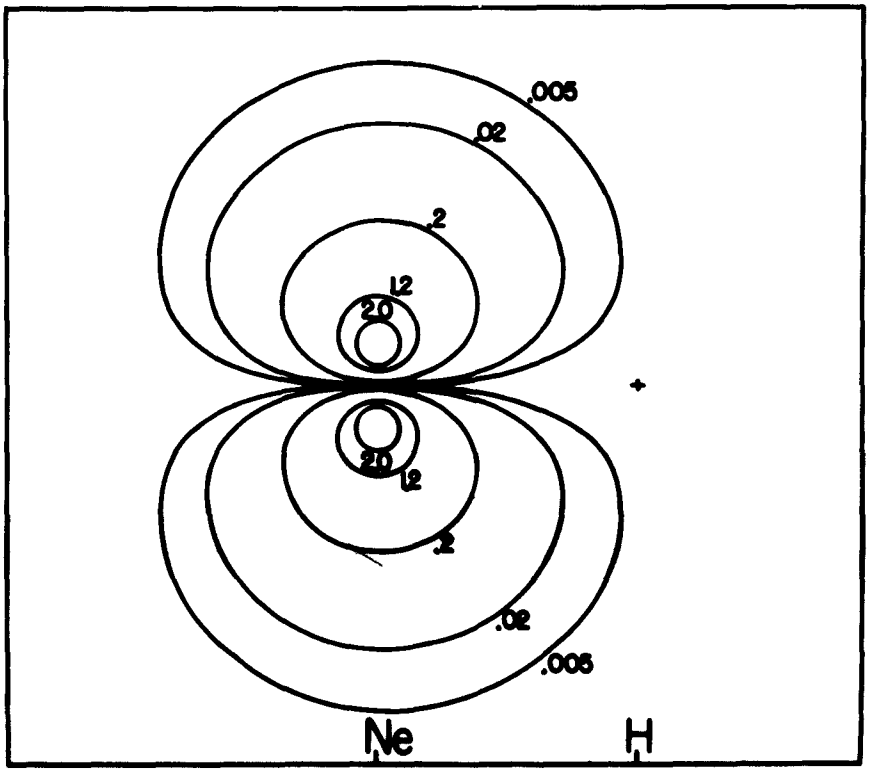

Figure 7d: Charge density contours for the 1π MO of NeH^+ (R = 1.83 Bohr).

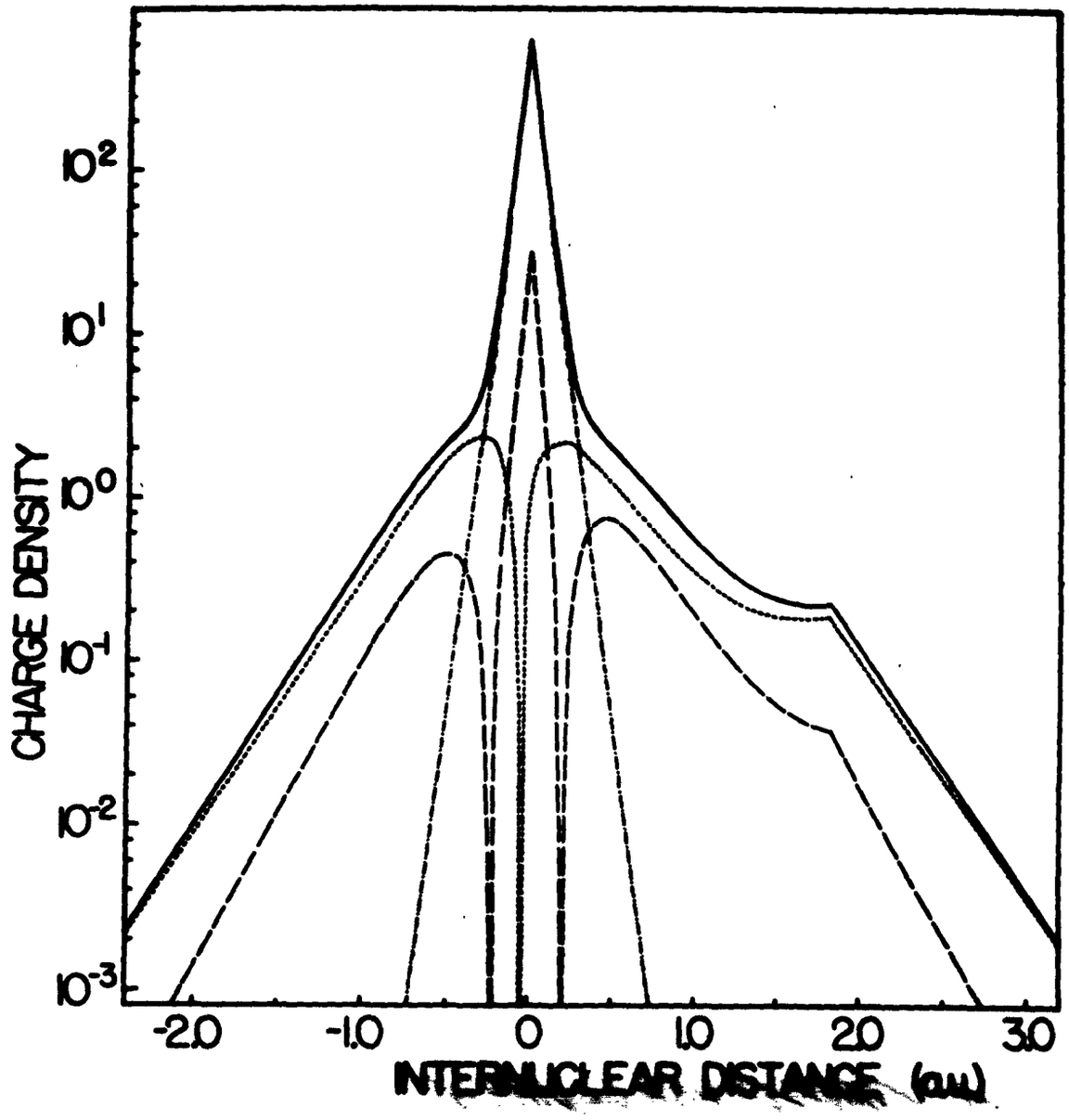

Fig. 8. Charge density for NeH^+ along the internuclear axis.

——— Charge density of the total wavefunction.
—·—·—·— Charge density of the 1σ - MO
— — — — Charge density of the 2σ - MO
------- Charge density of the 3σ - MO

Reprinted from THE PHYSICAL REVIEW, Vol. 136, No. 4A, A962–A965, 16 November 1964
Printed in U. S. A.

Rare-Gas and Hydrogen Molecule Electronic States, Noncrossing Rule, and Recombination of Electrons with Rare-Gas and Hydrogen Ions*

ROBERT S. MULLIKEN
Laboratory of Molecular Structure and Spectra, Department of Physics, University of Chicago, Chicago, Illinois
(Received 23 June 1964)

Recent experimental work on helium jets has indicated that excited atoms result usually from collisional-radiative electron capture by atom ions ($A^+ + 2e \rightarrow A^* + e$; etc.) rather than by dissociative recombination by molecule ions ($A_2^+ + e \rightarrow A^* + A$), while for the heavier rare gases, the latter process is apparently relatively important. It is shown in the present paper that the theoretically expected forms of the potential curves of excited He_2 and other rare-gas molecules make dissociative recombination improbable for He_2^+ but more probable for the other rare-gas diatomic ions. Available spectroscopic data and theoretical considerations make it fairly sure that many of the familiar excited states of He_2 have high maxima in their potential curves, but that no pure repulsion curves, except the one for two normal He atoms, exist below the energy of $He^+ + He$. Besides the stable states with stable He_2^+ core ($1\sigma_g^2 1\sigma_u$, $^2\Sigma_u^+$) plus a Rydberg electron, there must be others with a core ($1\sigma_g 1\sigma_u^2$, $^2\Sigma_g^+$) which *per se* is unstable but which on addition of an electron in a sufficiently strongly bound Rydberg orbital is stable; consideration of these states makes possible a reasonable explanation of the Hornbeck-Molnar effect in helium. Statements analogous to those about potential curves and electron recombination in helium are applicable also to a large extent for hydrogen.

FOLLOWING Bates,[1,2] it was rather generally accepted[3] that the relatively rapid recombination rate of electrons into excited states of atomic rare-gas ions in discharge afterglows can be explained only by assuming that the major responsible process is "dissociative recombination":

$$A_2^+ + e \rightarrow A^* + A. \qquad (1)$$

Recently, however, the general usefulness of this explanation has been seriously questioned, and a "collisional-radiative" mechanism,[4]

$$A^+ + 2e \rightarrow A^{**} + e; \quad A^{**} \rightarrow A^* + h\nu; \quad \text{etc.} \qquad (2)$$

has been found to explain many results previously interpreted by Eq. (1). Experimental work on helium jets[5] indicates that mechanism (2) and not (1) is dominant in these for the recombination of electrons with helium ions.[6] For neon,[3] however, there seems to be good evidence for the importance of Eq. (1). As will now be shown, theoretical considerations on the forms of the potential curves of the excited states of He_2 and of other rare-gas diatomic molecules indicate that these curves are such as to make dissociative recombination of electrons [Eq. (1)] improbable for He_2^+ except for higher vibrational states but, tentatively, entirely likely [though not to the exclusion of Eq. (2)] for the other rare-gas diatomic ions.

In 1932, I published a potential-curve diagram[7] for He_2 which included many repulsive states such that electron capture into them by He_2^+ would have resulted in dissociative electron recombination. However, the existence of such states contradicted the "noncrossing rule" for potential curves of any one electronic species. In 1932 confidence in the noncrossing rule was much less secure than now, and there was evidence which seemed to indicate its violation for certain states of He_2. Namely, near their minima the potential curves of the electronic states $A3d\sigma$, $^3\Sigma^+_u$, $A3d\pi$, $^3\Pi_u$ and $A3d\delta$, $^3\Delta_u$, where the He_2^+ core A has the normal-state configuration $1\sigma_g^2\, 1\sigma_u$ and the excited electron is in a Rydberg MO (molecular orbital), all lie close together with energies which for $v=0$ are above that of two normal He atoms by amounts $I - D^+ - X$ eV, where $X = 1.574$, 1.550, and 1.491 for $3d\sigma$, $3d\pi$, and $3d\delta$, respectively. (I = ionization energy of He atom, v = vibrational quantum number, D^+ = dissociation energy of He_2^+ into $He^+ + He$.) Now if the $3d\sigma$, $^2\Sigma^+_u$ and $3d\pi$, $^2\Pi_u$ states dissociate in the manner expected from simple linear-combination-of-atomic-orbitals (LCAO) MO theory and the noncrossing rule, they would both dissociate to $He(1s^2) + He(1s2p, {}^3P)$, with energy $I - 3.623$ eV,[8] but the $A3d\delta$, $^3\Delta_u$ state necessarily goes to

* This work was assisted by the U. S. Office of Naval Research, Physics Branch under Contract Nonr-2121 (01).
[1] D. R. Bates, Phys. Rev. 77, 718 (1950).
[2] D. R. Bates, Phys. Rev. 78, 492 (1950).
[3] For example, W. A. Rogers and M. A. Biondi, Phys. Rev. 134, A1215 (1964), on helium; T. R. Connor and M. Biondi, Bull. Am. Phys. Soc. 9, 184 (1964), on neon.
[4] D. R. Bates, A. E. Kingston, and R. W. P. McWhirter, Proc. Roy. Soc. (London) A267, 297 (1962); A270, 155 (1962); N. D'Angelo, Phys. Rev. 121, 505 (1961); S. Byron, R. C. Stabler, and P. I. Bortz, Phys. Rev. Letters 8, 376 (1962).
[5] C. B. Collins and W. W. Robertson, J. Chem. Phys. 40, 2202, 2208 (1964); F. E. Niles and W. W. Robertson, *ibid.* 40, 2909 (1964).
[6] Further, experimental results obtained by E. E. Ferguson, F. C. Fehsenfeld, and A. L. Schmeltekopf at the National Bureau of Standards in Boulder show that the molecular and atomic emissions in helium afterglows have the same dependence on electron temperature in the millimeter pressure range, which has led them to believe that dissociative recombination is not a significant process under the conditions where it has generally been thought to occur (private communication from Dr. Ferguson).
[7] R. S. Mulliken, Rev. Mod. Phys. 4, 1 (1932), Fig. 49, p. 61. In this figure, $D^+ = 2.6$ eV was assumed for He_2^+.
[8] This ignores a minor complication which does not alter the essential conclusions reached here. Namely, the potential curve of the $A3s$, $^3\Sigma^+_u$ state, in order to dissociate to $1s^2 + 1s3s$, ^3S as it tends to do, would have to cross that of the $A3d\sigma$, $^3\Sigma^+_u$ state (see Fig. 1). But the interaction matrix element is probably large enough near the prospective crossing point so that the $A3s$, $^3\Sigma^+_u$ shortcuts and actually dissociates into $1s^2 + 1s2p\sigma$, ^3P, leaving the $A3d\sigma$, $^3\Sigma^+_u$ to dissociate into $1s^2 + 1s3s$, ^3S. Analogous statements hold for $4p\sigma$, $^3\Sigma^+_g$ and $4f\sigma$, $^3\Sigma^+_g$, whose curves are shown in Fig. 1.

$He(1s^2)+He(1s3d, {}^3D)$, at an energy $I-1.513$ eV. Now if, for example, $D^+=2.1$ eV,[9] the energies of the $v=0$ level of the $A3d\sigma$, $^3\Sigma^+_u$ and $A3d\pi$, $^3\Pi_u$ states would be almost equal to that of the separate atoms $He(1s^2)+He(1s2p, {}^3P)$: see Fig. 1. This expectation seemed in 1932 (Ref. 7, footnote 147) to be inconsistent with the close similarity of the potential curves of the two Rydberg states mentioned to that of the $A3d\delta$, $^3\Delta_u$ state, which pointed to the conclusion that all three states dissociate alike to $He(1s^2)+He(1s3d, {}^3D)$. The $^3\Sigma^+_u$ and $^3\Pi_u$ curves would then have to violate the noncrossing rule and cross other repulsion curves of the same species (see Fig. 49 of Ref. 7). Electron capture into such repulsion curves could give rise to dissociative recombination.

Careful reconsideration has convinced me that the reason for the close proximity and similarity of the potential curves of the three Rydberg states mentioned is that at the equilibrium distance R_e the Rydberg MO is still nearly a united-atom $3d$ atomic orbital (AO). This conviction has been in fact a key clue to a better understanding of diatomic Rydberg states in general.[10]

The anomaly discussed above is resolved if the $3d\pi$, $^3\Pi_u$ and $3d\sigma$, $^3\Sigma^+_u$ curves at first nearly follow the $3d\delta$, $^3\Delta_u$ curve (which is very similar to the A curve of He_2^+), but as R increases, fall below the latter, reach a maximum or hump of as much as 0.5 eV or possibly even 1 eV height, and from there[8] go down to their dissociation asymptotes as R increases. As a matter of fact, there are indications pointing toward such behavior. Namely, R_e increases slightly and the vibration frequency ω_e and the energy fall slightly as one proceeds from $3d\delta$ to $3d\pi$ to $3d\sigma$. These deviations are just in the direction expected if there is already a *small* tendency away from the united-atom AO toward the respective LCAO forms $\delta_g 3d$, $\pi_g 2p$, and $\sigma_g 2p$ (that is, $3d\delta_a+3d\delta_b$, $2p\pi_a-2p\pi_b$, and $2p\sigma_a+2p\sigma_b$) which the MO's should tend to assume as R increases, on the way toward respective dissociation[8] to $1s^2+1s3d\delta$, ^3D or $1s2p\pi$, ^3P or $1s2p\sigma$, ^3P.

In general, any Rydberg state which at R_e is well described as $1\sigma_g^2\ 1\sigma_u\ x$ must undergo two kinds of changes as $R\to\infty$; (1) the x MO goes over to an LCAO form $y+y$ or $y-y$; (2) the wave function goes over toward $1\sigma_g^2 1\sigma_u(y\pm y)+\lambda 1\sigma_g 1\sigma_u^2(y\mp y)$, with $\lambda\to 1$ as $R\to\infty$. The $1\sigma_g$ and $1\sigma_u$ MO's have the respective forms $\sigma_g 1s$ and $\sigma_u 1s$, that is, $1s+1s$ and $1s-1s$. For $\lambda=1$ we attain the covalent Heitler-London state $He+He^*(1s\ y)$, while for $\lambda=-1$ we have the ion-pair state $He^++He^-(1s^2y)$ or, since $He^-(1s^2y)$ is unstable, just He^++He+e. All states except those with unpromoted x MO's (that is, $y=x$ and $x\to x+x$) probably have obligatory humps,[11] *unless it turns out* that D^+ is much larger than 2.1 eV.[9,12,13] All the foregoing state-

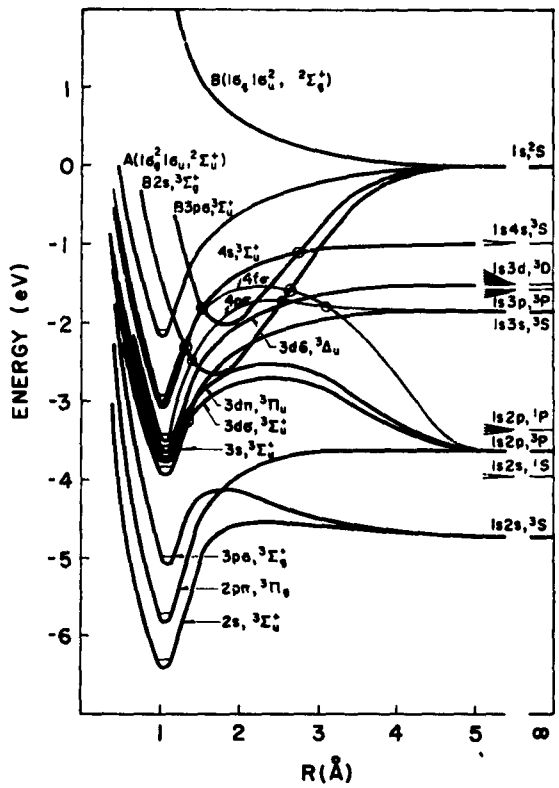

FIG. 1. Potential curves of He_2^+ and of some triplet states of He_2. For the ten lower states shown, which have A core, the curve shapes near their minima and their depths relative to the A curve of He_2^+ are based on experimental data, except for $4p\sigma$ and $4f\sigma$. The absolute depths of all these curves are based on an *assumed* value (Ref. 9) of 2.1 eV for the dissociation energy D^+ of the $v=0$ level of He_2^+. The forms of the B-core curves, and of the A-core curves at larger R values, have no more than qualitative justification. Circles, for example where $A3s$ intersects $A3d\sigma$, and where $A4s$ intersects $B\ 3p\sigma$ (twice), indicate crossings which, although not so shown, *should* be avoided according to the noncrossing rule (see Ref. 8, and text). For every triplet state of He_2 a corresponding singlet state exists, but to avoid confusion these are omitted in Fig. 1.

[9] A thoroughly reliable value of D^+ is not yet available (Ref. 12); however, experimental data of E. A. Mason and J. T. Vanderslice, J. Chem. Phys. 29, 361 (1958), are in good agreement with $D^+=2.16$ eV, while the best available theoretical calculation, by P. C. Reagan, J. C. Browne, and F. A. Matsen, J. Am. Chem. Soc. 84, 2650 (1962), after subtracting 0.1 eV for zero-point energy, gives $D^+\gtrsim 2.04$ eV.

[10] See R. S. Mulliken, J. Am. Chem. Soc. 86, 3183 (1964) for parts I–V; parts VI and VII to be published later.

[11] Meaning a hump which is necessary if a potential curve which is He_2^+-like near R_e because the Rydberg MO is united-atom-like is to connect smoothly with the proper dissociation products indicated by LCAO theory and the noncrossing rule. The occurrence of small *non*obligatory humps is also possible, as is suggested by theoretical calculations on the $A2s$, $^3\Sigma^+_u$ and $^1\Sigma^+_u$ states by R. A. Buckingham and A. Dalgarno [Proc. Roy. Soc. (London) A213, 327 (1952)], and by G. H. Brigman, S. J. Brient, and F. A. Matsen [Phys. Rev. 132, 307 (1963)] for the $^3\Sigma^+_u$ state, and supported by some experimental indications for the $^1\Sigma^+_u$ state, and by apparently conclusive spectroscopic evidence [J. L. Nickerson, Phys. Rev. 47, 707 (1935); Y. Tanaka and K. Yoshino, J. Chem. Phys. 39, 3081 (1963)] for the $^1\Sigma^+_u$ state.

[12] Intensive new studies of the He_2 spectrum by M. L. Ginter in this laboratory may throw light on this question; papers on the $A2s$ and $A3p\sigma$ singlet and triplet states will be published soon.

[13] An inspection of the data on the Rydberg states of H_2, where $D^+=2.648$ eV, makes it fairly certain that the $3d\sigma$ and $3d\pi$ states of H_2 have obligatory humps (perhaps 1 eV in height); but the $3p\sigma$, $^1\Sigma_u^+$ state probably has no hump. Further, H_2 should have Rydberg states with B core (i.e., $1\sigma_u$, $^2\Sigma^+_u$ core) with character-

ments apply equally well to excited singlet as to corresponding triplet states.

Thus if the Rydberg MO is unpromoted (for example, $2s$, which tends to take on the LCAO form $\sigma_g 2s$ as R increases, so that dissociation is to $1s^2$ plus $1s2s$; or $2p\pi$, which tends toward $\pi_u 2p$ and dissociates to $1s^2+1s2p$; or $3d\delta$, as discussed above), a potential curve with *no* obligatory hump is expected. But if it is promoted (e.g., $3p\sigma$, which tends to $\sigma_u 2s$, so that a $A3p\sigma$, $^3\Sigma^+_g$ and $^1\Sigma^+_g$ should dissociate to $1s^2+1s2s$, ^3S and ^1S, respectively; or $3d\sigma$ or $3d\pi$, as discussed above), a hump is expected if D^+ is near 2.1 eV. However, for Rydberg MO's with $n>3$ in united-atom description, except $4f\sigma$, atomic dissociation products with $n\geq 3$ for the excited atoms are required, and no more than *small* obligatory humps are expected. (For $A4f\sigma$, $^3\Sigma^+_g$ and $^1\Sigma^+_g$, larger obligatory humps may be expected.[8]) Figure 1 shows schematically how some of the lower triplet-state potential curves might look, with humps drawn in a plausible way including a small nonobligatory hump[11] in the $A2s$, $^3\Sigma^+_u$ state. [*Note added in proof.* Recent theoretical calculations by Browne[12a] confirm the conclusions reached here on the existence of obligatory humps in the $A3d\pi$, $^3\Pi_g$ and $^1\Pi_g$ states of He_2, and also on those predicted[13] for the analogous $1\sigma_g 3d\pi$, $^3\Pi_u$ and $^1\Pi_u$ states of H_2. Browne has made variational calculations using mixed $1s2p\pi$ and $1s3d\pi$, plus $1s^2$, Heitler-London states for He_2, and mixed $2p\pi$ and $3d\pi$, plus $1s$, for H_2, and obtains humps of heights from 0.4 to 0.6 eV. Calculations[12a] by Browne, on the $2s$, $^1\Sigma^+_u$ and $3d\sigma$, $^3\Sigma^+_g$ and $^1\Sigma^+_g$ states of He_2 also agree with the conclusions reached here.]

On the basis of the preceding considerations, there seems to be no reasonable doubt that, on the one hand, *all* excited states of He_2 of the type $A\ x$, ^3X or ^1X, where x is an excited (here Rydberg) MO, have potential curves with stable minima supporting at least several vibrational levels, and that, on the other hand, if we consider the potential curves for the approach of a normal atom $1s^2$ and an excited atom $1s\ y$, ^3Y or ^1Y, *all* of these correlate, probably very often over a hump, with stable excited molecular states of the type $A\ x$, ^3X or ^1X.

One should now consider Rydberg states of the type $B\ x$, ^3X and ^1X, where the B core is $1\sigma_g\ 1\sigma_u^2$, $^2\Sigma^+_g$, corresponding to the repulsive potential curve of He_2^+ (see Fig. 1). Assuming the term values for any Rydberg MO x in a $B\ x$ state to be roughly the same *at small R values* as for a corresponding $A\ x$ state, one concludes unavoidably that the potential curves of the lowest $B\ x$ states, at least for $2s$, $2p\pi$, and $3p\sigma$, must have stable minima which lie well below the energy of normal He^+ plus He in spite of the repulsive character of the core. Further, the $B\ x$ states should all tend to dissociate to (virtual) excited He^- plus He^+, hence actually, since excited He^- is unstable, to He plus electron plus He^+. Plausible guesses for the forms of two such curves (for the triplet states with $x=2s$ and $3p\sigma$) are shown in Fig. 1.

It is seen from Fig. 1 that a curve like that of $A4s$, $^3\Sigma^+_u$ (as well as higher and perhaps also some lower $^3\Sigma^+_u$ curves[14]) tends to intersect the $B3p\sigma$ curve at two points. Validity of the noncrossing rule would require that these intersections should be avoided, and new curves should result. However, if two atoms are moving fast enough toward each other on a potential curve which crosses another curve of the same electronic species, the atoms may with high probability remain on the first curve if the electronic interaction matrix element is small enough. The required conditions may well be fulfilled at the outer of the two intersections of the $A4s$ with the $B3p\sigma$ curve in Fig. 1, but then at the inner intersection, the much larger matrix element may suffice to produce an avoided crossing, hence for the approaching atoms a change-over from the $A4s$ to the $B3p\sigma$, $^3\Sigma^+_u$ curve. Then when the latter crosses curve A of the normal state of the ion (see Fig. 1), a radiationless transition $B3p\sigma$, $^3\Sigma^+_u \rightarrow A^*+e$ is not unlikely. Here A^* means a *vibrating* state of the He_2^+ ion.

The foregoing discussion, although speculative as to quantitative aspects, should be qualitatively correct. It furnishes a reasonable explanation of the Hornbeck-Molnar (HM) effect,[15,16] whereby He_2^+ ions are formed by reactions of the type

$$He(1s^2)+He^*(1s\ y) \rightarrow He_2^+ + e. \qquad (3)$$

The HM effect occurs only for He^* states within 1 or 2 eV of ionization; that is, it does not occur except when y is a Rydberg AO with $n\geq 3$ or perhaps (there is considerable experimental uncertainty[15] as to the exact limit) with $n\geq 4$. The experimental evidence suggests that the effect becomes increasingly strong for higher n. That it should not begin before $n=3$ or 4 is in harmony with the discussion of $B\ x$ potential curves given above.[16a] Although the HM mechanism for the formation of He_2^+ is important at low pressures (perhaps under 0.1 mm Hg), three-body mechanisms become dominant at higher pressures.[16]

In view of the existence of the HM effect, its inverse, which would be a dissociative recombination, should also occur. However, according to the preceding discussion the HM effect should lead only to *vibrating* He_2^+ molecules, with more vibration the higher n is for the

istics similar to those of He_2. Also, the formation of excited atoms by collisional-radiative electron capture by H^+ should predominate over dissociative recombination by H_2^+ in much the same way as for helium.

[12a] J. C. Browne (private communication).

[14] Depending on the actual form of the $B\ 3p\sigma$ curves, which can be estimated only roughly, and depending also on what is the true value of D^+.

[15] J. A. Hornbeck and J. P. Molnar, Phys. Rev. 84, 621 (1951).

[16] J. S. Dahler, J. L. Franklin, M. S. B. Munson, and F. H. Field, J. Chem. Phys. 36, 3332 (1962).

[16a] *Note added in proof.* R. K. Curran, J. Chem. Phys. 38, 2974 (1963), has shown that the effect occurs very weakly at $n=3$ with $l\geq 1$, much more strongly at $n=4$, and still more strongly at $n=5$.

y AO in Eq. (3). Hence, only vibrating He_2^+ molecules should be capable of dissociative recombination by inverse HM processes. It is not evident whether or not these would occur at a rate which (for vibrating He_2^+) would compete seriously with collisional-radiative electron capture. There exists also another possibility of dissociative recombination, but again only for vibrating He_2^+ ions. Namely, for ions with high vibrational amplitude, electron capture into the vibrational continuum at or above the top of the hump of an $A\ x$ state having an obligatory hump in its potential curve could occur with considerable probability.

Thus it appears that dissociative recombination to give He* *may* be able to compete seriously with collisional-radiative He_2^* formation under conditions where He_2^+ ions in high vibrational levels are abundant, but that for He_2^+ ions which are in their low or lowest states of vibration, electron recombination should be almost entirely nondissociative. In this connection it is of interest that the observed band spectra of He_2 hitherto reported in the literature, obtained usually in a mildly condensed discharge at 20 mm pressure, more or less, involve mainly $v=0$. Bands with $v=1$ are in general much weaker, and in only one case was a $v=2$ level seen. However, Ginter by a very thorough search for weaker bands has recently found states with v as high as 5.[12] Since the main process by which band-emitting He_2^* molecules are formed is probably[5] from He_2^+ ions in a manner analogous to Eq. (2), and since in view of the Franck-Condon principle (taken in connection with the fact that all the Ax potential curves have R_e values very similar to that of He_2^+) v should in most cases remain unchanged during electron capture, the strong predominance of $v=0$ states in the observed spectra suggests that most He_2^+ ions under the usual conditions where He_2 bands are observed are also in the level $v=0$.[17]

[*Note added in proof.* A new paper by Collins and Robertson[17a] reports that in a helium afterglow at sufficiently high pressures collisional-radiative formation of $1s2p$, ^3P helium atoms from He^+ ions is increasingly supplemented by a process which they conclude is one of "collisional-radiative recombination of He_2^+ into one or more molecular states dissociating into one of the $2p$ atomic states," yet is not direct dissociative recombination in the usual sense. The authors suggest that the observed phenomena may be explained by some sort of dissociation of the $4p\sigma$, $^3\Sigma^+_g$ state into $He(1s^2)+He^*(1s,2p,^3P)$.[8] This may be *energetically* possible for $4p\sigma$, $^3\Sigma^+_g$, still more so for $4f\sigma$, $^3\Sigma^+_g$ and other states (see Fig. 1), and perhaps could occur through (collision-induced?) predissociation. Direct dissociation via a repulsive curve seems to be ruled out by Fig. 1. A need for further work is indicated.]

The theoretical reasoning on potential curves which leads to the conclusion that dissociative recombination of electrons should, as is observed, be unimportant in helium gas if the vibrational excitation of He_2^+ ions is low, is not applicable to the other rare gases, because of the more complicated outer shells and excited states of their atoms. In fact, plausible tentative potential curves drawn some time ago for the Xe_2 molecule but not yet published[18] indicate that Eq. (1) may well compete with or under suitable conditions predominate over Eq. (2) in the rare gases other than helium. Instead of just one attractive $^2\Sigma^+_u$ and one repulsive $^2\Sigma^+_g$ as in He_2^+, there are for all the other rare-gas molecule ions four states $^2\Sigma^+_u$, $^2\Pi_g$, $^2\Pi_u$, and $^2\Sigma^+_g$ (or six if one counts substates $^2\Pi_{3/2}$ and $^2\Pi_{1/2}$ separately) derived from the normal state of the atomic ion (^2P, with substates $^2P_{3/2}$ and $^2P_{1/2}$) plus the neutral atom. Of these states, probably only the lowest, the $^2\Sigma^+_u$ (analogous to the $^2\Sigma^+_u$ of He_2^+) is attractive. By the attachment of an electron in a Rydberg MO to any of these states of the molecule ion, various molecular Rydberg states are obtained. The resulting potential curve diagram is extremely complicated. Many curves tend to cross but the noncrossing rule, here especially potent because of strong spin-orbit couplings, should often or usually prevent this for states of any one J,j-like or case c species. It is fairly sure that many of the resulting potential curves are repulsive, thus permitting dissociative capture of electrons by molecule-ions.

Further details on the Rydberg states of He_2 will be given in Parts VI–VII of Ref. 10, and, it is hoped, on those of heavier rare gases in a later paper. My interest in the electron recombination problem was stimulated by discussion with Dr. E. E. Ferguson of some of the latter's experimental results on helium jets, and I am, further, much indebted to Dr. Ferguson for valuable criticisms and suggestions.

[17] But possibly dissociative recombination could be wholly responsible for the observed scarcity of molecules with $v>0$ in the band spectra. In my opinion, this seems unlikely.

[17a] C. B. Collins and M. M. Robertson, J. Chem. Phys. (to be published).

[18] Referred to by O. Schnepp and K. Dressler, J. Chem. Phys. 33, 49 (1960), and by other writers. I hope that an understanding of the nature of potential curves of diatomic molecular Rydberg states gained in recent studies (Ref. 10) will reduce the uncertainties involved so that better estimated curves for Xe_2 can be drawn.

Reprinted from THE JOURNAL OF CHEMICAL PHYSICS, Vol. 40, No. 12, 3596-3598, 15 June 1964
Printed in U. S. A.

Octopole Moment of Methane*

JOHN J. SINAI
Laboratory of Molecular Structure and Spectra, Department of Physics, University of Chicago, Chicago, Illinois
(Received 24 February 1964)

The octopole moment of methane is calculated using three different LCAO–MO–SCF wavefunctions. The numerical method of calculation is illustrated. Results are compared with the experimental value of James and Keenan, as well as the theoretically computed value of Turner *et al.* who used the one-center-expansion-method wavefunction of Saturno and Parr. A brief discussion of these different wavefunctions and the octopole moments obtained from them is given.

FOR a system of electrons represented by a single determinant wavefunction constructed from products of orthornormal functions, the total electronic charge density is, in atomic units,

$$\rho(\mathbf{r}) = -\sum_{i=1}^{N} |\Phi_i(\mathbf{r})|^2. \tag{1}$$

Here the $\Phi_i(\mathbf{r})$'s are the orthonormal functions, and the summation extends over all electrons of the system. If the total charge distribution of the system, including any nuclei possesses tetrahedral symmetry, it can be expanded simply in terms of tetrahedral harmonics. The different terms in such an expansion can be identified as the components of a multipole charge distribution, and under certain conditions, multipole moments of this distribution can be defined. This idea has been carried through and discussed in detail by James and Keenan.[1]

Since the electronic wavefunction for the equilibrium configuration of the ground state of methane has tetrahedral symmetry, the total electronic charge density also has this symmetry, and an expression for the octopole moment of methane can be obtained from the treatment of James and Keenan.

The total charge distribution for methane is taken to be the charges of the nuclei plus the total electronic charge density given by Eq. (1). In atomic units,

$$\rho_T(\mathbf{r}) = \sum_{i=1}^{5} q_i \delta(\mathbf{r}-\mathbf{r}_i) - \sum_{i=1}^{10} |\Phi_i(\mathbf{r})|^2. \tag{2}$$

The situation of the nuclei with respect to the coordinate system used is such that the nuclei are located at

$$\mathrm{C}(0, 0, 0),$$

$$\mathrm{H}_1(-a, a, a),$$

$$\mathrm{H}_2(a, -a, a),$$

$$\mathrm{H}_3(a, a, -a),$$

$$\mathrm{H}_4(-a, -a, -a),$$

where $2a$ is the side of a cube centered on the carbon nucleus.

Then by Eqs. (3.2) and (3.8) of James and Keenan,

$$\rho_{ni}(\mathbf{r}) = \int d\Omega \rho_T(\mathbf{r}) T_{ni}^{A}, \tag{3}$$

where the T_{ni}^{A} are the normalized surface harmonics (tetrahedral harmonics) of degree n and symmetry type A, and the $\rho_{ni}(\mathbf{r})$ are the expansion coefficients.

By Eq. (3.10) of Ref. 1, one has for the 2^n multipole moment

$$I_n = (4\pi/2n+1)^{\frac{1}{2}} \int d\mathbf{v} \rho_T(\mathbf{r}) r^n T_{ni}^{A}. \tag{4}$$

* Research reported in this publication was supported by Advanced Research Projects Agency through the U.S. Army Research Office (Durham), under Contract No. DA-11-022-ORD-3119, and by a grant from the National Science Foundation, NSF GP 28 Research.

[1] H. M. James and T. A. Keenan, J. Chem. Phys. 31, 12 (1959).

By Eq. (3.9) of Ref. 1, this becomes for $n=3$,

$$I_3=\left(\frac{4\pi}{7}\frac{105}{4\pi}\right)^{\frac{1}{2}}\int d\mathbf{v}xyz\rho_T(\mathbf{r}) \quad (5)$$

$$=(15)^{\frac{1}{2}}\sum_{i=1}^{5}q_ix_iy_iz_i+(15)^{\frac{1}{2}}\int d\mathbf{v}\rho(\mathbf{r})xyz \quad (6)$$

$$=26.311+(15)^{\frac{1}{2}}\int d\mathbf{v}\rho(\mathbf{r})xyz. \quad (7)$$

The electronic contribution to the octopole moment is given by the integral

$$I_{3e}=(15)^{\frac{1}{2}}\int d\mathbf{v}xyz\rho(\mathbf{r}) \quad (8)$$

$$=-2(15)^{\frac{1}{2}}\int d\mathbf{v}xyz\sum_{1}^{5}|\Phi_i(\mathbf{r})|^2. \quad (9)$$

The summation over all the molecular orbitals reduces to a sum over the distinct orbitals because methane is a closed-shell system. The calculation was performed using spherical polar coordinates centered on the carbon nucleus. In this system we have

$$I_{3e}=-\frac{(15)^{\frac{1}{2}}}{2}\int_0^{2\pi}d\phi\int_0^{\pi}d\vartheta\int_0^{\infty}dr\,r^5\sin2\vartheta\sin^2\vartheta\sin2\phi \times\sum_{1}^{5}|\Phi_i(\mathbf{r})|^2. \quad (10)$$

This triple integral was evaluated numerically using Gauss' method of approximate quadrature. The reason for this particular choice is developed in the ensuing discussion. Consideration of the symmetry properties of the integrand discloses that the integration over the angular variable ϕ can be reduced, resulting in a somewhat more tractable numerical calculation. Firstly, the ϕ integration is seen to be the sum of two equal contributions over the intervals $(0, \pi)$ and $(\pi, 2\pi)$. Secondly, in using Gauss' method, it has been found advisable for reasons of convergence to adjust the limits of integration so that the integrand attains a maximum near or at the ends of the interval(s) of integration. Thus the range $(0, \pi)$ is divided into four intervals such that the integrand is maximum at one end of the interval and the integrals over these intervals are equal. This division of the ϕ integration into the intervals, $(0, \pi/4)$, $(\pi/4, \pi/2)$, $(\pi/2, 3\pi/4)$, and $(3\pi/4, \pi)$ is defined by planes passing through the two C–H axes and the y axis. The equality of the integrals over these intervals comes about because the z axis is a fourfold axis of symmetry T_d, and produces the final reduction of the ϕ integration into eight equal parts.

The θ interval is naturally divided into two parts $(0, \theta_1)$ and (θ_1, π) by the C–H axis for each of these integrals.

The r integration is divided into three regions, $0<r<RCH$, $RCH<r<RCH+8$, and $RCH+8<r<RCH+16$. RCH is the distance between the carbon nucleus and a hydrogen nucleus. The first region constitutes the "interior" of the molecule. The cutoff is chosen at $r=RCH$ because the charge density "peaks" at the hydrogen nuclei. The integration over the second region is expected to pick up the remaining contribution to the octopole moment. The last region is expected to yield little if anything, and this integration is intended mainly to show convergence of the calculation with respect to the r integration.

The integration over all space has now been reduced to a set of six integrals over a limited volume of space. The advantage here is that a smaller number of integration (grid) points can be used in the calculation which results in a significant saving in machine time. Thus we have for the electronic contribution to the octopole moment:

$$\begin{aligned}I_{3e}=-4(15e)^{\frac{1}{2}}\Bigg[&\int_0^{\pi/4}d\phi\int_0^{\theta_1}d\vartheta\int_0^{RCH}drF(r\theta\phi)\\&+\int_0^{\pi/4}d\phi\int_{\theta_1}^{\pi}d\vartheta\int_0^{RCH}drF(r\theta\phi)\\&+\int_0^{\pi/4}d\phi\int_{RCH}^{RCH+8}\int_0^{\theta_1}d\vartheta F(r\theta\phi)\\&+\int_0^{\pi/4}d\phi\int_{RCH}^{RCH+8}\int_{\theta_1}^{\pi}d\theta F(r\theta\phi)\\&+\int_0^{\pi/4}d\phi\int_{RCH+8}^{RCH+16}dr\int_0^{\theta_1}d\vartheta F(r\theta\phi)\\&+\int_0^{\pi/4}d\vartheta\int_{RCH+8}^{RCH+16}dr\int_{\theta_1}^{\pi}d\vartheta F(r\theta\phi)\Bigg], \quad (11)\end{aligned}$$

where

$$F(r\theta\phi)=r^5\sin2\vartheta\sin^2\vartheta\sin2\phi\sum_{i=1}^{5}|\Phi_i(\mathbf{r})|^2. \quad (12)$$

Three different electronic wavefunctions computed in the LCAO–MO–SCF scheme are considered, one given by Krauss,[2] another by Woznik,[3] and the third by Sinai.[4] The difference between the first two is that Krauss used Gaussian-type atomic functions in constructing the molecular orbitals, whereas Woznik used Slater-type orbitals. In both calculations the total electronic energy was optimized with respect to the orbital exponents. The best wavefunction obtained by Woznik yielded a slightly lower value for the total energy than that by Krauss with a smaller number of atomic orbitals. For both wavefunctions $RCH=2.0665$ a.u. Sinai[4] used the smallest possible set of atomic orbitals in his calculation; $1S$, $2S$, $2P_x$, $2P_y$, $2P_z$ Slater orbitals centered on the carbon nucleus and a $1S$ orbital centered on each of the hydrogen nuclei. The calculation was performed for $RCH=2.0$ a.u. with no variation of the orbital exponents.

[2] M. Krauss, J. Chem. Phys. 38, 564 (1963).
[3] B. J. Woznik, Solid-State and Molecul... Theory Group, MIT, Quart. Prog. Rept. 47, 107 (1963).
[4] J. J. Sinai, J. Chem. Phys. 39, 1575 (1963).

As each of the integrals in Eq. (11) was evaluated using Gauss' method of approximate quadrature, the variables of integration were transformed so that each integral is over the interval (0, 1).

The six integrals, Eq. (11), were then considered in pairs, each pair being characterized by the limits of the r integration. To eliminate unnecessary detail we take the first pair,

$$-RCH(15)^{\frac{1}{2}}\pi e\left[\theta_1\int_0^1 dw\int_0^1 du\int_0^1 dt F(uwt)\right.$$
$$\left.+(\pi-\theta_1)\int_0^1 du'\int_0^1 dw\int_0^1 dt F(u'wt)\right], \quad (13)$$

as a paradigm. The r integration here is taken over (0, 2.0665) for the Krauss and Woznik wavefunctions and (0, 2.0) for Sinai's. The angular integrations are as previously explained.

Numerical quadrature consists of replacing the integrals with polynomials. Equation (13) then becomes

$$-RCH(15)^{\frac{1}{2}}\pi e[\theta_1\sum_i^I\sum_j^J\sum_k^K A_iB_jC_kF(u_iw_jt_k)$$
$$+(\pi-\theta_1)\sum_i^I\sum_j^J\sum_k^K A_iB_jC_kF(u_i'w_jt_k)]. \quad (14)$$

The weight factors A_i, B_j, and C_k, and the points u_i, w_j, t_k are known and readily available.[5]

For convenience, the limits of summations were set equal ($I=J=K=N$) so that $A_i=B_i=C_i$. The function $F(u_iw_jt_k)$ was evaluated at the grid points by determining the values of r, ϕ, and θ for the known u_i, w_j, and t_k, and then using these to compute $F(u_iw_jt_k)$. The entire procedure was carried out by a FORTRAN program written for the IBM 7094. A pilot calculation to check out the program was carried out for $I=J=K=6$ with the help of T. Kinyon.

The different integrals using the MIT (Woznik) wavefunction were evaluated for different grid sizes to establish convergence of the procedure, to determine the "best" grid size to use with the Gaussian orbitals program as this calculation could be extremely costly because of the large number of atomic orbitals, and to provide yet another check on the program.

RESULTS

1. Woznik Wavefunction

Octopole moment $=I_3$

$=23.0989$ (electronic contribution)

-26.3106 (nuclear contribution)

$=-3.2117e-a_0^3$

$I_3=-0.476\times10^{-24}e\cdot\text{cm}^3$.

Total electronic energy

$=-40.1810$ a.u.

2. Krauss Wavefunction

Octopole moment $=I_3$

$=-26.3106+22.464e-a_0^3$

$=-3.847e-a_0^3$

$I_3=-0.570\times10^{-24}e\cdot\text{cm}^3$.

Total electronic energy

$=-40.166$ a.u.

3. Sinai Wavefunction

Octopole moment $=I_3$

$=-23.85+17.87e-a_0^3$

$=-5.98e-a_0^3$

$=-0.886\times10^{-24}e\cdot\text{cm}^3$.

Total electronic energy

$=-39.863$ a.u.

DISCUSSION

In a comparison of the results we see that the octopole moment is much more sensitive to the wavefunction than is the total electronic energy. The differences among the wavefunctions become most apparent through an examination of the resulting total electronic charge densities.[6] If we compare the Woznik and Krauss wavefunctions in this way we see that Krauss' has a flatter structure at the nuclei than does Woznik's. Further, it extends over a smaller region of space. These differences show up quantitatively in the different values of the octopole moment. Quite possibly an extension of the set of Gaussian atomic orbitals to compensate for this difference would easily pick up the difference in energy.

The value obtained from Sinai's wavefunction falls right in line with the other two values as judged by the total electronic energy given by his wavefunction.

The radical difference between these values and that obtained from a one-center-expansion wavefunction[7] ($-1.8\times10^{-24}e\cdot\text{cm}^3$) clearly demonstrates the weakness of that approach; namely, in correctly representing the electronic charge distribution. Finally, it is to be noted that the three values of the octopole moment presented here agree well with the value of $\pm0.504\times10^{-24}e\cdot\text{cm}^3$ deduced by James and Keenan[1] from their theory of phase transitions in solid heavy methane.

ACKNOWLEDGMENTS

The author is grateful to Dr. B. J. Ransil for initiating this particular calculation and to Dr. Y. N. Chiu for helpful comments on the manuscript.

[5] P. Davis and P. Rabinowitz, J. Res. Natl. Bur. Std., **56**, 35 (1956).

[6] J. J. Sinai and B. J. Ransil (to be published).

[7] A. G. Turner, A. F. Saturno, P. Hauk, and R. G. Parr, Paper presented at the meeting of the American Chemical Society in New York City, 1960.

Generalization of Laplace's Expansion to Arbitrary Powers and Functions of the Distance between Two Points*

R. A. SACK
Department of Mathematics, Royal College of Advanced Technology, Salford, England
(Received 16 August 1963)

In analogy to Laplace's expansion, an arbitrary power r^n of the distance r between two points $(r_1, \vartheta_1, \varphi_1)$ and $(r_2, \vartheta_2, \varphi_2)$ is expanded in terms of Legendre polynomials of $\cos \vartheta_{12}$. The coefficients are homogeneous functions of r_1 and r_2 of degree n satisfying simple differential equations; they are solved in terms of Gauss' hypergeometric functions of the variable $(r_</r_>)^2$. The transformation theory of hypergeometric functions is applied to describe the nature of the singularities as r_1 tends to r_2 and of the analytic continuation of the functions past these singularities. Expressions symmetric in r_1 and r_2 are obtained by quadratic transformations; for $n = -1$ and $n = -2$; one of these has previously been given by Fontana. Some three-term recurrence relations between the radial functions are established, and the expressions for the logarithm and the inverse square of the distance are discussed in detail. For arbitrary analytic functions $f(r)$, three analogous expansions are derived; the radial dependence involves spherical Bessel functions of $(r_<\partial/\partial r_>)$ of of related operators acting on $f(r_>)$, $f(r_1 + r_2)$ or $f[(r_1^2 + r_2^2)^{\frac{1}{2}}]$.

1. INTRODUCTION

THE inverse distance r^{-1} between two points Q_1 and Q_2, specified by the polar coordinates $(r_1, \vartheta_1, \varphi_1)$ and $(r_2, \vartheta_2, \varphi_2)$ with reference to a common origin O, is given by the well-known Laplace expansion

$$r^{-1} = r_>^{-1} \sum_{l=0}^{\infty} (r_</r_>)^l P_l(\cos \vartheta_{12}), \tag{1}$$

where

$$r_< = \min (r_1, r_2), \qquad r_> = \max (r_1, r_2), \tag{2}$$

$$\cos \vartheta_{12} = \cos \vartheta_1 \cos \vartheta_2 + \sin \vartheta_1 \sin \vartheta_2 \cos (\varphi_1 - \varphi_2), \tag{3}$$

and the $P_l(x)$ are the Legendre polynomials. In many physical problems, the distance between Q_1 and Q_2 may be required to powers other than the inverse first, and an expansion analogous to (1) is required for such cases. One way of approaching the problem is to preserve the expansion in powers of $(r_</r_>)$; the expression

$$r^{-2\nu} = r_>^{-2\nu} \sum_{l=0}^{\infty} (r_</r_>)^l C_l^{\nu}(\cos \vartheta_{12}) \tag{4}$$

serves to define the angular dependence as Gegenbauer polynomials of the argument[1] (cf. B 3.15[2]); but for three-dimensional problems it is more convenient to preserve the dependence on the angles, and to redefine the dependence on the radii, and the writer is not aware that the corresponding expansion

$$V_n = r^n = \sum_l R_{nl}(r_1, r_2) P_l(\cos \vartheta_{12}) \tag{5}$$

has been given in the general case. If n is a positive even integer, V_n is the $\frac{1}{2}n$th power of

$$r^2 = r_1^2 + r_2^2 - 2r_1 r_2 \cos \vartheta_{12}, \tag{6}$$

and the expansion (5) is a finite series terminating with $l = \frac{1}{2}n$; the form of the radial functions R_n is independent of the comparative values of r_1 and r_2. For odd positive values of n, recurrence relations based on (1) and (6) have occasionally been quoted; the expressions for $n = 1$ have been given explicitly by Jen.[3]

The purpose of the present paper is to derive the explicit terms in the expansion (5) for the general case. For variations of the positions of the points Q_1 and Q_2, the function V_n appears as the solution of the partial differential equation

$$\nabla_1^2 V_n = \nabla_2^2 V_n = n(n+1) V_{n-2}; \tag{7}$$

the corresponding differential equation for the radial functions R_{nl} following from (5) and (7), together with simple additional conditions of dimensionality and continuity, are solved in Sec. 2 in terms of Gauss' hypergeometric function

$$F(\alpha, \beta; \gamma, x) = 1 + \sum_1^{\infty} \frac{(\alpha)_s (\beta)_s}{(\gamma)_s s!} x^s, \tag{8}$$

where

$$(\alpha)_0 = 1; \quad (\alpha)_s = \alpha(\alpha+1) \cdots (\alpha+s-1) = \Gamma(\alpha+s)/\Gamma(\alpha). \tag{9}$$

* This work was begun at the Laboratory of Molecular Structure and Spectra, University of Chicago, supported by Office of Naval Research Contract Nonr-2121(01), continued at Salford, and completed at the Theoretical Chemistry Institute, University of Wisconsin, Madison, Wisconsin, supported by National Aeronautics and Space Administration Grant NsG-275-62(4180).

[1] L. Gegenbauer, Wien. Sitzung. 70, 6, 434 (1874); 75, 891 (1877).

[2] Bateman Manuscript Project, *Higher Transcendental Functions*, edited by A. Erdélyi (McGraw-Hill Book Company, Inc., New York, 1953). Sections and formulas in this work are directly referenced by the letter B.

[3] C. K. Jen, Phys. Rev. 43, 540 (1933).

In Sec. 3, the extensive transformation theory of the hypergeometric function is applied to express the R_n in a variety of forms and to study their behavior, expecially in the asymptotic case $r_1 \to r_2$. The results obtained are asymmetric in $r_<$ and $r_>$, but by means of quadratic transformations can be expressed in several symmetric forms; one of these transformations has recently been derived by Fontana[4] on the basis of group-theoretical arguments.

In Sec. 4, Gauss' relations between contiguous hypergeometric functions are used to establish recurrence relations between the R_{nl}, and the case of the logarithm and the inverse square are discussed in greater detail in Sec. 5.

The results obtained in Sec. 3 are rewritten in Sec. 6 in a symbolic form, independent of the power n, but involving powers or functions of differential operators; this yields an expansion theorem for an arbitrary analytic function $f(r)$. The more general problem that the function depends on the relative orientation of Q_1 and Q_2 as well as on their distance are considered in a separate paper.

2. MATHEMATICAL DERIVATION

Substitution of (7) into (5) leads to

$$\frac{\partial^2 R_{nl}}{\partial r_1^2} + \frac{2}{r_1}\frac{\partial R_{nl}}{\partial r_1} - l(l+1)\frac{R_{nl}}{r_1^2} = \frac{\partial^2 R_{nl}}{\partial r_2^2} + \frac{2}{r}\frac{\partial R_{nl}}{\partial r_2} - l(l+1)\frac{R_{nl}}{r_2^2}. \tag{10}$$

Furthermore, the R_{nl} are homogeneous functions of degree n in the variables r_1 and r_2, and since V_n is a continuous function if $r_< = 0$, they must contain the factor $r_<^l$ so that

$$R_{nl}(r_1, r_2) = r_<^l r_>^{n-l} G_{nl}(r_</r_>), \tag{11}$$

where $G_{nl}(x)$ is an analytic function for $0 \le x < 1$. Expressing G_n as a power series,

$$G_{nl}(r_</r_>) = \sum_s c_{nls}(r_</r_>)^s, \tag{12}$$

and substituting (10) into (11), we obtain the recurrence relations

$$(s+2)(2l+s+3)c_{n,l,s+2} = (n-2l-s)(n-s+1)c_{nls}. \tag{13}$$

The sequence of coefficients thus begins with $s = 0$, as the other possibility $s = -2l-1$ would violate the continuity condition, and hence $c_{nls} = 0$ for odd s, and for even $s = 2\nu$,

$$c_{n,l,2\nu} = \frac{(l-\frac{1}{2}n)_\nu(-\frac{1}{2}n-\frac{1}{2})_\nu}{(l+\frac{3}{2})_\nu \nu!} c_{nl0}, \tag{14}$$

where $(\alpha)_\nu$ is defined in (9). Hence, with the definition (8) for Gauss' hypergeometric function, (11), (12), and (14) yield

$$R_{nl}(r_1, r_2) = K(n, l) r_<^l r_>^{n-l} \times F(l-\tfrac{1}{2}n, -\tfrac{1}{2}-\tfrac{1}{2}n; l+\tfrac{3}{2}; r_<^2/r_>^2). \tag{15}$$

The coefficients $K(n, l)$ are most easily determined by considering the case $\vartheta_{12} = 0$ when all the $P_l(\cos\vartheta_{12}) = 1$:

$$V_n = |r_> - r_<|^n = r_>^n \sum_\lambda \binom{n}{\lambda}\left(\frac{-r_<}{r_>}\right)^\lambda; \tag{16}$$

comparison of the coefficients of $r_<^\lambda r_>^{n-\lambda}$ in (15) and (16) yields

$$\frac{n(n-1)\cdots(n-\lambda+1)}{\lambda!} = K(n, \lambda) + K(n, \lambda-2)\frac{(\lambda-2-\frac{1}{2}n)(-\frac{1}{2}-\frac{1}{2}n)}{\lambda-\frac{1}{2}} + K(n, \lambda-4)\frac{(\lambda-4-\frac{1}{2}n)_2(-\frac{1}{2}-\frac{1}{2}n)_2}{(\lambda-\frac{5}{2})_2 2!} + \cdots. \tag{17}$$

Considered as a function of n, the left-hand side is a polynomial of degree λ; it follows by induction that each $K(n, l)$ must be a polynomial in n of degree l at most.

Now for positive even n, the series (17) breaks off at $l = \frac{1}{2}n$, and conversely for any value of l, $K(n, l)$ vanishes for $n = 0, 2, \cdots 2l-2$. Hence it must be a multiple of $n(n-2)\cdots(n-2l+2)$ or of $(-\frac{1}{2}n)_l$, and since by virtue of (1) all $K(-1, l)$ are unity, the general solution is

$$K(n, l) = (-\tfrac{1}{2}n)_l/(\tfrac{1}{2})_l. \tag{18}$$

3. SOLUTION FOR THE RADIAL FUNCTIONS AND THEIR TRANSFORMATIONS

The Eqs. (15) and (18) show that radial functions R_{nl} in the expansion (5) are given as

$$R_{nl}(r_1, r_2) = \frac{(-\frac{1}{2}n)_l}{(\frac{1}{2})_l} r_>^n \left(\frac{r_<}{r_>}\right)^l \times F\left(l-\tfrac{1}{2}n, -\tfrac{1}{2}-\tfrac{1}{2}n; l+\tfrac{3}{2}; \frac{r_<^2}{r_>^2}\right). \tag{19}$$

The hypergeometric functions (8) are finite series, i.e., they are polynomials in x, if either α or β is a negative integer or zero. This implies that, for all positive odd integer values of n, the series for R_{nl} break off, and if $n = -1$, they consist of the leading

[4] P. R. Fontana, J. Math. Phys. 2, 825 (1961).

term only, in agreement with (1). For positive even n, the series are finite for $l \leq \frac{1}{2}n$; for $l > \frac{1}{2}n$, the factor $(-\frac{1}{2}n)_l$ ensures that R_{nl} vanishes identically.

Of the numerous transformations of the hypergeometric function, the following are especially relevant in the present context [cf. (B 2.9.1, 2); (B 2.10.1, 2)]:

$$F(\alpha, \beta; \gamma; x)$$

$$= (1-x)^{\gamma-\alpha-\beta} F(\gamma-\alpha, \gamma-\beta; \gamma; x), \tag{20a}$$

$$= \frac{\Gamma(\gamma)\Gamma(\gamma-\alpha-\beta)}{\Gamma(\gamma-\alpha)\Gamma(\gamma-\beta)} \times F(\alpha, \beta; \alpha+\beta-\gamma+1; 1-x)$$

$$+ \frac{\Gamma(\gamma)\Gamma(\alpha+\beta-\gamma)}{\Gamma(\alpha)\Gamma(\beta)} (1-x)^{\gamma-\alpha-\beta} \times F(\gamma-\alpha, \gamma-\beta; \gamma-\alpha-\beta+1; 1-x), \tag{20b}$$

$$= \frac{\Gamma(\gamma)\Gamma(\beta-\alpha)}{\Gamma(\beta)\Gamma(\gamma-\alpha)} (-x)^{-\alpha} \times F(\alpha, 1-\gamma+\alpha; 1-\beta+\alpha; x^{-1})$$

$$+ \frac{\Gamma(\gamma)\Gamma(\alpha-\beta)}{\Gamma(\alpha)\Gamma(\gamma-\beta)} (-x)^{-\beta} \times F(\beta, 1-\gamma+\beta; 1-\alpha+\beta; x^{-1}). \tag{20c}$$

The first, if applied to (19), yields

$$R_{nl}(r_1, r_2) = \frac{(-\frac{1}{2}n)_l}{(\frac{1}{2})_l} \frac{r_<^l (r_>^2 - r_<^2)^{n+2}}{r_>^{l+n+4}} \times F\left[l+2+\tfrac{1}{2}n, \tfrac{3}{2}+\tfrac{1}{2}n; l+\tfrac{3}{2}; \frac{r_<^2}{r_>^2}\right], \tag{21}$$

which shows that the functions F are invariant against the substitution $n \to -n-4$. Thus the coefficients R are rational functions of r_1 and r_2 for odd integer n whatever its sign, and also for negative even n as long as $l < \frac{1}{2}|n| - 1$, though in the latter case, the expansion (5) does not break off as with positive even n.

The transformation (20b) applied to (19) yields

$$R_{nl}(r_1, r_2) = \frac{2^{n+1}(l+\frac{1}{2})(-\frac{1}{2}n)_l}{(1+\frac{1}{2}n)_{l+1}} r_<^l r_>^{n-l} \times F\left[l-\tfrac{1}{2}n, -\tfrac{1}{2}-\tfrac{1}{2}n; -1-n; \frac{r_>^2 - r_<^2}{r_>^2}\right] - \frac{2l+1}{2^{n+3}(n+2)} \frac{r_<^l (r_>^2 - r_<^2)^{n+2}}{r_>^{l+n+4}} \times F\left[l+\tfrac{1}{2}n+2, \tfrac{3}{2}+\tfrac{1}{2}n; n+3, \frac{r_>^2 - r_<^2}{r_>^2}\right]. \tag{22}$$

Here the gamma products have been simplified with the use of (9) and Legendre's duplication formula (B 1.2.15)

$$\Gamma(2z) = 2^{2z-1}\pi^{-\frac{1}{2}}\Gamma(z)\Gamma(z+\tfrac{1}{2}). \tag{23}$$

The expansion (22) shows the nature of the branch point for fractional n as $r_<$ approaches $r_>$; we see that for $n \leq -2$, the individual functions R_{nl} are divergent, though they remain integrable as long as $n > -3$.

For integer n, (22) needs special interpretation since either one series contains terms with the indeterminate factor 0/0, or else both series possess infinite coefficients. In particular, if the function F in (19) represents a polynomial in $r_<^2/r_>^2$, it transforms into a polynomial in the variable $(r_>^2 - r_<^2)/r_>^2$; this corresponds to the terminating part of that series in (22) which has negative parameters; the terms of this series resume when the denominator in (8) also vanishes, a passage to the limit shows that the ratio 0/0 is to be interpreted as $\frac{1}{2}$, and the resumed terms exactly cancel the other series (22). On the other hand, for the nonterminating series R_{nl} in (19), at negative even n the infinities of the two series cancel out, leading to logarithmic terms in agreement with (B 2.10.12, 13).

The transformation (20c) when applied to (19) leads to

$$R_{nl} = \frac{(-\frac{1}{2}n)_l}{(\frac{1}{2})_l} (-1)^{\frac{1}{2}n} \cos\tfrac{1}{2}n\pi \quad r_<^{n-l} r_>^l \times F\left(l-\tfrac{1}{2}n; -\tfrac{1}{2}-\tfrac{1}{2}n; \tfrac{3}{2}+l; \frac{r_>^2}{r_<^2}\right) + \frac{\Gamma(l+\frac{3}{2})\pi^{\frac{1}{2}}}{\Gamma(-\frac{1}{2}n)\Gamma(2+l+\frac{1}{2}n)} (-1)^{\frac{1}{2}(n+1)} r_<^{n+l+1} r_>^{-1-l} \times F\left(-1-l-\tfrac{1}{2}n, -\tfrac{1}{2}-\tfrac{1}{2}n; \tfrac{1}{2}-l; \frac{r_>^2}{r_<^2}\right), \tag{24}$$

the constant factor of the first series having been simplified by means of the relation (B 1.2.6)

$$\Gamma(z)\Gamma(1-z) = \pi/\sin\pi z. \tag{25}$$

Equation (24) shows the nature of the analytic continuation of R_{nl} from $r_1 < r_2$ to $r_1 > r_2$, or conversely. As expected, this agrees with the true expression (19) for $r_1 > r_2$ only if n is a nonnegative even integer; in this case, the second series in (24) has zero coefficient. For the nonterminating series R_{nl} in the case of negative even n, the second term in (24) has a purely imaginary coefficient of indeterminate sign; the true function (19) for $r_1 > r_2$ corresponds to the first term in (24) only, and is therefore not the analytic continuation of R_{nl} for

$r_1 < r_2$, but its Cauchy principal value with respect to the logarithmic singularity at $r_1 = r_2$.

The relations between the three parameters occurring in the hypergeometric function in (19) allow additional, quadratic transformations to be applied to the R_{nl}. Thus, application of (B2.11.34,36),

$$F(\alpha, \beta; \alpha - \beta + 1; x) = (1 + x)^{-\alpha} \times F[\tfrac{1}{2}\alpha, \tfrac{1}{2}\alpha + \tfrac{1}{2}; \alpha - \beta + 1; 4x(1 + x)^{-2}] \quad (26a)$$

$$= (1 + x^{\frac{1}{2}})^{-2\alpha} F[\alpha, \alpha - \beta + \tfrac{1}{2}; 2\alpha - 2\beta + 1; \times 4x^{\frac{1}{2}}(1 + x^{\frac{1}{2}})^{-2}], \quad (26b)$$

to (19) leads to

$$R_{nl}(r_1, r_2) = \frac{(-\frac{1}{2}n)_l}{(\frac{1}{2})_l} \frac{(r_1 r_2)^l}{(r_1^2 + r_2^2)^{l-\frac{1}{2}n}} \times F\left[\tfrac{1}{2}l - \tfrac{1}{2}n, \tfrac{1}{2}l - \tfrac{1}{4}n + \tfrac{1}{2}; \tfrac{3}{2} + l; \frac{4r_1^2 r_2^2}{(r_1^2 + r_2^2)^2}\right], \quad (27a)$$

$$= \frac{(-\frac{1}{2}n)_l}{(\frac{1}{2})_l} \frac{(r_1 r_2)^l}{(r_1 + r_2)^{2l-n}} \times F\left[l - \tfrac{1}{2}n, 1 + l; 2 + 2l; \frac{4r_1 r_2}{(r_1 + r_2)^2}\right]. \quad (27b)$$

These expressions are completely symmetric in r_1 and r_2, the asymmetry in (19) in the two variables is related to the transformations inverse to (26) and (27) [cf. (B 2.11.6, 31)], which involve square roots which must be taken with a fixed sign. This leads to variables of the form

$$\frac{r_1^2 + r_2^2 - |r_1^2 - r_2^2|}{r_1^2 + r_2^2 + |r_1^2 - r_2^2|} \text{ and } \left[\frac{r_1 + r_2 - |r_1 - r_2|}{r_1 + r_2 + |r_1 - r_2|}\right]^2, \quad (28)$$

both of which equal $r_<^2/r_>^2$ of (2). Similar considerations apply to the factor outside the hypergeometric function. Fontana[4] has derived a formula equivalent to (27a) by group-theoretical methods, and given explicit expressions for $R_{-1,l}$ and $R_{-2,l}$ in terms of double factorials; a number of numerical results given in Fontana's paper thus appear as special cases of (26). For positive even n, the functions F in (27) reduce to polynomials; but for odd n, they are infinite series, so that the main advantage of (19) and (21) is lost by this transformation.

Hypergeometric functions which admit of quadratic transformations such as (26) are related to Legendre functions. Comparison of (27a) with (B 3.2.41) shows that the $R_{nl}(r_1, r_2)$ can be expressed in terms of associated Legendre functions of the second kind $Q_l^\mu[(r_1^2+r_2^2)/(2r_1r_2)]$, where $\mu = -1-\frac{1}{2}n$. Since, however, the various definitions of Q_l^μ for fractional μ involve differing phase angles, this approach is not studied further.

4. RECURRENCE RELATIONS

Any three contiguous hypergeometric functions, i.e., whose parameters differ by an integer only, satisfy a linear recurrence relation; hence there exists a linear relation between any three radial functions $R_{nl}(r_1, r_2)$, provided the values of l differ by integers and those of n, by even integers. Thus application of (B 2.8.31) to (27b) yields

$$(4 + 2l + n)(2l - 2 - n)R_{n+2,l} + 2(2 + n)^2(r_1^2 + r_2^2)R_{nl} - n(n + 2)(r_1^2 - r_2^2)^2 R_{n-2,l} = 0, \quad (29)$$

of (B 2.9.3) and (B 2.8.45) to (19)

$$\frac{r_1^2 + r_2^2}{r_1 r_2} R_{nl} - \frac{l + 2 + \frac{1}{2}n}{l + \frac{3}{2}} R_{n,l+1} - \frac{l - 1 - \frac{1}{2}n}{l - \frac{1}{2}} R_{n,l-1} = 0, \quad (30)$$

and of (B 2.8.35) to (27a)

$$(r_1^2 + r_2^2)R_{nl} - \frac{2l + 1}{l - \frac{1}{2}} r_1 r_2 R_{n,l-1} - \frac{2 + l + \frac{1}{2}n}{1 + \frac{1}{2}n} R_{n+2,l}. \quad (31a)$$

Elimination of $R_{n,l-1}$ or R_{nl} from (30) and (31a) leads to

$$(r_1^2 + r_2^2)R_{nl} - \frac{2l + 1}{l + \frac{3}{2}} r_1 r_2 R_{n,l+1} + \frac{l - 1 - \frac{1}{2}n}{1 + \frac{1}{2}n} R_{n+2,l} = 0, \quad (31b)$$

and

$$r_1 r_2 \left[\frac{R_{n,l+1}}{l + \frac{3}{2}} - \frac{R_{n,l-1}}{l - \frac{1}{2}}\right] - \frac{R_{n+2,l}}{1 + \frac{1}{2}n} = 0, \quad (31c)$$

respectively, and application of (29) to (31a) and (31b) yields

$$n(r_1^2 - r_2^2)^2 R_{n-2,l} = (2l + 2 + n)(r_1^2 + r_2^2)R_{nl} - (2l + 1)(2l - 2 - n)r_1 r_2 R_{n,l-1}/(l - \tfrac{1}{2}), \quad (32a)$$

$$= -(2l - n)(r_1^2 + r_2^2)R_{nl} + (2l + 1)(4 + 2l + n)r_1 r_2 R_{n,l+1}/(l + \tfrac{3}{2}); \quad (32b)$$

with a renewed application of (30), this leads to

$$\frac{n(r_1^2 - r_2^2)^2 R_{n-2,l}}{r_1 r_2} = 2\frac{(l + 1 + \frac{1}{2}n)_2}{l + \frac{3}{2}} R_{n,l+1} - 2\frac{(l - 1 - \frac{1}{2}n)_2}{l - \frac{1}{2}} R_{n,l-1}. \quad (32c)$$

All these formulas are three-term recurrence relations, independent of the relative magnitudes of r_1 and r_2. As mentioned in the introduction, use has previously been made of (6) to express $R_{n+2,l}$ in terms of $R_{nl}, R_{n,l-1}$ and $R_{n,l+1}$; such formulas are, of necessity, four-term recurrence relations.

5. EXPLICIT FORMULAS FOR THE LOGARITHM AND THE INVERSE SQUARE

The expansion for $\log r$ corresponding to (5),

$$\log r = \sum R_{\log,l}(r_1, r_2)P_l(\cos\vartheta_{12}), \qquad (34)$$

is most easily deduced from the limiting process

$$\log r = \lim \partial(r^n)/\partial n, \qquad \text{as} \quad n \to 0. \qquad (35)$$

The factor $(-\frac{1}{2}n)_l$, which occurs in the expressions for R_{nl}, vanishes for $n = 0$, $l > 0$, but gives a nonzero derivative; hence for all $l > 0$ we obtain from (19), (21), and (27),

$$R_{\log,l} = -\frac{(l-1)!}{(\frac{1}{2})_{l-1}}\left(\frac{r_<}{r_>}\right)^l F\left(l, -\tfrac{1}{2}; l+\tfrac{1}{2}; \frac{r_<^2}{r_>^2}\right), \qquad (36a)$$

$$= -\frac{(l-1)!}{(\frac{1}{2})_{l-1}}\frac{r_<^l(r_>^2 - r_<^2)^2}{r_>^{l+4}}$$

$$\times F\left(l+2, \tfrac{1}{2}; l+\tfrac{1}{2}; \frac{r_<^2}{r_>^2}\right), \qquad (36b)$$

$$= -\frac{(l-1)!}{(\frac{1}{2})_{l-1}}\left(\frac{r_1r_2}{r_1^2+r_2^2}\right)^l$$

$$\times F\left[\tfrac{1}{2}l, \tfrac{1}{2}l+\tfrac{1}{2}; l+\tfrac{3}{2}; \frac{4r_1^2r_2^2}{(r_1^2+r_2^2)^2}\right], \qquad (36c)$$

$$= -\frac{(l-1)!}{(\frac{1}{2})_{l-1}}\frac{(r_1r_2)^l}{(r_1+r_2)^{2l}}$$

$$\times F\left[l, l+1; 2l+2; \frac{4r_1r_2}{(r_1+r_2)^2}\right]. \qquad (36d)$$

For $l = 0$, the differentiation must be applied to the other factors; (19) and (27) yield

$$R_{\log,0} = \log r_> + \sum \frac{(r_</r_>)^{2s}}{2s(2s-1)(2s+1)}, \qquad (37a)$$

$$= \log(r_1+r_2) - \tfrac{1}{2}\sum \frac{1}{s(s+1)}\frac{(4r_1r_2)^s}{(r_1+r_2)^{2s}}, \qquad (37b)$$

$$= \tfrac{1}{2}\log(r_1^2+r_2^2) - \tfrac{1}{8}\sum \frac{1}{s(s+\frac{1}{2})}\left(\frac{2r_1r_2}{r_1^2+r_2^2}\right)^{2s}, \qquad (37c)$$

the index of summation running from 1 to ∞ in all cases. These series can be summed, leading to

$$R_{\log,0} = \log|r_1 - r_2| + \frac{(r_1+r_2)^2}{4r_1r_2}\log\frac{r_1+r_2}{|r_1-r_2|} - \tfrac{1}{2}. \qquad (38a)$$

Similarly, (36) can be summed for $l = 1$, with the result

$$R_{\log,1} = \frac{3}{16}\left(\frac{r_1^2-r_2^2}{r_1r_2}\right)^2 \times \log\frac{r_1+r_2}{|r_1-r_2|} - \frac{3}{8}\left(\frac{r_1^2+r_2^2}{r_1r_2}\right). \qquad (38b)$$

Differentiation of (30) yields, with (35), for $l > 0$,

$$\frac{r_1^2+r_2^2}{r_1r_2}R_{\log,l} - \frac{2l+4}{2l+3}R_{\log,l+1} - \frac{2l-2}{2l-1}R_{\log,l-1} + \delta_{l,1} = 0, \qquad (39)$$

$\delta_{l,m}$ being the Kronecker symbol. Similarly, (19) can be easily summed for $n = -2$ leading to

$$R_{-2,0} = \log[(r_1+r_2)/|r_1-r_2|](2r_1r_2)^{-1}, \qquad (40a)$$

$$R_{-2,1} = \tfrac{3}{4}(r_1^{-2}+r_2^{-2}) \times \log[(r_1+r_2)/|r_1-r_2|] - \tfrac{3}{2}(r_1r_2)^{-1}. \qquad (40b)$$

The recurrence relations (30) remain valid for $n = -2$, but in (31) the limiting ratio $R_{n+2,l}(1+\frac{1}{2}n)^{-1}$ is to be interpreted as $2R_{\log,l}$ $(l > 0)$; similarly in (32), R_{nl}/n tends to $R_{\log,l}$ as n tends to zero and $l > 0$.

6. EXPANSION FORMULAS FOR ARBITRARY FUNCTIONS OF r

The expansion (19) has the advantage that n occurs, as an exponent, for $r_>$ only, and, within each gamma product, only in the numerator. This allows the algebraic products to be expressed as products of the operator $(\partial/\partial r_>)$. In fact, we can equate

$$(-\tfrac{1}{2}n)_{l+s}(-\tfrac{1}{2}-\tfrac{1}{2}n)_s\, r_>^{n-1-2s} = \frac{(-)^l}{2^{s+2s}}r_>^l\left(\frac{1}{r_>}\frac{\partial}{\partial r_>}\right)^l\left[\frac{1}{r_>}\left(\frac{\partial}{\partial r_>}\right)^{2s} r_>^{n+1}\right] \qquad (41)$$

so that (19) can be written as

$$R_{nl} = (-r_<r_>)^l(2l+1)\sum_{s=0}^{\infty}\frac{r_<^{2s}}{(2s)!!\,(2s+2l+1)!!} \times \left(\frac{1}{r_>}\frac{\partial}{\partial r_>}\right)^l\left[\frac{1}{r_>}\left(\frac{\partial}{\partial r_>}\right)^{2s} r_>^{n+1}\right], \qquad (42)$$

where

$$(2k)!! = 2\cdot4\cdots2k = 2^k k!,\ 0!! = (-1)!! = 1, \qquad (43)$$
$$(2k+1)!! = 1\cdot3\cdots(2k+1) = 2^{k+1}(\tfrac{1}{2})_{k+1}.$$

This suggests, for any function $f(r)$ which can be represented as a finite or infinite sum of powers,

not necessarily integer,

$$f(r) = \sum c_n r^n, \tag{44}$$

i.e., for essentially all well-behaved functions $f(r)$, that

$$f(r) = \sum_{l=0}^{\infty} f_l(r_>, r_<) P_l(\cos \vartheta_{12}), \tag{45}$$

where

$$f_l = (2l+1)(-r_< r_>)^l \sum_{s=0}^{\infty} \frac{r_<^{2s}}{(2s)!!\,(2s+2l+1)!!} \times \left(\frac{1}{r_>}\frac{\partial}{\partial r_>}\right)^l \left\{\frac{1}{r_>}\left(\frac{\partial}{\partial r_>}\right)^{2s} [r_> f(r_>)]\right\}. \tag{46}$$

This formula can be written symbolically by means of the modified spherical Bessel functions

$$i_l(z) = \sum_{s=0}^{\infty} \frac{z^{l+2s}}{(2s)!!\,(2l+2s+1)!!} = \left(\frac{\pi}{2z}\right)^{\frac{1}{2}} I_{l+\frac{1}{2}}(z) \tag{47}$$

[this is not the notation given in (B 7.2.6)] as

$$f_l = (2l+1)(-r_< r_>)^l \left(\frac{1}{r_>}\frac{\partial}{\partial r_>}\right)^l \times \left\{\frac{1}{r_>}\frac{i_l(r_< \partial/\partial r_>)}{(r_< \partial/\partial r_>)^l}[r_> f(r_>)]\right\}. \tag{48}$$

Similarly, (27) can be turned into an operational expansion if we introduce the new variables $\rho = (r_1^2 + r_2^2)^{\frac{1}{2}}$ and $r_+ = r_1 + r_2$. Thus (27a) leads to

$$f_l = \sum_s \frac{(-r_1 r_2)^{l+2s}(2l+1)}{(2s)!!\,(2s+2l+1)!!}\left(\frac{1}{\rho}\frac{\partial}{\partial \rho}\right)^{l+2s} f(\rho) = (2l+1) i_l\left[-\frac{r_1 r_2}{\rho}\frac{\partial}{\partial \rho}\right] f(\rho). \tag{49}$$

Similarly, (27b) yields

$$f_l = \frac{1}{(2l-1)!!} \times \sum \frac{2^s(-r_1 r_2)^{l+s}(1+l)_s}{s!\,(2+2l)_s}\left(\frac{1}{r_+}\frac{\partial}{\partial r_+}\right)^{l+s} f(r_+) = \frac{1}{(2l-1)!!}\left(-\frac{r_1 r_2}{r_+}\frac{\partial}{\partial r_+}\right)^l \times \Phi\left(1+l; 2+l; \frac{-2r_1 r_2}{r_+}\frac{\partial}{\partial r_+}\right) f(r_+), \tag{50}$$

where Φ is the confluent hypergeometric function (B 6). In both (49) and (50), the product $r_1 r_2$ is to be treated as a constant on differentiation. The equivalence of (49) and (50) follows from the connection of $\Phi(\alpha; 2\alpha; 2z)$ and the Bessel functions (B 6.9.10),

$$I_\nu(z) = [(\tfrac{1}{2}z)^\nu/\Gamma(\nu+1)]e^{-z}\Phi(\tfrac{1}{2}+\nu; 1+2\nu; 2z), \tag{51}$$

which with (47) turns (50) into

$$f_l = (2l+1) i_l\left(-\frac{r_1 r_2}{r_+}\frac{\partial}{\partial r_+}\right) \exp\left(-\frac{r_1 r_2}{r_+}\frac{\partial}{\partial r_+}\right) f(r_+). \tag{52}$$

Taylor's expansion, which can be written operationally

$$\exp(h\partial/\partial z) f(z) = f(z+h), \tag{53}$$

and the identity

$$(z^{-1}\partial/\partial z) = 2\partial/\partial(z^2), \tag{54}$$

show that (52) is equivalent to

$$f_l = (2l+1) i_l\left(-\frac{r_1 r_2}{r_+}\frac{\partial}{\partial r_+}\right) f[(r_+^2 - 2r_1 r_2)^{\frac{1}{2}}], \tag{55}$$

which is another way of writing (49).

The convergence of the expansions (42), (49), and (50) are not discussed in detail. Qualitively we can say that, for any function $f(r)$ which is analytic for $|r| < M$, the expansions converges as long as $|r_1| + |r_2| < M$. If $f(r)\cdot r^{-n} (n \neq 0)$ tends to a finite nonzero limit as r tends to zero, this does not affect the convergence for $r_1 \neq r_2$, and even when $r_1 = r_2$, (22) shows that we can expect convergence as long as $n > -2$.

For two types of functions $f(r)$, the expansions (42), (49), and (50) factorize. Let $f(r)$ be a spherically symmetric solution of the wave equation,

$$\nabla^2 f = r^{-1}\partial^2(rf)/\partial r^2 = -k^2 f, \tag{56}$$

i.e., a spherical Bessel function of order zero of the first, second, or third kind (B 7.2.6),

$$j_0(kr) = \sin(kr)/(kr), \quad y_0(kr) = -\cos(kr)/(kr), \quad h_0^{(1)}(kr) = -ie^{ikr}/(kr), \quad h_0^{(2)}(kr) = ie^{-ikr}/(kr), \tag{57}$$

where the same relation as (47) holds between the pairs of functions j_l and $J_{l+\frac{1}{2}}$, y_l and $Y_{l+\frac{1}{2}}$, and h_l and $H_{l+\frac{1}{2}}$. Then in view of (56), the recurrence relations (B 7.11.7–10),

$$w_l(z) = (-z)^l (z^{-1}d/dz)^l w_0(z), \qquad w = j, y, h^{(1)}, h^{(2)}, \tag{58}$$

and the series expansion for $j_l(z)$ which differs from (47) only by the factor $(-)^s$, (45), and (46), lead to

$$w_0(kr) = \sum_l (2l+1) j_l(kr_<) w_l(kr_>) P_l(\cos \vartheta_{12}), \qquad w = j, y, h^{(1)}, h^{(2)}, \tag{59}$$

which is Gegenbauer's addition theorem[1] (B 7.15.28, 30) particularized to spherical Bessel functions. For the modified Bessel functions i_l and $k_l = (\pi/2z)^{\frac{1}{2}} K_{l+\frac{1}{2}}$, the corresponding results are, in view of (B 7.2.43)

and (B 7.11.20),

$$i_0(kr) = \sum (-)^l(2l+1)i_l(kr_<)i_l(kr_>)P_l(\cos\vartheta_{12}), \quad (60)$$
$$k_0(kr) = \sum (2l+1)i_l(kr_<)k_l(kr_>)P_l(\cos\vartheta_{12})$$

(cf. B 7.6.3); the latter serves as the basis of the zeta-function expansion about a common center in the method by Barnett and Coulson[6] for evaluating molecular integrals.

If $f(r)$ is a Gaussian function,

$$f(r) = \exp(-kr^2), \quad (r^{-1}\partial/\partial r)f(r) = -2kf(r), \quad (61)$$

the expansions (49) and (50) factorize, with the result

$$\exp(-kr^2) = \sum (2l+1)i_l(2kr_1r_2) \times \exp[-k(r_1^2+r_2^2)]P_l(\cos\vartheta_{12}), \quad (62)$$

or, on dividing by the common exponential,

$$\exp(2kr_1r_2\cos\vartheta_{12}) = \sum (2l+1)i_l(2kr_1r_2)P_l(\cos\vartheta_{12}). \quad (63a)$$

For imaginary values of k, this becomes

$$\exp(2ikr_1r_2\cos\vartheta_{12}) = \sum i^l(2l+1)j_l(2kr_1r_2)P_l(\cos\vartheta_{12}); \quad (63b)$$

these two formulas are equivalent to Sonine's expansion (B 7.10.5) for $\nu = \frac{1}{2}$; (63b) is equivalent to the well-known expansion for a three-dimensional plane wave in terms of spherical harmonics.

ACKNOWLEDGMENT

The writer wishes to thank Dr. A. W. Weiss, Dr. P. R. Fontana, and Professor E. Hylleraas for stimulating discussions and advice.

[6] M. P. Barnett and C. A. Coulson, Phil. Trans. Roy. Soc. **A243**, 221 (1951).

Three-Dimensional Addition Theorem for Arbitrary Functions Involving Expansions in Spherical Harmonics*

R. A. SACK
Department of Mathematics, Royal College of Advanced Technology, Salford, England†
and
Theoretical Chemistry Institute, University of Wisconsin, Madison, Wisconsin
(Received 16 August 1963)

For any vector $\mathbf{r} = \mathbf{r}_1 + \mathbf{r}_2$ an expansion is derived for the product of a power r^N of its magnitude and a surface spherical harmonic $Y_L^M(\vartheta, \varphi)$ of its polar angles in terms of spherical harmonics of the angles (ϑ_1, φ_1) and (ϑ_2, φ_2). The radial factors satisfy simple differential equations; their solutions can be expressed in terms of hypergeometric functions of the variable $(r_</r_>)^2$, and the leading coefficients by means of Gaunt's coefficients or $3j$ symbols. A number of linear transformations and three-term recurrence relations between the radial function are derived; but in contrast to the case $L = 0$, no generally valid expressions symmetric in r_1 and r_2 could be found. By interpreting the terms operationally, an expansion is derived for the product of $Y_L^M(\vartheta, \varphi)$ and an arbitrary function $f(r)$. The radial factors are expansions in derivatives of $f(r_>)$; for spherical waves, they factorize into Bessel functions of r_1 and r_2 in agreement with the expansion by Friedman and Russek. The $3j$ symbols are briefly discussed in an unnormalized form; the new coefficients are integers, satisfying a simple recurrence relation through which they can be arranged on a five-dimensional generalization of Pascal's triangle.

1. INTRODUCTION

IN the preceding paper,[1] a generalization was derived of Laplace's expansion for the inverse distance between two points Q_1 and Q_2, specified by the vectors $\mathbf{r}_1$ and $\mathbf{r}_2$ or the spherical polar coordinates $(r_1, \vartheta_1, \varphi_1)$ and $(r_2, \vartheta_2, \varphi_2)$. It was shown that in the expansion for an arbitrary power of the distance in terms of Legendre polynomials of $(\cos \vartheta_{12})$,

$$|r_2 - r_1|^n = \sum R_{nl}(r_1, r_2) P_l(\cos \vartheta_{12}); \qquad (1)$$

the radial functions R_{nl} can be expressed in terms of hypergeometric functions of the argument $(r_</r_>)^2$, and by giving the expressions an operational interpretation, an addition theorem was obtained, valid for arbitrary analytic functions of $|\mathbf{r}_2 - \mathbf{r}_1|$.

A more general addition theorem would apply to functions $H(\mathbf{r}_2 - \mathbf{r}_1)$ or $H(\mathbf{r}_2 + \mathbf{r}_1)$, depending on the direction as well as on the magnitude of the vector argument. In Cartesian coordinates, such an expansion is given by Taylor's theorem in three variables; in many physical applications, however, it is of advantage to specify the dependence on the angles in terms of spherical harmonics. These harmonics can be defined in several ways in terms of the associated Legendre functions $P_l^m(x)$,

$$P_l^{|m|}(x) = (-)^m (1 - x^2)^{\frac{1}{2}|m|} [d^{|m|} P_l(x)/dx^{|m|}];$$
$$P_l^{-m}(x) = (-)^m P_l^m(x)[(l - m)!/(l + m)!]. \qquad (2)$$

The most useful definitions are for the unnormalized harmonics

$$\Theta_l^m(\vartheta, \varphi) = e^{im\varphi} P_l^{|m|}(\cos \vartheta), \qquad (3a, b)$$
$$\Omega_l^m(\vartheta, \varphi) = e^{im\varphi} P_l^m(\cos \vartheta),$$

and the normalized form

$$Y_l^m(\vartheta, \varphi) = [(2l + 1)(l - m)!/4\pi(l + m)!]^{\frac{1}{2}} \times e^{im\varphi} P_l^m(\cos \vartheta). \qquad (3c)$$

The functions $P_l(\cos \vartheta_{12})$ in (1) can be written as

$$P_l(\cos \vartheta_{12}) = \sum_{m=-l}^{l} (-)^m \Omega_l^{-m}(\vartheta_1, \varphi_1) \Omega_l^m(\vartheta_2, \varphi_2), \qquad (4)$$

with corresponding expressions in terms of Θ or Y (cf. B 3.11.2).[2]

The purpose of the present paper is to derive the expansion for the product of a spherical harmonic and a power of the radius

$$V_{NML} = r^N \Omega_L^M(\vartheta, \varphi)$$
$$= \sum R(N, L, l_1, l_2, M, m_1, m_2; r_1, r_2) \times \Omega_{l_1}^{m_1}(\vartheta_1, \varphi_1) \Omega_{l_2}^{m_2}(\vartheta_2, \varphi_2), \qquad (5)$$

and its generalization for functions of the type $f(r)\Omega_L^M(\vartheta, \varphi)$. In contrast to I, the vector $\mathbf{r} = (r, \vartheta, \varphi)$ denotes the *sum* of $\mathbf{r}_1$ and $\mathbf{r}_2$; the corresponding expressions for the difference $(\mathbf{r}_2 - \mathbf{r}_1)$ differ from those in (5) at most by a sign, corresponding to the parity of l_1. The spherical harmonics in (5) could equally well be expressed in terms of Θ or Y; the

* Supported in part by National Aeronautics and Space Administration Grant NsG-275-62(4180). This work was begun at the Laboratory of Molecular Structure and Spectra, University of Chicago, Chicago, Illinois, Supported by Office of Naval Research Contract Nonr-2121(01).
† Permanent address.
[1] R. A. Sack, J. Math. Physics 5, 246 (1964). (Hereafter referred to as I).
[2] Bateman Manuscript Project, *Higher Transcendental Functions*, edited by A. Erdélyi (McGraw-Hill Book Company, Inc., New York, 1953). Formulas in this work are directly referenced by the prefix B.

corresponding radial functions R_Θ and R_Υ differ from $R \equiv R_\Omega$ only by a factor which is easily calculated from (2) and (3). In view of the transformation properties of the normalized functions Y, their use would have the advantage that the azimuthal quantum numbers $\mathfrak{m} = M, m_1, m_2$ can affect the expressions R_Υ only through the Wigner coefficients or $3j$-symbols.[3-5] The writer's personal preference is for the functions Ω, as they do not necessitate the use of square roots; the place of the $3j$-symbols is then taken by unnormalized $3j$-coefficients which have the advantage of being integers; as shown in the Appendix, they can be arranged on a five-dimensional generalization of Pascal's triangle.

For some specific cases, expansions of the type (5) have been given before; an addition theorem for solid spherical harmonics ($N = L$ or $N = -L-1$) have been given by Rose,[6] and for spherical waves by Friedman and Russek;[7] more recently similar results have been rederived by Seaton.[8] The radial functions in the expansion (5) for the general case could be obtained by combining these results with those of I, i.e., by considering the product

$$V_{NLM} = r^n \cdot r^L \Omega_L^M(\vartheta, \varphi), \qquad n = N - L, \tag{6}$$

but this would involve the summation of multiple infinite series. Instead, the derivation of the functions R for arbitrary values of N are based, as in I, on the solution of the set of differential equations

$$\nabla_1^2 V_{NLM} = \nabla_2^2 V_{NLM}, \tag{7a}$$

$$\nabla^2 V_{NLM} = (N - L)(N + L + 1) V_{N-2,LM}. \tag{7b}$$

These solutions are again expressible in terms of hypergeometric functions, and leading coefficients are determined by comparison with special known cases; it is found that these constants can always be expressed in terms of integrals of products of three harmonics which may be given in their normalized or unnormalized forms. An alternative method of deriving these coefficients could be based on the transformation properties of the spherical harmonics, but neither this approach, nor any other group-theoretical arguments are employed in this paper. The only use made of the extensive theory of normalized harmonics[3-5] is of the relation between the integrals over triple products (Gaunt's coefficients)[9,10] and the $3j$-symbols, and the results obtained in terms of the functions Ω are reformulated in terms of the normalized harmonics Y.

The solutions of the Eqs. (7) satisfying the appropriate continuity conditions will be derived in Sec. 2, and the results discussed in Sec. 3. A selected number of recurrence relations are given in Sec. 4, and in Sec. 5 the formulas are given an operational form, applicable to arbitrary functions of r. The special case that one of the vectors points in the direction of the polar axis is considered in a later paper.

2. MATHEMATICAL DERIVATION

To avoid an excessive use of subscripts, formulas in this section are derived for the range $r_2 > r_1$ only. The dimensionality of (5) requires that the functions R be of the form

$$R(N, \mathfrak{l}, \mathfrak{m}; r_1, r_2) = r_1^{l_1} r_2^{N-l_1} \sum c_{Ns}(r_1/r_2)^s. \tag{8}$$

The differential equation (7a) substituted in (5) leads to

$$\frac{\partial^2 R}{\partial r_1^2} + \frac{2}{r_1}\frac{\partial^2 R}{\partial r_1} - l_1(l_1+1)\frac{R}{r_1^2} = \frac{\partial^2 R}{\partial r_2^2} + \frac{2}{r_2}\frac{\partial R}{\partial r_2} - l_2(l_2+1)\frac{R}{r_2^2}, \tag{9}$$

which together with (8) yields the recurrence relations

$$(s+2)(2l_1+s+3)c_{N,s+2} = (N - l_1 - l_2 - s)(N - l_1 + l_2 + 1 - s)c_{Ns}. \tag{10}$$

The leading term in the power series (8) is of degree $s = 0$, since the other possible solution, beginning with $s = -2l - 1$, would lead to a singularity as $r_1 \to 0$. As in I, the solution is best expressed in terms of Gauss' hypergeometric function

$$F(\alpha, \beta; \gamma; z) = \sum_0^\infty (\alpha)_w (\beta)_w z^w / [(\gamma)_w w!], \tag{11}$$

where[11]

$$(\alpha)_0 = 1; \quad (\alpha)_w = (\alpha; w) = \alpha(\alpha+1)\cdots \times (\alpha + w - 1) = \Gamma(\alpha + w)/\Gamma(\alpha). \tag{12}$$

[3] E. P. Wigner, *Group Theory and Its Application to the Quantum Mechanics of Atomic Spectra* (Academic Press Inc., New York, 1959).
[4] A. R. Edmonds, *Angular Momentum in Quantum Mechanics* (Princeton University Press, Princeton, New Jersey, 1957).
[5] M. E. Rose, *Elementary Theory of Angular Momentum* (John Wiley & Sons, Inc., New York, 1961).
[6] M. E. Rose, J. Math. and Phys. 37, 215 (1958).
[7] B. Friedman and J. Russek, Quart. Appl. Math. 12, 13 (1954).
[8] M. J. Seaton, Proc. Phys. Soc. 77, 184 (1961).
[9] J. A. Gaunt, Phil. Trans. Roy. Soc. A228, 151 (1929).
[10] M. Rotenberg, R. Bivins, N. Metropolis, and J. K. Wooten, *The 3-j and 6-j Symbols* (Technology Press, Cambridge, Massachusetts, 1959).
[11] The archaic form $(\alpha; w)$ is employed mainly when w carries a subscript.

If we abbreviate

$$\Lambda = \tfrac{1}{2}(L + l_1 + l_2), \qquad \lambda = \Lambda - L, \qquad \lambda_1 = \Lambda - l_1, \qquad \lambda_2 = \Lambda - l_2, \tag{13}$$

and use n as defined in (6), the solutions (8) and (10) can be expressed in the form

$$R(N, 1, \mathrm{m}; r_1, r_2) = K(N, 1, \mathrm{m}) r_1^{l_1} r_2^{N-l_1} F[\tfrac{1}{2}(l_1 + l_2 - N), \tfrac{1}{2}(l_1 - l_2 - 1 - N); l_1 + \tfrac{3}{2}; r_1^2/r_2^2], \tag{14a}$$

$$= K(N, 1, \mathrm{m}) r_1^{l_1} r_2^{n+L-l_1} \times F(\lambda - \tfrac{1}{2}n, -\tfrac{1}{2} - \tfrac{1}{2}n - \lambda_1; l_1 + \tfrac{3}{2}; r_1^2/r_2^2). \tag{14b}$$

As the functions Ω_l^m have the parity of l on inversion, $(\vartheta, \varphi) \to (\pi - \vartheta, \pi + \varphi)$, $K(n, 1, \mathrm{m})$ can take nonzero values only if

$$L - l_1 - l_2 = \text{even}, \tag{15}$$

and hence all the quantities defined in (13) are integers. The leading coefficients K in (14 a,b) satisfy the recurrence relation, in view of (7b):

$$n(n + 1 + 2L)K(N - 2, 1, \mathrm{m}) = (n - 2\lambda)(n + 1 + 2\lambda_1)K(N, 1, \mathrm{m}). \tag{16}$$

This means that K depends on n through the factors

$$(-\tfrac{1}{2}n; \lambda)(-\tfrac{1}{2} - \tfrac{1}{2}n - L; \lambda_2); \tag{17}$$

the only other way K could depend on n would be through an additional, periodic, factor of period 2; but, according to the results of I, the factor r^n in (6) does not show any such periodicity and the solid harmonics are independent of n; hence (17) describes the full dependence of K on n. To find the absolute value of $K(N, 1, \mathrm{m})$ we first consider the case $N = L$ or $n = 0$. Making use of (B 3.7.25) and its converse

$$P_l^m(\cos\vartheta)e^{im\varphi} = \frac{i^m(l + m)!}{2\pi l!} \times \int_0^{2\pi} [\cos\vartheta + i\sin\vartheta\cos(\varphi - \psi)]^l e^{im\psi}\, d\psi, \tag{18a}$$

$$[\cos\vartheta + i\sin\vartheta\cos(\varphi - \psi)]^l = \sum_m \frac{l!}{i^m(l + m)!} P_l^m(\cos\vartheta)e^{im(\varphi - \psi)}, \tag{18b}$$

we obtain for the solid harmonics, by means of the binomial theorem,

$$r^L\Omega_L^M(\vartheta, \varphi) = \frac{i^M(L + M)!}{2\pi L!}\int_0^{2\pi} (z_1 + ix_1\cos\psi + iy_1\sin\psi + z_2 + ix_2\cos\psi + iy_2\sin\psi)^L e^{iM\psi}\, d\psi = \sum (L + M)!\,[(l_1 + m_1)!\,(l_2 + m_2)!]^{-1} \times r_1^{l_1} r_2^{l_2}\Omega_{l_1}^{m_1}(\vartheta_1, \varphi_1)\Omega_{l_2}^{m_2}(\vartheta_2, \varphi_2), \tag{19}$$

the sum to be taken over all

$$m_1 + m_2 = M; \qquad l_1 + l_2 = L. \tag{20 a,b}$$

This is the unnormalized form of Rose's addition theorem.[6] Multiplication by r^n gives rise to terms for which (20b) is no longer satisfied. For positive even n, Eq. (19) of I shows that in the expansion (1) for $|\mathbf{r}_1 + \mathbf{r}_2|^n$, the radial coefficient of P_λ is $\lambda!(r_1r_2)^\lambda/(\frac{1}{2})_\lambda$ for $\lambda = \frac{1}{2}n$, and vanishes for $\lambda > \frac{1}{2}n$. Hence the leading term in $R(l_1 + l_2, 1, \mathrm{m})$, in view of (6), (13), and (19), is made up of terms

$$\frac{\lambda!\, r_1^{l_1} r_2^{l_2}}{(\frac{1}{2})_\lambda}\sum_\mu (-)^\mu \frac{(L + M)!}{(\lambda_2 + m_1 + \mu)!\,(\lambda_1 + m_2 - \mu)!} \times \Omega_{\lambda_2}^{m_1+\mu}(1)\Omega_{\lambda_1}^{m_2-\mu}(2)\Omega_\lambda^{-\mu}(1)\Omega_\lambda^{\mu}(2). \tag{21}$$

The product of two surface harmonics of the same coordinates (ϑ, φ) can be expressed as a sum of spherical harmonics,[9-8,9,12,13]

$$\Omega_l^m\Omega_\lambda^\mu = \frac{(2l)!\,(2\lambda)!\,(l + \lambda)!\,(l + \lambda - m - \mu)!}{(2l + 2\lambda)!\,l!\,\lambda!\,(l - m)!\,(\lambda - \mu)!} \times \Omega_{l+\lambda}^{m+\mu} + \cdots \Omega_{l+\lambda-2}^{m+\mu} + \cdots. \tag{22}$$

This leading term can be found most easily by a comparison of the leading coefficients of $P_l^m(x)$, which in view of (2) and Rodrigues' formula (B 3.6.16), are

$$P_l^m(x) = (-)^m(1 - x^2)^{m/2} \times [(2l)!/2^l l!\,(l - m)!]x^{l-m} + \cdots. \tag{23}$$

The leading coefficient K in (14) for $N = l_1 + l_2$ thus becomes, in view of (21) and (22),

$$K(l_1 + l_2, 1, \mathrm{m}) = (-)^{\Lambda+M} \times \frac{(L + M)!\,(l_1 - m_1)!\,(l_2 - m_2)!\,(2\lambda)!\,l_1!\,l_2!}{\lambda_1!\,\lambda_2!\,\lambda!\,(\frac{1}{2})_\lambda(2l_1)!\,(2l_2)!} \times U\begin{pmatrix} L & l_1 & l_2 \\ -M & m_1 & m_2 \end{pmatrix}, \tag{24}$$

where the symbols U represent the sums

$$U\begin{pmatrix} L & l_1 & l_2 \\ -M & m_1 & m_2 \end{pmatrix} = \sum_\mu (-)^{-\Lambda+\mu+M} \times \binom{2\lambda}{\lambda + \mu}\binom{2\lambda_1}{\lambda_1 - m_2 + \mu}\binom{2\lambda_2}{\lambda_2 + m_1 + \mu}, \tag{25}$$

provided (20a) holds. They are related to the Wigner $3j$-symbols[8-6]

$$U\begin{pmatrix} j_1 & j_2 & j_3 \\ m_1 & m_2 & m_3 \end{pmatrix} = \begin{pmatrix} j_1 & j_2 & j_3 \\ m_1 & m_2 & m_3 \end{pmatrix} \times \left[(2\Delta + 1)!\prod_{s=1}^{3}\frac{(2\lambda_s)!}{(j_s - m_s)!\,(j_s + m_s)!}\right]^{\frac{1}{2}}, \tag{26}$$

[12] L. Infeld and T. E. Hull, Rev. Mod. Phys. 23, 21 (1951).
[13] E. A. Hylleraas, Math. Scand. 10, 189 (1962).

where, for this equation only, we have put

$$\Lambda = \tfrac{1}{2}(j_1 + j_2 + j_3); \qquad \lambda_s = \Lambda - j_s \geq 0 \quad (s = 1, 2, 3). \tag{27}$$

In the present context these unnormalized $3j$-symbols are required for integral values of $\mathbf{l}$, $\mathbf{m}$, and $\boldsymbol{\lambda}$ only, but, as shown in the Appendix, their definition (25) also covers the case of half-integer parameters. For integer Λ they are invariant under a permutation of (1, 2, 3) in (26), and under a simultaneous change of sign of all the m_s.

The expression (24) can be simplified by the explicit use of Gaunt's coefficients[9,10] for the integral over the product of three associated Legendre functions. If we put

$$I_\Omega\begin{pmatrix} L & l & l' \\ M & -m & -m' \end{pmatrix} = \int_{-1}^{1} P_L^M(x) P_l^{-m}(x) P_{l'}^{-m'}(x)\, dx, \tag{28}$$

where the azimuthal numbers add up to zero, these integrals can be expressed in terms of the U's as[9]

$$I_\Omega\begin{pmatrix} L & l_1 & l_2 \\ M & -m_1 & -m_2 \end{pmatrix} = \frac{(-)^\Lambda 2(l_1 - m_1)!\,(l_2 - m_2)!\,(L + M)!\,\Lambda!}{(2\Lambda + 1)!\,\lambda_1!\,\lambda_2!\,\lambda!} \times U\begin{pmatrix} L & l_1 & l_2 \\ M & -m_1 & -m_2 \end{pmatrix}, \tag{29}$$

so that (24) becomes

$$K(l_1 + l_2, \mathbf{l}, \mathbf{m}) = \frac{(-)^M \lambda!\,(\tfrac{1}{2}; \Lambda + 1)}{(\tfrac{1}{2}; l_1)(\tfrac{1}{2}; l_2)} I_\Omega\begin{pmatrix} L & l_1 & l_2 \\ M & -m_1 & -m_2 \end{pmatrix}. \tag{30}$$

Using (17), we find, for the leading coefficient for arbitrary N,

$$K(N, \mathbf{l}, \mathbf{m}) = (-)^\lambda \frac{(-\tfrac{1}{2}n; \lambda)(-\tfrac{1}{2} - \tfrac{1}{2}n - L; \lambda_2)}{\lambda!\,(-\tfrac{1}{2} - \Lambda; \lambda_2)} \times K(l_1 + l_2, \mathbf{l}, \mathbf{m}) = (-)^{\lambda + M} \frac{(l_2 + \tfrac{1}{2})(-\tfrac{1}{2}n; \lambda)(\tfrac{3}{2} + \tfrac{1}{2}n; L)}{(\tfrac{1}{2}; l_1)(\tfrac{3}{2} + \tfrac{1}{2}n; \lambda_1)} \times I_\Omega\begin{pmatrix} L & l_1 & l_2 \\ M & -m_1 & -m_2 \end{pmatrix}. \tag{31}$$

3. DISCUSSION OF THE RADIAL FUNCTIONS R

According to (14) and (31), the radial functions R in the expansion (5) are given, for $r_2 > r_1$, by

$$R(N, \mathbf{l}, \mathbf{m}; r_1, r_2) = K'(\mathbf{l}, \mathbf{m}) R'(N, \mathbf{l}; r_1, r_2), \tag{32}$$

where

$$K'(\mathbf{l}, \mathbf{m}) = (-)^{\lambda + M}(l_1 + \tfrac{1}{2})(l_2 + \tfrac{1}{2}) \times I_\Omega\begin{pmatrix} L & l_1 & l_2 \\ M & -m_1 & -m_2 \end{pmatrix}, \tag{33}$$

$$R'(N, \mathbf{l}; r_1, r_2) = \frac{(-\tfrac{1}{2}n; \lambda)(\tfrac{3}{2} + \tfrac{1}{2}n; L)}{(\tfrac{1}{2}; l_1 + 1)(\tfrac{3}{2} + \tfrac{1}{2}n; \lambda_1)} r_1^{l_1} r_2^{N - l_1} \times F(\lambda - \tfrac{1}{2}n, -\tfrac{1}{2} - \tfrac{1}{2}n - \lambda_1; l_1 + \tfrac{3}{2}; r_1^2/r_2^2), \tag{34}$$

and the symbols are explained in (6), (11)–(13), (25), (28), and (29); for $r_1 > r_2$, the subscripts 1 and 2 should be interchanged. Equation (32) factorizes the functions $R(N, \mathbf{l}, \mathbf{m})$ into a constant K', independent of N or n, and a function R', independent of the azimuthal quantum numbers $\mathbf{m}$. The precise separation is, to some extent, arbitrary, since any dependence on $\mathbf{l}$ or $\boldsymbol{\lambda}$ only can be drawn into either factor; the selection (33), (34) was chosen primarily to give the recurrence relations of Sec. 4 their simplest form. In the case of spherical symmetry,

$$L = M = \lambda_1 = \lambda_2 = 0, \quad m_1 = -m_2 = m, \quad l_1 = l_2 = \lambda = l, \quad K' = (-)^{l+m}(l + \tfrac{1}{2}), \tag{35}$$

and the R' differ from the functions R_{nl} of (1) and I only by a factor $(l + \frac{1}{2})^{-1}$.

If the spherical harmonics in (5) are given in their normalized form Y_l^m, (3c), the analogous radial functions R_Y can be factorized as in (32),

$$R_Y(N, \mathbf{l}, \mathbf{m}; r_1, r_2) = K_Y'(\mathbf{l}, \mathbf{m}) R'(N, \mathbf{l}; r_1, r_2), \tag{36}$$

where R' remains unaltered as in (34), whereas in view of (3c) and (26),

$$K_Y'(\mathbf{l}, \mathbf{m}) = 2\pi(-)^\lambda (LM\,|Y_{l_1}^{m_1}|\,l_2 m_2). \tag{37}$$

Here

$$(LM\,|Y_l^m|\,l'm') = (-)^M[(2l + 1)(2l' + 1)(2L + 1)/4\pi]^{\frac{1}{2}} \times \begin{pmatrix} L & l & l' \\ -M & m & m' \end{pmatrix}\begin{pmatrix} L & l & l' \\ 0 & 0 & 0 \end{pmatrix} = \iint [Y_L^M(\vartheta, \varphi)]^* Y_l^m(\vartheta, \varphi) Y_{l'}^{m'}(\vartheta, \varphi) \times \sin\vartheta\, d\vartheta\, d\varphi \tag{38}$$

is the integral of the product of three normalized harmonics taken over the whole unit sphere.[10] In view of the properties of the $3j$-symbols, the coefficients K', and hence the radial functions R, are nonzero only if the conditions

$$|l_1 - l_2| \leq L \leq l_1 + l_2 \tag{39}$$

are satisfied, as well as (15) and (20a). The functions R also vanish, in view of (13), (32), and (34), if

$$L \leq N < l_1 + l_2, \quad n \text{ even}, \tag{40a}$$

or

$$-L \leq N + 1 < l_1 - l_2, \quad n \text{ odd}, \quad r_2 > r_1. \tag{40b}$$

The hypergeometric series are polynomials if

$$N \geq l_1 + l_2, \quad n \text{ even},$$

or

$$N \geq l_1 - l_2 - 1, \quad n \text{ odd}; \tag{41}$$

if either equality holds, they reduce to the leading term unity. The particular case $N = L$ has been discussed in (19) and (20); if $N = -L - 1$, the only nonvanishing functions in (5) for $r_2 > r_1$ are those for which $l_2 = L + l_1$, and for these we have, in view of (22) or from Refs. 9 and 11,

$$I_0\begin{pmatrix} L, & l_1, & L + l_1 \\ M, & -m_1, & m_1 - M \end{pmatrix} = (-)^{M-m_1} \times \frac{2(2L)!\,(2l_1)!\,(l_1 + L)!\,(l_1 + L + m_1 - M)!}{(2l_1 + 2L + 1)!\,L!\,l_1!\,(L - M)!\,(l_1 + m_1)!}, \tag{42}$$

so that (5) and (32)–(34) yield

$$r^{-L-1}\Omega_L^M(\vartheta, \varphi) = \sum_{l,m} (-)^{l+m} \frac{(l + L + m - M)!}{(l + m)!\,(L - M)!} r_1^l r_2^{-L-l-1} \times \Omega_l^m(\vartheta_1, \varphi_1)\Omega_{L+l}^{M-m}(\vartheta_2, \varphi_2). \tag{43}$$

This corresponds to the expansion for normalized "irregular" solid harmonics given by Rose[6] and recently by Chiu.[14]

As in I, the transformation theory of the hypergeometric functions can be applied to the expression (34) for the functions R'. Thus (B 2.9.1, 2) or Eq. (20a) of I leads to

$$R'(N, 1; r_1, r_2) = \frac{(-\frac{1}{2}n; \lambda)(\frac{3}{2} + \frac{1}{2}n; L)}{(\frac{1}{2}; l_1 + 1)(\frac{3}{2} + \frac{1}{2}n; \lambda_1)} \frac{r_1^{l_1}(r_2^2 - r_1^2)^{N+2}}{r_2^{N+4+l_1}} \times F(\Lambda + 2 + \tfrac{1}{2}n, \tfrac{3}{2} + \tfrac{1}{2}n + \lambda_2; l_1 + \tfrac{3}{2}; r_1^2/r_2^2), \tag{44}$$

which shows that the radial functions are also rational in r_1 and r_2 if $\frac{1}{2}(l_1 + l_2 + N) + 1$ or $\frac{1}{2}(l_1 - l_2 + N + 1)$ are negative integers. Similarly (B 2.10.1) or (20b) of I yield

$$R'(N, 1; r_1, r_2) = \frac{2^{n+1}(-\frac{1}{2}n; \lambda)(\frac{3}{2} + \frac{1}{2}n; L)(2 + n; L)}{(1 + \frac{1}{2}n; \Lambda + 1)(\frac{3}{2} + \frac{1}{2}n; \lambda_1)(\frac{3}{2} + \frac{1}{2}n; \lambda_2)} r_1^{l_1} r_2^{N-l_1} \times F(\lambda - \tfrac{1}{2}n, -\tfrac{1}{2} - \tfrac{1}{2}n - \lambda_1; -n - 1 - L; (r_2^2 - r_1^2)/r_2^2) + \left[-\frac{(-)^{\lambda_1}(\frac{3}{2} + \frac{1}{2}n; L)}{(n + 2; L + 1)2^{n+2}} \frac{r_1^{l_1}(r_2^2 - r_1^2)^{N+2}}{r_2^{N+4+l_1}} \right] \times F\left(\Lambda + 2 + \tfrac{1}{2}n, \tfrac{3}{2} + \tfrac{1}{2}n + \lambda_2; n + 3 + L; \frac{r_2^2 - r_1^2}{r_2^2}\right), \tag{45}$$

where the coefficients have been simplified in view of the properties of the gamma function (B 1.2.6) and (B 1.2.15), or (23) and (25) of I. This equation shows the nature of the branch point as r_1 approaches r_2; the difficulties arising for integer values of n have been discussed in I, following Eq. (22); the result is either a polynomial or a series involving logarithmic terms.

In the case $L = 0$, it was shown in I that, by means of quadratic transformations applied to the hypergeometric functions, the radial functions R_{nl} could be expressed in several forms symmetric in r_1 and r_2, involving power series in $r_1r_2/(r_1 + r_2)^2$ or in $r_1r_2/(r_1^2 + r_2^2)$. The same transformations can be applied whenever $l_1 = l_2$, regardless of the value of L; for general values of l_1 and l_2, (34) shows that even the leading coefficients are different as $r_1 < r_2$ or $r_1 > r_2$. In consequence, it is unlikely that analogous simple symmetric expansions exist in the general case. On the other hand, the leading coefficients in (45) are invariant for $r_1 \gtrless r_2$, and together with the symmetry of the recurrence relations derived below, this suggests the existence of symmetric expansions involving power series in the two arguments $r_1r_2/(r_1^2 + r_2^2)$ and $(r_1^2 - r_2^2)/(r_1^2 + r_2^2)$ or similar variables, though presumably involving the one variable only to a finite power depending on $|l_1 - l_2|$. So far the writer has been unable to derive such expansions.

Quadratic transformations for arbitrary hypergeometric functions have recently been derived by Kuipers and Meulenbeld[15] in terms of generalized hypergeometric functions or MacRobert's E functions, [cf. (B 4) and (B 5)]. This generalization, however, is not quite relevant to the problem at this stage, as it corresponds to a generalization of the transformation from (27a) to (27b) of I, and not of the transformation from (19) to (27).

[14] Y. N. Chiu, J. Math. Phys. 5, 283 (1964).

[15] L. Kuipers and B. Meulenbeld, J. London Math. Soc. 35, 221 (1960).

It might be considered that the expansion (5) would simplify if one of the vectors, say $\mathbf{r}_1$, points in the direction of the polar axis; for this choice all the Legendre functions of $\cos\vartheta_1$ are 1 or 0, according as $m_1 = 0$ or $m_1 \neq 0$, and hence for all nonvanishing terms, $m_2 = M$. The individual terms in (5) are therefore considerably simpler than in the general case; on the other hand, because of the restrictions imposed on $\mathbf{r}_1$, the rotational quantum number l_1 ceases to be meaningful and any consistent expansion making use of this restriction should reasonably involve an implicit summation over l_1, i.e., over products involving $3j$-symbols. From an analytic point of view, these symbols are generalized hypergeometric series[9,16] [cf. also (B 4)] of unit argument and all integer parameters, and any expansion involving such functions is likely to lead back to functions of at least the same, and possibly higher, complexity. This has indeed been found to be the case, and in order not to complicate any further the mathematical apparatus required for the present paper, the case $\vartheta_1 = 0$ is to be considered separately in a later publication.

4. RECURRENCE RELATIONS

The relations between contiguous hypergeometric functions (B 2.8.28–45) can be used, as in I, to derive linear recurrence relations between any three radial functions R' for which L, l_1, l_2 and $\frac{1}{2}N$ differ by integers only; the recurrence formulas between the coefficients K' of (33) or (37) are known from the theory of angular momentum.[3–8,9,10] Equation (14a) shows that the functions F depend on n and L only through their sum N; according to (34),

$$\frac{R'(N, L+2, l_1, l_2)}{R'(N, L, l_1, l_2)} = \frac{3+N+L}{L-N} = -\frac{3+n+2L}{n}. \tag{46}$$

It is therefore sufficient to derive any further relations for varying values of the angular quantum numbers L, l_1, and l_2 only, leaving

$$n = N - L = \text{const}; \tag{47}$$

the value of N can then be increased or decreased in steps of 2 by means of (46). In view of the larger number of independent parameters, the number of recurrence relations for even small changes in 1 are considerable; we therefore confine our attention to the following special cases:

(i) Between any two of the three functions R', none of the numbers L, l_1, and l_2 differ by more than unity.

(ii) One of the angular quantum numbers remains constant, the second varies by at most unity, and the third by at most two units.

There are eight inequivalent three-term recurrence relations of type (i) and 12 of type (ii); for the sake of brevity, only those parameters are indicated which differ from L, l_1, l_2, e.g., $R'(L+, l_1-) = R'(L+1, l_1-1, l_2)$ [cf. (B 2.9)], and N is understood to vary according to (47). The formulas are

$$(\tfrac{3}{2}+\tfrac{1}{2}n+L)(r_2^2-r_1^2)R' = (\lambda_1+\tfrac{3}{2}+\tfrac{1}{2}n)r_2R'(L+, l_2+) - (\lambda_2+\tfrac{3}{2}+\tfrac{1}{2}n)r_1R'(L+, l_1+), \tag{48a}$$

$$= (\lambda-1-\tfrac{1}{2}n)r_2R'(L+, l_2-) - (\Lambda+2+\tfrac{1}{2}n)r_1R'(L+, l_1+), \tag{48b}$$

$$= (\Lambda+2+\tfrac{1}{2}n)r_2R'(L+, l_2+) - (\lambda-1-\tfrac{1}{2}n)r_1R'(L+, l_1-), \tag{48c}$$

$$= -(\tfrac{3}{2}+\lambda_2+\tfrac{1}{2}n)r_2R'(L+, l_2-) + (\lambda_1+\tfrac{3}{2}+\tfrac{1}{2}n)r_1R'(L+, l_1-); \tag{48d}$$

$$(\tfrac{1}{2}+\tfrac{1}{2}n+L)^{-1}R' = (\lambda-\tfrac{1}{2}n)^{-1}[r_2R'(L-, l_2+) + r_1R'(L-, l_1+)], \tag{49a}$$

$$= (\tfrac{1}{2}+\tfrac{1}{2}n+\lambda_1)^{-1}[r_2R'(L-, l_2-) - r_1R'(L-, l_1+)], \tag{49b}$$

$$= (\tfrac{1}{2}+\tfrac{1}{2}n+\lambda_2)^{-1}[-r_2R'(L-, l_2+) + r_1R'(L-, l_1-)], \tag{49c}$$

$$= (\Lambda+1+\tfrac{1}{2}n)^{-1}[r_2R'(L-, l_2-) + r_1R'(L-, l_1-)]; \tag{49d}$$

$$(l_2+\tfrac{1}{2})R' = (\tfrac{1}{2}+\tfrac{1}{2}n+L)r_2[R'(L-, l_2+)+R'(L-, l_2-)], \tag{50a}$$

$$= r_2[(\Lambda+2+\tfrac{1}{2}n)(\lambda_1+\tfrac{3}{2}+\tfrac{1}{2}n)R'(L+, l_2+) - (\lambda-1-\tfrac{1}{2}n)(\lambda_2+\tfrac{3}{2}+\tfrac{1}{2}n) \times R'(L+, l_2-)]/[(\tfrac{3}{2}+\tfrac{1}{2}n+L)(r_2^2-r_1^2)], \tag{50b}$$

$$= (r_2/r_1)[-(\lambda_1+\tfrac{3}{2}+\tfrac{1}{2}n)R'(l_1-, l_2+) + (\lambda-1-\tfrac{1}{2}n)R'(l_1-, l_2-)], \tag{51a}$$

$$= (r_2/r_1)[(\Lambda+2+\tfrac{1}{2}n)R'(l_1+, l_2+) + (\tfrac{3}{2}+\tfrac{1}{2}n+\lambda_2)R'(l_1+, l_2-)]; \tag{51b}$$

[16] P. E. Bryant, *Tables of Wigner 3j-Symbols* (Res. Rept. 60-1, published by University of Southampton, Southampton, England, 1960).

Errata: Following (47), value of L at constant N

$$(L+n+2)(\tfrac{3}{2}+\tfrac{1}{2}n+L)r_2R'$$
$$=(\tfrac{1}{2}+\tfrac{1}{2}n+L)_2(r_2^2-r_1^2)R'(L-,\,l_2-)$$
$$+(\lambda-1-\tfrac{1}{2}n)(\lambda_2+\tfrac{1}{2}n+\tfrac{3}{2})R'(L+,\,l_2-), \quad (52a)$$
$$=-(\tfrac{1}{2}+\tfrac{1}{2}n+L)_2(r_2^2-r_1^2)R'(L-,\,l_2+)$$
$$+(2+\Lambda+\tfrac{1}{2}n)(\lambda_1+\tfrac{1}{2}n+\tfrac{3}{2})R'(L+,\,l_2+). \quad (52b)$$

The other six relations of the type (ii) are obtained by an interchange of the subscripts 1 and 2 in (50)–(52). Although the resulting equations are invariant on interchanging (l_1, r_1) and (l_2, r_2), their derivation is not symmetrical; thus (50) follows from (B 2.8.32, 37), but the corresponding equations for varying l_1 follow from

$$\gamma(\gamma-1)[F(\gamma-)-F]=\alpha\beta zF(\alpha+,\,\beta+,\,\gamma+) \quad (53)$$

and from (B 2.9.1, 2). Equations (49 a,b) follow from (B 2.8.38, 43), and (48c, d) from (B 2.8.35, 42); the remaining relations are derived from these by linear elimination, though to prove (51), the values of L in (48) and (49) must be lowered or raised.

It should be remembered in applying the recurrence relations (48)–(52), that they do not apply to the full radial functions R of (32); these latter vanish whenever the triangular condition (39) is violated because of the factor K' in (33), whereas the factors R' have perfectly well defined, usually nonzero, values in accordance with (46) regardless of the relative values of L, l_1, and l_2, provided only (15) is satisfied.

5. AN OPERATIONAL EXPANSION FOR ARBITRARY FUNCTIONS

As in I, the way in which the power N enters into the expressions (32)–(34) allows the functions $R'(N, 1; r_1, r_2)$ to be expressed in operational form. For $r_2 > r_1$, the expressions differ according to the relative magnitudes of L and l_2. For the factor in the general term in (34), which depends on N, we have, using (11)–(14),

$$(-)^{l_2}2^{l_2+2s}(\tfrac{1}{2}L-\tfrac{1}{2}N;\lambda+s)$$
$$\times(-\tfrac{1}{2}-\tfrac{1}{2}N-\tfrac{1}{2}L;\lambda_2+s)r_2^{N-l_2-2s}$$
$$=r_2^{-1-l_2}\left(\frac{1}{r_2}\frac{\partial}{\partial r_2}\right)^{L-l_2}r_2^L$$
$$\times\left[\frac{\partial^2}{\partial r_2^2}-\frac{L(L+1)}{r_2^2}\right]^{\lambda+s}r^{N+1}, \quad L\geq l_2, \quad (54a)$$
$$=r_2^{l_2}\left(\frac{1}{r_2}\frac{\partial}{\partial r_2}\right)^{l_2-L}r_2^{-1-L}$$
$$\times\left[\frac{\partial^2}{\partial r_2^2}-\frac{L(L+1)}{r_2^2}\right]^{\lambda_2+s}r^{N+1}, \quad L\leq l_2. \quad (54b)$$

Hence any function $f(r)$, which can be represented as a power series in r, we can expand, in analogy to (5),

$$f(r)\Omega_L^M(\vartheta,\varphi)=\sum K'(1,\mathrm{m})f'(1;r_1,r_2)$$
$$\times\Omega_{l_1}^{m_1}(\vartheta_1,\varphi_1)\Omega_{l_2}^{m_2}(\vartheta_2,\varphi_2), \quad (55)$$

where K' is given by (33), or by (37) if normalized surface harmonics are used. For the radial functions we obtain from (34) and (54)

$$f'(1;r_1,r_2)$$
$$=2(-)^\lambda\sum_s\frac{r_1^{l_1+2s}g_s(1;r_2)}{(2l_1+2s+1)!!\,(2s)!!}, \quad r_2>r_1 \quad (56)$$

(for the double factorials see (43) of I), where

$$g_s(1;r_2)=r_2^{-1-l_2}\left(\frac{1}{r_2}\frac{d}{dr_2}\right)^{L-l_2}r_2^L$$
$$\times\left[\frac{d^2}{dr_2^2}-\frac{L(L+1)}{r_2^2}\right]^{\lambda+s}[r_2f(r_2)], \quad L\geq l_2, \quad (57a)$$
$$=r_2^{l_2}\left(\frac{1}{r_2}\frac{d}{dr_2}\right)^{l_2-L}r_2^{-1-L}$$
$$\times\left[\frac{d^2}{dr_2^2}-\frac{L(L+1)}{r_2^2}\right]^{\lambda_2+s}[r_2f(r_2)], \quad L\leq l_2. \quad (57b)$$

Alternatively, the powers of the operator $(r_2^{-1}d/dr_2)$ can be put last, with the result

$$g_s(1,r_2)=\frac{1}{r_2}\left[\frac{d^2}{dr_2^2}-\frac{l_2(l_2+1)}{r_2^2}\right]^{\lambda+s}\frac{1}{r_2^{l_2}}$$
$$\times\left[\frac{1}{r_2}\frac{d}{dr_2}\right]^{L-l_2}[r_2^{L+1}f(r_2)], \quad L\geq l_2, \quad (58a)$$
$$=\frac{1}{r_2}\left[\frac{d^2}{dr_2^2}-\frac{l_2(l_2+1)}{r_2^2}\right]^{\lambda_2+s}r_2^{l_2+1}$$
$$\times\left[\frac{1}{r_2}\frac{d}{dr_2}\right]^{l_2-L}\left[\frac{f(r_2)}{r_2^L}\right], \quad L\leq l_2. \quad (58b)$$

The quadratic operators occurring in (57) and (58) can be factorized, but not expressed as squares; hence the operational factorization of f_1 in (48) of I, in terms of Bessel functions of a differential operator, does not appear to have a simple analog in the general case.

The expressions (56)–(58) factorize analytically if f is a spherical Bessel function,

$$f(r)=w_L(kr), \qquad w_L=i_L,\,y_L,\,h_L^{(1)},\,h_L^{(2)} \quad (59)$$

in the usual notation, satisfying

$$[d^2/dr^2-L(L+1)/r^2][rf(r)]=-k^2rf(r). \quad (60)$$

In view of (B 7.2.44–46, 52, 53) and (B 7.11.5–13),

we have

$$(z^{-1}d/dz)^s[z^{-l}w_l(z)] = (-)^s z^{-l-s}w_{l+s}(z),$$
$$(z^{-1}d/dz)^s[z^{l+1}w_l(z)] = z^{l+1-s}w_{l-s}(z), \tag{61}$$

so that (56) and (57) or (58) yield

$$f'(1; r_1, r_2) = 2j_{l_1}(kr_1)w_{l_2}(kr_2), \qquad r_2 \geq r_1. \tag{62}$$

Substituting this into (55) and making use of (33) or (37), we find an expansion equivalent to the expansion theorem for spherical waves derived by Friedman and Russek[7]; apparent discrepancies are due to the differing definitions of the spherical harmonics. For modified spherical Bessel functions, the expressions corresponding to (62) become, in view of (B 2.7.19–22),

$$f = i_l(kr); \qquad f' = 2(-)^{\lambda}i_{l_1}(kr_1)i_{l_2}(kr_2),$$
$$f = k_l(kr); \quad f' = 2(-)^{\lambda_2}i_{l_1}(kr_1)k_{l_2}(kr_2), \quad r_2 \geq r_1. \tag{63}$$

It should be borne in mind that the actual signs in the expansion (55) are not necessarily those given in (62) or (63) in view of the changes in sign occurring in (33) and (37).

The algebraic recurrence relations (48)–(52) are not directly applicable to the operational expansion terms (55)–(58); it should, nevertheless, be possible to derive recurrence relations for the functions $f'(1)$, if necessary involving more than three terms. Such relations might lead to a considerable simplification in the evaluation of the radial functions.

APPENDIX: THE UNNORMALIZED 3j-SYMBOLS

The theory of the Wigner $3j$-symbols is well established[3–5] and their values have been extensively tabulated[10,16]; it may therefore appear futile to return to the use of unnormalized harmonics and $3j$-symbols associated with these. However, the use of integers has its advantages, compared with expressions involving square roots, and from this point of view, the symbols U introduced in (25) may be found useful. Their definition is easily generalized to any set of integral or half-integral parameters (j_s, m_s), provided $m_1 + m_2 + m_3 = 0$, all the $(j_s + m_s)$ as well as $2\Lambda = j_1 + j_2 + j_3$ are integers, and the triangular relation (39) holds for the j's. Using the abbreviations (27), we define

$$U\begin{pmatrix} j_1 & j_2 & j_3 \\ m_1 & m_2 & m_3 \end{pmatrix} = \sum_{\mu} (-)^{\sigma-\Lambda+\mu}\binom{2\lambda_1}{\lambda_1+\mu} \times \binom{2\lambda_2}{\lambda_2 - m_3 + \mu}\binom{2\lambda_3}{\lambda_3 + m_2 + \mu}, \tag{A1}$$

where

$$\sigma \equiv 2j_1 + m_2 - m_3 \equiv m_1 + 2m_2 \equiv -m_1 - 2m_3 \pmod 2, \tag{A2}$$

and the sum is to be taken over all integral or half-integral values of μ (depending on λ_1) for which all the binomial coefficients are nonzero. The relation of these quantities to Wigner's normalized $3j$-symbols[3–5] is given in (26); like the latter they are invariant under a cyclic permutation of (1, 2, 3), and are multiplied by $(-)^{2\Lambda}$ for a noncyclic permutation or for the transformation $\mathbf{m} \to -\mathbf{m}$. On the other hand, the constant numerator in the sum (A1) destroys the Regge symmetries[17] of the symbols under permutation of the triples $2\lambda_s, j_s+m_s, j_s-m_s$.

Against this loss of symmetry, the definition (A1) has the advantage that all the terms in the sum are integers which, even for $\Lambda = 16$, never exceed 10^9. For $j_1 = j_2 + j_3$, i.e., $\lambda_1 = 0$, the sum reduces to a single term,

$$U\begin{pmatrix} j_2 + j_3, & j_2, & j_3 \\ -m_2 - m_3, & m_2, & m_3 \end{pmatrix} = (-)^{j_2+j_3-m_2+m_3}\binom{2j_2}{j_2+m_2}\binom{2j_3}{j_3+m_3}. \tag{A3}$$

In view of the property of the binomial coefficients

$$\binom{N}{M} = \binom{N-1}{M-1} + \binom{N-1}{M}, \tag{A4}$$

the definition (A1) entails the recurrence formula

$$U\begin{pmatrix} j_1 & j_2 & j_3 \\ m_1 & m_2 & m_3 \end{pmatrix} = U\begin{pmatrix} j_1, & j_2 - \tfrac{1}{2}, & j_3 - \tfrac{1}{2} \\ m_1, & m_2 - \tfrac{1}{2}, & m_3 + \tfrac{1}{2} \end{pmatrix} - U\begin{pmatrix} j_1, & j_2 - \tfrac{1}{2}, & j_3 - \tfrac{1}{2} \\ m_1, & m_2 + \tfrac{1}{2}, & m_3 - \tfrac{1}{2} \end{pmatrix}; \tag{A5}$$

the equivalent formula for the normalized $3j$-symbols has been given by Edmonds.[4] Apart from signs, the relation (A5) is similar to that obtaining in Pascal's triangle; and since for $j_3 = 0$ the absolute values of U are binomial coefficients, the whole set of coefficients U can be regarded as a five-dimensional generalization of Pascal's triangle. The numbers can thus be generated by means of (A3) and (A5); for work with electronic computers, this would appear more convenient than the more usual representation of the squares of the normalized symbols as products and ratios of powers of primes.[10,16] A more detailed discussion of the symbols U is given elsewhere.

[17] T. Regge, Nuovo Cimento 10, 545 (1958).

Reprinted from
JOURNAL OF MATHEMATICAL PHYSICS VOLUME 5, NUMBER 2 FEBRUARY 1964
Printed in U.S.A.

Two-Center Expansion for the Powers of the Distance Between Two Points*

R. A. SACK
Laboratory of Molecular Structure and Spectra, University of Chicago, Chicago, Illinois
and
Department of Mathematics, Royal College of Advanced Technology, Salford, England†
(Received 16 August 1963)

The powers r^n of the distance between two points specified by spherical polar coordinates relating to two different origins, or of the modulus of the sum of three vectors, are expanded in spherical harmonics of the angles. The radial factors satisfy simple partial differential equations, and can be expressed in terms of Appell functions F_4, and Wigner or Gaunt's coefficients. In the overlap region, first discussed by Buehler and Hirschfelder, the expressions are valid for integer values of $n \geq -1$, but in the other regions, for arbitrary n. For high orders of the harmonics, individually large terms in the overlap region may have small resulting sums; as a consequence the two-center expansion is of limited usefulness for the evaluation of molecular integrals. Expansions are also derived for the three-dimensional delta function within the overlap region, and for arbitrary functions $f(r)$, valid outside that region.

1. INTRODUCTION

THE inverse distance between two points Q_1 and Q_2 specified by the polar coordinates $(r_1, \vartheta_1, \varphi_1)$ and $(r_2, \vartheta_2, \varphi_2)$ with respect to a common origin O, is given by the well-known Laplace expansion in powers of $r_</r_>$ and in terms of Legendre polynomials of the mutual direction cosine $(\cos \vartheta_{12})$. For powers other than the inverse first, analogous expansions exist *either* in powers of $r_</r_>$ *or* in $P_l(\cos \vartheta_{12})$; in the former case the angular dependence is given by Gegenbauer polynomials of $(\cos \vartheta_{12})$[1]; in the latter case, the writer has shown in two recent papers that the radial dependence can be expressed by means of Gauss' hypergeometric function[2]

$$F(\alpha, \beta; \gamma; z) = \sum \frac{(\alpha)_w (\beta)_w}{(\gamma)_w w!} z^w; \tag{1a}$$

$$(\alpha)_w = (\alpha; w) = \alpha(\alpha + 1) \cdots (\alpha + w - 1) = \Gamma(\alpha + w)/\Gamma(\alpha). \tag{1b}$$

In many physical problems, it is more convenient to express the positions of Q_1 and Q_2 in spherical polars about two different origins O_1 and O_2 in such a way that the polar axes and the planes defining $\varphi = 0$ are kept parallel. If the coordinates of O_2 with respect to O_1 are given by $(r_3 = a, \vartheta_3, \varphi_3)$, expansions for the inverse distance in terms of spherical harmonics of the angles have been given by Carlson and Rushbrooke, by Rose, and by Buehler and Hirschfelder.[3-6] The precise form of the expressions depends on the specific definition of the spherical harmonics; in the present context, the most useful are the unnormalized forms

$$\Theta_l^m(\vartheta, \varphi) = e^{im\varphi} P_l^{|m|}(\cos \vartheta), \tag{2a}$$

$$\Omega_l^m(\vartheta, \varphi) = e^{im\varphi} P_l^m(\cos \vartheta), \tag{2b}$$

and the normalized form

$$Y_l^m(\vartheta, \varphi) = [(2l + 1)(l - m)!/4\pi(l + m)!]^{\frac{1}{2}} \times e^{im\varphi} P_l^m(\cos \vartheta). \tag{2c}$$

Buehler and Hirschfelder[5] consider in detail the case $\vartheta_3 = 0$ and put

$$|Q_1Q_2|^{-1} = \sum B(l_1, l_2, |m|; r_1, r_2, a) \times \Theta_{l_1}^{-m}(\vartheta_1, \varphi_1)\Theta_{l_2}^m(\vartheta_2, \varphi_2)$$
$$[l_1, l_2 = 0, 1, \cdots; \quad -l_< \leq m \leq l_<; \quad l_< = \min(l_1, l_2)]. \tag{3}$$

They have shown that the form of the radial func-

* Supported in part by Office of Naval Research Contract Nonr-2121(01). This work was completed at the Theoretical Chemistry Institute, University of Wisconsin, Madison, Wisconsin, supported by National Aeronautics and Space Administration Grant NsG-275-62(4180).
† Permanent address.
[1] L. Gegenbauer, Wien. Sitzung. 70, 6, 434 (1874); 75, 891 (1877).
[2] R. A. Sack, J. Math. Phys. 5, 245 (1964); 5, 252 (1964). (Hereafter referred to as I and II, respectively).
[3] B. C. Carlson and G. S. Rushbrooke, Proc. Cambridge Phil. Soc. 46, 215 (1950).
[4] M. E. Rose, J. Math. and Physics 37, 215 (1958).
[5] R. J. Buehler and J. O. Hirschfelder, Phys. Rev., 83, 628 (1951); 85, 149 (1952).
[6] J. O. Hirschfelder, C. F. Curtiss and R. B. Bird, *Molecular Theory of Gases and Liquids* (John Wiley & Sons, Inc., New York, 1954).

tions B differs according to the relative values of r_1, r_2 and $r_3 = a$; there are, in fact, four distinct regions defined by the following inequalities [see Fig. 1(a)]:

$$S_0: |r_1 - r_2| \leq r_3 \leq r_1 + r_2; \quad S_1: r_1 \geq r_2 + r_3, \qquad S_2: r_2 \geq r_1 + r_3; \quad S_3: r_3 \geq r_1 + r_2. \tag{4}$$

The same arguments apply to the more general expansions for arbitrary values of the angle ϑ_3 and of the power n of r.

$$r^n = \sum_{l,m} [{}_3R(n; l_1, l_2, l_3, m_1, m_2, m_3; r_1, r_2, r_3) \times \prod_1^3 \Omega_{l_i}^{m_i}(\vartheta_i, \varphi_i)]; \tag{5}$$

if either of the definitions (2a) or (2c) is used for the spherical harmonics, the corresponding radial functions differ from those in (5) by constants only; the subscripts Θ or Y are added to ${}_3R$ in such cases.

For the inverse first power $n = -1$, the functions ${}_3R \equiv {}_3R_i$ vanish in each of the "outer" regions S_i $(i = 1, 2, 3)$ unless

$$l_i = l_j + l_k; \quad l_s \geq 0 \qquad (s = 1, 2, 3), \tag{6a}$$

and

$$m_i + m_j + m_k = 0, \; |m_s| \leq l_s \quad (s = 1, 2, 3); \tag{6b}$$

throughout this paper, (i, j, k) denote permutations of (1, 2, 3). If (6) is satisfied, ${}_3R_i$ consists of a single term,

$${}_3R_i = {}_3K_i(-1; l_i, l_j, l_k, m_i, m_j, m_k) r_j^{l_j} r_k^{l_k} / r_i^{l_i+1}, \tag{7}$$

where the coefficients ${}_3K_i$ can be expressed in terms of Wigner coefficients[3,4] or as ratios of factorials.[5,6]

For the overlap region S_0, Buehler and Hirschfelder[5,6] found an expression for B_0 as a double power series in r_1/a and r_2/a for which they tabulated the coefficients as ratios of integers for $0 \leq m \leq l_1 \leq l_2 \leq 3$. They could not derive a generally valid formula in this region, though in their later paper (second paper of Ref. 5) they gave a (rather cumbersome) generating function for the function B_0.

The aim of the present paper is to derive generally valid expressions for B_0 or ${}_3R_i$ in all the regions; but for the sake of greater symmetry, the vector $\mathbf{r} = (r, \vartheta, \varphi)$ in (5) is to be understood to mean, not the vector Q_1Q_2, i.e. $\mathbf{r}_2 + \mathbf{r}_3 - \mathbf{r}_1$, but the vector sum $\mathbf{r}_1 + \mathbf{r}_2 + \mathbf{r}_3$; the corresponding radial functions ${}_3R$ differ only by the factor $(-)^{l_1}$.[3] As in I and II, the functions are derived as solutions of sets of

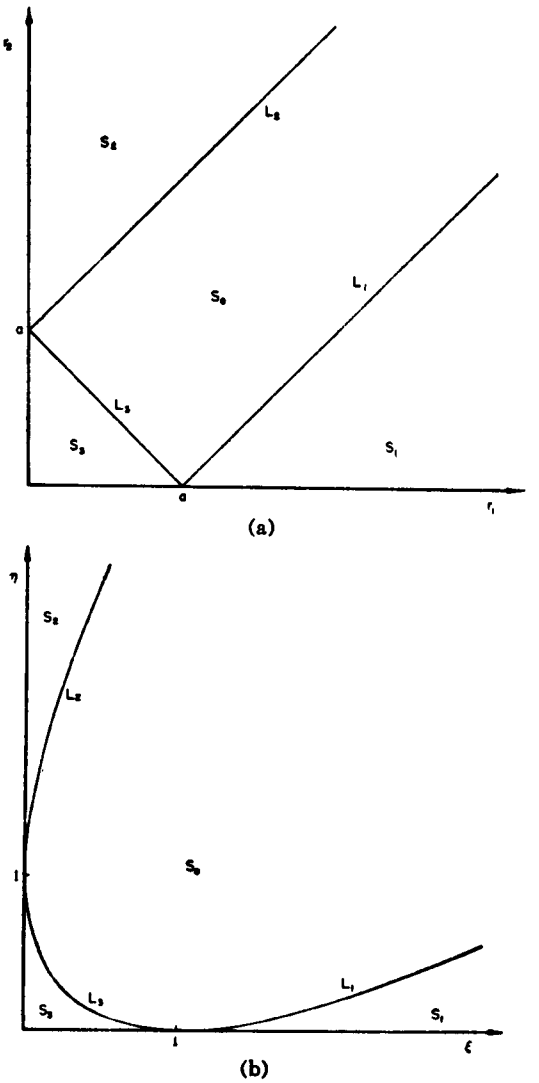

FIG. 1. The four regions S_0, S_1, S_2, S_3 and their boundaries. (a) as functions of r_1 and r_2; (b) as functions of ξ and η.

partial differential equations; they can be expressed in terms of the Appell functions F_4, which form a generalization to two variables of the hypergeometric function (1):

$$F_4(\alpha, \beta; \gamma, \gamma'; \xi, \eta) = \sum \frac{(\alpha)_{u+v}(\beta)_{u+v}}{(\gamma)_u(\gamma')_v u!\, v!} \xi^u \eta^v, \tag{8}$$

summed over all nonnegative values of u and v. The theory of these functions is given in detail in the monographs by Appell and Kampé de Fériet[7,8];

[7] P. Appell, "Sur les fonctions hypergéometriques de plusieurs variables" in *Mémorial des Sciences Mathématiques*, Fasc. 3, (Gauthier-Villars, Paris, 1925).

[8] P. Appell and J. Kampé de Fériet, *Fonctions hypergéometriques et hypersphériques, Polynômes d' Hermite* (Gauthier-Villars, Paris, 1926).

most of the relevant formulas are to be found in Chap. 5 of the Bateman Manuscript Project,[9] but for the benefit of the reader, all the formulas utilized in the present paper will be collected in the Appendix. The differential equations do not involve the azimuthal quantum numbers m, and hence the nature of the functions ${}_2R$ does not depend on these numbers; they can only affect the leading coefficients. In the outer regions, these constants can be determined from the results of I and II, and in the inner region S_0, indirectly, by means of certain linear relations between Appell functions along critical lines. They can be expressed, as in II, by means of $3j$-symbols, Wigner coefficients, or integrals of triple products of spherical harmonics (Gaunt's coefficients).[10-11]

It is found that for $n = -1$ the functions ${}_2R \equiv {}_2R_0$ appear in the region S_0 with nonzero coefficients whenever

$$|l_1 - l_2| \leq l_3 \leq l_1 + l_2, \quad l_1 + l_2 + l_3 = \text{even}, \tag{9}$$

so that by confining attention to this case, it would not be possible to determine the leading coefficients in this region, unless at least one of Eqs. (6a) is satisfied. In consequence, the general case (5) is considered from the start; the resulting formulas are valid for arbitrary values of n in the outer regions, but in S_0 only for integer $n \geq -1$. The formulas obtained for S_1, S_2, and S_3 can be put into an operational form which permit generally valid expansions to be derived in these regions for any function of r; this is done in Sec. 4. Within S_0, on the other hand, the Laplacean operator applied to the expansion for r^{-1} does not vanish; this gives an analogous expansion for the three-dimensional Dirac delta function and its derivatives.

2. MATHEMATICAL DERIVATION

The functions r^n satisfy the differential equation

$$\nabla_1^2(r^n) = \nabla_2^2(r^n) = \nabla_3^2(r^n) = n(n+1)r^{n-2}, \tag{10}$$

which, when substituted into (5), yields

$$\left[\frac{\partial^2}{\partial r_s^2} + \frac{2}{r_s}\frac{\partial}{\partial r_s} - \frac{l_s(l_s+1)}{r_s^2}\right] {}_2R(n, 1, \mathrm{m})$$

$$= \text{invariant} \quad (s = 1, 2, 3), \tag{11a}$$

$$= n(n+1)\, {}_2R(n-2, 1, \mathrm{m}). \tag{11b}$$

Furthermore, all the ${}_2R$ are homogeneous functions of the variables r_s of degree n, and in the region S_i they are regular as r_j and r_k tend to zero; hence they must be of the form

$${}_2R_i = r_j^{l_j} r_k^{l_k} r_i^{n-l_j-l_k} G_i(n, 1, \mathrm{m}; r_j/r_i, r_k/r_i), \tag{12}$$

where

$$G_i(n, 1, \mathrm{m}) = \sum C_{\mu\nu}(n, 1, \mathrm{m})(r_j/r_i)^\mu (r_k/r_i)^\nu. \tag{13}$$

Substitution of (11) into (12) and (13) leads to the recurrence relations

$$(\mu+2)(2l_j+\mu+3)C_{\mu+2,\nu}(n)$$

$$= (\nu+2)(2l_k+\nu+3)C_{\mu,\nu+2}(n), \tag{14a}$$

$$= (n+1+l_i-l_j-l_k-\mu-\nu)$$

$$\times (n-l_i-l_j-l_k-\mu-\nu)C_{\mu\nu}(n), \tag{14b}$$

$$= n(n+1)C_{\mu\nu}(n-2). \tag{14c}$$

This defines G_i as an Appel function F_4 in the variables

$$\xi = r_j^2/r_i^2, \qquad \eta = r_k^2/r_i^2: \tag{15}$$

$$G_i(n, 1, \mathrm{m}) = K_i(n, 1, \mathrm{m})F_4(\Lambda - \tfrac{1}{2}n,$$

$$\lambda_i - \tfrac{1}{2} - \tfrac{1}{2}n;\ l_j + \tfrac{3}{2},\ l_k + \tfrac{3}{2};\ \xi, \eta), \tag{16}$$

where we abbreviate

$$\Lambda = \tfrac{1}{2}(l_1 + l_2 + l_3), \quad \lambda_s = \Lambda - l_s$$

$$(s = 1, 2, 3). \tag{17}$$

In view of (11a) and (12), it is easily shown that the function G_i satisfies the set of differential equations of Appell's function (A2) (see Appendix), with the variables and parameters defined in (15)–(17). Hence, according to (A3), the complete set of solutions satisfying the differential equations for ${}_2R(n, 1, \mathrm{m})$ becomes

$$\Psi_{i0} = r_i^n (r_j/r_i)^{-l_j-1}(r_k/r_i)^{-l_k-1} F_4(-\Lambda - \tfrac{1}{2}n - \tfrac{3}{2},$$

$$-\lambda_i - 1 - \tfrac{1}{2}n;\ \tfrac{1}{2} - l_j,\ \tfrac{1}{2} - l_k;\ \xi, \eta), \tag{18a}$$

$$\Psi_{ii} = r_i^n (r_j/r_i)^{l_j}(r_k/r_i)^{l_k} F_4(\Lambda - \tfrac{1}{2}n, \lambda_i - \tfrac{1}{2}n - \tfrac{1}{2};$$

$$\tfrac{3}{2} + l_j, \tfrac{3}{2} + l_k; \xi, \eta), \tag{18b}$$

$$\Psi_{ij} = r_i^n (r_j/r_i)^{-l_j-1}(r_k/r_i)^{l_k} F_4(\lambda_j - \tfrac{1}{2}n - \tfrac{1}{2},$$

$$-\lambda_k - 1 - \tfrac{1}{2}n;\ \tfrac{1}{2} - l_j,\ \tfrac{3}{2} + l_k;\ \xi, \eta), \tag{18c}$$

$$\Psi_{ik} = r_i^n (r_j/r_i)^{l_j}(r_k/r_i)^{-l_k-1} F_4(\lambda_k - \tfrac{1}{2}n - \tfrac{1}{2},$$

$$-\lambda_j - 1 - \tfrac{1}{2}n;\ \tfrac{3}{2} + l_j,\ \tfrac{1}{2} - l_k;\ \xi, \eta). \tag{18d}$$

[9] Bateman Manuscript Project, *Higher Transcendental Functions*, edited by A. Erdélyi (McGraw-Hill Book Company, Inc., New York, 1953). Formulas in this work are directly referenced by the prefix B.

[10] See Refs. 3–5 and 10 of II.

[11] J. A. Gaunt, Phil. Trans. Roy. Soc. **A228**, 157 (1929).

Here the first subscript in notation Ψ_{ti} indicates which radius r_t occurs in the denominator of the definitions (15) for ξ and η, and the second subscript shows that Ψ_{ti}/r_i^n becomes singular as $r_t \to 0$; if $t = 0$, this ratio becomes singular, whichever radius tends to zero. Further we denote the function ${}_2R$ in the region S_w by ${}_2R_w$ as in (12), and the coefficients of (18) in the expression for ${}_2R_w$ by K_{wti}:

$$ {}_2R_w(n, \mathrm{l}, \mathrm{m}) = \sum_t K_{wti}(n, \mathrm{l}, \mathrm{m})\Psi_{ti}(n, \mathrm{l}). \qquad (19) $$

In view of (A1) the Appell functions in the outer regions are convergent only if $i = w$, and the regularity of ${}_2R_i$ for small values of r_j and r_k requires that the solution is of the form given by (12) and (16),

$$ K_{iti} \equiv 0, \qquad t \neq i; \qquad K_{iii} = K_i. \qquad (20) $$

In the region S_0, the series are always divergent unless they terminate; in those cases in which (18) leads to useful expansions, the choice of i is somewhat arbitrary. The nature of the functions Ψ of (19) being known from (18), it remains to calculate the coefficients K_i and K_{0ti}.

To determine K_i in S_i we provisionally combine $\mathbf{r}_j + \mathbf{r}_k$ to a vector $(r_{jk}, \vartheta_{jk}, \varphi_{jk})$; then according to (19) of I and the addition theorem for the $P_l(\cos\vartheta_{12})$ [(B 3.11.2)], we have

$$ r^n = \sum_{l,\mathrm{m}} \Big[r_i^{n-l} r_{jk}^l (-)^{l+\mathrm{m}} \Omega_l^{-\mathrm{m}}(\vartheta_i, \varphi_i)\Omega_l^{\mathrm{m}}(\vartheta_{jk}, \varphi_{jk}) $$

$$ \times \frac{(-\frac{1}{2}n)_l}{(\frac{1}{2})_l} F(l - \tfrac{1}{2}n, -\tfrac{1}{2} - \tfrac{1}{2}n; \tfrac{3}{2} + l; \frac{r_{jk}^2}{r_i^2}) \Big]. \qquad (21) $$

This expression involves r_{jk} only through the solid harmonics $r_{jk}^l\Omega_l^{\mathrm{m}}$ and through positive even powers $r_{jk}^{2\nu}$; both factors are regular functions of r_j and r_k. If these products, in turn, are expanded in spherical harmonics of (ϑ_j, φ_j) and (ϑ_k, φ_k), we see from (5) and (32)–(34) of II that the lowest power 2ν which contributes to terms for which $l_j + l_k - l = 2\lambda$ occurs for $\nu = \lambda$, irrespective of n. We have, from (5) and (30) of II,

$$ r_{jk}^{l+2\lambda}\Omega_l^{\mathrm{m}}(\vartheta_{jk}, \varphi_{jk}) = (-)^{\mathrm{m}} \sum r_j^{l_j} r_k^{l_k} \Omega_{l_j}^{\mathrm{m}_j}(\vartheta_j, \varphi_j)\Omega_{l_k}^{\mathrm{m}_k}(\vartheta_k, \varphi_k) $$

$$ \times \frac{(\frac{1}{2}; l_j + l_k + 1)\lambda!}{(\frac{1}{2}; l_j)(\frac{1}{2}; l_k)} I_0\begin{bmatrix} l & l_j & l_k \\ \mathrm{m} & -\mathrm{m}_j & -\mathrm{m}_k \end{bmatrix} + \cdots, \qquad (22) $$

where I_0 is Gaunt's coefficient[11]

$$ I_0\begin{bmatrix} l & l' & l'' \\ m & m' & m'' \end{bmatrix} = \int_{-1}^{1} P_l^m(x)P_{l'}^{m'}(x)P_{l''}^{m''}(x)\,dx. \qquad (23) $$

If we put $l = l_i$, $m = -m_i$, $\lambda = \lambda_i$, and use the abbreviations (17), the constant $K_i(n, \mathrm{l}, \mathrm{m})$ in (16) is found, from (21)–(23) and (1),

$$ K_i(n, \mathrm{l}, \mathrm{m}) = (-)^{l_i} \frac{(l_i + \frac{1}{2})(-\frac{1}{2}n; \Lambda)(-\frac{1}{2} - \frac{1}{2}n; \lambda_i)}{(\frac{1}{2}; l_i)(\frac{1}{2}; l_k)} $$

$$ \times I_0\begin{bmatrix} l_i & l_j & l_k \\ -m_i & -m_j & -m_k \end{bmatrix}. \qquad (24) $$

The radial functions ${}_2R_i$ in the outer regions are thus completely determined by (12), (16), and (24). The corresponding expressions in the overlap region S_0 can be obtained by means of the linear relation (A8) between the four solutions (A3) of the differential equations (A2) on the critical lines (A4) (see Fig. 1). These lines correspond exactly to the boundaries L_i separating the regions S_i from S_0, but the ${}_2R_w$ must be brought to a common set of variables before (A8) can be applied. In (18) we can transform Ψ_{ji}, on which ${}_2R_j$ solely depends, into a linear combination of Ψ_{ti} and Ψ_{tj} by means of (A6), but the resulting series are in general divergent. The only cases in which (A6) leads to an expression which can be usefully interpreted without recourse to contour integration, are those in which the initial series terminates, i.e., where α or β is a nonpositive integer; then (A6) shows that one of the series in the new variables has zero coefficient and the other terminates. Applying this argument to the set (18), we find we can deal with two cases:

(A) n is a nonnegative even integer; then r^n is analytic throughout and can be represented by a finite expansion common to all regions; the value of i in (18) and (19) is immaterial, and the result can be expressed in a form involving only positive powers of the r_s.

(B) n is an odd integer ≥ -1; then

$$ \Psi_{ji} = T_{ji}\Psi_{ii}; $$

$$ T_{ji} = (-)^{\frac{1}{2}+\frac{1}{2}n-\lambda_j} \frac{\Gamma(\frac{3}{2} + l_i)\Gamma(\frac{1}{2} + l_j)}{\Gamma(\Lambda - \frac{1}{2}n)\Gamma(2 + \frac{1}{2}n + \lambda_k)}. \qquad (25) $$

Now since ${}_2R_0 = {}_2R_s$ on $L_s (s = 1, 2, 3)$, the coefficients K_{0ti} in (19) can be determined from (24) and (A8) leading to

$$ K_{0ii} = \tfrac{1}{2}K_i, \quad K_{0ij} = \tfrac{1}{2}K_{jij} = \tfrac{1}{2}K_j/T_{ji}, $$

$$ K_{0ik} = \tfrac{1}{2}K_{kik} = \tfrac{1}{2}K_k/T_{ki}, \qquad (26) $$

$$ K_{0i0} = -\tfrac{1}{2}K_i $$

$$ \times \frac{\Gamma(\frac{3}{2} + l_i)\Gamma(\frac{3}{2} + l_k)\Gamma(1 + \frac{1}{2}n - \Lambda)\Gamma(\frac{3}{2} + \frac{1}{2}n - \lambda_i)}{\Gamma(\frac{1}{2} - l_i)\Gamma(\frac{1}{2} - l_k)\Gamma(2 + \frac{1}{2}n + \lambda_i)\Gamma(\frac{3}{2} + \frac{1}{2}n + \Lambda)}, \qquad (27a) $$

$$= (-)^{l_i+1}\tfrac{1}{2}(l_i+\tfrac{1}{2}) \times \frac{(\tfrac{1}{2};\, l_j+1)(\tfrac{1}{2};\, l_k+1)}{(1+\tfrac{1}{2}n;\, \lambda_i+1)\left(\frac{3}{2}+\frac{n}{2};\, \Lambda+1\right)} \times I_0\begin{bmatrix} l_i & l_j & l_k \\ -m_i & -m_j & -m_k \end{bmatrix}. \quad (27b)$$

The expression (27a) is meaningless $(0\cdot\infty)$ if $\lambda_i > \frac{1}{2} + \frac{1}{2}n$; nevertheless (27b) is valid for all values of l and m satisfying (6b) and (9); the result could first be derived for n raised by a sufficiently large even number for this difficulty to disappear, and then be extended by repeated application of (11b).

3. DISCUSSION OF RESULTS

As in II, it is convenient to factorize the expression for the functions ${}_2R$ in (5) in the form

$${}_2R(n, 1, \mathrm{m}; r_1, r_2, r_3) = {}_2K'(1, \mathrm{m})\ {}_2R'(n, 1; r_1, r_2, r_3), \quad (28)$$

where the constant ${}_2K'$ is independent of n and the values of r_s and comprises the complete dependence on m. The selection preferred by the writer is

$${}_2K'(1, \mathrm{m}) = (l_1+\tfrac{1}{2})(l_2+\tfrac{1}{2})(l_3+\tfrac{1}{2}) \times I_0\begin{bmatrix} l_1 & l_2 & l_3 \\ -m_1 & -m_2 & -m_3 \end{bmatrix}, \quad (29)$$

where the I_0 are Gaunt's coefficients[11] defined in (23), or if the unnormalized $3j$ symbols defined in (25) and (29) of II, and the abbreviations (17) are used,

$${}_2K'(1, \mathrm{m}) = 2(-)^{\Lambda}\frac{\Lambda!}{(2\Lambda+1)!} \times \prod_{s=1}^{3}\left[\frac{(l_s-m_s)!}{\lambda_s!}(l_s+\tfrac{1}{2})\right] \times U\begin{bmatrix} l_1 & l_2 & l_3 \\ -m_1 & -m_2 & -m_3 \end{bmatrix}. \quad (30)$$

The second factor ${}_2R'$ in (28) differs according to the region S_w; in the "outer" regions S_i we obtain, from (12), (16), (17), and (24),

$${}_2R'_i(n, 1; r_i, r_j, r_k) = (-)^{l_i} \times \frac{(-\tfrac{1}{2}n;\, \Lambda)(-\tfrac{1}{2}-\tfrac{1}{2}n;\, \lambda_i)}{(\tfrac{1}{2};\, l_j+1)(\tfrac{1}{2};\, l_k+1)}\left(\frac{r_j}{r_i}\right)^{l_j}\left(\frac{r_k}{r_i}\right)^{l_k} r_i^n \times F_4(\Lambda-\tfrac{1}{2}n, \lambda_i-\tfrac{1}{2}-\tfrac{1}{2}n;\, l_j+\tfrac{3}{2},\ l_k+\tfrac{3}{2};\, r_j^2/r_i^2,\, r_k^2/r_i^2). \quad (31)$$

In the overlap region S_0, the expressions for ${}_2R'$ are valid, according to the discussion of the previous chapter, only if n is an integer ≥ 1; two cases are to be distinguished:

(A) n even ≥ 0; then ${}_2R$ is the same expression in all four regions,

$${}_2R'_1 = {}_2R'_2 = {}_2R'_3 = {}_2R'_0. \quad (32)$$

(B) n odd ≥ -1; then according to (18), (19), (26), and (27),

$${}_2R'_0 = \tfrac{1}{2}({}_2R'_1 + {}_2R'_2 + {}_2R'_3) - \tfrac{1}{2}(-)^{l_i} \times \frac{(\tfrac{1}{2};\, l_j)(\tfrac{1}{2};\, l_k)}{(1+\tfrac{1}{2}n;\, \lambda_i+1)(\frac{3}{2}+\tfrac{1}{2}n;\, \Lambda+1)} \times r_i^n\left(\frac{r_i}{r_j}\right)^{l_j+1}\left(\frac{r_i}{r_k}\right)^{l_k+1} F_4\left(-\tfrac{3}{2}-\tfrac{1}{2}n-\Lambda,\ -1-\tfrac{1}{2}n-\lambda_i;\, \tfrac{1}{2}-l_j,\, \tfrac{1}{2}-l_k;\, \frac{r_j^2}{r_i^2}, \frac{r_k^2}{r_i^2}\right). \quad (33)$$

Equations (31) and (33) show that for odd n those functions which represent ${}_2R'$ in the outer regions appear with half their coefficient in the overlap region and vanish in the other outer regions; the last term in (33), which is specific to S_0, could equally well be expressed in terms of Appell functions with r_j or r_k in the denominator of the arguments, the results being a polynomial in each case.

If the spherical harmonics in (5) are given in their normalized form (2c), the corresponding radial functions ${}_2R_\Upsilon$ factorize, in analogy to (28), into functions ${}_2R'$, which are the same as in (31) and (33), and constants ${}_2K'_\Upsilon$ given, in view of (2) and (29), (30),

$${}_2K'_\Upsilon = (-)^{m_1}4\pi^2(l_1, -m_1\,|\,Y^{m_3}_{l_3}|\,l_2, m_2), \quad (34a)$$

$$= 2\pi^{\frac{1}{2}}[(2l_1+1)(2l_2+1)(2l_3+1)]^{\frac{1}{2}} \times \begin{bmatrix} l_1 & l_2 & l_3 \\ m_1 & m_2 & m_3 \end{bmatrix}\begin{bmatrix} l_1 & l_2 & l_3 \\ 0 & 0 & 0 \end{bmatrix}, \quad (34b)$$

in terms of integrals of products of three harmonics over the unit sphere or of (normalized) $3j$-symbols [cf. (37), (38) and Ref. 10 of II].

The main application of the expressions derived in this paper is likely to be the evaluation of integrals for the interaction between two "charge" distributions referred to different origins and interacting with a negative power of the distance,

$$\iint \rho_1(\mathbf{r}_1)\rho_2(\mathbf{r}_2)\ |Q_1Q_2|^n\ d^3\mathbf{r}_1\ d^3\mathbf{r}_2. \quad (35)$$

If the functions ρ are expanded in spherical harmonics,

$$\rho_u = \sum W_u(l_u, m_u; r_u)\Omega^{m_u}_{l_u}(\vartheta_u, \varphi_u), \quad u = 1, 2, \quad (36)$$

the expansion for $|Q_1Q_2|^n$ is given by (5) and (28)–(34), except for a factor $(-)^{l_3}$ in each term, as discussed in the introduction and by Carlson and Rushbrooke.[3] The orthogonality of the functions leads to straightforward integrations over the angles for common values of l_1, m_1, l_2, m_2, and the results have to be summed over all compatible values of l_3. The spherical harmonics of ϑ_3 and φ_3 are best left unnormalized, even if the expansion (36) is given in normalized harmonics; in particular, for the case considered by Buehler and Hirschfelder,[5] $\vartheta_3 = 0$, we have $\Omega = 1$ $(m_3 = 0)$, $\Omega = 0$ $(m_3 \neq 0)$.

For $n = -1$, the results in the outer regions have been known from previous work[3-6]; for other negative integer values of n and $\vartheta_3 = 0$, an expansion has been derived by Prigogine[12] by means of the appropriate Gegenbauer polynomials,[1] which were then reexpanded in terms of spherical harmonics; the resulting expressions are valid in the region S_3 only, though this limitation has not been noticed by Prigogine. The complete analysis of the expansions for general values of n and $\vartheta_3 = 0$, which implies a summation over l_3 in (5), leads to expressions for the radial factors which involve more complicated functions than the Appell polynomials used in the present paper, and for this reason is not discussed here.

The most important case considered is $n = -1$, for which we obtain, for ${}_2R'$ in (31) and (33),

$$ {}_2R'_i = (-)^{l_i} \times \frac{4(2l_i - 1)!!}{(2l_i + 1)!!\,(2l_k + 1)!!} \frac{r_j^{l_j} r_k^{l_k}}{r_i^{l_i+1}} \delta_{l_i, l_j + l_k}, \tag{37} $$

in agreement with previous work,[3-6] and for the overlap region S_0,

$$ \begin{aligned} {}_2R'_0 &= \tfrac{1}{2}({}_2R'_1 + {}_2R'_2 + {}_2R'_3) - (-)^{l_3} \\ &\times \frac{(2l_1 - 1)!!\,(2l_2 - 1)!!}{(2\lambda_3 + 1)!!\,2^\Lambda(\Lambda + 1)!} \left(\frac{a}{r_1}\right)^{l_1+1} \left(\frac{a}{r_2}\right)^{l_2+1} a^{-1} \\ &\times F_4(-1 - \Lambda, -\tfrac{1}{2} - \lambda_3; \tfrac{1}{2} - l_1, \\ &\times \tfrac{1}{2} - l_2; r_1^2/a^2, r_2^2/a^2), \end{aligned} \tag{38} $$

where $(2k)!! = 2^k k!$, $(2k - 1)!! = 2^k(\tfrac{1}{2})_k$ [cf. (43) of I]; the function F_4 in (38) represents a polynomial of degree $\Lambda + 1$ in ξ and η, or $2(\Lambda + 1)$ in (r_1/a) and (r_2/a). By substituting (29), (30), and (38) into (5) with the special value $\vartheta_3 = 0$, using the harmonics Θ of (2) instead of Ω, and summing over l_3, the writer has been able to reproduce and extend the list of coefficients tabulated by Buehler and Hirschfelder.[5,6]

The lack of an expansion for $n < -1$ valid within S_0 is a serious limitation to the applicability of the method to molecular problems; it precludes its use for the evaluation of relativistic corrections to Coulomb energies, for which $n = -2$, or of van der Waals energies $(n = -6)$ for interpenetrating or even closely approaching elongated distributions. The existence of expansions valid in S_0 for fractional n appears doubtful because of the highly complicated branch points of the function ${}_2R'_0$ corresponding to the physical singularity at $\mathbf{r} = 0$. On the other hand, if the relation

$$ \nabla^2(r^{-1}) = -4\pi\delta^3(r), \tag{39} $$

where δ^3 is the three-dimensional Dirac delta function, is applied to (37) and (38), an expansion for δ^3 is obtained, analogous to (5) and (28)–(33), with

$$ {}_2R'_i(\delta, 1) = 0, \qquad i = 1, 2, 3, \tag{40a} $$

$$ \begin{aligned} &{}_2R'_0(\delta, 1) \\ &= \frac{(-)^{l_3+1}(2l_1 - 1)!!\,(2l_2 - 1)!!}{\pi(2\lambda_3 - 1)!!\,2^{\Lambda-2}\Lambda!} \left(\frac{a}{r_1}\right)^{l_1+1} \left(\frac{a}{r_2}\right)^{l_2+1} a^{-3} \\ &\times F_4(-\Lambda, \tfrac{1}{2} - \lambda_3; \tfrac{1}{2} - l_1, \tfrac{1}{2} - l_2; r_1^2/a^2, r_2^2/a^2). \end{aligned} \tag{40b} $$

In contrast to (31) and (33), the functions ${}_2R'(\delta)$ are discontinuous along the boundaries L_i; hence, although the Laplacean operator could, in turn, be applied to δ^3, any integral making use of such an expansion for $\nabla^2(\delta^3)$ would have to be supplemented by line integrals taken along the L_i, and correspondingly for higher derivatives.

Even in such cases, where the complete expansion is known in S_0, its use for the numerical evaluation of integrals may give rise to considerable difficulties. The joint degree in r_1 and r_2 of the terms in ${}_2R'_0$,

$$ w = -2 - l_1 - l_2 + \mu + \nu, \tag{41} $$

may be positive as well as negative; on the other hand, for large values of $(r_1 + r_2)$, the functions cannot increase faster than with this sum raised to the nth power. Hence for $n = -1$, all those terms in a given ${}_2R'_0$ with a constant value of $w \geq 0$ must contain the factor $(r_1 - r_2)^{w+1}$, which, in view of (4), remains bounded. If, therefore, an attempt is made to evaluate the integrals in (35) and (36) term by term over the expansions for $1/r$ in (12) and (13), we obtain repeated integrals of

[12] I. Prigogine, *The Molecular Theory of Solutions* (North-Holland Publishing Company, Amsterdam, 1957).

the form

$$a^{l_1+l_2+1-\mu-\nu}C_{\mu\nu}\int r_1^{1-l_1+\mu}W_1(l_1, m_1; r_1)\,dr_1 \times \int r_2^{1-l_2+\nu}W_2(l_2, m_2; r_2)\,dr_2, \qquad (42)$$

with limits corresponding to the boundaries of S_0. These terms are likely to be largest for large μ and ν, but add up to a small sum when summed over constant values of w, thereby reducing the accuracy of any numerical method employed. To avoid this difficulty, we could first calculate ${}_2R_0'(-1, 1)$ over a grid in S_0, and evaluate the integrals by a suitable two-dimensional quadrature formula. This is bound to be more cumbersome than the repeated integration in (42), and also necessitates knowledge of recurrence formulas by which R_0 can be computed for large l from values with small l without loss of accuracy; the writer has been unable to derive such recurrence formulas, not only those involving three functions as suggested by Appell,[7,8] but even numerically useful formulas involving four or more terms.

The usefulness of the two-center expansion for molecular integrals would thus appear limited to the following special cases:

(a) The expansion for ρ_1 and ρ_2 only extend to small values of l, i.e., the charge distributions are atomic (Coulomb integrals). For this case, other methods are available, but the present approach seems to be competitive in simplicity and efficiency.

(b) Compared with the distance $r_3 = a$, ρ_1 and ρ_2 are sufficiently concentrated so that the integrand becomes negligible outside the region S_3. In this case, the two-center expansion is the most convenient method for the evaluation of the integrals; its usefulness could be increased considerably by numerical methods for the approximate evaluation of small, but not negligible contributions from the region S_0.

(c) The functions ρ_1 and ρ_2 are of such a nature that the integrals over S_0 of their products with the ${}_2R_0'$ can be evaluated analytically; this approach again necessitates the establishment of recurrence relations, in this case for the integrals. For exponential functions ρ, this method is to be treated in a separate paper.

In a recent paper, Fontana[13] has sketched a two-center expansion analogous to (27a) of I, which is independent of the region S_i, but introduces powers of $(r_1^2 + r_2^2 + r_3^2)$ in the denominator. The explicit formulas are not given by Fontana, and for the reasons discussed at the end of Sec. 3 of II, the writer considers that the expansion involves functions of greater complexity than those considered in the present series of papers.

More recently, Chiu[14] has derived some of the results of this paper by means of irreducible tensor algebra. Chiu also considers cases for which the functions depend on the angles of $\mathbf{r}_2 + \mathbf{r}_3 - \mathbf{r}_1$ provided $\vartheta_3 = 0$; a complete analysis of such cases would require the use of $6j$-symbols and has been purposely postponed by the writer.

4. AN EXPANSION THEOREM FOR ARBITRARY FUNCTIONS $f(r)$

As in I and II, the formula (31) for the functions ${}_2R_i'$ in the outer regions, though not (33) for ${}_2R_0'$, can be put in an operational form. For the factor in the general term of (31) and (8) which depends on n, we obtain

$$(-\tfrac{1}{2}n; \Lambda+u+v)(-\tfrac{1}{2}-\tfrac{1}{2}n; \lambda_i+u+v)r_i^{n-l_j-l_k-2u-2v} = \frac{(-r_i)^{l_i}}{2^{l_j+l_k+2u+2v}}\left(\frac{1}{r_i}\frac{\partial}{\partial r_i}\right)^{l_i}\frac{1}{r_i}\left(\frac{\partial}{\partial r_i}\right)^{2\lambda_i+2u+2v} r_i^{n+1}. \qquad (43)$$

Hence if we expand any function $f(r)$ which can be represented as a power series in r, we obtain in S_i in analogy to (5), (28), and (29),

$$f(r) = \sum [{}_2f'\cdot {}_2K'(\mathrm{l}, \mathrm{m})\cdot \prod \Omega_{l_i}^{m_i}(\vartheta_i, \varphi_i)], \qquad (44)$$

where

$${}_2f_i'(l; r_i) = \sum_{u,v} \frac{4r_i^{l_i}r_j^{l_j+2u}r_k^{l_k+2v}}{(2u)!!\,(2v)!!\,(2l_i+2u+1)!!\,(2l_k+2v+1)!!} \times \left(\frac{1}{r_i}\frac{\partial}{\partial r_i}\right)^{l_i}\frac{1}{r_i}\left(\frac{\partial}{\partial r_i}\right)^{l_j+l_k-l_i+2u+2v}[r_i f(r_i)], \qquad (45)$$

or using modified spherical Bessel functions $i_l(x)$,

$${}_2f_i' = 4r_i^{l_i}\left(\frac{1}{r_i}\frac{\partial}{\partial r_i}\right)^{l_i}\frac{1}{r_i}\frac{i_{l_j}(r_j\partial/\partial r_i)i_{l_k}(r_k\partial/\partial r_i)}{(\partial/\partial r_i)^{l_i}} \times [r_i f(r_i)]. \qquad (46)$$

As in I and II, this expression factorizes if $f(r)$ is a spherical Bessel function,

$$f(r) = w_0(Kr), \qquad w = j, y, h^{(1)}, h^{(2)}; \qquad (47)$$

then in view of (56)–(60) of I,

$${}_2f_i' = (-)^{\Lambda} j_{l_i}(Kr_i)j_{l_k}(Kr_k)w_{l_i}(Kr_i), \qquad (48)$$

[13] P. R. Fontana, J. Math. Phys. 2, 825 (1961).

[14] Y. N. Chiu, J. Math. Phys. (to be published).

and for the modified Bessel function $f(r) = i_0(Kr)$,

$$ {}_3f_i' = \prod_{s=1}^{3} i_{l_s}(Kr_s), \tag{49a} $$

and for the modified Bessel function of the second kind $f(r) = k_0(Kr)$,

$$ {}_3f_i' = (-)^{l'} i_{l_i}(Kr_i) i_{l_k}(Kr_k) k_{l_l}(Kr_l). \tag{49b} $$

For j_0 and i_0, which are even functions of the argument, the expansion is invariant on permuting (i, j, k) and is therefore also valid in S_0; for the other Bessel functions, the writer has been unable to find the expression appropriate to S_0.

ACKNOWLEDGMENTS

The writer wishes to thank Professor J. O. Hirschfelder, Dr. M. J. M. Bernal, and Dr. Y. N. Chiu for stimulating discussions and advice.

APPENDIX: PROPERTIES OF THE APPELL FUNCTIONS F_4

Appell's function F_4 as defined in (8) represents a polynomial in ξ and η of degree $|\alpha|$ or $|\beta|$ if α or β is a nonpositive integer. In all other cases, F_4 is an infinite series which converges for values ξ and η such that

$$ |\xi|^{\frac{1}{2}} + |\eta|^{\frac{1}{2}} < 1; \tag{A1} $$

for other values of the variables, the function can be defined in terms of contour integrals (cf. B 5.7.44 and B 5.8.9, 13). They satisfy the pair of differential equations (B 5.9.12),

$$ \begin{aligned} &\xi^2 \frac{\partial^2 Z}{\partial \xi^2} + 2\xi\eta \frac{\partial^2 Z}{\partial \xi\, \partial \eta} + \eta^2 \frac{\partial^2 Z}{\partial \eta^2} \\ &\quad + (\alpha + \beta + 1)\left(\xi \frac{\partial Z}{\partial \xi} + \eta \frac{\partial Z}{\partial \eta}\right) + \alpha\beta Z \\ &\quad = \xi \frac{\partial^2 Z}{\partial \xi^2} + \gamma \frac{\partial Z}{\partial \xi} = \eta \frac{\partial^2 Z}{\partial \eta^2} + \gamma' \frac{\partial Z}{\partial \eta}. \end{aligned} \tag{A2} $$

This set has, in general, four linearly independent solutions (p. 52 of Ref. 8),

$$ \begin{aligned} Z_0 &= \xi^{1-\gamma}\eta^{1-\gamma'} F_4(\alpha + 2 - \gamma - \gamma', \\ &\qquad \beta + 2 - \gamma - \gamma'; 2 - \gamma, 2 - \gamma'; \xi, \eta), \\ Z_i &= F_4(\alpha, \beta; \gamma, \gamma'; \xi, \eta), \\ Z_j &= \xi^{1-\gamma} F_4(\alpha + 1 - \gamma, \beta + 1 - \gamma; 2 - \gamma, \gamma'; \xi, \eta), \\ Z_k &= \eta^{1-\gamma'} F_4(\alpha + 1 - \gamma', \beta + 1 - \gamma'; \gamma, 2 - \gamma'; \xi, \eta); \end{aligned} \tag{A3} $$

but the four independent solutions of systems such as (A3) become linearly dependent with constant coefficients on certain critical lines (Sec. 12 of reference 8). For any function F_4 there exist at least three critical lines[18]

$$ L_i: \xi^{\frac{1}{2}} + \eta^{\frac{1}{2}} = 1; \quad L_j: \xi^{\frac{1}{2}} - \eta^{\frac{1}{2}} = 1; \quad L_k: \eta^{\frac{1}{2}} - \xi^{\frac{1}{2}} = 1, \tag{A4} $$

which form sections of a single parabola

$$ \xi^2 - 2\xi\eta + \eta^2 - 2\xi - 2\eta + 1 = 0. \tag{A5} $$

For variations of ξ and η along L_i, Appell has shown that $Z = Z[\xi, \eta(\xi)]$ taken as a function of ξ satisfies a third-order ordinary differential equation, instead of a fourth-order one, as along an arbitrary line; hence (A2) has only three linearly independent solutions on L_i. For the other lines, this dependence follows from the transformation (B 6.11.9),

$$ \begin{aligned} F_4(\alpha, \beta; \gamma, \gamma'; \xi, \eta) &= \frac{\Gamma(\gamma')\Gamma(\beta - \alpha)}{\Gamma(\gamma' - \alpha)\Gamma(\beta)} (-\eta)^{-\alpha} \\ &\times F_4\left(\alpha, \alpha + 1 - \gamma'; \gamma, \alpha + 1 - \beta; \frac{\xi}{\eta}, \frac{1}{\eta}\right) \\ &+ \frac{\Gamma(\gamma')\Gamma(\alpha - \beta)}{\Gamma(\gamma' - \beta)\Gamma(\alpha)} (-\eta)^{-\beta} \\ &\times F_4\left(\beta, \beta + 1 - \gamma'; \gamma, \beta + 1 - \alpha; \frac{\xi}{\eta}, \frac{1}{\eta}\right), \end{aligned} \tag{A6} $$

and a corresponding transformation to $(1/\xi, \eta/\xi)$. Appell has not explicitly stated the coefficients relating the functions (A3); the writer has been able to deduce them for restricted values of the parameters only. Considering their behavior near (1, 0) and (0, 1), we see that two of the functions are singular in the vanishing variable, and two analytic (for fractional values of γ and γ'); regarded as functions of the other variable, they are essentially hypergeometric series, and since (B 2.1.14)

$$ F(\alpha, \beta; \gamma; 1) = \Gamma(\gamma)\Gamma(\gamma - \alpha - \beta)[\Gamma(\gamma - \alpha) \times \Gamma(\gamma - \beta)]^{-1}, \quad \mathrm{Re}\,(\gamma) > \mathrm{Re}\,(\alpha + \beta), \tag{A7} $$

the only relation with constant coefficients which can hold on the line L_s of (4) is

$$ \begin{aligned} &\frac{\Gamma(\gamma)\Gamma(\gamma')}{\Gamma(\gamma + \gamma' - \alpha - 1)\Gamma(\gamma + \gamma' - \beta - 1)} Z_0 \\ &\quad + \epsilon_{si} \frac{\Gamma(2 - \gamma)\Gamma(2 - \gamma')}{\Gamma(1 - \alpha)\Gamma(1 - \beta)} Z_i \\ &\quad + \epsilon_{sj} \frac{\Gamma(\gamma)\Gamma(2 - \gamma')}{\Gamma(\gamma - \alpha)\Gamma(\gamma - \beta)} Z_j \\ &\quad + \epsilon_{sk} \frac{\Gamma(2 - \gamma)\Gamma(\gamma')}{\Gamma(\gamma' - \alpha)\Gamma(\gamma' - \beta)} Z_k = 0, \end{aligned} \tag{A8} $$

[18] P. Appell, J. Maths. Pures Appls., Ser. 3 10, 407 (1884).

where

$$\epsilon_{ss} = 1; \quad \epsilon_{st} = -1, \quad s \neq t. \tag{A9}$$

The precise form of (A8) for the lines L_l and L_k follows from that for L_i and (A6). On the other hand, a more careful investigation of the behavior of $F(\alpha, \beta; \gamma; x)$ near $x = 1$ [(B 2.10.1)], shows that (A8) is correct only if all the series terminate which appear with nonvanishing coefficients; otherwise terms of the form $(1 - \xi)^{\gamma-\alpha-\beta}$ enter into (A8) which do not add up to zero.

Appell has also stated (p. 19 of Ref. 8) that any three contiguous functions F_4 satisfy a linear recurrence relation, a total of 28 equations, if only one parameter at a time changes by unity; but the writer has been unable to find the complete set of such relations in the literature or to derive it, and he doubts the validity of Appell's statement.[16]

[16] Professor A. Erdélyi (private communication) has concurred with this opinion.

Reprinted from THE JOURNAL OF CHEMICAL PHYSICS, Vol. 41, No. 10, 3235–3249, 15 November 1964
Printed in U. S. A.

Rotation–Electronic Interaction in the Rydberg States of Diatomic Molecules*†

YING-NAN CHIU‡
Laboratory of Molecular Structure and Spectra, Department of Physics, University of Chicago, Chicago, Illinois
(Received 29 April 1964)

The theoretical foundation of Hund's coupling cases for the interaction between rotation and electronic motion is re-examined. The relationship between different cases is shown by angular-momentum coupling techniques. Rotational interaction terms neglected in the Born–Oppenheimer adiabatic type approximation and in the idealized Hund's cases are considered in particular. For application to Rydberg states, new and improved perturbed energy expressions of Λ doubling for spectroscopic use are derived up to the fourth order for a near Hund's Case b' diatomic molecule and up to the second order for a near Hund's Case d' diatomic molecule. Specific formulas are given for the p-term ($L=1$) and the d-term ($L=2$) complexes. For the approach towards cases intermediate between b' and d', secular determinants for this perturbation problem are formulated starting both from ideal case b' and from ideal case d' using two parameters, instead of one, for the d-term complex. These two approaches are shown to give equivalent results proving the consistency of the perturbations and assumptions used at both ends. The nature of these assumptions as well as the physical basis for the transition between Case b' and Case d' are shown.

I. INTRODUCTION

SINCE its formulation, the Born–Oppenheimer (B–O) separation[1] of nuclear and electronic motion has been a basis for the quantum-mechanical study of molecules of relatively heavy nuclei and for subsequent developments in this area.[2] Although introduced somewhat earlier,[3] the idealized Hund's coupling cases were essentially based on the averageability over electronic motion and the negligibility of some rotation–electronic interaction within the B–O separation framework. As spectroscopic measurement technique advances[4] and the high-speed computer calculation of electronic wavefunctions and energies improves[5] there is an increasing demand for exactness in the interpretation of rotation, vibration, and their interaction with electronic motion and for consideration of relativistic effects as well as spin interactions. Although *ab initio* nonadiabatic calculations including relativistic effects are available for the ground state of the hydrogen molecule,[6] for more complex molecules one still relies on the B–O adiabatic approximation but as a compensation takes into consideration the nonadiabatic interactions neglected in the separation of nuclear and electronic motion. Thus in the past, consideration of rotation electronic interaction led to the study of Λ doubling[7–9] while the above consideration and that of vibration–electronic (vibronic) interactions gave rise to isotope corrections in molecular spectra.[10,11]

More recently, studies in the weak interaction of neutral atoms[12] in forming repulsive states and similar studies at large internuclear separation[13] have invoked consideration of vibronic interactions and corrections due to relatively light nuclear masses. Studies of the binding energy of H_2 using an accurate electronic wavefunction[14] have called for considerations of relativistic effects. Studies of the fine structure of molecules have necessitated consideration of spin–orbit and spin–spin interactions.[15,16] Studies of high relative angular velocity collision have required consideration of rotation–electronic interaction.[17]

Modern angular momentum coupling techniques,[18a,19] have made possible clearer understanding of rotational

* This work was supported by a grant from the National Science Foundation, NSF GP 28 Research.
† Presented at the Symposium on Molecular Structure and Spectroscopy, Columbus, Ohio, June 1964.
‡ Present address: Department of Chemistry, The Catholic University of America, Washington, D. C.
[1] M. Born and J. R. Oppenheimer, Ann. Physik **84**, 457 (1927).
[2] M. Born and K. Huang, *Dynamical Theory of Crystal Lattices* (Oxford University Press, New York, 1954).
[3] F. Hund. Z. Physik **36**, 657 (1926); **40**, 742 (1927); **42**, 93 (1927).
[4] G. Herzberg and A. Monfils, J. Mol. Spectry. **5**, 482 (1960); W. Lichten, Phys. Rev. **120**, 848 (1960); **126**, 1020 (1962).
[5] W. Kolos and C. C. J. Roothaan, Rev. Mod. Phys. **32**, 219 (1960); B. J. Ransil, *ibid.* **32**, 239 (1960); S. Fraga and B. J. Ransil, J. Chem. Phys. **37**, 1112 (1962) and the intervening papers of Ransil *et al.*
[6] W. Kolos and L. Wolniewicz, Rev. Mod. Phys. **35**, 473 (1963).
[7] R. de L. Kronig, Z. Physik **46**, 814 (1927); **50**, 347 (1928); R. S. Mulliken and A. Christy, Phys. Rev. **38**, 87 (1931); M. H. Hebb, *ibid.* **49**, 610 (1936).
[8] E. Hill and J. H. Van Vleck, Phys. Rev. **32**, 250 (1928).
[9] J. H. Van Vleck, Phys. Rev. **33**, 467 (1929).
[10] J. H. Van Vleck, J. Chem. Phys. **4**, 327 (1936).
[11] V. A. Johnson, Phys. Rev. **60**, 373 (1941).
[12] T. Y. Wu and A. B. Bhatia, J. Chem. Phys. **24**, 48 (1956); T. Y. Wu, *ibid.*, p. 444; see also T. Y. Wu, R. L. Rosenberg and H. Sandstrom, Nucl. Phys. **16**, 432 (1960) for some corrections.
[13] A. Dalgarno and R. McCarroll, Proc. Roy. Soc. (London) **A237**, 383 (1956); **A239**, 413 (1957).
[14] W. Kolos and L. Wolniewicz, Acta Phys. Polon. **20**, 129 (1961).
[15] I. Kovacs, Can. J. Phys. **36**, 309 (1958); **36**, 329 (1958).
[16] P. R. Fontana, Phys. Rev. **125**, 220 (1962).
[17] W. R. Thorson, J. Chem. Phys. **39**, 1431 (1963).
[18] J. H. Van Vleck, Rev. Mod. Phys. **23**, 213 (1951).
[18a] *Note added in proof*: It has come to the author's attention that, with a different application in view, N. Mustelin, in a thesis entitled "On the Coupling of Angular Momenta in Diatomic Molecules with Applications to the Magnetic Hyperfine Structure" (Åbo Akademi, Åbo, Finland, October 1963), has developed some interesting formalisms which in some aspects are parallel to the treatment here.
[19] M. E. Rose, *Elementary Theory of Angular Momentum* (John Wiley & Sons, Inc., New York, 1961).

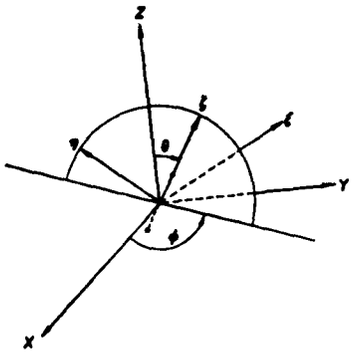

FIG. 1. Transformation from fixed space axis (x, y, z) system to moving molecular axis (ξ, η, ζ) system.

interaction. Recent interest in Rydberg states of molecules[20] and new spectroscopic measurements[21,22] make it worthwhile to derive more useful formulas for their interpretation. The object of the present work is to derive such formulas and to show the usefulness of angular momentum coupling techniques (1) in expressing the relationship between wavefunctions of different Hund's cases and (2) in treating the rotational interaction near Hund's Case d'.

II. BORN-OPPENHEIMER ADIABATIC APPROXIMATION

For a diatomic molecule consisting of two nuclei of masses M_a and M_b and f electrons of mass m, the Hamiltonian of motion (if we ignore the distinction between the two centers of mass of the nuclei and the molecule and discard the unquantized, uniform motion of the center of mass) may be written as

$$H=-\frac{\hbar^2}{2\mu r^2}\left[\frac{\partial}{\partial r}\left(r^2\frac{\partial}{\partial r}\right)-\mathbf{R}^2\right]-\frac{\hbar^2}{2m}\sum_i^f\nabla_i^2+V_{\text{nucl}}(r)+V_{\text{el, nucl}}(r_1\cdots r_f; r, \theta, \varphi), \quad (1)$$

where $\mu=M_aM_b/(M_a+M_b)$, r is the internuclear distance, and $V_{\text{nucl}}(r)=(z_az_b)/r$. The term $V_{\text{el, nucl}}$ comprises the ordinary electron–electron and electron–nuclear Coulomb potentials, where θ, φ are the polar and azimuth angles specifying the orientation of the figure axis (namely the molecular axis coincident with the vector $\mathbf{r}=\mathbf{r}_b-\mathbf{r}_a$) with respect to a set of space-fixed axes originating from the center of mass. In spherical polar coordinates, $\mathbf{R}$, the total angular momentum operator for the rigid rotation of the nuclei exclusive of the electrons, is defined by

$$\mathbf{R}^2=-\left[\frac{1}{\sin\theta}\frac{\partial}{\partial\theta}\left(\sin\theta\frac{\partial}{\partial\theta}\right)+\frac{1}{\sin^2\theta}\frac{\partial^2}{\partial\varphi^2}\right]. \quad (2)$$

As it is advantageous to express electronic coordinates relative to the moving molecular axis (figure axis) and to eliminate any θ, φ dependence from the potential energy expression, we use the molecular axis system[9,23–26] shown in Fig. 1. If we introduce spin-dependent

[20] R. S. Mulliken, J. Am. Chem. Soc. **86**, 3183 (1964).
[21] K. P. Huber, Helv. Phys. Acta **34**, 929 (1961); K. P. Huber and E. Miescher, *ibid.* **36**, 257 (1963).
[22] (a) J. W. C. Johns and G. Herzberg (to be published). (b) M. Ginter (to be published).

[23] I. I. Goldman and V. D. Krivchenkov, *Problems in Quantum Mechanics* (Pergamon Press, Ltd., London, 1961), pp. 207–211.
[24] L. P. Landau and E. M. Lifshitz, *Quantum Mechanics* (Pergamon Press, Ltd., London, 1958), pp. 279–281.
[25] R. de L. Kronig, *Band Spectra and Molecular Structure* (Cambridge University Press, New York, 1930), pp. 8–14.
[26] This amounts to a unitary (orthogonal for the space part) transformation that changes a set of space-fixed coordinates θ, ϕ, x_i, y_i, z_i $(i=1\cdots f)$, $S_1\cdots S_f$, to the following set of coordinates:

$$\theta=\theta,\ \phi=\phi,$$
$$\xi_i=-x_i\sin\phi+y_i\cos\phi,$$
$$\eta_i=-x_i\cos\theta\cos\phi-y_i\cos\theta\sin\phi+z_i\sin\theta,$$
$$\zeta_i=x_i\sin\theta\cos\phi+y_i\sin\theta\sin\phi+z_i\cos\theta,$$
$$\begin{pmatrix}\alpha_i\\ \beta_i\end{pmatrix}=D\begin{pmatrix}a_1\\ b_1\end{pmatrix}\cdots\begin{pmatrix}\alpha_f\\ \beta_f\end{pmatrix}=D\begin{pmatrix}a_f\\ b_f\end{pmatrix}\quad\text{or}\quad\sigma_1=DS_1\cdots\sigma_f=DS_f,$$

where D is a transformation matrix for spin (see below). Viewed as a coordinate transformation the partial differentiations (Refs. 23, 25), involved are obvious and straightforward for the space part. For the spin part as we assume the spin wavefunction to be entirely separable from the space wavefunction, it is easier to consider its transformation separately. To be able to use matrix notation for this transformation it appears more pertinent to consider D as a product of binary transformations $\mathbf{S}(\sigma_i; S_i)$ for the spin wavefunction which consists of spinors of Rank f (Ref. 24, pp. 195–198, pp. 200–201) rather than to consider D as a product of rotation matrices $D^k(\sigma_i; S_i)$ which is the transpose of $\mathbf{S}(\sigma_i; S_i)$ by definition (Ref. 19, pp. 67–72). Thus as far as the spin wavefunction χ transforms as $\mathbf{S}\chi(S_1\cdots S_i\cdots S_f)$, where explicitly

$$\chi(\sigma_1\cdots\sigma_i\cdots\sigma_f)=\mathbf{S}\chi(S_1\cdots S_i\cdots S_f)=\prod_i^f\sum_{S_i=a_i,b_i}\mathbf{S}(\sigma_i; S_i)\chi(S_1\cdots S_i\cdots S_f)$$

and the spin-dependent Hamiltonian $\mathcal{H}$ must transform as $\mathbf{S}\mathcal{H}\mathbf{S}^{-1}$ to preserve the eigenvalues. With the coordinate system defined in Fig. 1, the Euler angles (Ref. 24, p. 201) relating the moving molecular axes to the fixed space system are the following: for rotation around space fixed polar (z) axis the angle is $\phi+\pi/2$, for rotation around the new axis (ξ) the angle is θ, for rotation around the final new polar axis (ζ) the angle is zero. The corresponding rotation operator is[24] $\exp[ij_z0]\exp[ij_\xi\theta]\exp[ij_z(\phi+\pi/2)]=\exp[ij_z(\phi+\pi/2)]\exp[ij_\xi\theta]$. Instead of the lengthy Cayley-Klein parameter method [Ref. 24 and E. P. Wigner, *Group Theory and Its Application to the Quantum Mechanics of Atomic Spectra* (Academic Press Inc., New York, 1959), pp. 158–160] we introduce Pauli matrices (Ref. 24, p. 191) for the angular momentum operators j_z and j_ξ to get directly for $k=1\cdots f$

$$\begin{aligned}S(\sigma_k; S_k)&=\left\{\exp[\tfrac{1}{2}i\begin{pmatrix}1&0\\0&-1\end{pmatrix}(\phi+\pi/2)]\exp[\tfrac{1}{2}i\begin{pmatrix}0&1\\1&0\end{pmatrix}\theta]\right\}^T\\&=\begin{pmatrix}\cos\tfrac{1}{2}\theta & i\sin\tfrac{1}{2}\theta\\ i\sin\tfrac{1}{2}\theta & \cos\tfrac{1}{2}\theta\end{pmatrix}^T\begin{pmatrix}\exp[\tfrac{1}{2}i(\phi+\pi/2)] & 0\\ 0 & \exp[\tfrac{1}{2}i(\phi+\pi/2)]\end{pmatrix}^T\\&=\begin{pmatrix}\cos\tfrac{1}{2}\theta\exp[\tfrac{1}{2}i(\phi+\pi/2)] & i\sin\tfrac{1}{2}\theta\exp[-\tfrac{1}{2}i(\phi+\pi/2)]\\ i\sin\tfrac{1}{2}\theta\exp[\tfrac{1}{2}i(\phi+\pi/2)] & \cos\tfrac{1}{2}\theta\exp[-\tfrac{1}{2}i(\phi+\pi/2)]\end{pmatrix},\end{aligned}$$

where T denotes the transpose operation on the matrices. The partial differentiation of the space part, followed by differentiating $\mathbf{S}$ and matrix multiplication then (Ref. 25, p. 13) gives, for example,

$$\mathbf{S}[\partial/\partial\theta]_{sp}\mathbf{S}^{-1}=[\partial/\partial\theta]_{molec}-i(\mathbf{L}_\xi+\mathbf{S}_\xi)=[\partial/\partial\theta]_{molec}-i\mathbf{P}_\xi,$$

where sp and molec denote partial differentiations with space or molecular coordinates fixed, respectively. This shows that if we want the wavefunction to have spin associated with the molecular axis system (see text) then due to their equivalent properties under rotation, spin (e.g., $\mathbf{S}_\xi$) and orbital angular momentum come out together automatically as equal dynamical partners exerting similar gyroscopic effects.

interactions $W(S_i)$, then $\mathcal{H}=H+W(S_i)$, where $W(S_i)$ may still be referred either to the fixed space axes (in Latin alphabet) or to the moving molecular axes (in Greek alphabet) through a similarity transformation $\mathbf{S}W(S_i)\mathbf{S}^{-1}=W'(\sigma_i)$. Depending on whether the effect of electron spin on molecular motion is weak or strong we have the final spin Hamiltonian referred to either the space or molecular coordinates, respectively. The corresponding wavefunctions will naturally have spin coordinates referred to the same sets of axes, namely for a weak effect we have the total (nuclear plus electronic) wavefunction in the form of $\Psi(\xi_i\eta_i\zeta_i S_i; r, \theta, \varphi)$ which aside from other necessary assumptions leads to the spin condition for Hund's Case[27] *b* and for a strong effect we have $\Psi(\xi_i\eta_i\zeta_i\sigma_i; r, \theta, \varphi)$ which leads to Hund's Cases *a* or *c*.[27,28]

For the strong spin effect case, the Hamiltonian in the molecular axis system after appropriate spin transformations is the following[23,25,26]:

$$\mathcal{H}=-\frac{\hbar^2}{2\mu r^2}\left[\frac{\partial}{\partial r}\left(r^2\frac{\partial}{\partial r}\right)+\cot\theta\left(\frac{\partial}{\partial\theta}-i\mathbf{P}_\xi\right)+\left(\frac{\partial}{\partial\theta}-i\mathbf{P}_\xi\right)^2+\frac{1}{\sin^2\theta}\left(\frac{\partial}{\partial\varphi}-i\sin\theta\mathbf{P}_\eta-i\cos\theta\mathbf{P}_\zeta\right)^2\right]$$
$$-\frac{\hbar^2}{2m}\sum_i\left(\frac{\partial^2}{\partial\xi_i^2}+\frac{\partial^2}{\partial\eta_i^2}+\frac{\partial^2}{\partial\zeta_i^2}\right)$$
$$+V_{\text{nucl}}(r)+V_{\text{el,nucl}}(\xi_i\eta_i\zeta_i; r)+\mathbf{S}W(S_i)\mathbf{S}^{-1}, \quad (3)$$

where $\mathbf{P}_\xi=\mathbf{L}_\xi+\mathbf{S}_\xi=\sum_i(L_{i\xi}+S_{i\xi})$ is the ξ component of the total electronic (orbital and spin) angular momentum.[29] For a weak spin effect, we have $\mathbf{L}_\xi$ instead of $\mathbf{P}_\xi$ and $W(S_i)$ instead of $\mathbf{S}W(S_i)\mathbf{S}^{-1}$.

To consider the separation of nuclear motion we use Eq. (3) and include the spin motion in the electronic part. The Schrödinger equation from (3) may then be abbreviated as

$$\mathcal{H}\Psi=(H_{\text{nucl}}+H_{\text{el}})\Psi(\xi_i\eta_i\zeta_i\sigma_i; r, \theta, \varphi)=E\Psi. \quad (4)$$

If the complete set of electronic wavefunctions is available the total wavefunction in (4) may be expanded as a product of nuclear and electronic wavefunction as follows[2,6,13,30]:

$$\Psi(\xi_i\eta_i\zeta_i\sigma_i; r, \theta, \varphi)=\sum_n\phi_n(\xi_i\eta_i\zeta_i\sigma_i; r)F_n(r, \theta, \varphi), \quad (5)$$

where $\phi_n(\xi_i\eta_i\zeta_i\sigma_i; r)\equiv\Phi_n(\xi_i\eta_i\zeta_i; r)\chi_n(\sigma_i)$ satisfies the Schrödinger equation for electronic motion

$$H_{\text{el}}\phi_n=\left[-(\hbar^2/2m)\sum_{i\xi}\nabla_{i\xi}^2+V_{\text{el, nucl}}(\xi_i\eta_i\zeta_i; r)+W'(\sigma_i)\right]\phi_n=U_n(r)\phi_n, \quad (6)$$

and n stands for the assembly of quantum numbers involved (see below). Substitution of (5) into (6), yields the Schrödinger equation for nuclear motion, viz.,

$$[H_{\text{nucl}}+U_n(r)+C_{nn}-E]F_n(r, \theta, \varphi)=-\sum_{n'\neq n}C_{nn'}F_{n'}(r, \theta, \varphi), \quad (7)$$

where F_n will further be decomposed into $R_n(r)\Theta_n'(\theta, \varphi)$, and $C_{nn'}=\int\phi_n^*H_{\text{nucl}}\phi_{n'}d\tau_i\cdots d\tau_f$.

If we neglect the nondiagonal matrix elements of $\mathbf{C}$ on the right-hand side we get essentially the *adiabatic* Born approximation[2] as an improvement over the original Born–Oppenheimer approximation.[1] The neglected off-diagonal matrix elements then are treated as perturbations.

Such a consideration of the diagonal term alone is tantamount to a one-term expansion of Ψ in (5). Because of the axial electric field pertaining to a diatomic molecule, we may assume the projection Ω of the total electronic angular momentum (including spin) on the figure axis (Ω being the eigenvalue of $\mathbf{P}_\zeta$) to be quantized. Assuming the nuclear rotational wavefunction to be that of a symmetric top with the angular momentum along the symmetry axis equal to Ω,[31,32] we then have

$$\Psi_{nvJM\Omega}(\xi_i\eta_i\zeta_i\sigma_i; r, \theta, \varphi)=\phi_{nJ\Omega}(\xi_i\eta_i\zeta_i\sigma_i; r)F_{nvJM\Omega}(r, \theta, \varphi)=\phi_{nJ\Omega}(\xi_i\eta_i\zeta_i\sigma_i; r)R_{nvJ\Omega}(r)\Theta_{\Omega M}^J(\theta)e^{iM\varphi}, \quad (8)$$

where n denotes the assembly of electronic quantum numbers other than Ω. Substitution of (8) into (3) yields, aside from the Schrödinger equation for electronic motion already given in (6), the following

[27] G. Herzberg, *Molecular Spectra and Molecular Structure. I. Spectra of Diatomic Molecules* (D. Van Nostrand Company, Princeton, New Jersey, 1950), pp. 219–226.

[28] Kovacs (Ref. 15) expressed his spin-orbit interaction operators in a molecular axis system (Case *a*) hence his expansion of Case *b* wavefunctions in terms of Case *a* wavefunctions for the subsequent evaluation of matrix elements. Fontana,[16] however, expressed his spin-orbit and spin-spin interaction in the fixed space axis system (Case *b*) and expressed his Case *b* wavefunctions in terms of space-fixed spin wavefunctions by angular-momentum coupling.

[29] As long as $\mathbf{P}_\xi=\sum_i L_{i\xi}+\sum_i S_{i\xi}=\sum_i(L_{i\xi}+S_{i\xi})=\mathbf{L}_\xi+\mathbf{S}_\xi=\sum_j j_{j\xi}$, no distinction of Russell-Saunders and *j–j* coupling need be made here.

[30] A. Fröman, J. Chem. Phys. 36, 1490 (1962).

[31] W. R. Thorson, J. Chem. Phys. 34, 1744 (1961).

[32] Note, however, our definition of the electronic and nuclear Hamiltonian is different from that of Refs. 30 and 6. The separation of electronic and nuclear wavefunctions following the separation of the Hamiltonian is somewhat arbitrary. By giving a different meaning to the set of wavefunctions, one does no more than attribute a new but consistent set of meanings to the spectroscopic states. After appropriate perturbations are taken into account the final result of the energy and wavefunction should be the same.

equation for nuclear motion:

$$\left\{-\frac{\hbar^2}{2\mu r^2}\left[\frac{1}{\sin\theta}\frac{\partial}{\partial\theta}(\sin\theta)\frac{\partial}{\partial\theta}+\frac{1}{\sin^2\theta}\left(\frac{\partial}{\partial\varphi}-i\Omega\cos\theta\right)^2\right]-W_{\rm rot}(r)\right\}\Theta_{\Omega M}{}^{J}(\theta)e^{iM\varphi}=0, \quad (9)$$

and

$$\left\{-\frac{\hbar^2}{2\mu r^2}\frac{\partial}{\partial r}\left(r^2\frac{\partial}{\partial r}\right)+U_n(r)+W_{\rm rot}(r)+C_{nn}-E\right\}R_{n\nu J\Omega}(r)=0. \quad (10)$$

Equation (9) is the differential equation of a symmetric top with eigenvalues[33]

$$W_{\rm rot}(r)=(\hbar^2/2\mu r^2)[J(J+1)-\Omega^2], \quad (11)$$

and the eigenfunction may be formally identified to be the rotation matrix,[34] aside from a normalization constant

$$\Theta_{\Omega M}{}^{J}(\theta)e^{iM\varphi}=[(2J+1)/8\pi^2]^{\frac{1}{2}}D_{M\Omega}{}^{J}(\varphi,\theta,\psi)=[(2J+1)/8\pi^2]^{\frac{1}{2}}e^{iM\varphi}d_{M}{}^{J}(\theta)e^{i\Omega\psi}, \quad (12)$$

where ψ may be set to zero.[35–37] Such identification facilitates the calculation of matrix elements using standard angular momentum methods[16,38] without recourse to explicit forms of Jacobi polynomials. The detailed form of the operator $C_{nn'}$ consists of two parts:

$$C_{nn'}=\int\phi_{nJ\Omega}{}^{*}(H_1+H_2)\phi_{n'J\Omega}d\tau_i d\sigma_i. \quad (13)$$

The expression of H_1 may be shown to be[39]

$$-\frac{1}{2}\frac{\hbar^2}{2\mu r^2}\Big[e^{-i\psi}\left(\frac{\partial}{\partial\theta}+\cot\theta\mathbf{P}_\xi+\frac{i}{\sin\theta}\frac{\partial}{\partial\varphi}\right)(-\mathbf{P}_\eta-i\mathbf{P}_\xi)+e^{i\psi}\left(-\frac{\partial}{\partial\theta}+\cot\theta\mathbf{P}_\xi+\frac{i}{\sin\theta}\frac{\partial}{\partial\varphi}\right)(-\mathbf{P}_\eta+i\mathbf{P}_\xi)+\text{two similar terms}$$

obtained by interchanging the contents of the first and second parenthesis in each of the above terms$\Big]$

$$=-\tfrac{1}{2}B(r)[J_-P_-+J_+P_++P_-J_-+P_+J_+]\Rightarrow -B(r)[J_-P_-+J_+P_+], \quad (14)$$

[33] H. Eyring, J. Walter, and G. Kimball, *Quantum Chemistry* (John Wiley & Sons, New York, 1944), pp. 260–261.

[34] A. R. Edmonds, *Angular Momentum in Quantum Mechanics* (Princeton University Press, Princeton, New Jersey, 1957), pp. 8, 55. Note although the definition of Euler angles is different here, it is irrelevant in this connection. Note also the rotation matrix here is the complex conjugate of that defined in Ref. 19.

[35] In Fig. 1 and Footnote 26, although we have tacitly used the Euler angle definitions and coordinate systems consistent with those of Landau and Lifshitz,[24] Kronig,[25] Van Vleck,[9] and Goldman (Ref. 23, p. 208), where the second Euler angle θ is generated by rotation with respect to the new x axis instead of the y axis, it should be recognized that rotation of the first Euler angle by $\phi+\pi/2$ here to a new x axis (ξ) is equivalent to rotation by ϕ to a new y axis (coincident with ξ here). With this recognition, ϕ, θ, and ψ are consistent with the definition of Euler angles of Rose (Ref. 19, p. 50), Edmonds,[34] and Wigner,[26] where the angle θ is generated by rotation with respect to the new y axis. Also ϕ, θ are easily seen to be the usual azimuth and polar angle of the vector $\mathbf{r}$ in spherical polar coordinates.

[36] Reference 34, p. 55; pp. 64–67.

[37] See Ref. 34, p. 62 and Ref. 19, p. 55 and p. 75. If ψ is retained the factor $\exp(i\Omega\psi)$ is redundant as it also occurs in the electronic wavefunction. But as far as evaluation of matrix elements over rotational wavefunctions is concerned, if the proper normalization constant $(2\pi)^{-\frac{1}{2}}$ for ψ is included, this redundancy is no handicap. Because vector or tensor operators[16,26] [Ref. 24, pp. 296–298] on decomposition into products using the rotational transformation of Fig. 1 always contains the same ψ dependence in the electronic and rotational parts, thus no embarrassing occasion ever arises when the selection rule for the electronic part contradicts that of the rotational part for the same operator. It is perhaps more sagacious to use electronic coordinate systems (such as the elliptical coordinate system) so that ψ is an independent variable and $\exp(i\Omega\psi)$ may be factored out and absorbed into the rotational wavefunction.

[38] L. Y. Chow Chiu, J. Chem. Phys. **40**, 2276 (1964); see also Y.-N. Chiu, J. Math. Phys. **5**, 283 (1964).

[39] See Ref. 23, pp. 218–220 for derivation of the ladder operators $J_\pm$ in terms of moving molecular coordinates. However, Goldman's Euler angles are defined differently compared with ours [Ref. 35 and our Eq. (12)]. With our definition of Euler angles we shall denote the right-handed moving axes system by $\xi'\eta'\zeta'$. The primed coordinate system is of greater generality, being the same as that of Rose,[26] hence our choice of this. For $\psi=0$, we have $\xi'=-\eta$, $\eta'=\xi$, $\zeta'=\zeta$ and $P_{\xi'}=P_\eta$; $P_{\eta'}=P_\xi$; $P_{\zeta'}=P_\zeta$ (see Fig. 1). But the designation of ξ, η is arbitrary for practical purposes. The coordinate system of Fig. 1 is more convenient for our earlier reductions involving spin variables. The primed coordinate system here gives meaning to (14) more directly. In this system the angular momentum operators are, from the transformation of coordinates (Ref. 19, p. 50; p. 65),

$$\mathbf{J}_{\xi'}=-i\left(\sin\psi\frac{\partial}{\partial\theta}+\cos\psi\cot\theta\frac{\partial}{\partial\psi}-\frac{\cos\psi}{\sin\theta}\frac{\partial}{\partial\phi}\right),$$

$$\mathbf{J}_{\eta'}=-i\left(\cos\psi\frac{\partial}{\partial\theta}-\sin\psi\cot\theta\frac{\partial}{\partial\psi}+\frac{\sin\psi}{\sin\theta}\frac{\partial}{\partial\phi}\right),$$

$$\mathbf{J}_{\zeta'}=-i(\partial/\partial\psi).$$

From the above, the abnormal commutation rule[16] $\mathbf{J}_{\xi'}\mathbf{J}_{\xi'}-\mathbf{J}_{\xi'}\mathbf{J}_{\xi'}=-i\mathbf{J}_{\eta'}$ immediately follows. Under such an abnormal commutation rule which differs from the normal one by the sign on the right-hand side, the matrix elements $\langle\Omega\mp1\,|\,J_\pm\,|\,\Omega\rangle$ are equivalent to the matrix elements $\langle\Omega\mp1\,|\,J_\mp\,|\,\Omega\rangle$ for normal commutation rules. (See, for example, Ref. 18, Ref. 19, pp. 24–27.) With this information the derivation of (14) and part of (15) may be easily perceived as follows. Starting from (1) we recognize that $\mathbf{R}^2$ is a scalar invariant under coordinate transformation and may be expressed in any coordinate system. In the moving coordinate system

$$(\hbar^2/2\mu r^2)\mathbf{R}^2=B(r)\mathbf{R}^2=B(\mathbf{J}-\mathbf{P})^2=B[\mathbf{J}^2-\mathbf{J}\cdot\mathbf{P}-\mathbf{P}\cdot\mathbf{J}+\mathbf{P}^2]$$

$$=B[(\mathbf{J}^2-2\mathbf{J}_{\zeta'}\mathbf{P}_{\zeta'}+\mathbf{P}_{\zeta'}{}^2)-(\mathbf{J}_{\xi'}\mathbf{P}_{\xi'}+\mathbf{J}_{\eta'}\mathbf{P}_{\eta'}+\mathbf{P}_{\xi'}\mathbf{J}_{\xi'}+\mathbf{P}_{\eta'}\mathbf{J}_{\eta'})+(\mathbf{P}_{\xi'}{}^2+\mathbf{P}_{\eta'}{}^2)]$$

$$\Rightarrow B\langle J^2-P_\zeta{}^2\rangle-\tfrac{1}{2}B(J_+'P_-+P_-J_+'+P_+J_-'+J_-'P_+)+B(P_\xi{}^2+P_\eta{}^2)]$$

$$\Rightarrow B[J(J+1)-\Omega^2]-\tfrac{1}{2}B\langle J_-P_-+J_+P_++P_-J_-+P_+J_+\rangle+B\langle\mathbf{P}_\xi{}^2+\mathbf{P}_\eta{}^2\rangle,$$

where $P_\pm\Rightarrow\mathbf{P}_{\xi'}\pm i\mathbf{P}_{\eta'}=-\mathbf{P}_\eta\pm i\mathbf{P}_\xi$ and the first term corresponds to the symmetric-top eigenvalue. The second term corresponds to (14) with $J_\pm$ already converted to follow normal commutation rules, namely, $\langle\Omega\pm1\quad J_\pm\,|\,\Omega\rangle=[(J\mp\Omega)(J\pm\Omega+1)]^{\frac{1}{2}}$.

so that clearly H_1 has no matrix elements diagonal in the electronic quantum number Ω or Λ.

The expression of H_2 may be shown by inspection[39] and differentiation to be

$$H_2=\frac{\hbar^2}{2\mu r^2}\left[(\mathbf{P}_\xi^2+\mathbf{P}_\eta^2)-2r\frac{\partial}{\partial r}-r^2\frac{\partial^2}{\partial r^2}-\frac{2r^2}{R(r)}\frac{\partial R(r)}{\partial r}\frac{\partial}{\partial r}\right]. \tag{15}$$

We are interested in second- and higher-order perturbation splitting of the degenerate (with respect to $\pm\Lambda$) energy values of the system[40] due to the off-diagonal perturbation matrix element of H_1 which we rewrite as

$$\begin{aligned}[H_1]_{nn'}&\equiv\langle nv\Omega J\mid H_1\mid n'v'\Omega' J\rangle\equiv H_1(\Omega;\Omega')\\&=A^2\int R^*_{nvJ\Omega}(r)D_{M\Omega}{}^{J*}\phi^*_{nJ\Omega}B(r)\\&\quad\times(J_-P_-+J_+P_+)R_{n'v'J\Omega}(r)\\&\quad\times D^J{}_{M\Omega'}\phi_{n'J\Omega'}r^2dr\sin\theta d\theta d\varphi d\psi d\tau_i\cdots d\tau_f,\end{aligned} \tag{16}$$

where A is the normalization constant for $D_{M\Omega}{}^J$ in Eq. (12). Upon integration over the rotational wavefunctions one immediately obtains[39] for $\Omega'=\Omega\pm1$

$$-\langle nv\Omega J\mid BP_\mp\mid n'v'\Omega\pm J\rangle[(J\pm\Omega+1)(J\mp\Omega)]^{\frac{1}{2}}, \tag{17}$$

or

$$-\langle nv\Omega J\mid 2BP_y\mid n'v'\Omega\pm1 J\rangle[(J\pm\Omega+1)(J\mp\Omega)]^{\frac{1}{2}}. \tag{18}$$

This matrix element was first given by Van Vleck[41] using wavefunctions in the form of Jacobi polynomials. Van Vleck also made the pure precession assumption equivalent to a united-atom model for the electronic state of a diatomic molecule. In this model the electronic angular momentum (L) is well defined. With this and the assumption of equal $r(=r_0)$ for initial and final states (17) becomes, neglecting spin

$$-B_0[(L\mp\Lambda)(L\pm\Lambda+1)]^{\frac{1}{2}}[(N\mp\Lambda)(N\pm\Lambda+1)]^{\frac{1}{2}}, \tag{19}$$

where $B_0=\hbar^2/2\mu r_0^2$.

III. HUND'S COUPLING CASES FOR THE INTERACTION OF ROTATION AND ELECTRONIC MOTION

In Hund's Case a, the electron spin σ expressed in the molecular coordinate system is intimately connected with molecular motion and has a well-defined projection Σ along the figure axis. This, together with the well-defined projection Λ of electronic orbital angular momentum, constitutes $\Omega=\Lambda+\Sigma$ which is a good quantum number characterizing the state. Therefore, in our many-term expansion (5) we delete the sum over Ω on the right-hand side and add Ω, Λ, Σ to the quantum numbers of the final state on the left to read $\Psi_{nvJM\Omega\Lambda\Sigma}$ as in (8).

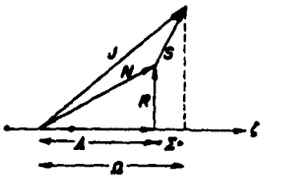

FIG. 2. Spin decoupling from Hund's Case a to form Hund's Case b.

In Hund's Case b the electron spin S expressed with respect to the space coordinate system is not coupled to the figure axis, and hence has no well-defined projection along it. Therefore, we use (8) but with Λ in the place of Ω and with an additional quantum number $\mathbf{N}=\mathbf{\Lambda}+\mathbf{R}$ to read $\Psi_{nvJMN\Lambda}$.

In such an idealized picture we are looking at Case b as resulting from Case a through spin uncoupling. The difference in Cases b and a then lies in the presence in the latter of the gyroscopic effect of spin treated as a dynamical coordinate having transformation properties similar to that of the space coordinates.[26] Such a treatment of spin is consistent with the classical relativistic consideration which among other terms also gives rise to the magnetic interactions $W(S_i)$ [see Eq. (3)] used in connection with Hund's Case c.[42]

The purely gyroscopic effect of spin may be expressed as $-2B\mathbf{J}\cdot\mathbf{S}$ coming from $-2B\mathbf{J}\cdot\mathbf{P}=-2B\mathbf{J}\cdot(\mathbf{L}+\mathbf{S})$. As such it is held responsible for the rotational distortion of spin multiplets for Hund's cases between a and b.[5,43] As the perturbation similar to (14) omitted in the separation of the wave equation, it is held responsible for the expansion of Case b wavefunctions in terms of those of Case a after solving the secular equation.[15,44] On the other hand, instead of solving secular equations to find eigenfunctions, the decoupling of spin from Case a may be viewed as the coupling of J with the inverse[18] spin vector $\mathbf{S}'=-\mathbf{S}$ to give an angular momentum vector $\mathbf{N}$ (Fig. 2), which is conserved in Case b. Writing $\mathbf{N}=\mathbf{J}+(-\mathbf{S})$ and omitting vibration and other irrelevant quantum numbers, we get the wavefunction in N representation (i.e., Case b) as a linear combination of Case a wavefunctions, using angular-momentum coupling with the figure axis as the quantization axis,

$$\begin{aligned}&\Psi_{nvJMN\Lambda}(\xi_i\eta_i\zeta_i S_i;r,\theta,\varphi)\\&\quad=\Psi_{N\Lambda}=\sum_{\Sigma'}^{S'}C(J,S',N;\Omega,\Sigma',\Lambda)\psi_{J\Omega}\chi_{S'\Sigma'},\end{aligned} \tag{20}$$

[39] The degeneracy of the symmetric-top eigenvalue is obvious from (11). For degeneracy of the electronic energy, see Ref. 35, p. 202.

[41] Reference 9, pp. 476–480. Note in the normalization of Jacobi polynomials in Van Vleck's Eq. (16), there appears to be a misprint of the factorial sign; namely, $(1+\delta+S+2\rho)!$ should read $(1+\delta+S+2\rho)$. See also Ref. 34, pp. 58–62.

[42] Inclusion of spin as a dynamical coordinate will give (i) the gyroscopic effect of spin[26] on molecular motion manifested in Eq. (3) and (ii) magnetic interactions $W(S_i)$, which consist of spin-rotational, spin-own-orbit, spin-other-orbit and spin-spin interactions.

[43] Reference 24, pp. 288–289; Ref. 25, pp. 47–48.

[44] R. Schlapp, Phys. Rev. 39, 806 (1932), especially pp. 811–812.

where $\Sigma' = -\Sigma$; $\psi_{J\Omega} \equiv \Phi_{n\Lambda}(\xi_i\eta_i\zeta_i; r) R_{nvJ\Omega}(r) A D_{M\Omega}^{J}$, and the C's are Clebsch–Gordan (vector coupling) coefficients.[46] Using (20), we have obtained[46] wavefunctions essentially equivalent to those of Kovacs[18] except for the over-all signs of some states (i.e., ${}^3\Sigma^{\pm}_{J\pm1}$ states) due to different definitions. Our Eq. (20) is perfectly general and may be used for any multiplet states. The phase convention as obtained from Clebsch–Gordan coefficients is naturally a consistent one.

In Hund's Case *c*, the spin–orbit interaction is strong compared with the spin–axis and the electrostatic orbit–axis interactions. As a consequence the projections Λ and Σ of $\mathbf{L}$ and $\mathbf{S}$, respectively, on the figure axis are not separately defined. Instead, the projection Ω of the angular momentum $\mathbf{j}(=\mathbf{L}+\mathbf{S})$ is a good quantum number. Thus in the wave equation (3) we should formally use $\mathbf{j}_i$ in place of $\mathbf{P}_i$. However, in the subsequent reduction to a symmetric top Eq. (9), the properties of $\mathbf{j}$ as manifested through its projection Ω are the same as those of Case *a*. The angular momentum $\mathbf{j}$, if approximately defined in an idealized case, hence is an internal electronic property and may be absorbed into the quantum number n, making it unnecessary to specify Russell–Saunders or j–j coupling in (3) as noted in Footnote 29.

With the introduction of spin–orbit interaction in the Hamiltonian, spin is not separately a good quantum number; the $L-S$ or Russell–Saunders representation is inadequate. When the spin–orbit interaction is large but not *very* large we have the j representation which may be obtained from the angular momentum coupling of $\mathbf{L}$ and $\mathbf{S}$. Thus we have for Case *c* [see Eq. (5) and (20)]

$$\Psi_{nJM\Omega}(\xi_i\eta_i\zeta_i\sigma_i; r, \theta, \varphi)$$

$$= \sum_{LS}\sum_{\Sigma} W_{LSj_i} C(LSj; \Lambda\Sigma\Omega)\, \psi_{J\Omega}\chi_{S\Sigma}$$

$$= A\sum_{LS}\sum_{\Sigma} W_{LSj_i} C(LSj; \Lambda\Sigma\Omega)\, \phi({}^{2S+1}\Lambda_\Omega) R_{nvJ} D_{M\Omega}^{J}, \quad (21)$$

where the summation over LS characterized by the coefficient W_{LSj_i} will eventually lead to the j–j-type coupling representation if spin–orbit interaction is very large.

As a very special example, if L is defined we consider a p-term ($L=1$) electron, we have the relationship between a state of Case *c* (with $j=\frac{3}{2}$, $\Omega=\frac{1}{2}$) and states of Case *a* as follows, namely, neglecting the sum over L and S in W:

$$\Psi_{n\frac{1}{2}JM\frac{1}{2}} = A\{C(1\tfrac{1}{2}\tfrac{3}{2}; 1, -\tfrac{1}{2}, \tfrac{1}{2})\phi({}^2\Pi_{\frac{1}{2}}) + C(1\tfrac{1}{2}\tfrac{3}{2}; 0, \tfrac{1}{2}, \tfrac{1}{2})\phi({}^2\Sigma_{\frac{1}{2}})\} R_{nvJ\frac{1}{2}} D_{M\frac{1}{2}}^{J}. \quad (22)$$

The contents inside the curly brackets constitute the electronic wavefunction of Case *c* in terms of those of Case *a*.

The spin multiplicity is still assumed to be preserved. This is, of course, the extreme, idealized case which may be obtained as the j representation merely from the consideration of commuting operators. The size of spin–orbit interaction need not appear in the coefficient. For intermediate cases, first-order mixing coefficients will then depend on the size of the spin–orbit interaction parameter A. An example may be found in Eq. (56) of Van Vleck[9] for the Λ doubling of a ${}^2\Pi_{\frac{1}{2}}$ state intermediate between Cases *a* and *c*, obtained by the superposition of spin–orbit perturbation on rotational perturbation.

For Hund's Case *d*, L and S are both decoupled from the figure axis and are approximately defined while Λ and Σ are no longer valid quantum numbers. We therefore sum over Λ in the many-term expansion (5) to give the representation of Case *d* wavefunctions in terms of those of Case *b*, or neglecting the coupling of spin for the time being

$$\Psi_{nLRNM}(\xi_i\eta_i\zeta_i S_i; r, \theta, \varphi) = A\sum_{\Lambda} C_{LNR}\phi_{nL\Lambda}(\xi_i\eta_i\zeta_i S_i; r) R_{nLvN\Lambda} D_{M\Lambda}^{N}. \quad (23)$$

As $D_{M\Lambda}^{N}$ represents the eigenfunction of angular momentum $\mathbf{N}$ and $\phi_{nL\Lambda}$ represents the eigenfunction of angular momentum $\mathbf{L}$, (23) may be viewed as the coupling of $\mathbf{N}$ and $\mathbf{L}'(=-\mathbf{L})$ to form $\mathbf{R}$ (see Fig. 3) and the expansion coefficient C_{LNR} may be formally identified to be $C(NLR; \Lambda, -\Lambda, 0)$. We discuss this

[46] See Ref. 19, Chap. III and p. 225 for the table of Clebsch–Gordan coefficients necessary for a triplet state.

[46] As an example for a ${}^2\Pi$ state translated into Kovacs notation our (20) for Case *b* $N = J \pm 1$ reads

$$\Psi_{N,\Lambda-\frac{1}{2}} = \psi({}^2\Pi_{J\pm\frac{1}{2}}{}^{\Lambda-\frac{1}{2}}) = \sum_{\Sigma} C(J, 1, J\pm1; \Omega, -\Sigma, +1)\psi_{J\Omega}\chi_{1,-\Sigma}$$
$$= \sum_{\Sigma} C(J, 1, J\pm1; \Omega, -\Sigma, +1)\phi({}^2\Pi_\Omega) R_{nv} U_{J\Omega}$$

$$\Psi_{N,\Lambda-\frac{3}{2}} = \psi({}^2\Pi_{J\pm\frac{1}{2}}{}^{\Lambda-1})$$
$$= \sum_{\Sigma} C(J, 1, J\pm1; -\Omega, +\Sigma, -1)\phi({}^2\Pi_{-\Omega}) R_{nv} U_{J,-\Omega},$$

where $U_{J\Omega}$ corresponds to our $A D_{M\Omega}^{J}$ and

$$\phi({}^2\Pi_\Omega) \equiv \Phi_{n,\Lambda-\frac{1}{2}}(\xi_i\eta_i\zeta_i; r)\chi_{1,-\Sigma} \equiv \phi(\xi_i\eta_i\zeta_i\sigma_i; r)$$

is a Case *a* wavefunction. The two Clebsch–Gordan coefficients for $\pm\Omega$ states are equal in magnitude and sign. Adding and subtracting the above two equations yields

$$\psi({}^2\Pi_{J\pm\frac{1}{2}}{}^{\pm}) = 1/\sqrt{2}[\psi({}^2\Pi_{J\pm\frac{1}{2}}{}^{\Lambda-\frac{1}{2}}) \pm \psi({}^2\Pi_{J\pm\frac{1}{2}}{}^{\Lambda-\frac{3}{2}})],$$

which is to be compared with Kovacs results. For $N = J$ states, the two Clebsch–Gordan coefficients in the expansions for $+\Omega$ and $-\Omega$ states are of equal magnitude but opposite signs, it is necessary to define

$$\psi({}^2\Pi_J{}^{\pm}) = -1/\sqrt{2}[\psi({}^2\Pi_J{}^{\Lambda-\frac{1}{2}}) \mp \psi({}^2\Pi_J{}^{\Lambda-\frac{3}{2}})]$$

to agree with Kovacs results. This shows that to be consistent one should consider Kovacs expression belonging to the ${}^2\Pi_J{}^{\pm}$ state as that belonging to the ${}^2\Pi_J{}^{\mp}$ state, only so will the expressions on both sides of the equation give the *same* eigenvalue under inversion.

case (also known as Case d' according to Mulliken) in detail in Sec. VI.

IV. ROTATIONAL PERTURBATIONS OF IDEAL HUND'S CASE b

For the rotational perturbation (Λ doubling) near Hund's Case b, the basic off-diagonal matrix element $H_1(\Lambda; \Lambda\pm1)$ of Eq. (16) was evaluated by Van Vleck.[9] For higher (2Λth) order Λ doubling, the matrix element $H_1^{(2\Lambda)}(\Lambda; -\Lambda)$ connecting doubly degenerate states of $\pm\Lambda$ was also given by Van Vleck.

As the off-diagonal matrix element $H_1(\Lambda; -\Lambda)$ which governs the Λ doubling width $[=2H_1(\Lambda; -\Lambda)]$ is of 2Λth order,[9] for $\Lambda=2$ it appears also necessary to consider the diagonal matrix elements $H_1(\Lambda; \Lambda)$ up to the fourth order. Due to the selection rule of H_1, the third-order energy vanishes. We give the energy up to the fourth order for Δ, Π, and Σ states. Thorson,[17] in a study of high-energy, high-angular velocity scattering, has also considered the fourth-order energy for the Σ state. To derive these higher-order energies, we use the more concise expressions given by Dalgarno[47] which are equivalent to the more general expressions of Condon and Shortley.[48]

For Case b (and Case b' when spin is neglected) we give the general perturbed energy formulas including electronic, rotational, and their interaction energy, but neglecting vibrational energy as follows:

$$\Lambda^{\pm}\text{ state: } E_\Lambda+B[N(N+1)-\Lambda^2+\langle \mathbf{P}_\xi^2\rangle_{Av}+\langle \mathbf{P}_\eta^2\rangle_{Av}] +\sum_{\sigma=1}^{\infty} H_1^{(2\sigma)}(\Lambda;\Lambda)\pm H_1^{(2\Lambda)}(\Lambda;-\Lambda), \quad (24)$$

where E_Λ is the electronic energy for a stationary molecule with a Rydberg electron in a Λ state, the average of $\mathbf{P}_\xi^2+\mathbf{P}_\eta^2$ over the electronic wavefunction comes from Eq. (15), and $\mathbf{P}$ is set to $\mathbf{L}$ for Case b'. The master formula for the 4th order ($\sigma=2$) energy, by the selection rule of H_1, and in our notation reads

$$H_1^{(4)}(\Lambda;\Lambda)=\sum_{\Lambda'}{}'\sum_{\Lambda''}{}'\sum_{\Lambda'''}{}'\frac{H_1(\Lambda;\Lambda')H_1(\Lambda';\Lambda'')H_1(\Lambda'';\Lambda''')H_1(\Lambda''';\Lambda)}{E(\Lambda\Lambda')E(\Lambda\Lambda'')E(\Lambda\Lambda''')} -\sum_{\Lambda'}{}'\sum_{\Lambda''}{}'\frac{H_1(\Lambda;\Lambda')H_1(\Lambda';\Lambda)H_1(\Lambda;\Lambda'')H_1(\Lambda'';\Lambda)}{[E(\Lambda,\Lambda')]^2E(\Lambda\Lambda'')}, \quad (25)$$

where the primes on the summation signs indicate that none of the summation indices Λ', Λ'', or Λ''' may be equal to $\pm\Lambda$. The definition of the energy separation is $E(\Lambda\Lambda')=E_\Lambda-E_{\Lambda'}$. The summation over the other electronic quantum number n and the vibrational quantum number v is omitted for brevity and we are to understand that $H_1(\Lambda;\Lambda')\equiv H_1(nv\Lambda; n'v'\Lambda')$.

When the matrix elements in (24) are evaluated over the rotational wavefunctions [see Eq. (18)], we have the following energy expressions up to the fourth order for Δ, Π, Σ states ($\Lambda=2, 1, 0$). For $\Lambda=2$ (the $\Delta^{\pm}$ states):

$$\begin{aligned}
E_\Delta^{\pm}=E_\Delta&+B[N(N+1)-2^2+\langle \mathbf{P}_\xi^2\rangle_{Av}+\langle \mathbf{P}_\eta^2\rangle_{Av}]+\left\{\frac{4[BP_y(\Delta\Phi)]^2}{E(\Delta\Phi)}(N-2)(N+3)+\frac{4[BP_y(\Delta\Pi)]^2}{E(\Delta\Pi)}(N-1)(N+2)\right\}\\
&+\left\{\frac{4[BP_y(\Delta\Pi)]^2(N-1)(N+2)}{[E(\Delta\Pi)]^2}\left[\frac{4[BP_y(\Pi\Sigma)]^2N(N+1)}{E(\Delta\Sigma)}-\frac{4[BP_y(\Delta\Pi)]^2(N-1)(N+2)}{E(\Delta\Pi)}\right]\right\}\\
&+\left\{\frac{16[(BP_y(\Delta\Phi)]^2[BP_y(\Phi\Gamma)]^2(N-2)(N+3)(N-3)(N+4)}{[E(\Delta\Phi)]^2E(\Delta\Gamma)}\right.\\
&\quad-\frac{16[BP_y(\Delta\Phi)]^2[BP_y(\Delta\Phi)]^2}{[E(\Delta\Phi)]^3}(N-2)^2(N+3)^2\\
&\quad-\frac{16[BP_y(\Delta\Phi)]^2[BP_y(\Delta\Pi)]^2}{[E(\Delta\Phi)]^2E(\Delta\Pi)}(N-2)(N+3)(N-1)(N+2)\\
&\quad\left.-\frac{16[BP_y(\Delta\Pi)]^2[BP_y(\Delta\Phi)]^2}{[E(\Delta\Pi)]^2E(\Delta\Phi)}(N-1)(N+2)(N-2)(N+3)\right\}\\
&\pm\left\{\frac{16[BP_y(\Delta\Pi)]^2[BP_y(\Pi\Sigma)]^2(N-1)(N+1)(N+2)N}{[E(\Delta\Pi)]^2E(\Delta\Sigma)}\right\}, \quad (26)
\end{aligned}$$

[47] *Quantum Theory*, edited by D. R. Bates (Academic Press Inc., New York, 1961), Vol. I, p. 182.
[48] E. U. Condon and G. H. Shortley, *The Theory of Atomic Spectra* (Cambridge University Press, New York, 1935), pp. 34-35.

where the first curly bracket with N dependence up to the second order represents second-order effects, the second and third curly brackets represents fourth-order effects, and the last curly bracket with $\pm$ sign represents Λ-doubling effects. For $\Lambda=1$ (the $\Pi^{\pm}$ states):

$$E_{\Pi}^{\pm}=E_{\Pi}+B[N(N+1)-1+\langle \mathbf{P}_{\xi}^{2}\rangle_{av}+\langle \mathbf{P}_{\eta}^{2}\rangle_{av}]+\left\{\frac{4[BP_{y}(\Pi\Delta)]^{2}}{E(\Pi\Delta)}(N-1)(N+2)+\frac{4[BP_{y}(\Pi\Sigma)]^{2}}{E(\Pi\Sigma)}N(N+1)\right\}$$

$$+\left\{\frac{16[BP_{y}(\Pi\Delta)]^{2}[BP_{y}(\Delta\Phi)]^{2}}{[E(\Pi\Delta)]^{2}E(\Pi\Phi)}(N-1)(N+2)(N-2)(N+3)\right.$$

$$-\frac{16[BP_{y}(\Pi\Delta)]^{2}[BP_{y}(\Pi\Delta)]^{2}}{[E(\Pi\Delta)]^{3}}(N-1)^{2}(N+2)^{2}-\frac{16[BP_{y}(\Pi\Sigma)]^{2}[BP_{y}(\Pi\Sigma)]^{2}}{[E(\Pi\Sigma)]^{3}}N^{2}(N+1)^{2}$$

$$-\frac{16[BP_{y}(\Pi\Delta)]^{2}[BP_{y}(\Pi\Sigma)]^{2}}{[E(\Pi\Delta)]^{2}E(\Pi\Sigma)}(N-1)(N+2)N(N+1)-\frac{16[BP_{y}(\Pi\Sigma)]^{2}[BP_{y}(\Pi\Delta)]^{2}}{[E(\Pi\Sigma)]^{2}E(\Pi\Delta)}$$

$$\left.\times N(N+1)(N-1)(N+2)\right\}\pm\left\{\frac{4[BP_{y}(\Pi\Sigma)]^{2}}{E(\Pi\Sigma)}N(N+1)\right\}, \quad (27)$$

while for $\Lambda=0$ (the Σ^{+} state):

$$E_{\Sigma}^{+}=E_{\Sigma}+B[N(N+1)+\langle \mathbf{P}_{\xi}^{2}\rangle_{av}+\langle \mathbf{P}_{\eta}^{2}\rangle_{av}]+\left\{\frac{8[BP_{y}(\Sigma\Pi)]^{2}}{E(\Sigma\Pi)}N(N+1)\right\}$$

$$+\left\{\frac{32[BP_{y}(\Sigma\Pi)]^{2}[BP_{y}(\Pi\Delta)]^{2}}{[E(\Sigma\Pi)]^{2}E(\Sigma\Delta)}(N-1)N(N+1)(N+2)-\frac{64[BP_{y}(\Sigma\Pi)]^{4}}{[E(\Sigma\Pi)]^{3}}N^{2}(N+1)^{2}\right\}, \quad (28)$$

where we have arbitrarily chosen the Σ state of the Rydberg electron in question to be Σ^{+} by assuming a Σ core. In (28) we have also assumed the degeneracy of $\pm\Lambda$ states in the energy denominators. The $\pm$ signs in (26) and (27) are to be read consistently for the Λ-doubling states, while the term $BP_{y}(\Lambda;\Lambda\pm1)$ is defined as in (18). With the assumption of pure precession[9] [see also Sec. VII for discussions and Eqs. (18) and (19) for matrix elements of P_{y}], $n=n'$ and $v=v'$ we have the following specific formulas:

Specific formula for $L=2$,

Δ^{+} state: $E_{\Delta}^{+}=E_{\Delta}+B[N(N+1)-2]$

$$+\frac{4B^{2}}{E(\Delta\Pi)}[N(N+1)-2]+\frac{48B^{4}(N-1)(N)(N+1)(N+2)}{[E(\Delta\Pi)]^{2}E(\Delta\Sigma)}-\frac{16B^{4}(N-1)^{2}(N+2)^{2}}{[E(\Delta\Pi)]^{3}},$$

Δ^{-} state: $E_{\Delta}^{-}=E_{\Delta}+B[N(N+1)-2]+\frac{4B^{2}}{E(\Delta\Pi)}[N(N+1)-2]-\frac{16B^{4}(N-1)^{2}(N+2)^{2}}{[E(\Delta\Pi)]^{3}}$,

Π^{+} state: $E_{\Pi}^{+}=E_{\Pi}+B[N(N+1)+4]-\frac{4B^{2}}{E(\Delta\Pi)}[N(N+1)-2]+\frac{12B^{2}N(N+1)}{E(\Pi\Sigma)}+\frac{16B^{4}(N-1)^{2}(N+2)^{2}}{[E(\Delta\Pi)]^{3}}$

$$-\frac{36B^{4}N^{2}(N+1)^{2}}{[E(\Pi\Sigma)]^{3}}-24B^{4}(N-1)N(N+1)(N+2)\left\{\frac{1}{[E(\Pi\Delta)]^{2}E(\Pi\Sigma)}+\frac{1}{[E(\Pi\Sigma)]^{2}E(\Pi\Delta)}\right\},$$

Π^{-} state: $E_{\Pi}^{-}=E_{\Pi}+B[(N(N+1)+4]-\frac{4B^{2}}{E(\Delta\Pi)}[N(N+1)-2]+\frac{16B^{4}(N-1)^{2}(N+2)^{2}}{[E(\Delta\Pi)]^{3}}$

$$-\frac{36B^{4}N^{2}(N+1)^{2}}{[E(\Pi\Sigma)]^{3}}-24B^{4}(N-1)N(N+1)(N+2)\left\{\frac{1}{[E(\Pi\Delta)]^{2}E(\Pi\Sigma)}+\frac{1}{[E(\Pi\Sigma)]^{2}E(\Pi\Delta)}\right\},$$

Σ^{+} state: $E_{\Sigma}^{+}=E_{\Sigma}+B[N(N+1)+6]-\frac{12B^{2}N(N+1)}{E(\Pi\Sigma)}+\frac{24B^{4}(N-1)N(N+1)(N+2)}{[E(\Sigma\Pi)]^{2}E(\Sigma\Delta)}+\frac{144B^{4}N^{2}(N+1)^{2}}{[E(\Pi\Sigma)]^{3}}$. (29)

Specific formulas for $L=1$

$$\Pi^+ \text{ state:} \quad E_\Pi{}^+ = E_\Pi + B[N(N+1)] + \frac{4B^2(N)(N+1)}{E(\Pi\Sigma)} - \frac{4B^4N^2(N+1)^2}{[E(\Pi\Sigma)]^3},$$

$$\Pi^- \text{ state:} \quad E_\Pi{}^- = E_\Pi + B[N(N+1)] - \frac{4B^4N^2(N+1)^2}{[E(\Pi\Sigma)]^3},$$

$$\Sigma^+ \text{ state:} \quad E_\Sigma{}^+ = E_\Sigma + B[N(N+1)+2] - \frac{4B^2N(N+1)}{E(\Pi\Sigma)} + \frac{16B^4N^2(N+1)^2}{[E(\Pi\Sigma)]^3}. \tag{30}$$

V. CASE *b* APPROACH TO INTERMEDIATE STATES BETWEEN CASES *b* AND *d*

For cases intermediate between *b* and *d*, approaches from both ends exist in the literature[49] (see below). To characterize the energy of an electronic state of a given Λ, both of these approaches make use of a *single* parameter A that represents the magnitude with which the electronic orbital motion is coupled to the figure axis. Our work represents a remedy for the inadequacy of the one-parameter approach.

In an approach from Case *b*, Kovacs and Budo[49] used the following diagonal matrix element for a state of quantum number Λ:

$$A\Lambda^2 + B[N(N+1) - \Lambda^2 + L(L+1) - \Lambda^2], \tag{31}$$

where $A\Lambda^2$ takes the place of E_Δ of our Eq. (24), and $L(L+1)-\Lambda^2$ comes from the average over $\mathbf{P}_\xi^2 + \mathbf{P}_\eta^2$ after using the pure precession assumption and neglecting the spin. This makes the above formula actually represent Case *b'*. Such use of *one* parameter A aside from a constant shift of energy levels is equivalent to the first-order perturbation treatment given by Hund[50] (see also Sec. VI) and is not justified for term complexes of $L \geq 2$.

In an approach from Case *d*, Dieke[51] following Hill and Van Vleck[52] computed the explicit diagonal and off-diagonal matrix element (over rotation-electronic wavefunctions) for the operator[53] $A\cos^2\alpha$ which we rewrite as $A(\mathbf{N}_f \cdot \mathbf{L})^2$, where $\mathbf{N}_f$ is the unit vector along the figure axis. In a stationary Case *b* diatomic molecule, the average of this operator, of course, reduces to $A\Lambda^2$, where Λ is the projection of $\mathbf{L}$ on $\mathbf{N}_f$. We show (Sec. VI) that this operator merely corresponds to the first contribution term of an infinite multipole expansion, and is clearly an inadequate representation of the whole situation.

We choose to use energy parameters. Such use of energy as a parameter has also been made previously[21,22] in a Case *b* approach. We define

$$\begin{aligned} &\mathbf{\Sigma} \equiv E_\Sigma, \\ &\mathbf{\Pi} \equiv E_\pi - E_\Sigma \equiv E(\Pi\Sigma), \qquad \mathbf{\Pi}' \equiv \mathbf{\Pi}/B, \\ &\mathbf{\Delta} \equiv E_\Delta - E_\Sigma \equiv E(\Delta\Sigma), \qquad \mathbf{\Delta}' \equiv \mathbf{\Delta}/B, \\ &\nu \equiv \mathbf{\Delta} - \mathbf{\Pi} \equiv E_\Delta - E_\pi, \qquad \nu' \equiv \nu/B. \end{aligned} \tag{32}$$

For a *d*-term complex ($L=2$) of a Rydberg electron with a Σ core (neglecting spin), the 5×5 secular determinant factors into a 2×2 and a 3×3 secular determinant equation, each involves the mixing of states of the same Kronig reflection (σ_v) symmetry "+" or "−." For the "−" states the two-by-two secular equation reads

$$\begin{array}{c|cc} & \Delta^- & \Pi^- \\ \hline \Delta^- & \nu + B[N(N+1)-2] - w & -2B[(N+2)(N-1)]^{\frac{1}{2}} \\ \Pi^- & -2B[(N+2)(N-1)]^{\frac{1}{2}} & B[N(N+1)+4] - w \end{array} = 0, \tag{33}$$

where Δ^-, Π^- at extreme left labels the states involved, $w = E - E_\Pi$ and $B_\Delta = B_\Pi = B$. The solution of this quadratic equation immediately yields

$$\begin{aligned} E_\Delta{}^- &= E_\Pi + B\{\nu'/2 + N(N+1) + 1 + [(2N+1)^2 + (\nu')^2/4 - 3\nu']^{\frac{1}{2}}\}, \\ E_\Pi{}^- &= E_\Pi + B\{\nu'/2 + N(N+1) + 1 - [(2N+1)^2 + (\nu')^2/4 - 3\nu']^{\frac{1}{2}}\}. \end{aligned} \tag{33a}$$

[49] I. Kovacs and A. Budo, Hung. Acta Phys. 1, No. 4, 1 (1949).
[50] See F. Hund, Z. Physik 63, 719 (1930); where the first-order energy reads $-a^2K(L^2+L-3\Lambda^2)$.
[51] C. H. Dieke, Z. Physik 57, 71 (1929).
[52] E. Hill and J. H. Van Vleck, Phys. Rev. 32, 250 (1928); pp. 267–272.
[53] Matrix elements for this operator may also be computed by the angular momentum coupling techniques such as those in (i) Landau and Lifshits, Ref. 24, p. 105 and p. 295; (ii) M. E. Rose, Ref. 19, p. 117.

Analytic formulas same as (33a) may be obtained from the Case d' approach (Sec. VI). This is because we have used the pure precession assumption in the evaluation of the off-diagonal matrix element $H_1(\Delta^-;\Pi^-)=\frac{1}{2}[H_1(+2;+1)+H_1(-2;-1)]$ and in the evaluation of the part of the diagonal matrix element that involves L, namely $\langle \mathbf{P}_\xi^2\rangle_{Nv}+\langle \mathbf{P}_\eta^2\rangle_{Nv}$. For the "+" state the three by three secular equation with state labels reads

$$\begin{array}{c} \\ \Delta^+ \\ \Pi^+ \\ \Sigma^+ \end{array}\begin{vmatrix} \mathbf{\Delta}+B[N(N+1)-2]-w' & -2B[(N-1)(N+2)]^{\frac{1}{2}} & 0 \\ -2B[(N-1)(N+2)]^{\frac{1}{2}} & \mathbf{\Pi}+B[N(N+1)+4]-w' & -2B[3N(N+1)]^{\frac{1}{2}} \\ 0 & -2B[3N(N+1)]^{\frac{1}{2}} & B[N(N+1)+6]-w' \end{vmatrix}=0, \tag{34}$$

where $w'=E-E_\Sigma$. While this 3×3 symmetric secular equation may be solved numerically by standard computer methods, after the fashion of Kovacs and Budo,[49] we consider it helpful to give explicit series solutions in terms of the over-all B's. Thus[50]

$$E_{\Delta^+}=B\left[\frac{\mathbf{\Delta}'+\mathbf{\Pi}'+8}{3}+N(N+1)\right]+a^{\frac{1}{2}}-\frac{b}{2a}-\frac{3b^2}{8a^{\frac{1}{2}}}-\sum_{n=3}^{\infty}\frac{3}{2n}\binom{\frac{3}{2}n-\frac{5}{2}}{n-1}\frac{b^n}{a^{\frac{1}{2}(3n-1)}}+E_\Sigma,$$

$$E_{\Pi^+}=B\left[\frac{\mathbf{\Delta}'+\mathbf{\Pi}'+8}{3}+N(N+1)\right]+\frac{b}{a}+\sum_{n=3}^{\infty}[1-(-)^n]\frac{3}{2n}\binom{\frac{3}{2}n-\frac{5}{2}}{n-1}\frac{b^n}{a^{\frac{1}{2}(3n-1)}}+E_\Sigma,$$

$$E_{\Sigma^+}=B\left[\frac{\mathbf{\Delta}'+\mathbf{\Pi}'+8}{3}+N(N+1)\right]-a^{\frac{1}{2}}-\frac{b}{2a}+\frac{3b^2}{8a^{\frac{1}{2}}}+\sum_{n=3}^{\infty}(-)^n\frac{3}{2n}\binom{\frac{3}{2}n-\frac{5}{2}}{n-1}\frac{b^n}{a^{\frac{1}{2}(3n-1)}}+E_\Sigma,$$

where the binomial coefficient

$$\binom{\frac{3}{2}n-\frac{5}{2}}{n-1}\equiv\binom{l}{m}=\frac{l!}{(l-m)!\,m!} \tag{34a}$$

and

$$a=(B^2/6)[\mathbf{\Delta}'^2+\mathbf{\Pi}'^2+v'^2-(12v'+4\mathbf{\Pi}'+16\mathbf{\Delta}')+32+24(2N+1)^2]$$

$$b=(B^3/27)\{[v'^2-12v'-45+9(2N+1)^2][10-(\mathbf{\Delta}'+\mathbf{\Pi}')]+[\mathbf{\Pi}'^2-4\mathbf{\Pi}'-23+27(2N+1)^2]$$

$$\times[(v'+\mathbf{\Delta}')-14]+[\mathbf{\Delta}'^2-16\mathbf{\Delta}'+64][(\mathbf{\Pi}'-v')+4]\}. \tag{35}$$

VI. ROTATIONAL PERTURBATIONS OF IDEAL HUND'S CASE d' AND CASE d' APPROACH TO INTERMEDIATE STATES

The Λ-doubling effect near Hund's Case d was first considered by Hill and Van Vleck[52] and subsequently by Dieke[51] both using one parameter A to represent the magnitude of coupling of orbital motion to the figure axis. As an improvement, we use energy as a parameter and develop a formalism that permits the use of any necessary number of parameters.

Neglecting spin for the time being, we consider Hund's Case d' and assume the orbital angular momentum $\mathbf{L}$ of the Rydberg electron to be completely decoupled from the figure axis. In other words, the core potential is assumed to have a spherical symmetry and $\mathbf{L}^2$ commutes with the Hamiltonian to make $\mathbf{L}$ a good quantum number. In this case the total angular momentum $\mathbf{N}$ of the system is simply the resultant of the electron orbital angular momentum $\mathbf{L}$ and the nuclear orbital angular momentum $\mathbf{R}$, the latter coming from the rigid rotation of the bare nuclei. Conversely $\mathbf{R}$ is the difference of $\mathbf{N}$ and $\mathbf{L}$. In terms of the standard notation for vector coupling of angular momenta (Fig. 3) we have $\mathbf{R}=\mathbf{N}-\mathbf{L}=\mathbf{N}+\mathbf{L}'$, where $\mathbf{L}'$ is the negative of $\mathbf{L}$ and has the signs of its components reversed compared with the latter. More explicitly we rewrite (23)

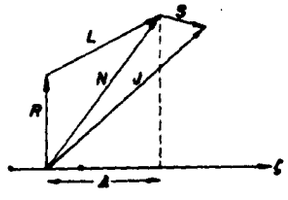

FIG. 3. L decoupling from Hund's Case b to form Hund's Case d.

[50] I. Kovacs and S. Singer, Physik. Z. 43, 362 (1942).

to read

$$\Psi_{R,0}=\sum_{\Lambda=-L'}^{L'} C(N, L', R; \Lambda, -\Lambda, 0) D_{N\Lambda}\phi_{L',-\Lambda}, \quad (36)$$

where we have omitted the vibrational wavefunction $R_{nvN\Lambda}$ and other irrelevant quantum numbers. $\Psi_{R,0}$ is the wavefunction for the rigid rotation of nuclei. Since R, the nuclear orbital angular momentum, is perpendicular to the figure axis, the former naturally has zero component along the latter. C is the vector coupling (Clebsch–Gordan) coefficient.[55] From Eq. (12),

$$D_{N\Lambda}=[(2N+1)/8\pi^2]^{\frac{1}{2}}D_{M\Lambda}^{N}$$

is the normalized wavefunction for a symmetric top expressed in terms of Euler angles. $\phi_{L\Lambda}$ is the normalized electronic wavefunction expressed with respect to the moving molecular coordinate axes.

A perturbation that causes Hund's Case d to deviate towards Case b also causes L to be more coupled to the figure axis. In other words, the core potential deviates from a spherical symmetry towards an axial symmetry. Such coupling with the figure ($\mathbf{N}_f$) axis was expressed by Hill and Van Vleck[52] as

$$A\langle(\mathbf{L}\cdot\mathbf{N}_f)^2\rangle \Rightarrow A\Lambda^2. \quad (37)$$

The square of Λ then accounts for the $\pm\Lambda$ double degeneracy in a stationary molecule. However, we can also view the above in a different manner. Because of equivalent transformation properties[56] of the angular momentum vector and the position vector of an electron, the matrix elements of these operators are equivalent except for a proportionality constant. For this to be valid, one expresses the operator in irreducible spherical tensor form, namely,

$$A'[3(\mathbf{L}\cdot\mathbf{N}_f)^2-\mathbf{L}^2]=A'[3L_f^2-\mathbf{L}^2] \quad (38a)$$

$$\Rightarrow A'[3\cos^2\theta_{ln}-1], \quad (38b)$$

where θ_{ln} is the angle between $\mathbf{L}$ and the unit vector ($\mathbf{N}_f$) along the figure axis. Eq. (38b) may be shown to be equivalent to

$$-\tfrac{1}{4}\rho A'[3\cos^2\theta_{\rho n}-1]=-\tfrac{1}{2}\rho A' P_2(\cos\theta_{\rho n}), \quad (39)$$

where $\theta_{\rho n}$ is the angle between the electron position vector $\boldsymbol{\rho}$ and $\mathbf{N}_f$ and differs from θ_{ln} by $\pi/2$ as $\boldsymbol{\rho}$ is perpendicular to $\mathbf{L}=\boldsymbol{\rho}\times\mathbf{P}$. The proportionality constant can be gotten simply by evaluating the first operator (38) in Hill and Van Vleck's formalism[52] (with their $j=N$, $j_r=R$ and their $k=L=1$) and evaluating the second operator (39) over our wavefunctions in (36) for $L=1$ (see below), and then comparing results. When converted to an operator in the position space of the electron as above, the coupling perturbation of Van Vleck $A(\mathbf{L}\cdot\mathbf{N}_f)^2$ is suggestive of the electrostatic nature of such perturbation. In fact if we consider a united atom[57] model as representative of Hund's Case d, the axial perturbation on the spherically symmetric field due to the separation of nuclei is the following (2^k) multipole-type potential expansion for a (linear) distribution of (two) charges (Z_a and Z_b), where Z_a and Z_b may be considered to be the effective positive charge of the partially shielded nuclei.[58]

$$H_p=e^2\left\{\frac{Z_a+Z_b}{\rho} - \sum_{k=0}^{\infty}[Z_a(\rho_<)^k+(-)^k Z_b(\rho_<)^k]\frac{P_k(\cos\theta)}{\rho_>^{k+1}}\right\}. \quad (40)$$

Here $\rho_<$ and $\rho_>$ are the larger or the smaller of ρ and $R/2$, R is the separation between the nuclei a and b [denoted as r in Eqs. (1)–(10)], and $\boldsymbol{\rho}$ is the position vector of the Rydberg electron which perceives this perturbing potential. As the spherical harmonics with odd k will yield[19] a vanishing Clebsch–Gordan coefficient $C(LkL;\ 000)$ when evaluated over any two rotation–electronic states with the same good quantum number L in a first order perturbation theory, only term with even k remain. The first contributing term for $L\neq 0$ has $k=2$ which is precisely of the form of the coupling perturbation term in (55) that gives rise to $A(\mathbf{L}\cdot\mathbf{N}_f)^2$ or $A\Lambda^2$ dependence. More precisely the dependence up to R^2 of the perturbed energy can be shown[57] to be, for $L\neq 0$, coming from the $k=2$ term in the expansion for $\rho>R/2$, namely,

$$\Delta E=\frac{Z_aZ_b}{(Z_a+Z_b)}\left\langle\frac{1}{\rho^3}\right\rangle\frac{L(L+1)[3\Lambda^2-L(L+1)]}{(2L-1)L(L+1)(2L+3)}R^2$$

$$\equiv A'[3\Lambda^2-L(L+1)], \quad (41)$$

which is equivalent to the formula given by Hund[50] for an approximate one-electron state (without electron–electron interaction) in the orbital approximation of a many-electron molecule ab. Here A is assumed to be a function dependent on the principal quantum number of the united-atom orbital n, the orbital angular momentum quantum number L and internuclear separation R but independent of Λ. For a hydrogenlike orbital

$$A'=\frac{2Z_aZ_b(Z_a+Z_b)^2}{a_0^3n^3L(L+1)(2L-1)(2L+1)(2L+3)}R^2. \quad (41a)$$

From (37) and (38) it is seen that $3A'=A$.

With increasing separation of R, higher-order multipoles and higher-order perturbation theory will give

[55] For the algebraic expressions of C involving L up to 2, see E. U. Condon and G. H. Shortley, Ref. 48, pp. 76–78, or J. C. Slater *Quantum Theory of Atomic Structure* (McGraw-Hill Book Company, Inc., New York, 1960), Vol. I, pp. 92–94. However, note a misprint here in the expression (in Slater's notation) for $S=2$, $J=L-2$, $M_s=0$ inside the square root ($L+M+1$) should read ($L+M-1$). For $L=3$, see D. L. Falkoff, G. S. Collakay, and R. E. Sells, Can. J. Phys. **30**, 253 (1952).

[56] V. Heine, *Group Theory in Quantum Mechanics* (Pergamon Press, New York, 1960), p. 152.

[57] W. A. Bingel, J. Chem. Phys. **30**, 1250 (1959); see also P. M. Morse and E. C. Stuekelberg, Phys. Rev. **33**, 932 (1929).

[58] For the H_2 molecule this corresponds to a demi-H_2^+ core for a H_2 Rydberg MO. See R. S. Mulliken, Ref. 20. The charge distribution, of course, must have cylindrical symmetry.

rise to the other powers of R dependence. When higher orders are included, the total effect is manifested in the electronic energy expression

$$\phi_\Lambda H_p \phi_\Lambda = E_\Lambda. \tag{41b}$$

We have noted that the perturbations (40) are diagonal in Λ. If we apply these perturbations to our Case d wavefunctions (36), we have, from the orthonormal property of $D_{N\Lambda}$ the following nonvanishing matrix elements[50]:

$$\Delta R=0;\ \Psi_{R,0}H_P\Psi_{R,0}=\sum_{\Lambda=-L}^{L}|C(NLR;\ \Lambda-\Lambda 0)\ |^2\ E_\Lambda,$$

$$\Delta R=\pm 2;\ \Psi_{R,0}H_P\Psi_{R\pm 2,0}=\sum_{\Lambda=-L}^{L}C(NLR;\ \Lambda-\Lambda 0)\,C(NLR\pm 2;\ \Lambda-\Lambda 0)\,E_\Lambda. \tag{42}$$

From these nonvanishing matrix elements, we have the general formula for a state of given R up to the second order:

$$E_R=BR(R+1)+H_p(R;\ R)+\frac{[H_p(R;\ R+2)]^2}{E(R;\ R+2)}+\frac{[H_p(R;\ R-2)]^2}{E(R;\ R-2)}$$

$$=BR(R+1)+H_p(R;\ R)-\frac{[H_p(R;\ R+2)]^2}{B[4R+6]}+\frac{[H_p(R;\ R-2)]^2}{B[4R-2]}. \tag{43}$$

More explicitly we write the state wavefunction (36) for the p-term complex ($L=1$) as

$$R=N+1;\ \Psi_{N+1,0}=\left[\frac{N}{2(2N+1)}\right]^{\frac{1}{2}}D_{N,1}\phi_{L,1}+\left[\frac{N+1}{2N+1}\right]^{\frac{1}{2}}D_{N,0}\phi_{L,0}+\left[\frac{N}{2(2N+1)}\right]^{\frac{1}{2}}D_{N,-1}\phi_{L,-1},$$

$$R=N;\ \Psi_{N,0}=[\tfrac{1}{2}]^{\frac{1}{2}}D_{N,1}\phi_{L,1}-[\tfrac{1}{2}]^{\frac{1}{2}}D_{N,-1}\phi_{L,-1},$$

$$R=N-1;\ \Psi_{N-1,0}=\left[\frac{N+1}{2(2N+1)}\right]^{\frac{1}{2}}D_{N,1}\phi_{L,1}-\left[\frac{N}{2N+1}\right]^{\frac{1}{2}}D_{N,0}\phi_{L,0}+\left[\frac{N+1}{2(2N+1)}\right]^{\frac{1}{2}}\times D_{N,-1}\phi_{L,-1}. \tag{44}$$

Using the definition of energy parameters (32), the energies E_R's for the above states up to the second order are then:

$$R=N+1\text{ state:}\quad B(N+1)(N+2)+H_p(N+1;\ N+1)+\frac{[H_p(N+1;\ N-1)]^2}{B[4N+2]}\rightarrow\Pi^+,$$

$$R=N\quad\text{state:}\quad BN(N+1)+H_p(N;\ N)\rightarrow\Pi^-,$$

$$R=N-1\text{ state:}\quad B(N-1)(N)+H_p(N-1;\ N-1)-\frac{[H_p(N-1)(N+1)]^2}{B[4N+2]}\rightarrow\Sigma^+, \tag{45}$$

where the matrix elements are

$$H_p(N+1;\ N+1)=\frac{N}{2N+1}\Pi+\Sigma,$$

$$H_p(N;\ N)=\Pi+\Sigma,$$

$$H_p(N-1;\ N-1)=\frac{N+1}{2N+1}\Pi+\Sigma,$$

$$[H_p(N+1;\ N-1)]^2=[H_p(N-1;\ N+1)]^2=\frac{N(N+1)}{(2N+1)^2}\Pi^2, \tag{46}$$

and the arrow indicates the correlation[51] to the states of Case b [Eq. (30)] for a Σ core.

[50] Off-diagonal matrix elements for $\Delta R=\pm 1$ can be shown to be zero from the properties of the Clebsch-Gordan coefficients (Ref. 19, p. 38 and p. 42). We write

$$\Psi_{R,0}H_p\Psi_{R\pm 1,0}=\sum_{\Lambda=1}^{L}C(NLR;\ -\Lambda,\ +\Lambda,\ 0)\,C(NLR\pm 1;\ -\Lambda,\ +\Lambda,\ 0)\,E_{-\Lambda}$$

$$+C(NLR;\ 000)\,C(NLR\pm 1;\ 000)\,E_0+\sum_{\Lambda=1}^{L}C(NLR;\ \Lambda,\ -\Lambda,\ 0)\,C(NLR\pm 1,\ \Lambda,\ -\Lambda,\ 0)\,E_\Lambda.$$

Because $E_\Lambda=E_{-\Lambda}$, on changing the signs of Λ the first term cancels the last term. The second term vanishes because one of the sum either $(N+L+R)$ or $(N+L+R\pm 1)$ must be odd and the corresponding Clebsch-Gordan coefficient for this is zero.

In the above formulas use has been made of the orthonormal condition of the Clebsch-Gordan coefficients to separate one energy parameter $E_\Sigma(=\Sigma)$ which is later eliminated on the diagonal by being absorbed into the energy variable W' of the secular equation. Thus for a p-term complex ($L=1$) we need only one parameter (number of parameters is equal the number of Λ's in the summation that ranges from $\Lambda=1$ to L or L in number), for a d-term complex ($L=2$) we need two parameters, etc. After eliminating the parameter E_Σ by letting $W'=E-E_\Sigma$ as was done in (34), we see that the secular equation obtained by using the matrix elements of (46)

$$|H_p(R;R')-W'\delta_{R,R'}|=0 \qquad R'=R,\ R\pm 2 \qquad (47)$$

is identical to that of Hill and Van Vleck,[50,52] with their $A=E_\pi-E_\Sigma=\Pi$, a conclusion wholly consistent with (41) and (41a).

The energies E_R's for the five states of a d-term complex ($L=2$) up to the second order are the following

$$\begin{aligned}
R=N+2 \text{ state:}\quad & B(N+2)(N+3)+H_p(N+2;N+2)+\frac{[H_p(N+2;N)]^2}{B[4N+6]}\rightarrow\Delta^+,\\
R=N+1 \text{ state:}\quad & B(N+1)(N+2)+H_p(N+1;N+1)+\frac{[H_p(N+1;N-1)]^2}{B[4N+2]}\rightarrow\Delta^-,\\
R=N \quad \text{state:}\quad & BN(N+1)+H_p(N;N)-\frac{[H_p(N;N+2)]^2}{B[4N+6]}+\frac{[H_p(N;N-2)]^2}{B[4N-2]}\rightarrow\Pi^+,\\
R=N-1 \text{ state:}\quad & B(N-1)(N)+H_p(N-1;N-1)-\frac{[H_p(N-1;N+1)]^2}{B[4N+2]}\rightarrow\Pi^-,\\
R=N-2 \text{ state:}\quad & B(N-2)(N-1)+H_p(N-2;N-2)-\frac{[H_p(N-2;N)]^2}{B[4N-2]}\rightarrow\Sigma^+,
\end{aligned} \qquad (48)$$

where the matrix elements are

$$\begin{aligned}
H_p(N+2;N+2)&=\frac{N(N-1)}{2(2N+1)(2N+3)}\Delta+\frac{2N(N+2)}{(2N+1)(2N+3)}\Pi+\Sigma,\\
H_p(N+1;N+1)&=\frac{(N-1)}{(2N+1)}\Delta+\frac{(N+2)}{(2N+1)}\Pi+\Sigma,\\
H_p(N;N)&=\frac{3(N-1)(N+2)}{(2N-1)(2N+3)}\Delta+\frac{3}{(2N-1)(2N+3)}\Pi+\Sigma,\\
H_p(N-1;N-1)&\equiv\frac{N+2}{2N+1}\Delta+\frac{N-1}{2N+1}\Pi+\Sigma,\\
H_p(N-2;N-2)&\equiv\frac{(N+1)(N+2)}{2(2N-1)(2N+1)}\Delta+\frac{2(N-1)(N+1)}{(2N-1)(2N+1)}\Pi+\Sigma,\\
[H_p(N+2;N)]^2&=[H_p(N;N+2)]^2=\frac{3N(N+2)}{2(2N-1)(2N+1)(2N+3)^2}[(N-1)\Delta+2\Pi]^2,\\
[H_p(N+1;N-1)]^2&=[H_p(N-1;N+1)]^2=\frac{(N-1)(N+2)}{(2N+1)^2}[\Delta-\Pi]^2,\\
[H_p(N;N-2)]^2&=[H_p(N-2;N)]^2=\frac{3(N-1)(N+1)}{2(2N+1)(2N-3)(2N-1)^2}[(N+2)\Delta-2\Pi]^2,
\end{aligned} \qquad (49)$$

and the arrows in (48) indicate the correlation[49,51] to the states of Case b [Eq. (29)] with a Σ core.

To investigate cases intermediate between b and d from the Case d approach, we again form a secular equation similar to (47). This secular equation can be reduced to Dieke's secular equation[51] which was obtained from Hill and Van Vleck's one-parameter formalism,[50] if we make the assumption that $E_\Delta-E_\Sigma=4(E_\pi-E_\Sigma)\equiv 4A$. This last assumption of course stems from one parameter energy expression $E_\Delta=A\Lambda^2$ which is precisely what we try to avoid. Our 5×5 secular equation easily factors into a 2×2 secular equation involving the mixing of $R=N+1$ and $R=N-1$ states which corresponds to the mixing of Π^- and Δ^- states in Case b; and a 3×3 secular equation involving the mixing of $R=N+2$, $R=N$, and $R=N-2$ states which

corresponds to the mixing of Δ^+, Π^+, and Σ^+ states of Case b. The 3×3 secular equation is too complicated to warrant a series solution similar to that of (34)-(35). The 2×2 secular equation with appropriate labeling of R with $W'=E=E_\Sigma$, namely,

$$\begin{vmatrix} R=N+1 & \frac{N-1}{2N+1}\Delta+\frac{N+2}{2N+1}\Pi+B(N+1)(N+2)-W', & \frac{[(N-1)(N+2)]^{\frac{1}{2}}}{2N+1}(\Delta-\Pi) \\ R=N-1 & \frac{[(N-1)(N+2)]^{\frac{1}{2}}}{2N+1}(\Delta-\Pi), & \frac{N+2}{2N+1}\Delta+\frac{N-1}{2N+1}\Pi+B(N-1)N-W' \end{vmatrix}=0, \quad (50)$$

though very different in form from the secular equation (33) obtained by the Case b approach with pure precession assumption, may be easily shown to yield solutions identical to (33a). The equivalence of our present Case d approach to the Case b approach towards intermediate states then demonstrates the consistency of theoretical basis of the two cases and the correctness of perturbations involved in the transition between them.

VII. CONCLUDING REMARKS

We have developed, in Secs. IV, V, and VI, energy formulas for near ideal Cases b' and d' as well as for intermediate cases. For near Case b' and for the Case b' approach to intermediate states we have made use of Van Vleck's pure precession assumption[9] to evaluate the electronic matrix element, $2BL_y$ [See Eq. (19)]. Strictly speaking, these formulas then are applicable only to nonpenetrating Rydberg orbitals of relatively high n. We write the electronic term energy of a Rydberg state as follows:

$$-U_n(r)=T=R_yZ_c^2/n^{*2}=R_yZ_c^2/(n-\delta)^2, \quad (51)$$

where R_y is the Rydberg constant, Z_c charge of the core, δ is the quantum defect and $U_n(r)$ comes from Eq. (6) when the latter is written as a self-consistent field Schrödinger equation with core potential for a single Rydberg electron. For large n and consequently small magnitude of $U_n(r)$ the perturbation is significant. In these orbitals of large n, furthermore if the orbitals are nonpenetrating, the electron position vector ρ becomes consistently large, the core potential (40) loses its multipole character and appears as a spherically symmetric charge distribution to the electron. In this spherical central potential, the angular momentum L is defined and the Σ, Π, Δ states have nearly equal n^*'s which are close to the united atom n value.

When the rotational quantum number N is large, the rotational interaction [see Eqs. (26)-(28) for its dependence on N) will be large enough to decouple L from the figure axis, and the limiting formulas for perturbation near Hund's Case d are normally applicable. However, for penetrating Rydberg orbitals and for low N's where the pure precession assumption is not adequate, we have to go to near Case b and it may be necessary to distinguish B_Σ, B_π, $B_{\Sigma\pi}\cdots$, etc., and to reassess the magnetic dipole[60] matrix element $\langle\Lambda \mid Ly \mid \Lambda\pm1\rangle$ which does not take the simple form (19). This operator in spherical polar or in Eular angles,[39] or in elliptical coordinates[61] is to be evaluated over accurate electronic wavefunctions of molecular states in the appropriate coordinate systems. In the pure precession treatment with equal n's and L's, we are considering a rotational perturbation within the same term complex, for example, the matrix element $-\langle 3d\sigma_g \mid 2BLy \mid 3d\pi_g\rangle$, whereas the only known magnetic dipole matrix element for a real molecule appears to be that of $\langle 1s\sigma_g \mid L \mid 3d\pi_g\rangle$ of H_2^+ calculated by Dalgarno and McCarroll.[62] For complex molecules and for other molecular states the calculation at present is not practical because of the lack of accurate wavefunctions.

In the treatment of Hund's Cases b' and d', we have neglected electron spin and its coupling to the figure axis. Such decoupling of spin is especially justified for Rydberg states of high n where the spin–orbit interaction of the spin of the Rydberg electron of a $^1\Sigma$ core with its own orbit, is small. This is because the interaction is proportional to $\langle 1/\rho^3\rangle$ which in a central field approximation and with hydrogen-like atomic wavefunction becomes $Z^3/[n^3L(L+\frac{1}{2})(L+1)]$, where Z will be small in a united-atom approximation for relatively light molecules. The consequence of the above is of course the Case b representation. When spin is included for a Rydberg electron with a doublet core, we have singlet and triplet states each forming a separate Rydberg series. In that case, the difference in the space part of the singlet and the triplet states, as well as other refinements on the electronic state such as electron correlation, magnetic interactions will be manifested in the electronic matrix element of $2BL_y$. In the event of having made the pure precession assumption, these electronic properties will then be absorbed into

[60] See J. H. Van Vleck, Astrophys. J. **80**, 161 (1934) for a discussion and for some selection rules.

[61] The operators L_x, L_y, and $L_\pm$ in elliptical coordinates were given by Dalgarno and McCarroll[62] and also by Kolos and Wolniewicz.[6]

[62] A. Dalgarno and R. McCarroll, Proc. Phys. Soc. (London) **A70**, 502 (1957). The selection rule of $\Delta n=2$ and $\Delta L=2$ may be viewed as coming indirectly from the perturbation $P_2(\cos\theta)/\rho^3$ on the united atom [see Eq. (40)].

the effective spectroscopic constant B. As a last remark, if we replace Λ by $\Omega(=\Lambda+\Sigma)$ in all our equations, what was said about Hund's Case b' here applies to Hund's Case a (or c if L and S are strongly coupled) and about Hund's Case d' here applies to Hund's Case e.

ACKNOWLEDGMENTS

The author takes pleasure in thanking Professor Robert S. Mulliken, who sponsored this research, for helpful suggestions and discussions, Dr. L. Y. Chow Chiu for a preliminary reading of the manuscript, the referee for suggesting omissions of some introductory material which is necessary only for the uninitiated, Dr. M. L. Ginter, for some stimulating discussions and for a reading of the manuscript with suggestions for improving its presentation. The financial support of the National Science Foundation is gratefully acknowledged.

ELECTRIC QUADRUPOLE AND MAGNETIC DIPOLE RADIATION IN LINEAR MOLECULES. APPLICATIONS TO $^1\Pi - ^3\Pi$ TRANSITIONS.*

Ying-Nan Chiu†

Laboratory of Molecular Structure and Spectra
Department of Physics, University of Chicago
Chicago, Illinois 60637

ABSTRACT

The electric quadrupole and magnetic dipole operators of a rotating, linear molecule interacting with a radiation field are formulated, in the space-fixed and in the molecular coordinate systems, as contractions of irreducible spherical tensors. Radiative transition probabilities are obtained for the initial and final rotation-electronic states that are in Hund's coupling case a or b, using the normalized rotation matrix as the separated rotational wavefunction in the Born-Oppenheimer approximation. Line strength formulas are derived for (1) transitions between singlet case b states, in the case of an electric quadrupole, the $^1\Sigma - ^1\Sigma$, $^1\Pi - ^1\Sigma$, $^1\Delta - ^1\Sigma$, $^1\Pi - ^1\Pi$, $^1\Delta - ^1\Pi$, $^1\Phi - ^1\Pi$, $^1\Delta - ^1\Delta$, $^1\Phi - ^1\Delta$, and $^1\Gamma - ^1\Delta$ transitions; in the case of a magnetic dipole, the $^1\Pi - ^1\Phi$, $^1\Pi - ^1\Pi$, $^1\Delta - ^1\Pi$, $^1\Delta - ^1\Delta$ and $^1\Phi - ^1\Delta$ transitions (2) the $^1\Pi - ^3\Pi$(a) transitions (3) the $^1\Pi - ^3\Pi$(b) transitions. The master line strength formula as well as intensity distribution for different branches are given. In (2) and (3), some of the transitions are found to be dependent on the absolute Krönig reflection symmetry, giving, for molecules of unequal nuclei, an intensity alternation for the two Λ-doubling components. A discussion of this reflection symmetry and the inversion symmetry is given and a consistent set of molecular wavefunctions of a given symmetry is constructed for (1) singlet case b states and triplet case a states (2) triplet case b states expressed as linear combination of case a state wavefunctions through angular momentum coupling. The rotation-vibration spectra due to these higher multipole radiations are briefly discussed. A new view for the possibility of $\Delta\Lambda = 0$ (for $\Lambda \neq 0$) magnetic-dipole pure rotation spectra is advanced.

---

*This work was supported by a grant from the National Science Foundation, NSF GP-28 Research.

†Present Address: Department of Chemistry, The Catholic University of America, Washington 17, D. C.

I.. INTRODUCTION

The relatively "forbidden" higher multipole transitions are of interest in planetary and stellar spectra[1] and in molecular spectra where the electric dipole transition moment vanishes because of symmetry. Early theoretical work ranges from the magnetic dipole interpretation[2] of the atmospheric bands of oxygen to the calculation of the intensity distribution of the electric quadrupole rotation-vibration spectra[3] of H_2 in its ground electronic state. More recent experimental works of Wilkinson and Mulliken[4] and Wilkinson *et al.*[5] make it worthwhile to pursue further studies in this area. The theoretical line strength formulas we shall derive for diatomic molecules are equally valid for rotating, linear, polyatomic molecules when the interactions between rotation and vibration are not considered.

II. ELECTRIC QUADRUPOLE RADIATION

For a system of interacting charged particles such as the electrons and nuclei in a molecule, the Einstein spontaneous quadrupole emission probability $A_{n \to n'}$ for the transition from a state n to a state n' may be written as[3,6]

$$A_{n \to n'} = \frac{32\pi^6 \nu^5 \sum'_{M} \sum'_{M'} |\sum_i \overline{Q}_i(nM;n'M')|^2}{5\, hc^5\, g_n} , \qquad (1)$$

where $\overline{Q}_i$ is the electric quadrupole tensor for the i^{th} charged particle, the summation index M ranges through the g_n degenerate levels of the n state, and the other symbols have their usual meaning. If we consider only the degeneracy of the rotational levels explicitly, the line strength S(J,J') may be defined in terms of the quadrupole

---

[1] G. Herzberg, Astrophys. J. 87, 428 (1938).

[2] J. H. Van Vleck, Astrophys. J. 80, 161 (1934).

[3] H. M. James and A. S. Coolidge, Astrophys. J. 85, 438 (1938). Note here, I, J, and K stand for the molecular axes instead of the space axes.

[4] P. G. Wilkinson and R. S. Mulliken, Astrophys. J. 126, 120 (1957).

[5] P. G. Wilkinson, Communication with Professor R. S. Mulliken. $^1\Pi_g - {}^1\Sigma_g$ and $^3\Pi_g - {}^1\Pi_g$ transitions in N_2. See also Vanderslice, Wilkinson and Tilford, J. Chem. Phys. (to be published).

[6] E. C. Kemble, "The Fundamental Principles of Quantum Mechanics", Dover Publications Inc. (1958) pp. 462-469.

transition moment as follows:

$$S(J,J') = \sum_M \sum_{M'} |\sum_i \overline{Q}_i(JM;J'M')|^2 \quad , \tag{2}$$

where the indices M and M' range through the 2J+1 and 2J'+1 degeneracies of the initial and final states respectively.

The quadrupole tensor $\overline{Q}$ may be referred to an arbitrary space-fixed axis system ($\underset{\sim}{I}\ \underset{\sim}{J}\ \underset{\sim}{K}$) or to the molecular axis system ($n_\xi\ n_\eta\ n_\zeta$). Should Cartesian basis be used, $|\overline{Q}|^2$ represents the sum of the squares of the nine components of $\overline{Q}$. This has been the conventional treatment[3,6] we chose to express Q in the spherical basis[7] for the easier evaluation of the matrix elements. $|\overline{Q}|^2$ then represents the sum of the squares of the five independent components of the quadrupole tensor. In the molecular coordinate system[8] the electric quadrupole tensor of James and Collidge[3] may be written in the spherical basis as a contraction of irreducible tensors as follows:

$$\begin{aligned}\sum_i \overline{Q}_i &= \tfrac{2}{3} \sum_\lambda \sum_i e_i\, T_{2\lambda}(\xi_i\eta_i\zeta_i)\ T^*_{2\lambda}(\underset{\sim}{n}_\xi \underset{\sim}{n}_\eta \underset{\sim}{n}_\zeta) \\ &= (2/3)^{\frac{1}{2}} \sum_\mu \sum_\lambda \sum_i e_i\, T_{2\lambda}(\xi_i\eta_i\zeta_i) D^{2*}_{\mu\lambda}(\varphi\theta\psi) \\ &\times (2/3)^{\frac{1}{2}}\, T^*_{2\mu}(\underset{\sim}{I}\ \underset{\sim}{J}\ \underset{\sim}{K}) \quad ,\end{aligned} \tag{3}$$

where e_i is the charge of the i^{th} particle, $T_{2\lambda}$ is the λ^{th} component of the irreducible spherical tensor of the second rank;[7] in terms of the spherical harmonics on a unit sphere,[9] $T_{2\lambda} = (4\pi/5)^{\frac{1}{2}} Y_{2\lambda}$; the components $(2/3)^{\frac{1}{2}}\, T^*_{2\mu}\ (\underset{\sim}{I}\ \underset{\sim}{J}\ \underset{\sim}{K})$, are mutually orthonormal in as much as the unit vectors $\underset{\sim}{I}\ \underset{\sim}{J}\ \underset{\sim}{K}$ are orthonormal when one takes their mutual scalar products. $D^2_{\mu\lambda}$ is the rotation matrix[7] of the second rank and φ,θ,ψ are the Euler angles through which one rotates the space-fixed axis system to the molecular axis

---

[7] M. E. Rose, Elementary Theory of Angular Momentum, John Wiley and Sons, New York (1957).

[8] In the space-fixed axis system $\sum_i \overline{Q}_i = \frac{2}{3} \sum_\mu \sum_i e_i T_{2\mu}(x_i y_i z_i) T^*_{2\mu}(\underset{\sim}{I}\ \underset{\sim}{J}\ \underset{\sim}{K})$. Upon an inverse rotation to express the space coordinates (xyz) in terms of the molecular coordinates ($\xi\eta\zeta$), the above becomes $\sum_i \overline{Q}_i = (\frac{2}{3}) \sum_\lambda \sum_\mu \sum_i e_i D^2_{\lambda\mu}(-\psi-\theta-\varphi) T_{2\lambda}(\xi_i\eta_i\zeta_i) T^*_{2\mu}(\underset{\sim}{I}\ \underset{\sim}{J}\ \underset{\sim}{K})$ and is equivalent to the expression in (3) because (see Ref. 7, p. 54) $D^2_{\lambda\mu}(-\psi-\theta-\varphi) = D^{2*}_{\mu\lambda}(\varphi\theta\psi)$.

[9] Explicitly $T_{20}(a\ b\ c) = \frac{1}{2}[-aa - bb + 2cc)]$,
$T_{2,\pm 1}(a\ b\ c) = \mp(3/8)^{\frac{1}{2}}\ [(ac + ca) \pm i(bc + cb)]$,
$T_{2,\pm 2}(a\ b\ c) = (3/8)^{\frac{1}{2}}\ [aa - bb \pm i(ab + ba)]$.

system. We take as a generalized, initial state wavefunction[10-11]

$$\Psi_1 = (2J+1/8\pi^2)^{\frac{1}{2}} \sum'_{\Lambda} a_{\Lambda} \Phi_{nv\Lambda} D^{J*}_{M\Lambda}(\varphi\theta\psi) \quad , \tag{4a}$$

and final state wavefunction

$$\Psi_f = (2J'+1/8\pi^2)^{\frac{1}{2}} \sum'_{\Lambda'} b_{\Lambda'} \Phi_{n'v'\Lambda'} D^{J'*}_{M'\Lambda'}(\varphi,\theta,\psi) \quad , \tag{4b}$$

(See below for the reasons of taking a linear combination with summation indices Λ and Λ') and make use of the following formula for the integration, over Euler angles,[12] of the product of three rotation matrices,

$$\left[\frac{(2J+1)(2J'+1)}{8\pi^2}\right]^{\frac{1}{2}} \int D^{J'**}_{M'\Lambda'} D^{2*}_{\mu\lambda} D^{J*}_{M\Lambda} d\varphi \sin\theta d\theta d\psi = \left(\frac{2J+1}{2J'+1}\right)^{\frac{1}{2}} C(J2J';\Lambda\lambda\Lambda') \; C(J2J';M\mu M') \quad ,$$

where C is the Clebsch-Gordan vector-coupling coefficient.[7] We then get from Eqs. (2)-(3) the line strength

$$S(J,J') = \frac{2(2J+1)}{3(2J'+1)} \sum_M \sum_\mu \sum_{M'} \left[\sum'_{\Lambda} \sum_{\lambda} \sum_{\Lambda'} a_{\Lambda} b_{\Lambda'} (n'v'\Lambda' | Q_{2\lambda} | nv\Lambda) C(J2J';\Lambda\lambda\Lambda')\right]^2 C^2(J2J';M\mu M')$$

$$= \frac{2(2J+1)}{3} \left[\sum_{\Lambda'} \sum'_{\lambda} \sum'_{\Lambda} a_{\Lambda} b_{\Lambda'} (n'v'\Lambda' | Q_{2\lambda} | nv\Lambda) \; C(J2J';\Lambda\lambda\Lambda')\right]^2 \quad , \tag{5}$$

where the superscript, 2, on C denotes the square of the Clebsch-Gordan coefficient, $Q_{2\lambda} = \sum_i e_i \, T_{2\lambda}(\xi_i \eta_i \zeta_i)$, v is the vibrational quantum number, n stands for the assembly of electronic quantum numbers other than Λ, $(n'v'\Lambda' | Q_{2\lambda} | nv\Lambda)$ stands for the vibronic matrix element over vibrational and electronic wavefunctions. In singlet states of Hund's coupling case b[13] Λ stands for the projection of the total electronic orbital angular momentum along the molecular figure axis (n_ζ). In the event that we must consider the Kronig reflection symmetry, (see below) of the initial or final state wavefunction, the summation over the electronic quantum number Λ may be taken simply to mean that for $\Lambda \neq 0$, Λ assumes the values of $+\Lambda$ and $-\Lambda$ and $a_{\pm\Lambda} = b_{\pm\Lambda} = \pm 1/\sqrt{2}$. In states of Hund's coupling case a, Λ is set to Ω which is the projection of electronic orbital and spin angular momentum along the figure axis.[14] For a non-singlet case b

---

[10] L. Y. Chow Chiu, J. Chem. Phys. 40, 2276 (1964).

[11] Y. N. Chiu, "Rotation-Electronic Interaction in the Rydberg States of Diatomic Molecules", J. Chem. Phys. 41, 3235, (1964).

[12] Reference 7, p. 75.

[13] G. Herzberg, Spectra of Diatomic Molecules, (D. Van Nostrand Co., Princeton, N. J. (1931)), pp. 218-240.

[14] For the case of $\Omega = 0$, see Section IV.

state, the initial or final wavefunction may be expressed[11] as a linear combination (summation over Ω) of case a wavefunctions. For a Hund's case d' state, the wavefunction may be expressed[11] as a linear combination (summation over Λ) of case b' wavefunctions. For intermediate cases the wavefunction can always be expressed, by first order perturbation theory in terms of the wavefunctions of the idealized Hund's cases.

In the reduction to the first equation of (5), use was made of the orthogonality of the components of $T_{2\mu}(\underset{\sim}{I}\ \underset{\sim}{J}\ \underset{\sim}{K})$ to eliminate the corss terms composed of a product of different μ-components which represents the different components of the quadrupole tensor in the space-fixed coordinate system.[8] In the treatment of the interaction between radiation and matter[15-16] such non-mixing of different μ components follows from the orthogonality of the analogous components of the tensor $\underset{\sim}{\kappa}(\underset{\sim}{\Pi}_1 + \underset{\sim}{\Pi}_2)$ along the same space fixed coordinate system where for a transverse light wave Π_1 and Π_2 are the polarization vectors which together with $\underset{\sim}{\kappa}$, the propagation vector, form an orthogonal right handed axis system. In Eq. (5), one of the three summation indices, M,μ,M' is redundant; we may arbitrarily eliminate the index μ. In the reduction to the final form of Eq. (5), use was made of a very general sum rule for operators in the forms of tensors of any rank (ℓ), namely

$$\sum_{M'}\sum_{M} C^2(J\ell J';M,M'-M,M') = 2J'+1,\ \ell = 0,1,2,3\ \cdots \qquad (6)$$

which follows from the orthonormality[7] of the Clebsch-Gordan coefficients and the summation of M' over the 2J'+1 projections of J'. For the electric quadrupole tensor operators, $\ell = 2$, and for the magnetic dipole or electric dipole operator, $\ell = 1$.

From Eq. (5), in principle, all the Hönl-London type line-strength formulas[17] for $\Delta J = J' - J = -2, -1, 0, +1, +2$ (the O,P,Q,R,S branches) and for $\Delta\Lambda = \pm 2, \pm 1, 0$, should immediately follow. However, there is considerable cancellation in actual cases as well as some complication due to the differences in the Λ-doubling components (see below). We have computed some examples and they are shown in Table I. The formulas are labelled according to the case b designation and are, strictly speaking, good for

---

[15] J. S. Griffith, The Theory of Transition-Metal Ions, Cambridge University Press, London (1961), pp. 52-55.

[16] E. U. Condon and G. H. Shortley, The Theory of Atomic Spectra, Cambridge University Press, London (1957), pp. 93-97.

[17] Reference 13, pp. 127-128 and p. 208.

singlet, case b states only. However, by setting $\Lambda = \Omega$, it is clear from Eq. (5) that for transitions between the multiplet levels of two Hund's case a states, the same formulas for the J dependence are valid. The electronic and vibrational matrix elements, of course, differ. For example, the $^3\Pi_2(a) \leftarrow {}^3\Delta_3(a)$ transition will have the same J dependence as the $^1\Delta(b) \leftarrow {}^1\Phi(b)$ transition. (See Section V for more details.) In the formulas given, where the Kronig reflection symmetry (denoted by the superscript $\pm$) is not specified, the transition if occurs, will have the same line strength formulas for either of the Λ-doubling components.[18]

For the $^1\Pi - {}^1\Pi$ transition, writing $^1\Pi^{\pm} = (\frac{1}{2})^{\frac{1}{2}}\left[\Phi_{+1} D^{J*}_{M1} \pm \Phi_{-1} D^{J*}_{M-1}\right]$ we see that a complication arises because the Q_{22} component of the electronic quadrupole tensor operator connects the $\Lambda = +1$ or $^1\Phi_{+1}$ and the $\Lambda = -1$ or $^1\Phi_{-1}$ components. As a result in

---

[18] To show this, one needs only to know the relative Kronig reflection symmetry and the relative overall inversion symmetry (parity) of the final and initial states. As an example, consider the $^1\Delta - {}^1\Pi$ transition. From Eqs. (4a)(4b), if the final state wavefunction is $^1\Delta^{\pm} = (\frac{1}{2})^{\frac{1}{2}}A'\left[{}^1\Phi_2 D^{J'*}_{M'2} \pm {}^1\Phi_{-2} D^{J'*}_{M'-2}\right]$ with the eigenvalue (overall parity) of $\pm(-)^{J'}$ under the total inversion operation, the initial state wavefunction must be $^1\Pi = (\frac{1}{2})^{\frac{1}{2}} A\left[{}^1\Phi_1 D^{J*}_{M1} \pm (-)^{(J'-J)} {}^1\Phi_{-1} D^{J*}_{M-1}\right]$ so that under the inversion operation it will have the same eigenvalue (parity) of $\pm (-)^{J'-J}(-)^{J} = \pm (-)^{J'}$. This is the requirement for an electric quadrupole or a magnetic dipole transition. The line strength for the former is, according to Eq. (5), $(2/3)(2J+1)\left[({}^1\Phi_2|Q_{21}|{}^1\Phi_1) \frac{1}{2} \times C(J2J';112) + (-)^{J'-J}(\frac{1}{2})({}^1\Phi_{-2}|Q_{2-1}|{}^1\Phi_{-1})\ C(J2J';-1-1-2)\right]^2$. From the relationship between the vibronic matrix elements, which follows from our definition of the electronic state under the total inversion (see Section IV), for singlet states, $({}^1\Phi_{-2}|Q_{2-1}|{}^1\Phi_{-1}) = ({}^1\Phi_2|Q_{21}|{}^1\Phi_1)$ and from the relationship between the Clebsch-Gordan coefficients (see Ref. 7), $C(J2J';-1-1-2) = (-)^{J'-J+2}\ C(J2J';112)$, we reduce the line strength formula to $(2/3)(2J+1)(\Phi_2|Q_{21}|\Phi_1)^2|C(J2J';112)|^2$ an expression totally independent of the $\pm$ sign that specifies the Kronig reflection symmetry.

the transition matrix element[19] there are cross terms of the above kind which have signs of (±), dependent on the Kronig symmetry. Hence the two Λ-doubling components of molecules of unequal nuclei will have different line strength formulas,[19] and will give rise to line doublets of unequal intensities, in contrast to the electric dipole $^1\Pi - {}^1\Pi$ transitions[20] where the two components of a line doublet have equal intensities. An analogous dependence of the matrix element on the Kronig symmetry may be found in the fine structure formula[21] of the $^3\Pi_u^{\pm}(b) = (\frac{1}{2})^{\frac{1}{2}} \left[{}^3\Pi_u(\Lambda = +1) \pm {}^3\Pi_u\ (\Lambda = -1)\right]$ state of H_2 in Hund's coupling case b, where the $Y_2^{\pm 2}(\theta_{12}\varphi_{12})$ space component of the spin-spin interaction double tensor connects the $^3\Pi_u(\Lambda = +1)$ and $^3\Pi_u(\Lambda = -1)$ components.

III. MAGNETIC DIPOLE RADIATION

For magnetic dipole radiation, the Einstein spontaneous emission probability for the transition between the state n and n', may be written as[6,15]

$$A_{n \to n'} = \frac{64\pi^4 \nu^3 \sum'_M \sum_{M'} |\sum_i \underline{D}_i(nM;n'M')|^2}{3hc^3\, g_n} \quad , \tag{7}$$

where $\underline{D}_i = (e_i/2m_ic)\underline{j}_i = (e_i/2m_ic)(\underline{\ell}_i + \underline{s}_i)$ is the magnetic dipole vector for the i^{th} charged particle with mass m_i, charge e_i, orbital angular momentum $\underline{\ell}_i$ and spin angular momentum $\underline{s}_i$, the other symbols have the same meaning as those in Eq. (1). The magnetic dipole line strength is defined as follows:

$$S(J,J') = \sum_M \sum_{M'} |\sum_i \underline{D}_i(JM;J'M')|^2 \quad . \tag{8}$$

In spherical basis, the magnetic dipole vector in the molecular coordinate

---

[19] To use these formulas, one must know the absolute Kronig reflection symmetry and the absolute overall inversion symmetry of the states. Following footnote 18, let the final state be $^1\Pi^{\pm} = (\frac{1}{2})^{\frac{1}{2}} A' \left[\Phi_{+1}\, D^{J'*}_{M'+1} \pm \Phi_{-1}\, D^{J'*}_{M'-1}\right]$ and the initial state be $^1\Pi = (\frac{1}{2})^{\frac{1}{2}} A \left[\Phi_{+1}\, D^{J*}_{M+1} \pm (-)^{J'-J}\, \Phi_{-1}\, D^{J*}_{M-1}\right]$. The line strength according to Eq. (5) is $(1/4)(2/3)(2J+1)\left[(\Phi_{+1}|Q_{20}|\Phi_{+1})\ C(J2J';101) + (-)^{J'-J}(\Phi_{-1}|Q_{20}|\Phi_{-1})\ C(J2J';-10-1) + (-)^{J'-J}(\Phi_{+1}|Q_{22}|\Phi_{-1})\ C(J2J';-121) \pm (\Phi_{-1}|Q_{2-2}|\Phi_{+1})\ C(J2J';1-2-1)\right]^2$ an expression containing the ± sign that specifies the Kronig-symmetry of the final state.

[20] Reference 13, p. 268.

[21] P. R. Fontana, Phys. Rev. 125, 220 (1962). For a correction of a factor of two in these formulas, see L. Y. Chow Chiu, Ref. 10, footnote 20. The writer is indebted to L. Y. Chow Chiu for bringing up this point.

system[22] may be written as a contraction of irreducible tensors as follows:

$$\sum_i D_i = \sum_\lambda \sum_i (e_i/2m_ic)\ T_{1\lambda}(j_{i\xi}, j_{i\eta}, j_{i\zeta})\ T^*_{1\lambda}(n_\xi n_\eta n_\zeta) = \sum_\mu \sum_\lambda \sum_i (e_i/2m_ic)\ T_{1\lambda}(j_{i\xi}, j_{i\eta}, j_{i\zeta})\ D^{1*}_{\mu\lambda}(\varphi\theta\psi) T^*_{1\mu}(I\ J\ K), \tag{9}$$

where $T_{1\lambda}$ is the λ^{th} component of the irreducible spherical tensor of the first rank;[7,23] the components of $T_{1\mu}$ (I J K) are mutually orthonormal and $D^1_{\mu\lambda}$ is the totation matrix of the first rank. Using the same initial and final wavefunctions as in (4a)-(4b) and following the same reduction to Eq. (5), we get from Eqs. (8)-(9) the line strength

$$S(JJ') = \frac{(2J+1)}{(2J'+1)} \sum_M \sum'_\mu \sum_{M'} \left[\sum'_\Lambda \sum_\lambda \sum'_{\Lambda'} a_\Lambda b_{\Lambda'} (n'v'\Lambda' | D_{1\lambda} | nv\Lambda) \times C(J1J';\Lambda\lambda\Lambda) \right]^2 C^2(J1J';M\mu M') \tag{10}$$

$$= (2J+1) \left[\sum_\Lambda \sum_\lambda \sum_{\Lambda'} a_\Lambda b_{\Lambda'} (n'v'\Lambda' | D_{1\lambda} | nv\Lambda)\ C(J1J';\Lambda\lambda\Lambda') \right]^2 .$$

The J dependence of formula (10) for $\Delta J = J'-J = -1,0,1$ (the P,Q,R branches) and for $\Delta\Lambda = \pm 1,0$ is, aside from definitive factors, the same as that of the Hönl-London line strength formulas[17] for electric dipole transitions. For illustrative purposes, we have computed a few examples and have given these along with the master formulas in Table II. These formulas are equally applicable to electric dipole transitions, but the vibronic matrix elements of course must be different. In the examples given, there is no need to give the Kronig reflection symmetry for the states involved,

---

[22] In the space axis systems $\sum_i D_i = \sum_\mu \sum_i (e_i/2m_ic)\ T_{1\mu}(j_{ix}j_{iy}j_{iz})\ T^*_{1\mu}(I\ J\ K) = \sum_\lambda \sum_\mu \sum_i (e_i/2m_ic)\ D^1_{\lambda\mu}(-\psi,-\theta,-\varphi)\ T_{1\lambda}(j_{i\xi}j_{i\eta}j_{i\zeta})\ T^*_{1\mu}(I\ J\ K)$ and is equivalent to Eq. (9), see Refs. 7 and 8.

[23] In terms of the spherical harmonics on a unit sphere $T_{1\lambda} = (4\pi/3)^{\frac{1}{2}} Y_{1\lambda}$. Explicitly, $T_{10}(abc) = c$, $T_{1\pm1}(abc) = \mp (1/\sqrt{2})(a \pm ib)$.

as the formulas are completely independent of the ± sign that specifies this symmetry.[24] Therefore, for molecules of unequal nuclei the two Λ-doubling components of a line doublet for transitions among the states with $\Lambda \neq 0$, will have equal intensities. This follows from the fact that none of the components of the dipole vector can connect $^1\Phi_{+\Lambda}$ and $^1\Phi_{-\Lambda}$ to give rise to cross terms. However, when spin-orbit interactions are considered, in both electric dipole and magnetic dipole transitions of $^1\Pi(b) - {}^3\Pi_0(a)$ or $^3\Pi_1(a) - {}^3\Pi_0(a)$, such Kronig symmetry dependence does occur and it is considered in Section V. It will be noted that contrary to earlier thoughts[2,13] we have asserted that even for $\Delta\Lambda = 0$ (e.g. the $^1\Pi - {}^1\Pi$ and $^1\Delta - {}^1\Delta$ transitions) there should be magnetic dipole pure rotation spectra. Because for $\Lambda \neq 0$, it is clear that there is a magnetic dipole moment (L_ζ) which will be oscillating as long as the electrons receive the periodic perturbation of the radiation field and radiative transitions can occur as long as there is a difference in energy between the initial and final states. This difference does not have to be that in electronic energy but can be that due to the difference in rotational energies.

IV. THE ABSOLUTE REFLECTION AND INVERSION SYMMETRY OF MOLECULAR WAVEFUNCTIONS.

Many of the transition intensity formulas we have considered are dependent on the Kronig reflection symmetry of one of the states involved. These transitions are for example, $^1\Pi^{\pm}\ \underline{R},\underline{D},\underline{Q}\ {}^3\Pi_0(\underline{a})$; $^1\Pi^{\pm}\ \underline{Q}\ {}^3\Pi_1(\underline{a})$; and $^1\Pi^{\pm}\ \underline{R},\underline{D},\underline{Q}\ {}^3\Pi(\underline{b})$, where the ± sign denotes the Kronig reflection symmetry of the final state and the a's and b's inside

---

[24] To show this, consider, as an example, the magnetic dipole transition between the final state $^1\Sigma^{\pm}(J') = A'\,{}^1\Phi_0^{\pm}\, D^{J'*}_{M',0}$ and the initial state $^1\Pi = (\tfrac{1}{2})^{\frac{1}{2}} A\left[{}^1\Phi_{+1}\, D^{J*}_{M1} \pm (-)^{J'-J}\, {}^1\Phi_{-1}\, D^{J*}_{M-1}\right]$. The line strength according to (10) is $(2J+1)\tfrac{1}{2}\left[({}^1\Phi_0^{\pm}|D_{1-1}|{}^1\Phi_{+1})\, C(J1J';1\text{-}10) \pm (-)^{J'-J}\,({}^1\Phi_0^{\pm}|D_{11}|{}^1\Phi_{-1})\, C(J1J';-110)\right]^2$. Because $({}^1\Phi_0^{\pm}|D_{1-1}|{}^1\Phi_{+1}) = -(\pm)({}^1\Phi_0^{\pm}|D_{11}|{}^1\Phi_{-1})$ (Sec. IV) and $C(J1J';1\text{-}10) = (-)^{J'-J+1} C(J1J';-110)$, the line strength reduces to $2(2J+1)(\Phi_0^{\pm}|D_{11}|\Phi_{-1})^2\, C^2(J1J';-110)$, an expression independent of the ± sign that specifies the Kronig symmetry of the final state. For an electric dipole transition, the initial state should be $^1\Pi = (\tfrac{1}{2})^{\frac{1}{2}} A\left[{}^1\Phi_{+1}\, D^{J*}_{M1} \pm (-)^{J'-J+1}\, {}^1\Phi_{-1}\, D^{J*}_{M-1}\right]$. But as the electric dipole (R) matrix element $({}^1\Phi_0^{\pm}|R_{1-1}|{}^1\Phi_{+1}) = (\pm)({}^1\Phi_0^{\pm}|R_{11}|{}^1\Phi_{-1})$, the result is the same as above, but with D replaced by R.

the parentheses denote the Hund's coupling cases of the states concerned, R, D, and Q stand for the electric dipole, magnetic dipole and electric quadrupole, respectively. it therefore necessary to know the absolute Kronig symmetry and the absolute total inversion symmetry (overall parity) of the wavefunctions used. Our emphasis here is on the Kronig symmetry which for states of $\Lambda \neq 0$ we can only draw an analogy to the $^1\Sigma^{\pm}$ state by calling as our normalized (normalization constant A') singlet state wavefunction (ψ) in Hund's case b coupling

$$\psi(^1\Pi^{\pm}_{N'=J'}) = (\tfrac{1}{2})^{\frac{1}{2}}A'\left[1 \pm (-)^{J'}1\right]\Phi(^1\Pi_{+1})\ D^{J'*}_{M'1} = (\tfrac{1}{2})^{\frac{1}{2}}A'\left[\Phi(^1\Pi_1)\ D^{J'*}_{M'1} \pm \Phi(^1\Pi_{-1})\ D^{J'*}_{M'-1}\right], \quad (11)$$

which upon the total inversion operation i gives an eigenvalue[25-26] (overall parity) of $(\pm)(-)^{J'}$.

---

[25]The assertion that the wavefunction in Eq. (11) has this eigenvalue implies a very different (from the old convention), new definition of the electronic wavefunction, Φ, which now has the property that under the Kronig reflection operation with respect to a plane passing through the ξ-ζ axes (this operation is equivalent to changing the electronic azimuth angle from φ to $2\pi-\varphi$ or to $-\varphi$), $\sigma_v^{\xi\zeta}\Phi(^1\Pi_1) = (-)\Phi(^1\Pi_{-1})$ or more generally $\sigma_v^{\xi\zeta}\ ^1\Phi_{\pm\Lambda} = (-)^{\Lambda}\ ^1\Phi_{\mp\Lambda}$, for a singlet state. Similarly, under the reflection with respect to a plane passing the η-ζ axes (this operation is equivalent to changing φ to $\pi-\varphi$) $\sigma_v^{\eta\zeta}\Phi(^1\Pi_1) = \Phi(^1\Pi_{-1})$ or more generally $\sigma_v^{\eta\zeta}\ ^1\Phi_{\pm\Lambda} = {}^1\Phi_{\mp\Lambda}$. The most general definition of a singlet case b state of an arbitrary Λ and with a parity of $(\pm)(-)^{J'}$ is then $\psi(^1\Lambda^{\pm}_{N'=J'}) = (\tfrac{1}{2})^{\frac{1}{2}}\ A'\left[^1\Phi_{+\Lambda}\ D^{J'*}_{M'\Lambda} \pm {}^1\Phi_{-\Lambda}\ D^{J'*}_{M'-\Lambda}\right]$. Our kind of electronic wavefunctions have properties that correspond to the spherical harmonics (Ref. 7) used to represent the Slater atomic orbitals in the construction of molecular orbitals. In the old convention $\sigma_v^{\xi\zeta}\ \Phi_{\pm\Lambda} = \Phi_{\mp\Lambda}$ and $\sigma_v^{\eta\zeta}\Phi_{\pm\Lambda} = (-)^{\Lambda}\Phi_{\mp\Lambda}$. The most general definition of a singlet case b state in the old convention is $\underline{\psi}(^1\Lambda^{\pm}_{N'=J'}) = (\tfrac{1}{2})^{\frac{1}{2}}\ A'\left[^1\Phi_{+\Lambda}\ D^{J'*}_{M'\Lambda} \pm (-)^{\Lambda}\ \Phi_{-\Lambda}\ D^{J'*}_{M'-\Lambda}\right]$ so as to have the same eigenvalue under inversion of $(\pm)(-)^{J'}$. This kind of electronic wavefunctions appear in the correlated molecular wavefunctions where one simply represents the azimuth dependence as $\exp(\pm i\Lambda\varphi)$.

[26]There are two ways to bring about the total inversions of the coordinates of all particles referred to the space-fixed axis; namely to go from $x_i, y_i, z_i \rightarrow -x_i, -y_i, -z_i$ for all i: (1) The Euler angles (Ref. 7) change from α, β, γ to $\pi + \alpha$, $\pi - \beta$ and $\pi - \gamma$ respectively, with corresponding change of the molecular axes from n_ξ, n_η, n_ζ to $n_\xi, -n_\eta, n_\zeta$. The net effect on the electronic coordinates referred to the molecular axis system being that of the operation $\sigma_v^{\xi\zeta}$. Under such an inversion,

the rotational wavefunction changes from $D^J_{M\Lambda}$ to $(-)^{J-\Lambda} D^J_{M-\Lambda}$. (2) The Euler angles change to $\pi + \alpha$, $\pi - \beta$, and $2\pi - \gamma$ (or $-\gamma$) respectively with corresponding change of the molecular axes to $-n_\xi$, n_η, n_ζ. The net effect on the electronic coordinates is equivalent to $\sigma_v^{\eta\zeta}$. Under such an inversion the rotational wavefunction $D^J_{M\Lambda}$ changes to $(-)^J D^J_{M-\Lambda}$. When these transformation properties of the rotational wavefunctions and those of the new electronic wavefunctions (Ref. 25) are taken into account together, we get the eigenvalue (overall parity) of the state. The eigenvalues obtained from both ways of inversion are the same as they should be. In either cases $i\,\Phi_\Lambda D^J_{M\Lambda} = (-)^J \Phi_{-\Lambda} D^J_{M-\Lambda}$.

For triplet states of $\Lambda \neq 0$ we draw an analog to the $^3\Sigma^\pm$ state. Thus for Hund's case a state we have for $\Omega = 0$, 1, and 2, the state function (Φ) as follows:

$$\Phi(^3\Pi^\pm_\Omega) = (\tfrac{1}{2})^{\frac{1}{2}} A\left[\Phi(^3\Pi_\Omega) D^{J*}_{M\Omega} \pm \Phi(^3\Pi_{-\Omega}) D^{J*}_{M-\Omega}\right] \qquad (12)$$

which under total inversion gives an eigenvalue of $(-)(\pm)(-)^J$, the extra minus sign being due to the odd properties of the triplet-state spin eigenfunction under inversion.[27] For Hund's case b states, we express the state function (ψ) as a linear combination of the case a statefunctions (Φ) as follows[11,28]

$$\psi(^3\Pi^\pm_N) = (\tfrac{1}{2})^{\frac{1}{2}}\left[1 \pm (-)^{N_1}\right]\psi(^3\Pi^{\Lambda=1}_N) = (\tfrac{1}{2})^{\frac{1}{2}}\left[\psi(^3\Pi^{\Lambda=+1}_N) \pm \psi(^3\Pi^{\Lambda=-1}_N)\right] = \sum_\Omega b_{N\Omega}\, \Phi(^3\Pi^S_\Omega) \qquad (13)$$

where $b_{N\Omega} = C(J1N;\Omega,-\Sigma,+1)$ is the Clebsch-Gordan coefficient, $S = (\pm)(-)^{J+N+1}$ is the Kronig reflection-symmetry designation. The wavefunctions on either side of Eq. (13) under total inversion will <u>consistently</u> give the same eigenvalue (overall parity) <u>of</u> $(\pm)(-)^N$. Such <u>consistency</u> permits the generalized treatment that will follow. In the reduction to the final form of Eq. (13) use was made of the expression of the case b wavefunction (characterized by N and Λ) in terms of the case a wavefunctions (characterized by J and Ω) through a coupling of angular momentum[11] $\underset{\sim}{J}$ with $-\underset{\sim}{S}$($S = 1$ for a triplet), namely

---

[27] J. H. Van Vleck, Phys. Rev. <u>40</u>, 544 (1932), p. 559.

[28] Explicitly, $\psi(^3\Pi^\pm_{J+1}) = \sum_\Omega b_{J+1\Omega}\, \underset{\sim}{\Phi}(^3\Pi^\pm_\Omega)$, $\underset{\sim}{\psi}(^3\Pi^\pm_J) = \sum_\Omega b_{J\Omega}\, \underset{\sim}{\Phi}(^3\Pi^\mp_\Omega)$; $\underset{\sim}{\psi}(^3\Pi^\pm_{J-1}) = \sum_\Omega b_{J-1\Omega}\, \underset{\sim}{\Phi}(^3\Pi^\pm_\Omega)$. Compare these results of Kovacs (Can. J. Phys. <u>36</u>, 309, 1958) who gave a different definition for the $\underset{\sim}{\psi}(^3\Pi^\pm_J)$ state. The inconsistency introduced by this definition has been remarked upon by Chiu (Ref. 11).

$$\psi(^3\Pi_N^{\Lambda=\pm1}) = A \sum_\Omega C(J1N;\pm\Omega,\mp\Sigma,\pm1)\Phi(^3\Pi_{\pm\Omega}) D^{J*}_{M,\pm\Omega} \quad , \tag{14}$$

and

$$(-)^{N_1}\psi(^3\Pi_N^{\Lambda=+1}) = (-)^{J+N+1} A \sum_\Omega C(J1N;\Omega,-\Sigma,+1)\Phi(^3\Pi_{-\Omega}) D^{J*}_{M-\Omega}$$

$$= A \sum_\Omega C(J1N;-\Omega,+\Sigma,-1)\Phi(^3\Pi_{-\Omega}) D^{J*}_{M-\Omega} \equiv \psi(^3\Pi_N^{\Lambda=-1}) \quad . \tag{15}$$

V. APPLICATIONS TO THE $^1\Pi$ - $^3\Pi$(a) TRANSITIONS

Except for the complication due to the inversion property of a triplet-state spin eigenfunction,[27] the magnetic-dipole and electric quadrupole line strength formulas for the $^1\Pi$ - $^3\Pi_2$(a) and $^1\Pi^\pm$-$^3\Pi_1$(a) transitions where the triplet state is in Hund's coupling case a can be obtained from the $^1\Pi$ - $^1\Delta$, $^1\Pi^\pm$-$^1\Pi$ transitions in Tables I and II.

The case of $^1\Pi^\pm$-$^3\Pi_0$(a) transitions presents some new aspects[29] but follows essentially the same principles. We give the simplified and condensed master line strength formulas for these transitions in Table III. In the reduction to the master formulas the following relationships are used:

$$C(J\ell J';\Lambda\lambda\Lambda') = (-)^{-\Delta J+1} C(J\ell J';-\Lambda-\lambda-\Lambda'), \quad \Delta J \equiv J' - J,$$

$$\sigma_v^{\xi\zeta}\,\Phi(^3\Pi_\Omega) = (-)^{\Omega+1}\,\Phi(^3\Pi_{-\Omega}), \quad \sigma_v^{\xi\zeta}\,\Phi(^1\Pi_1) = (-)\Phi(^1\Pi_{-1}), \tag{16}$$

$$\sigma_v^{\xi\zeta} D_{1,\lambda} = (-)^{\lambda+1} D_{1,-\lambda}, \; D_{1,0} \equiv D_{1,-0}, \; \sigma_v^{\xi\zeta} Q_{2,\lambda} = (-)^{\lambda} Q_{2,-\lambda}, \; Q_{2,0} \equiv Q_{2,-0}.$$

[29] We take as the final state function $\psi(^1\Pi^\pm) = (\tfrac{1}{2})^{\frac{1}{2}} A'\left[\Phi(^1\Pi_1)\, D^{J'*}_{M'1} \pm \Phi(^1\Pi_{-1})\, D^{J'*}_{M'-1}\right]$ and as the initial state function $\Phi(^3\Pi_0) = (\tfrac{1}{2})^{\frac{1}{2}} A\left[\Phi(^3\Pi_{+0}) \pm (-)^{\Delta J+1}\,\Phi(^3\Pi_{-0})\right] D^{J*}_{M0}$. Both of these have the same parity of $(\pm)(-)^{J'}$ under inversion. The magnetic dipole or electric quadrupole line strength formula for the $^1\Pi^\pm$ - $^3\Pi_0$ transitions is, before any reduction or simplification, $S(J,J') = (1/4)(2J+1)\Big[(^1\Pi_1|F_{\ell 1}|^3\Pi_{+0})\; C(J\ell J';011) + (-)^{\Delta J+1}(^1\Pi_{-1}|F_{\ell-1}|^3\Pi_{-0})\; C(J\ell J';0\text{-}1\text{-}1) \pm (-)^{\Delta J+1}(^1\Pi_1|F_{\ell 1}|^3\Pi_{-0})\; C(J\ell J';011) \pm (^1\Pi_{-1}|F_{\ell-1}|^3\Pi_{+0})\; C(J\ell J';0\text{-}1\text{-}1)\Big]^2$ where for a magnetic dipole $\ell = 1$, $F_{\ell,\pm1} = D_{1,\pm1}$, and for an electric quadrupole $\ell = 2$, $F_{\ell,\pm1} = \frac{2}{3} Q_{2,\pm1}$. For an electric dipole (R), however, we must replace $(-)^{\Delta J+1}$ by $(-)^{\Delta J}$, set $F_{\ell,\pm1} = R_{1\pm1}$ and $\ell = 1$, where $R_{1,\pm1} = \mp(\tfrac{1}{2})^{\frac{1}{2}} \sum_i e_i(\xi_i \pm i\eta_i)$ which has the properties as follows: $\sigma_v^{\xi\zeta} R_{1,\lambda} = (-)^{\lambda} R_{1,-\lambda}$ with $R_{1,0} \equiv R_{1,-0}$ and $(^1\Pi_{\Lambda'}|R_{1,\Lambda'-\Omega}|^3\Pi_\Omega) = (-)(^1\Pi_{-\Lambda'}|R_{1,-\Lambda'+\Omega}|^3\Pi_{-\Omega})$.

From the last four relationships, and using the fact that the matrix elements should be invariant under the operation[30] $\sigma_v^{\xi\zeta}$, we get the relationships for the vibronic matrix elements, with $^1\Pi_{\Lambda'}$ standing for $\Phi(^1\Pi_{\Lambda'})$ etc.,

$$(^1\Pi_{\Lambda'}|D_{1,\Lambda'-\Omega}|^3\Pi_{\Omega}) = (^1\Pi_{-\Lambda'}|D_{1,-\Lambda'+\Omega}|^3\Pi_{-\Omega}) \quad ,$$

and (17)

$$(^1\Pi_{\Lambda'}|Q_{2,\Lambda'-\Omega}|^3\Pi_{\Omega}) = (-)(^1\Pi_{-\Lambda'}|Q_{2,-\Lambda+\Omega}|^3\Pi_{-\Omega}) \quad ,$$

where Λ' may be ±1, Ω may be ±2, ±1, ±0 and the notation is self-evident. In the same reduction we have used the following abbreviations:

$$\begin{aligned} \alpha &= (^1\Pi_{-1}|Q_{21}|^3\Pi_{-2}) \quad , \\ \beta &= (^1\Pi_{1}|Q_{20}|^3\Pi_{1}) \quad , \\ \gamma &= (^1\Pi_{1}|Q_{21}|^3\Pi_{+0}) \quad , \\ \delta &= (^1\Pi_{1}|Q_{21}|^3\Pi_{-0}) \quad , \\ \epsilon &= (^1\Pi_{1}|Q_{22}|^3\Pi_{-1}) \quad . \end{aligned} \tag{18}$$

For the case of a magnetic dipole, we replace $\alpha,\beta,\gamma,\delta$ by A,B,C, and D respectively, and replace $Q_{2\lambda}$ by $D_{1\lambda}$ in the above abbreviations.

In all formulas, the J dependence of the magnetic dipole transitions, is equally applicable to the electric dipole transition except when $(-)^{\Delta J+1}$ occurs, it must be replaced by $(-)^{\Delta J}$. The net effect is to replace D by -D. Explicit formulas for the different branches are computed and given in Tables IV and V where we have assumed a normal multiplet with the case a states, namely $^3\Pi_2$, $^3\Pi_1$, $^3\Pi_0$ correlate to the case b states $^3\Pi_{N=J+1}$, $^3\Pi_{N=J}$, $^3\Pi_{N=J-1}$, respectively.

VI. APPLICATIONS TO THE $^1\Pi$ - $^3\Pi$(b) TRANSITIONS

When the triplet state is of Hund's coupling case b we express the state function as a linear combination of case a wavefunctions as in Eq. (13). The magnetic-dipole master line strength formula is as follows:

$$\begin{aligned} &\text{For } ^1\Pi^{\pm} - ^3\Pi(b),\ S(J,J') = (2J+1)[(-)^{\Delta J+1} A\, b_{N2}\, C(J1J';-21-1) + \\ &B\, b_{N1}\, C(J1J';101) + C\, b_{N0}\, C(J1J';011) \pm (-)^{\Delta J+1} D\, b_{N0}\, C(J1J';011)]^2 \quad . \end{aligned} \tag{19}$$

---

[30] If we use the $\sigma_v^{\eta\zeta}$ operator, the relationships between the matrix elements so obtained are the same as they should be.

For $^1\Pi - {}^3\Pi^{\pm}(b)$, one simply replaces the coefficient of D, which is $\pm (-)^{\Delta J+1}$, by $\pm (-)^{J+N+1}$. For electric dipole transitions, one changes $(-)^{\Delta J}$ to $(-)^{\Delta J+1}$ in the above formulas. The electric-quadrupole master line strength formula is as follows:

$$\text{For } {}^1\Pi^{\pm} - {}^3\Pi(b),\ S(J,J') = (2/3)(2J+1)[(\pm)(-)^{\Delta J+1}\ \epsilon\ b_{N1}\ C(J2J';-121)$$
$$+ (-)^{\Delta J+1}\ \alpha\ b_{N2}\ C(J2J';-21-1)$$
$$+ \beta\ b_{N1}\ C(J2J';101) + \gamma\ b_{NO}\ C(J2J';011)$$
$$\pm (-)^{\Delta J+1}\ \delta\ b_{NO}\ C(J2J';011)]^2$$

For $^1\Pi - {}^3\Pi^{\pm}(b)$ one simply replaces the coefficients of δ and ϵ, which are $(\pm)(-)^{\Delta J+1}$ by $(\pm)(-)^{J+N+1}$. Explicit formulas for the different branches are given in Tables IV and V.

VII. DISCUSSIONS

In all of the initial and final state functions employed here, we have made use of the Born-Oppenheimer (B.O.) approximation to separate out the rotational wavefunction. If the B.O. approximation is valid, the vibronic matrix elements between different electronic states are small. In particular, for a linear molecule only the $Q_{20} = \frac{1}{2}\sum_{nuc\ell} e_{nuc\ell}(3z^2_{nuc\ell} - r^2_{nuc\ell})$ component of the nuclear vibrational matrix element contributes to the rotation-vibration spectra.

If rotation-electronic interaction is considered, states of the same J (or N) but different Ω (or Λ) are mixed into the statefunction, we then will have the P and R branches of the magnetic dipole as well as the electric quadrupole in $^1\Sigma^{\pm} - {}^1\Sigma^{\mp}$ transitions where the initial and final states are of different Kronig symmetry. For $^1\Sigma^{\pm} - {}^1\Sigma^{\pm}$ transitions where the initial and final states are of the same Kronig symmetry, there is, besides the electric-quadrupole O, Q and S branches ($\Delta J = -2,0,+2$) which exist anyway, a magnetic-dipole Q branch after rotation-electronic interaction is introduced.

It should be noted that for singlet-triplet transitions, as the spin magnetic dipole vector $S = \sum_i S_i$ is diagonal in the Russell-Saunders representation, there is no pure spin magnetic-dipole transition. All magnetic dipole transitions of this type must come through the spin-orbit interaction.[31] In our treatment here, spin-orbit interaction appears only in the electronic matrix elements.

---

[31] Only in multiplets involving more than two electrons will spin-spin interaction connect different multiplicities.

For homopolar diatomic molecules, the formulas for the electric quadrupole magnetic dipole transitions are of course applicable only to $^1\Pi_g$-$^3\Pi_g$ or $^1\Pi_u$-$^3\Pi_u$ transitions. In these cases, besides the normal intensity alternation due to the population difference governed by nuclear spin statistics, there is an additional intensity fluctuation due to the two different intensity formulas appropriate to the two Λ-doubling components. The derivation of the condensed formulas are straight-forward, once the principle behind it is mastered. Readers interested in the detailed steps are referred to four of the footnotes[18,19,24,29] each giving a different type of examples. Applications of the present technique to cases intermediate between Hund's case a and b and estimate of the electronic matrix elements will be treated in a future article.

ACKNOWLEDGMENT

The writer is indebted to Professor R. S. Mulliken who suggested this problem for stimulating discussions. The financial support of the National Science Foundation is gratefully acknowledged.

TABLE Ia. LINE STRENGTH FORMULAS FOR ELECTRIC QUADRUPOLE TRANSITIONS[1,2]

Master Formula S(J,J') =		$(2/3)Q_0^2(2J+1)C^2(J2J';000)$	$(4/3)Q_1^2(2J+1)C^2(J2J';011)$	$(4/3)Q_2^2(2J+1)C^2(J2J';022)$
$^1\Lambda_f' \leftarrow {}^1\Lambda_i(J)$	$^1\Lambda_i' \rightarrow {}^1\Lambda_f(J)$	$^1\Sigma(J') - {}^1\Sigma(J)$	$^1\Pi(J') - {}^1\Sigma(J)$	$^1\Delta(J') - {}^1\Sigma(J)$
O(J)	S(J-2)	$Q_0^2 \frac{J(J-1)}{(2J-1)}$	$Q_1^2 \frac{4J(J-2)}{3(2J-1)}$	$Q_2^2 \frac{(J-2)J-3)}{3(2J-1)}$
P(J)	R(J-1)	0	$Q_1^2 \frac{2(J+1)}{3}$	$Q_2^2 \frac{2(J-2)}{3}$
Q(J)	Q(J)	$Q_0^2 \frac{2J(J+1)(2J+1)}{3(2J-1)(2J+3)}$	$Q_1^2 \frac{2(2J+1)}{(2J-1)(2J+3)}$	$Q_2^2 \frac{2(2J+1)(J+2)(J-1)}{(2J-1)(2J+3)}$
R(J)	P(J+1)	0	$Q_1^2 \frac{2J}{3}$	$Q_2^2 \frac{2(J+3)}{3}$
S(J)	O(J+2)	$Q^2 \frac{(J+1)(J+2)}{(2J+3)}$	$Q^2 \frac{4(J+1)(J+3)}{3(2J+3)}$	$Q_2^2 \frac{(J+3)(J+4)}{3(2J+3)}$

[1]The symbol Q_λ stands for the vibronic matrix element $(n'v'\Lambda'|Q_{2\lambda}|nv\Lambda)$ with the appropriate Λ' and Λ values pertaining to the initial and final state and corresponding to the Λ' and Λ in the Clebsch-Gordan coefficient $C(J2J';\Lambda\lambda\Lambda')$, e.g. for $^1\Delta - {}^1\Sigma$ transitions $Q_2 = (n'v'2|Q_{22}|nv0)$, but for $^1\Pi^{\pm} - {}^1\Pi$ transitions $Q_2 = (n'v'1|Q_{22}|nv-1)$.

[2]The rotational quantum number that follows the branch designation always refers to the initial state. The branch designation is after that of Herzberg, namely the O, P, Q, R. S. branches correspond to $\Delta J = J_f - J_i = -2, -1, 0, +1, +2$ respectively.

TABLE Ib. LINE STRENGTH FORMULAS FOR ELECTRIC QUADRUPOLE TRANSITIONS

Master Formula S(J,J') =		$(2/3)(2J+1)[Q_0\ C(J2J';101) \pm (-)^{J'-J}\ Q_2\ C(J2J';-121)]^2$	$(2/3)Q_2^2(2J+1)C^2(J2J';112)$	$(2/3)Q_2^2(2J+1)C^2(J2J';123)$
$^1\Lambda_f' \leftarrow {}^1\Lambda_i(J)$	$^1\Lambda_i' \rightarrow {}^1\Lambda_f(J)$	$^1\Pi^{\pm}(J') - {}^1\Pi(J)$	$^1\Delta(J') - {}^1\Pi(J)$	$^1\Phi(J') - {}^1\Pi(J)$
O(J)	S(J-2)	$[Q_0 \pm Q_2/\sqrt{6}]^2 \times \frac{(J-2)(J+1)}{(2J-1)}$	$Q_1^2 \frac{2(J-2)(J-3)(J+1)}{3J(2J-1)}$	$Q_2^2 \frac{(J-2)(J-3)(J-4)}{6J(2J-1)}$
P(J)	R(J-1)	$[Q_0 \mp Q_2\ J/\sqrt{6}]^2 \times \frac{2}{J}$	$Q_1^2 \frac{(J+3)^2(J-2)}{3J(J+1)}$	$Q_2^2 \frac{(J+2)(J-3)(J-2)}{3J(J+1)}$
Q(J)	Q(J)	$[Q_0(3-J^2-J) \pm (3/2)^{\frac{1}{2}} \times Q_2\ J(J+1)]^2 \times \frac{2(2J+1)}{3(2J-1)J(J+1)(2J+3)}$	$Q_1^2 \frac{9(2J+1)(J-1)(J+2)}{(2J-1)J(J+1)(2J+3)}$	$Q_2^2 \frac{(2J+1)(J+3)(J-2)(J-1)(J+2)}{(2J-1)J(2J+3)(J+1)}$
R(J)	P(J+1)	$[Q_0 \pm Q_2(J+1)/\sqrt{6}]^2 \times \frac{2}{(J+1)}$	$Q_1^2 \frac{(J-2)^2(J+3)}{3J(J+1)}$	$Q_2^2 \frac{(J+3)(J+4)(J-1)}{3J(J+1)}$
S(J)	O(J+2)	$[Q_0 \pm Q_2/\sqrt{6}]^2 \times \frac{J(J+3)}{(2J+3)}$	$Q_1^2 \frac{2J(J+3)(J+4)}{3(J+1)(2J+3)}$	$Q_2^2 \frac{(J+3)(J+4)(J+5)}{6(J+1)(2J+3)}$

TABLE Ic. LINE STRENGTH FORMULAS FOR ELECTRIC QUADRUPOLE TRANSITIONS

Master Formula $S(J,J') =$		$(2/3)Q_0^2\ (2J+1)C^2(J2J';202)$	$(2/3)Q_1^2\ (2J+1)C^2(J2J';213)$	$(2/3)Q_2^2\ (2J+1)C^2(J2J';224)$
$^1A_f' \leftarrow {}^1A_i(J)$	$^1A_i' \rightarrow {}^1A_f(J)$	$^1\Delta(J') - {}^1\Delta(J)$	$^1\Phi(J') - {}^1\Delta(J)$	$^1\Gamma(J') - {}^1\Delta(J)$
O(J)	S(J-2)	$Q_0^2 \frac{(J-2)(J-3)(J+1)(J+2)}{(J-1)J(2J-1)}$	$Q_1^2 \frac{2(J-2)(J-3)(J-4)(J+2)}{3(J-1)J(2J-1)}$	$Q_2^2 \frac{(J-5)(J-4)(J-3)(J-2)}{6(J-1)(2J-1)J}$
P(J)	R(J-1)	$Q_0^2 \frac{8(J-2)(J+2)}{J(J-1)(J+1)}$	$Q_1^2 \frac{(J+5)^2(J-2)(J-3)}{3(J-1)J(J+1)}$	$Q_2^2 \frac{(J+3)(J-4)(J-3)(J-2)}{3(J-1)J(J+1)}$
Q(J)	Q(J)	$Q_0^2 \frac{2(J+1)(J+4)^2(J-3)^2}{3(2J-1)J(J+1)(2J+3)}$	$Q_1^2 \frac{25(2J+1)(J-2)(J+3)}{J(2J-1)(J+1)(2J+3)}$	$Q_2^2 \frac{(2J+1)(J+3)(J+4)(J-3)(J-2)}{(2J-1)J(J+1)(2J+3)}$
R(J)	P(J+1)	$Q_0^2 \frac{8(J-1)(J+3)}{J(J+1)(J+2)}$	$Q_1^2 \frac{(J-4)^2(J+3)(J+4)}{3J(J+1)(J+2)}$	$Q_2^2 \frac{(J+3)(J+4)(J+5)(J-2)}{3J(J+1)(J+2)}$
S(J)	O(J+2)	$Q_0^2 \frac{J(J-1)(J+3)(J+4)}{(J+1)(J+2)(2J+3)}$	$Q_1^2 \frac{2(J-1)(J+3)(J+4)(J+5)}{3(J+1)(J+2)(2J+3)}$	$Q_2^2 \frac{(J+3)(J+4)(J+5)(J+6)}{6(J+1)(J+2)(2J+3)}$

TABLE II. LINE STRENGTH FORMULAS FOR MAGNETIC DIPOLE TRANSITIONS[1,2]

Master Formula $S(J,J') =$		$2D_1^2(2J+1)C^2(J1J';011)$	$D_0^2(2J+1)C^2(J1J';101)$	$D_1^2(2J+1)C^2(J1J';112)$	$D_0^2(2J+1)C^2(J1J';202)$	$D_1^2(2J+1)C^2(J1J';213)$
$^1\Lambda_f' \leftarrow {}^1\Lambda_1(J)$	$^1\Lambda_1' \rightarrow {}^1\Lambda_f(J)$	$^1\Pi(J') - {}^1\Sigma(J)$	$^1\Pi(J') - {}^1\Pi(J)$	$^1\Delta(J') - {}^1\Pi(J)$	$^1\Delta(J') - {}^1\Delta(J)$	$^1\Phi(J') - {}^1\Delta(J)$
P(J)	R(J-1)	$D_1^2(J-1)$	$D_0^2\,\frac{(J-1)(J+1)}{J}$	$D_1^2\,\frac{(J-2)(J-1)}{2J}$	$D_0^2\,\frac{(J-2)(J+2)}{J}$	$D_1^2\,\frac{(J-3)(J-2)}{2J}$
Q(J)	Q(J)	$D_1^2(2J+1)$	$D_0^2\,\frac{(2J+1)}{J(J+1)}$	$D_1^2\,\frac{(2J+1)(J+2)(J-1)}{2J(J+1)}$	$D_0^2\,\frac{2(2J+1)}{J(J+1)}$	$D_1^2\,\frac{(2J+1)(J+3)(J-2)}{2J(J+1)}$
R(J)	P(J+1)	$D_1^2(J+2)$	$D_0^2\,\frac{J(J+2)}{(J+1)}$	$D_1^2\,\frac{(J+2)(J+3)}{2(J+1)}$	$D_0^2\,\frac{(J-1)(J+3)}{(J+1)}$	$D_1^2\,\frac{(J+3)(J+4)}{2(J+1)}$

[1]In the expression $D_\lambda^2\,(2J+1)C^2(J1J';\Lambda\lambda\Lambda')$, the symbol D_λ stands for $(n'v'\Lambda'|D_{1\lambda}|nv\Lambda)$, the vibronic matrix element. For other symbols, see the legend for Table I.

[2]For $\Delta\Lambda = 0$, the J dependence of our line strength formulas agrees with that of Hönl and London,[17] for $\Delta\Lambda = +1$, ours is two times that of Hönl and London. Judging from the identical form of our generalized master formula, our definition appears to be the more consistent. For transitions in and out of $^1\Sigma$ states, ours is four times that of Hönl and London, the additional factor of two comes from the vibronic matrix element.[24] These factors are important when one wants to compute the absolute line intensities.

TABLE III. MASTER LINE-STRENGTH FORMULAS FOR MAGNETIC DIPOLE AND ELECTRIC QUADRUPOLE TRANSITIONS.

(TRIPLET STATE IN CASE a)

$^1\Pi(J') \leftarrow {}^3\Pi_\Omega(J)$	$^1\Pi(N' = J') - {}^3\Pi_2(a)$	$^1\Pi^\pm(N' = J') - {}^3\Pi_1(a)$	$^1\Pi^\pm(N' = J') - {}^3\Pi_0(a)$
Magnetic Dipole $S(J,J') =$	$A^2(2J+1)C^2(J1J';-21-1)$	$B^2(2J+1)C^2(J1J';101)$	$(2J+1)[C \pm (-)^{\Delta J+1} L]^2$ $\times C^2(J1J';011)$
Electric Quadrupole $S(J,J') =$	$(2/3)\alpha^2(2J+1)C^2(J2J';-21-1)$	$(2/3)(2J+1)[\beta C(J2J';101)$ $\pm (-)^{\Delta J+1} \epsilon\, C(J2J';-121)]^2$	$(2/3)(2J+1)[\gamma \pm (-)^{\Delta J+1} \delta]^2$ $\times C^2(J2J';011)$

TABLE IV. MAGNETIC-DIPOLE LINE STRENGTH FORMULAS FOR $^1\Pi^{\pm}$—$^3\Pi$ TRANSITIONS[1,2]

$^1\Pi_f^{\pm} \leftarrow {}^3\Pi_1(J)$	$^1\Pi_1^{\pm} \rightarrow {}^3\Pi_f(J)$	$^3\Pi$(a)	$^3\Pi$(b)
$^OP(J)$	$^SR(J-1)$	$A^2 \frac{(J+1)(J+2)}{2J}$	$[A - 2B + (C \pm D)]^2 \frac{(J-1)(J+2)}{4(2J+1)}$
$^PQ(J)$	$^RQ(J)$	$A^2 \frac{(J-1)(J+2)(2J+1)}{2J(J+1)}$	$[A(J-1) + 2B - C \mp D)(J+1)]^2 (J+2)/[4(J+1)^2]$
$^QR(J)$	$^QP(J+1)$	$A^2 \frac{J(J-1)}{2(J+1)}$	$[AJ(J-1) + 2BJ(J+2) + (C \pm D)(J+1)(J+2)]^2 \frac{1}{4(J+1)^2(2J+1)}$
$^PP(J)$	$^RR(J-1)$	$B^2 \frac{(J-1)(J+1)}{J}$	$[A(J+2) - 2B - (C \pm D)J]^2 \frac{(J-1)}{4J^2}$
$^QQ(J)$	$^QQ(J)$	$B^2 \frac{(2J+1)}{J(J+1)}$	$[A(J-1)(J+2) + 2B + (C \mp D)J(J+1)]^2 \frac{(2J+1)}{4J^2(J+1)^2}$
$^RR(J)$	$^PP(J+1)$	$B^2 \frac{J(J+2)}{(J+1)}$	$[A(J-1) + 2B - (C \pm D)(J+1)]^2 \frac{(J+2)}{4(J+1)^2}$
$^QP(J)$	$^QR(J-1)$	$(C \pm D)^2 \frac{(J-1)}{2}$	$[A(J+1)(J+2) + 2B(J-1)(J+1) + (C + D)(J-1)J]^2 \frac{1}{4J^2(2J+1)}$
$^RQ(J)$	$^PQ(J)$	$(C \mp D)^2 \frac{2J+1}{2}$	$[A(J+2) - 2B - (C \mp D)J]^2 \frac{(J-1)}{4J^2}$
$^SR(J)$	$^OP(J+1)$	$(C \pm D)^2 \frac{J+2}{2}$	$[A - 2B + C \pm D]^2 \frac{(J-1)(J+2)}{4(2J+1)}$

[1]When the triplet state belongs to Hund's coupling case a, we have here assumed a normal multiplet. The case a states $^3\Pi_2$, $^3\Pi_1$ and $^3\Pi_0$ are correlated to the case b states of $^3\Pi_{N=J+1}$, $^3\Pi_{N=J}$ and $^3\Pi_{N=J-1}$, respectively. For an inverted multiplet, the intensity formulas for the ^QP, ^RQ, and ^SR branches should be interchanged with those of the ^OP, ^PQ and ^QR branches respectively for this case.

[2]The upper left-corner superscripts stand for the branch designations of N with N,O,P,Q,R,S,T corresponding to $\Delta N = N_f - N_1 = -3,-2,-1,0,1,2,3$ respectively.

TABLE V. ELECTRIC QUADRUPOLE LINE STRENGTH FORMULAS FOR $^1\Pi^{\pm}$—$^3\Pi$ TRANSITIONS[1]

$^1\Pi^{\pm} \leftarrow {}^3\Pi_i(J)$	$^1\Pi_i^{\pm} \rightarrow {}^3\Pi_f(J)$	$^3\Pi$(a)	$^3\Pi$(b)
$^N O(J)$	$^T S(J-2)$	$\alpha^2 \frac{2(J+2)(J+1)(J-1)}{3(J-1)(2J-1)}$	$[\mp\epsilon + \alpha\sqrt{2} + \beta\sqrt{6} - (\gamma \pm \delta)\sqrt{2}]^2 \frac{J(J+2)(J-2)}{6(2J-1)(2J+1)}$
$^O P(J)$	$^S R(J-1)$	$\alpha^2 \frac{(J-3)^2(J+2)}{3J(J-1)}$	$[\mp\epsilon J\sqrt{2} + \alpha(J-3) - 2\beta\sqrt{3} + (\gamma \pm \delta)(J+1)]^2 \times \frac{(J+2)}{6(J+1)(2J+1)}$
$^P Q(J)$	$^R Q(J)$	$\alpha^2 \frac{9(J-1)(J+2)(2J+1)}{J(J+1)(2J-1)(2J+3)}$	$[\mp\epsilon J(J+1)\sqrt{6} - (27)^{\frac{1}{2}}\alpha(J-1) + 2\beta(3-J^2-J) - (\gamma \pm \delta) \times (J+1)\sqrt{3}]^2 \frac{(J+2)}{6(J+1)^2(2J-1)(2J+3)}$
$^Q R(J)$	$^Q P(J+1)$	$\alpha^2 \frac{(J+4)^2(J-1)}{3(J+1)(J+2)}$	$[\mp\epsilon(J+1)(J+2)\sqrt{2} - \alpha(J-1)(J+4) + 2\beta(J+2)\sqrt{3} - (\gamma \pm \delta)(J+1)(J+2)]^2 \frac{J}{6(J+1)^2(J+2)(2J+1)}$
$^R S(J)$	$^P O(J+2)$	$\alpha^2 \frac{2(J+3)(J-1)J}{3(J+2)(2J+3)}$	$[\mp\epsilon J(J+2) - \alpha J(J-1)\sqrt{2} + \beta J(J+2)\sqrt{6} + (\gamma \pm \delta) \times (J+1)(J+2)\sqrt{2}]^2 \frac{(J+3)}{6(J+1)(J+2)(2J+1)(2J+3)}$
$^O O(J)$	$^S S(J-2)$	$[\beta\sqrt{6} \mp \epsilon]^2 \times \frac{(J-2)(J+1)}{6(2J-1)}$	$[\mp\epsilon + \alpha(J+2)\sqrt{2} + \beta\sqrt{6} + (\gamma \mp \delta)J\sqrt{2}]^2 \frac{(J-2)}{6J(2J-1)}$
$^P P(J)$	$^R R(J-1)$	$[\beta\sqrt{6} \pm \epsilon J]^2 \frac{1}{3J}$	$[\mp\epsilon J\sqrt{2} + \alpha(J+2)(J-3) - (12)^{\frac{1}{2}}\beta - (\gamma \pm \delta) \times J(J+1)]^2 \frac{1}{6J^2(J+1)}$

TABLE V. ELECTRIC QUADRUPOLE LINE STRENGTH FORMULAS FOR $^1\Pi^{\pm}$—$^3\Pi$ TRANSITIONS (Cont'd.)

$^1\Pi_f^{\pm} \leftarrow {}^3\Pi_1(J)$	$^1\Pi_1^{\pm} \rightarrow {}^3\Pi_f(J)$	$^3\Pi$(a)	$^3\Pi$(b)
$^Q{}_{Q(J)}$	$^Q{}_{Q(J)}$	$[\beta(3-J^2-J)\sqrt{2} \mp \epsilon\, J(J+1) \times \sqrt{3}]^2 \times \frac{(2J+1)}{3(2J-1)(2J+3)J(J+1)}$	$[\mp \epsilon\, J(J+1)\sqrt{6} - (27)^{\frac{1}{2}}\alpha(J-1)(J+2) + 2\beta(3-J^2-J) + (\gamma \mp \delta)J(J+1)\sqrt{3}]^2 \frac{(2J+1)}{6J^2(J+1)^2(2J-1)(2J+3)}$
$^R{}_{R(J)}$	$^P{}_{P(J+1)}$	$[\beta\sqrt{6} \mp \epsilon(J+1)]^2 \frac{1}{3(J+1)}$	$[\mp \epsilon\,(J+1)\sqrt{2} - \alpha(J+4)(J-1) + (12)^{\frac{1}{2}}\beta + (\gamma \pm \delta) \times J(J+1)]^2 \frac{1}{6J(J+1)^2}$
$^S{}_{S(J)}$	$^O{}_{O(J+2)}$	$[\beta\sqrt{6} \mp \epsilon]^2 \frac{J(J+3)}{6(2J+3)}$	$[\mp \epsilon\, -\alpha(J-1)\sqrt{2} + \beta\sqrt{6} - (\gamma \mp \delta)(J+1)\sqrt{2}]^2 \times \frac{(J+3)}{6(J+1)(2J+3)}$
$^P{}_{O(J)}$	$^R{}_{S(J-2)}$	$(\gamma \mp \delta)^2 \frac{2J(J-2)}{3(2J-1)}$	$[\pm \epsilon\,(J-1)(J+1) + \alpha(J+1)(J+2)\sqrt{2} - \beta(J-1)(J+1)\sqrt{6} -(\gamma \mp \delta)J(J-1)\sqrt{2}]^2 \frac{(J-2)}{6J(J-1)(2J-1)(2J+1)}$
$^Q{}_{P(J)}$	$^Q{}_{R(J-1)}$	$(\gamma \pm \delta)^2 \frac{J+1}{3}$	$[\pm \epsilon\, J(J-1)\sqrt{2} + \alpha(J-3)(J+2) + (12)^{\frac{1}{2}}\beta(J-1) + (\gamma \pm \delta) \times J(J-1)]^2 \frac{(J+1)}{6J^2(J-1)(2J+1)}$
$^R{}_{Q(J)}$	$^P{}_{Q(J)}$	$(\gamma \mp \delta)^2 \frac{(2J+1)}{(2J-1)(2J+3)}$	$[\pm \epsilon\, J(J+1)\sqrt{6} - (27)^{\frac{1}{2}}\alpha(J+2) - 2\beta(3-J^2-J) - (\gamma \mp \delta) \times J\sqrt{3}]^2 \frac{(J-1)}{6J^2(2J-1)(2J+3)}$
$^S{}_{R(J)}$	$^O{}_{P(J+1)}$	$(\gamma \mp \delta)^2 \frac{J}{3}$	$[\pm \epsilon\,(J+1)\sqrt{2} - \alpha(J+4) - 2\beta\sqrt{3} - (\gamma \mp \delta)J]^2 \frac{(J-1)}{6J(2J+1)}$
$^T{}_{S(J)}$	$^N{}_{O(J+2)}$	$(\gamma \mp \delta)^2 \frac{2(J+1)(J+3)}{3(2J+3)}$	$[\pm \epsilon\, -\alpha\sqrt{2} - \beta\sqrt{6} + (\gamma \mp \delta)\sqrt{2}]^2 \frac{(J-1)(J+1)(J+3)}{6(2J+1)(2J+3)}$

[1]The formulas given for $^3\Gamma$(a) are for a case a normal triplet. For an inverted triplet, the intensity formulas for the $^P{}_O$, $^Q{}_P$, $^R{}_Q$, $^S{}_R$ and $^T{}_S$ branches should be interchanged with those of the $^N{}_O$, $^O{}_P$, $^P{}_Q$, $^Q{}_R$ and $^R{}_S$ branches respectively. For other explanations, see legends for Table IV.

ON THE INTENSITY OF ELECTRIC DIPOLE TRANSITIONS*

Ying-Nan Chiu

Laboratory of Molecular Structure and Spectra
Department of Physics, University of Chicago
Chicago, Illinois 60637

and

Department of Chemistry
The Catholic University of America
Washington 17, D. C.**

ABSTRACT

A new method is proposed to derive the electric dipole transition intensity distributions for the electronic bands of diatomic molecules. The theoretical foundation of the use of the Hönl-London intensity formula and its shortcomings are discussed.

In the derivation of the intensity formula, it has been a common practice (Schlapp 1932, Kovács 1960, and James 1963), to equate the square of the transition dipole moment† $|R^{nn'}|^2 = |X^{nn'}|^2 + |Y^{nn'}|^2 + |Z^{nn'}|^2$ to three times $|Z^{nn'}|^2$, the square of the Z component of the electric dipole transition matrix element. The J dependence of the latter which gives rise to the line strength is usually taken from the Hönl-London formula (Herzberg 1931, p. 208). It is the purpose of this work to discuss the theoretical foundation and the inadequacy of this approach and to propose a general alternative method for computing the intensity formula for the electronic bands of diatomic (or linear) molecules.

From the interaction of radiation and matter, we know that the oscillating material (a molecule, for example) dipole may be referred to an arbitrary space-fixed axis system ($\underline{I}$, $\underline{J}$, $\underline{K}$) or to a molecular axis system (n_ξ, n_η, n_ζ). Thus $\underline{R} = X\underline{I} + Y\underline{J} + Z\underline{K} = \xi n_\xi + \eta n_\eta + \zeta n_\zeta$. We choose to use, instead of this Cartesian basis, a spherical basis (Rose 1957, pp. 63-67) for the easier evaluation of the matrix elements. In terms of this the Z component of the electric dipole vector reads

---

*This work was supported by a grant from the National Science Foundation, NSF GP-28.

**Present address.

†For brevity, we shall throughout use the coordinate axis symbol to denote the component of the electric dipole along this coordinate axis. For example, $Z = \sum_i e_i Z_i$ where e_i is the charge of the i^{th} particle.

$Z = \sum_\lambda D^1_{\lambda 0}(-\Psi, -\theta, -\varphi)\ V_{1\lambda}(\xi,\eta,\zeta) = \sum_\lambda D^1_{0\lambda}{}^*(\varphi,\theta,\Psi)\ V_{1\lambda}(\xi,\eta,\zeta)$ and the complete dipole in the space axis system** reads $\underset{\sim}{R} = \sum_\mu V_{1\mu}(X, Y, Z)\ V_{1\mu}{}^*(\underset{\sim}{I}, \underset{\sim}{J}, \underset{\sim}{K}) = \sum_\mu \sum_\lambda D^1_{\mu\lambda}{}^*(\varphi,\theta,\Psi)\ V_{1\lambda}(\xi,\eta,\zeta)\ V_{1\mu}{}^*(\underset{\sim}{I}, \underset{\sim}{J}, \underset{\sim}{K})$ where $D^1_{\mu\lambda}{}^*(\varphi,\theta,\Psi)$ is the rotation matrix (Rose 1957, p. 54, p. 60) and φ, θ, Ψ are the Euler angles through which one rotates the fixed space axis system to the molecular axis system. $V_{1\lambda}$ is the λ^{th} component of the spherical tensor of the first rank which constitutes the spherical basis.†

We shall consider explicitly only the intensity formula in the rotational structure of an electronic band of a diatomic molecule. For a singlet state in a Hund's coupling case b (Herzberg 1931, pp. 218-240), we write the initial state function as

$$\Psi_n = \left(\frac{2J+1}{8\pi^2}\right)^{\frac{1}{2}} \Phi_\Lambda\ D^J_{M\Lambda}{}^*(\varphi,\theta,\Psi)$$

and the final state function as

$$\Psi_{n'} = \left(\frac{2J+1}{8\pi^2}\right)^{\frac{1}{2}} \Phi_{\Lambda'}\ D^{J'}_{M'\Lambda'}{}^*(\varphi,\theta,\Psi)$$

where the rotational wavefunctions which are the rotation matrices, have 2J + 1 and 2J'+ 1 degeneracies represented by the indices M and M' respectively, which designate the space components. The square of the transition matrix element for the Z component of the dipole, after integrating out the rotational wavefunctions (Rose 1957), is

$$\sum_M \sum_{M'} |Z^{nn'}|^2 = \left(\frac{2J+1}{2J'+1}\right)(\Lambda'|R_1,\Lambda'-\Lambda|\Lambda)^2 C^2(J1J';\Lambda,\Lambda'-\Lambda,\Lambda') \times \sum_M \sum_{M'} C^2(J1J';MOM')\delta_{MM'}, \quad (1)$$

and for the dipole as a whole is

$$\sum_M \sum_{M'} |R^{nn'}|^2 = \left(\frac{2J+1}{2J'+1}\right)(\Lambda'|R_1,\Lambda'-\Lambda|\Lambda)^2 \times C^2(J1J';\Lambda,\Lambda'-\Lambda,\Lambda') \sum_M \sum_{M'} \sum_\mu C^2(J1J';M\mu M') , \quad (2)$$

where $R_{1,\lambda} = V_{1\lambda}(\xi,\eta,\zeta)$ and $(\Lambda'|R_{1,\Lambda'-\Lambda}|\Lambda)$ is the vibronic matrix element, the superscript 2 on C $(J1J';M\mu M')$, etc. denotes the square of the Clebsh-Gordan coefficient. As $M + \mu = M'$, one of the indices in Eq. 2 is redundant, we have therefore the sum rule‡

**In the molecular axis system $\underset{\sim}{R} = \sum_\lambda V_{1\lambda}(\xi,\eta,\zeta) V_{1\lambda}{}^*(n_\xi\ n_\eta\ n_\zeta) = \sum_\lambda \sum_\mu V_{1\lambda}(\xi,\eta,\zeta) D^1_{\mu\lambda}{}^*(\varphi,\theta,\Psi) V_{1\mu}{}^*(\underset{\sim}{I}, \underset{\sim}{J}, \underset{\sim}{K})$; the expression is identical.

†Explicitly, the first rank tensor (vector) components are the following:
$V_0(a,b,c) = c$, and $V_1(a,b,c) = \mp (1/\sqrt{2})(a \pm i\, b)$.

‡In fact for a tensor operator of any rank, ℓ, we have the most general sum rule as follows:
$\sum_M \sum_{M'} C^2(J\ell J';M,M'-M,M') = \sum_M \sum_\mu C^2(J\ell J';M,\mu,M+\mu) = \sum_\mu \sum_{M'} C^2(J\ell J';M'-\mu,\mu,M') = 2J'+1.$

of $\sum_M \sum_{M'} C^2(J1J';M,M'-M,M') = 2J'+1$, which is a generalization of the orthonormality of the Clebsch-Gordan coefficients and is the basis of the sum rule for vector operators given by Condon and Shortley (1951). In Eq. (1) because (Rose 1957, p. 38)

$$\sum_M C^2(J1J';MOM) = (2J'+1)/3 \sum_M C^2(JJ'1;M-MO) = (2J'+1)/3 ,$$

it is therefore perfectly valid to equate the results of Eq. (2) to three times that of Eq. (1). Although it will not be shown here, it is easily proved** that before taking square and summing over M and M' the matrix elements of the X, Y, and Z components are not isotropically equal.

In the reduction to Eq. (2), use has been made of the orthonormality of the different μ^{th} components of $V_{1\mu}$ ($\underset{\sim}{I}$, $\underset{\sim}{J}$, $\underset{\sim}{K}$) which follows from the orthonormality of the unit vectors along the rectangular coordinate axes $\underset{\sim}{I}$, $\underset{\sim}{J}$, and $\underset{\sim}{K}$.

For a general initial state wavefunction (Chiu 1964)

$$\Psi_n = A \sum_\Omega b_{n\Omega} \Phi_\Omega D^{J*}_{M\Omega}$$

and a final state wavefunction

$$\Psi_{n'} = A' \sum_{\Omega'} b_{n'\Omega'} \Phi_{\Omega'} D^{J'*}_{M'\Omega'} ,$$

where $A = (2J+1/8\pi^2)^{\frac{1}{2}}$ and $A' = (2J'+1/8\pi^2)^{\frac{1}{2}}$, the general line strength formula reads,

$$\sum_M \sum_{M'} |\underline{R}^{nn'}|^2 = (2J+1) \left[\sum_{\Omega'} \sum_\lambda \sum_\Omega b_{n'\Omega'} \; b_{n\Omega} \; (\Omega' | R_{1,\lambda} | \Omega) C(J1J';\Omega\lambda\Omega') \right]^2 \qquad (3)$$

From the relationship between the vibronic matrix elements such as

$$(-\Omega' | R_{1,-\lambda} | -\Omega) = (-)^S (\pm)^{S'} (\Omega' | R_{1,\lambda} | \Omega)$$

where S and S' depend on the operator R as well as the electronic wavefunction (see below) and from the relationship

$$C(J1J';-\Omega,-\lambda,-\Omega') = (-)^{\Delta J+1} \; C(J1J';\Omega,\lambda,\Omega')$$

one can eliminate the sum over negative Ω', λ and Ω without losing the correct sign. Whereas, the straightforward use of Hönl-London formulas which do not give explicitly the relationship between the J dependence for $+\Lambda$ and $-\Lambda$ states, as the Clebsch-Gordan

---

**For this purpose, one writes $X = (1/\sqrt{2}) \sum_\lambda \left[-D^{1*}_{1\lambda} + D^{1*}_{-1\lambda} \right] V_{1\lambda}(\xi,\eta,\zeta)$

and $Y = (1/\sqrt{2}) \sum_\lambda \left[D^{1*}_{1\lambda} + D^{1*}_{-1\lambda} \right] V_{1\lambda}(\xi,\eta,\zeta)$.

coefficients here do, may lead to errors of signs. For example in the ${}^1\Sigma_0^{\pm} \leftarrow {}^3\Delta_1$ (a) transitions, we have for the initial state

$$\Psi_n = A(1/\sqrt{2})\left[\Phi({}^3\Delta_{+1})\ D^{J*}_{M1} \pm (-)^{\Delta J}\ \Phi({}^3\Delta_{-1})\ D^{J*}_{M-1}\right]$$

and for the final state

$$\Psi_{n'} = A'\Phi({}^1\Sigma_0^{\pm})\ D^{J'*}_{M'0}$$

and we get the line strength, for $\Delta J = J' - J$,

$$\begin{aligned}\sum_M \sum_{M'} |R^{nn'}|^2 &= \tfrac{1}{2}(2J+1)\left[(0|R_{1,-1}|1)\ C(J1J';1\text{-}10)\right. \\ &\left. \pm (-)^{\Delta J}(0|R_{1,1}|\text{-}1)\ C(J1J';\text{-}110)\right]^2 \qquad (4) \\ &= 2(2J+1)(0|R_{1,1}|\text{-}1)^2\ C^2(J1J';\text{-}110)\ ,\end{aligned}$$

where $(0|R_{1,-1}|1) = \sigma_v^{\xi\zeta}(0|R_{1,-1}|1) = (\mp)(0|R_{1,1}|\text{-}1)$ and were we have made use of the relationships such as reflection with respect to the $\xi\zeta$ plane

$$\sigma_v^{\xi\zeta}\ \Phi({}^1\Sigma_0^{\pm}) = \pm\Phi({}^1\Sigma_0^{\pm}),\ \sigma_v^{\xi\zeta}\ R_{1,\lambda} = (-)^{\lambda}\ R_{1,-\lambda}$$

and

$$\sigma_v^{\xi\zeta}\ \Phi({}^3\Delta_{+\Omega}) = (-)^{\Omega+1}\ \Phi({}^3\Delta_{-\Omega})\ ,$$

inversion with respect to the coordinate origin

$$i\Phi({}^1\Sigma_0^{\pm})D_{M',0} = (\pm)(-)^{J'}\Phi({}^1\Sigma_0^{\pm})D^{J'*}_{M',0}$$

and

$$i\Phi({}^3\Delta_{+\Omega})D^{J*}_{M\Omega} = (-)^{J+1}\ \Phi({}^3\Delta_{-\Omega})D^{J*}_{M-\Omega}\ .$$

Eq. (4) is independent of the Kronig reflection symmetry of the ${}^1\Sigma$ state. The reason is that regardless of whether the upper state is ${}^1\Sigma^+$ or ${}^1\Sigma^-$ there is always a Λ-doubling component of the lower ${}^3\Delta_1$ state from which transition may take place. We thus take exception** to the Eq. (4a) of Kovacs (1960) which gives a line strength for

**Similar objections may be raised to the general line strength formulas (4b), the ${}^3\Sigma_1^{\pm} - {}^3\Delta_2$ and ${}^3\Sigma_0^{\pm} - {}^3\Delta_1$ transitions. However, these objections all appear to be a matter of minor technicality as the branch intensity given in Kovacs' tables actually makes no such discrimination against certain branches and are the same for Σ^+ and Σ^- states.

$^1\Sigma^{\pm}$ states proportional to $[1 \pm (-)^{\Delta J+\delta}]$ where δ is even for $^1\Sigma^+$ and odd for $^1\Sigma^-$ states. This latter line strength formula would then exclude P and R ($\Delta J \mp 1$) branches for the $^1\Sigma^{\pm}$ states if the $\pm$ signs are read consistently and δ is chosen as above. A more detailed discussion of our method, its extension to electric quadrupole and magnetic dipole transitions with application to the $^1\Pi^{\pm} - {}^3\Pi(a)$ and $^1\Pi^{\pm} - {}^3\Pi(b)$ transitions will be treated in a separate article.

REFERENCES

1. Chiu, Y. N., J. Chem. Phys. 41, 0000 (1964).
2. Condon, E. U. and Shortley, G. H., "The Theory of Atomic Spectra" (Cambridge University Press, London) pp. 71-73 (1951).
3. Herzberg, G., "Spectra of Diatomic Molecules" (D. Van Nostrand Co., Princeton, New Jersey, 1931).
4. James, T. C., J. Chem. Phys. 38, 1094 (1963).
5. Kovács, I., Can. J. Phys. 38, 955 (1960).
6. Rose, M. E., "Elementary Theory of Angular Momentum" (John Wiley, New York, 1957).
7. Schlapp, R., Phys. Rev. 39, 806 (1932).

ON THE VECTOR ADDITION THEOREM FOR THE EXPANSION OF SOLID SPHERICAL HARMONICS*

Ying-Nan Chiu**
Laboratory of Molecular Structure and Spectra
Department of Physics, University of Chicago
Chicago, Illinois 60637

Expansion of solid spherical harmonics $r_b^n Y_n^k(\theta_b,\varphi_b)$ or $r_b^{-n-1} Y_n^k(\theta_b,\varphi_b)$ of vector r_b referred to center b in terms of those on another center, as well as the expansion of solid spherical harmonics of the interelectronic vector $\underline{r}_{12}$ in terms of those of individual electron position vectors $\underline{r}_1$ and $\underline{r}_2$ are useful in the evaluation of molecular integrals that occur in the study of electric and magnetic interactions in molecules.

In a recent paper[1] (hereafter referred to as paper I), Chiu demonstrated the common principle behind the above kinds of expansions and showed the vector addition nature of solid spherical harmonics expansions through expressing them as coupling of irreducible spherical tensors. From this principle we shall reformulate in a clearer way the vector addition theorem and shall give a thumb rule for its ready application to physical problems. By use of this theorem one can easily write down any expansion of solid spherical harmonics, including those in existing literature.[2-9]

In essence the theorem says that given vectors $\underline{r}_{oa}$, $\underline{r}_{ob}$ in space and vector $\underline{r}_{ab}$ defined as $\underline{r}_{oa} - \underline{r}_{ob}$, the solid spherical harmonics of the above vectors couple to give one another as irreducible spherical tensors (aside from definitive constants) according to the vector addition model.

The definitive constants may be accounted for by defining[1] the irreducible tensor of regular solid spherical harmonics as

$$R_n^k(\underline{r}_b) \equiv [4\pi/(2N+1)!]^{\frac{1}{2}} r_b^n Y_n^k(\theta_b,\varphi_b) \qquad (1)$$

and the irreducible tensor of irregular solid spherical harmonics as

$$I_n^k(\underline{r}_b) \equiv [4\pi(2n)!]^{\frac{1}{2}} r_b^{-n-1} Y_n^k(\theta_b,\varphi_b) \qquad (2)$$

*This work was supported by a grant from the National Science Foundation, NSF GP 28 Research.

**Present Address: Department of Chemistry, Catholic University of America, Washington 17, D. C.

As an example of the theorem, according to the vector addition relationship $\underset{\sim}{r}_{ob} = \underset{\sim}{r}_{oa} + (-\underset{\sim}{r}_{ab})$ we have

$$R_n^k(\underset{\sim}{r}_{ob}) = \sum_{\ell=0}^{n} \sum_{m=-\ell}^{\ell} C(\ell,n-\ell,n;m,k-m,k)\, R_\ell^m(\underset{\sim}{r}_{oa})\, R_{n-\ell}^{k-m}(-\underset{\sim}{r}_{ab}) \qquad (3)$$

and

$$I_n^k(\underset{\sim}{r}_{ob}) = \sum_{\ell=0}^{\infty} \sum_{m=-\ell}^{\ell} C(\ell,n+\ell,n;m,k-m,k)\, R_\ell^m(\underset{\sim}{r}_{<})\, I_{n+\ell}^{k-m}(\underset{\sim}{r}_{>}) \qquad (4)$$

where $r_>$ and $r_<$ stand for the larger or smaller of $\underset{\sim}{r}_{oa}$ and $-\underset{\sim}{r}_{ab}$. The vectors stand for the lengths of themselves and the polar and azimuth angles [as in Eqs. (1) and (2)] made by them with respect to the mutually <u>parallel</u> sets of local axes at the origin of these vectors. Since the origin does not really come into the expression, $\underset{\sim}{r}_{oa}$, $\underset{\sim}{r}_{ob}$ and $\underset{\sim}{r}_{ab}$ may well be the sides of a triangle in space and <u>o</u> a space point, not any particular space-fixed origin.

For mnemonic purpose we have arbitrarily written the first irreducible tensor on the right hand side of (3) [or in (4), the tensor with the lesser argument $r_<$] as R_ℓ^m. But as the rank ℓ and the azimuth quantum number m are dummy indices, by changing their designation but keeping the relative magnitudes, one can reduce (3), (4) to (5.1a) and (10,1a) of paper I. $C(\ell,n\pm\ell,n;m,k-m,k)$ is readily identified to be the Clebsch-Gordan or Wigner vector coupling coefficient[10] which also gives the conservation of azimuth angular momentum quantum number on both sides. For an inverse vector we have $R_N^M(-\underset{\sim}{r}) = (-)^N R_N^M(\underset{\sim}{r})$ and $I_N^M(-\underset{\sim}{r}) = (-)^N I_N^M(\underset{\sim}{r})$.

As it stands Eqs. (3)-(4) may be viewed as the expansion of spherical harmonics of the vector $\underset{\sim}{r}_{ob}$ referred to the origin <u>o</u> in terms of those of $\underset{\sim}{r}_{oa}$ referred to the same origin and those of $\underset{\sim}{r}_{ab}$ referred to a different origin b. With repeated applications of (3) and (4) expansions in terms of vectors at yet another center may be obtained. This constitutes the two-center (bipolar) expansions[3,4] which along with the case of <u>unparallel</u> local axes systems have been treated at the end of paper I.

For $\underset{\sim}{r}_{ab}$ along the polar axis (3), and (4) represent the displacement theorem of Hobson;[2] for arbitrary orientation of $\underset{\sim}{r}_{ab}$ they lead to existing results in literature.[1,5,7,8,9]

From (3) and (4) it is clear that the rank of the second irreducible tensor on the right hand side, instead of a range of values can take only one value: $n-\ell$ for regular solid spherical harmonics expansions demanding that the ranks of the two tensors on the right add to give n which is the rank of the tensor on the left; $n+\ell$ for irregular solid spherical harmonics expansions demanding that these ranks subtract

to give n. This is of course a very special case of the coupling of angular momentum vectors as here we assert that the "wavefunctions" corresponding to all these vectors are spherical harmonics, which in truth the wavefunctions in composite space are not.[11] This limitation on the values of the ranks of tensors although resulting from detailed analysis[1] can be conceived as related to the dimensionality of the radial function r_b^n on the left hand side.

If a represents electron 1, b represents electron 2, then following (3) and (4) the expansion of r_{12} according to $\underset{\sim}{r}_{12} = \underset{\sim}{r}_1 + (-\underset{\sim}{r}_2)$ will give for n=k=0 the coulomb potential expansions, for n = 2, k = 0 and ±2 the electron magnetic dipole-dipole interaction operators.[6] Our (3) and (4) with arbitrary n and k are of course the more general and will give expansions for operators of higher (than dipole) magnetic multipole interactions.

REFERENCES

1. Y. N. Chiu, J. Math. Phys. 5, 283 (1964); referred to as paper I.
2. E. W. Hobson, The Theory of Spherical and Ellipsoidal Harmonics, (Chelsea Publishing Company, New York, 1955) pp. 140-141.
3. B. C. Carlson and G. S. Rushbrooke, Proc. Camb. Phil. Soc. 46, 626 (1950).
4. R. J. Buehler and J. O. Hirschfelder, Phys. Rev. 83, 628 (1951); 85, 149 (1952).
5. M. E. Rose, J. Math. and Phys. 37, 215 (1958).
6. R. M. Pitzer, C. W. Kern, and W. N. Lipscomb, J. Chem. Phys. 37, 267 (1962).
7. J. P. Dahl and M. P. Barnett, Quarterly Progress Report No. 48, Solid State and Molecular Theory Group, M.I.T., p. 53 (1963).
8. R. A. Sack, J. Math. Phys. 5, 000 (1964).
9. J. P. Dahl, Quarterly Progress Report No. 52, Solid State and Molecular Theory Group, M.I.T., p. 47 (1964). In the Eq. (10) here the undefined function $F_{nn}(r_a,R)$ can be absorbed in our definition of irreducible tensors, Eqs. (1) and (2). The summation index n_1 can take one value of N+n or N-n only as shown in our Eqs. (3) and (4) because this is not the ordinary case of coupling of angular momenta.
10. Algebraic expressions of the necessary coefficients are given in paper I, Ref. 1.
11. M. E. Rose, Elementary Theory of Angular Momentum, (John Wiley and Sons, New York, 1957), p. 61.

Reprinted from THE JOURNAL OF CHEMICAL PHYSICS, Vol. 41, No. 5, 1377–1382, 1 September 1964
Printed in U. S. A.

Isotope Shifts and the Vibrational Structure in Some Weaker Systems of N_2†

D. MAHON-SMITH
Department of Physics, University College, Dublin, Ireland
AND
P. K. CARROLL
Laboratory of Molecular Structure and Spectra, Department of Physics, University of Chicago, Chicago, Illinois

(Received 14 February 1964)

The emission spectrum of $^{15}N_2$ has been studied in the region 2000–9000 Å with a view to investigating the vibrational structure of some of the weaker systems. In the cases of the Herman infrared bands and the Gaydon–Herman green bands, it has been possible to decide between alternative vibrational schemes which have been suggested. Observations have also been made on the Goldstein–Kaplan and the $B'\rightarrow B$ systems. In the near-ultraviolet spectrum it is shown that the $h\rightarrow a$, $s'\rightarrow a$, $r'\rightarrow a$, $m\rightarrow a$, and $d\rightarrow a$ progression all arise from upper levels with $v>0$. The possibility that some of these progressions may belong to a single system is discussed. The vibrational schemes for the fifth positive and Kaplan's first and second systems have been confirmed. Some new bands of $^{15}N_2$ corresponding apparently to hitherto unobserved transitions are reported.

I. INTRODUCTION

IN the spectrum of N_2 there are still many systems of which our knowledge is far from complete.[1] For some of these the nature of the electronic states involved has not yet been established, while for others even the vibrational analysis is subject to considerable uncertainty. The present paper, which describes investigations of the spectrum of $^{15}N_2$ in the region 2000–9000 Å, is concerned with the vibrational structure of some of these less well understood systems. Part of the present data on the near ultraviolet spectrum has already been reported briefly.[2]

II. EXPERIMENTAL

Several sources were used in the course of the present experiments. For the Goldstein–Kaplan and for the $B'\rightarrow B$ systems, an ordinary transformer discharge through pure nitrogen was used. To excite the Herman infrared system and the Gaydon–Herman green bands rather specialized sources had to be employed. In the case of the former, the bands were studied in a weak low current subnormal-type discharge[3] while the green bands were found to be considerably enhanced in discharges cooled to liquid-nitrogen temperatures. For the near-ultraviolet bands, a mildly condensed discharge through pure nitrogen was used for all systems.

In the visible and near infrared the spectra were photographed on a small Wadsworth grating spectrograph, which gave a dispersion of about 8 Å/mm over the region studied. For the near-ultraviolet systems, a large Hilger quartz spectrograph which gave a dispersion of 4 A/mm at 2500 A was used.

III. HERMAN INFRARED SYSTEM

Using a low-current discharge cooled to liquid-nitrogen temperatures, Herman[4] observed eight bands degraded to shorter wavelengths in the region 7000–8600 A. A vibrational analysis was given and it was suggested that the system might arise from the singlet transition $v\rightarrow q\ ^1\Sigma_u^+$. Carroll and Sayers[3] studied the system under higher resolution and were able to identify six heads or features in each band. The possibility of a singlet transition was eliminated and a new vibrational scheme was proposed in which the v' values of Herman were reduced by unity.

In the present work the bands were studied with both $^{14}N_2$ and $^{15}N_2$ and the data for five bands of the system are given in Table I. The measurements for the first four bands refer to the long-wavelength head. In fact it was possible to measure between four and six heads in these bands and each $\Delta\nu$ value in Table I is the average of the isotopic shifts observed for corresponding heads. In the case of fifth band, due to overlapping by first positive structure, it was possible to give a reliable measurement for the short-wavelength head only. For the same reason the isotope shifts of the Herman bands in the region 7570–7440 Å could not be determined with any accuracy and so the data are not given.

Columns 4 and 5 of Table I show the isotope shifts calculated on the vibrational scheme of Herman and that of Carroll and Sayers, respectively. It is evident that the latter analysis is in fact the correct one.

IV. GAYDON–HERMAN GREEN SYSTEM

This system, occurring in the region 6400–5000 Å, is very similar in character and excitation conditions to

† This work assisted by the Office of Naval Research under Contract Nonr-2121(01) and by the U. S. Air Force, through Electronic Systems Division, Air Force Systems Command under Contract AF19(628)-2474.

[1] For a recent and detailed account of the band spectrum of N_2, see A. Lofthus, "The Molecular Spectrum of Nitrogen," Spectroscopic Report No. 2, University of Oslo, 1960.

[2] P. K. Carroll and D. Mahon-Smith, J. Chem. Phys. **39**, 237 (1963).

[3] P. K. Carroll and N. D. Sayers, Proc. Phys. Soc. (London) **A66**, 1138 (1953).

[4] R. Herman, Compt. Rend. **233**, 738 (1951).

TABLE I. Herman infrared system.

			Carroll–Sayers		Herman	
λ(Å)$^{14}N_2$	λ(Å)$^{15}N_2$	$\Delta\nu$ (obs)	$v'-v''$	$\Delta\nu$	$v'-v''$	$\Delta\nu$
8101.4	8102.0	1.3	0–0	3.4	1–0	32.4
7869.4	7877.8	13.9	2–2	16.0	3–2	39.9
7095.4	7123.9	56.8	2–0	59.9	3–0	84.4
7033.2	7062.9	60.1	3–1	62.2	4–1	84.1
8549[a]	8536.6[a]	−16.9	0–1	−20.0	1–1	9.3

[a] Short-wavelength head.

the Herman infrared system and will therefore be considered next. Gaydon[5] observed seven bands of the system while Herman[6] independently discovered the three strongest bands. Later another band at 5047 Å was reported[8] while Grün[7] using electron beam excitation observed 17 bands in all.

The tentative vibrational analysis proposed by Gaydon was quite different from that given by Herman. It is the most likely scheme and has been generally favored. The results of the present work are given in Table II where the measurements refer to the short-wavelength heads. Several features were in fact measured in each band and the tabulated $\Delta\nu$ is the average isotope shift. Column 4 gives the shifts calculated from the vibrational analysis of Gaydon and it is seen that the values are in excellent agreement with those observed experimentally. Gaydon's analysis is therefore established as being correct.

Both the green bands and the infrared bands discussed in the previous section are quite difficult to observe and require special conditions of excitation. Nothing is known about the electronic states involved and no transition between any of them and the other known states of N_2 has so far been observed. Until now the possibility at least existed that one or both of these systems might not be due to the nitrogen molecule. However the present work, apart from establishing the vibrational schemes for both of these systems, shows conclusively that N_2 must be the emitter.

V. $B'\,^2\Sigma_u^- - B\,^3\Pi_g$ INFRARED SYSTEM

It was with a view to studying this transition at a time when little was known about it that the present work on the spectrum of $^{15}N_2$ was initially undertaken. The first band was observed in emission from a nitrogen discharge[9] while later the system was found to be developed in cooled afterglow sources.[8] From a rotational analysis of the 8265.5-Å band, it was shown[9] that the B' state was $^3\Sigma_u^-$ while the same result was obtained[10] independently from a study of the far-ultraviolet forbidden transition $B'\leftarrow X$. Bayes and Kistiakowsky[11] observed the afterglow spectrum using $^{15}N_2$, and although their work was apparently carried out at quite low resolution, their results left little doubt as to the vibrational numbering in the B' state. The present more accurate data on different bands of the system observed in the discharge tube are presented merely as conclusive evidence for the vibrational analysis.

As the spectral region of interest is heavily covered by first positive bands the system is difficult to observe in discharge tube sources and with $^{14}N_2$ only one band (5−1) can be detected. However, in $^{15}N_2$ due to a favorable shift of both systems four bands could be observed and measured. The data for these bands are given in Table III and it is seen that the observed frequencies of the R_2 heads are in excellent agreement with those computed on the basis of the work of Bayes and Kistiakowsky.

TABLE II. The Gaydon–Herman green bands.

$v'-v''$	λ(Å)$^{14}N_2$	λ(Å)$^{15}N_2$	$\Delta\nu$(obs)	$\Delta\nu$(calc)
0–0	5574.5	5575.3	2.6	2.6
1–0	5308.6	5317.4	32.3	32.1
2–1	5271.1	5281.9	36.8	35.6
2–0	5073.3	5089.0	60.1	59.9
3–1	5047.1	5062.6	60.6	61.6

[5] A. G. Gaydon, Proc. Phys. Soc. (London) **56**, 85 (1944).
[6] R. Herman, Ann. Phys. (Paris) **20**, 241 (1945).
[7] A. E. Grün, Z. Naturforsch. **9a**, 1017 (1954).

VI. GOLDSTEIN–KAPLAN SYSTEM

This system consists of a long progression of bands extending from the green to the near ultraviolet. Normally the intermediate bands are not observed due to

TABLE III. The $B'\,^2\Sigma_u^- \rightarrow B\,^3\Pi_g$ bands. K_2 heads.

$v'-v''$	λ(Å)$^{15}N_2$	ν(cm^{-1})$^{15}N_2$	ν(cm^{-1}) calc
8–2	7035.8	14 209	14 202
8–3	7924.9	(12 615)[a]	12 616
4–0	8195.1	12 199	12 195
5–1	8402.5	11 898	11 901

[a] Computed from $^0R_{23}$ head. R_2 head obscured.

[8] F. LeBlanc, Y. Tanaka, and A. Jursa, J. Chem. Phys. **28**, 879 (1959); G. B. Kistiakowsky and P. Warneck, *ibid.* **27**, 1417 (1957). See also M. Brook, Scientific Report No. 2, Institute of Geophysics, University of California, Los Angeles (1953).
[9] P. K. Carroll, and H. E. Rubalcava, Nature (London) **184**, 119 (1959); Proc. Phys. Soc. (London) **76**, 337 (1960).
[10] P. G. Wilkinson, J. Chem. Phys. **32**, 1061 (1960). The transition was observed in emission by M. Ogawa and Y. Tanaka, *ibid.*, p. 922.
[11] K. D. Bayes and G. B. Kistiakowsky, J. Chem. Phys. **32**, 992 (1960).

the great strength of the second positive bands in the same region. Gaydon[6] in fact believed that two systems were present, one in the visible and one in the near ultraviolet. Recently rotational analyses[12] have been made of two of the ultraviolet bands and one of the visible bands and this work shows that both groups do in fact belong to a single system which has the well-known $B\ ^3\Pi_g$ state as the lower state. The upper state, C', was shown to be of Species $^3\Pi_u$ in which the coupling was almost pure Case *b*.

The vibrational quantum number of the upper level has been given the most natural value of $v=0$ but as some isolated ultraviolet progressions have been shown to arise from excited vibrational levels (see below), it seemed worthwhile to check the vibrational numbering in the C' state. It was also hoped to make an estimate of ω_e' from the isotopic shift. Furthermore, as the potential curve for the $C'\ ^3\Pi_u$ state must "cross" that of the $C\ ^3\Pi_u$ state, the possibility arises that an interaction between these two states of the same species might give rise to an anomalous isotopic shift. In particular it is conceivable that the C' state might behave like a higher vibrational level of the $C\ ^3\Pi_u$ state.

Due to the unfavorable shifts in the $^{15}N_2$ spectrum most of the Goldstein–Kaplan bands are rather badly obscured by strong second positive bands. In fact it was possible to make measurements on only three bands and these data are not of high precision. The results are given in Table IV and it is seen that to the accuracy of the measurements the shifts are accounted for by the isotopic displacements in the $B\ ^3\Pi_g$ state. This shows that the Goldstein–Kaplan bands arise from the $v=0$ level in the upper state and that there is no anomalous isotope shift.

Using a suitable mixture of isotopes some observations were also made with $^{14}N\ ^{15}N$ and in this case the shift in the 0–11 band could be measured quite accurately. By combining this with the calculated displacement in the $v=11$ level of the $B\ ^3\Pi_g$ state, the actual displacement of the upper level could be obtained. From the resulting value, 7 cm^{-1}, it was possible to estimate ω_e as $\approx$860 cm^{-1} for the $C'\ ^3\Pi_u$ state. The value obtained from the relationship $\omega_e=B^2/D^2$ is 651 cm^{-1} and, considering the uncertainties involved, these two results may be taken to be in reasonable agreement. Hamada[13] classified two weak bands in the near ultraviolet as the 1–4 and 1–5 transitions of the system. On this identification one estimates ω_e to be $\approx$1450 cm^{-1}, which is much greater than the values derived above. However, for independent reasons, it has been suggested[12] that the bands of Hamada do not belong to the Goldstein–Kaplan system, a view which seems to be confirmed by the present results. This is satisfactory because it is believed that the $C'\ ^3\Pi_u$ state either goes to the dissociation limit $^4S+^2D$ or else is predissociated by some state from this limit.

TABLE IV. The Goldstein–Kaplan bands. P_1 heads.

$v'-v''$	λ(Å) $^{14}N_2$	λ(Å) $^{15}N_2$	$\Delta\nu$ (cm^{-1}) obs	$\Delta\nu$ (cm^{-1}) calc. for $B\ ^3\Pi_g$
0–11	4728.4	4613.0	529	535
0–10	4432.3	4335.3	505	502
0–7	3707.1	(3653.7)[a]	394	386

[a] Calculated from P_2 head. P_1 head obscured.

[12] P. K. Carroll, Proc. Roy. Soc. (London) A272, 270 (1963).
[13] H. Hamada, Phil. Mag. 23, 25 (1937).

TABLE V. Progressions to $a\ ^1\Pi_g$. Wavelengths of heads.[a]

Transition	λ(Å) $^{14}N_2$	λ(Å) $^{15}N_2$
h–0	2281.5	2294.2
h–1	2371.6	2382.3
h–3	2569.5	2575.3
h–4	2678.7	2680.0
s'–0	2397.1	2407.9
s'–1	2496.8	2505.0
s'–2	2603.3	2608.6
r'–0	2671.7	2676.8
r'–1	2796.0	2797.5
m–1	2877.9	2883.4
m–2	3020.3	3021.5
d–0	2795.4	2802.9
d–1	2932.0	2935.2
d–2	3079.9	3078.4

[a] In this and in the subsequent Tables the wavelengths for $^{14}N_2$ are taken from Ref. 1.

VII. NEAR-ULTRAVIOLET BANDS

The main features of the N_2 spectrum from 2000 to 3000 Å are the second and fourth positive bands. Under suitable excitation conditions, however, numerous other bands appear which have been assigned to a considerable number of systems. These systems may be classified as falling mainly into two groups: (1) Those involving transitions from highly excited states to the well-known $a\ ^1\Pi_g$ state. Most of these systems consisted apparently of the $v'=0$ progression only. (2) Those arising from transitions between the $x\ ^1\Sigma_g^-$, $a'\ ^1\Sigma_u^-$, $y\ ^1\Pi_g$, $w\ ^1\Delta_u$, and $z\ ^1\Delta_g$ states.

a. $r'-a$, $s'-a$, and $h-a$ Bands

These three systems were first observed by Gaydon[14] while Herman[6] independently discovered the $h-a$ transition. Although working at fairly low resolution, Gaydon was able to analyze the fine structure of some bands in each transition. Subsequently Lofthus[15] studied the rotational structure under much higher resolution. In all three cases the upper states were shown to be $^1\Sigma_u^+$ and some anomalies in the rotational structure and in the vibrational intensities were reported.

[14] A. G. Gaydon, Proc. Roy. Soc. (London) A182, 286 (1944).
[15] A. Lofthus, Can. J. Phys. 35, 216 (1957).

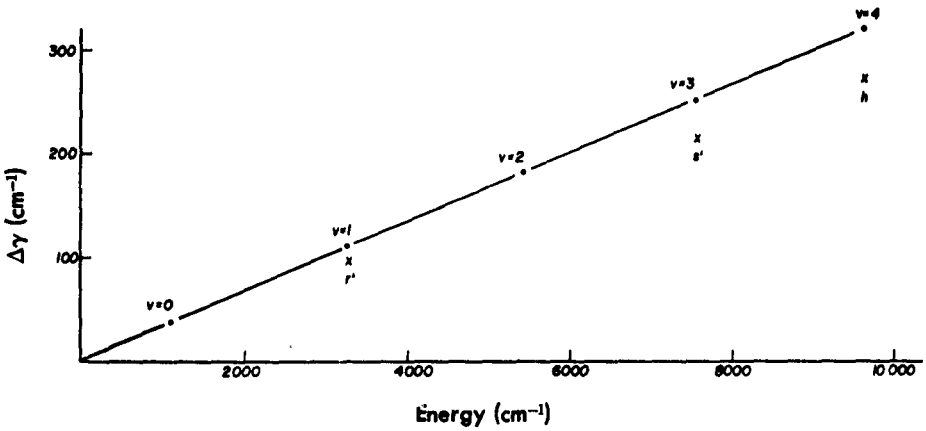

FIG. 1. Isotopic shifts as a function of vibrational energy. Crosses: observed shifts in the r', s', and h levels. Line: shifts calculated on the assumption that the r', s', and h levels belong to the same electronic state.

Table V gives the wavelengths of the heads of these bands measured in both $^{14}N_2$ and $^{15}N_2$. The most convenient way of treating the data is to combine the isotope shifts for the $a\ ^1\Pi_g$ state, which can readily be computed, with the observed band displacements and hence find the isotopic lowering of the upper levels. The results of this procedure are shown in Table VI. From these data it is at once evident that none of the upper levels corresponds to $v=0$. While it is fairly obvious that the value of v in the r' level is probably unity, the numbering of the other levels, for which the shifts are considerably greater, is less certain. However, the transitions involving s' and h could very reasonably be assigned to vibrational levels with $v=3$ and 4, respectively, and as the upper states are of the same species, $^1\Sigma_u^+$, it is just possible that the three progressions belong to a single system. The levels r', s', and h can in fact be fitted satisfactorily to a vibrational formula with $\omega_e=2191.5$ cm^{-1}, $x\omega_e=9.6_5$ cm^{-1}. Furthermore, as shown in Fig. 1, the isotopic shifts in the upper levels plotted against $G'(v)$ yield an essentially straight line which passes through the origin. (See, however, below.)

Nevertheless, several difficulties arise in considering the three progression as belonging to the same system: (1) The B values, although of similar magnitudes, do not decrease in the usual regular way with increasing v (see Table VI). (2) While the isotopic shifts in the upper levels plotted against $G'(v)$ give a straight line, their magnitudes are noticeably less than the computed values (see Fig. 1). (3) The $v'=2$ progression is not included in the analysis. This could be identified as the $k-a$ progression of Lofthus[16] as the upper state is of the correct species and energy, but the B value (1.425 cm^{-1}) would be quite anomalous. (The $k\rightarrow a$ bands were not observed in $^{15}N_2$ due, it seems, to their being displaced in such a way as to be obscured by adjacent strong bands. Such a shift would be consistent with $v'=2$.) (4) The $v=0$ progression is not observed. In particular the 0–0 band in both $^{14}N_2$ and $^{15}N_2$ should lie in a comparatively clear spectral region but no good evidence for its presence could be found. (5) The ω_e value is rather large, especially when compared with the rotational constants of the levels.

Despite these difficulties, the possibility that a single state is involved cannot be ruled out.[16] The anomalies listed above may be due to perturbations and predissociations[17] which are likely to be common at the high energies where the levels lie. If in fact a single state is involved, the vibrational structure at least would suggest that it is a Rydberg state as the ω_e value, 2191.5 cm^{-1}, is very close to that of the $X\ ^2\Sigma_g^+$ ground state of N_2^+ (2207.2 cm^{-1}).

b. $m\rightarrow a$ and $d\rightarrow a$ Bands

Herman[6] and Janin[18] observed two progressions of bands which were considered to arise from the levels

TABLE VI. Isotope shifts for the h, s', r', m, and d levels of N_2.

State	E^a (cm^{-1})	$\Delta\nu$ (cm^{-1})	Suggested v value	B (cm^{-1})[c]
$h\ ^1\Sigma_u^+$	112 767.7	274	4[b]	1.655
$s'\ ^1\Sigma_u^+$	110 656.5	215	3[b]	1.595
$r'\ ^1\Sigma_u^+$	106 368.3	98	1	1.711
$m\ ^1\Pi_u$	105 343.7	150	5 or 6	1.361
d ···	104 713.2	122	5 or 6	···

[a] Energy of level in $^{14}N_2$ relative to $v=0$ of the ground state.
[b] Assuming r', s', and h belong to a single system.
[c] For $^{14}N_2$.

[16] The ν_{00} for the single system would be 35 246 cm^{-1}.

[17] The r' level is known to be predissociated for $J>11$. The breaking off in rotational structure occurs at 13.214±0.003 eV which is just below the dissociation limit $^4S+^2P$ at 13.330 eV. The predissociation is therefore almost certainly due to a repulsive state from $^4S+^2D$. Consequently the predissociating state must be either triplet or quintet so that the process is an intersystem one. The appearance of bands from higher vibrational levels would therefore not be surprising. The predissociation also most likely falls into Case c^+ of Mulliken [J. Chem. Phys. 33, 247 (1960)]. Here the curves cross rather sharply so that on the Franck-Condon principle the reappearance of transitions from higher vibrational levels will be favored.

[18] J. Janin, Compt. Rend. 217, 392 (1943).

$v=0$ and 1 of a state d, the lower state of the transition being $a\ ^1\Pi_g$. The $v'=1$ progression was independently discovered by Gaydon[14] and was later studied under high resolution by Lofthus[15] who confirmed Gaydon's analysis of the upper state as $^1\Pi_u$. This particular level has been identified as the lowest observed vibrational level of the m state of Worley.[19]

In the present work the two progressions were observed in both $^{14}N_2$ and $^{15}N_2$ and the measurements are given in Table V, while the resulting isotopic displacements in the upper levels are given in Table VI. It is quite clear from the magnitudes of the shifts that the vibrational quantum numbers must be greater than 0 and 1. If the bands are assigned to a single system, the most likely values for v are 4 and 5. This interpretation, however, gives poor quantitative agreement with theory and would suggest a negative value of $x\omega_e$ for the upper state. For this reason it is believed that the two levels belong to different electronic transitions. This is supported by the fact that the vibrational interval, 640.3 cm^{-1}, would be too small to correspond to an extension of the m progression of Worley.

The vibrational numbering in the m state cannot be determined with great certainty because (a) the three bands observed in the far-ultraviolet spectrum show a somewhat anomalous spacing, and (b) the isotopic shift is known for only one level. The procedure adopted was to use the two equations $\Delta G(v+\frac{1}{2})=\omega_e-2x\omega_e(v+1)$ and $\Delta\nu=(1-\rho)\omega_e(v+\frac{1}{2})-(1-\rho^2)x\omega_e(v+\frac{1}{2})^2$; in the first of these, the lowest observed vibrational interval, 764 cm^{-1}, for the m state was introduced while in the second the observed isotopic shift was used. Over the likely range of $x\omega_e$ (say 4 to 12 cm^{-1}), the resulting value of v lies between 5 and 6. We can therefore say that the first observed level of the m state at 105 347 cm^{-1} has a vibrational quantum number of 5 or 6.

TABLE VII. Fifth positive system. $x\ ^1\Sigma_g^+-a'\ ^1\Sigma_u^-$.

$v'-v''$	λ(Å) $^{14}N_2$	λ(Å) $^{15}N_2$	$\Delta\nu$ (cm^{-1}) obs	$\Delta\nu$ (cm^{-1}) calc
2–2	2165.2	2166.4	−27	−29
1–1	2181.5	2182.3	−17	−18
0–0	2198.9	2199.1	−4	−6
2–3	2235.9	2234.9	21	29
0–1	2274.3	2272.0	44	44
1–3	2331.1	2326.6	82	88
1–4	2411.8	2404.6	124	119
2–6	2469.9	2460.6	153	151
1–5	2496.7	2486.5	164	168
0–4	[a]	2513.7		181
2–7	2556.2	2543.7	194	192
1–6	2586.6	2572.7	209	210
2–8	2647.1	2631.3	227	223
1–7	2681.5	2663.5	253	251

[a] Obscured in $^{14}N_2$ spectrum.

TABLE VIII. Kaplan's first system. $y\ ^1\Pi_g-a'\ ^1\Sigma_u^-$.

$v'-v''$	λ(Å) $^{14}N_2$	λ(Å) $^{15}N_2$	$\Delta\nu$ (cm^{-1})
0–3	2381.7	2374.0	136
1–4	2366.4	2360.2	110
0–2	2301.9	2297.1	92
0–1	2225.9	2223.8	43
0–0	2153.6	2154.0	−10

Little can be said about the d state except that it is an excited vibrational level. However, its energy 104 713 cm^{-1}, is very close to that of the second observed vibrational level in the l progression of Worley[19] at 104 702 cm^{-1}. If this identification is made and the procedure for the m state applied, one finds that vibrational quantum number to be 5 or 6, the latter value being slightly favored. The first member of the $l-X$ progression would therefore have $v=4$ or 5. However, the identification is quite tentative and for confirmation a rotational analysis of the $d-a$ bands would be required.

c. Other Bands Involving the $a\ ^1\Pi_g$ State

On the plates of $^{14}N_2$, several of the other singlet systems were present. In particular, bands of the $p'\rightarrow a$, $l\rightarrow a$, $k\rightarrow a$, $g\rightarrow a$, and $d'\rightarrow a$ transitions were observed. However, in these cases the analogous bands in $^{15}N_2$ could not be found or identified due to unfavorable shifts with respect to the strong second positive bands or due to blending with other structure. Conversely, some bands were found in $^{15}N_2$ whose analogs in $^{14}N_2$ are apparently not known. In particular, three bands degraded to shorter wavelengths at 2667.9, 2787.9, and 2916.7 Å are fairly obviously the $v-0$, $v-1$, and $v-2$ bands, respectively, of a new progression to the $a\ ^1\Pi_g$ state. The observed ΔG values for the lower state are 1612.0 and 1583.9 cm^{-1}, while those calculated for $a\ ^1\Pi_g$ in $^{15}N_2$ are 1610.8 and 1585.0 cm^{-1}. The bands have a structure rather similar to the $h-a$ and $s-a$ transitions so that the upper state is probably $^1\Sigma_u$. The new state lies at 106 760.7 cm^{-1} above the ground state of $^{15}N_2$; the corresponding energy for $^{14}N_2$ cannot be determined as only one vibrational level of unknown v is observed in the $^{15}N_2$ spectrum.

Several other new bands were found in both $^{14}N_2$ and $^{15}N_2$ but no satisfactory groupings or correlations could be made.

d. Fifth Positive and Related Systems

The lower state of the fifth positive bands,[14,20,21] $x\ ^1\Sigma_g^+\rightarrow a'\ ^1\Sigma_u^-$, is also the lower state of Kaplan's first system,[22,23] $y\ ^1\Pi_g\rightarrow a'\ ^1\Sigma_u^-$. Furthermore, it com-

[19] R. E. Worley, Phys. Rev. 64, 207 (1943). In the earlier note (Ref. 2) on the present results, it was suggested that the progression might not have m as the upper state. This was based on the B value, 1.461 cm^{-1}, given by Lofthus (Ref. 1, p. 25) for the near ultraviolet bands. In the original paper, however, the B value is given as 1.361 cm^{-1} which agrees well with Worley's value, 1.36 cm^{-1}, for the m state. This together with the other evidence shows that the upper state of the two transitions is in fact the same.

[20] A. Van der Ziel, Physica 1, 513 (1934).
[21] A. Lofthus, J. Chem. Phys. 25, 494 (1956).
[22] J. Kaplan, Phys. Rev. 46, 534, 631 (1934); 47, 259 (1935).
[23] A. Lofthus and R. S. Mulliken, J. Chem. Phys. 26, 1010 (1957).

TABLE IX. Kaplan's second system. $y\,^1\Pi_g - w\,^1\Delta_u$.

$v'-v''$	λ(Å) $^{14}N_2$	λ(Å) $^{15}N_2$	$\Delta\nu$ (cm^{-1})
0–4	2741.9	2728.0	186
1–5	2722.0	2709.4	171
0–3	2636.2	2626.6	138
1–4	2619.3	2610.3	132
0–2	2536.6	2530.8	90
1–3	2522.3	2517.2	81
0–0	2354.5	2355.2	−13
1–0	2263.4	2266.9	−69

bines both in emission[24] and absorption[25] with the ground state. All the observations leave no doubt as to the vibrational numbering of the a' state. The original numbering for the upper state x has been modified by Gaydon[14] and the satisfactory intensity distribution within the system indicates that the vibrational analysis is correct. However, as the system was well developed on the present plates, it seemed worthwhile to measure the isotopic shifts as a final check. The data are given in Table VII and the good agreement between the observed and calculated shifts shows in fact that the vibrational analysis is correct.

Kaplan's first system, $y \rightarrow a$, although moderately intense, is less extensive than the fifth positive system and there is consequently more uncertainty about the vibrational numbering of the upper state. Five bands were observed in the $^{15}N_2$ spectrum, the measurements for which are given in Table VIII. It is clear from the magnitudes of the shifts that the vibrational analysis is correct especially as the isotopic displacements of the levels in the lower state are known. The upper state will be considered in some more detail below.

Kaplan's second system involves a transition from from $y\,^1\Pi_g$, the upper state of the first system, to the $w\,^1\Delta_u$ state. In the present work, the results of which are given in Table IX, the second system was better developed than the first and it was therefore used for studying the vibrational structure of the y state. Due to the fact that only two vibrational levels are observed, it is not possible to determine the vibrational constants ω_e and $x\omega_e$. As in the case of single progressions therefore, the isotope shifts calculated for the lower state[26] were combined with the observed band displacements and the lowering of the upper levels were thus computed. The values obtained were 38 and 95 cm^{-1} which show that the vibrational levels involved are $v=0$ and $v=1$, respectivelv. It is also clear that the two progressions belong to the same system. This was the interpretation of Lofthus and Mulliken,[23] in spite of the anomalous behavior of the B values ($B_1 > B_0$).

In principle it should be possible to determine ω_e and $x\omega_e$ for the y state from the isotope shifts and the observed $\Delta G(\frac{1}{2})$ values. Attempts to do this were unsuccessful however. The reason, it is fairly clear, is that a vibrational perturbation is present in the $v=1$ level. Confirmation of this is provided by the fine structure analysis of the $v=1$ level by Lofthus and Mulliken.[23] They found that the rotational levels were considerably displaced from their normal course, the displacement varying smoothly as a function of J. It is this behavior which gives the anomalous B_1 value mentioned above and the effect is one which might well be expected as the result of a vibrational perturbation.

SUMMARY

The vibrational numbering of most of the weaker systems of nitrogen in the region 2000–9000 Å has been established or confirmed. In particular the vibrational analyses of the Herman infrared system, the Herman–Gaydon green system, the $B'-B$ bands, the Goldstein–Kaplan system, the fifth positive and Kaplan's first and second systems are now known with certainty. In the $v=1$ level of the $y\,^1\Pi_g$ state, evidence is found for a vibrational perturbation which can be correlated with the unusual rotational structure of this level.

The progressions in the near ultraviolet to the $a\,^1\Pi_g$ state show a curious behavior. The $m \rightarrow a$ and $d \rightarrow a$ progressions belong fairly definitely to different transitions and in each instance we have a single vibrational level of fairly high v (5 or 6) being excited. A similar effect may be taking place in the $r' \rightarrow a$, $s' \rightarrow a$, and $h \rightarrow a$ progressions, but in this case it is possible, but by no means certain, that the bands belong to a sin gle system. In any event, the behavior is not easy to explain. Because of the range of energies involved and because of the nature of the source, it is difficult to believe that selective excitation in the usual sense is occurring. It seems more likely that the effects are due to processes in the molecule itself and that their interpretation will depend on a fuller understanding of the high energy states of N_2 and the interactions between them.

ACKNOWLEDGMENT

We are grateful to Professor R. S. Mulliken for his interest in this work and for his helpful comments on the manuscript.

[24] M. Ogawa and Y. Tanaka, J. Chem. Phys. **30**, 1354 (1959); **32**, 754 (1960).

[25] P. G. Wilkinson and R. S. Mulliken, J. Chem. Phys. **31**, 674 (1959).

[26] In Ref. 23, the values of ω_e and $x\omega_e$ for the w state were given as 1548 cm^{-1} and 8 cm^{-1}, respectively. These proved unsatisfactory so the data were re-examined and the values $\omega_e = 1557.7$ and $x\omega_e = 11.5$ cm^{-1} derived. With the new constants the vibrational structure of both $^{14}N_2$ and $^{15}N_2$ could be represented within experimental error.

Reprinted from THE JOURNAL OF CHEMICAL PHYSICS, Vol. 42, No. 2, 561-568, 15 January 1965
Printed in U. S. A.

Spectrum and Structure of the He_2 Molecule. I. Characterization of the States Associated with the UAO's $3p\sigma$ and $2s$*

MARSHALL L. GINTER
Laboratory of Molecular Structure and Spectra, Department of Physics, University of Chicago, Chicago, Illinois
(Received 27 August 1964)

The He_2 band systems $3p\sigma$, $^{1,3}\Sigma_g^+ \rightarrow 2s$, $^{1,3}\Sigma_u^+$ are described in detail. The rotational and vibrational constants of the $2s$, $a\ ^3\Sigma_u^+$ and $A\ ^1\Sigma_u^+$ and $3p\sigma$, $c\ ^3\Sigma_g^+$ states are improved and the data for the A and c states extended from $v=1$ to $v=3$ and 4, respectively. The $3p\sigma$ $C\ ^1\Sigma_g^+$ state (identified for the first time) has been characterized through $v=5$. The apparent dissociation energy of the $c\ ^3\Sigma_g^+$ state is found to be $\sim$0.7 eV too high to be consistent with the theoretical dissociation energy of He_2^+. If the D_0 value for He_2^+ is correct, large maxima must be present in the potential curves of a number of electronic states of He_2. Also discussed is the observed and expected behavior of states associated with $np\sigma$ UAO's.

I. INTRODUCTION

WHILE the spectrum of the He_2 molecule was extensively investigated prior to 1935, few spectroscopic additions have appeared since that time. However, recent theoretical work on the Rydberg states of molecules[1] has drawn attention to the incompleteness of the existing experimental data, two of the more obvious deficiencies[2] being a general lack of vibrational information and the almost complete absence of transitions associated with $np\sigma$ MO's. Therefore, in order to remedy these defects and to clarify the behavior of the various molecular states at large internuclear distances, an extensive reinvestigation of the He_2 spectrum has been undertaken.

Although the entire He_2 spectrum between 2800–11 500 Å is under study, this paper is concerned primarily with the transitions $3p\sigma$, $^{1,3}\Sigma_g^+ \rightarrow 2s$, $^{1,3}\Sigma_u^+$ which occur in the region 7000–10 000 Å. For the He_2 molecule, the ground-state configuration[3] $1\sigma_g^2\ 1\sigma_u^2$ is unstable, but many stable states exist for configurations corresponding to the excitation of one of the $1\sigma_u$ electrons to a Rydberg MO, which can be best characterized by a UAO symbol. Transitions among these stable Rydberg electronic states produce a discrete spectrum on the long-wavelength side of about 3000 Å, while transitions to the unstable ground state produce the well known "Hopfield" continuum in the vacuum ultraviolet. The lowest-lying stable electronic states for He_2 are the $a\ ^3\Sigma_u^+$ and $A\ ^1\Sigma_u^+$ states of configuration $1\sigma_g^2 1\sigma_u 2s$. The lowest-lying stable states involving $np\sigma$ UAO's must be of the configuration $1\sigma_g^2 1\sigma_u 3p\sigma$, since the $1\sigma_u$ MO correlates as $r \rightarrow 0$ with the UAO form $2p\sigma$.[4] The only previously observed transitions involving $np\sigma$ MO's were the 0–0 and 1–1 bands[4] for the transitions $3p\sigma$, $c\ ^3\Sigma_g^+ \rightarrow 2s$, $a\ ^3\Sigma_u^+$, and several 0–0 bands[5] corresponding to transitions from higher members of the ns and nd triplet series to $3p\sigma$, $c\ ^3\Sigma_g^+$. In the present work it has been possible to obtain sufficient vibrational structure for the $c \rightarrow a$ transition to determine accurate molecular constants for both the c and a states and to make reasonable estimates of the apparent dissociation energy of the $c\ ^3\Sigma_g^+$ state. In addition, the previously unreported $3p\sigma$, $C\ ^1\Sigma_g^+ \rightarrow 2s$, $A\ ^1\Sigma_u^+$ transition has been observed and both the C and A states characterized.

II. EXPERIMENTAL

The conventional method[6] of producing the emission spectrum of He_2 consists of passing a mildly condensed discharge through flowing He gas at pressures of about 20–40 mm. However, in initial experiments it was found that the visible spectrum could be greatly enhanced by the *complete* removal of trace impurities of H_2 and argon. Thus, sealed discharge tubes filled to pressures of about 40 mm with assayed reagent-grade helium were used in the present work. These tubes have very long lifetimes,[7] while the resulting He_2 emission is completely free of atomic or molecular contaminants

* This work was supported by a grant from the National Science Foundation, NSF GP 28 Research, and by the U.S. Air Force Cambridge Research Laboratories, Office of Aerospace Research, under Contract AF19 (628)-2474. Preliminary discussions were presented at the Regional American Chemical Society meeting in Charlotte, North Carolina (1963), and at the Ohio State Symposium on Molecular Structure and Spectra in Columbus, Ohio (1964).

[1] R. S. Mulliken, J. Am. Chem. Soc. **86**, 3183 (1964); Parts VI and VII of this series (to be published).

[2] G. Herzberg, *Spectra of Diatomic Molecules* (D. Van Nostrand Company Inc., New York, 1950), 2nd ed., Vol. 1.

[3] United-atom orbital (UAO) symbols are used throughout this paper, since the Rydberg MO's (molecular orbitals) for He_2 in the region around r_e would correspond fairly closely to the united atom form. The He_2^+ core would more closely correspond to the LCAO form $\sigma_g 1s^2 \sigma_u 1s$. Since no confusion results, core symbols are often omitted and a single UAO symbol used to designate a Rydberg MO.

[4] W. F. Meggers and G. H. Dieke, J. Res. Natl. Bur. Std. **9**, 121 (1932).

[5] G. H. Dieke, S. Imanishi, and T. Takamine, Z. Physik **57**, 305 (1929).

[6] For an excellent discussion of the "conventional" procedures and apparatus, see R. E. Huffman, Y. Tanaka, and J. C. Larrabee, Appl. Opt. **2**, 617 (1963). While Huffman *et al.* describe optimization of the He_2 continuum in the 600–1100-Å region, similar conditions seem to apply to the visible He_2 spectrum obtained from discharge tubes using flowing He gas.

[7] One tube at least has been used over 600 h without any noticeable change in its spectral properties. In general, the tubes are Π-shaped, with tungsten electrodes sealed into their side arms. They are cleaned and filled by the same general procedures employed to make sealed Xe and Kr lamps for use in the vacuum ultraviolet; cf. P. G. Wilkinson and Y. Tanaka, J. Opt. Soc. **45**, 344 (1955).

and is at least several times more intense than the emission from similar tubes utilizing conventional flowing procedures. An air-blow spark gap in series with a 15 000-V transformer, together with a capacitance of about 1500 $\mu\mu$F supplied the condensed, disruptive discharge used in excitation of the spectrum, with the power input to the transformer being generally about 200 W.

The 7000–11 000-Å region of the spectrum was photographed in the first orders of two spectrographs: a 30-ft Paschen circle and a 3.4-m Ebert, with reciprocal dispersions of approximately 0.9 and 2.0 Å/mm, respectively. For spectrograms taken on the 30-ft circle, exposure times on hypersensitized $I-N$ and $I-M$ plates ranged from a few hours for the stronger bands to as much as 50 h for the weakest. Using the Ebert spectrograph, comparable exposures were obtained in about one-fourth the time required for the circle. The effective resolving power ranged from about 100 000 for the shorter exposures to about 70 000 for the longest, the higher figure being attained only on circle plates. Iron arc lines—superimposed before, during, and after the exposures—were used as standards, and measurements were made by the superposition of optical density profiles using a Grant spectrum line measuring comparator. In almost all cases, the spectrum lines were measured on three different circle plates and one Ebert plate, and the resulting wavenumbers averaged. In some regions, the maximum deviations in the "absolute" line positions determined from the four sets of data reached values as high as ± 0.03 cm^{-1}. However, the agreement of the relative positions of unblended lines was generally somewhat better, being in most instances within about ± 0.01 cm^{-1}.

III. ANALYSIS OF THE SPECTRUM AND EVALUATION OF MOLECULAR CONSTANTS

In any molecular spectrum which has its branch lines widely separated from one another, rotational analysis must precede everything but the most tentative electronic-state and vibrational-level estimates. In the case of $^4He_2$ this is particularly true, since ^{4}He has a nuclear spin of zero which requires alternate lines to be missing. Also, it should be noted that the triplet splitting for most of the electronic states of He_2 is too small to be resolved, the only known exception being the partial resolution of the splitting for the $2p\pi$, $^3\Pi_g$ state.

The wavenumbers of the lines of nine bands of the transition $3p\sigma$, $c\ ^3\Sigma_g^+ \rightarrow 2s$, $a\ ^3\Sigma_u^+$ and eleven bands of the transition $3p\sigma$, $C\ ^1\Sigma_g^+ \rightarrow 2s$, $A\ ^1\Sigma_u^+$ are given in Tables I and II. Since the triplet splitting is not resolved for the $c \rightarrow a$ transition, the triplet states necessarily must be treated in the same manner as the singlet states. Thus, the effective rotational constants for all bands were obtained by fitting the data in Tables I and II to the relation[7]

$$\Delta_2 F_v(N) = \sum_{i=0}^{2} a_i (N+\tfrac{1}{2})^{2i+1}, \tag{1}$$

where

$$a_0 = (4B_v - 6D_v + \tfrac{27}{8}H_v),$$

$$a_1 = -(8D_v - 28H_v),$$

and

$$a_2 = +12H_v. \tag{2}$$

The B_v, D_v, and H_v constants in (2) are the first three coefficients of the expansion of the rotational terms in the power series

$$F_v(N) = B_v N(N+1) - D_v N^2(N+1)^2 + H_v N^3(N+1)^3 + \cdots, \tag{3}$$

and the lower- and upper-state $\Delta_2 F_v(N)$'s are given by $R(N-1)-P(N+1)$ and $R(N)-P(N)$, respectively. In all cases, the a_i values were determined both by the method of least squares and by standard graphical procedures.[7] Using the method of least squares, one finds that the values of the constants in Eq. (1) are somewhat dependent on the total number of $\Delta_2 F_v(N)$'s used in their determination (i.e., the a_i's change slightly as one successively deletes from the calculations the $\Delta_2 F_v(N)$'s corresponding to the highest N values). As expected, this effect is small for a_0, but can be appreciable for a_1 and a_2. In each case, the various a_i values determined by different least-squares fits of the data were averaged with the results of the graphical method (the a_0 and a_1 being determined by intercept procedures).[8] The final values of B_v, D_v, and H_v obtained from (2) are listed in Table III.[9]

Band origins $\nu(v', v'')$ were obtained by fitting the data in Tables I and II to the relation

$$R(N)+P(N) = \sum_{i=0}^{2} b_i [N(N+1)]^i, \tag{4}$$

both by graphical methods[7] and by least squares, where

$$b_0 = 2\nu_{(v',v'')} + 2B_{v'} + 4D_{v'}. \tag{5}$$

Band origins obtained from the two methods of fitting (4) agreed to ± 0.01 cm^{-1} and fell into three sequences corresponding to $\Delta v = 0$, $+1$, and $+2$ as shown in Tables IV and V. It should be noted that the peculiar distribution of these tables is due to the rapid loss in photographic plate sensitivity to the long-wavelength side of about 8900 Å (11 200 cm^{-1}). This feature also accounts for the many $P(N)$ branches in Tables I and II which are much shorter than their associated $R(N)$ branches.

[7] F. H. Crawford and T. Jorgensen, Phys. Rev. 47, 358 (1935).

[8] As a further check, ΔB_v, ΔD_v, and ΔH_v values were calculated using the b_1, b_2, and b_3 coefficients obtained from the least-squares determinations of the band origins [Eq. (4)]. These resulting values were in agreement with the constants listed in Table III.

TABLE I. Wavenumbers of the bands of the $c\,^3\Sigma_g^+ \rightarrow a\,^3\Sigma_u^+$ transition of He_2.[a,b]

	(0–0)[c] $\nu_{(0-0)} = 10\,889.48$		(1–0) $\nu_{(1-0)} = 12\,369.50$		(1–1) $\nu_{(1-1)} = 10\,637.37$	
N	$R(N)$	$P(N)$	$R(N)$	$P(N)$	$R(N)$	$P(N)$
1	10 915.43	10 874.31	12 393.64	12 354.34	10 662.00	10 622.67
3	935.34	839.61	409.41	317.85	680.19	588.58
5	949.18	799.17	416.69	273.28	691.79	548.31
7	956.84	753.14	415.36	220.64	696.71	501.97
9	(958.17)	701.61	405.24	160.10	694.78	449.61
11	953.13	644.64	386.20	091.68	685.88	391.31
13	941.58	582.40	358.06	12 015.46	669.83	327.18
15	923.40	514.92	320.60	11 931.40	646.42	257.18
17	898.47	442.28	273.59	839.49	615.42	181.35
19	(866.66)	364.54	216.68	739.68		099.57
21	827.75	281.76	149.98[d]	631.80		
23	781.58	193.89	12 071.82	516.12[d]		
25	727.90	100.86	11 982.70	391.10		
27	666.37		881.48	257.40		
29	596.52		767.05	113.99		
31	517.86		638.51			

	(2–0) $\nu_{(2-0)} = 13\,741.22 \pm 0.06$		(2–1) $\nu_{(2-1)} = 12\,009.08$		(2–2) $\nu_{(2-2)} = 10\,354.74$	
N	$R(N)$	$P(N)$	$R(N)$	$P(N)$	$R(N)$	$P(N)$
1	(13 763.47)[e]	f	12 031.73	11 994.38	10 377.85	10 340.58
3	(774.52)	13 687.62	045.22	958.29	393.85	306.96
5	(774.52)	638.33	049.50	913.39	402.55	266.50
7	(763.47)[e]	(578.49)	044.40	859.70	403.88	219.22
9	f	507.78	029.51	797.26	397.46	165.27
11	705.19	426.49	12 004.79	726.08	383.20	104.50
13	658.17	334.41	11 969.86	646.14		
15	598.60	231.48	924.37	(557.23)		
17	525.98	13 117.47	867.79	459.31		
19	439.72	12 992.08	799.55	351.94		
21	338.82	854.81	718.76	234.76		
23	221.71	704.96	623.76	107.06		
25		540.99				

	(3–1) $\nu_{(3-1)} = 13\,256.64$		(3–2) $\nu_{(3-2)} = 11\,602.29$		(4–2) $\nu_{(4-2)} = 12\,698.13$	
N	$R(N)$	$P(N)$	$R(N)$	$P(N)$	$R(N)$	$P(N)$
1	13 276.95	13 241.95	(11 623.06)	11 588.20	12 715.94	12 683.93
3	285.02	203.53	(633.67)	552.14	719.44	645.00
5	280.64	153.17	(633.67)	506.25	708.40	592.10
7	263.56	090.83	(623.06)	(450.31)	682.12	525.02
9	233.38	13 016.46	(601.29)	384.42	639.98	443.52
11	189.65	12 929.95	568.03	308.36	580.82	347.01
13	131.79	830.96	522.64	221.83	503.04	234.62
15	13 058.97	719.13	464.39	124.53		104.98
17	12 970.19	593.86	392.40	016.13		
19	863.82	454.32				
21	(737.67)	299.03				
23		12 125.94				

[a] Parentheses denote blended lines.

[b] The estimated error of all band origin determinations, with the exception of the (2–0) band, is $\lesssim\sim\pm 0.02$ cm^{-1}.

[c] This band was reported in part by Meggers and Dieke (see Footnote 4). Because of the much higher dispersion and resolution of the instruments used in the present work, the values reported below may be more accurate than the previous data.

[d] Perturbed lines.

[e] Strongly overlapped by R_2 of $H\,^1\Sigma_u^+ - C\,^1\Sigma_g^+$ (0–0).

[f] Completely obscured by the 7281-Å line of He I.

TABLE II. Wavenumbers of the bands of the $C\,^1\Sigma_g^+ \rightarrow A\,^1\Sigma_u^+$ transition of He_2.[a,b]

	(0–0) $\nu_{(0-0)} = 10\,945.50$		(1–1) $\nu_{(1-1)} = 10\,726.57$		(1–0) $\nu_{(1-0)} = 12\,517.32$	
N	$R(N)$	$P(N)$	$R(N)$	$P(N)$	$R(N)$	$P(N)$
1	10 971.82	10 930.17	10 751.85	(10 712.00)	12 542.16	12 501.98
3	(10 992.25)[c]	895.20	771.06	677.48	559.13	465.52
5	11 006.70	(854.69)[d]	784.13	637.44	568.15	421.46
7	015.10	808.48	790.92	591.71	569.12	369.92
9	017.40	757.00	791.39	540.41	561.98	311.00
11	013.50	700.28	785.47	483.63	546.63	244.83
13	11 003.38	638.42	773.07	421.54	523.02	171.51
15	10 987.01	571.55	754.13	354.25	491.07	091.20
17	964.30	499.88	728.60	(281.76)	450.69	12 003.93
19	(935.34)	423.42			401.81	11 909.85
21	899.75	342.40			344.34	809.03
23		256.90			278.18	701.56
25					203.18	587.31
27					119.15	(466.31)
29					12 025.84	338.86
31					11 922.99	

	(2–0) $\nu_{(2-0)} = 14\,006.61 \pm 0.06$		(2–1) $\nu_{(2-1)} = 12\,215.80$		(2–2) $\nu_{(2-2)} = 10\,496.13 \pm 0.06$	
N	$R(N)$	$P(N)$	$R(N)$	$P(N)$	$R(N)$	$P(N)$
1	14 029.8[e]		12 239.55	12 200.89	10 520.35	
3	043.34	(13 953.66)	255.13	165.15	538.23	10 448.3
5	(046.59)	905.64	262.48	121.49	549.68	408.66
7	039.74	848.34	261.48	070.11	554.62	363.20
9	14 022.71	781.58	252.06	12 010.99	552.96	311.86
11	13 995.31	705.54	234.10	11 944.32	544.52	254.7
13	957.56	e	207.48	870.20	529.33	
15	909.07	525.73	(172.13)	788.65	507.18	
17	850.06	421.94	127.86	(699.79)		
19	780.13	309.19	074.60	603.64		
21	699.13	187.31	12 012.13	500.23		
23	607.03	13 056.31	(11 940.20)	389.58		
25		12 916.08	858.66	271.52		

	(3–1) $\nu_{(3-1)} = 13\,617.93$		(3–2) $\nu_{(3-2)} = 11\,898.22$		(4–2) $\nu_{(4-2)} = 13\,206.39$	
N	$R(N)$	$P(N)$	$R(N)$	$P(N)$	$R(N)$	$P(N)$
1	13 640.0[e]	13 602.9[e]	11 920.78	11 883.78	13 227.14	13 191.95
3	651.78	565.63	934.78	848.66	236.94	155.03
5	653.05	518.14	(940.20)	805.27	235.71	107.42
7	643.79	460.64	936.79	753.68	223.23	13 049.20
9	623.74	393.24	(924.37)	694.02	199.32	12 980.44
11	592.87	316.00	903.24	626.37	163.82	901.17
13	550.98	228.95	872.76	550.74	116.42	811.33
15	497.89	132.14	832.93	467.17	13 056.86	710.83
17	433.41	13 025.58	783.53	375.70	12 984.71	599.61
19	357.22	12 909.18	724.26	(276.28)	899.45	477.44
21	269.02	782.88	654.86	168.74	800.50	343.90
23	168.37	646.44	574.88			198.56
25	054.77	499.59	483.79			

TABLE II (*Continued*)

	(4–3) $\nu_{(4-3)}=11\ 558.42$		(5–3) $\nu_{(5-3)}=12\ 761.75$	
N	$R(N)$	$P(N)$	$R(N)$	$P(N)$
1	11 579.61	11 544.44		
3	591.78	509.83	12 788.34	12 711.17
5	594.70	(466.39)	783.81	663.04
7	588.13	(414.22)[f]	766.94	603.32
9	572.25	353.38	(737.67)	532.04
11	546.49	283.84	695.50	449.20
13	510.78	205.64	(639.98)	(354.85)
15	464.78	118.76	570.50	(247.84)
17			486.43	128.70

[a] Parentheses denote blended lines.
[b] The estimated error of all band origin determinations, with the exception of the (2-0) and (2-2) bands, is $\lesssim\sim\pm0.0?$ cm^{-1}.
[c] Overlapped by P_{16} of $f\,^3\Pi_u-c\,^3\Sigma_g^+$ (0-0).
[d] Overlapped by Q_8, P_{16} of $f\,^3\Pi_u-c\,^3\Sigma_g^+$ (0-0).
[e] Completely obscured by R_8, $H\,^1\Sigma_u^+-C\,^1\Sigma_g^+$ (0-0).
[f] Overlapped by P_8 of $f\,^3\Delta_u-c\,^3\Sigma_g^+$ (1-1).

The B_v and $\Delta G_{(v+\frac{1}{2})}$ data in Tables III–V were fitted by least squares to the usual $(v+\frac{1}{2})$ expansions[2] of the vibrational and rotational energies. For the $c\,^3\Sigma_g^+$ and $C\,^1\Sigma_g^+$ states, the *values* of these coefficients depended somewhat on the *number* of terms used in the expansions—a phenomenon occurring fairly frequently in the excited electronic states of light molecules (i.e., H_2, hydrides, etc.). For the states of He_2 in question, the deviations are relatively small and generally result from a rather rapid and monotonic decrease in the various effective constants. The values reported in Table VI correspond to the minimum set which reproduces the experimental data within the *estimated* errors.

IV. DISCUSSION

Since all of the stable electronic states of He_2 are Rydberg states, it is useful to preface this discussion

TABLE III. Rotational constants (cm^{-1}).[a]

	$a\,^3\Sigma_u^+$	$A\,^1\Sigma_u^+$	$c\,^3\Sigma_g^+$	$C\,^1\Sigma_g^+$
B_0	$7.586_2\pm0.001_0$	$7.671_0\pm0.001_0$	$6.852_0\pm0.002_0$	$6.945_2\pm0.001_2$
B_1	$7.348_7\pm0.001_5$	$7.446_4\pm0.001_0$	$6.556_4\pm0.001_0$	$6.699_8\pm0.001_0$
B_2	$7.098_6\pm0.001_8$	$7.218_0\pm0.001_5$	$6.224_1\pm0.001_3$	$6.441_6\pm0.001_8$
B_3		$6.985_5\pm0.002_1$	$5.837_0\pm0.001_5$	$6.166_7\pm0.001_5$
B_4			$5.340_0\pm0.001_0$	$5.867_6\pm0.001_5$
B_5				$5.530_0\pm0.001_5$
$D_0\times10^4$	$5.5_0\pm0.05$	5.43 ± 0.02	5.56 ± 0.02	$5.13\pm0.02_5$
$D_1\times10^4$	$5.6_1\pm0.04$	5.40 ± 0.03	5.76 ± 0.02	5.24 ± 0.01
$D_2\times10^4$	5.5 ± 0.1	5.41 ± 0.03	6.11 ± 0.08	5.32 ± 0.02
$D_3\times10^4$		5.40 ± 0.06	6.98 ± 0.05	5.56 ± 0.02
$D_4\times10^4$			8.57 ± 0.04	$5.8^3\pm0.03$
$D_5\times10^4$				6.60 ± 0.05
$H_0\times10^8$	2.5 ± 0.4	3.0 ± 0.1	$1.3_2\pm0.1_6$	$1.7_2\pm0.2$
$H_1\times10^8$	2.2 ± 0.5	2.5 ± 0.3	$-0.4_8\pm0.2_0$	$1.6_2\pm0.1_5$
$H_2\times10^8$		2.3 ± 0.4	-5.3 ± 0.9	1.0 ± 0.3
$H_3\times10^8$			-13.0 ± 1.5[b]	$0.0\pm0.1_5$
$H_4\times10^8$			-54.9 ± 2.0[b]	$-2.4_5\pm0.3$
$H_5\times10^8$				-6.2 ± 1.0

[a] The "errors" listed in this table are the maximum deviations from the average of the constants determined by different fitting procedures (see text). As such, they are a measure of reproducibility and internal consistency of the methods employed and probably give reasonable estimates of the *over-all* errors inherent in the molecular constant determinations.
[b] The *highest* rotational levels observed for these vibrational states are not fitted accurately by a three-coefficient expansion of $F_v(N)$. The need for a higher-order constant is evident in both the graphical and least-squares procedures, but the probable reasons for this deviation (see text) are such as to make its inclusion unwarranted. The H_v values reported here are determined after excluding the data for the highest N values.

TABLE IV. Deslandres table for the band origins (cm^{-1}) of the transition $3p\sigma$, $c\ ^3\Sigma_g^+ \rightarrow 2s$, $a\ ^3\Sigma_u^+$ of He_2.

	v''				
v'	0		1		2
0	10 889.48 (1480.02)				
1	12 369.50 (1371.72)	(1732.13)	10 637.37 (1371.71)		
2	13 741.22	(1732.14)	12 009.08 (1247.56)	(1654.34)	10 354.74 (1247.55)
3			13 256.64	(1654.35)	11 602.29 (1095.84)
4					12 698.13

TABLE V. Deslandres table for the band origins (cm^{-1}) of the transition $3p\sigma$, $C\ ^1\Sigma_g^+ \rightarrow 2s$, $A\ ^1\Sigma_u^+$ of He_2.

	v''							
v'	0		1		2		3	
0	10 945.50 (1571.82)							
1	12 517.32 (1489.29)	(1790.75)	10 726.57 (1489.23)					
2	14 006.61	(1790.81)	12 215.80 (1402.13)	(1719.67)	10 496.13 (1402.09)			
3			13 617.93	(1719.71)	11 898.22 (1308.17)			
4					13 206.39	(1647.97)	11 558.42 (1203.33)	
5							12 761.75	

TABLE VI. Molecular constants (cm^{-1}).

State	$a\ ^3\Sigma_u^+$	$A\ ^1\Sigma_u^+$	$c\ ^3\Sigma_g^{+a}$	$C\ ^1\Sigma_g^{+b}$
T_e	a	A	$a+11\,005.8_9$	$A+11\,050.8_7$
ω_e	1809.91	1861.27	1583.85	1653.43
$x\omega_e$	38.8_9	35.0_7	52.7_4	41.0_4
$y\omega_e$		-0.105_6	-1.256_6	0.354_9
$z\omega_e$			-0.487_6	-0.131_6
B_e	7.710_3	7.787_2	7.004_9	7.067_8
α_e	0.243_8	0.228_6	0.310_6	0.244_8
$\gamma_1 \times 10^1$			0.162_9	0.0117_9
$\gamma_2 \times 10^1$			-0.065_6	-0.0135_6
r_e(Å)	1.045_9	1.039_9	1.096_4	1.091_6

[a] The higher-order vibrational constants for this state seem somewhat anomalous. The three-constant least-squares fit, while not within the experimental errors (standard deviation=2.6) is more regular, and shows the trend more graphically: $G(v+\frac{1}{2}) = 1564.59(v+\frac{1}{2}) - 36.7_0(v+\frac{1}{2})^2 - 3.61_{28}(v+\frac{1}{2})^3$.

[b] The higher-order rotational constants for this state seem somewhat anomalous. While high-order constants are of questionable importance, such behavior probably reflects a slight "overfit" of the experimental data since the calculated standard deviation for this case is somewhat less than the estimated error. The next lower-order fit (standard deviation=0.006) is given by $B_v = 7.051_7 - 0.215_9(v+\frac{1}{2}) - 0.011_{82}(v+\frac{1}{2})^2$.

with a brief listing of several properties[10] of Rydberg states in general. For Rydberg states, (1) at low n, the bonding properties of the core—in this case, of He_2^+—are somewhat modified by the presence of the Rydberg electron, but to a rapidly decreasing extent as n increases; (2) the observed molecular constants (such as $\Delta G_{v+\frac{1}{2}}$, B_v, etc.) rather rapidly approach those of the core as n increases; and (3) penetration into the core occurs for Rydberg MO's when the core contains one or more MO's of the same species[11] (i.e., the Rydberg series has one or more "initial members" in the core). Further, the electronic states of He_2 obey the usual Rydberg relation for neutral molecules:

$$T = R/n^{*2} = R/(n-\delta)^2, \qquad (6)$$

where δ is the term defect, R is the Rydberg constant, n is the principal quantum number for the UAO state in question, and T is the term value.

Because of the general lack of vibrational data for He_2, consistent values of T usually have been obtained by fitting the convergence of the (0–0) bands of the previously observed Rydberg series.[2] Until this defect can be remedied, it is more practical to consider T_0 values (the energies necessary for the removal of the Rydberg electron from the $v=0$ level of the Rydberg state to that of He_2^+) when using Eq. (6), and the resulting n^* and δ values must be interpreted accordingly.

With the above statements in mind, there are several features of the behavior of the states associated with the $np\sigma$ Rydberg series which should be emphasized. Using the T_0 values for the $2s$ singlet and triplet states given by Herzberg,[2] the $\nu_{(0-0)}$'s from Tables IV and V and Eq. (6), one calculates $n^*=2.164$ and 2.285 for $3p\sigma$, $c\ ^3\Sigma_g^+$ and $3p\sigma$, $C\ ^1\Sigma_g^+$, respectively, where the large values of δ, 0.836 and 0.715, are of particular note.[11] Consideration of the variation of n^* values[1] with n for the states associated with the known $np\sigma$ series of H_2 would lead one to estimate $n^* \cong 3.24$ and 3.30 for the $4p\sigma$, $^3\Sigma_g^+$ and $^1\Sigma_g^+$ states, respectively, so that one would predict that these unreported states lie 23 650 and 24 230 cm^{-1} above the $2s$, $a\ ^3\Sigma_u^+$ state. Further, one sees from Tables IV–VI that the $\Delta G_{\frac{1}{2}}$ and B_e values for the $3p\sigma$, $^{1,3}\Sigma_g^+$ states lie slightly *below* the corresponding values estimated for the ground state of He_2^+, which are 1627.2 and 7.22 cm^{-1}, respectively.[2] Thus, for low n, the $np\sigma$ Rydberg electron–core interaction seems to produce resultant electronic states which are slightly less bonding than the He_2^+ core itself. This effect should decrease rapidly with increasing n, so that the $\Delta G_{\frac{1}{2}}$ and B_e values for higher members of the $np\sigma$ series should *increase* from those of the $3p\sigma$ UAO and rapidly approach their asymptotic He_2^+ values. Similar behavior is already well known for the ns and $np\pi$ series, except that the observed $\Delta G_{\frac{1}{2}}$ and B_e values decrease with increasing n and approach the asymptotic He_2^+ values from above, the Rydberg electron-core interaction for these series resulting in Rydberg states which are slightly more bonding than the He_2^+ core.

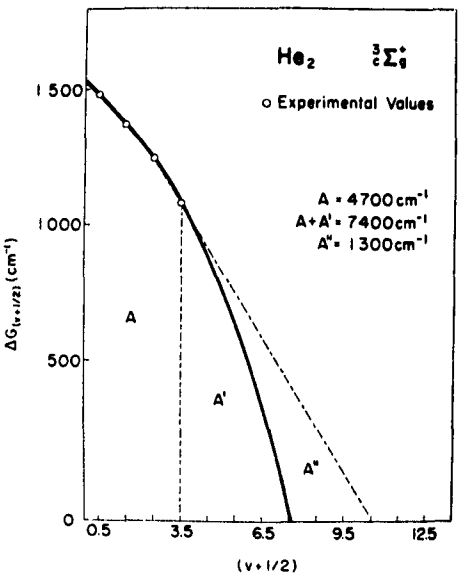

FIG. 1. Birge–Sponer extrapolation for the $3p\sigma$, $c\ ^3\Sigma_g^+$ state of He_2.

Another result of the previous lack of vibrational data was an inability to obtain even a reasonably accurate value for the dissociation energy of He_2 by direct means. Estimates[2] of D_0 from the relation $\omega_0^2/4x\omega_0$ yield $D_0 \cong 2.6$ eV for the $a\ ^3\Sigma_u^+$ state, but such estimates are at best only very approximate. In addition, it should be noted that there has been a major objection to a value as high as 2.6 eV, since this requires that the dissociation energy for He_2^+ be about 3.1 eV, which is 1 eV higher than the currently accepted theoretical values.[12] With the more extended vibrational data given in Tables IV and V, one can attempt better estimates. At present, the most advantageous case seems to be that of the $c\ ^3\Sigma_g^+$ state, the Birge–Sponer extrapolation for this state being reasonably short, as can be seen in Fig. 1. In this figure, the "most likely" extrapolation yields an apparent dissociation energy for the $c\ ^3\Sigma_g^+$ state of about 7400 cm^{-1}. The energy given by Area A'', the difference between a linear extrapolation of the last two experimental values and the "most likely" curve, can be used as a reasonable estimate of the error, while Area A corresponds to the energy of the last observed vibrational level. Since the $a\ ^3\Sigma_u^+$ state should dissociate into the same atomic terms as the $c\ ^3\Sigma_g^+$ state[1] (i.e., $1s2s$, $^3S+1s^2$, ^1S), one obtains from Fig. 1 and Table VI, an *apparent* dis-

[10] For further discussion of this material, see Refs. 1 and 2.

[11] In He_2, the $np\sigma$ and ns series have one "initial" member, $2p\sigma$ and $1s$, respectively, in the core and, therefore, will be penetrating. However, the $np\pi$ series has no core "ancestor" and should be nonpenetrating. The large term defect observed for the states associated with the $3p\sigma$ orbital is attributable in part to its penetrating properties (Ref. 1).

[12] P. C. Reagan, J. C. Browne, and F. A. Matsen, J. Am. Chem. Soc. 84, 2650 (1962). See also Ref. 13, Footnote 9.

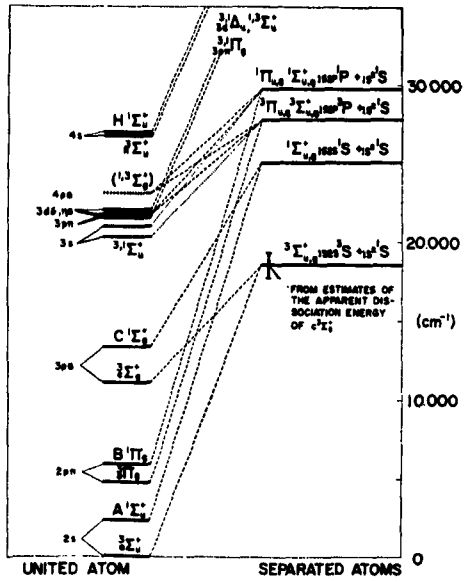

FIG. 2. Dissociation scheme for the lower electronic states of He_2. The relative positions of the $v=0$ levels of the lower electronic states of He_2 are taken from Table 39, Ref. 2, and from the present work. The apparent dissociation energy of the $c\,^3\Sigma_g^+$ state has been employed in estimating the relative positions of the molecular states and atomic term limits, and the correlations made assuming the validity of the noncrossing rule.

sociation energy of $2.2_6 \pm 0.1_8$ eV for the $a\,^3\Sigma_u^+$ state. This is still about 0.7 eV above a value necessary for agreement with the theoretical calculations on He_2^+; however, even if one uses the energy corresponding to the last observed vibrational level in Fig. 1 (which certainly must be above the lowest limit possible since rotational levels are known to $N \geq 13$ in $v=4$), the resulting D_0 for the $a\,^3\Sigma_u^+$ state would be only about 0.3 eV lower than the "best value." Thus, one is led to the conclusion that either the theoretical dissociation energy for He_2^+ is too low or the potential curves for the states associated with the $3p\sigma$ UAO exhibit rather high and broad potential maxima.

Because of the possibility of peculiarities in the potential energy curves for the $c\,^3\Sigma_g^+$ state, considerable effort has been made (1) to extend the existing vibrational data and (2) to extend the rotational analysis in the hope of unambiguously identifying predissociation phenomena. As yet, neither effort has been successful enough to warrant discussion here. It should be noted, however, that the lack of success in extension of the vibrational analysis is somewhat striking since the *weaker* transition $C\,^1\Sigma_g^+ \rightarrow A\,^1\Sigma_u^+$ has been extended to $v'=5$ (compare Tables IV and V), and this feature together with the behavior of the observed molecular constants suggests rather strongly that the $c\,^3\Sigma_g^+$ state predissociates by $v' \cong 5$ or 6.

Using the *apparent* dissociation limit of the $c\,^3\Sigma_g^+$ to fix the $1s2p$, $^3S+1s^2$, ^1S term limit, one can estimate the positions of the molecular states of He_2 relative to the known atomic terms, as shown in Fig. 2. As is obvious from Fig. 2, *all* of the excited states of He_2 should be intrinsically stable. This feature should remain even in the event that a rather high maximum exists in the $3p\sigma$, $^3\Sigma_g^+$ potential curve, since one would expect a similar maximum in the $4p\sigma$, $^3\Sigma_g^+$ potential curve.[12]

In a recent paper,[13] Mulliken has postulated the existence of rather high and broad potential maxima in a number of electronic states of He_2; in particular, the states associated with the $3p\sigma$, $3d\sigma$, $3d\pi$, and $4f\sigma$ Rydberg MO's (as well as their higher n-value homologs). Such considerations are compatible with the data presented here, although, as pointed out above, the experimental results would also be consistent with a higher value of D_0 for He_2^+ than is accepted currently. It is interesting to note, however, that present studies of transitions involving the $3d$ complex (i.e., especially the triplet members $3d\sigma$, $^3\Sigma_u^+$, $3d\pi$, $^3\Pi_u$, and $3d\delta$, $^3\Delta_u$) show that these states are *more* stable than expected from Fig. 2. In particular, the $3d\pi$, $^3\Pi_u$ state has vibrational levels which are quite stable at least through $v=3$, a level which is approximately *equal* to the energy of the $1s2p$, $^3P+1s^2$, ^1S term limit, if the $D_0(a\,^3\Sigma_u^+)$ estimated from the $c\,^3\Sigma_g^+$ state is valid, and which would be considerably *above* this limit, if one uses the current D_0 value for He_2^+ as a basis. In fact, the general behavior of the $3d\pi$, $^3\Pi_u$ state is that of a state tending to dissociate into a much higher term limit than is indicated in Fig. 2. Such a situation requires that either there is a high maximum (intrinsic or produced by avoided crossing) in the potential curve for this state or there must be a violation of the avoided crossing rule. Presently, the *experimental* evidence cannot distinguish between the two alternatives, although the theoretical considerations[13] make the former seem more plausible.

ACKNOWLEDGMENTS

The author is indebted to Professor R. S. Mulliken for suggesting the problem and for many stimulating discussions during its progress, to Dr. P. K. Carroll for many helpful comments and suggestions, and to Professor K. K. Innes for the use of his laboratory during several phases of the experimental work. Also, the assistance of Mrs. D. S. Ginter, Mrs. J. Maxwell, and Mr. T. Kinyon with measurements and calculations is gratefully acknowledged.

[12] R. S. Mulliken, "Rare-Gas Molecule Electronic States Noncrossing Rule and Recombination of Electrons with Rare-Gas Ions," Phys. Rev., to be published. Recently, J. C. Browne has calculated the theoretical potential curves for the $3p\sigma$, $^3\Sigma_g^+$ state and finds that this state has a potential maximum of the order of 0.8–0.9 eV, while the $3d\pi$, $^3\Pi_u$ state has a potential maximum of about 0.6 eV (private communications from J. C. Browne).

DISTRIBUTION LIST°

A. GOVERNMENT DISTRIBUTION

1. Department of Defense

Defense Documentation Center for
Scientific and Technical Information
Cameron Station Building
Alexandria, Virginia 22314 (20 copies)

Office of the Director of Defense
Defense Research and Engineering
Information Office, Library Branch
Pentagon Building
Washington, D. C. 20301 (2 copies)

2. Department of the Army

Chief of Ordnance, Hqs.
Department of the Army
Washington 25, D. C.
Attn: ORDGU-SE
For Transmittal to Canadian Joint Staff
2001 Connecticut Avenue
Washington 25, D. C.

Chief of Research and Development
Department of the Army
Washington 25, D. C.
Attn: Research Division

Chief of Ordnance, Hqs.
Department of the Army
Washington 25, D. C.
Attn: ORDTB-PS (2 copies)

Commanding General
Aberdeen Proving Ground
Maryland
Attn: BRL, Tech. Info. Division

Commanding General
Army Rocket and Guided Missile Agency
Redstone Arsenal, Alabama
Attn: ORDDW-MR

Commanding General
Frankfort Arsenal
Bridge-Tacont Streets
Philadelphia 37, Pennsylvania

Commanding General
Ordnance Weapons Command
Rock Island, Illinois
Attn: Research Branch

Commanding General, Hqs.
White Sands Missile Range
New Mexico
Attn: ORDS-OM-TL

Commanding General
U. S. Army Ordnance Missile
Redstone Arsenal, Alabama

Commanding Officer
U. S. Army Research Office
Box CM, Duke Station (2 copies)
Durham, North Carolina 27706

Commanding Officer
Chicago Ordnance District
632 So. Wabash Avenue
Chicago, Illinois
Attn: Mr. Morris Winer (2 copies)

Commanding Officer
Detroit Arsenal
Center Line, Michigan

Commanding Officer
Diamond Ordnance Fuse Laboratories
Washington 25, D. C.
Attn: Tech. Res. Sec. ORDTL-06.33

Commanding Officer
Ordnance Material Research Office
Watertown Arsenal
Watertown 72, Massachusetts

Commanding Officer
Picatinny Arsenal
Dover, New Jersey
Attn: Feltman Res. and Engr. Lab.

Commanding Officer
Rock Island Arsenal
Rock Island, Illinois
Attn: R and D Division

Commanding Officer
Springfield Armory
Springfield 1, Massachusetts

Commanding Officer
Watertown Arsenal
Watertown 72, Massachusetts
Attn: W. A. Laboratories

Commanding Officer
Watervliet Arsenal
Watervliet, New York

Director, U. S. Army Engr. Research
and Development Laboratories
Fort Belvoir, Virginia
Attn: Technical Documents Center

Information Processing Officer
U. S. Army Research Office (Durham)
Box CM, Duke Station
Durham, North Carolina 27706 (20 copies)

IRIA
University of Michigan
Willow Run Research Center
Ypsilanti, Michigan
Attn: Librarian

Office of the Chief Signal Officer
Engineering and Technical Division
Engineering Control Branch
Room 2B273, Pentagon Building
Washington 25, D. C.

Technical Reports Library
SCEL, Evans Signal Corps Lab.
Belmar, New Jersey

U. S. Army Chemical Warfare Labs.
Technical Library
Building 330, Room 200
Baltimore, Maryland
Attn: Librarian

U. S. Army R. and D. Liaison
USAREUR, Northern Area Command
APO 757
New York, New York

U. S. Army Signal Engineering Lab.
Fort Monmouth, New Jersey 07703
Attn: Technical Information Officer
(2 copies)

Watertown Arsenal
Watertown 72, Massachusetts
Attn: Rodman Laboratories

Watertown Arsenal
Watertown 72, Massachusetts
Attn: Dr. J. L. Martin

3. Department of the Navy

Chief, Bureau of Ships
Technical Library
Navy Department
Washington, D. C. 20360

Chief, Bureau of Naval Weapons
Department of the Navy
Washington, D. C. 20360
Attn: J. A. Mery, RREN-42

Chief of Naval Research
Office of Naval Research
Washington, D. C. 20360 (3 copies)
Attn: Physics Branch (421)

Commanding Officer
Office of Naval Research Branch Office
1030 East Green Street
Pasadena, California 91101

Commanding Officer
Office of Naval Research Branch Office
1000 Geary Street
San Francisco, California 94109

Commanding Officer
Office of Naval Research
219 South Dearborn Street
Chicago, Illinois 60604

Commanding Officer
Office of Naval Research Branch Office
495 Summer Street
Boston, Massachusetts 02210

Commanding Officer
Office of Naval Research Branch Office
207 West 24th Street
New York, New York 10011

Commanding Officer
Office of Naval Research Branch Office
Navy #100, Box 39, Fleet Post Office
New York, New York 09510 (2 copies)

Commanding Officer
Physics Division
U. S. Naval Ordnance Test Station
Inyokern, China Lake, California 93557

Commanding Officer
U. S. Naval Ordnance Laboratory
Corona, California 91720

Director
Research Department
U. S. Naval Ordnance Laboratory
White Oak, Silver Spring
Maryland 20900

Director
U. S. Naval Research Laboratory
Technical Information Officer
Code 2000, Code 2021
Washington, D. C. 20390 (6 copies)

Dr. P. G. Wilkinson
Navy Department
U. S. Naval Research Laboratory
Washington, D. C. 20390
Code (7140-C)

4. Department of the Air Force

Air Force Institute of Technology
Wright-Patterson Air Force Base
Ohio 45433
Attn: Library

Air Force Office of Scientific Research
Attn: SRIL
Washington, D. C. 20333

AFSWC, SWRP
Kirtland Air Force Base
New Mexico

Commander
Aeronautics Systems Division
Aeronautical Research Laboratory
Attn: Chief Scientist
Wright-Patterson Air Force Base
Ohio 45433

Commander
Aeronautics Systems Division
Wright-Patterson Air Force Base
Ohio 45433
Attn: Material Physics Division
Code ASRCP-31 (10 copies)

Systems Engineering Group
Deputy for Systems Engineering
Directorate of Technical Publications
and Specifications (SEP RR)
Wright-Patterson AF Base, Ohio 45433

Air Force Cambridge Research Laboratory
Laurence G. Hanscom Field
Attn: CRXL-R, Research Library
Bedford, Massachusetts

Commander
European Office, OAR
c/o American Embassy
Brussels, Belgium
Department of State
Washington 25, D. C.

Commanding General, AFSC
Attn: Air Force Office of
Scientific Research, AROC
Andrews Air Force Base
Washington 25, D. C. (2 copies)

Air Force Cambridge Research Labs.
Office of Aerospace Research
Technical Services Division
Attn: Research Library Branch
CRXL-R Stop #29
L. G. Hanscom Field
Bedford, Massachusetts

Deputy Chief of Staff
Plans and Operations
Headquarters, Aeronautical
Systems Division
Wright-Patterson Air Force Base
Ohio 45433
Attn: ASO

Director of Administrative Service
Headquarters, AFMDC
Hollomon Air Force Base, New Mexico
Attn: MDGRT

Director of Administrative Services
Headquarters, AWS
Scott Air Force Base, Illinois
Attn: AWSS/TIPD

Director, Air University
Maxwell Air Force Base
Alabama
Attn: Librarian

Director of Research and Development
Headquarters, United States Air Force
Washington, D. C. 20330

Director, Directorate of Technical
Services - RADC
Griffis Air Force Base
Rome, New York
Attn: RCSST

Director of Information Services
Headquarters, AFSC
Andrews Air Force Base
Washington 25, D. C.

DCS/Operations
Headquarters, AFCRL
Laurence G. Hanscom Field
Bedford, Massachusetts

Dr. T. Namioka
Air Force Cambridge Research Lab.
Attn: CR/AB
Laurence G. Hanscom Field
Bedford, Massachusetts

Dr. Yoshio Tanaka
Air Force Cambridge Research Lab.
Attn: CR/AB
Laurence G. Hanscom Field
Bedford, Massachusetts

DISTRIBUTION LIST

Executive Director
Air Force Office of Scientific Research
Washington, D. C. 20333
Attn: SRPP

Executive Secretary
Scientific Advisory Board
Office of the Chief of Staff
Headquarters, USAF
Washington, D. C. 20330

Headquarters, USAF
Attn: AFDDS
Washington 25, D. C.
For forwarding to U. S. Advisory
Groups SHAPE, ADTC, P. O. Box 174
The Hague, Netherlands
Attn: E. B. Staqles

Institute of Aeronautical Science
Two-East 64th Street
New York 21, New York

Librarian: Technical Library
Dugway Proving Ground
Dugway, Utah

Office of Aerospace Research
Headquarters, AFSC
Andrews Air Force Base
Washington 25, D. C.

Professor Joseph Kaplan
c/o Executive Secretary
Scientific Advisory Board
Office of the Chief of Staff
Headquarters, USAF
Washington, D. C. 20330

Wright Patterson Air Force Base
Attn: Air Force Material Laboratory
Dayton, Ohio 45433

5. Atomic Energy Commission

Argonne National Laboratories
Solid State Sciences Division
Argonne, Illinois 60440
Attn: Dr. Paul Bagus

Argonne National Laboratories
Solid State Chemistry Division
Argonne, Illinois 60440
Attn: Dr. Weldon G. Brown

Argonne National Laboratories
P. O. Box 299
Argonne, Illinois 60440
Attn: Dr. Fausto Fumi

Argonne National Laboratories
Solid State Sciences Division
Argonne, Illinois 60440
Attn: Dr. T. Gilbert

Argonne National Laboratories
Argonne, Illinois 60440
Attn: Dr. Gordon Goodman

Argonne National Laboratories
P. O. Box 299
Argonne, Illinois 60440
Attn: Dr. R. L. Platzman

Argonne National Laboratories
Solid State Chemistry Division
Argonne, Illinois 60440
Attn: Dr. Arnold C. Wahl

Argonne National Laboratories
Building 205
Argonne, Illinois 60440
Attn: Dr. T. F. Young

Brookhaven National Laboratories
Chemistry Department
Upton, Long Island, New York
Attn: Dr. Stanton Ehrenson

Brookhaven National Laboratories
Upton, Long Island, New York
Attn: Dr. Simon Freed

Brookhaven National Laboratory
Department of Chemistry
Upton, Long Island, New York
Attn: Dr. W. C. Hamilton

Brookhaven National Laboratories
Technical Information Division
Upton, Long Island, New York
Attn: Research Library

Carbide and Carbon Chemical Division
Central Reports and Information
Office (Y-12), P. O. Box P
Oak Ridge, Tennessee

Defense Atomic Support Agency
Washington 25, D. C.

Defense Atomic Support Agency
Sandia Base, New Mexico

Iowa State College
P. O. Box 14a, Station A
Ames, Iowa 50010
Attn: Prof. F. J. Spedding

Knolls Atomic Power Laboratory
P. O. Box 1072
Schenectady, New York
Attn: Documentation Librarian

Los Alamos Scientific Laboratory
P. O. Box 1663
Los Alamos, New Mexico
Attn: Report Librarian

Mound Laboratory
U. S. Atomic Energy Commission
P. O. Box 32
Miamisburgh, Ohio
Attn: Library and Record Center

Oak Ridge National Laboratory
Central Files
P. O. Box P
Oak Ridge, Tennessee

Oak Ridge National Laboratory
Metals and Ceramics Division
Post Office Box X
Oak Ridge, Tennessee 37831
Attn: Dr. Hubert W. Joy

Radiation Laboratory
Livermore, California
Attn: Dr. James E. Faulkner

Technical Information Service
P. O. Box 63
Oak Ridge, Tennessee
Attn: Reference Librarian (5 copies)

U. S. Atomic Energy Commission
New York Operations Office
P. O. Box 30, Ansonia Station
New York 23, New York
Attn: Division of Technical Info.
and Declassification Service

U. S. Atomic Energy Commission
Division of Biology and Medicine
Washington 25, D. C.
Attn: Dr. Leroy Augenstine

U. S. Atomic Energy Commission
Document Library
1901 Constitution Avenue N.W.
Washington 25, D. C.

U. S. Atomic Energy Commission
Technical Information Service
P. O. Box 62
Oak Ridge, Tennessee

U. S. Atomic Energy Commission
Library Branch, Technical Information
P. O. Box E
Oak Ridge, Tennessee

U. S. Atomic Energy Commission
P. O. Box E
Oak Ridge, Tennessee
Attn: Dr. Alvin M. Weinberg

University of California
Radiation Laboratory
Room 128, Building 50
Berkeley, California
Attn: Dr. R. K. Wakerling

University of Rochester
Atomic Energy Project
P. O. Box 287, Station 3
Rochester 7, New York
Attn: Technical Report-Control Unit

Western Reserve University
Atomic Energy Medical Research Project
School of Medicine, Room 365
Cleveland, Ohio 44106
Attn: Dr. H. L. Friedell

Westinghouse Electric Corporation
Atomic Power Division
P. O. 1468
Pittsburgh 30, Pennsylvania
Attn: Librarian

6. Department of Commerce

Director
National Bureau of Standards
Washington, D. C. 20234

National Bureau of Standards
Washington, D. C. 20234
Attn: Librarian

National Bureau of Standards
Washington, D. C. 20234
Attn: Dr. Harry C. Allen

National Bureau of Standards
Washington, D. C. 20234
Attn: Dr. A. M. Bass

National Bureau of Standards
107 West Building
Washington, D. C. 20234
Attn: Dr. Charles C. Beckett

National Bureau of Standards
Washington, D. C. 20234
Attn: Dr. Marian McLean Davis

National Bureau of Standards
Washington, D. C. 20234
Attn: Dr. Ugo Fano

National Bureau of Standards
Washington, D. C. 20234
Attn: Chemistry Division
Dr. Morris Krauss

National Bureau of Standards
Thermodynamics Section
Heat and Power Division
Washington, D. C. 20234
Attn: Dr. David E. Mann

National Bureau of Standards
Washington, D. C. 20234
Attn: Dr. Andrew Weiss

National Bureau of Standards
Boulder Laboratories
Boulder, Colorado 80301
Attn: Library

National Bureau of Standards
Infrared Spectroscopy Section
Atomic Physics Division
Washington, D. C. 20234
Attn: Dr. Thomas C. James

7. Other Government Agencies

Director
Advanced Research Projects Agency
The Pentagon
Room 3E 157
Washington, D. C. 20301

Central Intelligence Agency
2439 "E" Street
Washington 25, D. C.

Department of State
Office of International
Scientific Affairs
Washington 25, D. C.

Chief, Division of Scientific Services
U. S. Weather Bureau
24th and "M" Street, N.W.
Washington 25, D. C.

Director
National Science Foundation
Washington, D. C. 20550

Director
National Science Foundation
1951 Constitution Avenue
Washington, D. C. 20550
Attn: Chemistry

Library
U. S. Weather Bureau
Suitland, Maryland

National Aeronautics and
Space Administration
1520 "H" Street, N.W.
Washington, D. C. 20546
Attn: Librarian

National Advisory Committee
for Aeronautics
Lewis Research Center
Cleveland, Ohio
Attn: Chemistry (5 copies)

Scientific and Technical
Information Facility
Attn: NASA Representative
(SAK/DL-1429)
Attn: Sylvaine L. Kenyon, Chief
P. O. Box 5700
Bethesda, Maryland 20014 (2 copies)

Superintendent of Documents
U. S. Government Printing Office
Washington, D. C. 20402

Unit X, Document Expediting Project
Library of Congress
Washington 25, D. C.

B. DOMESTIC (NON-GOVERNMENT) DISTRIBUTION

Dr. William H. Adams
Department of Chemistry
Pennsylvania State University
University Park, Pennsylvania

Prof. Leland C. Allen
Department of Chemistry
Princeton University
Princeton, New Jersey

American Meteorological Society
Abstracts and Bibliography
P. O. Box 1736
Washington 13, D. C.
Attn: Mr. Malcolm Rigby

Dr. Avraham Amith
RCA Laboratories
David Sarnoff Research Center
Princeton, New Jersey

Prof. K. L. Andrew
Department of Physics
Purdue University
Lafayette, Indiana 47907

Prof. L. J. Andrews
Division of Chemistry
College of Agriculture
University of California
David, California

Applied Physics Laboratory
Johns Hopkins University
8621 Georgia Avenue
Silver Spring 19, Maryland
Attn: Director

Prof. R. M. Badger
Department of Chemistry
California Institute of Technology
Pasadena, California

Prof. M. P. Barnett
Department of Physics
Massachusetts Institute of Technology
Cambridge, Massachusetts 02100

DISTRIBUTION LIST

Prof. Gordon Barrow
Department of Chemistry
Case Institute of Technology
Cleveland, Ohio 44106

Dr. Rama Basu
Department of Chemistry
Indiana University
Bloomington, Indiana 47405

Prof. S. H. Bauer
Department of Chemistry
Cornell University
Ithaca, New York

Prof. Charles L. Beckel
Department of Physics
Georgetown University
Washington 7, D. C.

Prof. W. W. Beeman
Department of Physics
University of Wisconsin
Madison, Wisconsin 53706

Bell Telephone Laboratories
463 West Street
New York, New York 10014

Dr. Lloyd V. Berkner, President
Graduate Research Center of the Southwest
P. O. Box 8478
Dallas 5, Texas

Prof. R. Bersohn
Department of Chemistry
Columbia University
New York, New York 10027

Dr. Edmund Blau
Applied Physics Laboratory
Johns Hopkins University
8621 Georgia Avenue
Silver Spring 19, Maryland

Boeing Airplane Company
Wichita Division
Physical Sciences Staff
Plant # 1
Wichita, Kansas
Attn: J. R. Galli

Prof. L. M. Branscomb
Joint Institute for Laboratory Astrophysics
University of Colorado
Boulder, Colorado 80304

Dr. Robert G. Breene, Jr.
Physical Studies, Inc.
4761 Mad River Road
Kettering, Ohio 45429

Prof. Gregory Breit
Department of Physics
Yale University
New Haven, Connecticut

Prof. Leo Brewer
Department of Chemistry
University of California
Berkeley, California 94704

Dr. H. P. Broida
Department of Physics
University of California
Santa Barbara, California 94704

Prof. Anton B. Burg
Department of Chemistry
University of Southern California
3518 University Avenue
Los Angeles 17, California

Prof. Milton Burton
Radiation Laboratory
University of Notre Dame
Notre Dame, Indiana 46556

Prof. Melvin Calvin
Department of Chemistry
University of California
Berkeley, California 94704

Prof. Shang Yi Ch'en
Department of Physics
University of Oregon
Eugene, Oregon

Prof. Ying-Nan Chiu
Department of Chemistry
Catholic University of America
Washington 17, D. C.

Prof. George A. Clarke
Department of Chemistry
State University of New York
Buffalo 14, New York

Dr. E. Clementi
IBM Research Laboratory
Monterey and Cottle Roads
San Jose 14, California

Prof. Forrest F. Cleveland
Illinois Institute of Technology
3300 South Federal Street
Chicago, Illinois 60616

Prof. E. U. Condon
Department of Physics
University of Colorado
Boulder, Colorado 80304

Prof. Jesse B. Coon
Department of Physics
A and M College of Texas
College Station, Texas 77843

Dean Bryce L. Crawford, Jr.
School of Chemistry
University of Minnesota
Minneapolis, Minnesota 55455

DISTRIBUTION LIST

Dr. Paul C. Cross
Mellon Institute
4400 Fifth Avenue
Pittsburgh 13, Pennsylvania

Prof. B. P. Dailey
Department of Chemistry
Columbia University
New York 27, New York

Dr. F. W. Dalby
Radiation Physics Laboratory
E. I. du Pont de Nemours and Company
Wilmington 98, Delaware

Dr. T. P. Das
Department of Chemistry
University of California
Riverside, California

Prof. E. R. Davidson
Department of Chemistry
University of Washington
Seattle 5, Washington

Prof. D. M. Dennison
Department of Physics
University of Michigan
Ann Arbor, Michigan 48104

Prof. M. Dewar
Department of Chemistry
University of Texas
Austin, Texas 78712

Prof. G. H. Dieke
Department of Physics
Johns Hopkins University
Homewood Campus
Baltimore 18, Maryland

Dr. Karl Dittmer
American Chemical Society
1155 16th Street
Washington, D. C.

Father S. J. Dooling
Catholic University of America
Washington 17, D. C.

Prof. A. B. F. Duncan
Department of Chemistry
University of Rochester
River Campus Station
Rochester, New York

Mrs. Virginia L. Duncan
Lavoisier Library
E. I. du Pont de Nemours and Company
Central Research Department
Experimental R. Station
Wilmington 98, Delaware

Prof. W. M. Eberhardt
Department of Chemistry
Georgia Institute of Technology
Atlanta, Georgia

Prof. W. F. Edgell
Department of Chemistry
Purdue University
Lafayette, Indiana 47907

Dr. M. A. El-Sayed
Department of Chemistry
University of California
Los Angeles 24, California

Prof. Frank O. Ellison
Department of Chemistry
Carnegie Institute of Technology
Pittsburgh 13, Pennsylvania

Dean Henry Eyring
Department of Chemistry
University of Utah
Salt Lake City 1, Utah

Dr. Milton Farber, Vice-President
Research Laboratories
Rocket Power
3016 East Foothill Boulevard
Pasadena, California

Dr. P. Feng
Illinois Institute of Technology
Research Institute
Chicago, Illinois 60616

Prof. Eldon Ferguson
National Bureau of Standards
Boulder Laboratories
Boulder, Colorado 80301

Prof. Ricardo de Carvalho Ferrier
Department of Chemistry
Indiana University
Bloomington, Indiana 47405

Prof. George K. Fraenkel
Department of Chemistry
Columbia University
New York 27, New York

Dr. A. J. Freeman
National Magnet Laboratory
Massachusetts Institute of Technology
Cambridge, Massachusetts 02100

Prof. A. A. Frost
Department of Chemistry
Northwestern University
Evanston, Illinois 60201

General Dynamics/Convair
P. O. Box 1950
San Diego 12, California
Attn: Engineering Library
Mail Zone 6-157

General Electric Company
Space Sciences Laboratory
P. O. Box 8555
Philadelphia 1, Pennsylvania
Attn: Library Manager

DISTRIBUTION LIST

Geophysical Observatory
University of Alaska
College Alaska
Attn: Director

Prof. Leo Goldberg
Department of Astronomy
Harvard University
Cambridge, Massachusetts 02100

Prof. S. Golden
Department of Chemistry
Brandeis University
Waltham, Massachusetts

Prof. J. H. Goldstein
Department of Chemistry
Emory University
Emory, Georgia

Prof. Lionel Goodman
Department of Chemistry
Pennsylvania State University
University Park, Pennsylvania

Prof. Walter Gordy
Department of Physics
Duke University
Durham, North Carolina

Prof. M. Gouterman
Department of Chemistry
Harvard University
Cambridge, Massachusetts 02100

Prof. L. C. Green
Strawbridge Observatory
Haverford College
Haverford, Pennsylvania

Prof. John B. Greenshields
Department of Chemistry
Duquesne University
Pittsburgh, Pennsylvania

Prof. W. D. Gwinn
Department of Chemistry
University of California
Berkeley, California 94704

Prof. Stanley Hagstrom
Department of Chemistry
University of Indiana
Bloomington, Indiana 47405

Prof. R. S. Halford
Department of Chemistry
Columbia University
New York 27, New York

Prof. H. F. Hameka
Department of Chemistry
University of Pennsylvania
Philadelphia, Pennsylvania 19104

Prof. Frank C. Harris
Department of Chemistry
Stanford University
Palo Alto, California 94300

Prof. George R. Harrison
School of Science
Massachusetts Institute of Technology
Cambridge, Massachusetts 02100

Prof. L. J. Heidt
Department of Chemistry
Massachusetts Institute of Technology
Cambridge, Massachusetts 02100

Dr. Robert C. Herman
Research Laboratory
General Motors Corporation
Detroit, Michigan

Prof. Joel H. Hildebrand
Department of Chemistry
University of California
Berkeley, California 94704

Prof. J. O. Hirschfelder
Theoretical Chemistry Institute
Department of Chemistry
University of Wisconsin
Madison, Wisconsin 53706

Prof. J. R. Holmes
Department of Physics
University of Southern California
Los Angeles, California

Prof. D. F. Hornig
Department of Chemistry
Princeton University
Princeton, New Jersey

Dr. Winifred Huo
Department of Chemistry
Harvard University
Cambridge, Massachusetts 02100

Dr. Morton A. Hyman
IBM Systems Center
7220 Wisconsin Avenue
Bethesda 14, Maryland

Prof. K. K. Innes
Department of Chemistry
Vanderbilt University
Nashville, Tennessee

Institute of Aeronautical Sciences
2 East 64th Street
New York 21, New York

Prof. H. H. Jaffe
Department of Chemistry
University of Cincinnati
Cincinnati, Ohio 45221

Prof. H. M. James
Department of Physics
Purdue University
Lafayette, Indiana 47907

Dr. George J. Janz
Department of Chemistry
Rennselaer Polytechnic Institute
Troy, New York

DISTRIBUTION LIST

Prof. Joseph Kaplan
Physics Department
University of California
Los Angeles 24, California

Dr. A. M. Karo
Radiation Laboratory
University of California
Livermore, California

Prof. M. Karplus
Department of Chemistry
Columbia University
New York, New York

Prof. Michael Kasha
Department of Chemistry
Florida State University
Tallahassee, Florida

Dr. Joyce J. Kaufman
RIAS
7212 Bellona Avenue
Baltimore 12, Maryland

Prof. R. M. Keefer
Division of Chemistry
College of Agriculture
University of California
Davis, California

Prof. John Kilpatrick
Department of Chemistry
Rice University
Houston, Texas 77001

Prof. Martin Kilpatrick
Department of Physical Chemistry
Argonne National Laboratory
Building 200
Argonne, Illinois 60440

Dr. G. E. Kimball
Arthur D. Little Company
Cambridge 42, Massachusetts

Prof. R. B. King
Department of Physics
California Institute of Technology
Pasadena, California

Prof. G. B. Kistiakowsky
Department of Chemistry
Harvard University
Cambridge, Massachusetts 02100

Prof. W. Klemperer
Department of Chemistry
Harvard University
Cambridge, Massachusetts 02100

Prof. W. S. Koski
Department of Chemistry
Johns Hopkins University
Baltimore 18, Maryland

Prof. E. M. Kosower
Department of Chemistry
State University of New York
Stony Brook, New York

Prof. George Koster
Department of Physics
Massachusetts Institute of Technology
Cambridge, Massachusetts 02100

Prof. E. Miller Layton, Jr.
Department of Chemistry
Montana State College
Bozeman, Montana

Prof. Margaret N. Lewis
Department of Physics
University of Massachusetts
Amherst, Massachusetts

Prof. W. F. Libby
Department of Chemistry
University of California
Los Angeles 24, California

Dr. A. D. Liehr
Department of Theoretical Chemistry
Mellon Institute
4400 Fifth Avenue
Pittsburgh 13, Pennsylvania

Linda Hall Library
5109 Cherry Street
Kansas City 10, Missouri
Attn: Thomas Gillies, Document Div.

Prof. Bruno Linder
Department of Chemistry
Florida State University
Tallahassee, Florida

Prof. Henry Linschitz
Department of Chemistry
Brandeis University
Waltham, Massachusetts

Prof. W. N. Lipscomb
Department of Chemistry
Harvard University
Cambridge, Massachusetts 02100

Library
Abbott Laboratories
14th and Sheridan Road
North Chicago, Illinois
Attn: Dr. O. William Adams

Library
Arthur D. Little Company
30 Memorial Drive
Cambridge, Massachusetts

Prof. Chun C. Lin
Research Institute
Department of Physics
University of Oklahoma
Norman, Oklahoma 73069

DISTRIBUTION LIST

Prof. R. C. Lord
Department of Chemistry
Massachusetts Institute of Technology
Cambridge, Massachusetts 02100

Prof. Per-Olov Löwdin
Quantum Theory Project
Nuclear Science Building
University of Florida
Gainesville, Florida 32603

Prof. Peter G. Lykos
Department of Chemistry
Illinois Institute of Technology
Chicago, Illinois 60616

Prof. Julian E. Mack
Department of Physics
University of Wisconsin
Madison, Wisconsin 53706

Dr. Gulzari L. Malli
Department of Chemistry
Yale University
New Haven, Connecticut

Prof. R. A. Marcus
Institute of Mathematical Sciences
New York University
25 Waverly Place
New York, New York

Dr. R. J. Marcus
Stanford Research
Stanford, California 94300

Prof. Henry Margenau
Sloane Physics Laboratory
Yale University
New Haven 11, Connecticut

Prof. J. L. Margrave
Department of Chemistry
Rice University
Houston, Texas 77001

Prof. E. A. Mason
Institute of Molecular Physics
University of Maryland
College Park, Maryland

Prof. F. A. Matsen
Department of Chemistry
University of Texas
Austin, Texas 78712

Prof. Joseph E. Mayer
Department of Chemistry
School of Science and Engineering
University of California
LaJolla, California 92038

Prof. Harden McConnell
Department of Chemistry
Stanford University
Stanford, California 94300

Prof. S. P. McGlynn
Department of Chemistry
Louisiana State University
Baton Rouge, Louisiana 70803

Dr. A. D. McLean
IBM Research Laboratory
Monterey and Cottle Roads
San Jose, California

Dr. Donald Merrifield
Alma College
Los Gatos, California

Prof. D. H. A. Menzel
Harvard College Observatory
Harvard University
Cambridge, Massachusetts 02100

Prof. Albert Moscowitz
Department of Chemistry
University of Minnesota
Minneapolis, Minnesota 55455

Prof. Jules R. Moskowitz
Department of Chemistry
New York University
Washington Square
New York 3, New York

Prof. S. Mrozowski
Department of Physics
University of Buffalo
Buffalo, New York

Prof. Norbert Muller
Department of Chemistry
Purdue University
Lafayette, Indiana 47907

Dean J. F. Mulligan, S. J.
Rev. R. Clancy, S. J.
Fordham University
Department of Physics
New York, New York

Prof. G. M. Murphy
Department of Chemistry
New York University
Washington Square College
New York, New York

Prof. Boris Musulin
Department of Chemistry
College of Liberal Arts and Sciences
Southern Illinois University
Carbondale, Illinois 62903

National Research Council
Division of Physical Sciences
National Academy of Sciences
Washington 25, D. C.

National Research Council
2101 Constitution Avenue
Washington 25, D. C.

DISTRIBUTION LIST

Dr. R. K. Nesbet
IBM Research Laboratory
Monterey and Cottle Roads
San Jose, California

Prof. A. H. Nielsen
Department of Physics
University of Tennessee
Knoxville 16, Tennessee

Prof. H. H. Nielsen
Department of Physics
Ohio State University
Columbus, Ohio 43210

Prof. J. Rud Nielsen
Department of Physics
University of Oklahoma
Norman, Oklahoma 73069

Prof. W. A. Noyes, Jr.
Department of Chemistry
University of Texas
Austin, Texas 78712

Dr. L. E. Orgel
Salk Institute for Biological Studies
P. O. Box 9499, La Jolla
San Diego, California 92109

Dr. Rudolph Pariser
Jackson Laboratory
DuPont de Nemours and Company
P. O. Box 525
Wilmington 99, Delaware

Dr. J. M. Parks
Department of Chemistry
Room 60F, Noyes Laboratory
University of Illinois
Urbana, Illinois 61803

Prof. Robert G. Parr
Department of Chemistry
Johns Hopkins University
Baltimore, Maryland

Prof. Linus Pauling
Big Sur
California

Prof. Ralph G. Pearson
Department of Chemistry
Northwestern University
Evanston, Illinois 60201

Prof. Willis B. Person
Department of Chemistry
University of Iowa
Iowa City, Iowa 52240

Prof. John G. Phillips
Berkeley Astronomical Department
University of California
Berkeley, California 94704

Dr. W. D. Phillips
Central Research Department
Experimental Station
E. I. DuPont de Nemours and Company
Wilmington 98, Delaware

Prof. Paul Phillipson
Department of Physics
University of Colorado
Boulder, Colorado 80304

Prof. Lucy W. Pickett
Department of Chemistry
Mount Holyoke College
South Hadley, Massachusetts

Prof. G. C. Pimentel
Department of Chemistry
University of California
Berkeley, California 94704

President K. S. Pitzer
Department of Chemistry
Rice University
Houston, Texas 77001

Dr. Russell M. Pitzer
Department of Chemistry
California Institute of Technology
Pasadena, California 91109

Prof. Earle K. Plyler
Department of Physics
University of Florida
Tallahassee, Florida

The Polaroid Corporation
730 Main Street
Cambridge 39, Massachusetts
Attn: Librarian

Prof. J. A. Pople
Department of Chemistry
Carnegie Institute of Technology
Pittsburgh 13, Pennsylvania

Prof. Alexander I. Popov
Department of Chemistry
Michigan State University
East Lansing, Michigan 91965

Dr. W. J. Potts, Jr.
Spectroscopy Department
The Dow Chemical Company
Midland, Michigan

Princeton University
Princeton, New Jersey
Attn: Library, Periodicals Section

Princeton University
The James Forrestal Research
Center Library
Princeton, New Jersey
Attn: H. M. Smith

DISTRIBUTION LIST

Prof. Eugene Rabinowitch
Department of Biophysics
University of Illinois
Urbana, Illinois 61803

The Rand Corporation
1500 Fourth Street
Santa Monica, California
Attn: F. Gilmore

Prof. D. H. Rank
Department of Physics
Pennsylvania State College
State College, Pennsylvania

Prof. F. O. Rice
Department of Chemistry
University of Notre Dame
South Bend, Indiana 46556

Prof. O. K. Rice
Department of Chemistry
University of North Carolina
Chapel Hill, North Carolina

Prof. James W. Richardson
Department of Chemistry
Purdue University
Lafayette, Indiana 47907

Prof. W. W. Robertson
Department of Physics
University of Texas
Austin, Texas 78712

Prof. G. Wilse Robinson
Gates and Crellin Laboratory
California Institute of Technology
Pasadena 4, California

Dr. S. D. Ross
Research Laboratories
Sprague Electric Company
North Adams, Massachusetts

Dean Frederick D. Rossini
Notre Dame University
South Bend, Indiana 46556

Prof. Klaus Ruedenberg
Department of Chemistry
Iowa State University
Ames, Iowa 50010

Dr. R. C. Sahni
Department of Chemistry
New York University
University Heights
New York, New York

Prof. Paul N. Schatz
Department of Chemistry
University of Virginia
Charlottesville, Virginia

Prof. Charles W. Scherr
Department of Physics
University of Texas
Austin, Texas 78712

Prof. Edwin J. Schillinger, Chairman
Department of Physics
De Paul University
Chicago, Illinois 60614

Dr. D. M. Schrader
IBM Watson Scientific Computing Lab.
612 West 115th Street
New York 25, New York

Prof. Robert L. Scott
Department of Chemistry
University of California
Los Angeles, California

Prof. Harrison Shull
Department of Chemistry
University of Indiana
Bloomington, Indiana 47405

Dr. James L. Simmons
Department of Physics
Emory University
Atlanta, Georgia

Prof. W. T. Simpson
Department of Chemistry
University of Oregon
Eugene, Oregon

Prof. John J. Sinai
Department of Physics
University of Louisville
Belknap Campus
Louisville, Kentucky 40208

Dr. Oktay Sinanoglu
Department of Chemistry
Yale University
New Haven, Connecticut (2 copies)

Prof. John C. Slater
Department of Physics
Massachusetts Institute of Technology
Cambridge, Massachusetts 02100

Alfred P. Sloan Foundation
630 Fifth Avenue
Rockefeller Center
New York 20, New York

Prof. Darwin W. Smith
Chemistry Department
University of Florida
Gainesville, Florida

Dr. Richard P. Smith
Central Basic Research Laboratory
Esso Research and Engineering Company
Box 45
Linden, New Jersey

DISTRIBUTION LIST

Dr. L. C. Snyder
Bell Telephone Laboratory
Murray Hill, New Jersey

Dr. Jack Sokoloff
Lockheed Missiles and Space Division
Palo Alto, California

Prof. Rudolph Speiser
Department of Metallurgy
Ohio State University
Columbus, Ohio 43210

Prof. Lyman Spitzer, Jr.
Princeton University Observatory
Princeton, New Jersey

Prof. Andrew Streitwieser, Jr.
Department of Chemistry
University of California
Berkeley, California 94704

Prof. R. L. Strong
Department of Chemistry
Rensselaer Polytechnic Institute
Troy, New York

Prof. Miroslav Synek
Department of Physics
De Paul University
Chicago, Illinois 60614

Prof. Michael Szwarc
College of Forestry
State University of New York
Syracuse, New York

Prof. R. W. Taft, Jr.
Department of Chemistry
Pennsylvania State College
State College, Pennsylvania

Prof. Milton Tamres
Department of Chemistry
University of Michigan
Ann Arbor, Michigan 48104

Prof. H. Taube
Department of Chemistry
Stanford University
Stanford, California 94300

Prof. Howard S. Taylor
Department of Chemistry
University of Southern California
University Park
Los Angeles 7, California

Prof. William J. Taylor
Department of Chemistry
Ohio State University
Columbus, Ohio 43210

Prof. E. Teller
Lawrence Radiation Laboratory
University of California
Livermore, California

Prof. Walter Thorsen
Department of Chemistry
Massachusetts Institute of Technology
Cambridge, Massachusetts 02100

Prof. Charles H. Townes, Provost
Massachusetts Institute of Technology
Cambridge, Massachusetts 02100

Dr. Almon G. Turner
Department of Chemistry
Polytechnic Institute of Brooklyn
Brooklyn 1, New York

Prof. J. T. Vanderslice
Institute for Molecular Physics
University of Maryland
College Park, Maryland

Prof. J. H. Van Vleck
Department of Physics
Harvard University
Cambridge, Massachusetts 02100

Prof. K. Watanabe
Department of Physics
University of Hawaii
Honolulu, Hawaii

Dr. R. E. Watson
Bell Telephone Laboratories
Murray Hill, New Jersey

Prof. G. L. Weissler
Department of Physics
University of Southern California
Los Angeles 7, California

Prof. Samuel Weissman
Department of Chemistry
Washington University
St. Louis, Missouri 63130

Prof. John E. Wertz
Department of Chemistry
University of Minnesota
Minneapolis, Minnesota 55455

Prof. Eugene Wigner
Department of Physics
Princeton University
Princeton, New Jersey

Prof. E. Bright Wilson, Jr.
Department of Chemistry
Harvard University
Cambridge, Massachusetts 02100

Prof. J. G. Winans
Department of Physics
University of Buffalo
Buffalo, New York

Dr. Ta-You Wu
Department of Physics
Polytechnic Institute of Brooklyn
333 Jay Street
Brooklyn 1, New York

Dr. M. Yoshimine
IBM Research Laboratory
Monterey and Cottle Roads
San Jose, California

Dr. Clarence Zener
Westinghouse Research Laboratories
Beulah Road - Churchill Borough
Pittsburgh 35, Pennsylvania

C. UNIVERSITY OF CHICAGO DISTRIBUTION

Dean A. Adrian Albert
Eckhart Hall 111

Mr. James Bell
Laboratory of Molecular Structure
and Spectra

Prof. R. Stephen Berry
Department of Chemistry
GHJ 205

Dr. Paul E. Cade
Laboratory of Molecular Structure
and Spectra

Prof. S. Chandrasekhar
Department of Physics
R. I. 365

Chemistry Library
GHJ 204

Mr. Howard D. Cohen
Laboratory of Molecular Structure
and Spectra

Mr. Gurupada Das
Laboratory of Molecular Structure
and Spectra

Mr. John Detrich
Laboratory of Molecular Structure
and Spectra

Eckhart Library
Eckhart, 2nd Floor

Dr. M. L. Ginter
Laboratory of Molecular Structure
and Spectra

Mr. F. P. Huberman
Laboratory of Molecular Structure
and Spectra

Prof. Clyde A. Hutchison, Jr.
Department of Chemistry
R. I. 446

Prof. Mark G. Inghram
Department of Physics
Eckhart 208

Prof. Warren C. Johnson
Vice-President Special Projects
Administration 502

Dr. Joshua Jortner
Department of Chemistry
R. I. 361

Dr. Bhairav D. Joshi
Laboratory of Molecular Structure
and Spectra

Mr. Yong-Ki Kim
Laboratory of Molecular Structure
and Spectra

Mr. Marvin Kroll
Laboratory of Molecular Structure
and Spectra

Laboratory of Molecular Structure
and Spectra (20 copies)

Prof. Edward H. Levi
Provost of the University
Administration 502

Prof. Donald S. McClure
Department of Chemistry
R. I. L109

Mr. Joseph P. Olive
Laboratory of Molecular Structure
and Spectra

Prof. J. R. Platt
Department of Biophysics
R. I. 431

Dr. Y. V. Rao
Laboratory of Molecular Structure
and Spectra

Prof. Stuart A. Rice
Director, Institute for the Study
of Metals
R. I. 142

Mr. Hideo Sambe
Laboratory of Molecular Structure
and Spectra

Mrs. Eugenia Schwartz
Laboratory of Molecular Structure
and Spectra

Mr. Z. Sibincic
Laboratory of Molecular Structure
and Spectra

Mr. George A. Soukup
Laboratory of Molecular Structure
and Spectra

Prof. J. W. Stout
Department of Chemistry
R. I. 152

Mr. Theodore M. Switz
Director, Industrial Relations
Administration 501

Dr. W. L. Wessel
Laboratory of Molecular Structure
and Spectra

Prof. Leonard Wharton
Department of Chemistry
R. I. L104

Mr. Irving Wladawsky
Laboratory of Molecular Structure
and Spectra

Prof. W. H. Zachariasen
Department of Physics
Ryerson 154

D. FOREIGN (NON-GOVERNMENT) DISTRIBUTION

Dr. Asgar Ali
Quantum Chemistry Group
University of Uppsala
Uppsala, Sweden

Prof. Gentaro Araki
Department of Nuclear Engineering
Kyoto University
Yosida, Kyoto, Japan

Prof. R. K. Asundi
Spectroscopy Division
Atomic Energy Establishment Trombay
Block L, 414A Cadell Road
Bombay 28, India

Prof. Børge Bak
Kemisk Laboratorium V
H. C. Ørsted Institutet
5, Universitetsparken
University of Copenhagen
Copenhagen Ø, Denmark

*Dr. M. P. Barnett
Computer Unit
University College
University of London
London, W.C.1, England

*Dr. R. F. Barrow
Exeter College
Oxford University
Oxford, England

Prof. Otto Bastiansen
Institute of Theoretical Chemistry
Technical University of Norway
Trondheim, Norway

*Prof. D. R. Bates
Department of Applied Mathematics
The Queen's University
Belfast, Northern Ireland

Prof. Noel S. Bayliss
Department of Chemistry
University of Western Australia
Nedlands, Western Australia

*Dr. R. P. Bell
Department of Chemistry
Balliol College, Oxford University
Oxford, England

Prof. Ernst D. Bergmann
Scientific Department
Ministry of Defense
Hakirya, P. O. Box 7057
Tel-Aviv, Israel

Dr. H. J. Bernstein
Division of Physics
National Research Council of Canada
Ottawa 2, Ontario, Canada

Prof. D. L. Biermann
Fohringer Ring 6
Munich, Germany

Prof. Werner A. Bingel
Theoretical Chemistry Group
University of Göttingen
Bürgerstrabe 50 a
Göttingen, Germany

Prof. Fraser W. Birss
Department of Chemistry
University of Alberta
Edmonton, Alberta, Canada

*Dr. H. C. Bolton
Department of Theoretical Chemistry
Cambridge University
Cambridge, England

*Dr. S. F. Boys
University Chemical Laboratory
Cambridge University
Cambridge, England

Prof. Dr. G. Briegleb
Institut für Physikalische Chemie
Universität Würzburg
Würzburg, Germany

Prof. R. D. Brown
Department of Chemistry
Monash University
Clayton, Melbourne, Victoria
Australia

*Prof. A. D. Buckingham
Inorganic Chemistry Laboratory
The University of Oxford
Oxford, England

*Dr. J. H. Callomon
Department of Chemistry
University College
Gower Street, W.C.1
London, England

DISTRIBUTION LIST

*Prof. C. A. Coulson
Mathematical Institute
Oxford University
Oxford, England

*Prof. D. P. Craig
Department of Chemistry
University College
Gower Street, W.C.1
London, England

*Prof. A. Dalgarno
Department of Applied Mathematics
The Queen's University
Belfast, Northern Ireland

Prof. R. Daudel
Centre de Mecanique Ondulatoire
Appliquee
23, Rue du Maroc
Paris 19e, France

Dr. D. W. Davies
Laboratorium voor Anorganische
en Fysische Chemie
Ryksuniversiteit te Groningen
Groningen, The Netherlands

Dr. Jean Debiesse
Commissariat a l'Energie Atomique
69, Rue de Varenne
Paris VIIeme, France

Defence Scientific Information Service
Defence Research Board
Ottawa, Ontario, Canada

Prof. G. DeMaria
Instituto de Chimica Fisica
Universita di Roma
Rome, Italy

Dr. G. Diercksen
Institut für Physikalische Chemie
der J. W. Goethe Universitat
Robert-Mayer-Str. 11
6 Frankfurt 1, West Germany

Dr. A. E. Douglas
Division of Pure Physics
National Research Council of Canada
Ottawa 2, Ontario, Canada

Prof. Jules Duchesne
Institute d'Astrophysique
Universite de Liege
Coint Sclessin
Liege, Belgium

Prof. B. Edlen
Department of Physics
University of Lund
Lund, Sweden

Dr. M. A. El-Bayoumi
Faculty of Science, Moharrem Bey
Alexandria University
Alexandria, U. A. R.

Dr. M. Z. El-Sabban
Vaccine and Serum Institute
Agonza, Cairo, Egypt

*Prof. A. von Engel
Claredon Laboratory
University of Oxford
Oxford, England

*Dr. Dennis F. Evans
Imperial College of Science and
Technology
Department of Chemistry
London S.W.7, England

Prof. Inga Fischer-Hjalmars
Institute of Theoretical Physics
Norrtullsgatan 16
Stockholm V A, Sweden

Prof. Dr. Th. Förster
Laboratorium für Physikalische
Chemie and Electrochemie der
Technischen Hochschule
Stuttgart N, Germany

Dr. S. Fraga
Department of Chemistry
University of Alberta
Edmonton, Alberta, Canada

Prof. Yoshio Fujioka
Institute for Optical Research
Tokyo University of Education
400, 4-Chome, Hyakunin-Machi
Shinjuku-ku, Tokyo, Japan

*Prof. A. G. Gaydon
Chemical Engineering Department
Imperial College of Science and
Technology
London S.W.7, England

Dr. Giovanni Giacometti
Instituto de Chimica-Fisica
Via Lorendan 4a
Padova, Italy

*Prof. Victor Gold
Department of Chemistry
Kings College, University of London
Strand W.C.2, England

Prof. P. Goldfinger
Universite Libre de Brussels
50, Avenue F. D. Roosevelt
Brussels, Belgium

Dr. J. S. Griffith
Department of Theoretical Chemistry
Cambridge University
Cambridge, England

Prof. Rafael Grinfeld
Departamento de Fisica
Universidad Nacional de la Plata
Calle 115 y 49 - La Plata
Republica Argentian

DISTRIBUTION LIST

Prof. H. H. Guenthard
Institut für Organische Chemie
Eidgenössische Technische Hochschule
Zürich, Switzerland

*Prof. G. G. Hall
Department of Mathematics
University of Nottingham
Nottingham, England

Dr. N. S. Ham
Commonwealth Scientific and Industrial Research Organization
Division of Industrial Chemistry
Box 4331, G.P.O.
Melbourne, Australia

Prof. Dr. H. Hartmann
Institut für Physikalische Chemie der Universität Frankfurt-am Main
Robert Meyer Strasse 11
Frankfurt-am Main 1, Germany

Prof. Odd Hassel
Universitet Kjemiske Institut
Blindern-Oslo, Norway

Dr. Karl H. Hausser
Max-Planck-Institut für Medizinische Forschung
Institut für Chemie
Jahnstrasse 29
Heidelberg, Germany

Prof. E. Havinga
Department of Chemistry
University of Leiden
Leiden, The Netherlands

*Prof. R. J. R. Hayward
School of Chemistry
The University
Leeds 2, England

Prof. E. Heilbronner
Institut für Organische Chemie
Eidgenössische Technische Hochschule
Zürich, Switzerland

Dr. G. Herzberg
Division of Pure Physics
National Research Council of Canada
Ottawa 2, Ontario, Canada

Dr. K. Higasi
The Research Institute of Applied Electricity
Hokkaido University
Sapporo, Japan

*Sir Cyril H. Hinshelwood
Laboratory of Physical Chemistry
Oxford University
Oxford, England

Prof. G. Jan Hoijtink
Laboratory for Physical Chemistry
University of Amsterdam
Nwe Prinsengracht 12b
Amsterdam, The Netherlands

Prof. Erik Hulthén
Laboratory of Physics
University of Stockholm
Stockholm, Sweden

Prof. Lamek Hulthén
Institute for Applied Mathematics
Royal Institute of Technology
Stockholm, Sweden

Prof. F. Hund
Institut für Theoretische Physik der Universität Göttingen
Göttingen, Germany

Dr. Andrew Hurley
Chemical Physics Section
C.S.I.R.O.
Melbourne, Australia

Prof. S. Huzinaga
General Education Department
Kyushu University
Otubo-Machi, Fukuoka, Japan

Prof. E. A. Hylleraas
Institute for Theoretical Physics
Oslo University
Blindern, Oslo, Norway

Prof. Y. I'Haya
Department of Chemistry
University of Electro-Communications
Chofu-shi, Tokyo, Japan

*Prof. C. K. Ingold
Department of Chemistry
University College, Gower Street
London, W.C. 1, England

Prof. T. Inue
Department of Applied Physics
Faculty of Engineering
University of Tokyo
Tokyo, Japan

Dr. Laurens Jansen
Institut Battelle
7, Route de Drite
Geneva, Switzerland

Prof. J. Janin
Institut de Physique Generale
Universite de Lyon
Lyon, France

Dr. Chr. Klixbüll Jørgensen
Cyanamid European Research Institute
Cologny (Geneva), Switzerland

DISTRIBUTION LIST

Prof. M. L. Josien
Laboratoire De Chimie XIII
8, Rue Cuvier
Paris (Ve), France

Dr. D. Kastler
University of Saarbrücken
Saarbrücken, Germany

Prof. J. A. A. Ketelaar
Laboratorium voor Elektrochemie
Der Universitat Amsterdam
Amsterdam (Centrum), The Netherlands

Dr. M. Aslam Khan
Department of Physics
University of Karachi
Karachi, Pakistan

Prof. Oskar B. Klein
Institute for Mechanics and
Mathematical Physics
Narrtullsgatan 16
Stockholm, Sweden

Prof. Dr. G. Kortüm
Physikalisch-chemisches Institut
der Universität
Wilhelmstrasse 33
Tübingen, Germany

Prof. Masao Kotani
Department of Physics
University of Tokyo
Bunkyo-ku, Tokyo, Japan (2 copies)

Dr. Tanekazu Kubota
Shionogi Research Laboratory
Sagisu, Fukushima-ku
Osaka, Japan

Dr. Akira Kuboyama
Government Chemical Industrial
Research Institute, Tokyo
Shibuya-ku
Tokyo, Japan

Prof. Hans Kuhn
Physikalisch-chemisches Institüt
der Universität
Marbacher Weg 15
Marburg, Germany

Dr. Heinrich Labhart
CIBA, Gesellschaft für Chemische
Indistrie Basel
Basel, Switzerland

Prof. A. Lagerqvist
Laboratory of Physics
University of Stockholm
Stockholm, Sweden

Dr. H. Lemaire
Centre d'Etudes Nucleaires
de Grenoble
Chemin des Martyrs
Boite Postale Nr. 269
Grenoble [Isere], France

Library of Institute for Nuclear
Study
University of Tokyo
Tanashi-Machi - Kitatama-Gun
Tokyo, Japan

*Dr. J. W. Linnett
The Queen's College
Oxford University
Oxford, England

Dr. Ernst Lippert
Laboratorium für Physikalische Chemie
und Elektrachemie der Technischen
Hochschule
Stuttgart, Germany

Prof. W. Lochte-Holtgraven
Institut für Experimental-Physik
University of Kiel
Kiel, Germany

Dr. Alf Lofthus
Physical Institute
University of Oslo
Blindern-Oslo, Norway

*Prof. H. C. Longuet-Higgins
Department of Theoretical Chemistry
University of Cambridge
Cambridge, England

Prof. Per-Olov Löwdin
Quantum Chemistry Group
University of Uppsala
Uppsala, Sweden (2 copies)

Prof. W. Lüttke
Organisch Chemisches Institut
der Universität
Hospitalistrasse 8-11
Göttingen, Germany

*Prof. A. MacColl
Department of Chemistry
University College
London University, Gower Street
London, W.C. 1, England

Dr. L. Mackor
Koningklijke/Shell Laboratorium
Amsterdam, The Netherlands

Dr. Valerio Magnasco
Institute of Industrial Chemistry
University of Genoa
Genoa, Italy

DISTRIBUTION LIST

Dr. E. A. Magnusson
Science Department
A. M. College
Cooranbong N.S.
Western Australia

Prof. Dr. W. Maier
Physikalisches Institut der Universität
Katherinenstrasse 25
Freiburg im Breisgau, Germany

Prof. C. Manneback
27, Rue de la Tourelle
Brussels 4, Belgium

*Prof. S. F. Mason
School of Chemical Sciences
University of East Anglia
Norwich, England

*Prof. H. S. W. Massey
University College
University of London
London, England

Prof. C. A. McDowell
Department of Chemistry
University of British Columbia
Vancouver 8, B.C., Canada

*Prof. R. McWeeny
Quantum Theory Group
University of Keele
North Staffordshire, England

Prof. Dr. R. Mecke
Institut für Physikalische Chemie der
Universität Freiburg im Breisgau
Freiburg im Breisgau, Germany

Prof. E. Miescher
Department of Physics
University of Basel
Basel, Switzerland

Prof. S. I. Mizushima
Department of Chemistry
Faculty of Science
Tokyo University
Hongo, Tokyo, Japan

Dr. Roberto Moccia
Instituto Chimico della Universita
Via Mezzocannone 4
Napoli, Italy

Prof. Yonezo Morino
Department of Physical Chemistry
Faculty of Science
Tokyo University
Bunkyo-ku, Tokyo, Japan

Dr. James D. Morrison
Division of Chemical Physics
C.S.I.R.O.
Melbourne, Australia

Dr. Carl Moser
Centre de Mecanique Ondulatoire
Appliquee
155, Rue de Sevres
Paris 15e, France

*Prof. J. N. Murrell
Department of Chemistry
University of Sussex
Sussex, England

Prof. S. Nagakura
Institute of Science and Technology
University of Tokyo
No. 856, Komba-cho
Meguro-ku, Tokyo, Japan

Prof. R. Nakamura
Research Institute for Catalysis
Hokkaido University
Sapporo, Japan

Dr. N. A. Narasimham
Government of India
Atomic Energy Establishment Trombay
Chemical Division, Block L 414 A
Cadell Road
Bombay 28, India

Dr. S. M. Naude
South African Council for Scientific
and Industrial Research
P. O. Box 395
Pretoria, South Africa

Prof. R. W. Nicholls
Department of Physics
The University of Western Ontario
London, Ontario, Canada

Dr. W. C. Nieuwpoort
Phillips Research Laboratories
N. V. Phillips Gloerlampenfabrieken
Eindhavon, The Netherlands

Prof. K. Niira
Tokyo Institute of Technology
Oh-Okyama, Tokyo, Japan

Prof. Isamu Nitta
Science Department
Kwansei Gakuin University
Uegahara, Nishinomiya
Hyogo-Ken, Japan

*Prof. F. W. G. Norrish
Department of Physical Chemistry
Cambridge University
Cambridge, England

*Prof. R. S. Nyholm
Department of Chemistry
University College
London University, Gower Street
London, W.C. 1, England

DISTRIBUTION LIST

Dr. Kimio Ohno
Department of Chemistry
Hokkaido University
Sapporo, Japan

Dr. Yuzuru Ooshika
Physics Department
Kwansei Gakuin University
Nishinomiya, Japan

Prof. L. J. Oosterhoff
Department of Chemistry
University of Leiden
Leiden, The Netherlands

*Prof. W. J. Orville-Thomas
Edward Davies Chemical Laboratory
University College of Wales
Aberystwyth, Wales 7634

Prof. M. R. Padhye
Physics Department
Indian Institute of Technology
Powai Bombay, India

Prof. D. D. Pant
D. S. B. Government College
Naini Tal (U.P.)
India

Prof. Ruben Pauncz
Chemistry Department
Technion
Israel Institute of Technology
Haifa, Israel

*Dr. J. E. Peacock
Department of Chemistry
University of London King's College
Strand, W.C. 2,
London, England

Dr. C. L. Pekeris
Department of Applied Mathematics
The Weissman Institute
Rehovoth, Israel

*Dr. David Peters
Department of Chemistry
Royal Holloway College
University of London
Englefield Green, Surrey, England

Dr. Sigrid Peyerimhoff
Institut f. Theoretische Physik
Justus Liebig Universitaet
63, Giessen, Lahn
West Germany

Prof. J. C. Polanyi
Department of Chemistry
University of Toronto
Toronto 5, Ontario, Canada

*Prof. G. Porter
Department of Chemistry
Sheffield University
Sheffield, England

Dr. H. Preuss
Max-Planck-Institut
für Physik und Astrophysik
München 23 - Aumeisterstrasse 6
Germany

*Prof. W. C. Price
Department of Physics
University of London King's College
Strand, W.C. 2, London, England

Prof. Hans Primas
Institute für Physikalische Chemie
Eig. Technische Hochschule
Zürich, Switzerland

*Dr. H. O. Pritchard
Department of Chemistry
Manchester University
Manchester, England

*Prof. M. H. L. Pryce
Department of Physics
The University
Bristol, England

Prof. B. Pullman
Laboratoire de Chimie Theorique
Institut de Biologie Physico-Chimique
Universite de Paris
13, Rue Pierre Curie
Paris Ve, France

Dr. P. G. Puranik
Department of Physics
Osmania University
India

Prof. G. Racah
The Hebrew University
Jerusalem, Israel

Dr. D. A. Ramsay
Division of Pure Physics
National Research Council of Canada
Ottawa 2, Ontario, Canada

Prof. K. Rangadhawa Rao
College of Science and Technology
Andhra University
Waltair, (Andhra Pradesh)
India

*Prof. F. H. Read
The Physical Laboratories
The University
Manchester 13, England

DISTRIBUTION LIST

Dr. A. L. G. Rees
Division of Industrial Chemistry
Commonwealth Scientific and Industrial
Research Organization
Box 4331, G.P.O.
Melbourne, Australia

Prof. C. Reid
Department of Chemistry
University of British Columbia
Vancouver, Canada

*Dr. R. E. Richards
Laboratory of Physical Chemistry
Oxford University
Oxford, England

Dr. B. Rosen
Institut D'Astrophysique
Universite de Liege
Cointe-Sclessin, Belgium

*Dr. R. A. Sack
Department of Mathematics
Royal Technical College
Salford 5 Lancs, England

*Dr. Keith D. Sales
Department of Chemistry
Queen Mary College
London, England

Dr. L. G. Salomon
Central Laboratorium
Juliana laan 134
Delft, The Netherlands

Prof. Camille Sandorfy
Department of Chemistry
University of Montreal
Montreal, Canada

Prof. G. Scheibe
Physikalisch-Chemisches und
Elektrochemisches Institut der
Technischen Hochschule München
München 2, Germany

Dr. H. H. Schmidtke
Cyanamid European Research Institute
91 Route de la Capite
Cologny (Geneve), Switzerland

Prof. Otto Schnepp
Department of Chemistry
Institute of Technology
Haifa, Israel

Prof. Dr. H. Schüler
Forschungsstelle für Spektroskopie
In der Max-Planck Gesellschaft
Bunsenstrasse 10
Göttingen, Germany

Prof. Georg Maria Schwab
Institut für Physikalische Chemie
der Universität
Munich, Germany

Prof. F. Seel
Institut für Physikalische Chemie
der Universität Würzburg
Würzburg, Germany

Dr. I. Shavitt
Laboratory of Physical Chemistry
Israel Institute of Technology
Haifa, Israel

Prof. N. L. Singh
Department of Spectroscopy
Banaras Hindu University
Varanasi-5 (U.P.), India

*Dr. H. A. Skinner
Department of Chemistry
University of Manchester
Manchester, England

Prof. Dr. R. Suhrmann
Institut für Physikalische Chemie und
Electrochemie der Technischem
Hochschule Schleinitzstrasse
Braunschweig, Germany (20 b)

*Dr. G. B. B. M. Sutherland, Director
National Physical Laboratory
Teddington, England

*Dr. Leslie E. Sutton
Magdalen College, Oxford University
Oxford, England

Prof. P. Swings
Institut d'Astrophysique
Universite de Liege
Cointe-Schlessin
Liege, Belgium

*Prof. M. C. R. Symons
Department of Chemistry
The University
Leicester, England

Prof. N. R. Tawde
Department of Physics
Karnatak University
Dharwar, India

*Dr. B. A. Thrush
Department of Physical Chemistry
Cambridge University
Cambridge, England

*Dr. Colin Thomson
Department of Theoretical Chemistry
University Chemical Laboratory
Cambridge, England

DISTRIBUTION LIST

Prof. K. Tomita
Department of Physics
Kyoto University
Kyoto, Japan

Prof. H. Tsubomura
Faculty of Engineering Science
Toyonaka, Osaka, Japan

*Prof. A. R. Ubbelohde
Chemical Engineering Department
Imperial College of Science
and Technology
London, S.W.7, England

Dr. J. H. Van Der Waals
Koninklijke/Shell Laboratorium
Amsterdam, The Netherlands

Prof. Putcha Venkateswarlu
Department of Physics
Agricultural Gardens
Indian Institute of Technology
Kanpur, (U.P.) India

Prof. R. D. Verma
Department of Physics
University of New Brunswick
Fredericton, New Brunswick
Canada

Prof. B. Vodar
Laboratoires de Bellevue
Centre National de la
Recherche Scientific
1, Place Aristide-Briand
Bellevue, France

Prof. Ivar Waller
Institute of Mechanics and
Mathematical Physics
University of Uppsala
Trädgardsgatan 13
Uppsala, Sweden

*Prof. A. D. Walsh
Department of Chemistry
Queen's College
University of Saint Andrew
Dundee, Scotland

*Dr. E. Warhurst
Department of Chemistry
University of Manchester
Manchester, England

Prof. A. Weller
Scheikundig Laboratorium
der Vriji Universiteit
Amsterdam - Z
The Netherlands

Prof. H. L. Welsh
Department of Physics
University of Toronto
Toronto, Ontario, Canada

Prof. Antoine Zahlan
Department of Physics
American University of Beirut
Beirut, Lebanon

°Unless indicated otherwise, each addressee receives one copy.

*Through Office of Assistant Naval Attache for Research
Navy # 100, Box 39
Fleet Post Office
New York, New York 09510

All addressees are respectfully requested to notify the Laboratory of Molecular Structure and Spectra, Department of Physics, The University of Chicago, Chicago Illinois 60637, of any change of address.

UNCLASSIFIED
Security Classification

DOCUMENT CONTROL DATA - R & D

1. Originating Activity

Department of Physics
University of Chicago
Chicago, Illinois 60637

2a. Report Security Classification
UNCLASSIFIED

2b. Group

3. Report Title

LABORATORY OF MOLECULAR STRUCTURE AND SPECTRA TECHNICAL REPORT, 1964

4. Descriptive Notes

Annual Joint Technical Report of research accomplished during the period 1 January through 31 December, 1964.

5. Authors

Mulliken, R. S. and Roothaan, C. C. J. (Principal Investigators). See Table of Contents for the complete list of additional authors.

6. Report Date	7a. Total No. of Pages	7b. No. of References
1 January through 31 December, 1964	296	Approx. 200

8. Contract Nos.

a. Contract Nonr-2121 (01)
b. Project No. 014-101

a. Contract AF19(628)-2474
b. Project No. CRL-0346

a. Contract DA-11-022-ORD-3119
b. D/A Project No. 5b51-02-004
ARO (D) Project No. 3835-P
c. Task No. 4

a. Contract AF33(657)-8891
b. Project No. 7360
c. Task No. 736004

9a. Originators Report No.
LMSS TR 1964

9b. Other Report Nos.

10. Availability/Limitation Notices

Qualified requesters may obtain copies of this report from DDC.

11. Supplementary Notes

12. Sponsoring Military Activity

Office of Naval Research, Physics Branch
Washington, D. C. 20360

Office of Aerospace Research, United States AF
Laurence G. Hanscom Field, Bedford, Mass.

Army Research Office (Durham), Box CM,
Duke Station, Durham, North Carolina 27706

Research and Technology Division, Air Force
Systems Command, USAF, Wright-Patterson
Air Force Base, Ohio 45433

13. Abstract:

This is a collection of related, but independent, theoretical and experimental studies concerned with the electronic structure of atoms and molecules. Hartree-Fock or SCF wavefunctions are given for Neon-like and Argon-like ions, F_2, N_2, CO, BF, and NeH^+ and HeH^+ molecular ions. X-ray transition probabilities are also given for Nion-like and Argon-like ions and a number of molecular properties are given for F_2, CO, BF. The octopole moment of methane is calculated. Mathematical expressions are given for certain generalizations of Laplace's expansion. The rotational-electronic interaction for the Rydberg states of diatomic molecules is examined as is the electric quadrupole and magnetic dipole radiation in linear molecules ($^1\Pi$ - $^3\Pi$ transitions). Experimental studies are presented for some weak systems of N_2 and certain Rydberg states of He_2.

DD FORM 1 JAN 64 1473

UNCLASSIFIED
Security Classification

14. KEY WORDS	LINK A		LINK B		LINK C	
	ROLE	WT	ROLE	WT	ROLE	WT
Hartree-Fock Wave Functions						
Diatomic Molecules						
X-ray Transition Probabilities						
Rydberg States						
Rotational-Electronic Interaction						
Electric Quadrupole Radiation						
Helium Molecule						
Laplace Expansion						

INSTRUCTIONS

1. ORIGINATING ACTIVITY: Enter the name and address of the contractor, subcontractor, grantee, Department of Defense activity or other organization *(corporate author)* issuing the report.

2*a*. REPORT SECURITY CLASSIFICATION: Enter the overall security classification of the report. Indicate whether "Restricted Data" is included. Marking is to be in accordance with appropriate security regulations.

2*b*. GROUP: Automatic downgrading is specified in DoD Directive 5200.10 and Armed Forces Industrial Manual. Enter the group number. Also, when applicable, show that optional markings have been used for Group 3 and Group 4 as authorized.

3. REPORT TITLE: Enter the complete report title in all capital letters. Titles in all cases should be unclassified. If a meaningful title cannot be selected without classification, show title classification in all capitals in parenthesis immediately following the title.

4. DESCRIPTIVE NOTES: If appropriate, enter the type of report, e.g., interim, progress, summary, annual, or final. Give the inclusive dates when a specific reporting period is covered.

5. AUTHOR(S): Enter the name(s) of author(s) as shown on or in the report. Enter last name, first name, middle initial. If military, show rank and branch of service. The name of the principal author is an absolute minimum requirement.

6. REPORT DATE: Enter the date of the report as day, month, year; or month, year. If more than one date appears on the report, use date of publication.

7*a*. TOTAL NUMBER OF PAGES: The total page count should follow normal pagination procedures, i.e., enter the number of pages containing information.

7*b*. NUMBER OF REFERENCES: Enter the total number of references cited in the report.

8*a*. CONTRACT OR GRANT NUMBER: If appropriate, enter the applicable number of the contract or grant under which the report was written.

8*b*, 8*c*, & 8*d*. PROJECT NUMBER: Enter the appropriate military department identification, such as project number, subproject number, system numbers, task number, etc.

9*a*. ORIGINATOR'S REPORT NUMBER(S): Enter the official report number by which the document will be identified and controlled by the originating activity. This number must be unique to this report.

9*b*. OTHER REPORT NUMBER(S): If the report has been assigned any other report numbers *(either by the originator or by the sponsor)*, also enter this number(s).

10. AVAILABILITY/LIMITATION NOTICES: Enter any limitations on further dissemination of the report, other than those imposed by security classification, using standard statements such as:

(1) "Qualified requesters may obtain copies of this report from DDC."

(2) "Foreign announcement and dissemination of this report by DDC is not authorized."

(3) "U. S. Government agencies may obtain copies of this report directly from DDC. Other qualified DDC users shall request through _____."

(4) "U. S. military agencies may obtain copies of this report directly from DDC. Other qualified users shall request through _____."

(5) "All distribution of this report is controlled. Qualified DDC users shall request through _____."

If the report has been furnished to the Office of Technical Services, Department of Commerce, for sale to the public, indicate this fact and enter the price, if known.

11. SUPPLEMENTARY NOTES: Use for additional explanatory notes.

12. SPONSORING MILITARY ACTIVITY: Enter the name of the departmental project office or laboratory sponsoring *(paying for)* the research and development. Include address.

13. ABSTRACT: Enter an abstract giving a brief and factual summary of the document indicative of the report, even though it may also appear elsewhere in the body of the technical report. If additional space is required, a continuation sheet shall be attached.

It is highly desirable that the abstract of classified reports be unclassified. Each paragraph of the abstract shall end with an indication of the military security classification of the information in the paragraph, represented as *(TS)*, *(S)*, *(C)*, or *(U)*.

There is no limitation on the length of the abstract. However, the suggested length is from 150 to 225 words.

14. KEY WORDS: Key words are technically meaningful terms or short phrases that characterize a report and may be used as index entries for cataloging the report. Key words must be selected so that no security classification is required. Identifiers, such as equipment model designation, trade name, military project code name, geographic location, may be used as key words but will be followed by an indication of technical context. The assignment of links, roles, and weights is optional.

DD FORM 1 JAN 64 1473 (BACK)